O'ZBEKISTON RESPUBLIKASI
FANLAR AKADEMIYASI

Mexanika va inshootlar seysmik mustahkamligi instituti
MISMI

International Conference: Mechanics, Earthquake Engineering, Machinery Building

Международная конференция: Механика, Сейсмостойкость, Машиностроение

«Ensuring seismic safety and seismic stability of buildings and structures, applied problems of mechanics»

dedicated to the 90th anniversary of Academician T.R. Rashidov

«Обеспечение сейсмической безопасности и сейсмостойкости зданий и сооружений, прикладные задачи механики»

посвященная 90-летию академика АН РУз Т.Р. Рашидова

I-TOM

May 27-29, 2024. Tashkent, Uzbekistan
27-29 мая 2024 г. Ташкент, Узбекистан

Кабинет Министров Республики Узбекистан
Академия наук Республики Узбекистан
Институт механики и сейсмостойкости сооружений им. М.Т.Уразбаева
Институт сейсмологии им. Г.О. Мавлянова
Национальный университет Узбекистана им. Мирзо Улугбека
Самаркандский государственный университет
Ташкентский архитектурно-строительный университет
Самаркандский государственный архитектурно-строительный университет
Санкт-Петербургский политехнический университет Петра Великого
Калифорнийский университет в г. Беркли

СБОРНИК МАТЕРИАЛОВ МЕЖДУНАРОДНОЙ КОНФЕРЕНЦИИ: МЕХАНИКА, СЕЙСМОСТОЙКОСТЬ, МАШИНОСТРОЕНИЕ

ПО ПРОБЛЕМАМ

ОБЕСПЕЧЕНИЯ СЕЙСМИЧЕСКОЙ БЕЗОПАСНОСТИ И СЕЙСМОСТОЙКОСТИ ЗДАНИЙ И СООРУЖЕНИЙ, ПРИКЛАДНЫЕ ЗАДАЧИ МЕХАНИКИ

посвященная 90-летию академика АН РУз Т.Р. Рашидова
27-29 мая 2024 года

I – ТОМ

Ташкент

Сборник материалов международной научной конференции: Механика, Сейсмостойкость, Машиностроение по проблемам «Обеспечения сейсмической безопасности и сейсмостойкости зданий и сооружений, прикладные задачи механики», посвященной 90-летию академика АН РУз Т.Р. Рашидова.

Сборник материалов состоит из 3х томов:

I-Том содержит материалы секций 1 «Сейсмостойкость зданий и сооружений»,
2 «Инженерная сейсмология и сейсмический риск»;

II-Том содержит материалы секции 3 «Механика деформируемого твердого тела, геотехника»;

III-Том содержит материалы секций 4 «Механика жидкости, газа и многофазных сред»,
5 «Динамика и прочность машин».

В сборнике международной конференции представлены научные доклады из научно-исследовательских организаций и университетов Узбекистана, Казахстана, Кыргызстана, США, России, Таджикистана.

В сборнике материалы посвящены актуальным проблемам обеспечения сейсмической безопасности и сейсмостойкости зданий и сооружений, а также решению прикладных задач механики. Материалы сборника освещают широкий круг вопросов по междисциплинарным исследованиям проблем теоретической и прикладной механики: представлены последние инновационные результаты научных исследований, а также новейшие разработки и тенденции широкого спектра задач механики, включая эксперименты, численные результаты и приложения. Избранные доклады будут опубликованы в Узбекском журнале Проблемы механики, AIP Conference Proceedings и Magazine of Civil Engineering. В сборнике все статьи представлены в авторской редакции.

Сборник материалов будет полезен научным работникам, преподавателям, докторантам и студентам вузов.

Collection of materials of the International Scientific Conference: Mechanics, Seismic Resistance, Mechanical Engineering on the problems of "Ensuring Seismic Safety and Seismic Resistance of Buildings and Structures, Applied Problems of Mechanics", dedicated to the 90th anniversary of Academician of Academy of Sciences of RUz T.R. Rashidov

The collection of materials consists of 3 volumes:

Volume I contains materials of sections 1 “Seismic resistance of buildings and structures” and
2 “Engineering seismology and seismic risk”;

Volume II contains materials of section 3 “Mechanics of deformable rigid bodies, geotechnics”;

Volume III contains materials of sections 4 “Mechanics of liquids, gases, and multiphase media” and
5 “Dynamics and strength of machines.”

The proceedings of the International Conference of present scientific reports from research institutions and universities of Uzbekistan, Kazakhstan, Kyrgyzstan, the USA, Russia, and Tajikistan.

Materials of the collection of reports are devoted to current problems of ensuring seismic safety and seismic resistance of buildings and structures and solving applied problems of mechanics. The proceedings cover a wide range of issues in interdisciplinary research into problems of theoretical and applied mechanics: the latest innovative results of scientific research and the latest developments and trends in numerous mechanics problems, including experiments, numerical results, and applications. Selected reports will be published in the Uzbek Journal of Problems of Mechanics, AIP Conference Proceedings and Magazine of Civil Engineering. In the collection, all articles are presented in the author's edition.

The collection of reports will be useful to researchers, lecturers, doctoral students, and university students.

ОРГАНИЗАТОРЫ

Юлдашев Бехзод Садыкович
Президент Академии наук Республики Узбекистан

Закиров Батир Иркинович
Министр строительства и жилищно-коммунального хозяйства Республики Узбекистан

Кулдашев Абдулла Хамидуллаевич
Министр по чрезвычайным ситуациям Республики Узбекистан

Бекмирзаев Диёрбек Абдугаппорович
Заместитель начальника отдела координации вопросов обеспечения сейсмической безопасности Кабинет Министров Республики Узбекистан

ОРГАНИЗАЦИОННЫЙ КОМИТЕТ КОНФЕРЕНЦИИ

Юлдашев Бехзод Садыкович (*председатель*)
Президент Академии наук Республики Узбекистан, доктор физико-математических наук, профессор. Ташкент, Узбекистан

Султанов Карим Султанович (*сопредседатель*)
доктор физико-математических наук, профессор, директор Института механики и сейсмостойкости сооружений АН РУз. Ташкент, Узбекистан

Ватин Николай Иванович (*сопредседатель*)
доктор технических наук, профессор, Санкт-Петербургский политехнический университет Петра Великого. Санкт-Петербург, Россия

МЕЖДУНАРОДНЫЙ КОНСУЛЬТАТИВНЫЙ КОМИТЕТ

Нигматулин Р.И. – Академик РАН, д.ф.-м.н., профессор, Московский государственный университет имени М.В.Ломоносова. Москва, РОССИЯ

Марко Амабили – профессор, Инженерный факультет Университета Вестлейка, Ханчжоу, Китай.

Амаржит Сингх – профессор, Машиностроительный факультет, Национальный технологический институт Хамирпур, Индия.

Быковцев А.С. – д.т.н., профессор, Региональная академия естественных наук, Калифорния, США.

Рашид Зегаид – профессор, Университет Касди Мерба Уаргла, Уаргла, Алжир.

Бассас А. Тайах – профессор, Строительный факультет, Исламский университет Газы, Газа.

Энрике Да Сильва Пиззо – Строительство/Водные ресурсы, Факультет гидравлический измерений, Муниципальная санитарно-техническая компания Жуис де Фора, Минас Жераис, Бразилия.

Мирсаидов М.М. – Академик АН РУз, доктор технических наук, профессор, Национальный исследовательский университет "Ташкентский институт инженеров ирригации и механизации сельского хозяйства". Ташкент, Узбекистан.

Бахадиров Г.А. – профессор, Институт механики и сейсмостойкости сооружений АН РУз. Ташкент, Узбекистан.

Саурав Диксит – профессор, Профессиональный университет Ловли, Фагвара, Пенджаб, Индия

Тахиров Ш.М. – профессор, Калифорнийский Университет в Беркли, США.

Ху Донгшенг – профессор, Технологический университет Уханя, Ухань, Китай

Абиров Р.А. – старший научный сотрудник, Институт механики и сейсмостойкости сооружений АН РУз. Ташкент, Узбекистан.

ПРОГРАММНЫЙ КОМИТЕТ КОНФЕРЕНЦИИ

Абдуллабеков К.Н. Академик АН РУз. г. Ташкент.
Негматуллаев С.Х. Академик НАН РТ, г. Душанбе.
Мамасаидов М.Т. Академик НАН КР, г. Ош.
Ильичев В.А. Академик РААСН, г. Москва.
Алексеева Л.А. д.ф.-м.н., проф. г. Алматы.
Абдикаримов Р.А. д.ф.-м.н., проф. г. Ташкент.
Абдусаттаров А.А. д.т.н., проф. г. Ташкент.
Ахмедов А.Б. д.ф.-м.н., проф. г. Ташкент.
Бегалиев У.Т. д.т.н., проф. г. Бишкек.
Бегматов А.Б. д.ф.-м.н., проф. г. Ташкент.
Георгиевский Д.В. д.ф.-м.н., проф. г. Москва
Исаханов Е.А. д.т.н., проф. г. Алматы.
Исмаилов В.А. д.г.-м.н., проф. г. Ташкент.
Исмоилова С.И. д.т.н. г. Ташкент.
Исраилов М.Ш. д.ф.-м.н., проф. г. Грозный
Халджигитов А.А. д.ф.-м.н., проф. г. Ташкент
Хожметов Г.Х. д.т.н., проф. г. Ташкент.
Худайназаров Х.Х. д.т.н., проф. г. Ташкент.
Хужаев И.К. д.т.н., проф. г. Ташкент.
Хусанов Б.Э. д.ф.-м.н. г. Ташкент.
Хужаёров Б.Х. д.ф.-м.н., проф. г. Самарканд
Коршунова Н.А. д.ф.-м.н., проф. г. Ташкент.
Кузнецов С.В. д.ф.-м.н., проф. г. Москва
Маликов З.М. д.т.н., проф., г. Ташкент
Мухаммадиев Д.М. д.т.н., проф. г. Ташкент.
Мардонов Б.М. д.ф.-м.н., проф. г. Ташкент.
Мирзаев И.М. д.ф.-м.н., проф. г. Ташкент.
Москвитин Г.В. д.ф.м.н., проф. г. Москва.
Овчинникова Н.В. к.ф.-м.н. г. Москва.
Ризаев А.А. д.т.н., проф. г. Ташкент.
Усаров М.К. д.ф.-м.н., проф. г. Ташкент.
Ювмитов А.С. PhD., ст.н.с. г. Ташкент.
Уздин А.М. д.т.н., проф. г. Санкт-Петербург.
Жусупбеков А.Ж. д.т.н., проф. г. Астана.

СЕКРЕТАРИАТ

Нишонов Н.А. (отв. секр.)	PhD.	Ташкент
Ан Е.В.	PhD.	Ташкент
Джураева Н.Б.	PhD.	Ташкент
Логинов П.В.	PhD.	Ташкент
Набиев А.М.	PhD.	Ташкент
Умархонов С.И.	к.т.н.	Ташкент
Хамдамов М.	PhD.	Ташкент

ТУРСУНБОЙ РАШИДОВ
(1934 – 2020)

Видный ученый в области механики, доктор технических наук, профессор, академик Академии наук Республики Узбекистан, заслуженный деятель науки Республики Узбекистан, лауреат Государственной премии им. Абу Райхана Беруни в области науки и техники, лауреат премии Совета Министров СССР.

Турсунбай Рашидов родился 27 мая 1934 г. в городе Ташкенте. После окончания средней школы с золотой медалью в 1951 г. он поступил на физико-математический факультет Среднеазиатского государственного университета (ныне Национальный университет Узбекистана) и в 1956 г. окончил его с отличием по специальности «Механика». По окончании университета он прошел курс обучения в аспирантуре под руководством академика М.Т. Уразбаева и в 1959 г. был направлен в Институт механики АН РУз, где прошел трудовой путь от младшего научного сотрудника до директора института.

26 апреля 1966 г. – в день, когда произошло Ташкентское землетрясение Т.Рашидов был назначен директором Института механики и сейсмостойкости сооружений АН РУз и проработал в этой должности до 1974 года.

В период с 1966 по 1970 гг. под его руководством проведен обширный анализ сейсмических воздействий на сооружения в эпицентральной зоне Ташкентского землетрясения. В этот же период Турсунбай Рвпервые изложил динамическую теорию сейсмостойкости подземных сооружений и уточнил статическую теорию, созданную для подземных трубопроводов, им была установлена природа взаимодействия сооружения с окружающим грунтом, обладающим упруго-вязкопластическими свойствами.

Результаты этих исследований легли в основу его докторской диссертации «Вопросы динамической теории сейсмостойкости сложных систем подземных сооружений», которую он успешно защитил в июле 1971 г. под руководством выдающегося ученого-механика, члена-корреспондента АН СССР А.А. Ильюшина.

Огромное благотворное влияние на формирование Т.Р. Рашидова как ученого и организатора науки оказало постоянное внимание и забота его наставника, известного ученого-механика,

основателя нашего института – академика М.Т. Уразбаева. Во многом это определило дальнейший творческий путь Т.Р.Рашидова.

Успехи в научной деятельности Т.Р.Рашидова отразились на разработанной им теории и полученных авторских свидетельствах, которые легли в основу создания сейсмостойких конструкций метрополитена г.Ташкента, использовались при строительстве тоннелей БАМа, Софийского метрополитена, Каракумского канала, Рогунской ГЭС, а также при разработке нормативных документов в сейсмостойком строительстве, обуславливающих значительный экономический и социальный эффект. Уже в годы Независимости, изданные впервые в нашей республике строительные нормативы по сейсмостойкости напрямую связаны с именем Т. Рашидова.

В дальнейшем теория сейсмодинамики Т. Р. Рашидова нашла большое количество научных последователей и сделала его имя известным не только в нашей республике, но и за рубежом.

Созданная Т.Р. Рашидовым теория, впоследствии названная и признанная научной общественностью «Сейсмодинамической теорией подземных сооружений», явилась поворотным моментом в решении актуальной задачи современного строительства в условиях нарастающей урбанизации и естественного расширения зон сейсмичности.

Академик Рашидов Т.Р. проводил активную преподавательскую работу, являлся наставником молодых специалистов, руководителем многих научных работ. Им подготовлено 44 кандидата и 7 докторов наук. Один из них, Я.Н.Мубараков, избран действительным членом АН РУз, шестеро его учеников являются лауреатами Государственной премии Узбекистана им. Абу Райхана Беруни, а 15 – лауреатами премий Союза молодежи в области науки и техники.

Т.Р. Рашидов автор 17 монографий и более 520 научных статей, имеет 16 авторских свидетельств, был ответственным редактором более 70 сборников и монографий.

В должности академика-секретаря Отделения механики и процессов управления АН РУз (1979 – 1984 гг.), Главного ученого секретаря Президиума АН РУз (1984 – 1985 гг.) и вице-президента АН РУз (1985 – 1994 гг.) Т.Р. Рашидов сосредоточивал усилия коллективов подведомственных учреждений на решение важнейших фундаментальных и прикладных задач.

Наряду с научной, административной и педагогической деятельностью Т.Р. Рашидов вел большую общественную работу. Более 20 лет (с 1972 г.) он являлся Председателем Узбекского Республиканского Совета научно-технических обществ. По его инициативе при Узбекском Республиканском Совете был создан Дом техники по пропаганде и внедрению в производство достижений научно-технического прогресса. Он большое внимание уделял развитию и укреплению дружеских и творческих связей научно-технических обществ Узбекистана и зарубежных стран.

Еще одна сфера деятельности Т. Рашидова связана с проявлением большого интереса и заботы о сохранности архитектурных памятников на территории Узбекистана. Его энтузиазм в этой области позволил поднять и во многом решать вопросы сохранности и реконструкции исторических архитектурных памятников.

Академик АН РУз Т.Р. Рашидов, будучи членом Национального комитета по теоретической и прикладной механике СССР, Научного Совета по проблемам прочности и пластичности РАН, Межведомственного Совета по сейсмологии и сейсмостойкому строительству, а также председателем Узбекской секции Национального комитета по сейсмостойкому строительству, Научного Совета по проблемам механики, прочности и сейсмодинамики сооружений АН Республики Узбекистан, главным редактором Узбекского журнала «Проблемы механики», прилагал много усилий для поднятия авторитета и престижа науки как в Узбекистане, так и за его пределами.

Заслуги академика Т.Р. Рашидова отмечены рядом государственных наград. Он был награжден орденами «Знак Почета», «Мехнат Шухрати», юбилейной медалью «За доблестный труд» и памятным знаком «25 лет конституции Узбекистана». В 1978 г. ему было присвоено почетное звание «Заслуженный деятель науки Узбекистана».

Огромная трудоспособность, энтузиазм, любовь к Родине, увлеченность и преданность своему делу, исключительная требовательность к себе и своим сотрудникам снискали Т.Р. Рашидову заслуженное уважение и авторитет как коллектива, так и всей научной общественности республики.

Section A - Seismic resistance of buildings and structures (theory and experiment)
Секция А – Сейсмостойкость зданий и сооружений (теория и эксперимент)

ASSESSMENT OF SEISMIC STRENGTH OF TRANSPORT STRUCTURES BASED ON ELECTRONIC TECHNICAL PASSPORTS IN UZBEKISTAN

Bekmirzaev D.[1], Berdibaev M.[1], Botabaev N.[1], Rakhimjonov Z.[2]
[1]*Institute of Mechanics and Seismic Stability of Structures named after M.T.Urazbaev, Tashkent, Uzbekistan.*
[2]*Tashkent state Transport University. Tashkent, Uzbekistan.*
E-mail: mars.berdibaev@mail.ru

Abstract. *The article examines the sequence of seismic strength assessment and certification of transport structures on the basis of electronic technical passports. The main objectives of this research are as follows. First, assessment of the technical state of transport structures based on diagnostic results and periodic monitoring. Second, the technical condition of the transport structures is monitored in time to evaluate whether the existing structural defects are progressing or new defects are developing. Third, classification of transport structures according to their seismic state into seismically strong, requiring instrumental technical inspection and seismically weak types. Fourth, classification of transport structures into seismic vulnerability types and formation of electronic technical passports based on all collected data.*

Keywords. *Earthquake, transport structure, certification, seismic state, technical state, electron technical passport.*

1. Introduction.

Highway systems play a key role in providing mobility to society, especially during emergency situations, including earthquakes. Bridges in highway systems are susceptible to damage from earthquakes, causing traffic capacity loss leading to a serious impact on surrounding areas. To better prepare for such scenarios, it is important to estimate capacity loss and traffic disruptions from earthquakes [1].

Earthquake damage to a bridge can have severe consequences. Clearly, the collapse of a bridge places people on or below the bridge at risk, and it must be replaced after the earthquake unless alternative transportation paths are identified. The consequences of less severe damage are less obvious and dramatic, but they are nonetheless important. A bridge closure, even if it is temporary, can have tremendous consequences, because bridges often provide vital links in a transportation system. In the immediate aftermath of an earthquake, closure of a bridge can impair emergency response operations. Later, the economic impact of a bridge closure increases with the length of time the bridge is closed, the economic importance of the traffic using the route, the traffic delay caused by following alternate routes, and the replacement cost for the bridge. Damage usually results from a complex and interacting set of contributing variables. The details of damage often are obscured by the damage itself, so that some speculation is required in reconstructing the event. In many cases, the cause of damage can be understood only after detailed analysis, and, even then, the actual causes and effects may be elusive. Performance of a bridge structure during an earthquake is likely to be influenced by proximity of the bridge to the fault and site conditions. Both of these factors affect the intensity of ground shaking and ground deformations, as well as the variability of those effects along the length of the bridge. Furthermore, many of the sites were subject to liquefaction and lateral spreading, resulting in permanent substructure deformations and loss of superstructure support. Bridge seismic design practices have changed over the years, largely reflecting lessons learned from performance in past earthquakes [2].

According to the international geophysical reference book, every year in seismically dangerous areas of the globe, on average, about 700 earthquakes with a magnitude of at least 5 occur, about 90 with a magnitude of at least 6, and over 12 with a magnitude of 7 or more. Strong earthquakes with a magnitude of 5 to 8.5 lead to great destruction and loss of life. Over the entire history of mankind, about

80 million people died from earthquakes and their direct consequences - fires, tsunamis, landslides, etc. During the first quarter of the twentieth century, about half a million people died in five devastating earthquakes alone - in San Francisco and Arezano (1901), Messina (1908), Kanshu (1920) and Tokyo (1923). Over the next 25 years, earthquakes killed an average of 15 thousand people annually, and property damage amounted to hundreds of millions of US dollars.

For example, the 1923 Tokyo earthquake in Japan alone, with a magnitude of 8.2, claimed 143 thousand lives. During this earthquake, 1286261 buildings were destroyed, 447128 buildings burned down, 268 buildings were washed away by sea waves, hundreds of pipeline accidents were recorded, many bridges and 2270 river vessels were destroyed. The damage caused by the earthquake to Tokyo and its environs amounted to $3 billion in 1923 prices. The 1971 San Fernando earthquake (USA), magnitude 6.6, caused approximately $1 billion in damage. During the 1988 Spitak earthquake (Armenia), damage amounted to up to 20 billion rubles, more than 25 thousand people died and more than 100 thousand people received injuries of varying severity [3].

Chile is located on one of the most active subduction zones in the world. In fact, three major earthquakes of moment magnitude greater than M_w=8.0 have occurred within the last 8 years, namely, the 2010 Maule earthquake (M_w=8.8), the 2014 Iquique earthquake (M_w=8.2), and the 2015 Illapel earthquake (M_w=8.3). Because of this, the design, construction and overall seismic performance of the civil infrastructure in Chile are constantly being tested. In particular, highway bridges, which are essential structures for the transportation and communication among regions, were heavily damaged and some even collapsed during the 2010 Maule earthquake.

After the 2010 Maule earthquake, approximately 300 bridges were damaged and some of them even collapsed (Buckle, et al., 2012). Most of the bridges that were damaged during the earthquake corresponded to multi-span prestressed precast concrete (PC) girder bridges. The damage observed on those bridges was caused by large displacements of the superstructure relative to the substructure, leaving a large number of bridges with residual deck displacements, shear key damage, bearing damage, and damage in the web of precast girders as shown in Figure.1 [4-9].

Figure.1. - **Damage observed in highway bridges after the 2010 Maule earthquake**

International experience shows that every destructive earthquake leads to a change in building standards towards stricter requirements. At the same time, the deployment of a set of works to prepare

cities for natural disasters is currently hampered by the lack of information about the volume of necessary costs for carrying out protective measures of various significance [10].

The first shock of the Tashkent earthquake occurred at 5:22 a.m. on April 26, 1966. Intense vibrations lasted 6–7 seconds and were accompanied by an underground hum and light flashes. The outbreak was located directly under the city center at a depth of only 8 km, i.e. The epicenter of the earthquake, the magnitude of which was 8 score here, coincided with the urban center, which suffered the most. A large number of residential buildings, especially old adobe ones, were destroyed. Naturally, the first morning shock found the city's residents in their beds, which led to casualties. Schools, factories, hospitals and other buildings were destroyed [11].

Uzbekistan is located on one of the most active subduction zones in the Central Asia. Because of this, the design, construction and overall seismic performance of the civil infrastructure in Uzbekistan are constantly being tested. The territory of the Republic of Uzbekistan is divided into regions with a seismicity of 7, 8 and 9 score degrees (MSK-64) (Figure.2). Therefore, possible earthquakes affect the working condition of life structure systems, including bridge structures. An earthquake causes various dangerous deflection and stresses in the constructions of transport structures, and if there are various damages in the bridge structures during operation, this will reduce their earthquake resistance. Therefore, in the event of an earthquake, by ensuring the technical condition of transport facilities, possible damages can be prevented, and the risk of possible earthquakes can be assessed in advance, and the development of suitable measures for their protection is of great importance in reducing catastrophic events. [12-18].

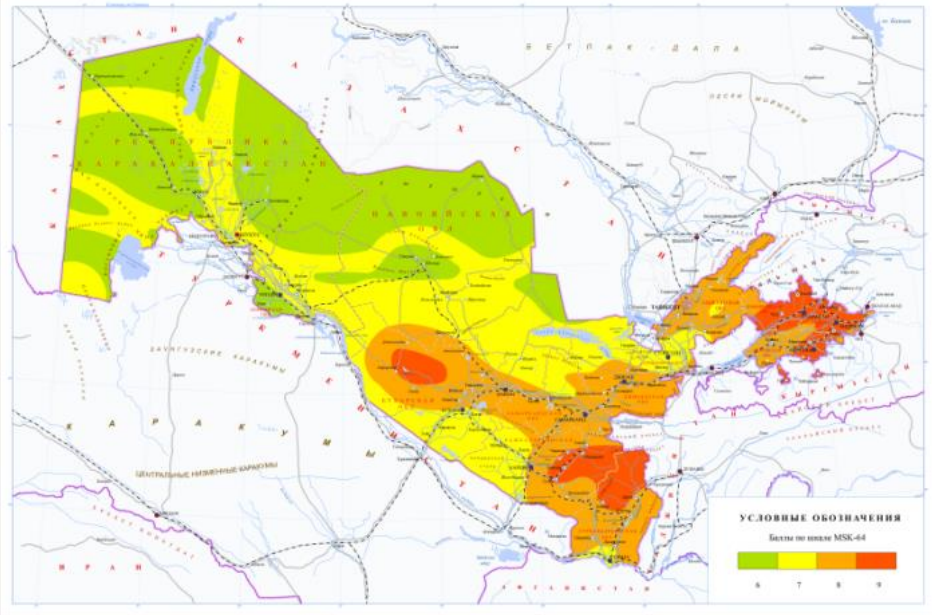

Figure 2. - **Seismic map of the territory of Uzbekistan [14-15]**

According to the country’s inventory results, there are 14331 bridge structures as of the beginning of 2019. Of these, 7628 (53.2%) are located on public roads, and 6703 (46.8%) are located on city roads, villages, and on-farm roads. It should be noted that a significant number of currently operating bridge structures were constructed in 1960-1970. It is related to the program of intensive cultivation of sown lands that took place in the Syrdarya, Jizzakh, Navoi, Bukhara regions and other regions of Uzbekistan during this period. As a result, about 70% of the currently operated bridges on public roads have a service life of more than 40 years and their condition is poor [19-21].

It is not possible to simultaneously improve the technical condition of all bridge structures. This requires significant funds and time. In addition to that, a strong political will and economic support from the government are needed. In recent years, the government of Uzbekistan has done a lot of work in this direction.

2. Methodology.

In order to carryout vulnerability analysis of bridges, an inventory of bridges is needed which should include information related to the characteristics of each bridge. In recent years, much attention has been paid to scientific and technical support and monitoring of the stress-strain state (SSS) of structures during construction and subsequent operation [22-23].

Table 1.

Information necessary for the formation of the electronic technical passport of the transport structure

№	**I. General information**
1	The date of filling out the electronic technical passport of the transport structure
2	Types of transport structures
3	Year of building of the transport structure
4	The organization that formed the electronic technical passport of the transport structure
5	Location of the transport structure (province, region or city)
6	The category of the road where the transport structure is located
7	The road where the transport structure is located (km, pk)
8	Cipher of the transport structure
9	Contact information (phone, email, website, etc.)
10	Geolocation coordinates of the transport structure (the Internet is obtained from the global information network using the Google Map program using mobile communication)
11	Water basin where the transport structure is located (river, canal, ditch, no)
	II. Technical parameters of the transport structures
12	Types by function performed by a transport structure
13	Types of transport structure by static scheme
14	Types of transport structure by length
15	Seismicity of the construction site (obtained from passport document or seismic zoning map, 6, 7, 8, 9, 9*)
16	Constructive solution of the superstructure intermediate device of the transport structure
17	Constructive solution of the support of the transport structure
18	The number of superstructures of the transport facility
19	The length of the superstructure
20	Bearing construction
21	Gabarite dimensions of the transport structure
22	The highest point of the transport structure
23	Repair of the transport structure
24	Year of reconstruction
25	Strengthened during reconstruction
26	The technical state of the transport structure on the day the passport is filled out
27	Technical state of the main load-bearing structures of the transport structure
28	The state of the transport structure has changed due to earthquakes
29	Passport and diagnostic documents of the transport structure
30	Pictures of the general state of the transport structure (total two sides (facade), general movement part)
31	Places where injury is present (damage to the main load-bearing structures)
32	Information on the implementation of strengthening and strengthening work in the transport structure
33	Final conclusion (I-seismic strength is moderate, II-seismic strength is satisfactory, III-seismic strength is unsatisfactory, an instrumental-technical inspection is required, IV-reinforcement is required, in pre-accident condition, in an emergency)

The main objectives of this research are as follows:

- determining the need to implement priority measures to take into account seismic risk, prevent socio-economic losses, to ensure safety and improve the quality of life of the population, sustainable socio-economic development;
- creating conditions for the sustainable functioning of the main social infrastructure facilities, life support systems and transport structures in Uzbekistan;
- achieving an acceptable level of seismic safety of transport structures in Uzbekistan;
- reducing possible economic, social and environmental damage from seismic impacts;

- creation of seismic resistance survey certificates for transport structures (bridges, overpass, flyover) in Uzbekistan;

- visual inspection of transport structures in Uzbekistan;

- identification of seismically vulnerable structures, in relation to which measures should first of all be developed to reduce the seismic risk of their further operation to an acceptable level;

- identification of the most earthquake-hazardous structures requiring priority demolition or strengthening;

- development of recommendations for further operation, seismic reinforcement or demolition of the structure;

- assessment of the expected degree of damage to structures depending on their design solutions, wear and seismic capacity under maximum seismic impacts;

- assessment of economic and social damage from the consequences of possible earthquakes, assessment of the economic costs of seismic reinforcement based on the degree of damage to structures during possible design earthquakes;

- preparation of a scientific and technical report.

The following information is required for the development of electronic technical passports of transport structures (Table 1).

The information in table 1 is obtained based on the results of technical diagnostics. After this information is fully entered into the platform, the transport facility is divided into seismically strong, requiring instrumental technical inspection and seismically weak types.

3. Results.

Information about transport facilities is entered into the platform and divided into types according to its seismic status. Figure 3 shows an overview of the platform.

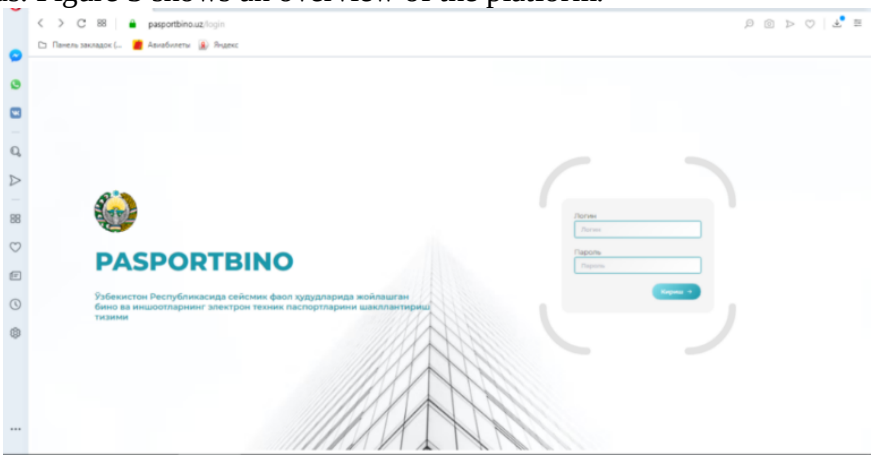

Figure 3. - **General view of the platform**

Monitoring of bridge structures is a system of monitoring the condition of bridge structures, which includes all types of surveys (measuring, geodetic, engineering, special) and instrumental measurements. As a result of monitoring, the technical condition of the bridge structure is determined, the reasons for the violation of its load-bearing capacity are established, and the ways and timing of decisions on the reconstruction or repair of the bridge structure are determined. Monitoring the technical condition of transport structures is long-term monitoring of parameters characterizing the stress-strain state of bridge structures in order to identify negative changes at an early stage, both during the construction stage and during operation.

The process of assessing the technical condition of artificial structures is very complex from a technological point of view. Carrying out certain types of measurements and tests is impossible without the use of special equipment, and the professional experience and qualifications of the specialist using it are of great importance. Inspection of the structure of artificial structures is carried out, as a rule, by a

group of experienced engineers who have a full range of necessary measuring instruments. The professionalism of the employees of this group allows us to minimize the time spent on carrying out the necessary diagnostic tests. Inspection and testing of bridges is carried out using non-destructive methods, visual and instrumental.

Visual examinations. They are an indispensable condition for carrying out work on the inspection and testing of bridges; they make it possible to record visible breaks in individual structural elements, various defects in the surface layer due to the influence of corrosion processes or mechanical static and dynamic loads. Particular attention is paid to the inspection of load-bearing units; magnifying devices are used if necessary.

Instrumental examinations. They make it possible to identify possible deviations of individual structural elements from the given initial positions, changes in the distances between them and violations of the linearity of surfaces due to deformation of the structure. For instrumental examinations, special instruments and devices are used, all data obtained is verified with the original design of the structure. All main load-bearing elements and structures are checked.

Acceptance surveys and tests of bridges are carried out for all new objects with individual structures of spans and supports. Before starting work, a test program for the bridge is developed, taking into account the specifics of its actual operation. Then, according to the Test Program approved by the Customer, all necessary work is carried out. In addition to full-scale measurements and tests, a verification calculation is carried out according to the test program to compare natural indicators with theoretical values.

Determination of the assessment of the technical condition of bridge structures should be carried out regularly throughout the entire period of their operation. Measures allow you to detect defects in a timely manner, prevent emergency situations and extend the service life of structures.

There is a marked difference in seismic design aspects of bridges and buildings. The reduced degree of indeterminacy of bridge structures leads to reduced potential of dissipating energy and load redistribution. In bridges, the superstructures (piers and abutments) are the main structural elements which provide resistance to seismic action. For energy dissipation, ductile behaviour is necessary during flexure of these structural elements under lateral seismic loads. This essentially means that the formation of plastic hinges or flexural yielding is allowed to occur in these elements during severe shaking to bring down the lateral design forces to acceptable levels [22]. Severe damages occurred by strong earthquake could be divided into 4 groups, such as collapse of spread foundation, collapse of substructure (column of pier, wall of abutment), collapse of bearing, and fall of superstructure [1].

Certification of a transport structure is the process of systematizing information about the constant or variable technical and operational characteristics of an object in a specific document, reflected in the form of a technical passport, which is a reporting document and is drawn up in the prescribed form. A bridge passport is a document based on legislation that records the main parameters of the structure. Its necessity arises when inspecting bridges from a construction or design organization, facility management or road maintenance department.

Certification of transport structures is the first stage of work to ensure the necessary and economically feasible level of seismic safety of operating construction projects in conditions of moral, physical and seismic deterioration of structures, changes in seismic hazard and design and construction standards in seismic areas. Certification of transport structures in seismic areas has two main goals: *a*) comparative assessment of the actual seismic resistance of buildings with the calculated seismicity of the territory (assessment of the seismic resistance deficit); *b*) identification of the most earthquake-hazardous objects that require priority strengthening, change of purpose or demolition of the building (seismic monitoring of the condition of the building stock). An important task is also the assessment of the vulnerability (vulnerability) of buildings or the probable degree of their damage under seismic impacts of various intensities, which is used in calculating seismic risk. It is known that the reliability of calculations depends not so much on the selected seismic risk model, but on the completeness and

reliability of the results of certification of buildings, which is one of the links in the methodological chain: seismic hazard – certification – vulnerability – seismic risk.

On the basis of electronic technical passports included in the platform, transport facilities are divided into types according to seismic vulnerability and their technical condition is evaluated. That is, they are divided into seismically strong, instrumental technical inspection required and seismically weak transport structures (Figure. 4).

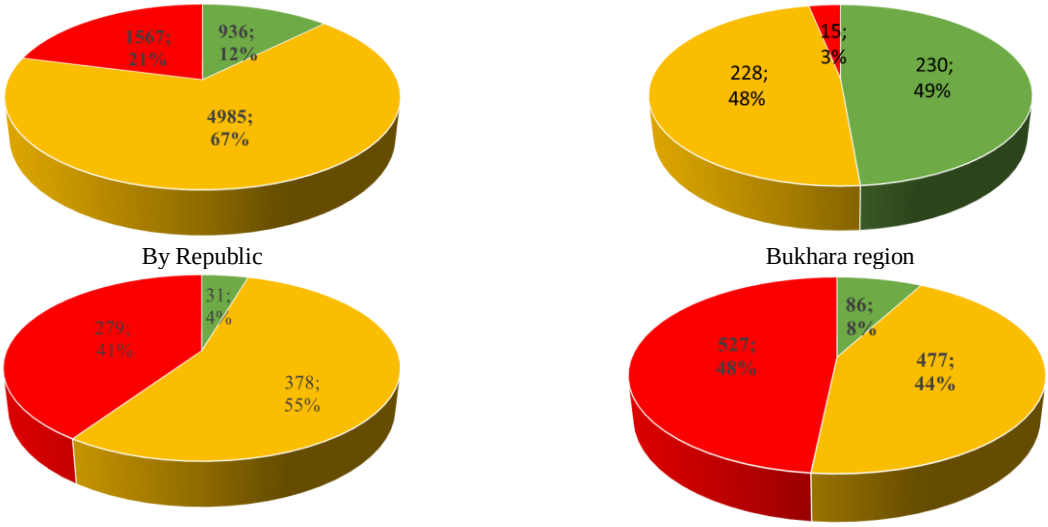

Figure.4. **Distribution of transport structures by seismic state in the cross section of the Republic and territories**

4. Conclusions.

This paper presented the results of studies which were conducted to determine seismic vulnerability of existing transport structures in Uzbekistan. The data of bridges and their structural systems were collected by diagnostic and structural monitoring surveys. All transport facilities in the republic were divided into seismically strong, requiring instrumental technical inspection, and seismically weak types based on their seismic condition. Based on the obtained results, an electronic technical passport on the seismic strength of transport facilities was formed.

The results of certification made it possible to identify earthquake-prone transport structures, assign priority objects for their seismic strengthening or demolition, and determine the amount of costs for strengthening seismic transport structures and demolition of dilapidated structure. Based on the Certification data received, state programs (for the demolition of dilapidated residential transport structures) were adjusted and dilapidated residential transport structures in Uzbekistan are being demolished and new earthquake-resistant residential transport structures are being built in their place. A classification of construction projects has been compiled based on the seismic scale MSK-64.

Based on the certification results, electronic passports of the surveyed transport structures were created with an assessment of their seismic vulnerability. Based on the results of certification, an electronic database was created on the seismic vulnerability of transport structures in Uzbekistan, which will improve the reliability of life support systems, reduce damage to transport structures and reduce population losses from destructive earthquakes.

References

1. *Cho J., Lee Y-J., Lee S.M., Song K.H.*, Wonho Suh. Analysis of Macroscopic Traffic Network Impacted by Structural Damage to Bridges from Earthquakes. Applied Sciences (Switzerland). 2021, 11, 3226. https://doi.org/10.3390/app11073226.
2. *Moehle J.P., Eberhard M.O.* Earthquake damage to bridges. Bridge Engineering: Seismic Design 2003.
3. *Apsemetov M.Ch., Murzakmatov D.K., Jenishbekov E.E., Shekeev A.O.* Study of damage road structures during strong earthquakes. News of OshTU, 2017 №3.

4. *Ramiro Bazaez*., *Alberto Vega*. Seismic Assessment of Repaired Bridges in Chile. The 2018 Structures Congress (Structures18). Songdo Convensia, Incheon, Korea, August 27 - 31, 2018.
5. *Kawashima K*., *Unjoh Sh*., *Hoshikuma J*., *Kosa K*. Damage characteristic of bridges due to 2010 Chile earthquake. Journal of Japan Society of Civil Engineers, Ser. A1 (Structural Engineering & Earthquake Engineering (SE/EE)). 2010.
6. Sofía A., *Ramiro B*., *Rodrigo A*., *Francisco H*. Seismic fragility assessment of Chilean skewed highway bridges. Engineering Structures 2021.
7. *Kawashima K*., *Unjoh Sh*., *Hoshikuma J*., *Kosa K*. Damage of bridges due to the 2010 Maule, Chile, earthquake. Journal of Earthquake Engineering 2011.
8. *Martínez A*., *Hube M*., *Rollins K*. Analytical fragility curves for non-skewed highway bridges in Chile. Engineering Structures 2017, Volume 141, pp. 530-542.
9. *Buckle I*., *Hube M*., *Chen G*., *Yen W*., *Ariasa J*. Structural Performance of Bridges in the Offshore Maule Earthquake of 27 February 2010. Earthquake Spectra, Volume 28, No. S1, pages S533–S552, June 2012.
10. Shokbarov E.M., Kulbaev B.B. Passportization of buildings and structures of the existing development of the city of almaty abstract. ISSN 2313-6669 «Science & Construction» 3(29) 2021. Doi: https://doi.org/10.33644/2313-6669-14-2021-3.
11. Wikipedia (2024): https://en.wikipedia.org/wiki/1966_Tashkent_earthquak.
12. *Erdik M*., *Rashidov T*., *Safak E*., *Turdukulov A*. Assessment of seismic risk in Tashkent, Uzbekistan and Bishkek, Kyrgyz Republic. Soil Dynamics and Earthquake Engineering, pp.473-486. August 2005.
13. *Ismailov V.A*., *Yodgorov S.I*., *Allayev, Sh.B*., *Mamarozikov T.U*., *Avazov, Sh.B*. Seismic microzoning of the Tashkent territory based on calculation methods. Soil Dynamics and Earthquake Engineering 2022.
14. *Artikov T.U*., *Ibragimov R.S*., *Ibragimova T.L*., *Kuchkarov K.I*., *Mirzaev M.A*. Quantitative Assessment Of Seismic Hazard For The Territory Of Uzbekistan According To The Estimated Maximum Ground Oscillation Rates And Their Spectral Amplitudes. Geodynamics & Tectonophysics Published By The Institute Of The Earth's Crust Siberian Branch Of Russian Academy Of Sciences 2018 VOLUME 9 ISSUE 4 PAGES 1173–1188.
15. *Artikov T.U*., *Ibragimov R.S*., *Ibragimova T.L*., *Mirzaev M.A*., *Artikov M.T*. Revealing the seismicity increase in interrelationships in various seismic zones in Uzbekistan as a case study. Geodesy and Geodynamics 2015, vol 6, № 5, 351-360
16. *Artikov T.U*., *Ibragimov R.S*., *Ibragimova T.L*., *Mirzaev M.A*. Complex of general seismic zoning maps OSR-2017 of Uzbekistan. Geodesy and Geodynamics 11 (2020), 273-292.
17. *Ismailov V.A*., *Yodgorov Sh.I*., *Mamarozikov T.U*. Seismic Risk Mapping for Uzbekistan. SSRN Electronic Journal 2022.
18. *Kishanov R*., *Bekmirzaev D*., *Nishonov N*., *Rakhmanov U*., *Ismailova G*. Response of underground polymer pipelines considering viscoelastic interaction under seismic impact. AIP Conference Proceedings 2612, 040032. https://doi.org/10.1063/5.0113061. 15 March 2023.
19. *Rashidov T*., *Baybulatov K*., *Bekmirzayev D*., *Takhirov S*., *Gayibov J*., Nishonov N. Comprehensive Program on Structural Assessment of Bridges in Uzbekistan. Vol. 3542. 2020 (Sendai, Japan: The 17th World Conference on Earthquake Engineering). P.3c–0013.
20. *Berdibaev M*., *Mardonov B*, *Nishonov N*. Calculation of beam road bridges for seismic loads taking into account the interaction of supports with the ground. Cite as: AIP Conference Proceedings 2612, 040017 (2023); https://doi.org/10.1063/5.0113617. Published Online: 15 March 2023.
21. *Berdibaev M*, *Mardonov B*, *Nishonov N*, *Baybulatov K*. The effect of a seismic wave on a two-span beam on rigid supports interacting with the ground. E3S Web of Conferences 401, 03070 / CONMECHYDRO – 2023. https://doi.org/10.1051/e3sconf/202340103070.
22. *Shermukhamedov U.Z*., *Karimova A.B*., *Zakirov B.S*. Calculation of Continuous Reinforced Concrete Bridges And Overpasses Inseismically Hazardous Areas. E3S Web of Conf. Volume 401, V International Scientific Conference "Construction Mechanics, Hydraulics and Water Resources Engineering" (CONMECHYDRO - 2023). https://doi.org/10.1051/e3sconf/202340101078.
23. *Shermukhamedov U*., *Mirzaev I*., *Karimova A*., *Askarova D*. Calculation of the stress-strain state of monolithic bridges on the action of real seismic impacts. E3S Web of Conferences 401, 05080. CONMECHYDRO – 2023. https://doi.org/10.1051/e3sconf/202340105080.
24. *Tandon M*. Economical Design Of Earthquake-Resistant Bridges. ISET Journal of Earthquake Technology, Paper No. 453, Vol. 42, No. 1, March 2005, pp. 13-20.

CALCULATION OF DYNAMIC CHARACTERISTICS DURING LONGITUDINAL-SHEAR VIBRATIONS OF MULTI-STORY BUILDINGS WITHIN THE FRAMEWORK OF A PLATE CONTINUUM MODEL

Isayev G.U.[1], Shamsiyev D.K.[1], Kurbanbayev M.K.[1]
[1]*Institute of Mechanics and Seismic Stability of Structures, Tashkent, Uzbekistan*
E-mail: isaev.gulomzhon@bk.ru

Abstract. *The article is devoted to the development of calculation methods within the framework of a continuum plate model of a multi-story building, under the assumption that its seismic vibrations can be modeled by the motion of a thick orthotropic cantilever plate, the deformation of which is described on the basis of the bi-moment theory of thick plates. Formulas are presented for determining the reduced moduli of elasticity, shear, and density of a plate model of a building. The first three natural frequencies of a multi-story building are calculated using the resonant method for given geometric and mechanical parameters.*

Keywords: *multi-storey building, continuum plate model, reduced moduli of elasticity, shear, and density, moments, forces, bi-moments, seismic impact, numerical method, resonance method, natural frequency*.

1. Introduction.

The development of dynamic spatial models of buildings and structures, the deformation of which is spatial, is one of the most complex current problems in the mechanics and dynamics of structures. At this stage of development of the theory of structures, various methods for calculating buildings and structures for seismic impacts were developed, considering various important factors. Such research includes the following scientific publications.

Article [1] is devoted to solving the problems of a four-story reinforced concrete frame building subjected to seismic loads, taking into account various irregularities. To assess the seismic characteristics of the structure, calculations were conducted considering the inelastic properties of the concrete and steel materials filling the walls.

The influence of [2] earthquakes of varying intensity and frequency on the seismic resistance of a wooden frame-type building, consisting of wooden vertical posts, lower and upper frames, bracing systems, and floor and roof elements. Seismic resistance was assessed based on experimental and theoretical studies. Article [3] considers the parametric bending of concrete-reinforced beam elements using the finite element method (FEM). Within the framework of the *Abaqus Finite Element Analysis* (FEA) software package, calculations were conducted of beams with a load applied in the middle of the span.Article [4] presents the results of a numerical study of the behavior of a multi-story reinforced concrete frame building under seismic influence. Numerical studies were conducted using the *LIRA* software package on a 9-story frame house.

The study in [5] proposes a method for using the polymer reagent POLIANCE in concrete, developed on the basis of waste from the production of polyacrylonitrile fibers. The results of the influence of the reagent on the capillary absorption of concrete are presented; it helps to ensure high resistance of cement concrete in saline environments.

References [6, 7] propose a methodology for experimental studies of curved reinforced concrete beams made of ordinary heavy concrete, equipped with fiberglass composite reinforcement. Data are presented on methods for measuring the resulting strains, cracks and deflections of prototype beams under the influence of transverse forces.

Article [8] is devoted to the calculation of structural elements of buildings and structures; scientific publications of many authors are devoted to this issue. The influence of displacements and inclinations of the axes of wall panels during their installation on the operation of large-panel structures is considered.

Articles [9, 10] are devoted to assessing the reliability of the design and construction of structures depending on the properties of the foundation soil of the construction site.

Reference [11] deals with the application of an active seismic protection system in the form of a seismic isolation sliding belt at the foundation level to ensure the seismic stability of a building or

structure. As a result of the calculations, the relative displacements, accelerations, and stress intensity in the most loaded structural elements were obtained.

In [12], the influence of the linear and nonlinear models of the base-soil interaction on the vibrations of the multi-storey building under seismic effects was studied.

In [13], vibrations of the buildings on the sliding foundation with dry friction was studied under the action of real earthquakes at the intensity of 8 and 9 on the MSK-64 scale.

Reference [14] considers the influence of moisture content of loess soil and soil foundations on sedimentary deformations. Subsidence of loess soils occurs due to a decrease in the strength parameters of soil and transform of the stressed state of soil [14-15].

The dynamic behavior of soils during the interaction of underground structures and building foundations with soil in a non-one-dimensional statement is considered in [16-17].

In [18-20], seismic vibrations of a building are modeled by the motion of a thick anisotropic cantilever plate, the deformation of which is described based on the bi-moment theory of thick plates [21].

2. Statement of the problem.

Longitudinal-shear vibrations of a multi-story building within the framework of a plate model of a multi-story building are considered in a Cartesian coordinate frame with variables x_1, x_2 and z. The origin is located in the lower left corner of the middle surface of the continuum plate model of a multi-story building. Let us direct the OX_1 and OX_2 axes in length and height, and the OZ –axis along the thickness (width of the building) of the plate model.

We describe the problem of longitudinal-shear vibrations of a multi-story building within the framework of the bi-moment theory of plate structures, developed in [18-20]. The basic system of equations of motion of the bi-moment theory of plate structures (multi-story buildings), which consists of equations for longitudinal, shear forces, and bi-moments and are described by nine unknown kinematic functions:

$$\overline{\psi}_k = \frac{1}{2h}\int_{-h}^{h} u_k dz, \quad \overline{\beta}_k = \frac{1}{2h^3}\int_{-h}^{h} u_k z^2 dz, \quad (k=1,2), \quad \overline{r} = \frac{1}{2h^2}\int_{-h}^{h} u_3 z dz, \quad \overline{\gamma} = \frac{1}{2h^4}\int_{-h}^{h} u_3 z^3 dz. \tag{1}$$

To formulate the problem of longitudinal-shear vibrations of a building within the framework of a continuous plate model of a multi-story building, we use the expressions of forces and bimoments proposed in [18-20].

We introduce longitudinal and shear forces N_{11}, N_{12}, N_{22} from stress $\sigma_{11}, \sigma_{12}, \sigma_{22}$, from stress:

$$\begin{aligned} N_{11} &= \int_{-h}^{h} \sigma_{11} dz = E_{11} H \frac{\partial \overline{\psi}_1}{\partial x_1} + E_{12} H \frac{\partial \overline{\psi}_2}{\partial x_2} + 2E_{13}\overline{W}, \\ N_{22} &= \int_{-h}^{h} \sigma_{22} dz = E_{12} H \frac{\partial \overline{\psi}_1}{\partial x_1} + E_{22} H \frac{\partial \overline{\psi}_2}{\partial x_2} + 2E_{23}\overline{W}, \\ N_{12} &= N_{21} = G_{12}\left(H \frac{\partial \overline{\psi}_2}{\partial x_1} + H \frac{\partial \overline{\psi}_2}{\partial x_1} \right). \end{aligned} \tag{2}$$

Similarly, expressions for the bi-moments generated by the longitudinal-shear plate model of the building are constructed, T_{11}, T_{22}, T_{12} from stress $\sigma_{11}, \sigma_{12}, \sigma_{22}$, they are defined as:

$$\begin{aligned} T_{11} &= \frac{1}{h^2}\int_{-h}^{h} \sigma_{11} z^2 dz = H\left(E_{11}\frac{\partial \overline{\beta}_1}{\partial x_1} + E_{12}\frac{\partial \overline{\beta}_2}{\partial x_2} + E_{13}\frac{2\overline{W} - 4\overline{r}}{H} \right), \\ T_{12} &= T_{21} = \frac{1}{h^2}\int_{-h}^{h} \sigma_{12} z^2 dz = HG_{12}\left(\frac{\partial \overline{\beta}_2}{\partial x_1} + \frac{\partial \overline{\beta}_1}{\partial x_2} \right), \\ T_{22} &= \frac{1}{h^2}\int_{-h}^{h} \sigma_{22} z^2 dz = H\left(E_{12}\frac{\partial \overline{\beta}_1}{\partial x_1} + E_{22}\frac{\partial \overline{\beta}_2}{\partial x_2} + E_{23}\frac{2\overline{W} - 4\overline{r}}{H} \right). \end{aligned} \tag{3}$$

Expressions for the intensities of transverse bi-moments generated by a longitudinal-shear plate model of a building are introduced, $\bar{p}_{13}$, $\bar{p}_{23}$ and $\bar{\tau}_{13}$, $\bar{\tau}_{23}$ from shear stresses σ_{13}, σ_{23}, determined by the following formulas:

$$\bar{p}_{k3} = \frac{1}{2h^2}\int_{-h}^{h}\sigma_{13}z dz = G_{k3}\left(\frac{\partial \bar{r}}{\partial x_k} + \frac{2(\bar{u}_k - \bar{\psi}_k)}{H}\right),$$
$$\bar{\tau}_{k3} = \frac{1}{2h^4}\int_{-h}^{h}\sigma_{23}z^3 dz = G_{k3}\left(\frac{\partial \bar{\gamma}}{\partial x_k} + \frac{2(\bar{u}_k - 3\bar{\beta}_k)}{H}\right), \quad (k=1,2). \tag{4}$$

The concept of bimoment intensities is also introduced $\bar{p}_{33}$ and $\bar{\tau}_{33}$ from normal stress σ_{33} according to the following formulas:

$$\bar{p}_{33} = \frac{1}{2h}\int_{-h}^{h}\sigma_{33} dz = E_{31}\frac{\partial \bar{\psi}_1}{\partial x_1} + E_{32}\frac{\partial \bar{\psi}_2}{\partial x_2} + E_{33}\frac{2\bar{W}}{H},$$
$$\bar{\tau}_{33} = \frac{1}{2h^4}\int_{-h}^{h}\sigma_{23}z^3 dz = E_{31}\frac{\partial \bar{\beta}_1}{\partial x_1} + E_{32}\frac{\partial \bar{\beta}_2}{\partial x_2} + E_{33}\frac{2\bar{W} - 4\bar{r}}{H} \tag{5}$$

Now, we present the basic system of equations for longitudinal vibrations of a plate model of a multi-story building, proposed in [13-15]. The system of differential equations of seismic vibrations of a multi-story building relative to longitudinal and shear forces (2) generated during longitudinal-shear vibrations of the plate model of the building is constructed in the following form:

$$\frac{\partial N_{11}}{\partial x_1} + \frac{\partial N_{12}}{\partial x_2} = \rho H \ddot{\bar{\psi}}_1, \qquad \frac{\partial N_{21}}{\partial x_1} + \frac{\partial N_{22}}{\partial x_2} = \rho H \ddot{\bar{\psi}}_2. \tag{6}$$

It should be noted that the system of two equations (6) contains three unknown functions $\bar{\psi}_1$, $\bar{\psi}_2$, $\bar{W}$.

The system of differential equations of seismic vibrations of a multi-story building relative to longitudinal and shear bi-moments (3), (4), generated during longitudinal-shear vibrations of the plate model of the building, is constructed in the following form:

$$\frac{\partial T_{11}}{\partial x_1} + \frac{\partial T_{12}}{\partial x_2} - 4\bar{p}_{13} = \rho H \ddot{\bar{\beta}}_1, \quad \frac{\partial T_{12}}{\partial x_1} + \frac{\partial T_{22}}{\partial x_2} - 4\bar{p}_{23} = \rho H \ddot{\bar{\beta}}_2. \tag{7}$$

The system of differential equations of seismic vibrations of a multi-story building relative to the intensities of transverse longitudinal and shear bi-moments (3), (4) and (5) is constructed in the following form:

$$\frac{\partial \bar{p}_{13}}{\partial x_1} + \frac{\partial \bar{p}_{23}}{\partial x_2} - \frac{2\bar{p}_{33}}{H} = \rho \ddot{\bar{r}}, \tag{8}$$

$$\frac{\partial \bar{\tau}_{13}}{\partial x_1} + \frac{\partial \bar{\tau}_{23}}{\partial x_2} - \frac{6\bar{\tau}_{33}}{H} = \rho \ddot{\bar{\gamma}}. \tag{9}$$

It should be noted that the systems of four equations (6) - (9) contain new six unknown functions $\bar{u}_1$, $\bar{u}_2$, $\bar{\beta}_1$ $\bar{\beta}_2$, $\bar{r}$, $\bar{\gamma}$.

Thus, the systems of six equations (6)-(9) contain nine unknown functions $\bar{u}_1$, $\bar{u}_2$, $\bar{\beta}_1$ $\bar{\beta}_2$, $\bar{r}$, $\bar{\gamma}$, $\bar{\psi}_1$, $\bar{\psi}_2$, $\bar{W}$. Therefore, three more equations are missing.

Three missing equations of motion of a plate model during longitudinal-shear vibrations of a multi-story building were constructed in [13-15] based on the method of expanding the displacement function into an infinite Maclaurin series. Considering six terms of the Maclaurin series, three approximate equations were constructed to determine generalized displacements $\bar{u}_1$, $\bar{u}_2$, $\bar{W}$, which are rewritten as follows:

$$\bar{u}_k = \frac{1}{4}\left(21\bar{\beta}_k - 3\bar{\psi}_k\right) - \frac{1}{20}H\frac{\partial \bar{W}}{\partial x_k}, \quad (k=1,2), \tag{10}$$

$$\overline{W} = \frac{1}{2}\left(21\bar{\gamma} - 7\bar{r}\right) - \frac{1}{30}H\left(\frac{E_{31}}{E_{33}}\frac{\partial \bar{u}_1}{\partial x_1} + \frac{E_{32}}{E_{33}}\frac{\partial \bar{u}_2}{\partial x_2}\right). \tag{11}$$

To represent the boundary conditions of the problem of longitudinal vibrations for multi-story buildings (10) - (11), we introduce the intensities of bi-moments $\bar{\sigma}_{11}$, $\bar{\sigma}_{22}$, $\bar{\sigma}_{12}$, $\bar{\sigma}^*_{11}$, $\bar{\sigma}^*_{22}$, determined by the formulas obtained in [20]. Bimoments $\bar{\sigma}_{11}, \bar{\sigma}_{12}$, $\bar{\sigma}_{22}$ have the following expressions:

$$\begin{aligned}
\bar{\sigma}_{11} &= \left(E_{11} - \frac{E_{13}}{E_{33}}E_{31}\right)\frac{\partial \bar{u}_1}{\partial x_1} + \left(E_{12} - \frac{E_{13}}{E_{33}}E_{32}\right)\frac{\partial \bar{u}_2}{\partial x_2}, \\
\bar{\sigma}_{22} &= \left(E_{21} - \frac{E_{23}}{E_{33}}E_{31}\right)\frac{\partial \bar{u}_1}{\partial x_1} + \left(E_{22} - \frac{E_{23}}{E_{33}}E_{32}\right)\frac{\partial \bar{u}_2}{\partial x_2}, \\
\bar{\sigma}_{12} &= G_{12}\left(\frac{\partial \bar{u}_1}{\partial x_2} + \frac{\partial \bar{u}_2}{\partial x_1}\right)..
\end{aligned} \tag{12}$$

$$\begin{aligned}
\bar{\sigma}^*_{11} &= -E_{11}H\frac{\partial^2 \overline{W}}{\partial x_1^2} - E_{12}H\frac{\partial^2 \overline{W}}{\partial x_2^2} + E_{13}\frac{60\left(7\overline{W} + 42\bar{r} - 105\bar{\gamma}\right)}{H} + \\
&+ E_{11}H\frac{\partial}{\partial x_1}\left(\frac{\bar{q}_1}{G_{13}}\right) + E_{12}H\frac{\partial}{\partial x_2}\left(\frac{\bar{q}_2}{G_{23}}\right),
\end{aligned} \tag{13}$$

$$\begin{aligned}
\bar{\sigma}^*_{22} &= -E_{12}H\frac{\partial^2 \overline{W}}{\partial x_1^2} - E_{22}H\frac{\partial^2 \overline{W}}{\partial x_2^2} + E_{23}\frac{60\left(7\overline{W} + 42\bar{r} - 105\bar{\gamma}\right)}{H} + \\
&+ E_{12}H\frac{\partial}{\partial x_1}\left(\frac{\bar{q}_1}{G_{13}}\right) + E_{22}H\frac{\partial}{\partial x_2}\left(\frac{\bar{q}_2}{G_{23}}\right).
\end{aligned}$$

Now let us write the boundary conditions on the free side and top faces of the multi-story building. On the side faces, the conditions for forces, moments, and bi-moments equal to zero are set:

$$\begin{gathered}
N_{11} = 0,\ \ N_{12} = 0,\ \ T_{11} = 0,\ \ T_{12} = 0,\ \ \bar{p}_{13} = 0,\ \ \bar{\tau}_{13} = 0, \\
\bar{\sigma}_{11} = 0;\ \ \bar{\sigma}_{12} = 0\ \ \bar{\sigma}^*_{11} = 0.
\end{gathered} \tag{15}$$

On the free upper face, the conditions for forces and bi-moments equal to zero are also specified:

$$\begin{gathered}
N_{12} = 0,\ \ N_{22} = 0,\ \ T_{12} = 0,\ \ T_{22} = 0,\ \ \bar{p}_{23} = 0,\ \ \bar{\tau}_{23} = 0, \\
\bar{\sigma}_{12} = 0;\ \ \bar{\sigma}_{22} = 0\ \ \bar{\sigma}^*_{22} = 0.
\end{gathered} \tag{16}$$

We take zero values as initial conditions.

Determine the reduced density and modulus of elasticity of the plate model according to the method given in [18-20].

The reduced density of the building is determined as follows. We determine the total volume and total volume of the elements of one floor of a multi-story building:

$$V_0 = ab_1H,\ V_1 = ab_1h_2 + (n-2)Hb_1h_2 + aHh_2, \tag{18}$$

Where a, H – are the length and width of the building; b_1 – the height of one floor of the building; k – the number of internal transverse walls of the building; h_1 - the thickness of external load-bearing walls; h_2 – the thickness of internal walls; h_{ov} – the overlap thickness.

In general, the given elastic characteristics and density of the building are determined by the following formulas:

$$\begin{aligned}
&E_1^{\text{given}} = \zeta_{11}E_0,\ \ E_2^{\text{given}} = \zeta_{22}E_0,\ \ E_3^{\text{given}} = \zeta_{33}E_0, \\
&G_{12}^{\text{given}} = \zeta_{12}G_0,\ \ G_{13}^{\text{given}} = \zeta_{13}G_0,\ G_{23}^{\text{given}} = \zeta_{23}G_0,\ \ \rho_{\text{given}} = \rho_0\varsigma_0.
\end{aligned} \tag{19}$$

It should be noted that the coefficient values ξ_{11}, ξ_{22}, ξ_{33}, ξ_{12}, ξ_{13}, ξ_{23}, ζ_0 for each cell (room) of a discrete part of the building are determined in the form of functions of two spatial variables, E_0, G_0 –

moduli of elasticity and shear of the strongest load-bearing panel of a cell of a discrete part of a building. Let us write the formulas for determining coefficients ξ_{11}, ξ_{22}, ξ_{33}, ξ_{12}, ξ_{13}, ξ_{23}, ζ_0 and given moduli of elasticity of a discrete part of the building:

$$\xi_{11}=\alpha\frac{S_{11}}{S_{01}},\quad \xi_{22}=\alpha\frac{S_{22}}{S_{02}},\quad \xi_{33}=\alpha\frac{S_{33}}{S_{03}},\ \xi_{12}=\alpha\frac{S_{12}}{S_{01}},$$
$$\xi_{13}=\alpha\frac{h_{nep}}{b_1}\lambda^*,\quad \xi_{23}=\alpha\frac{h_2}{a_1},\quad \zeta_0=\frac{V_1}{V_0}. \tag{20}$$

Where S_{01}, S_{02}, S_{03} – are the cross-sectional areas of the building in three coordinate planes of one floor of the building; S_{11}, S_{22}, S_{33} – the total cross-sectional areas of the slabs in the coordinate planes forming one floor of the building; λ^* – is the coefficient characterizing the voids in the cross-section of the floor slab. Coefficient α is determined depending on the cellular structure of the building structure.

Depending on the size of the slabs, rooms and the building itself, we determine the above areas using the methodology presented in [18-20], in the following form:

$$S_{01}=E_0b_1H,\quad S_{02}=E_0aH,\quad S_{03}=E_0ab_1, \tag{21}$$

$$S_{11}=b_1h_2E_b^{(2)}+Hh_{ov}E_{ov},\quad S_{12}=b_1h_2E_b^{(2)},$$
$$S_{22}=ah_2E_b^{(2)}+(k-2)Hh_2E_b^{(2)},\quad S_{33}=ah_2E_b^{(2)}+(k-2)b_1h_2E_b^{(2)}. \tag{22}$$

Where G_{ov} – is the building floor shear module; G_2 – internal wall shear module; $E_b^{(2)}$ – modulus of elasticity of internal walls; E_{ov} – modulus of elasticity of the floor.

3. Analysis of numerical results.

Let us assume that the seismic movement of soil occurs in the direction of the *OZ* axis (along the width of the building) in the form of movement of the base of the building:

$$u_0(t)=\frac{A_0}{2}(1-\cos(2\pi\nu_0 t)).$$

ν_0, A_0 – are the frequency and amplitude of external influence, k_c, g – earthquake seismicity coefficient and gravity acceleration.

Calculations for seismic impacts were performed within the framework of a plate continuum model of multi-story buildings. In calculations, the foundation of the building is considered absolutely rigid. Amplitude of external influence A_0 depends on the magnitude of the earthquake, which is determined from condition $A_0\omega_0^2=2k_cg$, Where k_c, g are the seismicity coefficient and gravitational acceleration, respectively. From here we find

$$A_0=\frac{2k_cg}{\omega_0^2}.$$

Note that the seismicity coefficient of 7, 8, and 9-magnitude earthquakes are equal, k_c=0.1.

The mechanical and geometric characteristics of the room panels and the external dimensions of the buildings must be specified as initial data. We assume that the external walls consist of reinforced concrete with an elastic modulus E=20000 MPa, density ρ=2500 kg/m^3, Poisson's ratio ν=0.3. We consider the internal walls to consist of expanded clay concrete with the following physical characteristics: modulus of elasticity E=7500 MPa, density ρ=1200 kg/m^3, Poisson's ratio ν=0.3.

The results of calculations of forced vibrations of a building within the framework of a thick plate model are presented for the following sizes of building slabs:

$$h_1=0.40m,\ h_2=0.25m,\ h_{ov}=0.2m,\ a_1=5m,\ b_1=3m,$$

The height and length of a multi-story building are assumed to be $b=nb_1$ and $a=30m$, respectively, and the width of the building varies.

The height for a nine-story, twelve-story and sixteen-story buildings is assumed to be a=30 m, a=40 m and a =51 m, respectively.

Using the initial data, the values of the reduced moduli of elasticity, shear, and density, given in Table 1, of multi-story buildings, calculated using formulas (17)-(20), were determined.

Consequently, the given characteristics of the building depend on the initial data and vary greatly depending on the specific task.

Table 1

Reduced elastic moduli of the continuum model of multi-story buildings for given initial data

Thickness	Modules of elasticity of a continuum model of a building					
$H\,(m)$	E_1^{given},MPa	E_2^{given},MPa	E_3^{given},MPa	$G_{12}^{\text{given}},MPa$	$G_{13}^{\text{given}},MPa$	$G_{23}^{\text{given}},MPa$
11	1545	1965	1220	458.2	320.0	240.0
13	1369	1789		387.7		
15	1240	1660		336.0		
18	1100	1520		280.0		

Let us present the results of calculations of displacements and stresses for a 16-story building.

Note that the natural frequencies of a multi-story building are determined using the resonance method. When determining the natural frequencies of a multi-story building, we gradually increase the frequencies of external influences until a gradual increase in displacements in the oscillatory process of the building is observed. As the value of the dimensionless frequency of external influence ω_0 approaches dimensionless natural frequency p_1 the values of displacements, forces, and moments increase sharply, which indicates a gradual transition to the resonant mode.

Let us present the results of calculations of the frequency, periods of oscillations and displacements of points for nine-, twelve- and sixteen-story buildings with longitudinal shear, near the resonant mode.

Below we present graphs of changes in normal and generalized displacements, from which the values of natural frequencies of multi-story buildings are determined. Graphs of changes in displacement and stress values were obtained for transverse vibrations of multi-story buildings in the resonant case during an earthquake of magnitude 7.

Figure 1 shows graphs of changes over time of normal displacement φ_1, in the middle of the top floor of a 16-story building near resonant oscillations with a frequency of p_1=3.52 *Hz*. As can be seen from the figures, when the external influence frequency values ν_0 very close to the natural frequency value p_1, there is an infinite increase in displacements.

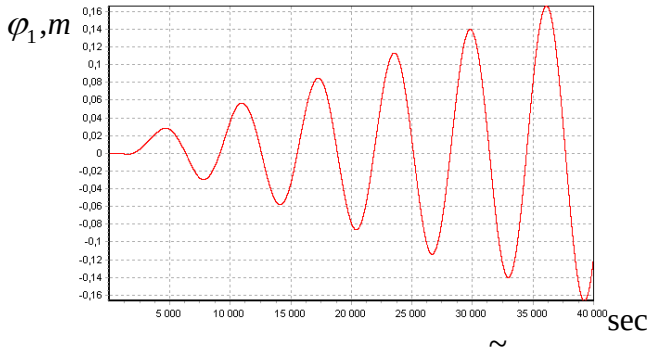

Figure 1 **Graph of normal displacement change $\tilde{r}$ in time in the middle of the top floor of a 16-story building with a width H=13 m at natural frequency p_1=3,52 Hz.**

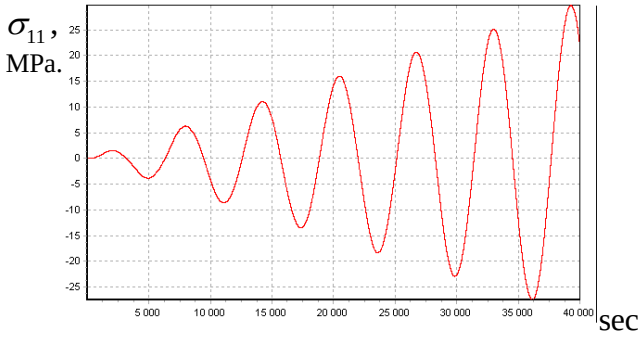

Figure 3 - **Graph of normal stress change σ_{11} in time in the middle of the first floor of a sixteen-story building with a width H = 13 m at a natural frequency p_1=3,52 Hz**

Figure 2 shows a graph characterizing changes in the maximum normal stress σ_{11} in the middle of the first floor of a sixteen-story building at time t. As established (Figure 2), in the middle of the first floor of the building, the maximum value of the normal stress was σ_{11}=27 MPa.

Similarly, using the resonance method, the second and third values of the natural frequency of a sixteen-story building with transverse dimensions are determined. Thus, the first three values of natural frequencies turned out to be

p_1=3.52 Hz, p_1=3.44 Hz and p_1=3.36 Hz,

and the periods of the fundamental tone of oscillations are:

$T_1=1/p_1$=0.2841 s, $T_1=1/p_1$=0.2907 s and $T_1=1/p_1= p_1$=0.2976 s.

Table 2.

The first three natural frequencies p_1, p_2, p_3 and periods of natural oscillations T_1, T_2, T_3 of nine-, twelve-, sixteen-story buildings, depending on three widths of the building

№	Number of floors	*H, m*	p_1, Hz	p_2, Hz	p_3, Hz	T_1, sec	T_2, sec	T_3, sec
1	9	11	7,70	20,61	33,91	0,1298	0,0485	0,0295
		13	7,63	20,31	33,25	0,1311	0,0492	0,0301
		15	7,58	20,12	32,82	0,1319	0,0497	0,0304
2	12	11	5,02	15,31	28,16	0,1992	0,0653	0,0355
		13	4,97	15,22	27,81	0,2012	0,0657	0,0359
		15	4,93	15,15	27,42	0,2028	0,0660	0,0365
3	16	13	3,52	11,51	23,02	0,2841	0,0868	0,0434
		15	3,44	11,41	22,83	0,2907	0,0876	0,0438
		18	3,36	11,31	22,44	0,2976	0,0884	0,0446

Calculations of natural frequencies were performed for nine-story and twelve-story buildings. Table 2 shows three values of natural frequencies p_1, p_2, p_3 and periods of natural oscillations T_1, T_2, T_3 of nine-, twelve-, sixteen-story buildings. For a nine-story and twelve-story building, the natural frequency is determined for three options for the building width H=11m, H=13m, and H=15m. For a sixteen-story building, the frequency of natural vibrations is determined for three options for the building width H=13m, H=15m, and H=18m.

Based on the results obtained, we note that the first natural frequencies of multi-story buildings under longitudinal shear vibrations are greater than the first natural frequency of the same building under transverse vibrations.

Table 3.

Values of the first natural frequency, maximum and minimum stresses of nine-, twelve-, sixteen-story large-panel buildings during an earthquake of magnitude 7-8-9

Number of floors	*H m*	k_s	ν_0, *Hz*	p_0 *Hz*	σ_{11}, *MPa*		σ_{22}, *MPa*,		σ_{33}, *MPa*	$\ddot{\tilde{r}}$, m/sek^2,	
					min	*max*	*min*	*max*		*min*	*max*
9	13	0.1	2.70	3.05	-2.42	2.43	-9.880	10.70	-8.43	-7.45	70.1
		0.2			-4.07	4.07	-20.11	21.20	-13.14	-14.9	13.3
		0.4			-6.52	6.55	-25.02	25.03	-16.31	-30.1	26.9
12	13	0.1	2.75	2.2	-1.90	2.00	-7.95	8.91	-6.74	-6.52	6.53
		0.2			-3.50	3.70	-14.8	16.0	-11.68	-12.5	13.2
		0.4			-7.10	7.55	-30.3	31.2	-23.35	-25.1	25.6
16	15	0.1	2.50	1.5	-0.9	0.8	-4.01	3.70	-3.22	-3.91	3.85
		0.2			-1.7	1.6	-8.00	7.61	-6.41	-6.92	6.95
		0.4			-3.59	3.31	-15.9	15.0	-10.32	-14.5	14.5

Here ν_0 and p_0 - resonant frequency. Calculations have shown that under external dynamic influences with a large amplitude, quite dangerous stresses appear in different upper levels of external walls during magnitude seven, eight and nine earthquakes.

4. Conclusions.

1. Within the framework of a continuous spatial plate model, the problem of determining the natural frequencies of multi-story buildings was formulated. Methods were developed for numerical solutions to the problem of seismic vibration based on the finite difference method and determining the natural frequencies of a multi-story building within the framework of the resonance method.

2. Based on the application of the resonance method, the first three values of the natural frequency of a multi-story building with the number of floors ranging from nine to forty were determined.

3. Based on the analysis of numerical results, it was established that the plate model is suitable for describing the dynamic behavior and calculating the stress-strain state of multi-story buildings under seismic impacts.

References

1. *Shendkar M., Beiraghi H., Mandal S.* Effect of irregularity on seismic design parameters of RC-infilled structures. Magazine of Civil Engineering. 2021. 108(8). Article No. 10807. DOI: 10.34910/MCE.108.7
2. *Belash T.A., Ivanova Zh.V.* Timber frame buildings with efficient junction designs for earthquake-prone areas. Magazine of Civil Engineering. 2019. 92(8). Pp. 84–95. DOI: 10.18720/MCE.92.7
3. *Manish Kewalramani, Osama Mohamed, Abdallah Badran.* Parametric finite element analysis to investigate flexural behavior of BFRP-FRC beams. Construction Materials and Technologies E3S Web Conf. Volume 347, 2022.
4. *Baisbay T. Yerimbetov, Berik M. Chalabayev, Yairakhan B. Kunanbayeva, Zhenisbek A. Ussenkulov, Zhenis I. Orazbayev, Zhumadilla A. Aldiyarov.* Seismic resistance of multi-storey reinforced concrete wall-frame structures at destructive earthquakes. Periodicals of Engineering and Natural Sciences Vol-7, № 4, December 2019, pp.-1582-1598.
5. *Goncharova N., Abobakirova Z., Davlyatov S., Umarov S., Mukhamedzanov A.* (2023). Polymer reagent in construction practice. In E3S Web of Conferences (Vol. 365, p. 02024). EDP Sciences.
6. *Akramov X., Davlyatov S., Umarov S., Abobakirova Z.* // Method of experimental research of concrete beams with fiberglass reinforcement for bending. In E3S Web of Conferences 2023 (Vol. 365, p. 02021). EDP Sciences.
7. *Goncharova N. I., Abobakirova Z. A., Mukhamedzanov A.R.* Capillary permeability of concrete in salt media in dry hot climate. / In AIP Conference Proceedings 2020 (Vol. 2281, No. 1, p. 020028). AIP Publishing LLC.
8. *Vatin N.I., Kuznetsov V.D., Nedviga E.S.* Installation errors in calculating large-panel buildings. Magazine of Civil Engineering. 2011. DOI:10.5862/mce.24.3.
9. *Pshenichkina, V.A., et al.* Methodology for assessing the seismic reliability of buildings with high floors. Bulletin of the Volgograd State University of Architecture and Civil Engineering. Series: Construction and Architecture 2011. 25. pp.50–56.
10. *Khachatryan, S.O.* Spectral-wave theory of earthquake resistance. / Earthquake engineering. Safety of facilities 2004. 3. pp.58–61.
11. *Oleg Mkrtychev.* Salima Mingazova. Analysis of the reaction of reinforced concrete buildings with a varying number of stories with a seismic isolation sliding belt to an earthquake// 2020. *IOP Conf. Ser.: Mater. Sci. Eng.* 869 052065.
12. *Khojmetov G., Mirzaev I., Yuvmitov A., Mirzahmedov M.* On Influence of Linear and Nonlinear Models of Foundation-Base Interaction on Vibrations of Multi-Storey Buildings at Seismic Impacts / Cite as: AIP Conference Proceedings 2022, 2432, 030071, https://doi.org/10.1063/5.0089506
13. *Ibrakhim Mirzaev, Anvar Yuvmitov, Malikjon Turdiev and Jakhongir Shomurodov*. Influence of the Vertical Earthquake Component on the Shear Vibration of Buildings on Sliding Foundations/ E3S Web of Conferences, 264, 02022 CONMECHYDRO – 2021. https://doi.org/10.1051/e3sconf/202126402022
14. *Bakhtiyar K., Barno R.* Numeric Simulation of Subsidence of Loess Soil under Wetting in a Limited Area // Journal of Advanced Research in Fluid Mechanics and Thermal Sciences.- 2023.- Vol.104.- Issue 2.- Pp.1-18. https://doi.org/10.37934/arfmts.104.2.118
15. *Bakhtiyar, K., Shovkat, N., Ozodaxon, K.* On One Method for Assessing the Soil Slopes Stability // AIP Conference Proceedings, 2022, 2637, 030012
16. *Khusanov B.E., Rikhsieva B.B.* Cylindrical shear waves in soil around underground pipelines // Journal of Physics: Conference Series. - 2022.- Vol.2182 (1). - P.012022. doi:10.1088/1742-6596/2182/1/012022
17. *Rikhsieva B., Khusanov B.* The Influence of Plastic Properties of the Surroundings on the Interaction Process of the "Cylindrical Body – External Medium" System // AIP Conf. Proc.- 2023.- Vol.2768.- P.020020. https://doi.org/10.1063/5.0150315
18. *Usarov M.,Usarov D., Mamatisaev G.* Calculation of a Spatial Model of a Box-Type Structure in the LIRA Design System Using the Finite Difference Method//Lecture Notes in Networks and Systems, 2022, 403 LNNS, pp:-1267–1275 https://doi.org/10.1007/978-3-030-96383-5_141
19. *Usarov M., Mamatisaev G.,Usarov D.* Calculation of the Box Structure of Large-Panel Buildings//AIP Conference Proceedings, 2023, 2612, 040014 DOI**:**10.1063/5.0116871
20. *Usarov M., Mamatisaev G., Ayubov G., Usarov D., Khodzhaev D.* Dynamic calculation of boxed design of buildings// IOP Conference Series: Materials Science and Engineering, 2020, 883(1), 012186
21. *Usarov M., Ayubov G., Usarov D., Mamatisaev G.* Spatial Vibrations of High-Rise Buildings Using a Plate Model // Lecture Notes in Civil Engineering , 2022, 182, pp. 403–418 https://doi.org/10.1007/978-3-030-85236-8_37

CONTRIBUTION AND INFLUENCE OF T.R. RASHIDOV'S WORKS ON THE FORMATION OF MATHEMATICAL SEISMODYNAMICS OF UNDERGROUND STRUCTURES

Israilov M.Sh.[1]

[1]*LLC: "Sensor Fusion and Monitoring Technologies".* California 94596, *USA*

E-mail: israiler@hotmail.com

Abstract: *The role and influence of T.R. Rashidov's works on the creation of mathematical seismodynamics of underground structures are discuss. Physically acceptable statements of seismic problems for the soil and their analytical solutions are given. These statements and solutions are based on the following propositions. First, on the transfer of boundary conditions from the surface of the Earth to a cylindrical surface that is coaxial to the surface of the pipeline. Second, on the proof of the dependence of the tangential stresses causing seismic movements of the pipeline only from the first terms of decomposition of soil displacement components in Fourier series on the angular coordinate (what leads the soil problem to an axisymmetric one). Third, on the assumption of quasi-one-dimensionality of soil deformation during the propagation of a longitudinal seismic wave along the pipeline. The solutions obtained lead to theoretical expressions for the force and coefficient of interaction of the pipeline with the ground. In particular, when the ratio of the wavelength to the diameter of the pipe is large, the law of proportionality of the interaction force to the relative displacement of the pipeline proposed by T.R. Rashidov is obtained.*

Keywords: *soil, pipeline, seismic problem, quasi-one-dimensional deformation, force of interaction.*

1. Introduction: the works of academician T.R. Rashidov and their role in mathematical seismodynamics

When studying the reaction of an underground structures, in particular, pipelines to seismic effects and clarifying the issues of their non-destruction, it is necessary to introduce a number of assumptions and hypotheses, the validity of which can be confirmed or not either experimentally or theoretically by formulating and solving problems about joint seismic vibrations of the soil and the structure. In the latter case, we will talk about the mathematical theory of seismic resistance of an underground structure (or, in short, about mathematical seismodynamics). Of course, such a division into engineering and mathematical theories of seismic resistance is to a certain extent conditional, however, it is convenient to distinguish approaches in substantiating the basic propositions and principles underlying these theories.

The main works of T.R.Rashidov, which address the theoretical aspects of seismodynamics of elongated underground structures, are the works of the 60s - 70s of the last century [1-9]. These works have made a significant contribution to the formation and development of mathematical seismodynamics of complex systems of underground structures. Let us note some of the fundamental issues raised in these works, the theoretical study of which was crucial for the formation and development of the named part of seismodynamics. They are as follows: (1) the definitions of seismic forces of interaction between an elongated structure (pipeline) and the soil during elastic and inelastic deformation of the soil; (2) the dependence of the force of interaction on the depth of the pipeline; (3) the existence of an attached mass during the motion of a body in the ground; (4) the possibility of considering the "soil - pipeline" system during longitudinal movements as a composite rod (i.e., elucidation of the conditions for the validity of the hypothesis of flat sections for longitudinal movements of such a system); and (5) the derivation of averaged differential equations of motion and averaged velocities of propagation of longitudinal waves in a pipeline with a periodic system of wells attached to the pipeline compartments using damping devices. Some of these problems were fully or partially solved in the works of Rashidov himself, while the other part determined the directions of further research carried out including under his supervision.

One of the main questions in the above list is the question about the force of interaction between the pipeline and the soil during seismic action. For elastic soil T. Rashidov proposed [2-5, 9] the law of proportionality of the force of interaction to the relative displacement of the pipeline, in which relative displacement is understood as the difference between the movements of soil particles in an incident seismic wave (away from the pipeline) in the direction of the pipeline axis and the motions of pipeline sections. Thus, the relative displacement is not understood in the law as the amount of slippage at the

boundary of soil contact with a pipe, which may not be there. The coefficient of proportionality in the named dependence is called the coefficient of interaction.

Due to the lack of external (in relation to the pipeline) statements and solutions at that time of seismic problems for soil, T. R. Rashidov and G. H. Khozhmetov proposed methods for experimental determining the interaction force and the coefficient of proportonality and also developed test setups for conducting appropriate experiments. These methods and setups are described in monographs by T.R. Rashidov [9] and T.R. Rashidov and G. H. Khozhmetov [10].

Let us note here what importance is the fulfillment of the law of proportionality of the interaction force of the pipeline with the soil to its relative displacement. When the soil and the pipeline material are linearly elastic the tangential stresses in the soil on the surface of the pipeline and, therefore, the force of interaction are represented by linear dependencies on the incident wave and the movement of the pipeline. Such a more general linear dependence (with two constants) does not complicate the theoretical study and solution of the problem of seismic vibrations of the pipeline, since in this case the equation of motion of the pipeline remains linear. However, the fact that the tangential stress and the force of interaction are proportional to the relative displacement significantly simplifies the experimental study of the law of interaction, reducing the task to determining only one constant from a test. This simplification becomes even more important in the case of inelastic deformation of the soil, when functions, rather than constants, are subject to experimental definition in the law of interaction.

The solution of the seismodynamic problem for the pipeline can be divided into two stages. Finding the force of interaction with the soil (experimentally or theoretically, by formulating and solving a seismic problem for the soil) at the first stage and solving the problem of forced vibrations of the pipeline under the influence of the found force of interaction – at the second. A fundamental contribution to the mathematical foundations of seismodynamics of underground structures was a investigation conducted by T. Rashidov together with A.A. Il'yushin and devoted to nonstationary longitudinal seismic vibrations of an endless pipeline [11]. In this work, for the first time in the literature, the self-similar mode of wave propagation along the pipeline is considered, when the motion characteristics are functions of the distance from the wave front. A.A. Il'yushin and T.R. Rashidov drew attention to the fact that a situation is possible when seismic waves in the ground propagate along the pipeline with velocity higher than the velocity of wave propagation in the pipeline (this case is called supersonic). Such an assumption cannot be taken into account purely formally, but requires a physically justified extension of the problem statement and leads to solutions that differ significantly in the nature of behavior from solutions for the subsonic case. These results are now classic in mathematical seismodynamics. They served and continue to serve as a model for subsequent research in this area.

2. Methods: theoretical investigation of the laws of seismic interaction of soil and pipeline

2.1. A brief history of the problem

The relation describing the proportional dependence of tangential stresses on shear displacements on the pipeline surface was proposed by L. M. Yemel'yanov [12] in 1951 when studying the forces of interaction between pipe and soil in the longitudinal motion of the pipeline by analogy with the same ratio between normal pressure and transverse displacement of the pipe in the theory of calculation of beams on an elastic base. Later (1953), R. I. Aronov [13] investigated this question in detail and gave a theory and methodology for conducting experiments to determine the proportionality coefficient in the above relation. It was believed that the longitudinal displacements of the pipe was caused by a change in the temperature of the metal of the pipe walls (heterogeneity of the temperature distribution along the pipe), or shortening of the pipeline compartments as a result of internal pressure (for example, in gas pipelines), or other reasons. Longitudinal displacements were measured in field experiments using the method of transverse sections of the pipeline. The named proportionality coefficient was identified with

the uniform shear coefficient introduced by D.D. Barkan [14] when studying shear movements and vibrations of rigid foundations of ground structures.

As noted above, in the law of proportionality proposed in the seismic problem by T.R. Rashidov, the force of the interaction of the soil with the pipe is proportional to the relative displacement and the coefficient of interaction in this case does not have such simple physical interpretations as in the problems studied by L.M. Yemel'yanov and R.I. Aronov and cannot be determined from the experiments described in [13].

Starting with the publication of A. Sakurai and T. Takahashi [15] (1969) a slightly different approach was also developed, however, leading to the same or similar results. In this approach the medium (soil) and the interaction with the medium are modeled by elastic springs. Then, in the problem of the longitudinal motion of an elongated underground structure, considered as a rod, the forces of interaction with the soil are proportional to the relative displacement, i.e., to the difference between the longitudinal displacements in the seismic wave and in the pipeline. Thus, the problem is reduced to the equation of forced vibrations of the rod containing an indefinite parameter - the stiffness of the springs. Numerous modifications and generalizations of this approach have been proposed [15], designed to take into account slippage between the pipeline and the soil [16-20], as well as the inelasticity of the soil by replacing the elastic spring in the soil model with a viscoelastic element [21, 22].

2.2. Formulation and analytical solution of an external problem for elastic soil

A rectilinear pipeline is considered as an infinitely long thick-walled cylinder (rod) of outer radius a. The motion of the pipeline and the elastic soil, surrounding it, is caused by a plane seismic wave propagating in the soil (medium) in the direction of the pipeline axis (Figure 1), which taken as the Oz axis of the cylindrical coordinate system (r, θ, z). This means that at a distance $r = R$, sufficiently far from the pipeline, the displacements of the medium $\boldsymbol{u}(u_r, u_\theta, u_z)$ are equal to the displacements in the incident wave, i.e.,

$$u_r|_{r=R} = 0,\ u_\theta|_{r=R} = 0,\ u_z|_{r=R} = w(z - ct). \tag{1}$$

Here c is the wave propagation velocity and t is the time.

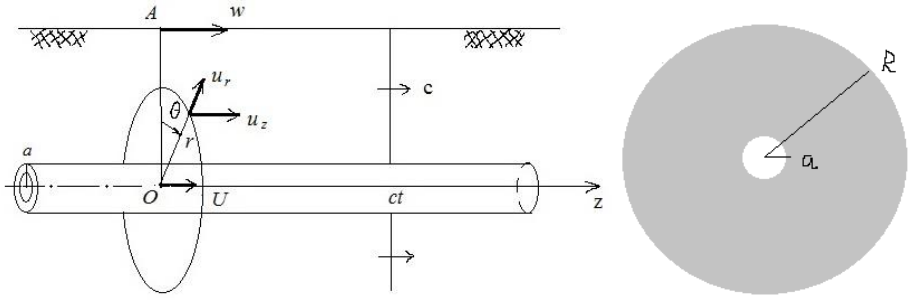

Figure 1. **Geometry of the problem**

As a rule, the depth of the pipeline is taken as the "remote" radius R and then w is the displacements, measured on the Earth's surface in the direction of the pipeline axis.

The boundary conditions on the contact surface of the pipeline and the soil are taken as

$$u_r|_{r=a} = 0,\ u_\theta|_{r=a} = 0, \quad u_z|_{r=a} = U(z, t), \tag{2}$$

where $U(z, t)$ means the axial displacement of the pipeline, determined from the equation of longitudinal vibrations of the rod. Physically, conditions (2) express the requirement of sticking on the contact surface of the soil and the pipeline. In solving an external problem for the soil (the problem of determining interaction forces), the influence of changes in the dimensions of the cross-sections of the pipeline during its longitudinal deformations is neglected (the first condition in (2)).

The latter assumption is valid for metal and concrete pipes due to the significant flexibility of the soil in comparison with the pipeline material. The necessary refinements in solving the external problem for the medium, taking into account the transverse deformations of the pipe in the case of flexible pipelines, can be easily implemented. The second condition in (2) expresses the fact that the torsion vibrations of circular cylinder are not to be excited under the action of plane waves.

Steady-state (or stationary) vibrations of the soil and the pipeline occur when a given incident seismic wave is represented as

$$w(z-ct) = w_0 e^{ik(z-ct)} = w_0 e^{i(kz-\omega t)}, \tag{3}$$

where ω is the frequency of seismic vibrations and $k = \omega/c$ is the wave number. Then the displacements of the soil and pipeline are expressed in a similar way, i.e.,

$$(u_r, u_\theta, u_z) = (U_r, U_\theta, U_z)\, e^{ik(z-ct)},\ U = U_0 e^{ik(z-ct)}. \tag{4}$$

1). The case $c = c_1$ when a given seismic wave w is a longitudinal wave [23]. Its propagation velocity is $c_1 = \sqrt{(\lambda+2\mu)/\rho}$, where (λ, μ) denote the Lame constants of the elastic soil and ρ is its density. In this case the problem for the medium is axisymmetric with $U_\theta = 0$ and the displacements U_r and U_z, which do not depend on the angular coordinate θ. Under these conditions, the Lame's equations of motion of the elastic soil are reduced in cylindrical coordinates to the next two equations

$$\begin{cases} \dfrac{d}{dr}\left(\dfrac{dU_r}{dr} + \dfrac{U_r}{r}\right) + ik\left[1 - \left(\dfrac{c_2}{c_1}\right)^2\right]\dfrac{dU_z}{dr} + k^2\left[1 - \left(\dfrac{c_2}{c_1}\right)^2\right]U_r = 0, \\ \dfrac{1}{r}\dfrac{d}{dr}\left(r\dfrac{dU_z}{dr}\right) + ik\left[\left(\dfrac{c_1}{c_2}\right)^2 - 1\right]\left(\dfrac{dU_r}{dr} + \dfrac{U_r}{r}\right) = 0. \end{cases} \tag{5}$$

relative to the nonzero components of the displacement vector. When deriving equations (5), it is taken into account that $\omega = kc_1$.

The boundary conditions for the amplitude functions (U_r, U_z) at $r = R$ and $r = a$, following from (1) and (2), are obvious by virtue of representations (3), (4),.

The method of "quasi-one-dimensional" deformation of the soil. A significant simplification of the formulated problem is obtained with the additional assumption that for the described soil motion, longitudinal deformations ε_{zz} (in the direction of motion of medium particles in a seismic wave) are predominant and by deformations ε_{rr} and $\varepsilon_{\theta\theta}$ can be neglected in comparison with ε_{zz} [24], i.e., when an approximate equality can be assumed for the tensor of soil deformations

$$(E) \equiv \begin{pmatrix} \varepsilon_{rr} & 0 & \varepsilon_{rz} \\ 0 & \varepsilon_{\theta\theta} & 0 \\ \varepsilon_{zr} & 0 & \varepsilon_{zz} \end{pmatrix} \approx \begin{pmatrix} 0 & 0 & \varepsilon_{rz} \\ 0 & 0 & 0 \\ \varepsilon_{zr} & 0 & \varepsilon_{zz} \end{pmatrix}. \tag{6}$$

In the considered case of steady-state oscillations (stationary motions), the specified property is provided if $|dU_r/dr| \ll |U_z|/\lambda$ and $|U_r/r| \ll |U_z|/\lambda$, where $\lambda = 2\pi/k$ is the length of the incident seismic waves. Then the second equation of the system (5) is allocated to a separate equation for U_z, namely

$$\frac{d^2U_z}{dr^2} + \frac{1}{r}\frac{dU_z}{dr} = 0. \tag{7}$$

Solution of the boundary value problem (7), (1), (2) (when in a stationary problem the displacements are represented by the relations (3), (4)) is

$$U_z(r) = \frac{\ln(r/a)}{\ln(R/a)}(w_0 - U_0) + U_0,\ \frac{dU_z(r)}{dr} = \frac{1}{r\ln(R/a)}(w_0 - U_0). \tag{8}$$

The tangential stress σ_{rz} on the pipeline surface, taking into account the boundary condition (2), is determined by the formula

$$(\sigma_{rz})|_{r=a} = \mu\left(\frac{\partial u_r}{\partial z} + \frac{\partial u_z}{\partial r}\right)\Big|_{r=a} = \mu\left(\frac{\partial u_z}{\partial r}\right)\Big|_{r=a} = \mu\left(\frac{dU_z}{dr}\right)\Big|_{r=a} e^{ik(z-c_1 t)}. \quad (9)$$

2). The case $c \neq c_1$ when the given function is the axial component of a seismic wave obliquely approaching the pipeline. In the case of an inclined fall the displacement vector in the incident wave is decomposed into a component parallel to the axis of the pipeline and a component perpendicular to it. Thus, the incident plane wave can be considered as the sum of two plane waves, which propagate along the Earth's surface $(r = R)$ in the direction of the pipe axis with a velocity c equal to $c_1/\sin\alpha$ or to $c_2/\sin\alpha$, depending on whether the initial wave is longitudinal or transverse (shear) with a propagation velocity of $c_2 = \sqrt{\mu/\rho}$. Here α is the angle formed by the front of an incident plane wave (or a plane of equal phase in the case of a stationary wave) with the axis of the pipeline. Therefore, if $c \neq c_1$ then the cases $c_2 < c < c_1$ and $c > c_1$ are possible.

The interaction of the pipeline and the wave, representing the second term in the above decomposition of the incident seismic wave, with displacements in the transverse direction to the pipe leads either to transverse motions of the pipeline together with the medium (without bending), or to its bending vibrations. The latter problem can be studied separately (see, for example, [25]) and is not considered here.

When the burial depth of the pipeline significantly exceeds its diameter, then even in the case of oblique fall of the incident wave, the longitudinal displacements on the surface $r = R$ might be considered as approximately the same. Hence, the function w (or w_0 in (3)) is independent from angle θ. Then the external problem for the soil is axisymmetric (as in case *1*) and leads to finding a solution to the system

$$\begin{cases} \frac{d}{dr}\left(\frac{dU_r}{dr} + \frac{U_r}{r}\right) + ik\left[1 - \left(\frac{c_2}{c_1}\right)^2\right]\frac{dU_z}{dr} + k^2\left[\left(\frac{c}{c_1}\right)^2 - \left(\frac{c_2}{c_1}\right)^2\right]U_r = 0, \\ \frac{1}{r}\frac{d}{dr}\left(r\frac{dU_z}{dr}\right) + ik\left[\left(\frac{c_1}{c_2}\right)^2 - 1\right]\left(\frac{dU_r}{dr} + \frac{U_r}{r}\right) + k^2\frac{c^2 - c_1^2}{c_2^2}U_z = 0. \end{cases} \quad (10)$$

under the same boundary conditions (1), (2). The system (10) coincides with (5) at $c = c_1$.

There are, of course, situations when the boundary conditions transfer to a cylindrical surface $(r = R)$, then the displacements w in (1) and, accordingly, w_0 in (3) are not constants in the same cross-sections even approximately, and they must be considered as functions of the angle θ. This is the case, for example, when a large-diameter tubular structure (say, a subway tunnel) lies at a shallow depth and when with an inclined fall of a seismic wave in the soil layer, lying above the structure, multiple reflected waves arise from the surface of the structure and the boundary of the half-space (the surface of the Earth). In this case, the problem is reduced to integrating of three Lame equations under boundary conditions (1), (2) and it can be solved by the Fourier method, decomposing the given function $w_0(\theta)$ and unknown functions into series by θ (the longitudinal displacement of the cross section of the rod U (or U_0) cannot depend on θ). At the same time, the following important fact is easily established: the resulting force acting on the pipeline and driving it is not affected by the coefficients of expansion of the displacement components in the Fourier series (coefficients at $\cos n\theta$ and $\sin n\theta$) for $n \geq 1$, i.e., this resultant force (calculated as an integral over the lateral surface of the pipe from the tangential stresses σ_{rz} is completely determined by the first coefficients of the Fourier series (for $n = 0$) of the displacement components.

In accordance with expression (9) for tangential stresses on the pipe surface, in order to find the specified resultant force, it is necessary to know only the first term $U_z^{(0)}(r)$ of the Fourier series expansion of the longitudinal displacement of the medium $U_z(r, \theta)$. But it cannot be determined independently, since the Lame equations (for the first coefficients of the series) include $U_r^{(0)}(r)$ and

$U_\theta^{(0)}(r)$ – the coefficients of the Fourier series of the other two components of the displacement vector of the medium. However, it is easily established that the differential equations for these functions decompose into a system of two equations with respect to $U_z^{(0)}$ and $U_r^{(0)}$, exactly coinciding with (10), and a separate equation for $U_\theta^{(0)}$:

$$\frac{d^2U_\theta^{(0)}}{dr^2}+\frac{1}{r}\frac{dU_\theta^{(0)}}{dr}+\left(m^2-\frac{1}{r^2}\right)U_\theta^{(0)}=0, \qquad m=k\sqrt{(c/c_2)^2-1}\,. \tag{11}$$

Therefore, due to homogeneous boundary conditions for $U_\theta^{(0)}$ from (1) and (2) we have $U_\theta^{(0)}\equiv 0$.

Thus, in the non-axisymmetric case, the problem reduces to the system (10) with respect to the functions $U_z^{(0)}$ and $U_r^{(0)}$. But in this case, in the boundary condition (1) for $U_z^{(0)}$ it is necessary to replace w_0 by the mean value (the first coefficient of the Fourier series) $\overline{w}_0=(2\pi)^{-1}\int_0^{2\pi}w_0(\theta)d\theta$ or, in other words, the boundary condition on the surface $r=R$ is sufficient to set in the integral form.

Further, applying, as above, the approach of quasi-one-dimensional deformation of the soil, i.e., considering the deformations ε_{rr} and $\varepsilon_{\theta\theta}$ small in comparison with ε_{zz}, we obtain that a separate equation for U_z is allocated from the system (10), namely

$$\frac{d^2U_z}{dr^2}+\frac{1}{r}\frac{dU_z}{dr}\pm p^2U_z=0, \qquad p\equiv\frac{k}{c_2}\sqrt{|c^2-c_1^2|}\,. \tag{12}$$

The Bessel equation (12) in combination with the boundary conditions (1), (2) for U_z leads to a separate problem for longitudinal displacements. The solving of the last problem is enough, in accordance with (9), to determine tangential stresses on the pipeline surface. The plus sign in (12) is taken in the case of *a*) $c>c_1$ and the minus sign in the case of *b*) $c_2<c<c_1$.

Solution of the problem (12), (1), (2) it is elementary written out and given in the cases under consideration by the relations:

$$a)\quad U_z=\frac{J_0(pr)}{\Delta_1}[Y_0(pR)U_0-Y_0(pa)w_0]-\frac{Y_0(pr)}{\Delta_1}[J_0(pR)U_0-J_0(pa)w_0], \tag{13}$$

$$\Delta_1=J_0(pa)Y_0(pR)-Y_0(pa)J_0(pR);$$

$$b)\quad U_z=\frac{I_0(pr)}{\Delta_2}[K_0(pR)U_0-K_0(pa)w_0]-\frac{K_0(pr)}{\Delta_2}[I_0(pR)U_0-I_0(pa)w_0], \tag{14}$$

$$\Delta_2=I_0(pa)K_0(pR)-K_0(pa)I_0(pR);$$

Here J_0, Y_0 mean Bessel functions of the first and second kind of zero order and I_0, K_0 are modified Bessel functions of the first and second kind of zero order.

3. Results and Discussion: Derivation of the proportionality law, theoretical values of the interaction coefficient

In the case of $c=c_1$, substituting the solution (8) of the boundary value problem for soil into formula (9), we have

$$(\sigma_{rz})|_{r=a}=\frac{\mu}{a\ln(R/a)}(w-U)\equiv k_z(w-U). \tag{15}$$

Thus, in this case on the contact surface of the soil and the pipeline the tangential stress is proportional to the ("global") relative displacement and the coefficient of this proportional dependence (called the coefficient of interaction of soil and pipeline) is given by the exact expression

$$k_z=\frac{\mu}{a\ln(R/a)}. \tag{16}$$

In the case of $c \neq c_1$ the tangential stress on the pipeline surface calculated by formula (9), as follows from formulas (13), (14), in the general case (for arbitrary values of the parameters included in the solutions) is not proportional to the relative displacement $w - U$, as it was the event in the above case $c = c_1$ (formulas (15), (16)). In the existing literature, this fact was not noticed and, as a result, the question of the existence of conditions when the "law of proportionality" is fulfilled remained unclear.

Now suppose that $pR \ll 1$ (then also pa $\ll 1$) or, equivalently, $R/\lambda \ll 1$, $a/\lambda \ll 1$, i.e., assume that the depth of the pipeline and its diameter are small compared to the length of the seismic wave. Then, it follows from solutions (13), (14) that the tangential stresses on the surface of the pipe, defined by the formula (9), have in both cases a and b the same asymptotic representation, namely

$$\mu^{-1}\sigma_{rz}|_{r=a} \approx \frac{1}{a\ln(R/a)}\left\{(w-U) + 2\left(\frac{pa}{2}\right)^2\left[U\ln\left(\frac{2}{pR}\right) - w\ln\left(\frac{2}{pa}\right)\right]\right\}. \qquad (17)$$

This asymptotic is obtained using well-known series for Bessel functions, included in solutions (13), (14), for small values of arguments (see, for example, [26], Chapter 5).

The condition of proportionality. As can be seen from (17), when the diameter and depth of the pipeline are significantly less than the length of the seismic wave, the tangential stresses on the contact surface of the pipeline and the soil are proportional to the relative displacement $w - U$ up to terms of the order $O(\varepsilon^2 \ln \varepsilon)$, where $\varepsilon = R/\lambda$. Moreover, the coefficient in this proportional dependence is determined by the same expression (16) as in the case of $c = c_1$.

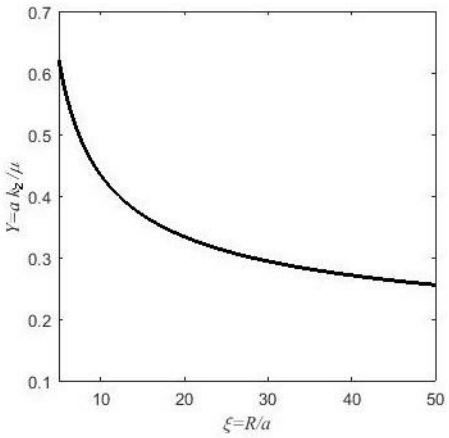

Figure 2. - **Graph of the dependence of the interaction coefficient on the ratio of the depth of the pipeline to its radius**

The above statement establishes the range of applicability and accuracy of the proportionality hypothesis in the case of propagation of seismic waves along the pipeline with an arbitrary velocity.

Note that the more general linear dependence (17) of tangential stresses on displacements w and U (with different multipliers in front of them) does not complicate the theoretical study and solution of the problem of seismic vibrations of the pipeline, since in this case the equation of pipeline motion remains linear. However, the fact that the stresses σ_{rz} are proportional to the relative displacement significantly simplifies the experimental study of the law of interaction, reducing the task to determining only one constant from experiment.

Figure 2 shows a graph of the dependence of the interaction coefficient on the ratio of the depth of the pipeline to its radius. It follows from formulas (16), (17) that $k_z \to 0$ as $R/a \to \infty$, however, it can be seen from the graph that the decrease in the interaction coefficient will be slow at $R/a \gtrsim 10$. Therefore, burying the pipeline to a depth greater than $10a$ may not have a meaningful effect to ensure earthquake resistance.

4. Conclusions

1. The issues raised in the works of T.R. Rashidov are discuss, the research and solution of which was a significant contribution to the creation of mathematical seismodynamics of underground structures.

2. The formulations of an external problems for elastic soil arising from the study of joint longitudinal seismic vibrations of soil and pipeline (elongated underground structure) are given. Their analytical solutions are obtained on the basis of a physically and mathematically justified assumption about the quasi-one-dimensionality of the soil deformation tensor in the considered cases.

3. These solutions lead to theoretical expressions for the forces of interaction between the pipeline and the soil. By means of asymptotic analysis (for large ratios of the depth of the pipeline to its radius)

the law of proportionality of the interaction forces to the relative displacement of the pipeline is derived. This result establishes the accuracy and the area of validity of engineering approaches in the study of the problem.

References

1. *Rashidov T.* Napryazheniya, voznikayushie v truboprovode pri sejsmicheskom vozdejstvii // Izv. AN UzSSR. Ser. tekhn. nauk. 1960, № 6. C. 36-40.
2. *Rashidov T.* Differentsial'noe uravnenie kolebaniya podzemnogo truboprovoda pri zemletryasenii // Dokl. AN UzSSR. 1962, № 9. C. 10-12.
3. *Rashidov T.* Issledovanie uslovii raboty podzemnykh truboprovodov pri zemletryaseniyah // Izv. AN UzSSR. Ser. tekhn. nauk. 1962, № 5. C. 44-52.
4. *Rashidov T.* Zavisimost' koeffitsienta ravnomernogo sdviga truboprovoda ot glubiny zalozheniya truboprovoda // Dokl. AN UzSSR. 1962, № 12. C. 16-18.
5. *Rashidov T.* Vliyanie glubin zalozheniya podzemnykh truboprovodov na ikh pri sejsmostojkost' i puti umen'sheniya ikh // Izv. AN UzSSR. Ser. tekhn. nauk. 1963, № 6. C. 35-40.
6. *Rashidov T.* Usiliya, voznikayushie v truboprovode pri zakrytykh prokhodakh //Dokl. AN UzSSR. 1963, №11.C.5-7.
7. *Rashidov T.* Prodol'nye dvizheniya zhestkoj podzemnoj truby v razlichnykh modelyakh grunta // Dokl. AN UzSSR. 1970, № 1.
8. *Il'yushin A.A., Rashidov T.* Uproshennye uravneniya sejsmodinamiki slozhnyh sistem podzemnykh sooruzhenii // Izv. AN UzSSR. Ser. tekhn. nauk. 1962, № 5. C. 44-52.
9. *Rashidov T.* Dinamicheskaya teoriya seismostoikosti slozhnykh sistem podzemnykh sooruzhenii. Tashkent: Izd-vo «FAN» UzSSR, 1973.
10. *Rashidov T., Khozhmetov G.Kh.* Seismostoikost' podzemnykh truboprovodov. Tashkent: Izd-vo «FAN» UZSSR,1985.
11. *Il'yushin A.A., Rashidov T.* O dejstvii sejsmicheskoj volny na podzemnyj truboprovod // Izv. Akad. nauk UzSSR. Ser. tekhn. nauk. 1971, no. 1, pp. 37-42.
12. *Emel'yanov L. M.* O prodol'nykh napryazheniyakh v podzemnykh gazoprovodnykh trubakh.Trudy VNIIGaz «Voprosy dobychi, transporta i pererabotki prirodnykh gazov».L.: Gostekhtopizdat, 1951. Pp. 177- 212.
13. *Aronov R. I.* Deistvitel'nye usloviya raboty konstruktsii stal'nykh truboprovodov // Trudy VNIIStroineft'. Vyp. V. M.-L.: Gostekhtopizdat, 1953. P. 54-72.
14. *Barkan D. D.* Dynamics of bases and foundations. N. Y.: McGraw - Hill, 1962.
15. *Sakurai A., Takahashi T.* Dynamic stress of underground pipelines during earthquakes. // Proc. 4th World Conf. Earthq. Engng. Chile: Santiago, 1969. P. 811-895. https://www.iitk.ac.in/nicee/wcee/article/4_vol2_B4-81.pdf
16. *Shinozuka M., Koike T.* Estimation of structural strains in underground lifeline pipes. // Lifeline Earthq. Engng.-Buried Pipelines, Seismic Risk, and Instrumentation. PVP-34. ASME. 1979. P. 31-48.
17. *Akiyoshi T., Fuchida K.* Seismic interaction of soil-pipeline system through the frictional interface // Proc.8th World Conf. Earthq. Engng. USA: San Francisco, 1984. P. 199-206. https://doi.org/10.1016/0261-7277(84)90024-X
18. *Nowak M., Hindy A.* Seismic analysis of underground tubular structures // Proc. 7th World Conf. Earthq. Engng. Turkey: Istambul, 1980. P. 287-294.
19. *O'Rourke M. J., Hmadi K. E.* Analysis of continuous buried pipelines for seismic wave effects // Earthquake Engineering and Structural Dynamics. 1988, **16**, p. 917-929. **DOI:** 10.1002/eqe.4290160611
20. *O'Rourke M. J., Liu X.* Response of buried pipelines subject to earthquake effects // Publ. Multidisciplinary Center for Earthquake Engineering Research (MCEER). Univ. of Buffalo: Buffalo, 1999.
21. *Mavridis G.A., Pitilakis K.D.* Axial and transverse seismic analysis of buried pipelines // Proc. 11th World Conf. Earthq. Engng. Mexico. 1996. Paper 1605.
22. *Dwivedi J. P., Singh V. P., Lal R. C.* Dynamic analysis of buried pipelines under linear viscoelastic soil conditions // Advanced Theoretical Applications of Mechanics. 2010, **3**(12), p. 551-558.
23. *Georgievskii D.V., Israilov M.Sh.* Sesmodynamics of Extended Underground Structures and Soils: Statement of the Problem and Self-Similar Solutions // Mechanics of Solids. 2015, **50**(4), p. 473-484. DOI: 10.3103/S0025654415040135
24. *Israilov M. Sh.* Seismodynamics of an underground pipeline // Proc. 15th World Conf. Earthq. Engng. Portugal: Lissabon. 2012. Paper 2125. WCEE2012_2125.pdf
25. *Toki K., Takada S.* Earthquake response analysis of underground tubular structures // Bulletin of the Disaster Prevention Res. Inst. Kyoto Univ. 1974, **24**(2). No 221, p. 107-125.
26. *Lebedev N. N.* Special functions and their applications. Prentice-Hall, Inc., 1965.

RECENT EARTHQUAKES IN TURKEY (2023) AND TAIWAN (2024): EARTHQUAKE SPECTRAL CHARACTERISTICS, SEISMIC WAVES, AND METHODS OF SEISMIC PROTECTION

Kuznetsov S.V.[1,2]
[1]*Moscow State University of Civil Engineering, Moscow, Russia*
[2]*Ishlinsky Institute for Problems in Mechanics, Moscow, Russia*
E-mail: kuzn-sergey@yandex.ru

Abstract*. The recent earthquakes in Turkey, occurred on February 6, 2023 and Taiwan, occurred on 03.04.2024, in Hualien region having extreme intensity (XI) by the modified Mercalli scale (MMS) caused extremely different subsequence, e.g. the death of more than 52,800 people in Turkey and Syria, as well as severe damages to the infrastructure, while in Taiwan the total death was 18 people, of which seven of these deaths were caused by land sliding, and less sever damages to the buildings. The appearance of an unusually strong delta-like S-wave pulse in the seismograms of these earthquakes and their consequences are analysed, and possible measures to mitigate the possible future high intensity earthquakes are discussed.*

Keywords*: Earthquake; seismogram; delta-pulse; spectrogram; seismicity; damage*

1. Introduction

1.1. Turkey-Syria earthquake of 06.02.2023. The recent earthquake (06.02.2023) of M_w7.8 and the subsequent strong aftershock M_w7.5, which took place in the Kahramanmaraş region of Turkey and in the nearby regions in Syria, had a relatively shallow hypocentre located within the sedimentary layers of the Earth's crust, about 10,000 meters below the ocean level [1, 2]. The estimated earthquake intensity in the cities Gaziantep and Kilis was XI on the modified Mercalli scale [3, 4]. The aftershocks continue and are likely to continue for about a year after the main shock [3].

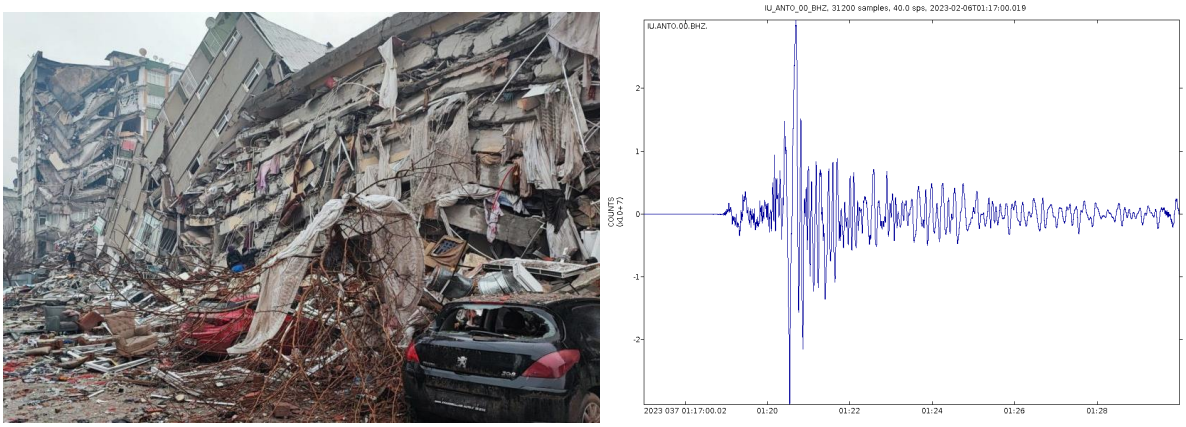

a)……b)

Figure 1. - a) Huge damages in Kahramanmaraş city; b) a horizontal component of the seismogram of the main shock at 01:17 GMT, Station IU ANTO, Ankara, Turkey; located about 235 km away from the epicentre

At least 15.73 million people and 4 million buildings were affected, more than 70 000 people were killed. About 164,000 buildings were either destroyed or severely damaged. All 15 buildings equipped with seismic isolating devices were destroyed.

The analysis of seismogram detected at different stations reveals the presence of a large horizontally polarized delta-like pulse located between 01:20 and 01:22; see Fig. 1a. It is associated with the arrival of the horizontally polarized large intensity and short duration S-wave. The authors' estimates indicate the duration of the peak pulses being ~100 ms. Considering this seismogram in a better resolution reveals that the two peaks actually consist of two delta-like pulses of almost equal amplitude and duration, as shown in Fig. 1b. Note that the resolution in the seismogram is limited by a sampling time $\Delta t \approx 50\,\text{ms}$ [5, 6].

1.2. Taiwan (Hualien region) earthquake of 03.04.2024. The recent earthquake in Hualien region of Taiwan (03.04.2024) of M_w7.4 and a large number of subsequent less strong aftershocks, three of

which were near or above M_w 6.0. The earthquake had a relatively shallow hypocentre located within the sedimentary layers of the Earth's crust, more than 15,000 meters below the ocean level.

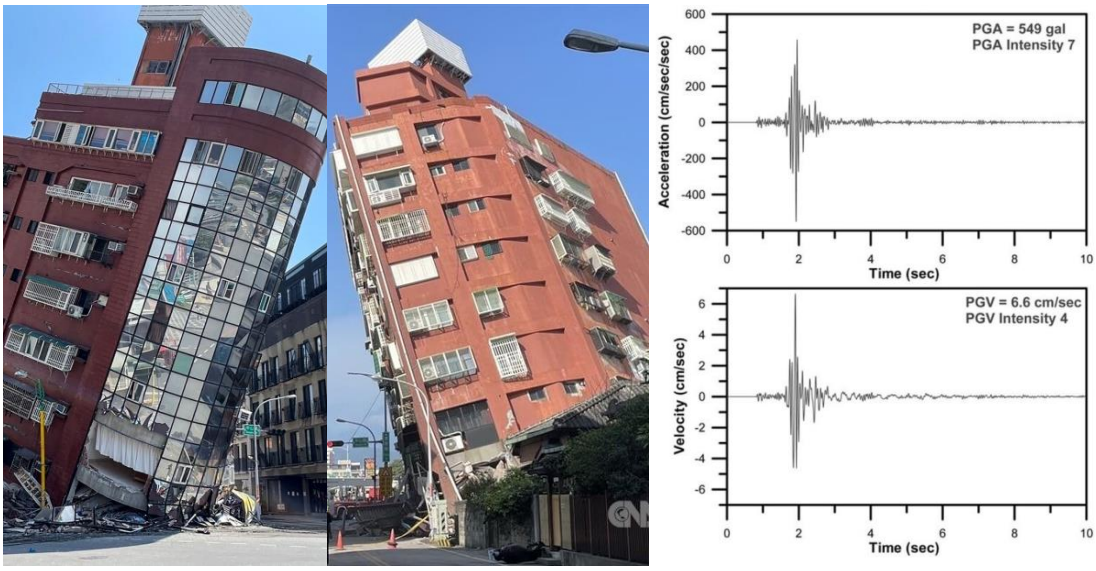

a)……b)

Figure 2. - a) Soil liquefaction caused uneven building settlements in Hualien city; b) an integral seismogram registered at station in Taipei, about 120 km from Hualien

1.3. Other high intensity earthquakes. TThe analogous extremely large pulses of relatively short duration have been also recorded at some strong earthquakes, caused high loss of life and severe destructions , e.g. Kobe M_w 6.9 earthquake, occurred on 17 January 1995 [7].

Sometimes large peaks appear at arrivals of large intensity Rayleigh, Rayleigh – Lamb, and horizontally polarized Love waves [8, 9]; see a seismogram of the Haitian M_w 7.0 earthquake of 12.01.2010; Fig. 3.

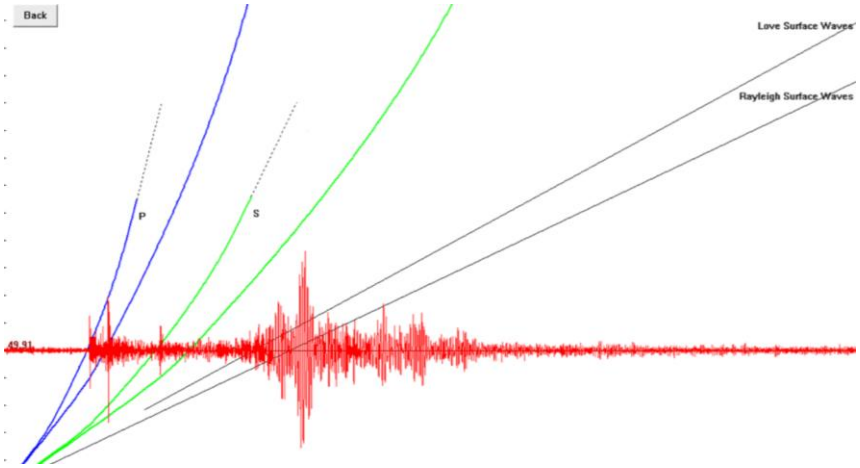

Figure 3. - Large intensity and low duration peaks associated with the arrival of Rayleigh – Lamb waves in Haitian M_w 7.0 earthquake of 12.01.2010 [10].

It should also be noted that the situation is much more typical when the recorded seismograms do not contain large impulses of such a short duration; see a sample of the typical seismogram in Fig. 4.

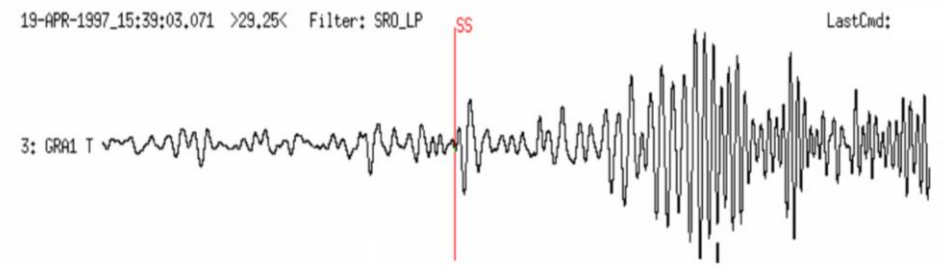

Figure 4. - The typical seismogram; an earthquake near island Severnaya Zemlya, occurred on 19 April 1997 [11]; red line indicates arrival of S-waves

2. What does a double delta-like pulse spectrum look like?

Consider integral Fourier transform of a single delta-like pulse, shown in Figs. 1b and 2b.

$$f^{\sim}(\omega)=\int_{-T}^{T} f(t)\exp\left(-i\omega t\right)dt\,, \tag{2.1}$$

where ω is the circular frequency; $f(t)$ is the function having finite support in the time-domain: supp $f=[-T;\,T]$

$$f(t)=\frac{p}{T}\times\begin{cases}t+T, & -T<t<0\\ T-t, & 0<t<T\end{cases}. \tag{2.2}$$

In Eq. (2.2) p is the amplitude multiplier. Herein, the pulse is shifted by T along the time-axis to avoid asymmetry, and thus, to have only real part in the Fourier spectrum.

Applying transformation (2.1) to function (2.2), yields the corresponding Fourier spectral function [12]

$$f^{\sim}(\omega)=pT\cdot\mathrm{sinc}^2\left(\frac{\omega T}{2}\right), \tag{2.3}$$

where

$$\mathrm{sinc}\left(t\right)=\frac{\sin t}{t}\,. \tag{2.4}$$

In view of Eq. (2.3), the plots for the corresponding Fourier spectra become; see Fig. 5.

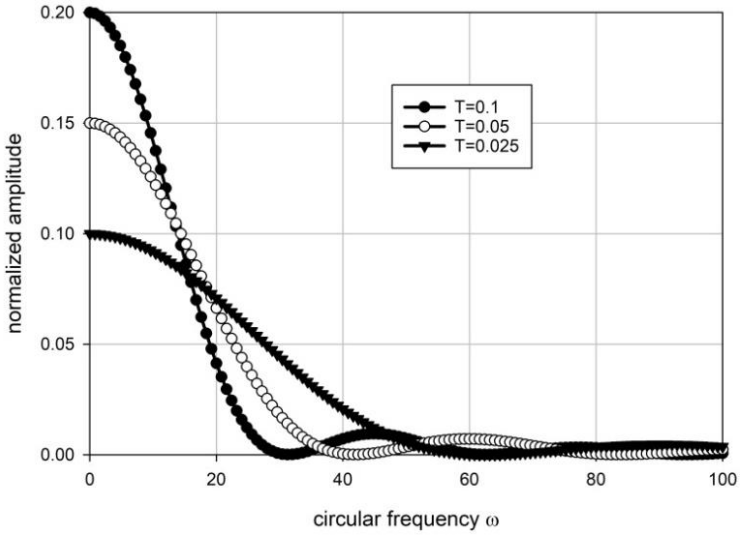

Figure 5. - Fourier spectrums of delta-like pulses at different T

The plot in Fig. 5 clearly indicates the substantial maximums at the zero frequency.

3. AFC for a typical seismic isolating device

Suppose a building is equipped with a typical seismic isolating device, modelled by Kelvin – Voigt model or a more refined Zener model, known also as the standard viscoelastic model [13, 14]; see Fig. 6a,b. The governing equations for both Kelvin – Voigt and Zener models may be represented in the Cauchy form [15]

$$\frac{d}{dt}\mathbf{Y}(t) = \mathbf{G}\cdot\mathbf{Y}(t) + \mathbf{U}(t), \tag{3.1}$$

where for Kelvin – Voigt model

$$\mathbf{Y}(t) = \begin{pmatrix} x(t) \\ v(t) \end{pmatrix}; \qquad \mathbf{G} = \begin{pmatrix} 0 & 1 \\ -k/m & -\eta/m \end{pmatrix}; \qquad \mathbf{U}(t) = \mathbf{U}_0 \exp(i\omega t). \tag{3.2}$$

Herein, $x(t)$ is the deflection of a mass; $v(t) = \dot{x}(t)$; η is the viscosity of a dashpot; k is the stiffness of a spring; m is the vibration mass; and, $\mathbf{U}_0$ is the amplitude of an external load. Note that $\mathbf{G}$ is a semi-stable matrix [15]. For Zener model with the auxiliary spring, the corresponding parameters become

$$\mathbf{Y}(t) = \begin{pmatrix} x_1(t) \\ x_2(t) \\ v_1(t) \end{pmatrix}; \qquad \mathbf{G} = \begin{pmatrix} 0 & 0 & 1 \\ k'/\eta & -k'/\eta & 0 \\ -(k+k')/m & k'/m & 0 \end{pmatrix}, \tag{3.3}$$

where $x_1(t)$, $v_1(t)$ are deflection and speed of the mass; $x_2(t)$ is the deflection of the auxiliary spring; and, k' is the auxiliary spring stiffness. Solving Eq. (3.1) at different excitation frequencies yields the amplitude-frequency characteristic (AFC); the typical AFC for Zener model is shown in Fig. 6c.

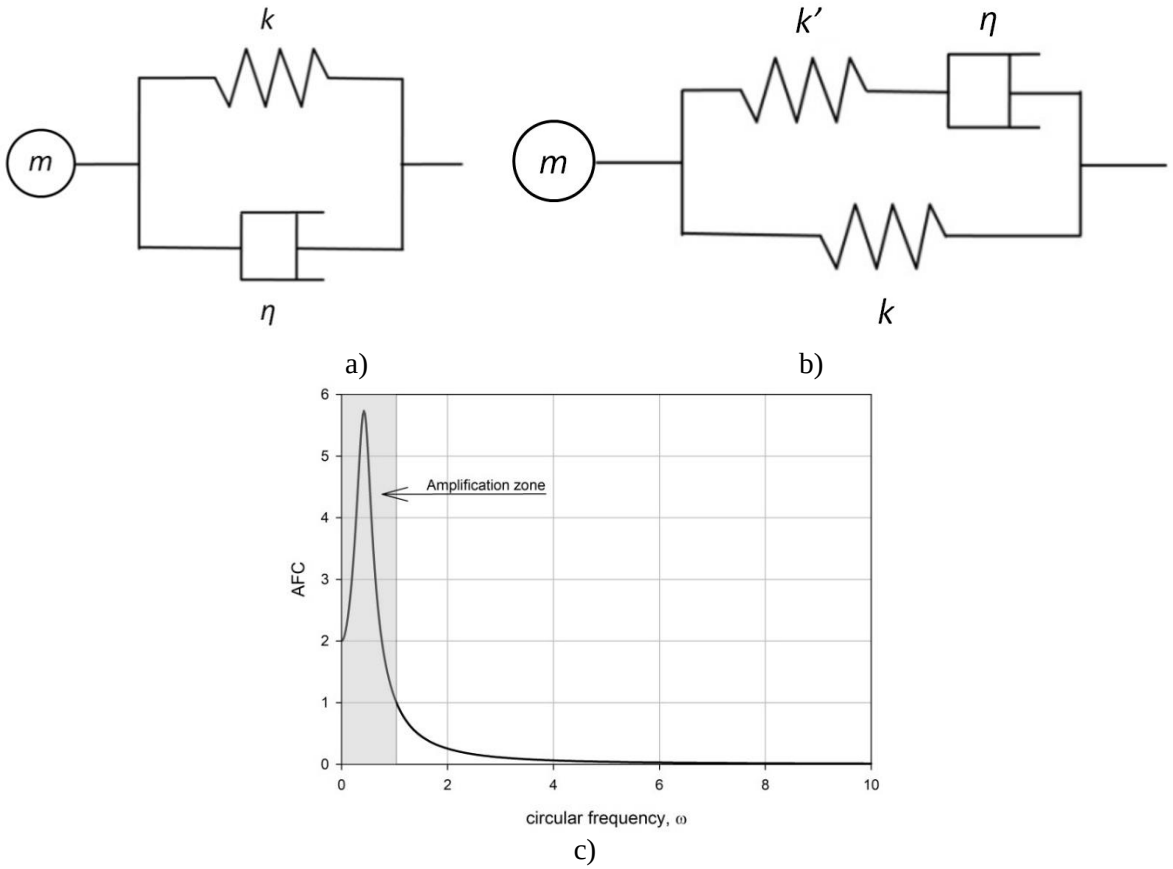

Figure 6. - a) Kelvin – Voigt model; b) Zener model; c) The typical AFC of a seismic isolating device modelled by Zener model; grey colour indicate amplification zone

The plot in Fig. 6c clearly demonstrates that the typical seismic isolating device being perfectly suited for damping relatively high frequencies ($\omega > 1$), generates considerable signal amplification in a smaller frequency range ($\omega < 1$), exactly, where the delta-like pulse spectrogram attains its maximum; see Fig. 4. Thus, the considered seismic isolating devices become not only useless at low frequencies, but instead, they amplify seismic signals in the low frequency range.

4. Collapse of a frame building without seismic isolation

Consider now the diffraction of the high intensity seismic delta-like S-wave into frame building without a seismic isolation.

The finite element (FE) analysis of the diffracted large amplitude and short duration S-wave pulse corresponding to 1g acceleration (~ 9.8 m/s^2) reveals, (i) the appearance of high intensity stress fields both in columns and slabs, especially on the lower floors; (ii) multiple damage zones appearing mostly at the back-fronts of the diffracted waves; and, (iii) collapse of the frame elements prior to the onset of vibration, when the standing waves are formed; see Fig. 7. The latter effect undermines the attempts to apply vibration dampers to mitigate high intensity and short duration delta-like impulse loadings.

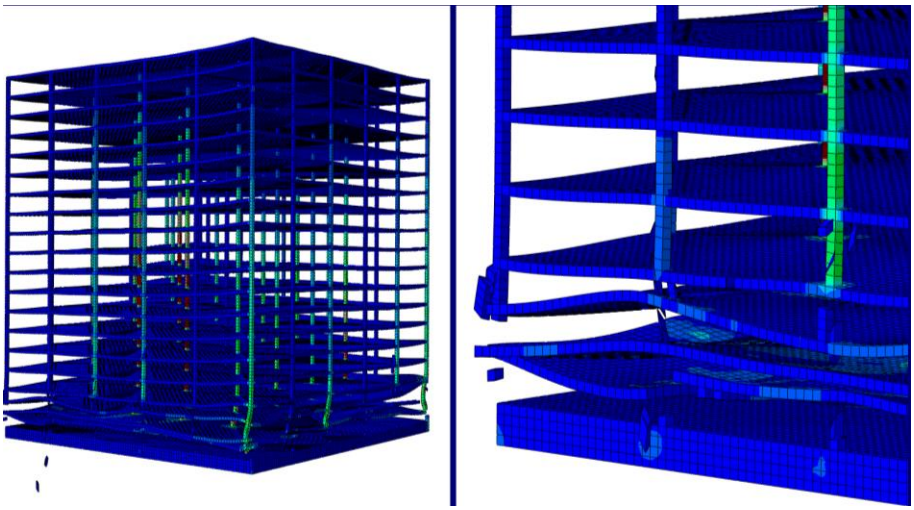

Figure 7. - Collapse of the frame building caused by the arrival of shock waves of high intensity; FE modelling

The slides in Fig. 7 demonstrate collapse of the building frame elements starting from the bottom floors, while the high-intensity S-wave propagates upward. Thus, the performed FEA along with numerous evidences [1 – 11] reveals a strong necessity for seismic protection against the considered types of short-duration seismic pulses.

5. How to get seismic protection at arrival of high intensity shock waves?

5.1 Seismic pads, an overview.

A natural question arises, on how to become seismically protected at the appearance of high intensity and short duration seismic pulses. That is especially important in view of the principal inability of the widely used seismic isolating devices to damp such short pulses.

Apparently, the first known natural seismic protection system capable of protecting from strong ground motions caused, by high intensity seismic waves, is the Imperial Hotel in Tokyo, designed in 1923 by Frank Lloyd Wright. The building was placed above a relict swamp, which acted as a seismic pad, protected the building from S-waves during the Great Kanto earthquake M_w 7.9–8.2, which occurred on 01.09.1923, the same year when the building was finished [16]. It is also known [17] that most of the surrounding buildings were destroyed by the earthquake. The principal scheme of the seismic pad is shown in Fig. 8.

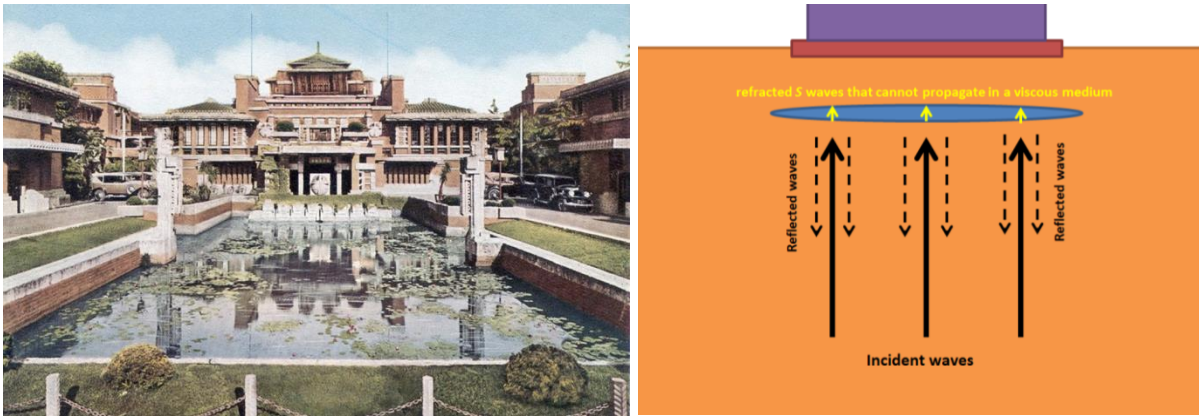

a) b)

Figure 8. - a) Imperial Hotel, Tokyo, 1923 [16]; b) The principal scheme of a relict swamp acting as a seismic pad

Currently, there are several approaches for mitigating the effect of the considered strong shock S-wave pulses. Some of these approaches are already developed, while others are still under development, including

(I) In case of foundations for bridges the following solution was developed, based on a seismic pad made of calibrated natural stones placed between pile heads and the bottom surface of the grillage. Thus, presumably for the first time for such large structures, the grillage was separated from the piles. This solution was used at constructing the Rion-Antirion bridge and some other long-span bridges [18, 19] by Geodynamique® (France). While such a pad could not reflect much seismic wave energy, because of small differences in acoustic impedances between seismic pad and reinforced concrete, it still could dissipate some of the wave energy within the pad ensured by the relative movement of the stones [20].

(II) A seismic protection system for buildings developed by Marathon Alliance® (Australia) relies on installation of a seismic pad either beneath the foundation slab (Fig. 9a) or splitting a grillage, in case of a pile foundation (Fig. 9b); see [21]. The developed seismic pads are made of granular metamaterials, ensuring reflection of the arriving seismic waves in a broad range of the corresponding spectral frequencies and absorbing mechanical energy of seismic waves within granular metamaterial; thus, more than 4 times attenuating wave energy that may still diffract into the building. The lifespan of these granular metamaterials is comparable with the lifespan of the protected structure due to the inorganic nature of the granules [21].

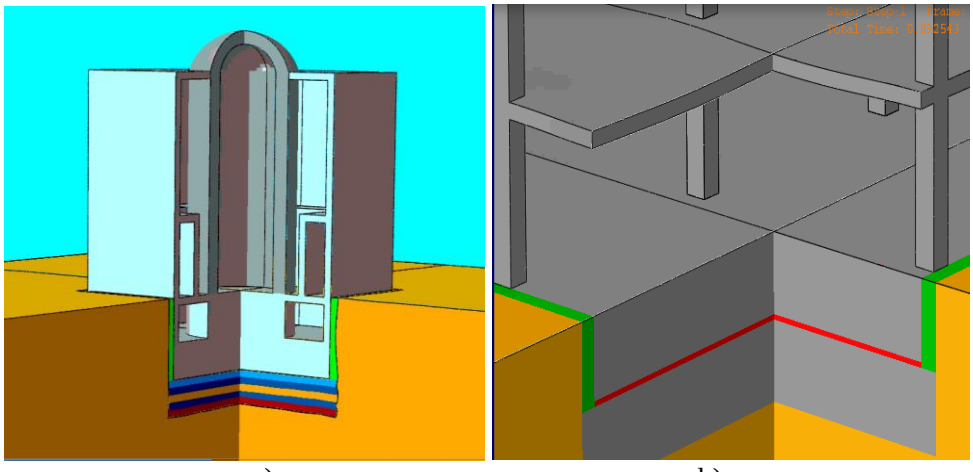

a) b)

Figure 9. - **Seismic pads for protecting a) NPP reactor building protected against both P- and S-shock waves, the composite pad made of the acoustically contrast layers (shown in different colours) is placed below the foundation structure [21]; b) splitting the foundation slab by a seismic pad (red).**

(III) Seismic pads especially constructed for seismic isolation of precision equipment, e.g. the use of elastomeric sheets coupled with mechanical sliders [22].

(IV) Seismic pads made of sheets of fluoroplastic, which have a very small friction coefficient and serve for achieving almost friction-free sliding surfaces [23, 24]. This approach can also be referred to the seismic protection by a meta-surface, since it is based on the concept of a sliding surface.

5.2 Seismic pads, basic principles

The considered seismic pads are capable for seismic protection from large intensity S-waves in a broad frequency range, moreover, as was previously mentioned, some kinds of pads are capable of protecting from both P- and S-waves. At least three basic principles ensuring the applicability and efficiency of the considered seismic pads could be stated,

(A) The acoustic impedance difference between ambient soil or concrete and granular metamaterial used for a typical seismic pad (not applicable to seismic pads made of fluoroplastic sheets). This principle ensures reflection of seismic wave energy at the interfaces between seismic pad and soil or concrete, thus decreasing the amount of wave energy diffracted into building. Note also that the reflection-refraction coefficients do not depend upon the wave frequency due to the Knott – Zoeppritz theory [25], the frequency independence provides a major advantage of the seismic pad over more common seismic isolating devices; see Sec 2.

(B) The formation and propagation of discontinuous shock wave fronts within the microstructure of a granular metamaterial, resulting in the substantial dissipation of wave energy inside the seismic pad [26]. This unusual effect is dominant in dissipating wave energy inside a granular metamaterial [27 – 29].

(C) The ability of relative movement of different granules inside the pad, which ensures additional attenuation of seismic wave energy [30]. Accounting dry friction at the contacting surfaces between granules, provides another source for dissipation of mechanical energy by the metamaterial [31].

6. Concluding remarks

The analysis of the seismograms of the recent devastating earthquake of M_w7.8 occurred on February 6, 20223 in the Kahramanmaraş region, revealed the appearance of an unusually strong delta-like S-wave pulse in the seismogram of the main shock. As was pointed out, the observed delta-like pulse corresponds to a large peak located at the zero frequency, making most of the widely used seismic isolating devices almost unusable, or even dangerous, at the appearance of delta-like pulses, since, as was shown, the considered seismic isolators amplify signals in the vicinity of zero frequency.

The analysis of the existing and being under development methods of seismic protection based on different seismic pads containing granular metamaterials, revealed the major benefits of these methods of seismic protection comparing to other types of seismic isolation, especially in regard of the appeared strong delta-like pulses in the earthquake seismograms.

References

1. USGS, 6 February 2023. "USGS earthquake catalogue". Archived from the original on 7 February 2023. (2023).

2. National Earthquake Information Center (6 February 2023). "M 7.8 - 26 km ENE of Nurdağı, Turkey". United States Geological Survey (2023). https://earthquake.usgs.gov/earthquakes/eventpage/us6000jllz/executive

3. *Emre Ö. et al.* (2018) Active fault database of Turkey. Bull. Earthquake Eng., 16: 3229–3275.

4. *Kawoosa V.M. Scarr, S. & Gerry, D.* (eds.). 10,000 tremors. Reuters. 2 March (2023).

5. *Kinoshita S.* (2012) Low-frequency and trend compensation of broadband seismograms, *Earth Planet Space*, 64: e5–e8.

6. *Larsonnier F. et al.* (2019) Comparison on seismometer sensitivity following ISO 16063-11 standard, In: *19th International Congress of Metrology*, Paper 27003.

7. *Singh N., Tampubolon D. & Yadavalli V.S.S.* (2002) Time series modelling of the Kobe-Osaka earthquake recordings. *Int. J. Math. Math. Sci*., 29(8): 467–479.

8. *Eberhard M.O. et al.* (2010) The M W 7.0 Haiti earthquake of January 12, 2010; USGS/EERI Advance Reconnaissance Team report. U.S. Geological Survey Report 2010–1048.

9. *Des Rochers R. et al.* (2011) Overview of the 2010 Haiti earthquake, *Earthquake Spectra*, 27(1, suppl. 1): 1–21.
10. Magnitude 7.0 HAITI Tuesday, January 12, 2010 at 21:53:09 UTC. IRIS (2010) https://www.iris.edu/hq/files/programs/education_and_outreach/retm/tm_100112_haiti/100112haiti.pdf
11. *Bormann P. & Wielandt E.* (2013) Seismic signals and noise. In: Bormann, P. (Ed.), *New Manual of Seismological Observatory Practice 2 (NMSOP2)*, Potsdam: GFZ, 1–62.
12. *Ye W. & Entezari A.* (2012) A geometric construction of multivariate sinc functions, IEEE Trans. Image Processing, 2(6): 2969–2979.
13. *Jóźwiak B., Orczykowska M. & Dziubiński M.* (2015) Fractional generalizations of Maxwell and Kelvin-Voigt models for biopolymer characterization, *PLoS ONE*, 10(11): Paper e0143090.
14. *Goldstein R.V. et al.* (2015) Study of forced vibrations of the Kelvin-Voigt model with an asymmetric spring, *Mech. Solids*, 50(3): 294–304.
15. *Kuznetsov S.V.* (2005) Fundamental and singular solutions of Lamé equations for media with arbitrary elastic anisotropy, *Quart. Appl. Math*., 63(3): 455–467.
16. *Smith K.* (1985) Frank Lloyd Wright and the Imperial Hotel: A postscript, *The Art Bulletin*, 67(2): 296–310.
17. *Hammer J.* (2011) The Great Japan earthquake of 1923, *Smithsonian Magazine*, May, Paper 1764539
18. *Dobry R. et al.* (2003) Damping/global energy balance in FE model of bridge foundation lateral response, *Soil Dynam. Earthquake Eng*., 23: 483–495.
19. *Teyssandier J.P., Combault, J. & Pecker, A.* (2000) Rion Antirion: le pontqui defieles seismes, *La Recherche*, 334: 42–46.
20. *Cremer C., Pecker A. & Davenne L.* (2001) Cyclic macro-element of soilstructure interaction: material and geometrical nonlinearities, *Int. J. Numer. Anal. Meth. Geomech*., 25(13): 1257–1284.
21. Granular metamaterials. Booklet. Marathon Allaince (2022): Adelaide, Australia. https://www.marathonalliance.com.au/metamaterials
22. *Begambre-Carrillo O.J. et al*. (2022) Passive seismic protection systems with mechanical metamaterials: A current review. *Struct. Eng. & Mech*., 82(4):Article 417.
23. *Mirzaev I. & Turdiev M.* (2021) Vibrations of buildings with sliding foundations under real seismic effects, *Constr. Unique Build. Struct*., 94: Article No 9407.
24. *Mirzaev I., Yuvmitov A., Turdiev M. & Shomurodov J.* (2021) Influence of the vertical earthquake component on the shear vibration of buildings on sliding, *E3S Web Conf*., 264: Article No 02022.
25. *Avesth P., Mukerji T. & Mavko G* (2005) *Quantitative Seismic Interpretation*. Cambridge University Press, Cambridge, UK.
26. *Lucchesi M. & Pagni A.* (2005) Longitudinal oscillations of bimodular rods, *Int. J. Struct. Stability Dynam*., 5(1): 37–54.
27. *Pelat A., Gautier F., Conlon S.C. & Semperlotti F.* (2020) The acoustic black hole: A review of theory and applications, *J. Sound Vibr*., 476: Paper 115316.
28. *Li S. et al.* (2019) Hybrid asynchronous absorbing layers based on Kosloff damping for seismic wave propagation in unbounded domains. *Comp. Geotech*., 109: 69–81.
29. *Li, S. et al.* (2021) Benchmark for three-dimensional explicit asynchronous absorbing layers for ground wave propagation and wave barriers. *Comp. Geotech*., 131: Paper 103808.
30. *Kuznetsov S.V.* (2020) Stoneley waves at the generalized Wiechert condition. *Z. Angew. Math. Phys*., 71(180): 1–11.
31. *Goldstein R.V. et al.* (2016) The modified Cam-Clay (MCC) model: cyclic kinematic deviatoric loading. Arch. Appl. Mech., 86(12): 2021–2031.

SEISMODYNAMICS OF SEGMENTED PIPELINE SYSTEMS

Mirzaev I.[1], Shomurodov Zh.F.[1], Kosimov E.A.[2], An E.V.[2]

[1]*Tashkent State Transport University, Tashkent, Uzbekistan*

[2]*Institute of Mechanics and Seismic Stability of Structures named after M.T.Urazbaev, Tashkent, Uzbekistan*

E-mail: ibrakhim.mir@mail.ru

Abstract: *The stress-strain state of segmented underground pipelines with regular joints under the impact of seismic waves is examined in the article. There are two types of calculation models of a segmented pipeline: the homogeneous model with the given characteristics and the "pipe-joint" model with its physical and mechanical characteristics. An explicit finite-difference scheme and finite element method with a time-domain implicit Newmark method were used. The results obtained using different models and both methods were compared for a one-dimensional problem. The dynamic processes in the pipeline are analyzed with abrupt and smooth changes in the velocity of particles in a given seismic wave propagating in soil. Calculations were conducted for different cases of the ratio of velocities of wave propagation in soil and segmented pipelines. The occurrence of high-frequency waves in a segmented pipeline is shown. The results of calculations of spatially located segmented pipeline systems were obtained and analyzed under the influence of real earthquakes.*

Keywords: *explicit scheme, implicit scheme, soil, interaction, segmented pipeline systems, seismic impact.*

1. Introduction

Underground pipeline systems are generally used to transport water, wastewater, oil, natural gas, and other materials. These pipelines are often called "lifelines" because they transport materials necessary to support life and maintain household [1-11]. Pipelines can be divided into continuous and segmented ones. Steel pipelines with welded joints are considered continuous, while segmented pipelines include cast iron, concrete, and asbestos-cement pipes with sealed or rubber gaskets [1-6, 22-24].

The seismic safety of embedded pipelines continues to attract the attention of researchers and practicing engineers. Important characteristics of underground pipelines are that they span large areas and are subject to numerous geotectonic hazards. Reviews of theoretical and experimental studies on mathematical modeling of dynamic processes in underground pipelines under the impact of seismic waves are given in [3-9, 20, 21].

Depending on the physical and mechanical properties of soil and the underground pipeline, velocity relations of wave propagation in soil and the underground pipeline embedded in it may be different. In [7, 19], it is shown that an inclined wave can be represented in the form of several longitudinal and transverse waves propagating along the pipeline at velocities greater than the velocity of the incident wave.

Analysis of strong earthquakes shows that damage and destruction of pipelines occur in the areas of pipe connection [12-15]. It is important to note that pipeline joints are the most vulnerable points in the pipeline system; the points where they turn and intersect are the most dangerous [1, 16-18]. Segmented pipeline systems with fragile joints fail during magnitude 7 and 8 earthquakes due to the destruction of joints.

One of the main factors determining the seismic resistance of underground pipelines is the flexibility of pipeline connections with complex joints and with each other. The seismic resistance of cast iron, reinforced concrete, asbestos-cement, concrete and polymer pipes significantly depends on the design, methods, and quality of jointing [1].

For segmented pipelines, especially the ones with large diameters and relatively thick walls, the observed seismic failure is most often associated with the failure of pipe joints. For example, in the monograph by M.J. O'Rourke et al. [1], it was reported that during the 1976 Tangshan earthquake, about 80% of pipe ruptures were associated with joints; six types of damage mechanisms were identified.

Axial extension, sometimes combined with relative angular rotation of joints, is a common failure mechanism in zones of tensile strain of soil. This is due to the fact that the shear strength of the joint sealing materials, or the frictional force due to the compression of the rubber gasket, is significantly less than the tensile strength of the pipe. That is, the segmental joint is the weak link. In areas of compressive soil stress, telescoping or failure of a socket or socket joint is a fairly common failure mechanism in, for example, concrete pipes. For segmented pipes of small diameter, failure was observed under the bending

along a circle in zones of soil curvature. For example, as noted by T. O'Rourke et al. (1991), more than 80% of small-diameter (100 to 200 mm or 4 to 8 in.) cast iron pipe ruptures in the Marina area following the 1989 Loma Prieta event were circular cracks in pipe segments near joints [15].

In [22] underground pipelines and their interaction with soil under seismic conditions are investigated. Continuous and segmented pipelines of different geometrical parameters are considered. The density, internal pressure of the pipe and density of the surrounding soil are taken into account. In continuous pipelines, the safety of the pipeline is checked against the force, while in segmented pipelines it is verified by the permanent ground deformation due to liquefaction. The results are presented in the form of strain and displacement curves for different pipe parameters and in each case the critical point for safety is identified. Based on the results, some considerations are given for the design of pipelines in the liquefied zone, which improve the capability of the pipeline to withstand the buoyancy force due to soil liquefaction.

In [23], the response of a segmented ductile iron pipeline crossing a fault is studied. All parts of the pipeline are inter-connected by K-type joints, which are flexible and widely used by water systems in Taiwan. Nonlinear finite element analysis considering large deformations was used. Full-scale tensile and compression tests of pipelines with K-type joints are carried out. The tension and compression of such joints are modeled by nonlinear springs and hard contact, respectively. The soil-pipeline interaction is simulated according to the ALA-ASCE guidelines. The main failure mode and failure range of a underground segmented pipeline with intersecting defects are presented and discussed.

In [24], a program is proposed to determine modified factors for segmented pipes in Chinese pipe seismic design code. A stochastic analysis method based on the finite element model of underground pipes and probability density evolution method is proposed to determine probability density functions of seismic responses of underground-segmented pipes. Using the proposed method, the stochastic seismic responses of three-segment pipes buried in four sites are calculated. Then, modified factors for segmented pipes are derived to modify the Chinese code.

Basically, all studies were conducted for single pipelines, neglecting the interaction between pipelines in the network.

Analysis of the research has shown that the problems of mathematical modeling of seismodynamic processes of underground segmented pipeline systems under static and dynamic impacts are currently insufficiently studied. Researchers have mainly considered one-dimensional problems when a seismic wave is represented by a given function. For this reason, the issues of calculating seismodynamic processes in a spatial system of segmented pipelines of complex structures based on real earthquake records have not been sufficiently studied. O'Rourke and Liu [1] noted that virtually no research has been conducted in this area.

Despite numerous studies performed in this direction, there are still a number of pressing problems associated with complex seismodynamic processes in underground structures.

2. Materials, methods, and object of study.

Fig. 1 shows the general structure of an underground pipeline with joints.

A study of the effect of a seismic wave propagating in soil on an underground segmented pipeline was conducted for an extended pipeline (a one-dimensional problem) and a spatial pipeline system (a three-dimensional problem).

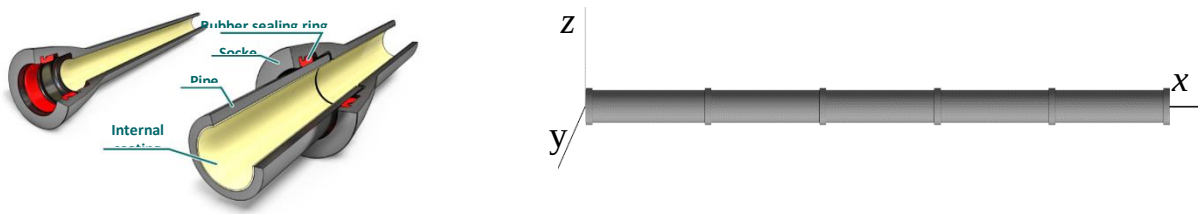

Figure 1. - **Segmented pipeline**

Consider the one-dimensional problem for an extended underground pipeline subject to seismic influences. Let a given plane longitudinal wave $v_g\left(t - x/c_g\right)$ propagate in soil at a velocity of c_g, the normal to the front of which is parallel to the axis of a pipeline of length L. The origin of the coordinate axis Ox is located at the left end of the pipeline.

The equations of longitudinal motion of the pipeline are written in velocities v and forces N, N_s

$$\begin{cases} \dfrac{\partial v}{\partial t} = \dfrac{1}{F\rho}\dfrac{\partial N}{\partial x} + \dfrac{\pi D}{F\rho}\tau, \\ \tau = k_x\left(u_g - u\right) \\ \dfrac{\partial N}{\partial t} = FE\dfrac{\partial v}{\partial x}, \ for the\ pipeline, \\ \dfrac{\partial N_s}{\partial t} = K_N\left(v_2 - v_1\right), \ for the\ joint. \end{cases} \tag{1}$$

With initial conditions

$$u\,|_{t=0} = 0 \ \text{ and } \ v\,|_{t=0} = 0. \tag{2}$$

To ensure combined operation of joints and pipes, the conditions of equality of displacements of the corresponding ends of pipes with displacements of the corresponding ends of joints are used $u_{ipr} = u_{is1}$, $u_{i+1pl} = u_{is2}$, $N_{ipr} = N_{is1}$, $N_{i+1pl} = N_{is2}$, where u_{ipr} is the displacement of the right end of the i-th pipe, u_{i+1pl} is the displacement of the left end of the (i+1)-th pipe, u_{is1}, u_{is2} are the displacements of the left and right ends of the i-th joint, N_{ipr} is the force on the right end of the i-th pipe, N_{i+1pl} is the force on the left end of i+1-th pipe, N_{is1}, N_{is2} are the forces on the left and right ends of the i-th joint. Here $K_N = \pi D_{st} l G_{st}/\delta$ is the stiffness coefficient of the joint; D_{st}, l is the average diameter and length of the joint gasket; δ is the thickness of the joint gasket; G_{st} is the shear modulus of the joint; v_1, v_2 are the particle velocities of the left and right ends of the joint; E, ρ are the elastic modulus and density of the pipeline material; v, u are the velocity and displacement of soil particles along the axis of the pipeline; v_g, u_g are the velocity and displacement of soil particles along the axis of the pipeline; D, F are the outer diameter and cross-sectional area of the pipeline; τ is the tangential stress that occurs on the contact surface of the pipeline with the soil.

The boundary conditions at the ends of an extended segmented pipeline system are stress-free:

$$\frac{\partial u}{\partial x}\,|_{x=0} = 0 \ \text{ and } \ \frac{\partial u}{\partial x}\,|_{x=L} = 0. \tag{3}$$

Strains in the pipeline and joint are defined as follows

$$\varepsilon = \frac{N}{EF}, \ \ \varepsilon_{st} = \frac{N_s}{K_N l}.$$

Here ε is the pipeline strain, ε_{st} is the shear strain in the joint.

System of equations (1) is approximated by finite differences [6]. Based on the resulting equations, we determine the velocity, displacement of particles, and strain in the pipeline.

The spatial problem for an underground segmented pipeline system subject to seismic impacts is posed only for a pipeline system interacting with soil, where propagating three-component seismic waves are specified. Since the length of the seismic wave is greater than the diameter of the pipeline, the latter is modeled as a rod working in tension-compression, torsion, and bending, considering shear strain; the interaction with the surrounding soil is modeled using various simplified models. The seismic impact propagating in soil is transferred to the pipeline through a combination of elastic and viscous contact elements. The spatial system of underground pipelines interacting with soil can be divided into linear sections of pipelines, massive nodes, and joint contacts. Joint contacts can be rigid or flexible. A finite element method for solving seismic dynamics problems for such structures was proposed [5]. When

calculating the problems posed, the following numerical methods were used: the finite element method for spatial coordinates and the time-domain implicit Newmark type scheme of the finite difference method.

To solve a system of algebraic equations, the Cholesky method was used for profile storage of the stiffness matrix of the spatial system of an underground pipeline [5].

To perform calculations, a set of programs for studying the seismodynamics of complex underground pipeline systems was developed, designed to automate the solution to such problems [5].

3. Results and discussion

For a one-dimensional problem, the following mechanical and geometric parameters of an extended segmented pipeline made of cast iron pipes and rubber gaskets were selected under the impact of the harmonic wave $v_g = v_{gm} \cdot cos\left(\pi(t - x/c_g)/t_0\right) \cdot H\left(t - x/c_g\right)$, v_{gm}=0.19m, t_0=0.165s. The parameters of the cast iron pipe: modulus of elasticity E=1.2·10^{5}MPa; material density ρ=7·10^{3}kg/m^3; pipeline length L=1000m; pipe segment length L_{seg}=5m; outer diameter D_n=0.5m; internal diameter d =0.48m; coefficient of linear interaction with soil k_x=1·10^{4}kN/m^3; and parameters for the rubber joint, they are E_r=2 MPa; ρ_r=930kg/m^3; l=0.05m; δ=0.01m; longitudinal rigidity K_N =5.42·10^{3}kN/m.

Let us present the results when the pipeline has rubber joints every 5 meters, i.e. L_{seg}=5m. Let the velocities of wave propagation in the soil c_g=500m/s and in the pipe segment c_{seg}=4150m/s. For this case, fig. 2 shows the comparison of forces when calculating the joint (100m) and the pipe (102.5m) by explicit and implicit schemes. The results obtained by explicit and implicit difference schemes differ in the joint up to 1.6%, and in the pipe up to 3.1%. It follows that the implicit time difference scheme can be used in calculations for seismic effects of spatial systems of segmented pipelines.

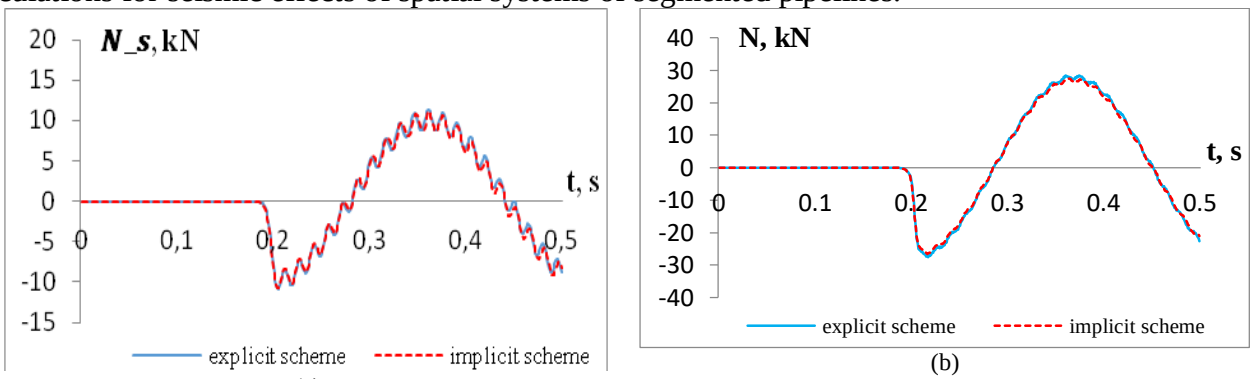

Figure 2. - **Comparison of forces in the joint (a) and pipeline (b), calculated by explicit and implicit schemes**

Let c_g=1000 m/s. In this case, the results showed that obtained by explicit and implicit difference schemes differ in the joint up to 0.7%, and in the pipe up to 5%. N_s=8.374 kN, N=16.06 kN in the explicit scheme, N_s= 8.31 kN, N=15.2 kN in the implicit scheme.

The wave propagation velocity in the soil of 1000 m/s exceeds the average wave propagation velocity in the pipeline of 492 m/s, therefore the difference in the amplitudes of high-frequency oscillations increases to 6473 N in the joint and to 4345 N in the pipe compared to 2326 N and 481 N, accordingly, at c_g=500 m/s. At c_g=300 m/s the oscillations of forces in joints and pipes are not noticeable. This implies the influence of the value of the wave propagation velocity in the soil compared to the value of the average wave propagation velocity in the pipeline. It is impossible to conduct such studies and obtain results using an averaged pipeline model.

Now consider the case when steel pipes 5 meters long each are connected by rubber joints. Let c_g=1000m/s in the soil, c_{seg}=5000m/s in the steel pipe, then taking into account the rubber joints, the average wave propagation velocity in the segmented pipeline is c_p=720m/s.

Fig. 3*a* shows the displacements of soil particles and both ends of the joint at a distance of 500 meters from the left end of the pipeline. Fig. 3*b* shows the change in the values of the relative displacements of the ends of this joint over time. As a result of the influence of the harmonic wave propagating in soil, the resulting stress wave in a segmented pipeline reaches a stationary mode at a distance of 35 meters. The joints lead to the formation of a high-frequency wave, which is associated with a discontinuity in the particle velocity at the wavefront in soil and a higher wave propagation velocity in soil compared to the reduced (averaged) wave propagation velocity in a segmented pipeline. In this case, the maximum strain in soil is ε_{gm} =0.0002. Moreover, if the average strain in a segmented pipeline is calculated from the relative displacement of the ends of one segment, then ε_{max}=0.0003. Thus, we come to the conclusion that in a segmented pipeline for $c_g > c_p$ the maximum average strain in the segmented pipeline is 1.5 times higher than the maximum strain in soil. If we perform the calculation using the reduced (averaged) model of a segmented pipeline, then this difference is 2 times higher [6]. Calculations have shown that if there is no velocity jump at the seismic wave fronts, high-frequency waves are not observed.

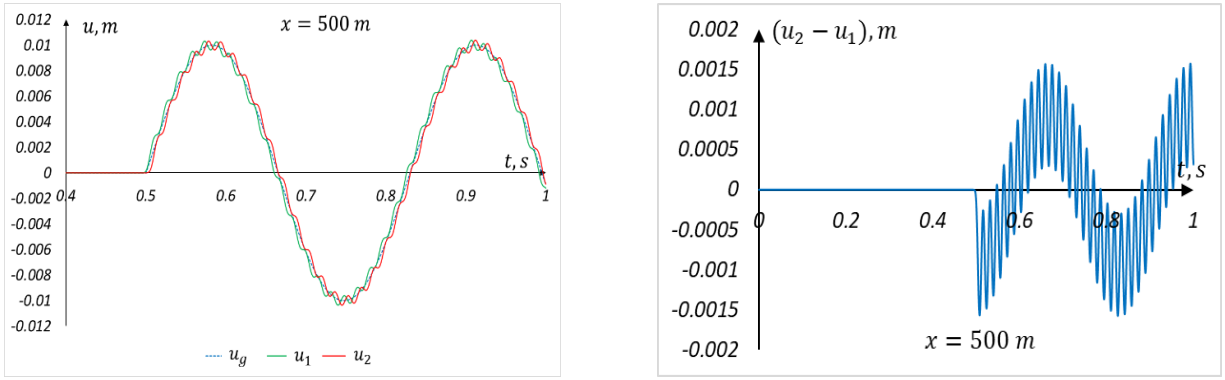

(a) (b)

Figure 3. - **Displacements of the ground particles and both ends of the joint**

Fig. 4 shows the strain: in the joint at point x=500m, $\varepsilon_{st} = (u_2-u_1)/\delta$ is the shear strain of the rubber gasket of the joint and the longitudinal strain of the pipe at point x=504m. It can be seen that the strain in the joint ε_{st} is significantly greater than in the pipeline ε, the ratio of their maximum values is 29673. This is due to the fact that the rigidity of the joint is much less than the rigidity of the pipe. Therefore, the joints are mostly deformed and the pipes behave almost like a rigid body. In this case, the maximum forces in the pipeline and joint do not differ so much, $N_{max}/N_{s,max}$=1.8.

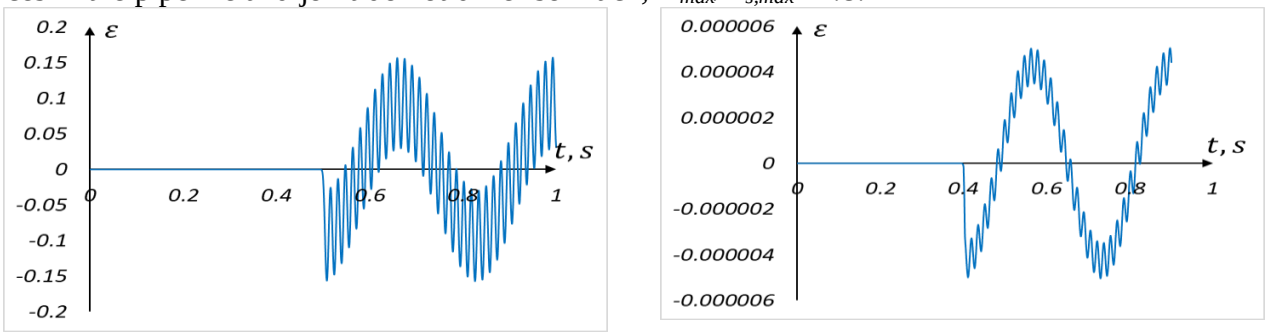

(a) (b)

Figure 4. - **Joint shear strain (a) and pipeline strain (b).**

If a given wave is represented as $v_g = v_{gm} \cdot sin(\pi(t - x/c_g)/t_0) \cdot H(t - x/c_g)$, then we get the result shown in fig. 5. In this case, it is clear that the maximum strain in joints is very large compared to the maximum strain in the pipeline, $max(\varepsilon_{st})/max(\varepsilon)$=22407. However, with this type of seismic wave, high-frequency waves with high amplitudes are not observed in the pipeline. In this case, the averaged strain for one segment does not practically differ from the strain in soil, as in the model of a segmented pipeline with averaged characteristics [6].

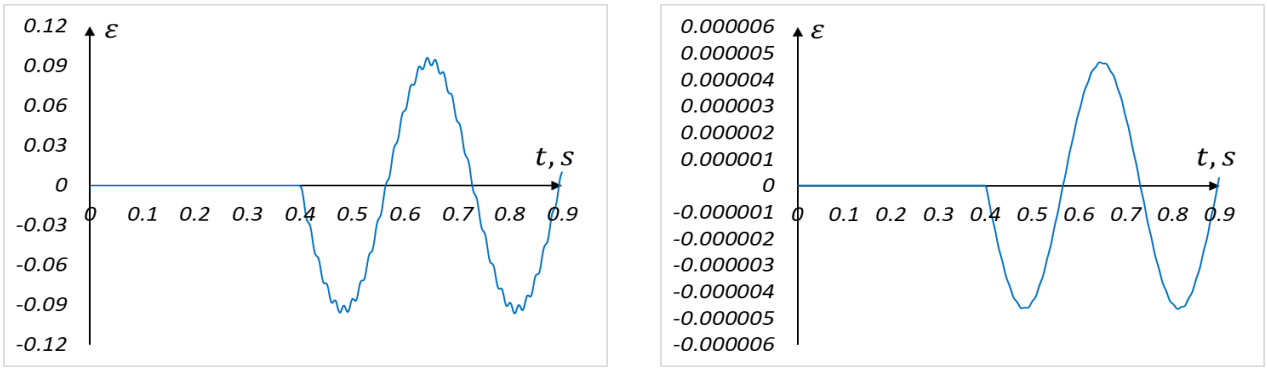

(a) (b)

Figure 5. - **Joint shear strain (a) and pipeline strain (b).**

Now we simulate the segmented pipeline as a homogeneous pipeline with averaged characteristics for previously specified pipe and joint. Let the velocity of wave propagation in soil be c_g =1000m/s, and in the pipeline its calculated value is c=720m/s.

From the above results, it is clear that when the velocity of wave propagation in soil exceeds the propagation velocity in the segmented pipe, if there is a jump (a rupture) or a sharp change of the seismic wave velocity, then high-frequency waves appear in the pipeline in the linear model of the "pipe-soil" system and the maximum strain in the pipe exceeds the maximum strain in soil. Since there is no sharp change of the velocity of soil particles in a seismic wave in real earthquakes, such processes are not observed and the strain in the pipeline is equal to the strain in soil [6]. For $c_g<c_p$, even with a jump or sharp change of the velocity of the seismic wave, high frequency waves are not observed in the pipeline.

Now consider the problem of the impact of a three-component seismic wave in the form of records of real earthquakes on an underground pipeline system of cast iron pipes with rubber gaskets with butt joints connected at different angles (fig. 6). Here Roman numerals (I, II, III, IV) indicate the numbers of segmented pipelines in the system of spatial pipelines. Let us denote the distances from the joint for each segmented pipeline by l_1, l_2, l_3 and l_4. We do not take into account the slippage of the rubber gasket relative to the pipe.

The instrumental records of an earthquake with an intensity of 9 points on the MSK-64 scale that occurred in 1976 in Gazli, Uzbekistan were used in calculations [5].

The mechanical and geometric parameters of the pipeline system are presented as: for cast iron pipes: E=1.2·10^{5}MPa; ρ=7·10^{3}kg/m^3; length of one branch L=100m; L_{seg}=5m; D=0.5m; d=0.48m; coefficients of linear interaction with the soil: longitudinal coefficient k_x=1·10^4 kN/m^3 and transverse coefficients k_y=4.07·10^4 kN/m^3, k_z=4.07·10^4 kN/m^3; for rubber joint gasket: E_r=2MPa; ρ_r=930kg/m^3; l=0.05m; δ=0.01m; longitudinal rigidity K_N=5.42·10^{3}kN/m; transverse rigidity K_Q=1.35·10^{4}kN/m; bending rigidity K_{M_u} =6.09 kN·m; torsional rigidity K_{M_k} =5.42·10^{2}kN·m; flexible joints (I-joint, II-joint, III-joint, IV-joint) of pipes from the rigid joint are at a distance of 0.3 m. Fig. 6 shows examples of segmented pipelines joints connected at different angles in a system of spatial underground pipelines. The results are presented in fig.7–9.

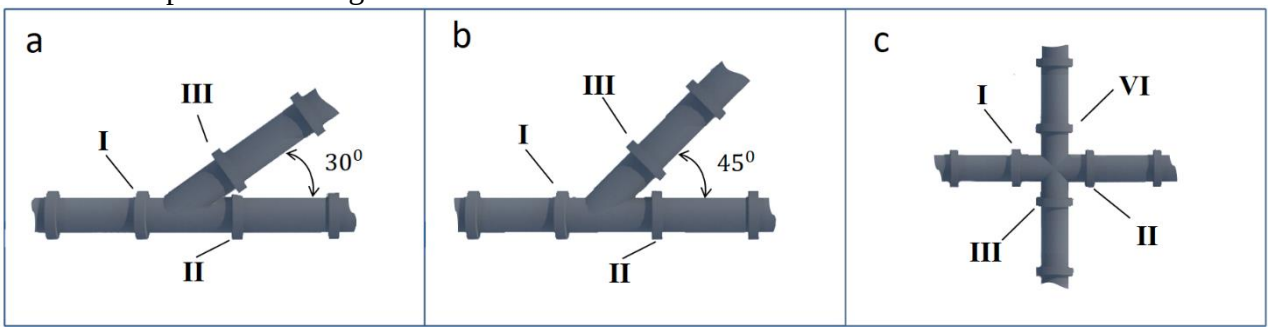

Figure 6. - **Examples of pipeline connections**

Fig. 6*a* shows a spatial underground pipeline system connected through joint at an angle of 30° to a straight-line section of pipeline. The values of forces occurring in joints: I-joint, II-joint, III-joint (fig. 7*a*) and in pipes at a distance of 22 m from the rigid joint of pipes (fig. 7*b*) are given. The rubber gasket in the joint reduces the forces and moments of forces by several times, the physical and mechanical parameters of the rubber are of great importance in this process. It is also clear from the results that the values of the generated forces in the joints and pipes also depend on the pipe joint angles.

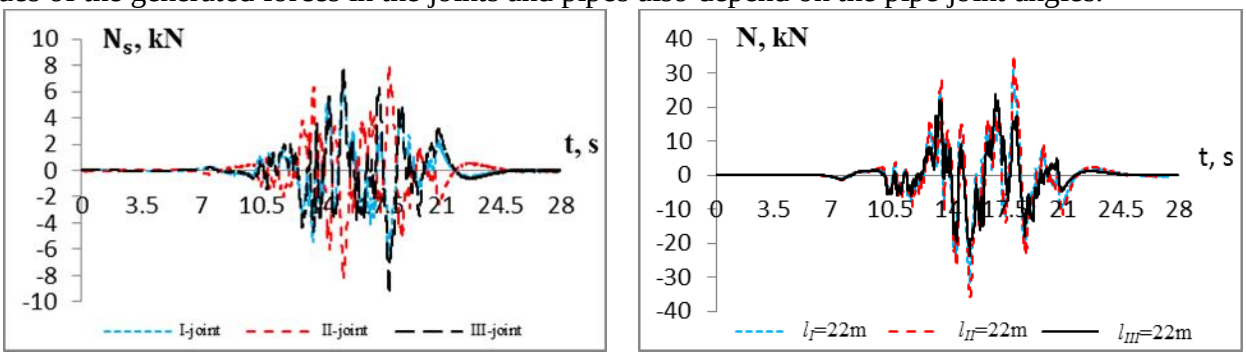

(a) (b)

Figure 7. - **(a) Forces in joints and (b) forces in pipelines at distances of 22m from the rigid joint**

Fig. 8 shows the case of seismic wave impact at an angle α=0° to the coordinate axis *OX* of the underground pipeline for a spatial underground pipeline system connected through joint at an angle of 45° to a straight-line section of pipeline (fig. 6*b*). Maximum values of forces occur in joints (I-joint, II-joint, III-joint) and in pipes at a distance of 22 m from the rigid joint of pipes are given. The relative displacements in joints (I-joint, II-joint, III-joint) are 0.0013, 0.0041, 0.0014 m respectively and the relative rotations with respect to local axes for the joints are: I-$1.67\cdot10^{-9}$, $5.1\cdot10^{-4}$, $6.2\cdot10^{-4}$, II-joint $1.46\cdot10^{-9}$, $5.5\cdot10^{-4}$, $4.7\cdot10^{-4}$, III-joint $6.42\cdot10^{-7}$, $3.9\cdot10^{-4}$, $2.9\cdot10^{-4}$ radians. These results show that during an earthquake with an intensity greater than 9 points on the MSK-64 scale, the relative rotations are small due to the significant length of seismic waves, and the relative approaches of pipes in joints do not exceed the value of 0.0041 m. Thus, it is necessary to establish a gap in joints at least 0.05 m.

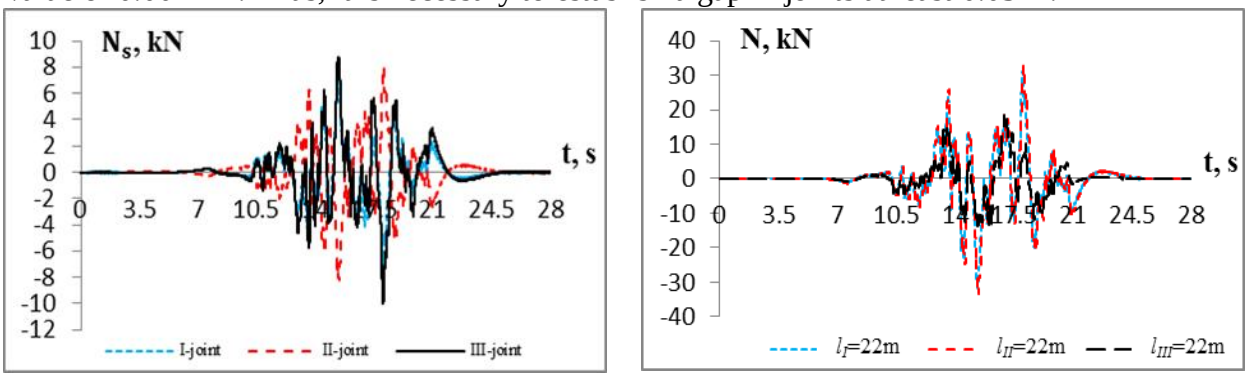

(a) (b)

Figure 8. - **(a) Forces in joints and (b) forces in pipelines at distances of 22m from the rigid joint**

Fig. 9 shows the case of seismic wave impact at an angle α=0° to the coordinate axis *OX* of the underground pipeline for a spatial underground pipeline system connected through joint at an angle of 90° relative to each other (fig. 6*c*). Maximum values of forces occur in joints (I-joint, II-joint, III-joint, IV-joint) and in pipes at a distance of 22 m from the rigid joint of pipes are given. From fig. 9, it is seen that if the seismic impact acts parallel to the axis of the pipeline, then the forces in the longitudinal pipeline much exceed the forces in the transverse pipeline. This effect is due to the fact that the transverse pipeline is perpendicular to the direction of seismic wave propagation, and small vibrations in it are due to the connection of the pipelines to each other.

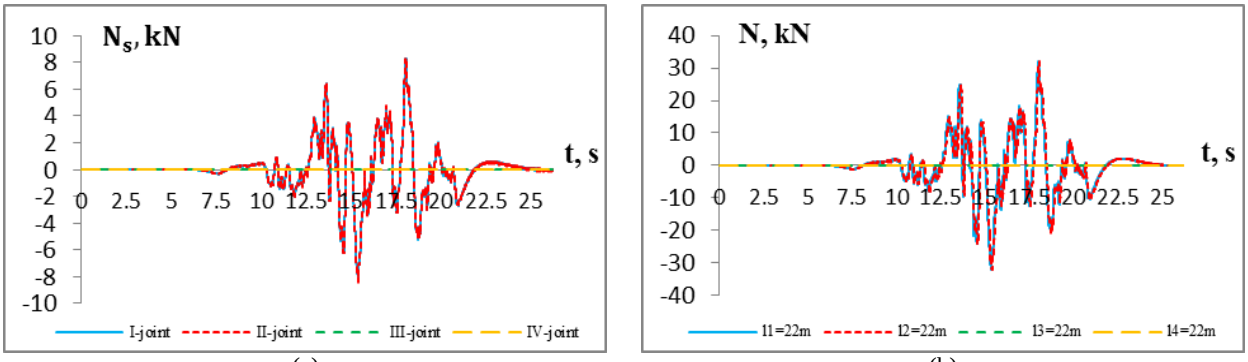

(a) (b)

Figure 9. - **(a) Forces in joints and (b) forces in pipelines at distances of 22m from the rigid joint**

Table 1 presents the maximum values of forces in joints (I-joint, II-joint, III-joint, IV-joint) of the cross-shaped system of underground segmented pipelines and in pipes at the distances of 22m from the rigid joint shown in fig. 9, based on various records of real earthquakes. In the calculations presented in table 1, records of real earthquakes with intensities of 7-10 points on the MSK-64 scale were used.

Table 1.

Results of the impact of various earthquakes on pipelines connected through rigid joint

No.	Records of real earthquakes	I-joint (kN)	II-joint (kN)	III-joint (kN)	IV-joint (kN)	l_I=22 m (kN)	l_{II}=22 m (kN)	l_{III}=22 m (kN)	l_{IV}=22 m (kN)
1	Filippias (Greece) 7 points	0.434	0.436	0.000479	0.00106	1.68	1.69	0.000379	0.00045
2	Manjil (Iran) 8 points	2.01	2.01	0.00501	0.00767	7.78	7.82	0.00279	0.00353
3	Erzincan (Turkey) 9 points	6.11	6.1	0.00525	0.00949	23.6	23.7	0.00371	0.00378
4	Gazli (Uzbekistan) 9* points	8.23	8.24	0.0345	0.0369	32.1	32.3	0.0197	0.0226

From the calculation results, it is clear that an increase of the intensity of earthquakes causes an increase of forces occurring in underground pipelines and joints. This, in turn, leads to the destruction of underground segmented pipelines during severe and very severe earthquakes.

4. Conclusion

Seismodynamic processes in segmented one-dimensional and spatial underground pipelines were analyzed in this study. A spatial underground pipeline system connected through a rigid joint at different angles to a straight pipeline section was considered. The seismic waves propagating in the pipeline were taken as harmonic ones and from records of real earthquakes with intensities of 7-10 points on the MSK-64 scale. The values of forces occurring in flexible joints and in pipes were obtained and presented in the form of graphs and table. It is revealed that the increase of the intensity of earthquakes causes an increase in the forces occurring in underground pipelines and flexible joints.

If the wave propagation velocity in soil exceeds the wave propagation velocity in the pipeline and there is a jump (a rupture) or a sharp change in the velocity of seismic wave in that case high-frequency waves appear in the pipeline and the maximum strain in the pipe exceeds the maximum strain in soil.

The flexible joints reduce the forces and moments of forces in the pipeline by several times, the physical and mechanical parameters of the gasket are of great importance in this process.

It was determined that if the seismic impact acts parallel to the axis of the pipeline then the forces in the longitudinal pipeline much exceed the forces in the transverse pipeline. This effect is due to the fact that the transverse pipeline is perpendicular to the direction of seismic wave propagation, and small vibrations in it are due to the connection of the pipelines to each other.

It is shown that during an earthquake with an intensity greater than 9 points on the MSK-64 scale, the relative rotations are small due to the significant length of seismic waves, and the relative approaches of pipes in joints do not exceed the value of 0.0041 m. Thus, it is necessary to establish a gap in joints at least 0.05 m.

The impact of an earthquake itself does not cause large approaches of pipes and angular rotation in the flexible joints of segmented pipelines, and also reduces the forces and moments of forces in the pipeline elements. This is due to the fact that segmented pipelines, unlike continuous pipelines, are less rigid and more flexible. Hazards for segmented pipelines are landslides due to earthquakes, soil scouring, mudflows, cracks and other consequences, as well as sandy soil surrounding the underground pipeline under which voids form during pipeline operation.

References

1. *O'Rourke M.J., Liu X.* Seismic design of buried and offshore pipelines / «Elsevier» Amsterdam, 2012.
2. *Wei Liu, Chunjie Huang, Yunchang Wang, Peixin Shi.* Seismic analysis of connections of buried continuous pipelines // Advances in Civil Engineering. 2020, Vol. 2020(3), 8839380. https://doi.org/10.1155/2020/8839380
3. *Nishonov N., Bekmirzaev D., Ergashov A., Rakhimjonov Z., Khurramov A.* Underground polymeric l-shaped pipeline vibrations under seismic effect, In: Proceedings of E3S Web of Conferences CONMECHYDRO, 2021, 264, 02037. https://doi.org/10.1051/e3sconf/202126402037.
4. *Vasileios E. Melissianos, Georgios P. Korakitis, Charis J. Gantes, George D. Bouckovalas*. Numerical evaluation of the effectiveness of flexible joints in buried pipelines subjected to strike-slip fault rupture // Soil Dynamics and Earthquake Engineering. 2016, 90. pp. 395-410.
5. *Mirzaev I., Nishonov N., Bekmirzaev D., Kosimov E.* Seismodynamics of the Cross-Shaped Underground Pipeline under Real Earthquakes, In: Proceedings of AIP Conference. 2022, 2432, 030107. https://doi.org/10.1063/5.0089585.
6. *Mirzaev I., Shomurodov J.F.* Unsteady waves in an extended underground pipeline under seismic action // Computational Technologies. 2023, vol. 28, No. 3, pp. 10-24. https://doi.org/10.25743/ICT.2023.28.3.002.
7. *Israilov M.Sh.* Action of an Oblique Seismic Wave on an Underground Pipeline // Mechanics of Solids. 2022, vol. 57, No. 5, pp. 1006-1015. https://doi.org/10.3103/S0025654422050089.
8. *Tsinidis G., Di Sarno L., Sextos A., Furtner P.* A critical review on the vulnerability assessment of natural gas pipelines subjected to seismic wave propagation. Part 1: Fragility relations and implemented seismic intensity measures // Tunnelling and Underground Space Technology. 2019, (86), pp. 279-296. https://doi.org/10.1016/j.tust.2019.01.025.
9. *Mardonov B., Mirzaev I., Nishonov N., An E., Kosimov E.* Study of the uplift of buried pipelines in liquefied soils based on the earthquake record, In: Proceedings of E3S Web of Conferences TT21C-2024. 2024, vol. 515, 04009. https://doi.org/10.1051/e3sconf/202451504009.
10. *Cen H., Huang D., Liu Q., Zong Z., Tang A.* Application research on risk assessment of municipal pipeline network based on random forest machine learning algorithm // Water. 2023, 15(10), 1964. https://doi.org/10.3390/w15101964.
11. *Psyrras N.K., Sextos A.G.* Safety of buried steel natural gas pipelines under earthquakeinduced ground shaking: A review // Soil Dynamics and Earthquake Engineering. 2018, (106). pp. 254-277. https://doi.org/10.1016/j.soildyn.2017.12.020.
12. *Yousife D.F., Aldefae A.H., Zubaidi S.L., Humaish W.H., Sinichenko E.K.* Static and seismic performance of buried pipelines: a review, In: Proceedings of E3S Web of Conferences. 2021, vol. 318, p.10.
13. *Gautam S. Nair, Suresh R. Dash, Goutam Mondal* Review of Pipeline Performance during Earthquakes since 1906 // J. Perform. Constr. Facil. 2018, 32(6), 04018083.
14. *Massimina Castiglia, Filippo Santucci de Magistris, Filippo Onori, Junichi Koseki* Response of buried pipelines to repeated shaking in liquefiable soils through model tests // Soil Dynamics and Earthquake Engineering. 2021, vol. 143.
15. *O'Rourke T.D., Jeon S.S., Toprak S., Cubrinovski M., Hughes M., Van Ballegooy S., Bouziou D.* Earthquake Response of Underground Pipeline Networks in Christchurch, NZ // Earthquake Spectra. 2014, vol. 30, Issue 1. pp. 183-204.
16. *Bekmirzaev D.A., Kishanov R.U., Mansurova N.Sh.* Mathematical Simulation and Solution of the Problem of Seismo–Dynamics of Underground Pipelines // International Journal of Emerging Trends in Engineering Research. 2020, vol. 8. No. 9. https://doi.org/10.30534/ijeter/2020/22892020.
17. *Gersena Banushi, Brad P. Wham.* Deformation capacity of buried hybrid-segmented pipelines under longitudinal permanent ground deformation // Can. Geotech. J. 2021, Vol. 58, pp. 1095-1117. https://doi.org/10.1139/cgj-2020-0049.
18. *Neelima Satyam, Durga Prasad.* Analysis of continuous and segmented pipeline in liquefiable soil, In: Proceedings of the 5th International Conference on Integrity-Reliability-Failure, Porto/Portugal, 24-28 July 2016, pp. 585-594.

19. *Kouretzis G.P., Bouckovalas G.D., Karamitros D.K.* Seismic verification of long cylindrical underground structures considering Rayleigh wave effects // Tunneling Underground Space Technol. 2011, vol. 26, issue 6, pp. 789-794. https://doi.org/10.1016/j.tust.2011.05.001.
20. *Halkijevic I., Vouk D., Posavcic H., Mostecak H.* Damage assessment of water supply networks due to seismic events using vulnerability functions // GRAĐEVINAR. 2021, 73(7), pp. 737-749, https://doi.org/10.14256/JCE.3185.2021
21. *Xu R., Jiang R., Qu T.J.* Review of dynamic response of buried pipelines // Journal of Pipeline Systems Engineering and Practice. 2021, 12(2). https://doi.org/10.1061/(ASCE)PS.1949-1204.0000527.
22. *Neelima Satyam, Durga Prasad.* Analysis of continuous and segmented pipeline in liquefiable soil // Proceedings of the 5th International Conference on Integrity-Reliability-Failure, Porto/Portugal 24-28 July 2016. Pp.585- 594. Paper Ref: 6317.
23. *Huang C.W., Chou K.W., Liu G.Y., Chung L.L., Yeh C.H., Lin T.J., Hung H.Y.* Analysis on a crossing-fault buried segmented pipeline with flexible joint behaviors from experimental tests //15WCEE Lisboa 2012. Pdf. 2651.
24. *Wei Liu, Zhaoyang Song, Huiquan Miao.* Modified factor for segmented pipes in chinese pipe seismic design code based on probability density evolution method // KSCE Journal of Civil Engineering (2018) 22(3):951-961. DOI 10.1007/s12205-018-1370-2

ON EARTHQUAKE RESISTANCE OF FRAME-SKELETON BUILDINGS CONSTRUCTED WITHIN THE FRAMEWORK OF BUILDING STANDARDS SNiP II-A.12-69

Sagdiev Kh.S.[1], Yuvmitov A.S.[1], Akhundjanov D.G.[1], Egamberdiev B.O.[2]
[1]Institute of Mechanics and Seismic Stability of Structures named after M.T. Urazbaev, Tashkent, Uzbekistan
[2]Fergana Polytechnic Institute, Fergana, Uzbekistan
E-mail: imssan@mail.ru

Abstract: *The article presents the results of measurement-and-survey and instrumental-calculation studies of seismic resistance of frame-skeleton buildings erected following regulatory documents that were in force in 1969-1981 when designing buildings and structures in seismic areas. The results of studies of the seismic safety of two and three-story buildings of a frame system are analyzed, a comparison of actual parameters and design requirements is conducted with the data of currently valid regulatory documents, and the corresponding conclusions are made. The general conclusions briefly summarize the results of previously conducted studies, indicate the need to develop technical data sheets for operating facilities, and recommend the organization of an engineering seismometric service in newly constructed high-rise buildings to obtain reliable information about the performance of the structures during earthquakes.*

Keywords: *frame-skeleton building, space-planning and structural solution, standards, instrumental and calculated data, strength and dynamic characteristics, general conclusions and recommendations.*

1. Introduction.

Considering the aftermaths of strong earthquakes, the Republic has accumulated significant experience in earthquake-resistant construction of buildings and structures in regions of high seismicity and unfavorable soil conditions. Dynamic theories and methods for calculating the seismic resistance of underground and aboveground structures with various design solutions were developed, building codes and regulations, construction technologies, and building materials were improved. These methods are used in the design and construction of buildings and structures in seismic areas, and in technical expertise of operating facilities. At the same time, it should be noted that there are certain shortcomings in the regulatory documents for construction in seismic areas. The current standards do not account for such factors as the wave pattern of the impact of seismic loads; non-homogeneous properties of building materials; nonlinear vibrations of structural elements; real conditions of the structure interaction with the soil foundation and mutual influence of structural elements during earthquakes. Observation of damage and destruction of buildings and structures during strong earthquakes and their analysis indicate existing shortcomings in the technology of seismic-resistant construction, research methods used, and building codes applied in the design of buildings and structures, and insufficient accuracy of seismic hazard assessment in the territories of the regions. This is confirmed by the results of the consequences of strong earthquakes in recent years in Turkey, Morocco, Afghanistan, Japan, etc.

Reducing possible damage during strong earthquakes in the Republic largely depends on the seismic vulnerability of buildings and structures in use and ensuring their sufficient strength, taking into account their low seismic resistance compared to the real seismic hazard. This especially concerns

buildings and structures operated within/beyond their service life [1-13], since their design does not meet modern requirements of earthquake-resistant construction standards [14] designed after surveying the consequences of recent strong earthquakes. For reliable operation of buildings and structures, an important factor is the forecast of the strength life of load-bearing structures and seismic safety of buildings, determined by instrumental and calculation methods considering the actual state of structures. Currently, in the regions of the republic, buildings are in use that were constructed with different design solutions and from different building materials and in accordance with old building codes and regulations [15-22]. A major part of these buildings [1-13] does not meet the requirements of the standards currently in force in the Republic for the design of buildings and structures in seismic areas.

2. Formulation of the problem.

It is known that the frame of a building consists of columns (posts), beams (crossbars), and floors connected into a solid skeleton of a spatial frame. All these elements are subject to vertical and horizontal (seismic) loads. In addition to these elements, buildings have wall structures, which to a certain extent also participate in joint work with the frame. Depending on the design solutions of the wall fillings and their connection with the building frame, they can be divided into several design schemes.

The first is a frame scheme, representing a system of columns, crossbars, floor slabs and anti-seismic belts, rigidly connected to each other. In this case, wall structures (frame filling, hitch panels, brick and plaster partitions, etc.) must be connected to the frame in such a way as not to prevent the frame from deforming under seismic impact. Then the rigidity and stability of the building must be fully ensured by the frame itself. Here one should pay attention to the fact that the filling of the frame is considered in the calculations only as an inertial load, which contributes, on the one hand, to an increase in the seismic load, and on the other, to its reduction due to an increase in the period of natural oscillations. Generally, the first factor has a greater influence on the value of the calculated seismic load, since the seismic load is directly proportional to the mass of the system, while the dynamic coefficient β is inversely proportional to the square root of this mass.

The operating principle of the second frame-bracing scheme of a frame building is similar to the frame scheme with the only addition that the horizontal rigidity of the building increases due to diagonal connections, usually made of metal or reinforced concrete. In this case, part of the horizontal forces is transferred from the columns to these connections. A feature of the frame-bracing scheme is the limitation of frame displacements.

The third scheme is a frame system with stiffness diaphragms. This scheme is characterized by the fact that an increase in rigidity of the frame system is achieved by introducing vertical stiffness walls, and installing interior railings, elevator shafts, and staircases. Unlike previous schemes, this one provides for a rigid connection of the diaphragm (walls) with the frame along the entire perimeter of the filling, which allows the filling to be included in the operation of the frame under seismic impacts to the extent of its load-bearing capacity.

Regarding the structural schemes of frame buildings, it should be noted that frame-braced schemes, as well as frame schemes with stiffening diaphragms, are recommended to be used mainly in high-rise buildings under significant horizontal loads. Structural solutions for frame buildings depend not only on the schemes discussed above; they are also determined by the methods of structure construction.

This article presents the results of an examination and study of space-planning and design solutions of frame-skeleton two- and three-story structures built in accordance with the SNIP II-A.12-69 standards. Based on the conducted instrumental and computational studies, the dynamic characteristics of buildings and the soil properties of their construction sites were determined; the results of calculations for seismic impacts of 8 and 9-points intensity, and assessment of compliance with the requirements of current standards for the design of buildings and structures in seismic areas are presented.

3. Research results and their analysis.

To assess the seismic resistance of skeleton buildings of the frame system following the requirements of the current standards of earthquake-resistant construction, the operated frame buildings of secondary schools and preschool educational institutions (PEIs), built according to "SNiP II-A.12-69 Construction in seismic areas" were selected as objects of study. For each object, the results of measurement and survey and instrumental and calculation studies and their analysis are presented separately according to the requirements of current standards.

1. The two-story frame building of preschool educational institution №27 is located at the address: Tashkent, Shaykhantakhur district, Center-27, Gulobod street. The building of the PEI is L-shaped and consists of two blocks separated by an aseismic joint. The structural system of reinforced concrete frame-skeleton blocks was built in 1974 without a basement. Here we present the results of studies of the main building (block 1), intended for group premises for children. The building is rectangular in plan measuring 12x54 m and is not divided into compartments by an aseismic joint. The block in plan has a protrusion in the form of a console with a length of 1.4 m. The building consists of typical rooms by floors (Fig. 1). The height from the floor to the ceiling slab is 3.1 m, to the transverse load-bearing crossbar - 2.7 m.

The skeleton of the building is reinforced concrete, of frame system, with rigid joints in the transverse and longitudinal directions. In the longitudinal direction of the building, there are multi-span frames with a pitch of 6 m, and in the transverse direction, there are two-span frames with a pitch of 6+6 m. The main load-bearing structures are reinforced concrete columns with a cross-sectional area of 0.3x0.3 m. The main load-bearing beams are transverse ones on which floor slabs and partitions rest. Transverse crossbars have dimensions: 0.3x0.4 m. Transverse frames are connected to longitudinal crossbars (links) of cross-section 0.3x0.2 m. Wall enclosures are external panels made of hitched expanded clay concrete slabs 0.3 m thick. Internal partitions built from brick separate interior rooms and corridors.

Floors and ceilings are made of prefabricated reinforced concrete hollow-core slabs, supported by transverse frames. The roof has an attic. The supporting structures of the roof (rafters and lathing) are wooden. A double-slope metal roof is made of corrugated sheets with water drainage and free discharge onto the blind area using a drainpipe. The staircases are structurally identical, double-flight, reinforced concrete with a flight width of 1.2 m. Prefabricated reinforced concrete flights with platforms were used. The staircases rest on the frame crossbars.

The technical condition of the building is satisfactory.

A comparison of the actual data with the margin data of the current standards shows that the structural design of the blocks corresponds to the standards of earthquake-resistant construction in terms of space-planning and design solutions.

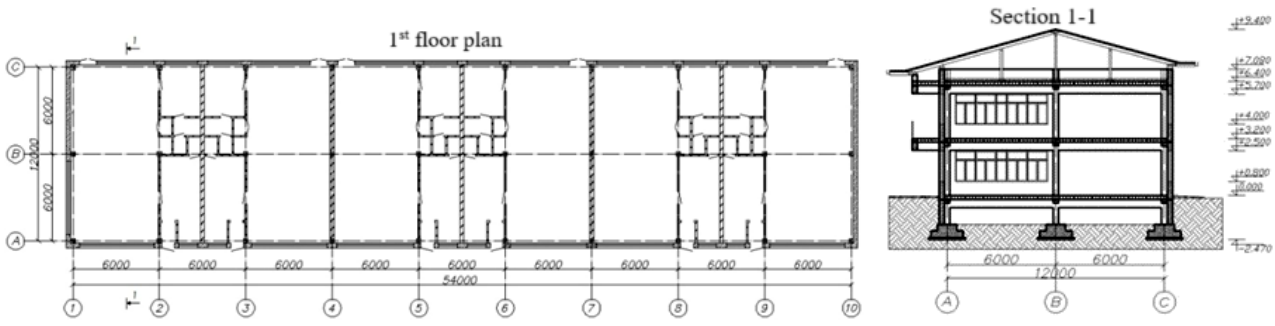

a) b)

Figure 1. **Floor plan (a) and cross-section (b) of the building**

2. The two-story frame building of preschool educational institution №14 was built in 1976 without a basement and is located at the address: Andijan, 3rd micro-district. The building of the preschool educational institution is L-shaped and consists of two blocks intended for group premises for children (block 1) and administrative and service premises (block 2). The building of the first block is rectangular in plan, measuring 12x72 m and has a protrusion in the form of a console with a length of 1.4 m. The second block is rectangular in plan, 12x12 m.

The blocks are connected using crossbars with rigid joints. The frame of the blocks is connected using reinforced concrete crossbars and floor slabs at the points of transition from the end of the first block to the end of the second block. The blocks are not separated by an aseismic joint. The children's block is divided with an aseismic joint into two compartments of the same size: 12x36 m. Here we present the results of an instrumental and computational study of the divided compartment of the children's block of the building (Fig. 2).

The skeleton of the building is reinforced concrete, of frame system, with rigid joints in the transverse and longitudinal directions. The height from the floor to the ceiling slab is 2.9 m, and to the transverse load-bearing beam 2.5 m. In the longitudinal direction of the building, there are multi-span frames with a pitch of 6 m, and in the transverse direction, there are two-span frames with a pitch of 6+6 m. The main load-bearing structures are reinforced concrete columns with a cross-sectional area of 0.3x0.3 m. The main load-bearing crossbars are transverse on which the floor and roof slabs rest. The dimensions of the transverse crossbar are 0.3x0.45 m. The transverse frames are connected to longitudinal crossbars (links) with a cross-section of 0.3x0.2 m.

Wall enclosure presents external panels made of hitched expanded clay concrete panels 0.3 m thick. Internal brick partitions separate internal rooms and a corridor. Floors and ceilings are made of prefabricated reinforced concrete multi-hollow slabs, supported by transverse frames. The roof is an attic. The load-bearing structures of the roof (rafters and lathing) are wooden. A double-slope wavy metal roof is made of corrugated sheets with water drainage and free discharge onto the blind area using a drainpipe. All staircases are structurally identical, external, double-flight, reinforced concrete with a flight width of 1.2 m. The flights of stairs rest on the frame crossbars.

The technical condition of the block building is satisfactory.

A comparison of the actual values of the structural systems of PEIs with the margin parameters of KMK 2.01.03-19 standards shows that the buildings comply with earthquake-resistant construction standards, except for the connection of blocks at the transition points where the staircase is located.

The design solution does not meet the requirements of KMK 2.01.03-19, clause 3.1.1. The building must have a geometrically correct shape in plan. If there are projections, they, as a rule, should not exceed 6 m in plan for frame buildings. In this case, the projection of the second block relative to the first block is 12 m.

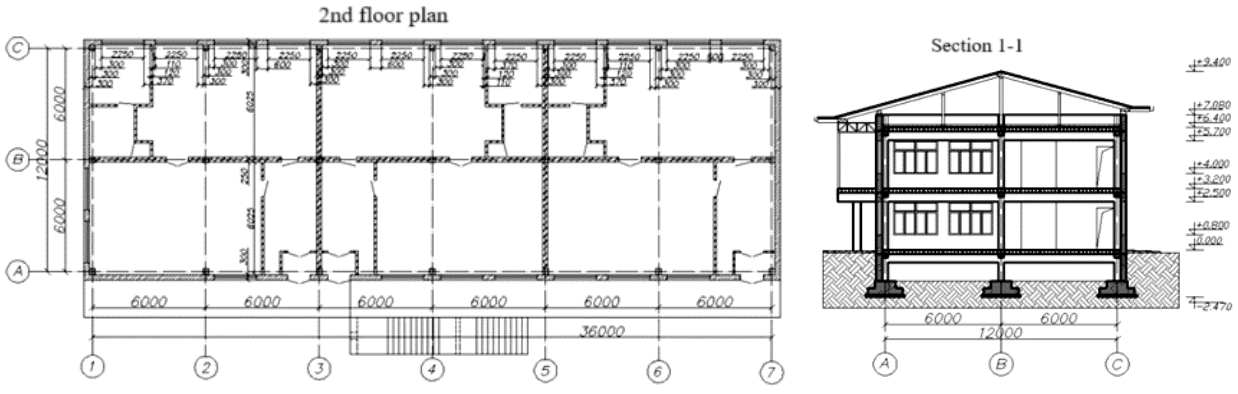

a) b)

Figure 2. **Floor plan (a) and cross-section (b) of the building**

3. Three-story frame building of school №248. The school building was erected in 1975 in the Mirzo-Ulugbek district of Tashkent and consists of ten blocks separated by anti-seismic joints. The buildings are one-, two- and three-story with floor heights of 3.3, 4.15 and 6.4 m, without a basement, some blocks have technological channels. The skeletons of the building blocks are reinforced concrete, single- and double-span, of frame system with rigid joints in the transverse and longitudinal directions. Aseismic joints in buildings are constructed in violation of the requirements of KMK 2.01.03-19, i.e. there is no complete separation between the blocs. As an example, we present the results of an inspection of a three-story building and the compliance of its parameters with the requirements of current earthquake-resistant construction standards. The building is rectangular in plan with dimensions of 9.0x87.0 m (Fig. 3) and is divided into two compartments with dimensions of 9.0x36.0 m and 9.0x51.0 m using an aseismic joint. The building has a floor height of 3.3 m. Transverse and longitudinal frames and rigid disks of slabs provide the spatial stability of the skeleton. The transverse frames bear the vertical load.

Columns are prefabricated reinforced concrete standard-type with a cross-section of 0.3x0.3 m. The grid of columns is 6.0x6.0 m, 3.0x6.0 m and 3.0x3.0 m. In the longitudinal direction of the building, there are multi-span frames (links) with a pitch of 3 and 6 m, and in the transverse direction, there are two spans with a pitch of 6+3 m. To connect the crossbars with the supporting frames, there are special free ends of reinforcement in the crossbar part of the columns. To fit the longitudinal crossbars, the columns also have free ends for reinforcing bars. The columns of the outer rows have embedded fittings for fastening wall panels.

The crossbars of the load-bearing transverse frames are prefabricated reinforced concrete of rectangular cross-sections, 0.4 m high and 0.3 m wide, of standard type. For the installation of the floor disc, free ends of the rod are provided in the crossbars for anchoring the reinforcement ends from the slabs. The upper and lower longitudinal reinforcement of the crossbars protrudes at the ends beyond the edges of the crossbars for connection with the free ends of the reinforcement from the columns in the frame rigid joints. Prefabricated reinforced concrete longitudinal crossbars, with a cross-section of 0.3x0.35 m are attached to the columns with the free ends of the reinforcement and monolithic rigid joints.

The floors and roofing of the building are made of prefabricated reinforced concrete round-hollow-core prestressed slabs of several standard sizes. The rigidity of the floor discs is provided by anchoring the free ends of reinforcement into monolithic reinforced concrete anti-seismic belts, reinforced with flat frames with longitudinal reinforcement. The flat frames of the chords are attached to the free ends of the reinforcement of the load-bearing crossbars.

The wall enclosure is made of hitched expanded clay concrete panels of rectangular section 0.3 m thick and of brickwork. Ordinary, wall and corner prefabricated panels of the standard series were used. It is recommended to carry out routine repairs of the wall panels and restore the fastening of the wall panels. To keep the panels from shifting out of plane, it is recommended to weld plates to the outside tables.

The partitions in the building are made of brick with a thickness of 0.12 m, plaster thickness - 0.8 and 0.16 m. When examining the masonry of the partitions between the rooms, no reinforcement was found, the fastening of the brick partitions to the frame structures was not arranged, and the gaps between the upper edges of the partitions and floor structures were observed. Due to the lack of fastening, cracks formed at the junctions of the partitions with the supporting structures. There were no gaps between the edges of the partitions and the load-bearing structures, which is why cracks formed at the junctions of the partitions with the frame elements.

It was recommended that brick partitions with through cracks and damaged plaster partitions be dismantled and rebuilt, and the partitions be secured to load-bearing structures following the requirements of the building codes.

All staircases are structurally the same - two-flight, reinforced concrete with a flight width of 1.15 m. The flights of stairs rest on the frame crossbars. Reinforced concrete frames are installed to support the intermediate flights.

Expansion joints between the blocks are covered with prefabricated reinforced concrete slabs of solid section with a thickness of 0.12 m and a plan size of 2.85 x 2.4 m. These slabs at both ends rest freely on metal tables made of rolling corners attached to longitudinal and transverse crossbars frames of adjacent compartments (Fig. 4, c).

When analyzing the design of aseismic joints, it was found that the joints correspond to the designed ones. The design solution does not meet the requirements of KMK 2.01.03-19, clause 3.1.3. "At the seismicity of the site 8-points or higher, it is not allowed to combine aseismic joints with displacement compensation due to the gap of the free-lying span structure of adjacent compartments".

In general, the inspection did not reveal any significant defects or damage that would reduce the load-bearing capacity of the building structure of the block.

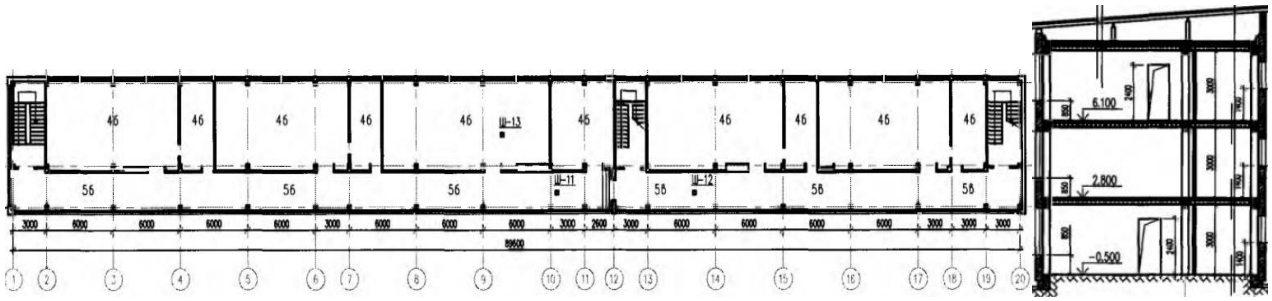

a) b)

Figure 3. **Floor plan (a) and cross-section (b) of the building**

When determining the dynamic characteristics of buildings, a Mobile engineering seismometric station was used, developed as part of a scientific project [23]. Using the mobile station, a series of instrumental measurements of microseismic vibrations of buildings were conducted. Based on the results of instrumental measurements, the periods and decrements of attenuation of natural vibrations of buildings in the longitudinal and transverse directions were determined:

№27:	T_{long}=0,27 sec, δ_{long}=0,15;	T_{tr}=0,20 sec, δ_{tr}=0,26.
№14:	T_{long}=0,20 sec, δ_{long}=0,19;	T_{tr}=0,17 sec, δ_{tr}=0,34.
№248:	T_{long} = 0,21 sec, δ_{long}=0,27;	T_{tr}=0,33 sec, δ_{tr}=0,12.

As seen from the above data, the periods of free vibrations of buildings depend on the geometric dimensions; and in two-story frame buildings in the longitudinal direction, they are greater than in the transverse direction. When compared with calculated data, it was found that the period of the fundamental tone of natural vibrations of buildings in theoretical calculations is greater than the periods obtained from measurements of microseismic vibrations. This discrepancy is explained by the fact that in calculations, it is almost impossible to consider the real states of all structural elements, and in the mode of micro oscillations the dynamic stiffness is determined by the initial elastic modulus, which is always greater than the calculated one.

Instrumental measurement methods [11-13] determined the wave propagation velocities and mechanical properties of soils of the construction site. According to the data obtained, the preliminary seismicity of the construction sites of the surveyed buildings can be attributed to 8 and 9-point zones with the predominant frequency of ground vibrations from 2 to 4 Hz and the thickness of the top soil layer in the range of 4.0 ÷ 9.0 m.

Using non-destructive inspection procedures [24-26], the strength of concrete and the characteristics of structural elements of skeleton-frame buildings were determined in the following

ranges: concrete of columns of class B20 - B30, concrete of monolithic joints B15 - B20; and actual concrete strength of crossbars B25 - B30.

The results of instrumental and calculation studies were used to perform verification calculations of skeleton-frame buildings under seismic impacts. The seismicity of the building construction site according to the microseismic zoning map of the cities of Tashkent and Andijan was taken as 8 and 9-points, respectively. Calculations of buildings for seismic loads were conducted using the LIRA 9.6 software package. In the calculations, the building was taken as a spatial diagram with the corresponding finite elements (Fig. 4). According to the calculation results, the displacements of buildings along the longitudinal and transverse axes are, respectively:

PEI №27:	14,3 mm < (1/200)l = 35,4 mm; 10,6 mm < (1/200)l = 35,4 mm;
PEI №14:	41,1 mm > (1/200)l =35,4 mm; 17,6 mm < (1/200)l = 35,4 mm;
School №248	76,0 mm > (1/200)l = 49,5 mm; 68,6 mm > (1/200)l = 49,5 mm.

From the calculation results, it is clear that the displacements of the frame of the building of PEI No. 27 along the longitudinal and transverse axes are within standard limits. The displacements of the building of PEI No. 14 along the longitudinal axis exceed the allowable value, and the displacements of the building of school No. 248 along the longitudinal and transverse axes exceed their allowable values following the existing standards.

The load-bearing capacity of reinforced concrete columns of the frame of buildings of preschool educational institution No. 14 and school No. 248 is not ensured and reinforcement of floor columns is required. It is recommended to strengthen the columns by installing a reinforced concrete frame and bringing the cross-section to 400x400 mm accepted in the current standards. During reconstruction, it is not allowed to increase the proportion of constant loads compared to those accepted in the calculations, and when installing partitions and floors, it is recommended to use lightweight materials.

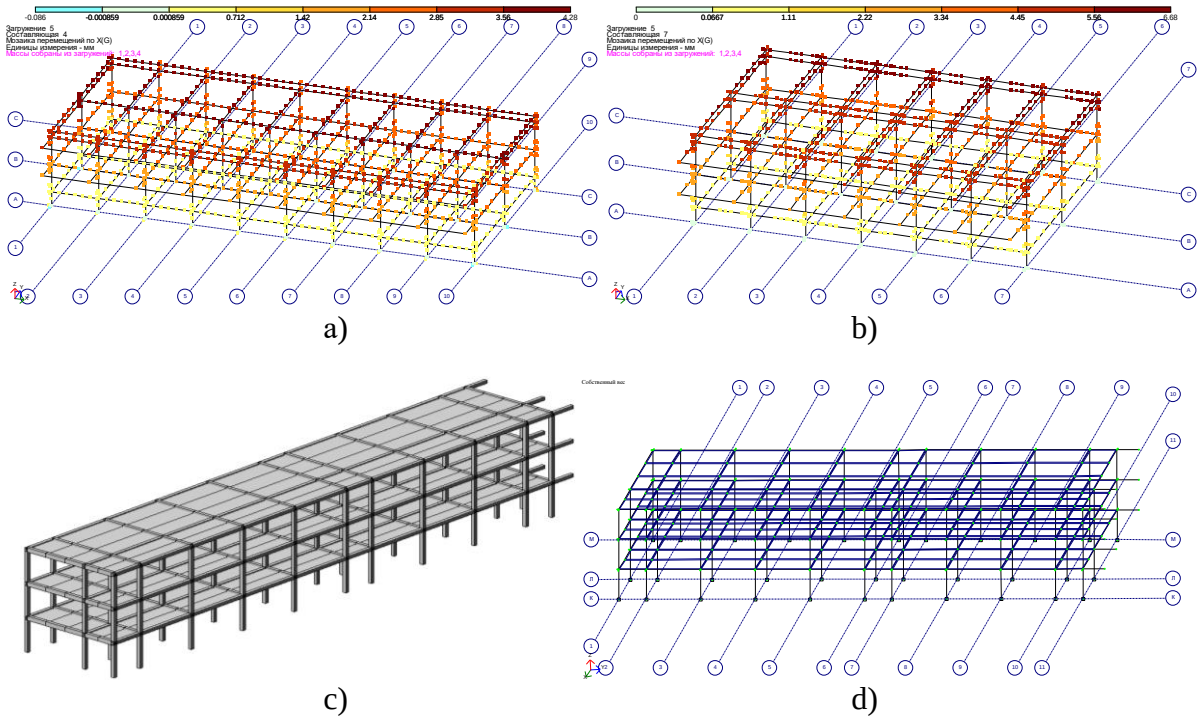

Figure 4. **Design diagrams of building frames: a – PEI No. 27; b – PEI No. 14; c and d – general view and design diagram of the frame of the 2nd compartment of the building of school No. 248**

4. Conclusion.

Conducted studies of the seismic resistance of operating reinforced concrete skeleton-frame buildings, constructed following SNiP II-A.12-69 norms, operating in the period from 01.03.1963 to

01.07.1970, showed that their parameters corresponded to the requirements of current standards, except for the use of aseismic joints. The building of preschool educational institution No. 14 has an L-shape in plan and is not divided into separate blocks using an aseismic joint, which does not meet the requirements of KMK standards 2.01.03-19, clause 3.1.1. "The building must have a geometrically correct shape in plan. If there are protrusions, they, as a rule, should not exceed 6 m in plan for frame buildings". The protruding part of the building relative to the main part is 12 m.

A comparison of the actual values of the structural systems of the skeleton-frame three-story building of school No. 248 with the margin parameters according to KMK 2.01.03-19 shows that the buildings comply with the standards of earthquake-resistant construction, except for the design solution of the aseismic joint between the compartments. The aseismic joint between the compartments is covered with prefabricated reinforced concrete slabs and at both ends they are freely supported by metal tables made of rolling corners attached to the crossbars of the longitudinal and transverse frames of the adjacent compartments, which do not meet the requirements for the design of the aseismic joint for 8 and 9-point seismicity of the construction sites.

When analyzing the design of the aseismic joint, it was found that the design of the joints does not meet the requirements of KMK 2.01.03-19, clause 3.1.3. "At the seismicity of the site is 8 points or higher, it is not allowed to combine aseismic joints with displacement compensation due to the gap of the free-lying span structure of adjacent compartments".

The results of verification calculations of skeleton-frame buildings showed that the displacement of buildings under seismic impacts exceeded their permissible value according to current standards. The load-bearing capacity of reinforced concrete columns of the building frame is not ensured and reinforcement of floor columns is required. It is recommended that the columns be strengthened by installing a reinforced concrete frame and bringing the cross-section to the accepted values stated in the current standards. When recalculating the frame considering the reinforcement of the columns in the specified way, a redistribution of stresses occurs, and the reinforcement of the columns must be performed to the entire height of the building. The load-bearing capacity of the reinforced concrete crossbars of the frame is ensured; reinforcement of the crossbars is not required. During reconstruction, it is not allowed to increase the proportion of constant loads compared to those accepted in the calculations, and when installing partitions and floors, it is recommended to use lightweight materials.

5. General conclusions and recommendations.

In the Republic, since the 1950s, building codes and rules for the design of buildings and structures in seismic areas have been regularly updated, considering the results of scientific and technical research and new technologies for earthquake-resistant construction and building materials; recording the intensity of seismic vibrations by region and seismic impact on objects for various purposes, and studying the consequences of past earthquakes. Using instrumental and calculation methods, we inspected buildings constructed in the first half of the twentieth century before the application of earthquake-resistant construction standards and buildings erected following the standards TU-58-48, PSP 101-51, SN-8-57, SNiP II-A.12- 62 and SNIP II-A.12-69. As part of the research, the general seismic vulnerability of buildings was determined depending on the building codes and rules used during their construction.

1. The surveyed buildings, built in the first half of the last century, generally do not meet the requirements of the current standards for the design and construction of buildings and structures in seismic areas. According to the design solutions, the buildings have complex configurations; they are H-shaped, U-shaped, L-shaped, and T-shaped in plan; the protruding parts are not separated from the main part of the building structure. During earthquakes, a complex deformation process may occur in the structural system of buildings, i.e. the associated structural elements in the joints between the protruding and main parts of the building will simultaneously work in compression-tension, bending and torsion, which can lead to cracks (damage) in the joints of the longitudinal and transverse walls. It would be

necessary to install seismic joints between parts of buildings; these regulations were not accepted at that time in construction technology in seismic regions.

In the buildings, there is no aseismic belt installed in the floors and there are no aseismic joints along the length of the building to divide it into separate compartments. All buildings have wooden floors, which does not provide spatial rigidity of the building structure, and is an important point in ensuring the seismic resistance of structures. In addition to those listed, according to certain actual parameters, the surveyed buildings do not meet such requirements of earthquake-resistant construction standards as length and height; pitch of transverse walls, and width of the walls. The design solutions of the inspected buildings do not comply with the design requirements of KMK 2.01.03-19 standards: strip foundations are made of brickwork, lintels are made of brickwork, the connecting walls are not reinforced, etc.

2. In the regions of the Republic, the main part of the operated facilities are buildings and structures constructed in the second half of the twentieth century after the Second World War due to the significant growth of industry, the expansion of cities and settlements, and the aftermaths of strong earthquakes (Chatkal, 1946 and Tashkent, 1966). Under normal operating conditions, many buildings and structures of mass construction (housing, municipal, educational, medical, industrial and other) are at the limit of their design service life. It should also be noted that individual buildings and structures have already exhausted their service life as a result of their operation in negative conditions and the impact of man-made and natural phenomena. Operating buildings and structures have low seismic resistance since they were built according to old regulatory requirements that were in force during the period of their construction, and did not consider the consequences of destructive earthquakes in recent decades. According to the results of the research, it was revealed that the brick buildings built in 1950-60, in some respects, do not meet the requirements of the current earthquake-resistant construction standards, such as length and height of the building; the pitch of transverse walls and spans; the width of the walls between the window openings; dividing the building with anti-seismic joints does not comply with the limit data of KMK 2.01.03-19. It should also be noted that in many buildings, the spacing of transverse walls is irregular and not all transverse walls have structural connections with all longitudinal walls, which leads to a non-uniform distribution of stresses in the building structure system.

As for certain characteristics of design solutions, the surveyed buildings do not meet the requirements of the current standards for the design of buildings and structures in seismic areas. For example, according to clause 3.5.12 of KMK 2.01.03-19 “Reinforcing meshes with a total cross-sectional area of longitudinal reinforcement of 1 cm2 and a length of 1.5 m must be laid in the joints of walls in masonry for every 700 mm in height at the design seismicity of 7-8 points and 500 mm - at seismicity of 9-points and higher. Sections of walls and columns above attic floors with a height of more than 400 mm must be strengthened and reinforced with monolithic reinforced concrete inclusions anchored in an anti-seismic belt.” Some buildings do not meet the requirements of the standards of clause 3.5.6 “In buildings with load-bearing walls two or more floors high, in addition to external longitudinal walls, there must be at least one internal longitudinal wall”.

To ensure the seismic safety of buildings, it is recommended to conduct a detailed instrumental and calculation study considering the state of structural elements and soil conditions of construction sites. The use of research results in practice and the implementation of recommendations to ensure the seismic safety of buildings in use will significantly mitigate seismic risk and damage during possible strong earthquakes.

3. The studies have shown that buildings and structures with different space-planning and design solutions operating in the Republic were built in accordance with the requirements of regulatory documents that were in force during their construction period. Buildings erected before 1970 were built mainly of baked bricks with longitudinal, transverse or mixed load-bearing walls. Since the mid-60s, after the Tashkent earthquake in 1966, reinforced concrete elements have predominated in the load-bearing structures of buildings in use. The results of the studies showed that skeleton buildings of the

frame system in terms of actual parameters and design requirements correspond to the requirements of earthquake-resistant construction, except for the design solution of anti-seismic joints and the results of calculations for seismic loads. In this regard, it is recommended to strengthen the columns by installing a reinforced concrete frame in accordance with the requirements of current standards for earthquake-resistant construction.

4. The main purpose of the inspection of buildings and structures is to certify the technical condition of buildings and structures as a whole, and their operational suitability, to obtain information about compliance with current regulatory requirements, to determine deviations from the norms, and to develop recommendations for their further reliable operation. When studying the technical condition of buildings and structures, the initial information is the design and technical documentation of construction and major repairs (reconstructions) carried out during the operation of the facilities. Unfortunately, during survey work on many objects, neither technical passports nor construction and reconstruction projects were found, i.e. there were no initial and subsequent documents of building structures, which complicated survey research to assess the seismic resistance of objects. It should also be noted that until recently, there were no laws or regulations in the republic obliging owners to issue a technical passport of a building or structure; in some cases, registration took place based on the results of an inspection of building structures or monitoring the technical condition of the facility. In this regard, the Resolution of the Cabinet of Ministers of the Republic of Uzbekistan PKM No. 405 dated June 30, 2021 was issued, which reflects the methodological recommendation we developed for the certification of buildings and structures. Currently, work is underway to create an integration platform for electronic technical passports of buildings and structures in the regions of the republic. The technical passport of the building must be a mandatory document for the use of the building and its surrounding area after commissioning and before decommissioning. As a rule, the developer must draw up the technical passport of a building upon its commissioning, and its further maintenance must be carried out by the operating organization. Regardless of the purpose of the building or legal status, any object must have a technical passport. The technical passport of the building must contain the main technical characteristics, for example, the year of construction, overall dimensions, design solutions, structural materials, area and the number of floors of the building, date of construction, date of major repairs, walls, ceilings, roofs, dynamic and strength characteristics of structures, etc.

5. In recent years in the Republic, the intensity of construction of buildings and structures has increased significantly, especially in the city of Tashkent; construction of high-rise buildings of more than 16 floors with a height of more than 50 m with new structural systems, technical solutions, elements and connections (links) began with the application of special seismic protection systems. At the same time, overall dimensions, space-planning and design solutions of objects do not comply with the provisions of the current norms of KMK 2.01.03-19 clause 1.1; their design and construction should be carried out according to special technical conditions developed by specialized research organizations authorized State body for architecture, urban planning and construction. In accordance with the Decree of the President of the Republic of Uzbekistan PU No. 144 dated May 30, 2022, the scientific and technical examination of the design documents of these objects is entrusted to the Institute of Mechanics and Seismic Stability of Structures named after M.T Urazbaev of the Uzbekistan Academy of Sciences.

It should be noted here that the main criterion for assessing the seismic resistance of high-rise buildings is their experimental testing and studying the impact of past earthquakes of varying intensities. Studying the impact of weak earthquakes on high-rise buildings using instrumental methods will make it possible to predict their behavior during strong earthquakes, evaluate the building materials used in design and construction, methods of theoretical research, the accuracy of calculation results for seismic loads, and the operation of the structural system. Bearing in mind the relevance of this issue, KMK 2.01.03-19 clause 1.9 provides: “To obtain reliable information about the operation of structures during earthquakes and vibrations of soils adjacent to buildings, in projects of typical buildings of mass development, buildings with fundamentally new structural decisions of especially critical structures, in

agreement with the State Authority of the Republic of Uzbekistan for Architecture, Urban Planning and Construction, Engineering Seismometric Service (ESS) stations should be installed ..." Monitoring high-rise buildings during their operation and recording vibrations of objects during earthquakes is of great practical importance in the subsequent development of design and technical documents and construction, as well as in studying the condition of building structure elements based on the impacts of earthquakes.

In conclusion, it should be noted that the manifestation of unfavorable phenomena on earth, the increase in megalopolises, large-scale industries, vehicle numbers, the expansion of energy production, and other processes lead to a deterioration of the environmental situation, a decrease in green areas, air pollution, etc. Especially large-scale production of gas and oil, the construction of large-scale dams with many billions of cubic meters of water lead to a change in the stressed state of tectonic plates and an increase in the intensity of strong earthquakes. It must be borne in mind that the process of earthquakes will continue until the earth cools down and there is no life on the earth, which indicates the need to take preventive measures to ensure seismic safety. In this regard, it would be advisable to conduct regular seismic risk assessments, monitor the condition of buildings and structures, appropriate supervision during the design and construction of buildings and structures for various purposes, and periodically update regulatory documents on the design and construction of buildings and structures in seismic areas.

References

1. *Sagdiev Kh.S., Saidiy S.A., Akhmedov M.A., Teshaboev Z.R.* Assessment of seismic resistance of standard brick buildings built in 1950-1960 // J. Problems of Mechanics. No. 4, 2012, p. 40-44.
2. *Sagdiev Kh.S., Rumi D.F., Saidiy S.A., Teshaboev Z.R.* Assessment of seismic resistance of multi-storey brick buildings, based on the results of calculations using one-dimensional and three-dimensional models. International symposium "Earthquake-resistant construction using light steel structures", November 27, 2014, Tashkent.
3. *Sagdiev Kh.S., Teshaboev Z.R., Khabibullin A.Sh.* Assessment of seismic resistance of buildings built according to old building codes and regulations // J. Problem. mechan. No. 2, 2015, p. 67-71.
4. *Sagdiev Kh.S., Saidiy S.A., M.A. Akhmedov, Teshaboev Z.R.* Instrumental and calculation assessment of seismic resistance of standard brick buildings built in 1960-1970 // J. Problems of mechanics. No. 2, 2015, p. 90-94.
5. *Sagdiev K. S. et al.* Simulation of the structure of a multistory building with seismic isolation and the testing technique on a laboratory bench under dynamic ((seismic) impacts) //E3S Web of Conferences. – EDP Sciences, 2023. – T. 402. – C. 07024.
6. *Yuvmitov, A., Akhundjanov, D., Abdurakhmanov, U., Khasanova, N., & Egamberdiev, B.* (2023). Study of stress-strain state of structures and assessment of seismic safety of Ismoil Somoni Mausoleum in Bukhara. In E3S Web of Conferences (Vol. 452, p. 06007). EDP Sciences.
7. *Sagdiev Kh.S.* Methodological recommendation for the development of technical passports of buildings and structures. Journal "Problems of Mechanics". Tashkent, 2019. No. 1, p. 90-95.
8. *Sagdiev Kh.S., Galiaskarov V.A., Yuvmitov A.S.* Instrumental study of the consequences of an earthquake in a complex connection joint of a frame building. Scientific and practical journal: Architecture. Construction. Design. – Tashkent, 2020. – No. 1. – pp. 187-192.
9. *Mirzaev, I., Sagdiev, K., Yuvmitov, A., Turdiev, M., & Egamberdiev, B.* (2024). Experimental determination of dynamic coefficient of amonton-coulomb dry friction. Facta Universitatis, Series: Mechanical Engineering.
10. *Sagdiev Kh.S., Yuvmitov A.S., Teshaboev Z.R., Galiaskarov V.A., Sherniyozov Kh.O., Mirzakabilov B.N., Sobirov Z.Zh.* Assessment of seismic safety of preschool educational buildings institutions in Tashkent and recommendations for their further operation. Journal "Problems of Mechanics". Tashkent, 2022. No. 2, pp. 39-53.
11. *Sagdiev Kh.S., Yuvmitov A.S., Galiaskarov V.A., Teshaboev Z.R., Sobirov Z.Zh., Sherniyozov Kh.O., Mirzakabilov B.N.* Assessment of the seismic resistance of buildings built before the application of the requirements of earthquake-resistant construction standards. Journal "Problems of Mechanics". Tashkent, 2023. No. 1. – P. 100–118.
12. *Sagdiev Kh.S., Yuvmitov A.S.* Dynamic characteristics of buildings of various design solutions and soil properties of the construction site. Journal "Problems of Mechanics". Tashkent, 2023. No. 4. – P. 9–26.
13. *Sagdiev KH. S., Yuvmitov A. S., Egamberdiev B. O. & Toshpulatov S. U.* Experimental and computational studies of earthquake resistance of buildings constructed in the second half of the XX century and recommendations for their further operation. Journal of Engineering and Technology (JET) ISSN (P): 2250-2394; ISSN (E): Applied Vol. 14, Issue 1, Jun 2024, 21-32.
14. KMK 2.01.03-19. Construction in seismic areas. 2019 Ministry of Construction of the Republic of Uzbekistan, Tashkent. Put in force 03/01/2020

15. TU-58-48. Technical conditions for the design of buildings and structures for seismic areas. Ministry of Construction of Heavy Industry Enterprises of the USSR. - M: Stroyizdat, 1949. Start date: December 30, 1948
16. PSP 101-51. Regulations on construction in seismic areas. Gosstroyizdat, 1951. Put in force November 1, 1951.
17. SN–8–57. Norms and rules for construction in seismic areas. Gosstroyizdat, 1957. Put in force November 1, 1957.
18. SNiP II-A.12-62. Construction in seismic areas. Gosstroyizdat, 1963. Put in force 03/01/1963.
19. SNiP II-A.12-69. Construction in seismic areas. Gosstroy USSR. M.: Stroyizdat, 1970. Put in force 07/01/1970.
20. SNiP II-7-81. Construction in seismic areas. Gosstroy USSR. M.: Stroyizdat, 1982. Put in force January 1, 1982.
21. KMK 2.01.03-96. Construction in seismic areas. State Committee for Architecture and Construction of the Republic of Uzbekistan. Tashkent: 1996. Put in force 03/01/1996.
22. *Rashidov T.R., Khozhmetov G.Kh., Sagdiev Kh.S., Kondratyev V.A.* On the issue of adjusting the standards for earthquake-resistant construction of the Republic of Uzbekistan // Problems of Mechanics No. 1, 2012, pp. 99-108.
23. Report on research work on the topic: "Improving the methodology for experimental studies of seismic resistance of structures by modernizing laboratory and experimental equipment and determining the patterns of deformation of a structure under the action of static and dynamic loads." Code: FA-A14-F021. Tashkent, 2016, 210 p.
24. GOST 17424-90. Ultrasonic methods of non-destructive testing. Moscow, 1990
25. GOST 22690-88. Concrete. Determination of strength by mechanical methods of non-destructive inspection procedure. Moscow, 1988.
26. GOST 18105-86. Concrete. Strength control rules. Moscow, 1986.

MONITORING THE STATE OF DAMS THROUGH SATELLITE AND IN SITU OBSERVATIONS AND THEORETICAL STUDIES

Salyamova K.D.[1], Tashmatov K.A.[2], Nishonov N.A.[1], An E.V.[1]
[1]Institute of Mechanics and Seismic Stability of Structures named after M.T. Urazbaev, Tashkent, Uzbekistan
[2] Center for Space Monitoring and Geoinformation Technologies LLC, Tashkent, Uzbekistan
E-mail: klara_51@mail.ru

Abstract. *A technique is proposed for determining the condition of a high dam using space monitoring, instrumentation, and theoretical research. Photo recordings of the condition of the hydro-technical structure are provided. During engineering and geodetic observations, deformations in the crest were identified. The data of processed satellite radar images taken in 2019 – 2023 were analyzed; according to the results of radar images, ground settlement was observed in areas of the crest. The stress-strain state of the dam under basic loads was studied using the finite element method. The results of the distribution of vertical displacements and normal stresses of the dam were plotted in the form of graphs; they show the subsidence of the dam in the area of the upstream slope. It is shown that the results of space monitoring confirm the results of engineering and geodetic observations and theoretical studies.*

Keywords: *high dam, space monitoring, engineering and geodetic observations, finite element method, subsidence.*

1. Introduction

Our republic has created a unique complex of hydro-technical structures (HTS), including dams and other structures, which are among the most important objects of the country's economy. In our republic, reservoirs play an important role: they are necessary for the production of electricity, for satisfying the needs of agriculture with water, for supplying fresh water to the population, and, in general, for the sustainable functioning of other sectors of the national economy.

The territory of Uzbekistan has seismicity of 7, 8, and 9 points. Today, 273 large hydraulic structures of categories I, II, and III are in operation in Uzbekistan, including 54 large earth dams (mostly earth-fill ones), with a total reservoir capacity of 20 km^3. More than 28 hydroelectric power plants (HPP) were built 60-70 years ago. In particular, the Bozsu HPP that operates on the Bozsu canal was built in 1923, Akkavak-2 HPP (1930 - 1940), Farkhad HPP (1949), Charvak HPP (1977), Gissarak HPP (1986), Karkidon reservoir (1962 - 1964), Kattakurgan reservoir (1942), etc. The seismicity of the sites ranged from 6 to 9 points.

Currently, one of the main tasks of water use is the reliable and rational operation of previously constructed and operating hydraulic structures. The condition of these structures directly depends on the results of generalized monitoring of their operation and technical state. At present, a large number of dams around the world are in the stage of planning or building due to the needs of countries' economies. In our republic, due to the lack of water, the design of the following reservoirs was resumed: a cascade

of reservoirs above and below (Zarchopa 1, 2) of the Tupolang hydroelectric power station, on the rivers Tupolang Darya, Naryn, Chatkal, Ugam, and Pskem. Maintaining the proper functioning and safety of dams throughout their life is a complex and never-ending task.

The aftermaths of the earthquake are dangerous displacements and stress concentrations in vulnerable areas of reservoir dams, due to the development of cracks, peeling of the protective layer of concrete, corrosion, etc. (the amount of damage may exceed the maximum permissible values established by the current design standards (SNiP)) [1], leading to a decrease in the seismic resistance of dams. Thus, the reliability and safety of dams are largely determined by the stresses and strains that appear under various loads and seismic impacts. Therefore, a preliminary forecast of the stress-strain state of a structure, considering its design features, characteristics of the structure itself, and the underlying foundation makes it possible to identify areas where the permissible safety margins are exceeded; thus, it is necessary to conduct appropriate revision.

In addition to monitoring the condition of dams by analyzing visual and field observations using control and measuring equipment (CME), large volumes of detailed cartographic materials that can be obtained using satellite-based means of observation of water bodies (reservoirs and their dams, the surrounding area), which allow to promptly identify the nature of changes and trace the intensity of processes occurring in them with sufficiently high accuracy. Therefore, obtaining and processing information on the state of water bodies using space methods is an urgent task for many regions, including Uzbekistan.

Space technology, due to its effectiveness in monitoring entire infrastructure without the need to install local control centers, allows the integration and improvement of monitoring capabilities provided by ground-based methods. Classical topographic methods have two main disadvantages: the inability to obtain complete information about the deformations of an object and the difficulty of observation with the required regularity in hard-to-reach places. New satellite-assisted methods overcome these shortcomings, allowing complete and continuous control of the movement of a structure without the need for access to the structure [2 – 5].

Luzi G. et al. [6] described two new remote sensing methods based on radar interferometry technology that can be used in monitoring dams. The first method uses synthetic aperture radar (SAR) data to produce 2D images. The second technology uses Real Aperture Radar (RAR) and can be used to measure objects (displacements) in a specific direction. In M. Alba et al. [7], the Cancano dam (Alta Valtellina, Italy) was investigated by two radar methods, RAR and SAR.

Al-Sadik B. and Al-Kanani Y. in [8], focused on assessing the displacement of the Mosul Dam in northern Iraq. A detailed review of the ongoing process of destabilization of the Mosul Dam was conducted in [8, 9].

The method of space radar interferometry with synthetic aperture (SAR, InSAR) is a new space geodetic tool for monitoring strains on the Earth's surface [10–15]. InSAR can provide dense observations over large spatial scales over long periods, providing a more complete analysis of dam deformation characteristics.

References [16, 17] are devoted to the study of the collapse of the Sardoba dam in Uzbekistan. In [17], the study was performed on three sets of data from Earth observation: (1) ICESat-2 data, necessary to understand the topographic features in the area under study; (2) Sentinel-1 multi-geometry SAR data to extract pre-crash deformation along the vertical and horizontal east-west directions; (3) optical images from Sentinel-2 satellites and Global Precipitation Measurement (GPM) products, used to study pre-disaster environmental conditions. Possible causes of dam failure were analyzed from the point of view of both physical and human factors. The differential settlement of approximately 60 mm detected by InSAR at the breach site is an indication of internal embankment erosion, which is a physical factor contributing to the breach. The opportunity to prevent a breakthrough was missed due to the lack of conventional monitoring methods. The authors of [16] revealed that the Sardoba water structure experienced local uneven settlement of ~4.7 cm near the breakthrough area using optical and SAR

imagery and modeling tools. Researchers in [17] noted that neither ground-based observations nor satellite GPM products showed extreme ground surface precipitation in the region, eliminating the possibility of rainfall-induced overflow. The settlement rate of the embankment does not tend to decay, indicating that the dam is undergoing a phase of primary consolidation of complete settlement. A maximum subsidence of ~270 mm (~0.8% of the dam height) occurred on the north bank when the reservoir was flooded. A group of authors [16, 17] showed that InSAR could recognize a precursor to failure by detecting movement of the ground surface and that strain signals can help warn of risks and avoid dam failure.

The monitoring using space observations, which is developing now in the Republic of Uzbekistan is expected to be tested at high earth dams of hydroelectric power stations (Charvak, Tupolang, Rezaksai, Gissarak, Angren), and then at dams' reservoirs. Below we propose a research method; the main results of radar interferometric monitoring using as an example a selected reservoir (the monitoring is performed by the Center for Space Monitoring and Geoinformation Technology under the Uzbekcosmos Agency) are compared with engineering and geodetic observations (provided by JSC "Hydroproject" of the Republic of Uzbekistan), and theoretical calculations (performed in the Institute of Mechanics and Seismic Stability of Structures named after M.T. Urazbaev, Uzbekistan Academy of Sciences). This study is a continuation of the research presented in [18, 19]. The ongoing research is conducted in pursuance of the objectives of the Decree of the President of the Republic of Uzbekistan No. PF-144 "On measures to further improve the seismic safety system of the Republic of Uzbekistan" dated May 30, 2022, specified in paragraph 43 of Appendix 2.

2. Materials and methods of satellite radar interferometry

Satellite radar interferometry InSAR uses the effect of interference of electromagnetic waves and is based on mathematical processing of several coherent amplitude-phase measurements of the same area of the earth's surface with a spatial shift of the radiating antenna during several successive surveys. In multi-time or multi-pass radar surveys, the methods of permanent reflectors or the PSI - Persistent Scatterer Interferometry method, well described in the literature [20], and the SBAS - Small Baselines Subset method [21] are used.

The input data for processing using specialized software systems is an interferometric pair (or multi-pass series) of radar images taken in identical survey geometry. The space and time bases limit the ability to interferometrically process a pair (or series) of radar images.

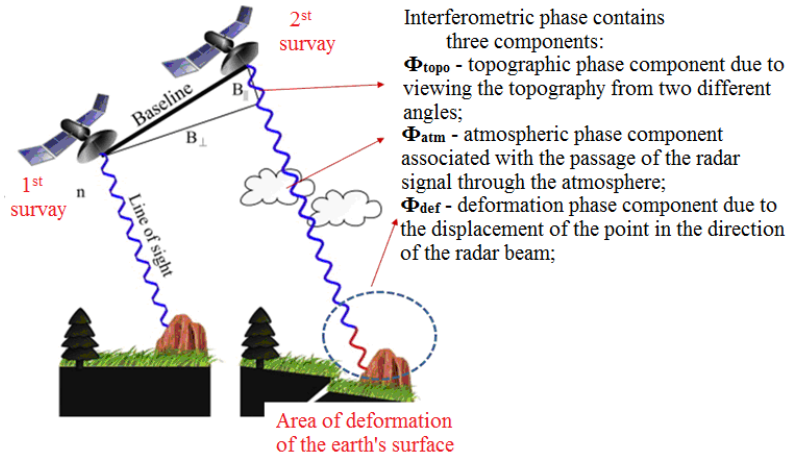

Figure 1. – **Scheme of space photography of an interferometric pair of radar images**

The space basis (or baseline) is the distance between the orbital positions of the radar when capturing the images that make up the interferometric pair. The smaller the value of the perpendicular component of the baseline (Fig. 1), the higher the degree of reliability of the model of displacements of

the earth's surface. In the case of a baseline equal to zero, the interferogram calculated from such a pair of images generally contains only the displacement phase and does not contain the relief phase.

The time base is the time interval that elapsed between the capture of images that make up an interferometric pair. The concept of a time base is directly related to such an important problem as time decorrelation, which arises due to changes that occur during the time between surveys in relief, vegetation, humidity, roughness, and other properties of the surface reflected by the radar beam.

As a result, the processing of radar images comes down to calculating the phase difference of the reflected signal from the same object for repeated observation (shooting) dates and its subsequent conversion into a change in relief height. As a result of using a set of interferograms for different shooting dates, it is possible to track the dynamics of vertical displacements of points on the earth's surface, that is, to construct a map of displacements or displacement rates for the studied period.

The technologies for using these methods and the logic of the processing have much in common (Fig. 2), but, depending on the tasks, the use of one or another method must be justified.

The PS method is suitable for built-up urban areas, and the density of permanent scatterers in undeveloped areas drops significantly. Therefore, SBAS is the best method for analyzing areal displacements on undeveloped surfaces.

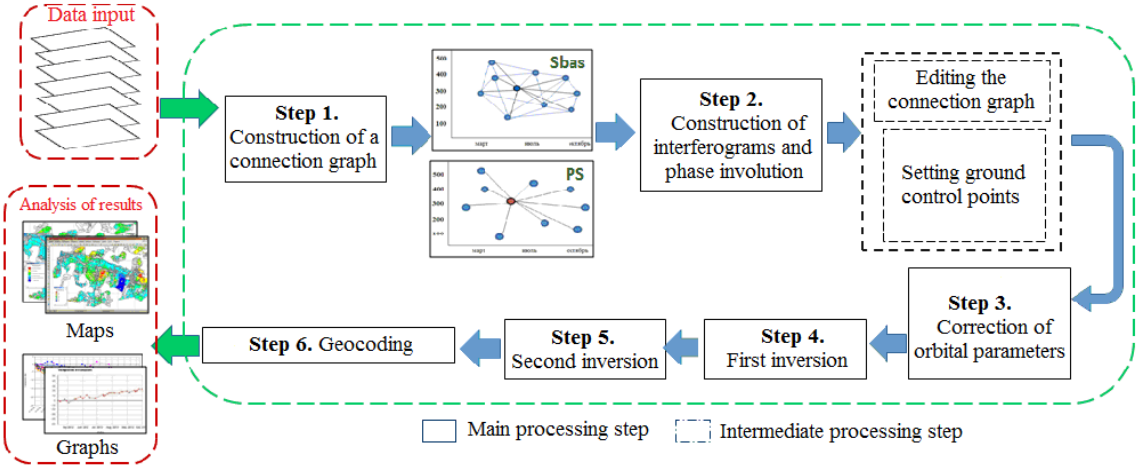

Figure 2. – **Technological chain for processing multi-pass radar data using PS and SBas methods**

3. Results of the study

3.1 *Geodetic observations*

Figure 3 – **Reservoir of the selected object**

The object under study is a large hydraulic engineering facility located in an 8-point seismic zone. The dam is erected from local materials, has a loamy core, and retaining prisms made of rockfill or combined (pebbles with stone surcharge). The main purpose is to produce electricity and regulate water consumption for irrigation and the energy needs of the national economy.

Below we present photographs of the state of the hydraulic structure (provided by the Center for Space Monitoring and Geoinformation Technology under the Uzbekcosmos Agency and JSC "Hydroproject" of the Republic of Uzbekistan). It is shown that along the dam crest, there are cracks in the concrete pavement and parapet. There are local traces of reshaping of the downstream slope as a result of compaction and sliding of the rock fill (see Fig. 4). Cracks and subsidence were observed on the concrete fastenings of the upstream slope, indicating the formation of cavities under fastenings (see Fig. 5).

Figure 4. – **Local traces of reshaping of the downstream slope as a result of compaction and sliding of rockfill from the downstream side**

Figure 5. – **Cracks and subsidence of reinforced concrete fastenings from the upstream side**

To diagnose the stability of the dam in the first observation cycle (7 - 22 May 2022), observations were conducted based on engineering and geodetic studies. The displacements of the structure foundation and the body of the reservoir dam were determined.

As indicated in the technical report, as the dynamics of the structure's subsidence enters the stabilization phase, the observation cycle is shortened and the time interval increases. In large hydraulic facilities, the observation cycle is extended to once a year.

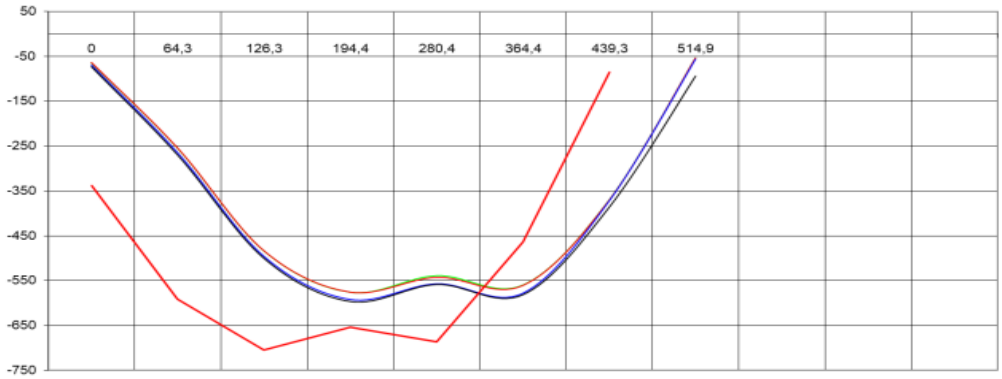

Figure 6. – **Vertical deformation of the upper berm at level H-1110 m**

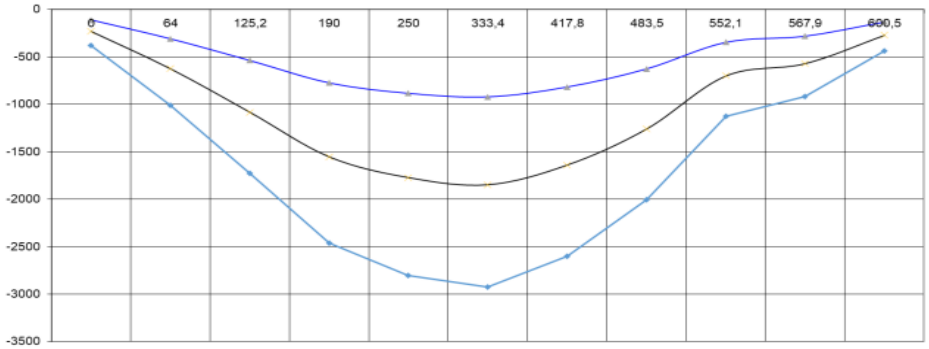

Figure 7. – **Vertical deformation observed in the dam crest of the reservoir**

When conducting engineering and geodetic observations at the site, all 73 strains were identified, including in the body of the dam and 5 marks on the berm at level H-1110m.

3.2 *Results of interferometric processing*

Data from processed space radar images were analyzed. As a result of studies of the reservoir conducted from January 2019 to March 2023, a total of 2,687 control points were identified on the dam and the water area of the reservoir; the maximum subsidence in the study area was observed on the left bank of the reservoir at -94.15mm; the point of the maximum rise was recorded at +80.20mm on the right bank. In the cross-section of the area under study, the average annual deformation was -0.1 mm.

Figure 8. – **Results of the analysis of space monitoring of the selected reservoir object**

It can be seen that the results of space monitoring confirm the results of engineering and geodetic observations. Subsidence was observed at points 1100 m of the upper crest.

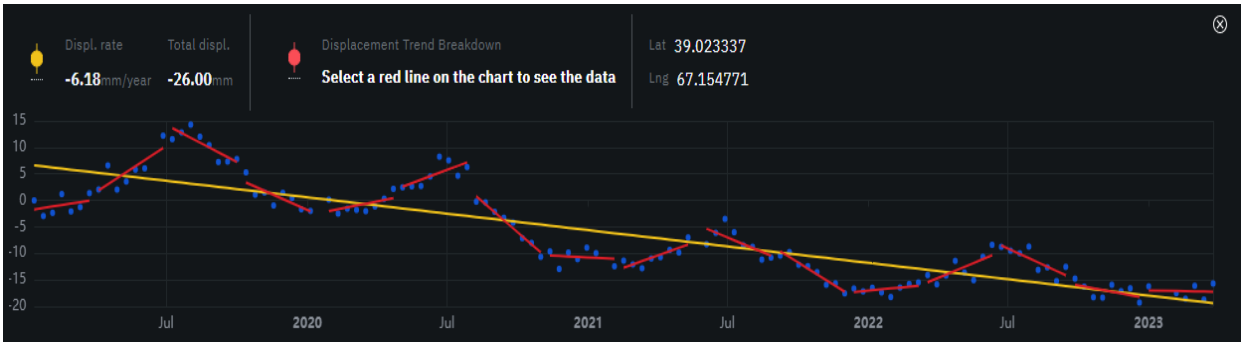

Figure 9. – **The maximum subsidence of the dam recorded in 2019-2023.**

The deformation of all points of the dam was -2.75 mm over the observation period, and the annual average was -0.65 mm. It should be noted that seasonal displacements were observed as well. The lowest point of dam subsidence was -26 mm and the average annual value was -6.18 mm.

Space observations must be combined with safety standards (with criterion values) and theoretical results of calculations considering climate changes depending on the time of year.

3.3 *Theoretical results*

When studying the stress-strain state (SSS) of a dam, a well-founded approach to the choice of calculation model and calculation method is required, allowing the consideration of the real geometry, design features of the structure, real properties of the material, static loads, and dynamic impact characteristics of the area where the object is located.

Based on the above, the authors considered a plane calculation model representing the cross-section of the dam. To determine the SSS of the dam under the impact of basic loads (dead weight and hydrostatic pressure), the finite element method (FEM) was used. This method allows one to consider the heterogeneity of the structure, its actual geometry, and various boundary conditions.

The geometric parameters of the dam model and the physical and mechanical characteristics of materials for each section of the dam were taken from the design documentation.

The equilibrium equations of converging forces at all nodes of the system give a matrix system of high-order algebraic equations in the following form [22]:

$$[K]\{q\}=\{Q\}+\{P\}\ . \qquad (1)$$

where [K] is the global stiffness matrix; $\{q\}$ – is the vector of displacements of model nodes; {Q} – is the self-weight matrix; {P} is the matrix of surface hydrostatic load from water on the upstream slope to the normal backwater level and on the bedrock surface in front of the dam.

The system of algebraic equations (1) was solved using the Gauss method. Next, using the Cauchy relations, the strain components in the element were determined, and, based on the resulting strains, using Hooke's law, the stress components were determined.

The results of the distribution of vertical displacements and normal vertical stresses of the dam are presented in Figure 10.

a) vertical displacements, m

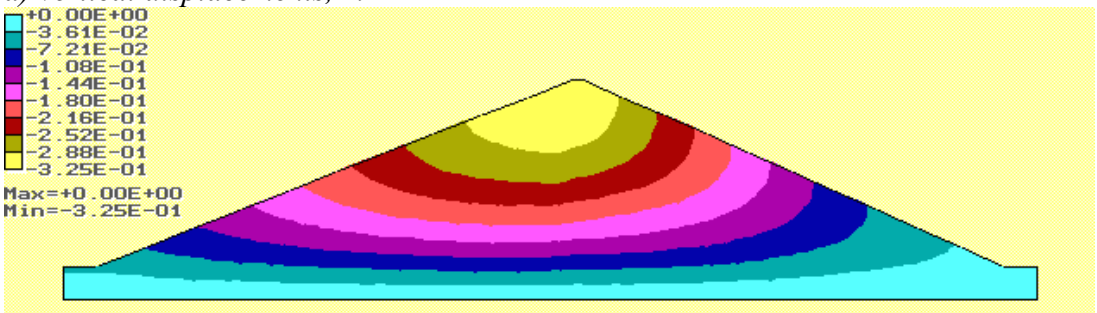

b) vertical stresses σ_y, MPa

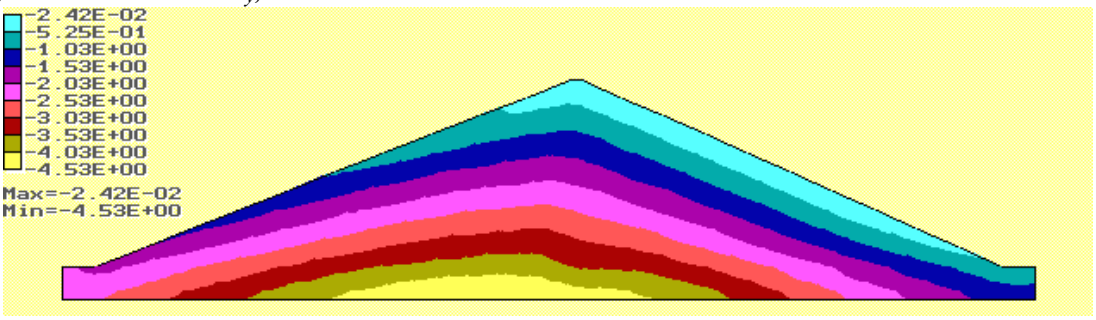

Figure 10. – **Distribution of fields of vertical displacements (a) and normal stresses (b) in the dam considering the dead weight and hydrostatic pressure**

Figure 10, *a* shows the dam subsidence, where vertical displacements (*v*) are presented. The maximum subsidence on the crest is 30 cm. The settlement is asymmetrical - the upper slope area, where hydrostatic pressure is applied, is subject to greater subsidence. From Fig. 10 *b*, it is clear that the vertical stresses along the surface of the downstream slope are only 0.024 MPa.

4. Conclusions

This study is a continuation of ongoing research on determining the condition of high hydro-technical structures. Uzbekistan has launched a system of continuous space monitoring of ground deformations and displacements (settlements) observed at dams; the system is relevant and vital for the reliable operation of dams, especially those located in seismic areas.

Note that space-monitoring data must comply with the results of engineering and geodetic observations and safety criteria. Therefore, this paper proposes a method for determining the condition of a high dam using space monitoring, instrumentation, and theoretical studies.

Photo recordings of the condition of the hydraulic structure are presented. During engineering and geodetic observations, deformations (settlements) were identified on the crest; as a result, individual cracks were noted in the reinforced concrete pavement and parapet. This indicates the formation of cavities under the fastening. Local traces of reshaping of the lower slope due to compaction and sliding of the rock fill were also discovered.

The methods of satellite radar interferometry PSI - Persistent Scatterer Interferometry and SBAS - Small Baselines Subset are presented. Data from processed space radar images taken in 2019–2023 were analyzed. According to the results of space monitoring, ground subsidence was observed in the crest areas.

The stress-strain state of a high dam under basic loads (dead weight and hydrostatic pressure) was studied using the finite element method (FEM), which allows considering the real geometry, design features of the structure, real properties of the material, static loads, and dynamic impact characteristics of the area where the object is located. The results are presented in the form of graphs of the distribution of vertical displacements and normal vertical stresses of the dam, with account for dead weight and hydrostatic pressure. From the results, it follows that the region of the upstream slope, where hydrostatic pressure is applied, is subject to greater subsidence.

Thus, it is shown that the results of space monitoring confirm the results of engineering and geodetic observations and theoretical studies. Therefore, the proposed methodology is appropriate for the dams under operation and design to predict their condition under basic loads and special combinations of loads following regulatory documents.

References

1. ShNK 2.06.11-04 Construction in seismic areas. Hydraulic structures. Goskomarchitekstroy, 2004, Tashkent, 54 p.
2. Di Pasquale A., Corsetti M., Guccione P., Lugli A., Nicoletti M., Nico G., Zonno M. (2013) Ground-based radar interferometry as a supporting tool I natural and man-made disasters. In: Proceedings of the 33rd annual EARSeL symposium, Matera, Italy, 3–6 June 2013
3. Nico G., Corsetti M., Di Pasquale A., Donnarumma D., Dotti L. Fiorentino L., Nicoletti M. (2013) On the monitoring of dams by means of ground-based radar interferometry. In: Proceedings of the 9th ICOLD European Club Symposium, Venice, Italy, 10–12 April 2013
4. Bonano M, Manunta M, Marsella M, Lanari R (2012) Long term ERS/ ENVISAT deformation time-series generation at full spatial resolution via the extended SBAS technique. Int J Remote Sens 33 (15):4756–4783. doi:10.1080/01431161.2011.638340
5. Calò FF, Ardizzone F, Castaldo R, Lollino P, Tizzani P, Guzzetti F, Manunta M (2014) Enhanced landslide investigations through advanced DInSAR techniques: the Ivancich case study, Assisi, Italy. Remote Sens Environ 142:69–82. doi:10.1016/j.rse.2013.11.003
6. Luzi, G. Advanced Techniques for Dam Monitoring/G. Luzi, M. Crosetto, O. Monserrat// research gate, 2010.
7. Structural monitoring of a large dam by terrestrial laser scanning/ M. Alba, L. Fregonese, F. Prandi, M. Scaioni, P. Valgoi// International Archives of Photogrammetry, Remote Sensing and Spatial Information Sciences, 2006.
8. Al-Sadik, B. S. Displacement Computation of Mosul Dam by Using Free Geodetic Network Adjustment/ B. S. Al-Sadik ,Y. H. Al-Kanani // 2010/10/01 -journal of engineering - Baghdad university ER
9. Milillo, P., Burgmann, R., Lundgren, P., Salzer, J., Perissin, D., Fielding, E., Biondi, F., Milillo, G., 2016, Space geodeti c monitoring of engineered structures: The ongoing destabilization of the Mosul dam, Iraq., Scientific Reports, 6, DOI:10.1038/srep37408
10. Biggs, J., Wright, T.J., 2020. How satellite InSAR has grown from opportunistic science to routine monitoring over the last decade. Nat. Commun. 11 (1) https://doi.org/ 10.1038/s41467-020-17587-6.
11. Cigna, F., Tapete, D., 2021a. Present-day land subsidence rates, surface faulting hazard and risk in Mexico City with 2014–2020 Sentinel-1 IW InSAR. Remote Sens. Environ. 253, 112161. https://doi.org/10.1016/j.rse.2020.112161.
12. Cigna, F., Tapete, D., 2021b. Satellite InSAR survey of structurally-controlled land subsidence due to groundwater exploitation in the Aguascalientes Valley, Mexico. Remote Sens. Environ. 254, 112254. https://doi.org/10.1016/j.rse.2020.112254.
13. Haghshenas Haghighi, M., Motagh, M., 2019. Ground surface response to continuous compaction of aquifer system in Tehran, Iran: Results from a long-term multi-sensor InSAR analysis. Remote Sens. Environ. 221, 534–550. https://doi.org/10.1016/j. rse.2018.11.003.
14. Lu Z., Dzurisin D., Lu Z., Dzurisin D., 2014. InSAR Imaging of Aleutian Volcanoes. In: InSAR Imaging of Aleutian Volcanoes. Springer, Berlin Heidelberg, pp. 87–345. https://doi.org/10.1007/978-3-642-00348-6_6.
15. Wang T., Shi Q., Nikkhoo M., Wei S., Barbot S., Dreger D., Bürgmann R., Motagh, M., Chen, Q.F., 2018. The rise, collapse, and compaction of Mt. Mantap from the 3 September 2017 North Korean nuclear test. Science 361, 166–170. https://doi.org/ 10.1126/science.aar7230.
16. Lei Xie, Wenbin Xu, Xiaoli Ding, Roland Bürgmann, Sanjay Giri, Xiaoge Liu. A multi-platform, open-source, and quantitative remote sensing framework for dam-related hazard investigation: Insights into the 2020 Sardoba dam collapse // International Journal of Applied Earth Observations and Geoinformation 111 (2022) 102849
17. Xiao, R., Jiang, M., Li, Z., He, X., 2022, New insights into the 2020 Sardoba dam failure in Uzbekistan from Earth observation, International Journal of Applied Earth Observation and Geoinformation, 107, 102705
18. Salyamova K., Toshmatov K., Nishonov N., An E., "Seismic stress state of a high earth dam using the spectroscopic method" in E3S Web Conf, 431, 03008 (2023).
19. Salyamova K., An E., Nishonov N., Toshmatov K., Turdikulov K., "Long-term monitoring of earth dam of the Charvak hydroelectric power plant (HPP) considering the water level of the reservoir" in E3S Web Conf, 462, 02050 (2023).
20. Hooper A., Persistent Scatterer Radar Interferometry for Crustal Deformation Studies and Modeling of Volcanic Deformation: Doctoral Thesis // Stanford University. – 2006. – P. 144
21. Lanari R. et al. An overview of the small baseline subset algorithm: A DInSAR technique for surface deformation analysis // Deformation and Gravity Change: Indicators of Isostasy, Tectonics, Volcanism, and Climate Change. – 2007. – P. 637-661. doi:10.1007/s00024-007-0192-9
22. Zienkiewicz O.C., Taylor R.L. The finite element, Butterworth-Heinemann (2000), 690 p.

STRUCTURAL RESPONSE OF THE HUMBOLT BAY BRIDGE TO THE RECENT SEISMIC EVENTS: ANALYSIS OF STRONG MOTION DATA.

Takhirov Sh[1], Gilani A.[2], Ergashev Z.[3], Abdiashimuly K.[4]

[1]*Structures Lab and Center for Smart Infrastructure, University of California at Berkeley, Berkeley, California, USA*
Miyamoto International, Sacramento, California, USA
Transport University, Tashkent, Uzbekistan
[4]*JSC Kazakhstan Highway Research Institute (KazDorNII), Astana, Kazakhstan*
E-mail: takhirov@berkeley.edu

Abstract: *The paper is focused on the analysis of the structural performance of the Humbolt Bay Bridge in Eureka (California, USA). The bridge was instrumented by accelerometers in 1996 to monitor and assess its structural performance in response to earthquakes. Out of three spans, the span called Samoa Channel Bridge was studied. The structural performance of the bridge during a few seismic events since 2014 is studied. It was shown that taking into account the spectral demand on top of the piers is very important for assessing the motions of the bridge's deck. Since the bridge represents a nonlinear system, the variation of the spectral demand over the range of resonant frequencies needs to be taken into account. This is especially important for spectral acceleration rapidly increasing within the frequency variability range, which is discussed in the paper based on the examples of a few seismic events after 2014.*

Keywords: *bridge, deck, pier, strong motion data, real-time monitoring, Humbolt Bay Bridge, seismic response.*

1. Introduction

The importance of structural health monitoring of bridges is discussed by using an example of the Humbolt Bay Bridge in Eureka, California, USA. Because of the range and sensitivity limitation of accelerometers, the monitoring can be arranged in two ways. First, it can be built as a network of very sensitive accelerometers monitoring the bridge's response to ambient vibrations: traffic, wind load, small excitations from nearby construction, and so on. Second, a set of accelerometers with a relatively higher range and lower sensitivity can be used to develop a network that monitors the shaking of the bridge during strong motion excitations. An example of the second one is discussed herein for a common bridge typology.

The main objective of the paper is to demonstrate the advantages of structural health monitoring (SHM) of bridges and promote their utilization in both Uzbekistan and Kazakhstan. A strong need for the application of SHM technologies to bridges was shown in the recently completed extensive program assessing the structural condition of bridges in Uzbekistan [1,2]. In addition, it is especially important for the ongoing effort in Kazakhstan aiming at the development of digital twins of major components of transportation infrastructure (see [3,4] as representative examples). In this case, in addition to the overall 3D geometry of the object, data related to its structural performance characteristics can be added. The latter is very important for well-calibrated modeling of bridges [5], complemented by component testing [6].

The construction of the Humbolt Bay Bridge in Eureka started in 1968 and was completed in 1971 [7-9]. It is located about 440 km north of San Francisco. It consists of three structures with the following names: (1) Eureka Channel Bridge, (2) Middle Channel Bridge, and (3) Samoa Channel Bridge [4], as presented in Figure 1 (Google Earth). This study is focused on the longest structure, the Samoa Channel Bridge. It underwent a structural retrofit in 2006 [9].

The bridge consists of 20 spans, varying from 36.6 m to 68.6 m long [7]. Its total length is 764.1m. [7]. The bridge is 10.4 m wide and carries two lanes of traffic. The bridge superstructure consists of a concrete deck and two prestressed concrete beams. In 2006 [9], the bridge was seismically retrofitted by strengthening the columns and foundation elements.

Figure 1. – **Three spans of the Humbolt Bay Bridge.**

2. Materials, methods, and object of study.

Based on the information provided in [7], the Samoa Channel Bridge was instrumented for the first time in 1996 with twenty-six accelerometers and a set of three accelerometers to record free-filed motion. More instrumentation was added throughout the years, with one of the latest additions in 2002 bringing the total number of sensors to 33 [9]. The locations of the sensors are presented in Figure 2 (reproduced from [10]). The data collected by the sensors was analyzed in the Matlab environment [11].

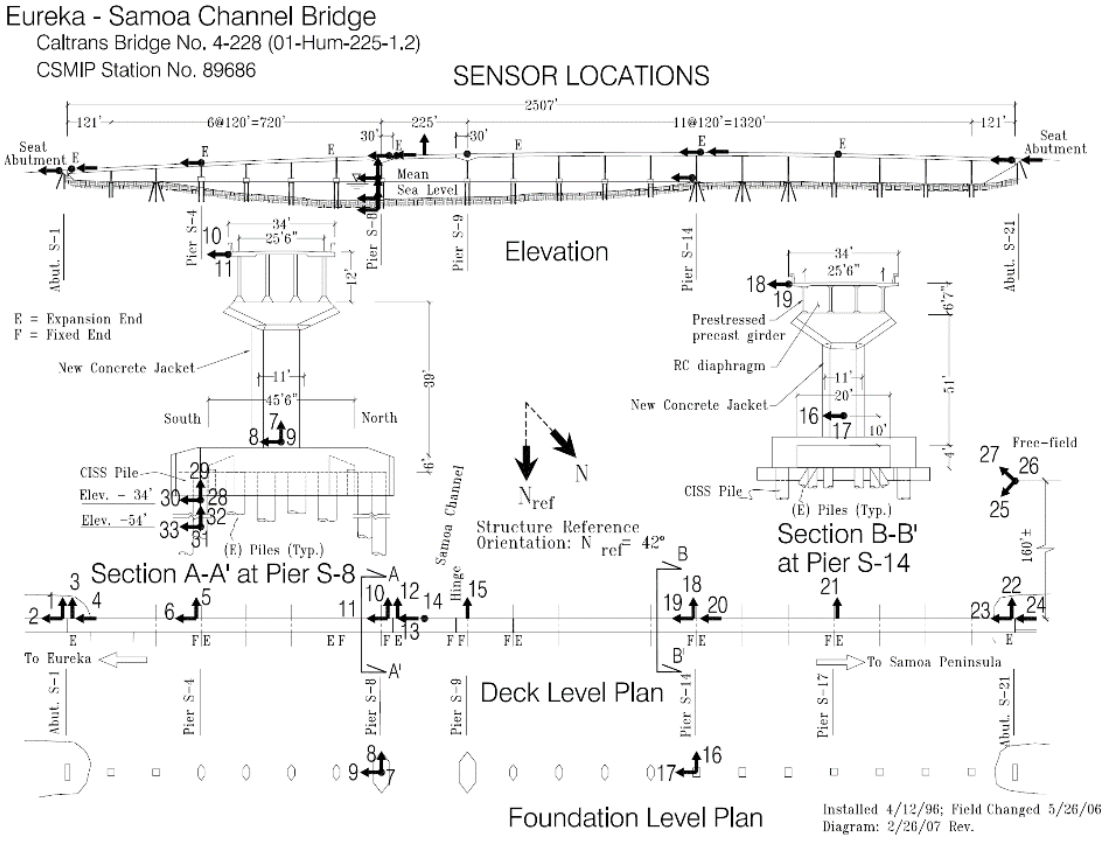

Figure 2. – **Layout of accelerometer locations [10].**

3. Problem statement.

The bridge represents a complex system with complex behavior that involves considering (1) the soil-structure effects of the supporting piers [12-15], (2) the motion of the deck with respect to the piers

[16-17], (3) the interaction of the adjacent bridge frames via expansion joints [18-21]. In addition, for long bridges such as the structure considered in this report, the seismic input would vary at the bridge piers, and this needs to be considered as well.

An extensive monitoring system was introduced to understand this performance and monitor possible changes. The changes can be related to the deterioration of the bridge over time or can be a result of seismic upgrades aimed at improving its structural performance. This paper is focused on analyzing the bridge performance in recent earthquakes, namely after 2014.

4. Results and discussion.

The effect of strong motions on the performance of the Samoa Channel Bridge was studied earlier [9], but this study is mainly based on all earthquake records up to 2014. In recent years, the bridge has experienced a few earthquakes, and it is noted that the structure is located in a region that can be subjected to very large earthquakes as a result of the fault rupture in the Cascadia Subduction Zone. A complete list is provided in Table 1 [22]. A special name was given to each dataset, which is provided in the last column of Table 1. It is worth noting that two datasets were missing sensor data for the accelerometer's location on or above Pier S-8. Hence, they were not used in the study. Therefore, as shown in the table, the study focused on the bridge responses to seven earthquakes (excluding numbers 4 and 5).

Table 1.

List of recent earthquakes (after 2024) [22]

No	Epicentral Distance (km)	Ground PGA (g)	Earthquake Name	Magnitude	Earthquake Origin Time (UTC)	Dataset name
1	25.5	0.054	BlueLake	4.7MW	7/21/2016 23:09	BL-16
2	20.1	0.017	humboldthill	4.6MW	3/22/2018 16:24	HH-18
3	91.6	0.011	Petrolia	5.8MW	3/9/2020 2:59	P-20
4	49.1	0.043	Petrolia	6.2MW	12/20/2021 20:10	
5	39.3	0.210	Ferndale	6.4MW	12/20/2022 10:34	
6	35.5	0.011	Ferndale	4.5MW	3/21/2023 23:18	F1-23
7	19.1	0.027	McKinleyville	3.8MW	8/13/2023 15:28	MV-23
8	30.9	0.019	Ferndale	4.7MW	9/30/2023 15:26	F2-23
9	57.0	0.023	Petrolia	4.7MW	10/16/2023 10:20	P-23

The response of the bride to a few earthquakes was studied earlier [9], and resonant frequencies of the bridge were estimated. It was observed that there is a large variation of resonant frequencies, as shown in Table 2.

Table 2.

Resonant frequencies estimated for a few seismic events that happened before 2024 [9]

	Longitudinal Direction				Transverse Direction			
Event\Sensor No	31	28	9	11	33	30	8	10
Ferndale, 2007	0.93	0.93	1.26	1.26	NA	0.93	0.93	0.93
Trinidad, 2007	0.90	0.90	1.23	1.23	NA	0.93	0.93	0.93
Willow Creek, 2008	0.90	0.90	0.93	0.93	0.93	0.90	0.90	0.90
Trinidad, 2008	NA	0.93	1.23	1.23	NA	0.93	0.93	0.93
Ferndale, 2020	0.68	0.68	0.78	0.78	NA	NA	0.68	0.68

Table 2 shows [9] that the frequency of the deck right above Pier S-8 depends on the level of excitation and varies from 0.78 Hz to 1.26 Hz for the longitudinal direction and from 0.68 Hz to 0.93 Hz for the transverse direction. It is worth noting that the results were somewhat close to each other except for the last one obtained for the 2020 Ferndale earthquake. This was attributed [9] to the nonlinear

performance of the bridge. This study is focused on data collected by Sensors 10 and 11, which are shown in bold in Table 2. They correspond to deck accelerations above Pier S-8. As presented in Figure 2, Sensor 10 is oriented in the transverse direction, whereas Sensor 11 is oriented in the longitudinal direction.

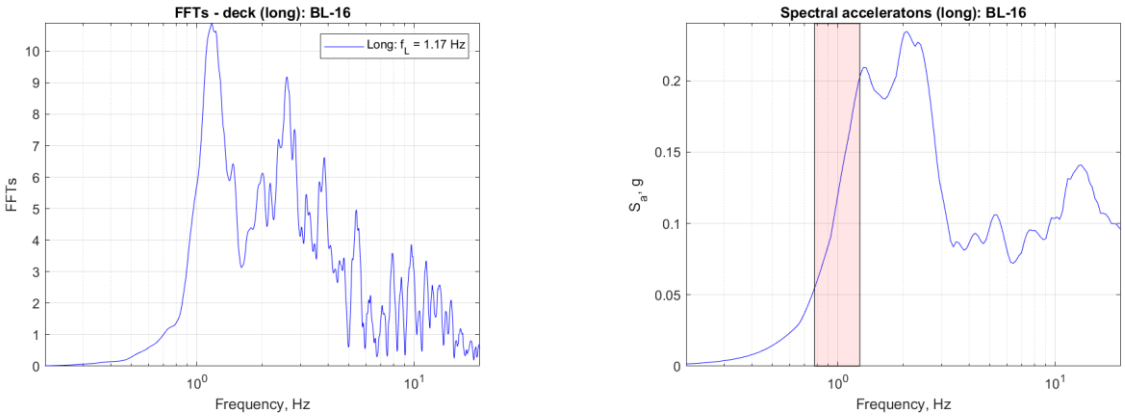

Deck: longitudinal axis (Sensor 11) Pier: longitudinal axis (Sensor 9)

Figure 3. – **FFTs of the deck and spectral accelerations on Pier S-8: longitudinal axis during Event Bl-16.**

Figure 3 provides the deck's Fast Fourier Transforms (FFTs) and spectral accelerations on Pier S-8 in the longitudinal direction. The shadowed zone in the right image corresponds to the range of the resonant frequency variability estimated in [9]. Both plots show the bridge's response recorded during the 2016 Blue Lake earthquake (Event BL-16 in Table 2). The resonant frequency was estimated at 1.17 Hz, which remains within the frequency variability range of (0.78 Hz ÷ 1.26 Hz) reported in [9].

Figure 4 presents the bridge's response during the same seismic event in the transverse direction. Similar to Figure 3, the shadowed zone corresponds to the variability range of the resonant frequencies adapted from [9] without an outlier. The range of frequency variability is much narrower in the transverse direction than in the longitudinal direction (the right images in Figure 4 and Figure 3, respectively). The resonant frequency in the transverse direction was estimated at 0.87 Hz, which remains within the frequency variability range of (0.68 Hz ÷ 0.93 Hz) reported earlier [9].

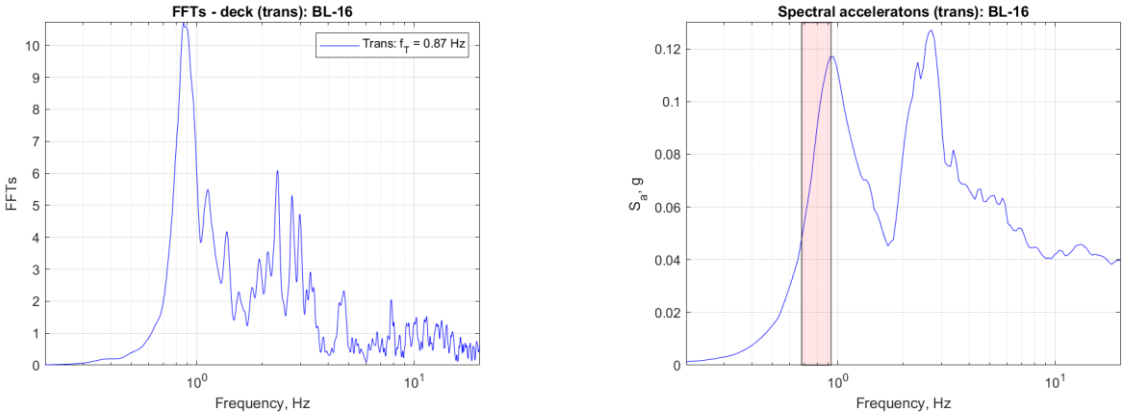

Deck: transverse axis (Sensor 10) Pier: transverse axis (Sensor 8)

Figure 4. – **FFTs of the deck and spectral accelerations on Pier S-8: transverse axis during Event Bl-16.**

These results are presented for Sensors 10 and 11, located on the deck supported by Pier 8. Sensors 12 and 13 were installed on the deck between Pier S-8 and Pier S-9 with an expansion joint on the former side. The FFTs for these two sensors are presented in Figure 5. The resonant frequency in the longitudinal direction was estimated at 1.28 Hz, which is slightly higher than the frequency variability range of (0.78 Hz ÷ 1.26 Hz) reported in [9]. It is worth noting that these sensors were not used in the earlier analysis [9], and this small discrepancy is considered acceptable. The resonant frequency in the transverse

direction was estimated at 0.87 Hz, which remains within the frequency variability range of (0.68 Hz ÷ 0.93 Hz) reported earlier [9].

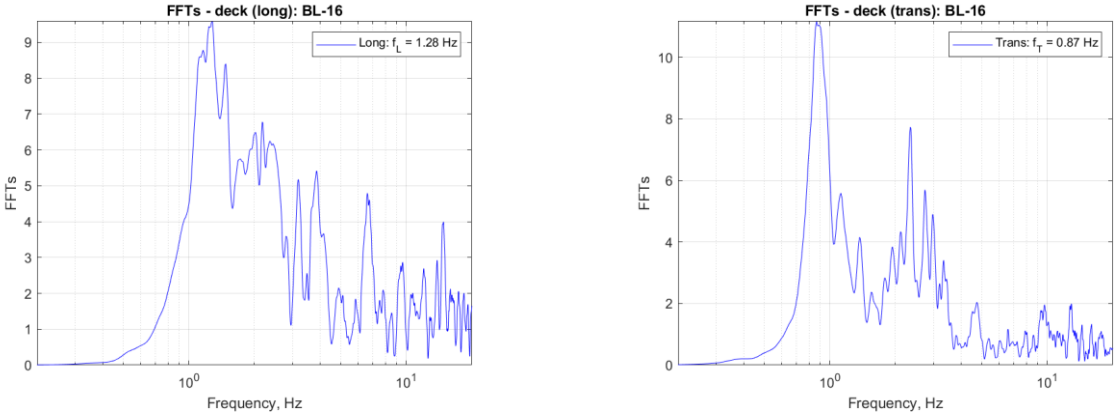

Deck: transverse axis (Sensor 13) Pier: transverse axis (Sensor 12)

Figure 5. – **FFTs of the deck between Pier S-8 and Pier S-9: longitudinal and transverse directions during Event Bl-16.**

The FFTs and spectra for the 2018 Humboldt Hill earthquake are provided in Figure 6 and Figure 7 for the longitudinal and transverse directions of the bridge, respectively. The resonant frequency was estimated at 1.14 Hz in Figure 6, which remains within the frequency variability range of (0.78 Hz ÷ 1.26 Hz) reported in [9]. Based on the results shown in Figure 7, the resonant frequency in the transverse direction was estimated at 0.93 Hz, which remains within the frequency variability range of (0.68 Hz ÷ 0.93 Hz) reported earlier [9].

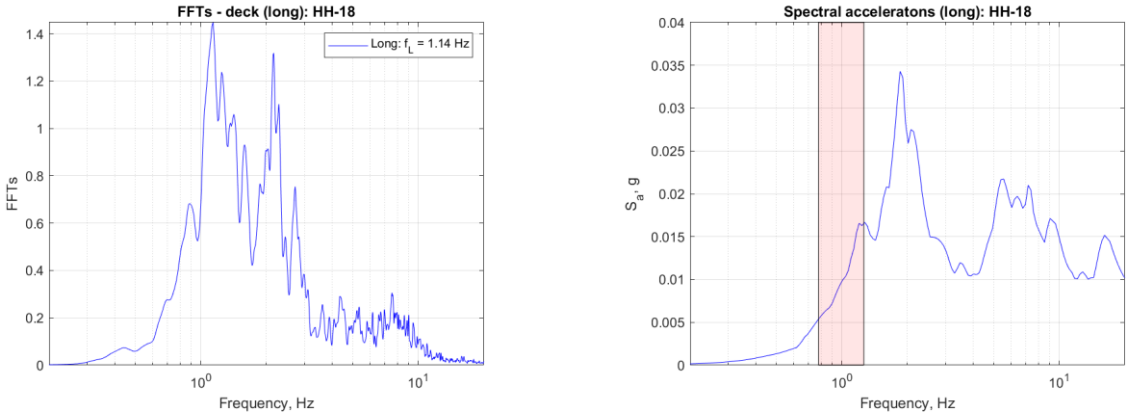

Deck: longitudinal axis (Sensor 11) Pier: longitudinal axis (Sensor 9)

Figure 6. – **FFTs of the deck and spectral accelerations on Pier S-8: longitudinal axis during Event HH-18.**

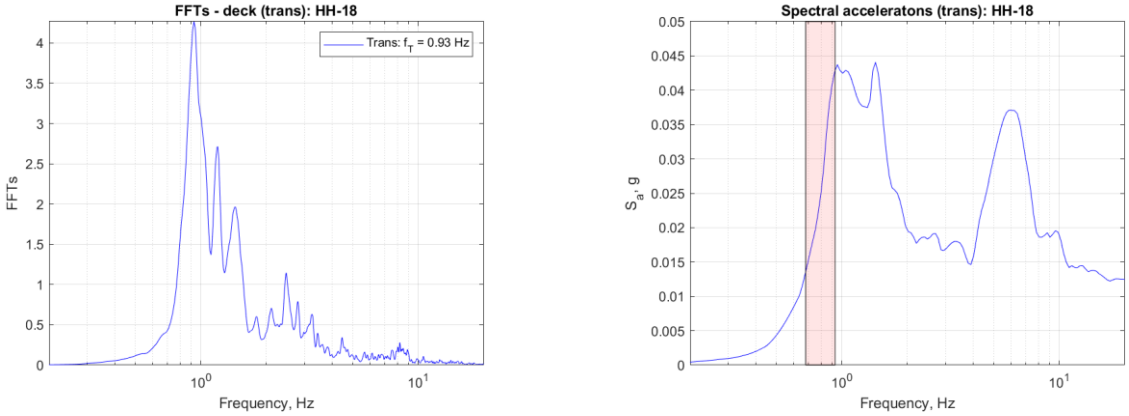

Deck: transverse axis (Sensor 10) Pier: transverse axis (Sensor 8)

Figure 7. – **FFTs of the deck and spectral accelerations on Pier S-8: transverse axis during Event HH-18.**

The FFTs of the deck between Pier S-8 and S-9 (deck#8 when counted from Pier S-1 toward Pier S-9) are presented in Figure 8. The resonant frequency was estimated at 1.21 Hz in Figure 8, which remains within the frequency variability range of (0.78 Hz ÷ 1.26 Hz) reported in [9]. Based on the results shown in Figure 9, the resonant frequency in the transverse direction was estimated at 0.93 Hz, which also remains within the frequency variability range of (0.68 Hz ÷ 0.93 Hz) [9].

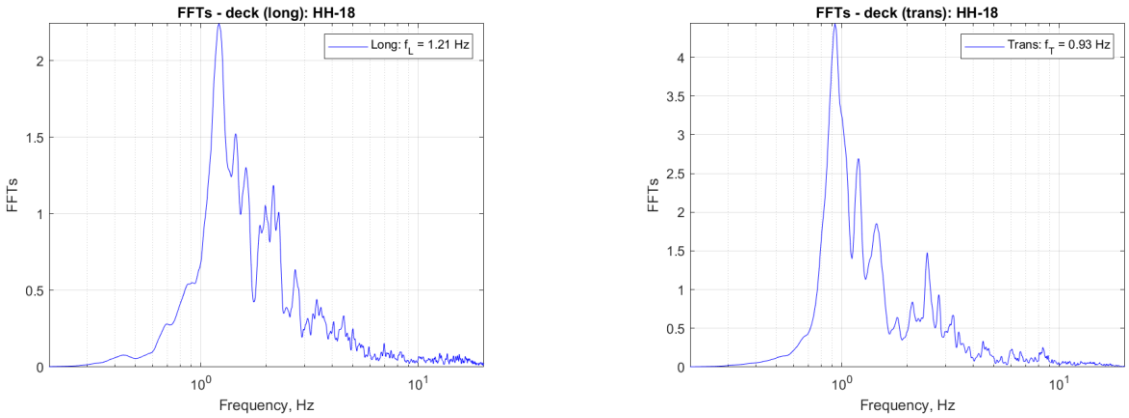

Deck: transverse axis (Sensor 13) Pier: transverse axis (Sensor 12)

Figure 8. – **FFTs of the deck between Pier S-8 and Pier S-9: longitudinal and transverse directions during Event HH-18.**

An example of the bridge's response to one more event is shown in Figure 9 and Figure 10. As shown in these plots, in the case of the March 9, 2023 Ferndale earthquake, the resonant frequencies were slightly greater than those reported earlier [9].

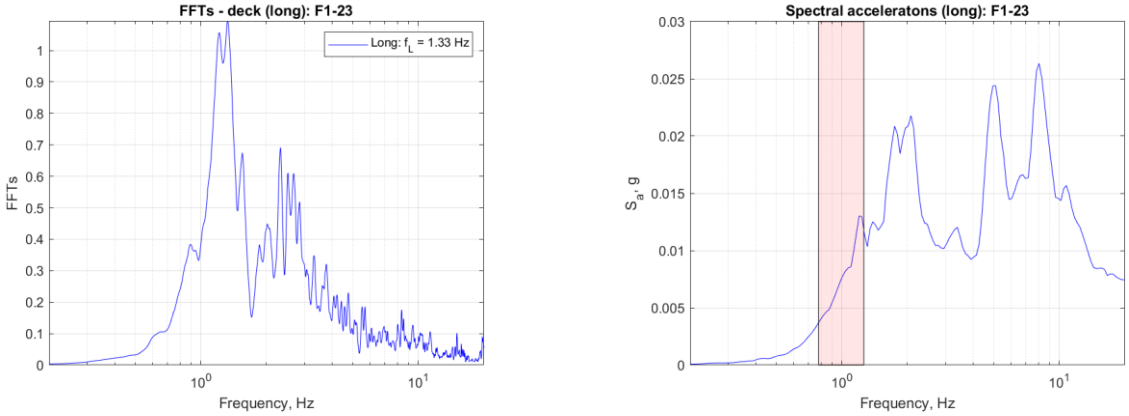

Deck: longitudinal axis (Sensor 11) Pier: longitudinal axis (Sensor 9)

Figure 9. – **FFTs of the deck and spectral accelerations on Pier S-8: longitudinal axis during Event F1-23.**

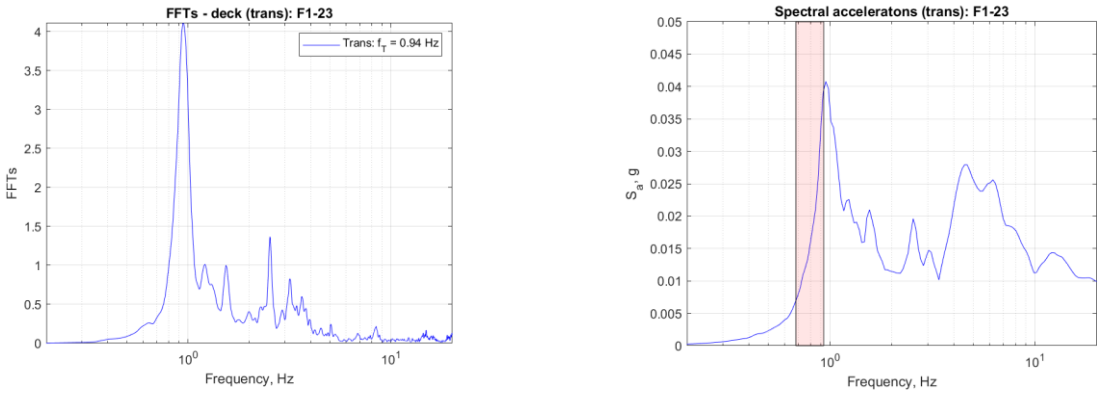

Deck: transverse axis (Sensor 10) Pier: transverse axis (Sensor 8)

Figure 10. – **FFTs of the deck and spectral accelerations on Pier S-8: transverse axis during Event F1-23.**

The results for the deck (deck#7) right above Pier S-8 are shown in Figure 9 and Figure 10. The results for the neighboring deck (deck#8) are shown in Figure 11.

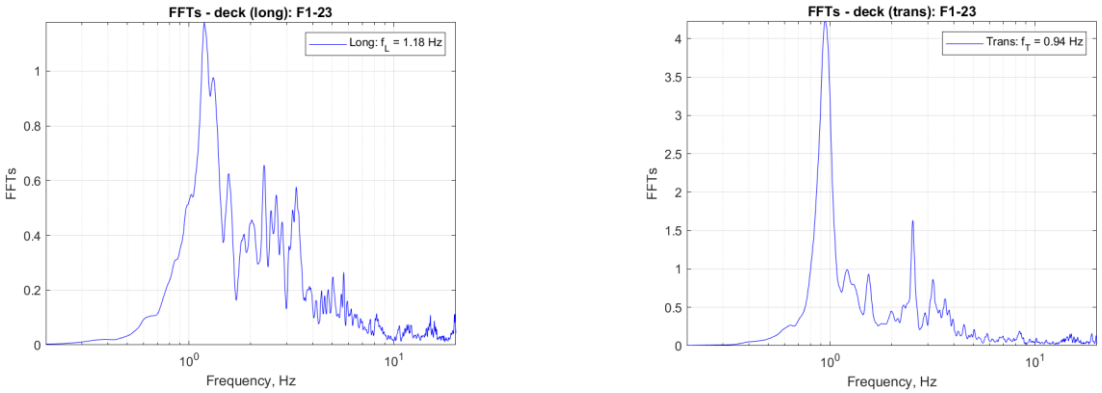

Deck: transverse axis (Sensor 13) Pier: transverse axis (Sensor 12)

Figure 11. – **FFTs of the deck between Pier S-8 and Pier S-9: longitudinal and transverse directions during Event F1-23.**

Figure 12 summarizes the estimated resonant frequencies for both decks. The shadowed boxes correspond to the frequency variability ranges published earlier [9]. This paper utilized a new set of data, and it shows that the frequencies are closer to the high end of the respective ranges, which might be related to the bridge's ongoing reinforcements, interactions between the decks, and other nonlinearities.

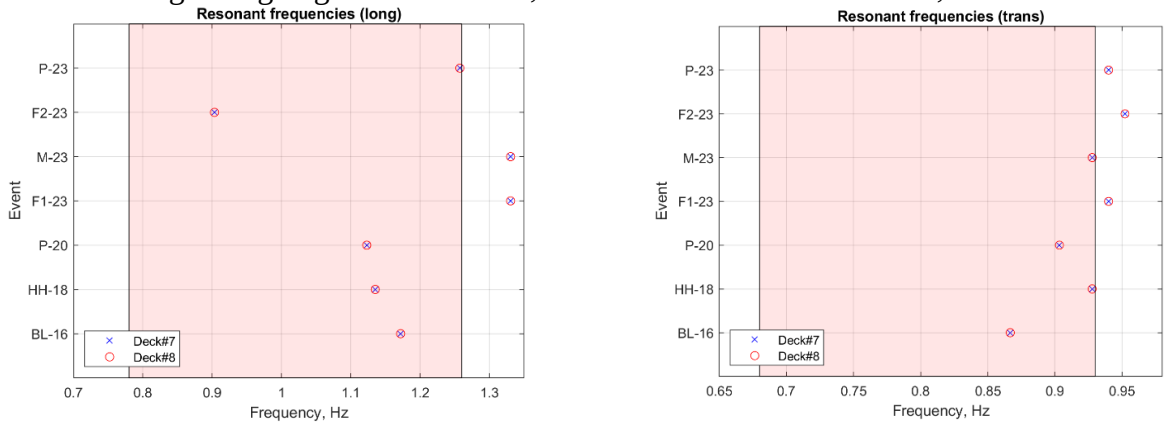

Longitudinal (Sensors 11 and 13) Transverse (Sensor 10 and 12)

Figure 12. – **Summary of the estimated resonant frequencies for two neighboring decks.**

Based on the results of this paper and the previous publication [9], it can be concluded that the resonant frequencies of the bridge can greatly depend on the intensity of the event and its frequency content. The bridge's response is nonlinear because of the presence of the seismic isolators, expansion joints, and overall nonlinear performance of the concrete support structure and the decks. To separate the effects from each other and investigate the benefits of each device in detail, having more extensive instrumentation is beneficial. For example, the residual displacement between the decks cannot be obtained in a reliable way from the acceleraton data. Therefore, having position transducers would be beneficial for that.

5. Conclusions

Because of the expansion joints, the seismic isolators, the deck's material, and the material of the supporting piers and cracking of concrete elements, the bridge's structural performance is nonlinear. As a result, there is a large variability in the dominant frequency of the bridge's response. It was reported earlier [9] for a set of earthquakes before 2014. The large variability of the resonant frequencies in both longitudinal and transverse directions is confirmed again for a new set of seismic events after 2014. Based on the results of this work, it was concluded that the resonant frequencies of the bridge can greatly

depend on the intensity of the event and its frequency content. The need for more extensive instrumentation to investigate the benefits of the seismic isolation and expansion joints is shown. Position transducers could be beneficial for measuring residual displacements or impact loading when the clearance in the expansion joint is obstructed or blocked. The sensing technology is rapidly progressing, and new sensors are coming to market (see [23] as an example) that can enrich data collection and expand the structural health monitoring of bridges in a significant way.

6. Acknowledgements

Special thanks are due to Sensor Fusion and Monitoring Technologies, LLC (USA) for partially sponsoring the analysis of the strong motion data.

References

1. *Rashidov, T.; Baybulatov, K.; Bekmirzayev, D.;Takhirov, S.; Gayibov, J.; and Nishonov, N.* (2020). Comprehensive Program on Structural Assessment of Bridges in Uzbekistan. 17th World Conference on Earthquake Engineering, 17WCEE, Sendai, Japan - September 13th to 18th 2020.
2. *Baybulatov, H.; Gayibov, J., Berdibaev, M.* (2019): Results of diagnostics of bridge structures, subject to repair and reconstruction works on roads of the Fergana region. Problems on Mechanics (ISSN 2010-7250), 2019, No. 1, pp. 71-74 (in Russian).
3. *Takhirov, S., Nugmanova, A., Koshimkhanov, D.* (2023). Application of Multi-Sensor Road Feature Detection and Mapping in Kazakhstan and Development of Pole Detection and Analysis Procedure. Proceedings of ISAS 2023 - 7th International Symposium on Innovative Approaches in Smart Technologies.
4. *Takhirov, S., and Robert Kayen, K.* (2021). Point Clouds of Bridge Generated by Terrestrial Laser Scanner and Images via Structure from Motion Technique: Comparison Study. HORA-2021, the 3rd International Congress on Human-Computer Interaction, Optimization and Robotic Applications, June 11-13, 2021, Turkey.
5. *Rashidov, T., Takhirov, S., Gilani, A., and Kudratov, S.* (2020). Automated meshing and finite element modelling of bridges from point clouds with subsequent model updating based on ambient vibration data. The 17th World Conference on Earthquake Engineering, 17WCEE, Sendai, Japan, September 13-18 2020.
6. *Shermukhamedov, U.Z., Ergashev, Z.Z., Takhirov, S.M., Abdullaev, A.A.* (2023). Improving reliability of uzbekistan's transport infrastructure facilities under impact of natural hazards by analysis of its vulnerability, monitoring and modeling. COMPDYN Proceedings, 2023.
7. https://www.strongmotioncenter.org/cgi-bin/CESMD/stationhtml.pl?staID=CE89686&network=CGS (last accessed on 04/17/2024).
8. *Wang, N., Elgamal, A., Lu, J.* (2022). Seismic response of the Eureka Channel Bridge-Foundation system, Soil Dynamics and Earthquake Engineering, Volume 152, 2022, 107015, ISSN 0267-7261, https://doi.org/10.1016/j.soildyn.2021.107015.
9. *Taciroglu, E., Shamsabadi, A., Abazarsa, F., Nigbor, R.L., Ghahari, F.S.* (2014). Comparative Study of Model Predictions and Data from Caltrans-CGS Bridge Instrumentation Program: A Case Study on the Eureka-Samoa Channel Bridge. Final Report No. CA14-2418 for California Department of Transportation (Caltrans), Department of Civil and Environmental Engineering, University of California, Los Angeles, March 2014.
10. https://www.strongmotioncenter.org/NCESMD/photos/CGS/lllayouts/ll89686.pdf (last accessed on 04/21/2024). MathWorks. Matlab Version R2020a; 2020.
11. *Dhar, Sreya, Dasgupta, Kaustubh* (2019). Seismic Soil Structure Interaction for Integral Abutment Bridges: a Review. Transportation Infrastructure Geotechnology. VL.6, IS.4, pp: 249-267.
12. *Wang, N., Elgamal, A., and Shantz, T.* (2017). Recorded seismic response of the Samoa Channel Bridge-foundation system and adjacent downhole array. Soil Dynam Earthq Eng 2017; 92: 358–76.
13. *Kim Y, Jeong S.* (2011). Analysis of soil resistance on laterally loaded piles based on 3D soil–pile interaction. Comput Geotech;38(2):248–57.
14. *Shirgir, V., Ghanbari, A., & Shahrouzi, M.* (2016). Natural Frequency of Single Pier Bridges Considering Soil-Structure Interaction. Journal of Earthquake Engineering, 20(4), 611–632. https://doi.org/10.1080/13632469.2015.1104754.
15. *Domaneschi, M., Martinelli, L.* (2014). Extending the Benchmark Cable-Stayed Bridge for Transverse Response under Seismic Loading. March 2014. Journal of Bridge Engineering 19(3), DOI: 10.1061/(ASCE)BE.1943-5592.0000532.
16. *Chen, X., Xu, G., Lin, C., Sun, H., Zeng, X., Chen, Z.* (2021). A comparative study on lateral displacements of movable T-deck and Box-deck under solitary waves, Structures, Volume 34, 2021, Pages 1614-1635, ISSN 2352-0124, https://doi.org/10.1016/j.istruc.2021.08.084.

17. *Malhotra, P.K., Huang, M.J., Shakal, A.F.* (1995). Seismic interaction at separation joints of an instrumented concrete bridge. Earthq Eng Struct Dynam. 1995; 24(8): 1055–67.
18. *Li, J.; Wen, F.; Chen, J.; Yang, C.; Du, W.; Xu, L.; Li, P.* (2023) Experimental Study of Bridge Expansion Joint Damage Based on Natural Frequency. Sensors, 23, 6437. https://doi.org/10.3390/s23146437.
19. *Busel, A., Krotau, R.* (2016). The Design and Composition of Expansion Joints on Big-span Bridges with Intensive Heavy-duty Traffic, Transportation Research Procedia, Volume 14, Pages 3953-3962, ISSN 2352-1465, https://doi.org/10.1016/j.trpro.2016.05.488.
20. *Li, J., Wen, F., Chen, J., Yang, C., Du, W., Xu, L., Li, P.* (2023). Experimental Study of Bridge Expansion Joint Damage Based on Natural Frequency. Sensors (Basel). Jul 16;23(14):6437. doi: 10.3390/s23146437. PMID: 37514731; PMCID: PMC10384253.
21. https://www.strongmotioncenter.org (search results for station No 89686, last accessed on 04/17/24).
22. *Takhirov S., Gilani A., Allen J.* (2020). Evaluation of Cost-Effective Lidar Scanner for Deformation Monitoring of Buckling Restrained Brace in a Full-Scale Seismic Qualification Experiment. In the Proceedings of 8th International Conference on Advances in Experimental Structural Engineering. Christchurch, New Zealand, 3-5 February 2020.

CALCULATION OF NATURAL FREQUENCIES OF MULTI-STORY BUILDINGS UNDER TRANSVERSE VIBRATIONS WITHIN THE FRAMEWORK OF A CONTINUUM PLATE MODEL

Usarov M.K.[1], Usanov F.A.[1], Askarkhodjaev Sh. I.[1]
[1]Institute of Mechanics and Seismic Stability of Structures, Tashkent, Uzbekistan
E-mail: umakhamatali@mail.ru

Abstract. *The article is devoted to solving the problem of determining natural frequencies, periods of oscillation and movement of points of a multi-story building, using the resonant method. The dynamic behavior of the building near the resonant regime is described within the framework of a continuum plate model developed within the framework of the biomoment theory of thick plates. The problem is solved using an explicit finite difference method. To compare the numerical results, the same problem was solved within the framework of the plate model of the Timoschenko theory.*

Keywords: *multi-storey building, continuum model, bimoment theory, resonant state, reduced elastic moduli, seismic impact, numerical method.*

1. Introduction.

The development of dynamic spatial models and methods for dynamic calculation of multi-story buildings, the deformation of which is spatial in nature, is one of the urgent problems of the science of structural dynamics and mechanics. In recent years, in the field of seismic resistance of structures, various methods for calculating a building for seismic impacts have been developed, considering various important factors. Such research includes a number of published scientific works.

The study in [1] deals with the issue of determining the natural vibration frequencies of modular buildings. The dependence between the first cross-frequency of one-storey buildings and the frequency of a single block is determined. The article shows the effect of the ratio of rigidity of horizontal and vertical elements of a building on the value of the first natural vibration frequency. The analytical formula for the determination of the first natural vibration frequency is proposed and substantiated.

Reference [2] investigated the natural frequency and modes of vibration of a multi-story office building with a foundation system and analyzed the influence of the vibration mode on the dynamic characteristics of the structure.

In [3], the calculation of a multi-storey monolithic concrete building for an earthquake is discussed. The problem is solved in the time domain using the direct dynamic method.

The study in [4] presents the results of a dynamic analysis of an 11-story steel moment-resisting building with sliding pin connections as beam-column connections, considering influential self-centering factors such as the continuity of MRFs and gravity columns and column base, and the flexibility of the diaphragm.

Article [5] proposes a model for calculating the seismic resistance of a building, considering its self-variable rigidity during an earthquake; the model takes into account the soil characteristics of the region, architectural and design features, and the general stage of construction.

The study in [6] presents the results of numerical observations of the behavior of a multi-story reinforced concrete wall frame structure under a special combination of loads, considering the seismic impact of a destructive earthquake. Article [7] considers the situation when a multi-storey building is subject to equivalent static and dynamic analysis. For the purpose of the study, the building was modeled using SAP2000 software. For dynamic analysis, a building was subjected to ground motion to obtain the building's response. The results are presented in displacement form.

Reference [8] describes the modified dynamic inelastic analysis, a method that can help account for the dynamic characteristics of structures using mode shapes during inelastic analysis. The steps to perform a modified dynamic inelastic analysis are described, and the proposed method is applied to examples of seven- and fifteen-story buildings. A common practice is to design high-rise buildings in such a way that the safety margin available after the formation of plastic hinges is designed to withstand earthquakes, avoiding the collapse of structures [9]. Pushover analysis is commonly used for static inelastic analysis of a structure [10]. In this method, the lateral load is increased with the same profile to determine the inelastic capacity of the structure. At each increment of lateral load, the plastic hinge sequence and the elastoplastic behavior of each element were determined without dynamic consideration of the structure [11].

In [12-14], the behavior and stress-strain state of structures and soils were investigated, considering the nonlinear deformation of soils around the structures and showed the existence of a near-contact layer of soil near the contact, in which it can play the role of self-protection for structures. To solve the problems, the numerical finite difference method was used and results were obtained for elastoplastic interaction problems taking into account dynamic processes for the design of structures and soil.

Articles [15-16] are devoted to dynamic calculations of elements of a box-shaped structure of buildings for seismic resistance, considering its spatial operation under the action of dynamic influences specified by the movement of their lower part by a sinusoidal law. The equations of motion are given for each of the plate and beam elements of the box-shaped building structure based on the Kirchhoff-Love theory. Expressions are given for forces, moments and stresses of plate elements that balance the movement of box elements, as well as boundary conditions and conditions for full contact through displacements and force factors in the contact zones of plate and beam elements.

References [17-18] are devoted to the dynamic calculation of box-shaped building structures for seismic resistance, considering the spatial operation of box-shaped elements under the influence of dynamic influence. The development of spatial calculations and the study of vibrations of box-type structural elements taking into account various factors is an urgent task in structural mechanics.

The studies in [19-20] are devoted to the numerical solution of the problem of transverse vibrations of a multi-story building within the framework of a continuous plate model of a solid slab under seismic influence. As a dynamic model of the building, a cantilever anisotropic plate is proposed, the theory of which was developed within the framework of the three-dimensional dynamic theory of elasticity and considers not only structural forces and moments but also bi-moments.

In [21], the development of the bi-moment theory and method for calculating thick plates within the framework of the three-dimensional theory of elasticity are discussed. The presented basic relationships and equations of motion of the plate are constructed considering the forces, moments and bimoments arising due to the nonlinearity of the law of distribution of displacements and stresses along the thickness of the plate. Article [22] proposes a dynamic continuous plate model of a multi-story building in the form of a cantilever orthotropic slab, developed within the framework of the Timoshenko plate theory, which describes seismic vibrations of buildings. Formulas are given for determining the reduced moduli of elasticity, shear, and density of a plate model of a building. Transverse natural and forced vibrations of a nine-story building under magnitude nine seismic impacts are considered.

Seismic vibrations of a multi-story building within the framework of a plate model are considered in a rectangular Cartesian coordinate system x_1, x_2 and z. For convenience, the origin of coordinates is located in the lower left corner of the middle surface of the continuum plate model of a multi-story building. Let us direct the OX1 and OX2 axes along the length and height, and the OZ axis along the width of the plate model of a multi-story building.

The problem of transverse vibrations of a multi-story building is an antisymmetric problem of the bimoment theory of plate structures, developed in [23]. The system of equations for transverse vibrations consists of six equations regarding shear forces, bending and torque moments and bimoments, as well as three more kinematic equations obtained by satisfying the conditions on the front surfaces of plate structures.

2. Materials, methods and object of study.

In the calculations, we assume zero initial conditions of the problem. The geometric characteristics of the room panels and the external dimensions of the buildings must be specified as initial data. To obtain specific numerical results, the mechanical characteristics of the structure of the considered plate model of a multi-story building must also be known.

Determination of the reduced density and elasticity moduli of the plate model according to the method given in [19]. The reduced density of the building is determined by the following formula:

$$m_{\text{пр}} = \rho_{\text{пл}} V_1 = \rho_{\text{пр}} V_0 . \tag{1}$$

Here V_1 – volume of slabs forming one floor of a building. V_0 – volume of one floor of the building. Considering the geometric parameters of the building in question, to calculate these volumes, we obtain the following formulas

$$V_0 = ab_1 H,\ V_1 = ab_1 h_2 + (n-2)Hb_1 h_2 + aHh_2, \tag{2}$$

Here a, H – building length and width; b_1 – height of one floor of a building; k – number of internal transverse walls of the building; h_1 - thickness of external load-bearing walls; h_2 – thickness of internal walls; h_{nep} – floor thickness.

In general, the given elastic characteristics and density of the building are determined by the following formulas:

$$\begin{aligned} &E_1^{\text{пр}} = \zeta_{11} E_0,\ E_2^{\text{пр}} = \zeta_{22} E_0,\ E_3^{\text{пр}} = \zeta_{33} E_0, \\ &G_{12}^{\text{пр}} = \zeta_{12} G_0,\ G_{13}^{\text{пр}} = \zeta_{13} G_0, G_{23}^{\text{пр}} = \zeta_{23} G_0,\ \rho_{\text{пр}} = \rho_0 \varsigma_0 . \end{aligned} \tag{3}$$

It should be noted that the coefficient values ξ_{11}, ξ_{22}, ξ_{33}, ξ_{12}, ξ_{13}, ξ_{23}, ζ_0 for each cell (room) of a discrete part of the building are determined as functions of two spatial variables, E_0, G_0 – moduli of elasticity and shear of the strongest load-bearing panel of a cell of a discrete part of a building.

Let us write the formulas for determining coefficients ξ_{11}, ξ_{22}, ξ_{33}, ξ_{12}, ξ_{13}, ξ_{23}, ζ_0 of reduced moduli of elasticity of a discrete part of the building:

$$\begin{aligned} &\xi_{11} = \alpha \frac{S_{11}}{S_{01}},\quad \xi_{22} = \alpha \frac{S_{22}}{S_{02}},\quad \xi_{33} = \alpha \frac{S_{33}}{S_{03}},\ \xi_{12} = \alpha \frac{S_{12}}{S_{01}}, \\ &\xi_{13} = \alpha \frac{h_{nep}}{b_1} \lambda^*,\ \ \xi_{23} = \alpha \frac{h_2}{a_1},\ \ \zeta_0 = \frac{V_1}{V_0}. \end{aligned} \tag{4}$$

Here S_{01}, S_{02}, S_{03} – cross-sectional area of the building in three coordinate planes of one floor of the building; S_{11}, S_{22}, S_{33} – total cross-sectional areas of slabs in coordinate planes forming one floor of the building; λ^* – coefficient characterizing the voids in the cross section of the floor slab. Coefficient

α is determined depending on the cell-type structure of the building structure.

Depending on the size of the slabs, rooms, and the building itself, the above areas are determined using the methodology presented in [21], in the following form:

$$S_{01} = E_0 b_1 H, \quad S_{02} = E_0 a H, \quad S_{03} = E_0 a b_1, \tag{5}$$

$$S_{11} = b_1 h_2 E_b^{(2)} + H h_{nep} E_{nep}, \quad S_{12} = b_1 h_2 E_b^{(2)},$$
$$S_{22} = a h_2 E_b^{(2)} + (k-2) H h_2 E_b^{(2)}, \quad S_{33} = a h_2 E_b^{(2)} + (k-2) b_1 h_2 E_b^{(2)}. \tag{6}$$

Here G_{nep} – building floor shear modulus; G_2 – internal wall shear modulus; $E_b^{(2)}$ – modulus of elasticity of internal walls; E_{nep} – floor elastic modulus.

We assume that the external walls consist of reinforced concrete with an elastic modulus $E = 20000\text{MPa}$, density $\rho = 2500\ \text{kg/m}^3$, Poisson's ratio $\nu = 0.3$.

We consider the internal walls to consist of expanded clay concrete with the following physical characteristics: modulus of elasticity $E = 7500\text{MPa}$, density $\rho = 1200\ \text{kg/m}^3$, Poisson's ratio $\nu = 0.3$.

The results of calculations of forced vibrations of a building within the framework of a thick plate model are presented for the following sizes of building slabs:

$$h_1 = 0.40\,м, \quad h_2 = 0.25\,м, \quad h_{\text{пер}} = 0.2\,м, \quad a_1 = 5\,м, \quad b_1 = 3\,м,$$

The given elastic characteristics and densities of a multi-story building are determined by formulas (1) - (6).

Tables 1 and 2 show the elastic characteristics of the building and the coefficients to determine the given elastic characteristics.

Table 1

Reduced elastic characteristics of the building and coefficients to determine the reduced elastic characteristics

Thickness	Coefficients and elastic characteristics of the building						
H (м)	ξ_0	ξ_{11}	ξ_{12}	ξ_{13}	ξ_{22}	ξ_{23}	ξ_{33}
11	0.102	0.129	0.095		0.164		
13	0.101	0.114	0.081		0.149		
15	0.100	0.103	0.070		0.138		
18	0.099	0.092	0.058		0.127		
20	0.098	0.086	0.053	0.067	0.121	0.05	0.102
22	0.098	0.081	0.048		0.116		
24	0.097	0.077	0.044		0.112		
26	0.097	0.074	0.040		0.109		
28	0.096	0.071	0.038		0.106		

Consequently, the given building characteristics depend on the initial data and vary greatly depending on the specific task at hand. The height and length of a multi-story building are assumed to be $b = nb_1$ and $a = 30m$, respectively, and the length, width, and thickness of the foundation are $a_0 = 40m, b_0 = 25m$, and $H_0 = 1m$. Building width H varies. As the value of the dimensionless frequency of external influence ν_0 approaches dimensionless natural frequency p_1, the values of displacements, stresses, forces, and moments increase sharply, which indicates a gradual transition to the resonant mode.

Table 2

Given elastic characteristics of the building

Thickness	Elastic characteristics of the building					
H (м)	**E_1**	**E_2**	**E_3**	**G_{12}**	**G_{13}**	**G_{23}**
11	1545	1965	1220	458.2	320.0	240.0
13	1369	1789		215.4	177.8	133.3
15	1240	1660		129.2	123.1	92.31
18	1100	1520		82.35	94.12	70.59
20	1030	1450		60.00	76.19	57.14
22	972.7	1393		45.82	64.00	48.00
24	925.0	1345		36.21	55.17	41.38
26	884.6	1305		29.37	48.48	36.36
28	850.0	1270		24.32	43.24	32.43

3. Statement of the problem.

The seismic impact on a multi-story building is set by a given law in the form of acceleration of the base of a multi-story building. Let us assume that the base points move by the given law of movement $u_0(t)$ with acceleration $\ddot{u}_0(t)$, and the lower part of a multi-story building moves in the horizontal direction along with the base.

The movement of the base of a multi-story building $\ddot{u}_0(t)$ is given by the harmonic law in the following form:

$$\ddot{u}_0(t) = a_0 \cos(\omega_0 t), \tag{7}$$

Here $a_0 = k_c g$ - maximum acceleration and $\omega_0 = 2\pi\nu_0$ – circular frequency of the soil base, k_c and ν_0 - earthquake magnitude coefficient and natural frequency of external influence, respectively.

From the differential dependence of the displacement u_0 in time (2), it is possible to determine the displacement of the base of the building in the following form:

$$u_0(t) = \frac{A_0}{2}(1 - \cos(\omega_0 t)). \tag{8}$$

Here A_0 – amplitude of movement of the base, determined by the following formula:

$$A_0 = \frac{2k_c g}{\omega_0^2}. \tag{9}$$

Note that the seismicity coefficient of a magnitude nine earthquake is $k_c = 0{,}4$.

4. Analysis of numerical results.

Below we present graphs of changes in normal and general displacements, from which the values of natural frequencies are determined, see Table 3. Graphs of changes in the values of displacement and stress were obtained for transverse vibrations of multi-story buildings in the resonant case during an earthquake of magnitude 8. $(k_c = 0.2)$. Let us present the results of calculations of natural frequencies, displacements, and stresses for a 9-story building.

Calculations of displacement and stress were performed for the following values: frequency of external influence $\nu_0 = 3.2$ Hz. The amplitude of the external impact is determined for a nine-story building during an eight-magnitude earthquake $(k_c = 0.2)$ according to the formula $A_0 = \frac{2k_c g}{\omega_0^2} = \frac{2 \cdot 0.2 \cdot 9.8}{20.01^2} = 0.0097\text{m}.$

Figure 1 shows graphs of changes over time *t* of normal displacement values $\tilde{r}$ at the highest point of a nine-story building near resonant oscillations with a frequency p_1=3.301 Hz.

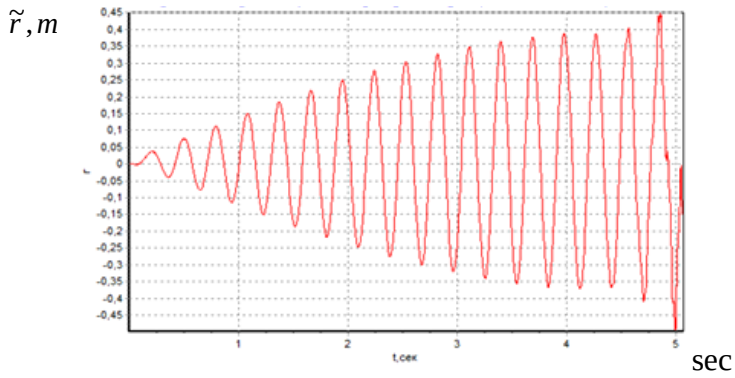

Figure 1 – **Graphs of changes over time *t* of normal displacement values $\tilde{r}$ at the highest point of a nine-story building near resonant oscillations with a frequency p_1=3.301 Hz.**

As seen from Figure 1, when the external impact frequency values ν_0 are very close to the natural frequency value p_1, then there is an infinite increase in displacements.

Figure 2 shows graphs of changes in the values of the generalized transverse shear function $\tilde{\psi}_2$ at the midpoint of the upper level of a nine-story building when oscillating with a frequency p_1=3.201 Hz (a beating state).

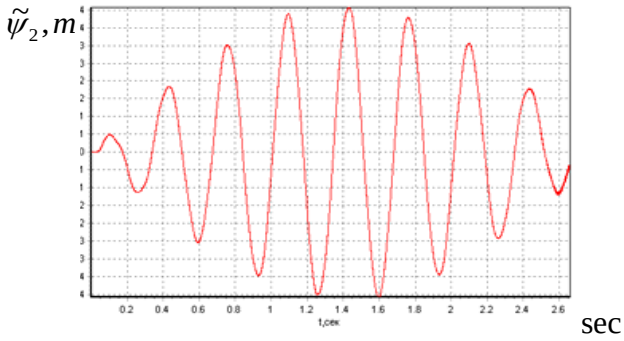

Figure 2 – **Law of change in the generalized transverse shear function $\tilde{\psi}_2$ at the midpoint of the upper level of a nine-story building when oscillating with a frequency p_1=3.201 Hz (a beating state).**

According to the graph, it can be seen that for a nine-story building, the displacement value at the edges of the upper level of the ninth floor of the building is $\tilde{\psi}_2$=4 cm.

Figure 3 shows a graph of changes over time *t* in normal stress values σ_{11} at the lowest point of a nine-story building near resonant oscillations with a frequency p_1=3.401 Hz.

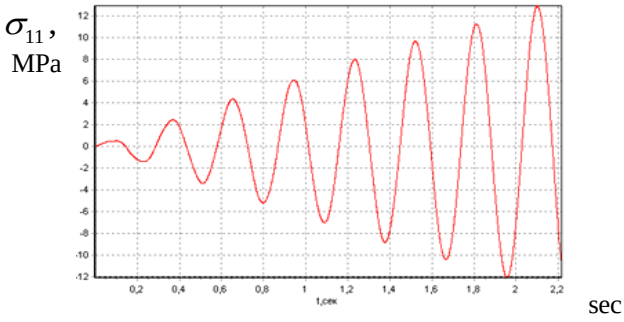

Figure 3 - **Graphs of changes in normal stress σ_{11} in a resonant case in time, in the middle of the first floor of a nine-story building.**

As seen from Figure 3, when the external impact frequency values ν_0 are very close to the natural frequency value p_1, then there is an infinite increase in stress σ_{11}.

Figure 4 shows the law of change over time *t* of normal stress values σ_{22} at the lowest point of a nine-story building near resonant oscillations with a frequency p_1=3.401 Hz.

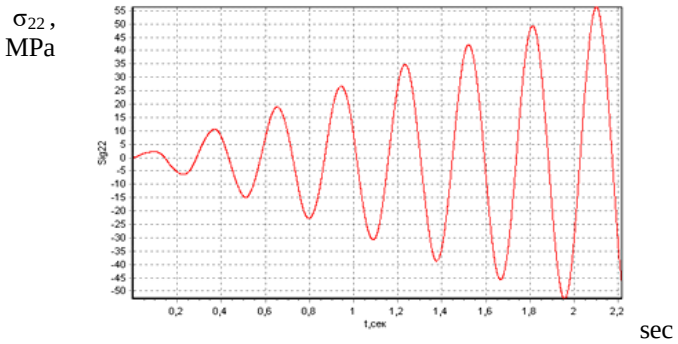

Figure 4 - **Graphs of changes in normal stress σ22 at a resonant time event in the middle of the first floor of a nine-story building.**

As seen from Figure 4, when the external impact frequency values ν_0 are very close to the natural frequency value p_1, then there is an infinite increase in stress σ_{22}.

Let us present the results of calculations of frequency and oscillation periods for nine to twenty-story buildings near the resonant mode. The dynamic characteristics of a multi-story building are determined by the resonance method. The frequency values of external impact, starting from a certain small value, gradually increase. The value of the dimensionless frequency of external impact ω_0 approaches dimensionless natural frequency p_1; this indicates a gradual transition to the resonant mode. Using the finite difference method, a technique for dynamic calculation of multi-story buildings with different numbers of floors was developed. Let us present the results of calculations of the frequency, periods of oscillation, and displacements of points for nine-, twelve-, sixteen- and twenty-story buildings, near the resonant mode.

Table 3 shows the first three values of natural frequencies p_1, p_2, p_3 and periods of natural oscillations T_1, T_2, T_3 of nine-, twelve-, sixteen and twenty-story buildings.

Table 3.

First three natural frequencies p_1, p_2, p_3 and periods of natural oscillations T_1, T_2, T_3 of sixteen- and twenty-storey buildings, depending on three building widths

№	Number of floors	b, m	H, m	p_1, Hz	p_2, Hz	p_3, Hz	T_1,sec	T_2,sec	T_3,sec
1	9	27	11	3.301	11.20	36.55	0.303	0.089	0.027
			13	3.402	11.52	36.85	0.294	0.086	0.027
			15	3.700	12.21	37.65	0.270	0.082	0.027
	12	36	11	1.911	7.702	15.43	0.526	0.130	0.065
			13	2.303	8.201	16.51	0.434	0.122	0.061
			15	2.501	8.600	17.32	0.400	0.116	0.058
2	16	48	13	1.301	5.800	12.50	0.768	0.172	0.080
			15	1.611	6.301	13.22	0.620	0.158	0.075
			18	1.802	6.704	13.91	0.554	0.149	0.071
	20	60	18	0.901	4.304	9.203	1.109	0.232	0.108
			20	1.002	4.503	9.504	0.998	0.222	0.105
			22	1.201	4.601	9.802	0.832	0.217	0.102

Now, we present the results of calculations of forced vibrations of high-rise buildings within the framework of the continuum plate model according to Timoshenko's theory.

Table 4 shows the first three numerical values of the natural vibration frequencies of buildings with the number of storeys 9, 12, 16, 20, using a continuum model of the building.

Table 4.

Natural frequencies of three vibration modes of buildings in the continuum model

№	Number of floors	b, m	H, m	p_1, Hz	p_2, Hz	p_3, Hz	$T_1, \sec$	$T_2, \sec$	$T_3, \sec$
1	9	27	11	0.65	3.15	9.10	1.54	0.32	0.11
2	12	36	13	2.05	3.35	4.65	0.49	0.30	0.22
3	16	48	15	1.4	3.10	3.62	0.71	0.32	0.28
4	20	60	18	1.0	2.52	3.81	1.00	0.40	0.26

Note that the seismicity coefficient of an eight-magnitude earthquake is k_c=0.2

Now we present the results of calculations of displacements, accelerations and stresses obtained during forced vibrations of multi-story buildings and foundations under seismic impacts with an intensity of 9 points, with the frequency of external influence of the soil conditions of our republic. When determining the reduced moduli of elasticity and shear of external walls, taking into account window openings, we apply the methodology given in [15] in the form of approximate formulas:

$$E_1^{\text{given}} = E_1\left(1-\frac{\eta}{\eta_0}\right),\ E_2^{\text{given}} = E_2\left(1-\frac{\eta}{\eta_0}\right),\ \ G_{12}^{\text{given}} = G_{12}\left(1-\frac{\eta}{\eta_0}\right),\ \ G_{13}^{\text{given}} = G_{13}\left(1-\frac{\eta}{\eta_0}\right). \tag{10}$$

where E_1, E_1, G_{12}, G_{13} – elasticity and shear moduli of external walls, η, η_0 - constant odds.

To solve the problem numerically, the finite difference method was chosen. To approximate the derivatives of displacements along spatial coordinates, we will use the formulas of central difference schemes.

We select the calculation steps based on spatial coordinates and time as follows:

$$\Delta x_1 = \frac{a}{N},\ \Delta x_2 = \frac{b}{M},\quad c\Delta t \le \min(\Delta x_1, \Delta x_2)\cdot$$

where introduced $c = \sqrt{E/\rho}$.

Note that in the contact zone of a rigid foundation and a multi-story building, rather large contact compressive and tensile stresses are generated. The height for nine-story, twelve-story and sixteen-story buildings is assumed to be 30 m, 40 m and 51 m, respectively. Calculations were performed for multi-story buildings during magnitude nine earthquakes, which are specified through the corresponding seismicity coefficients ks. In the calculations, the building walls, floors and coverings are considered to consist of reinforced concrete. Let us present the results of stress calculations at the lowest points of load-bearing walls of multi-story buildings.

Calculation results for a 9-story building.

The height and width of the building are assumed to be equal *b*=30 *m*, *a*=30 *m* and *H=13m* respectively. Let us present the numerical results of stresses obtained during transverse vibrations of a 9-story building during a magnitude 9 earthquake.

In Figures 5. and 6 show graphs characterizing changes in the maximum normal voltage σ_{11}, σ_{22} in the middle of the first floor of a nine-story building from time t, corresponding to magnitude nine earthquakes $k_c = 0{,}4$ and $\nu_0 = 2{,}7.$

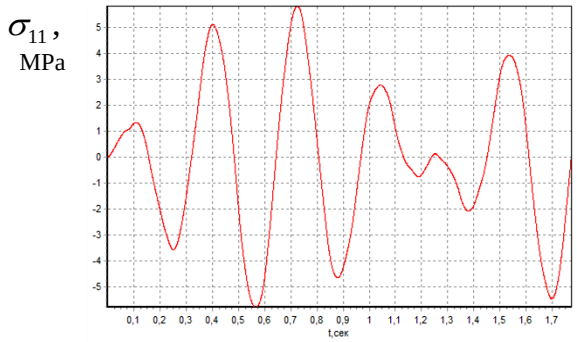

Figure 5 - **Graph of changes in normal voltage σ_{11} in time in the middle of the first floor of a nine-story building.**

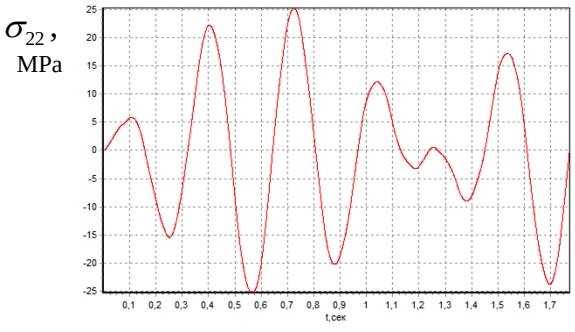

Figure 6 - **Graph of changes in normal voltage σ_{22} in time in the middle of the first floor of a nine-story building.**

Table 5 shows the minimum and maximum stress values obtained during transverse vibrations of a 9-story building.

Table 5.

Values of the first natural frequency, maximum and minimum stresses of a 9-story large-panel building during earthquakes with a magnitude of 7-8-9 points

№	*H, m*	k_s	ν_0, *Hz*	p_0, *Hz*	σ_{11}, MPa		σ_{22}, MPa		$\ddot{\tilde{r}}$, $m/\sec^2$,	
					min	ma x	min	max	min	max
1	13	0.1	2.7	3.05	-2.42	2.43	-9.880	10.70	-7.45	70.1
2		0.2			-4.07	4.07	-20.11	21.20	-14.9	13.3
3		0.4			-6.52	6.55	-25.02	25.03	-30.1	26.9

The height and width of the building are taken to be *b=30 m* and *a=30 m*, respectively. Note that the minimum and maximum values of tangential and normal stresses were found during forced transverse vibrations in the middle and quarter of the length *a = 30 m* of the multi-story high-rise building under consideration.

Calculation results for a 12-story building.

Let us present the numerical results of stresses obtained during transverse vibrations of a 12-story building during a magnitude 9 earthquake. The height and width of the building are taken to be b=40 m and a=30 m H=13, respectively.

Graphs of maximum stresses in the middle of the first floor of a twelve-story building versus time t during magnitude nine earthquakes are presented. $k_c = 0{,}4$.

Figures 7 and 8 show a graph characterizing changes in the maximum normal stress σ_{11}, σ_{22} in the middle of the first floor of a twelve-story building from time *t*, corresponding to magnitude nine earthquakes $k_c = 0{,}4$ and $\nu_0 = 2{,}7$.

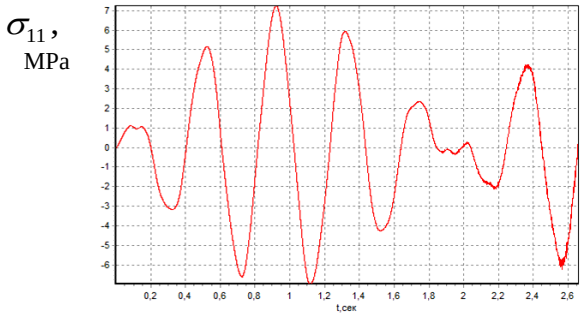

Figure 7 - **Normal voltage change graph σ_{11} in time in the middle of the first floor of a twelve-story building.**

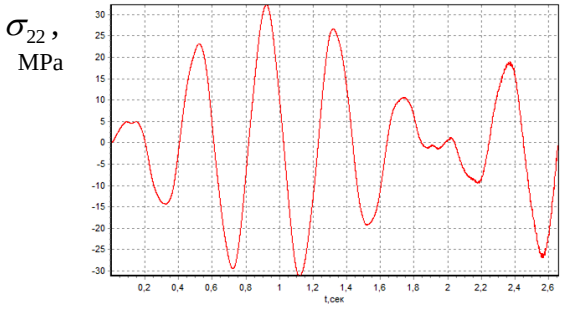

Figure 8 - **Graph of changes in normal voltage σ_{22} in time in the middle of the first floor of a twelve-story building.**

Table 6 shows the minimum and maximum stress values obtained during transverse vibrations of a 12-story building. The height and width of the building are taken to be *b=40 m* and *a=30 m*, respectively. Note that the minimum and maximum values of tangential and normal stresses were found during forced transverse vibrations in the middle and quarter of the length *a = 30 m* of the multi-story high-rise building under consideration.

Table 6

Values of the first natural frequency, maximum and minimum stresses of a 12-story large-panel building during an earthquake of 7-8-9 magnitude

№	*H, m*	k_s	ν_0, *Hz*	p_0, *Hz*	σ_{11}, MPa		σ_{22}, MPa		$\ddot{\bar{r}}$, $m/\sec^2$,	
					min	max	min	max	min	max
1	13	0.1	2.7	2.2	-1.90	2.00	-7.95	8.91	-6.52	6.53
2		0.2			-3.50	3.70	-14.8	16.0	-12.5	13.2
3		0.4			-7.10	7.55	-30.3	31.2	-25.1	25.6

Calculation results for a 16-story building.

The height and width of the building are taken equal to *b=51 m*, *a=30 m* and *H=15 m*, respectively. Let us present the numerical results of stresses obtained during transverse vibrations of a 16-story building during a magnitude 9 earthquake.

Figures 8 and 9 show graphs characterizing changes in the maximum normal stress σ_{11}, σ_{22} in the middle of the first floor of a 16-story building from time t during magnitude nine earthquakes $k_c = 0{,}4$ and $\nu_0 = 2{,}7$.

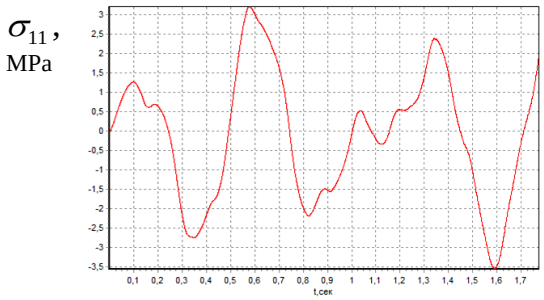

Figure 8 - **Graph of changes in normal voltage σ_{11} in time in the middle of the first floor of a sixteen-story building.**

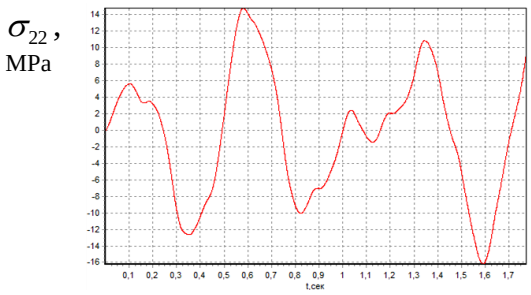

Figure 9 - **Normal voltage change graph σ_{22} in time in the middle of the first floor of a sixteen-story building.**

Table 7 shows the minimum and maximum stress values obtained during transverse vibrations of a 16-story building. The height and width of the building are taken to be b=51m and a=30m H=15, respectively.

Table 7

Values of the first natural frequency, maximum and minimum stresses of a 16-story large-panel building during an earthquake of 7-8-9 magnitude.

№	*H,m*	k_s	ν_0, *Hz*	p_0, *Hz*	σ_{11}, МПа		σ_{22}, МПа		$\ddot{\bar{r}}$, $м/сек^2$,	
					min	max	min	max	min	max
1	15	0.1	2.7	1.5	-0.9	0.8	-4.01	3.70	-3.91	3.85
2		0.2			-1.7	1.6	-8.00	7.61	-6.92	6.95
3		0.4			-3.59	3.31	-15.9	15.0	-14.5	14.5

Calculation results for a 20-story building.

The height and width of the building are taken to be a=30m, b=72m and H=18m, respectively. Let us present the numerical results of stresses obtained during transverse vibrations of a 20-story building during a magnitude 9 earthquake.

Figures 10 and 11 show graphs characterizing changes in the maximum normal stress σ_{11}, σ_{22} in the middle of the first floor of a twenty-story building from time t during magnitude nine earthquakes $k_c = 0{,}4$ and $\nu_0 = 2.7$.

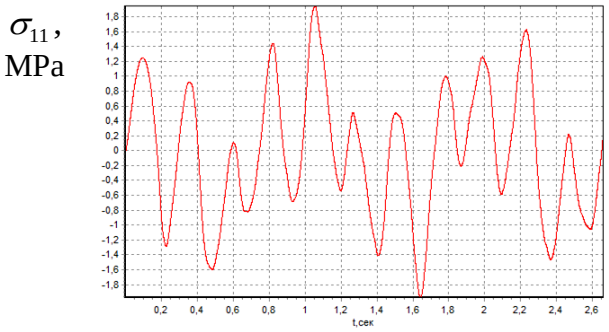

Figure 10 - Graph of changes in normal voltage σ_{11} in time in the middle of the first floor of a twenty-story building.

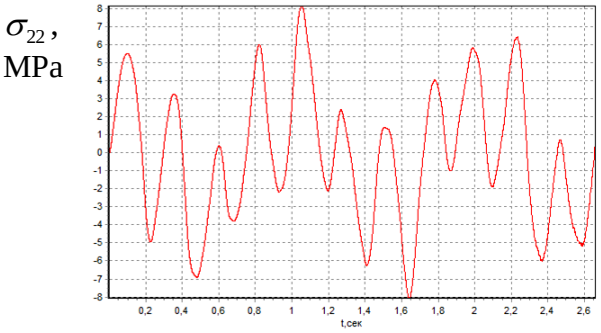

Figure 11 - Normal voltage change graph σ_{22} in time in the middle of the first floor of a twenty-story building.

Table 8 shows the minimum and maximum stress values obtained during transverse vibrations of a 20-story building. The height and width of the building are taken to be a=30m, b=72m and H=18m, respectively. Note that the minimum and maximum values of tangential and normal stresses were found during forced transverse vibrations in the middle and quarter of the length a = 30 m of the multi-story high-rise building under consideration.

Table 8

Values of the first natural frequency, maximum and minimum stresses of a 20-story large-panel building during earthquakes of magnitude 7-8-9.

№	H, m	k_s	ν_0, Hz	p_0, Hz	σ_{11}, MPa		σ_{22}, MPa		$\ddot{\tilde{r}}$, $m/\sec^2$,	
					min	ma x	min	max	min	max
1	18	0.1	2.7	0.905	-0,45	0,45	-2	2	-7.95	8.55
2		0.2			-0,9	0,9	-4	4	-16.0	16.7
3		0.4			-1,8	1,8	-8	8	-30.6	31.8

5. Conclusion.

Formulas are given for determining the elastic characteristics of a plate model of multi-story buildings, considering their design features.

For various options of geometric dimensions, numerical results of calculations of displacements and stresses under transverse vibrations of multi-story buildings were obtained.

Based on the application of the resonance method, the first three values of the natural frequency of a multi-story building with the number of floors ranging from nine to twenty floors were determined.

Based on the analysis of numerical results, it was established that the plate model is suitable for describing the dynamic behavior and calculating the stress-strain state of multi-story buildings under seismic impacts.

References

1. *Vyacheslav Shirokov, Igor Kholopov, Aleksey Solovejv.* // Determination of the Frequency of Natural Vibrations of a Modular Building / XXV Polish – Russian – Slovak Seminar “Theoretical Foundation of Civil Engineering. 2016,”. doi: 10.1016/j.proeng.2016.08.218
2. *T N T Chik, M F Zakaria, M A Remali and N A Yusof.* // Vibration Response of Multi Storey Building Using Finite / Element Modelling IOP Conf. Series: Materials Science and Engineering. 2016, 136 012037 doi:10.1088/1757-899X/136/1/012037

3. *Oleg V. Mkrtycheva, Guram A. Dzhinchvelashvilia, Marina S. Busalova.* Calculation of a multi-storey monolithic concrete building on the earthquake in nonlinear dynamic formulation / XXIV R-S-P seminar, Theoretical Foundation of Civil Engineering 2015, (24RSP) doi: 10.1016/j.proeng.2015.07.039

4. *S. Ramhormozian, G. C. Clifton, T. Good & S. Jiang, G.A. MacRae.* Dynamic time history analysis of a low damage multi-storey building incorporating the seismic friction dampers using a proposed simplified multi degree of freedom model: Is selfcentring really a concern? / Pacific Conference on Earthquake Engineering and Annual NZSEE Conference 2019.

5. *Jacob Bloch, Moshe Danieli, Iakov Iskhakov, Yuri Ribakov.* Taking into account the structure self-variable stiffness for estimation of existing buildings' seismic resistance / 13th World Conference on Earthquake Engineering 2004 Vancouver, B.C., Canada August 1- 6, 2004 Paper No. 1753.

6. *Baisbay T. Yerimbetov, Berik M. Chalabayev, Yairakhan B. Kunanbayeva, Zhenisbek A. Ussenkulov, Zhenis I. Orazbayev, Zhumadilla A. Aldiyarov.* Seismic resistance of multi-storey reinforced concrete wall-frame structures at destructive earthquakes / Periodicals of Engineering and Natural Sciences 2019 Vol. 7, No. 4, December 2019, pp.1582-1598

7. *N. Ganesh, B. Sushma, C. Lokeswar Reddy, S. Rafiulla Khadri, M. Thaheer Basha.* Dynamic analysis of multi-storey building / A Mini Project Report Submitted in Partial Fulfillment of the Requirement for the Degree of Bachelor of technology in Civil Engineering Nandyal 2023, 518 501, A. P., INDIA, P 45.

8. *Sangdae Kim, Youngkyu Ju, Wonkee Hong.* Seismic evaluation of high-rise buildings by modified dynamic inelastic analysis method / Department of Architectural Engineering, Korea University, Seoul, South Korea 2000 P-8

9. *Ju Y.K., Hong W.K., Kim S.D., Park C.L.* "Investigation on inelastic behavior of tall buildings based on efficient analysis algorithm", Journal of KSSC, 1998, Vol. 10, No. 1, pp.115-123.

10. *Allahabidi R. Powell G.H.* "DRAIN- 2DX: User Guide", Report 1988, No. UCB/EERC-88/06, EERC, University of California, Berkeley, CA.

11. *Bracci J.M., Kunnath S.K. Reinhorn A.M.* "Seismic performance and retrofit evaluation of reinforced concrete structures", Jr of S.E., ASCE, 1997, Vol. 123, No. 1, pp.3-10.

12. *Rikhsieva B.B., Khusanov B.E.* On Solution of Static Elastoplastic Problems Considering Dynamic Processes* // 15th International IEEE Scientific and Technical Conference Dynamics of Systems, Mechanisms and Machines, Dynamics - Proceedings, 2021, pp. 1-5, doi: 10.1109/Dynamics52735.2021.965369

13. *Rikhsieva B.B., Khusanov B.E.* Numerical analysis of shear interaction of an underground structure with soil // Journal of Physics: Conference Series.- 2021.- Vol.2131(3).- P.032093. doi:10.1088/1742-6596/2131/3/032093

14. *Rikhsieva B., Khusanov B.* Simulation of soil behavior under longitudinal motion of underground pipeline in one-dimensional statement. / E3S Web Conf.- 2023.- Vol.383.- P.04091. https://doi.org/10.1051/e3sconf/202338304091

15. *Usarov M., Mamatisaev G., Usarov D.* Calculation of the box structure of large-panel buildings / AIP Conference Proceedings 2023, 2612, 040014 / https://doi.org/10.1063/5.0116871

16. *Usarov M., Usarov D., Mamatisaev G.* Calculation of a Spatial Model of a Box-Type Structure in the LIRA Design System Using the Finite Difference Method, Lecture Notes in Networks and Systems 2022, 403 LNNS, pp- 1267–1275 https://doi.org/10.1007/978-3-030-96383-5_141

17. *Usarov M., Mamatisaev G.,Ayubov G.,Usarov D., Khodzhaev D.* Dynamic calculation of boxed design of buildings, IOP Conference Series: Materials Science and Engineering, 2020, 883(1), 012186 doi:10.1088/1757-899X/883/1/012186

18. *Mirsaidov M., Usarov M., Mamatisayev G.* Calculation methods for plate and beam elements of box-type structure of building, E3S Web of Conferences 2021, 264, 03030 // https://doi.org/10.1051/e3sconf/202126403030

19. *Makhamatali Usarov, Giyosiddin Mamatisaev, Davronbek Usarov.* Calculation of compelled fluctuations of panel buildings, E3S Web of Conferences 2023, 365CONMECHYDRO - 2022, 02002 / https://doi.org/10.1051/e3sconf/202336502002

20. *Usarov M., Ayubov G., Usarov D., & Mamatisaev G.* // Spatial Vibrations of High-Rise Buildings Using a Plate Model, Lecture Notes in Civil Engineering this link is disabled, 2022, 182, pp. 403–418 https://doi.org/10.1007/978-3-030-85236-8_37

21. *Usarov M.K., Usanov F.A., Usarov D.M., Isaev G.U., Toshmatov E.S.* Estimation of the stress-strain state of orthotropic plates on elastic foundation using the bimoment theory, E3S Web of Conferences 2023, 402, 07020, https://doi.org/10.1051/e3sconf/202340207020

22. *Ayubov G.T., Mamatisaev G.I., Usanov F.A., Askarhodjaev Sh.I., Urinov B.* Seismic resistance evaluation of multi-story buildings using the modern LIRA-SAPR SP, E3S Web of Conferences 2023, 402, 07019, https://doi.org/10.1051/e3sconf/202340207019

23. *Usarov M.K.* Bimoment theory of thick anisotropic plates. Monograph - Tashkent: publishing house "Fan ziyosi", 2022. - 246 p.

AMPLITUDE-FREQUENCY RESPONSE OF SEISMIC-ISOLATED HIGHWAY BRIDGES AT DIFFERENT COMBINATIONS OF SPAN LINKS

Uzdin A.M.[1], Shermukhamedov U.Z.[2], Rakhimjonov Z.K. [2], Gulomov D.I.[2]

[1]*Emperor Alexander I St. Petersburg State Transport University.*
Saint Petersburg, Russia
[2]*Tashkent State Transport University, Tashkent, Uzbekistan*
E-mail: ulugbekjuve@mail.ru

Abstract*: The features of calculating seismic resistance and studying the amplitude-frequency response of seismically isolated road bridges with various combinations of superstructure links are discussed in the article. An example of constructing the amplitude-frequency response of a system is given: a rigid support part on one span and a seismic isolating support part on the other, and seismic isolating support parts on both spans resting on a support. Possible options for installing isolating supporting parts are indicated and the case of simple seismic isolation, when fixed supporting parts are replaced with isolating ones, is considered in detail. The setting of the rigidity and damping of seismic isolation is determined by the allowable displacements of spans relative to supports.*

Keywords: *amplitude-frequency response, span structure, rigid supporting part, seismic isolating supporting part, damper, road bridge, seismic load, seismic impact.*

Introduction

In Uzbekistan, like in other countries, bridge supports are constructed with sturdy and heavy structures. The support body must be designed to withstand seismic loads, which in turn results in an increase in the load. Therefore, it is advisable to use special methods of seismic protection, particularly by incorporating movable supporting parts that offer seismic isolation, to protect the piers.

Issues on improving the methodology for calculating transport structures, in particular bridges, for seismic resistance are currently acquiring special relevance in connection with the widespread development of construction in seismic areas. The works of K.S. Zavriev [1], G.N. Kartsivadze [2], G.S. Shestoperov [3], A.A. Amosov [4], O.N. Eliseev, A.M. Uzdin [5–7], E.N. Kurbatsky [8], I.O. Kuznetsova [9], U.Z. Shermukhamedov [10, 11], T.V. Zhgutov [12], and others are devoted to methods for calculating bridges for seismic impacts.

In [13], the problem of harmonic oscillations of a linear damped system with inhomogeneous damping was considered. An example of constructing the amplitude-frequency response of a system with two dynamic vibration absorbers and three peaks in the amplitude-frequency response is given. The proposed formulas for calculating displacements are convenient for constructing the amplitude-frequency response of damped systems with viscous, hysteretic, and mixed types of damping. Based on the developed methodology, options for the technical implementation of the proposed seismic protection systems for bridges are proposed. This solution concerning a specific bridge is discussed.

The impact of adjustment errors on the efficiency of dynamic dampers of various masses was studied in [14]. Three types of damper are given there as an example. The obtained estimates make it possible to significantly simplify the task of designing seismic protection devices for bridges since they give the designer a wide opportunity to choose the size and rigidity of the designed elements of seismic protection devices.

At present, in the world practice of earthquake-resistant construction, the most important issue is to conduct dynamic calculations of structures based on seismograms of earthquakes. Such calculations are especially important when designing seismic damping and isolation systems for large multi-span bridges, unique buildings, and other critical objects, when assessing the damageability of structures, etc. Currently, two opposing approaches have emerged when modeling based on calculated accelerograms: modeling the impact on the construction site and modeling the impact on the structure. In [15], the kinematic, spectral, and energy properties of the impact are highlighted. The values of the energy characteristics I_A, CAV, SED, the harmonicity ratio $\boldsymbol{\kappa}$ and base accelerations PGA should be set to correspond to the values of the same characteristics at the construction site with a given adequacy. The

impact hazard assessment for a structure is conducted using spectra of kinematic quantities and work spectra of plastic strain forces.

Statement of the problem

Proposals for seismic isolation of a road bridge are discussed in this article. Span structures with a length of 33 m and a weight of 1343.8 tons rest on channel piers having a height of 5.200 m. The intermediate piers rest on a pile foundation 16 m long; the piles are connected using monolithic reinforced concrete grillages. The bridge scheme is shown in Fig. 1. The scheme of intermediate piers is shown in Fig. 2

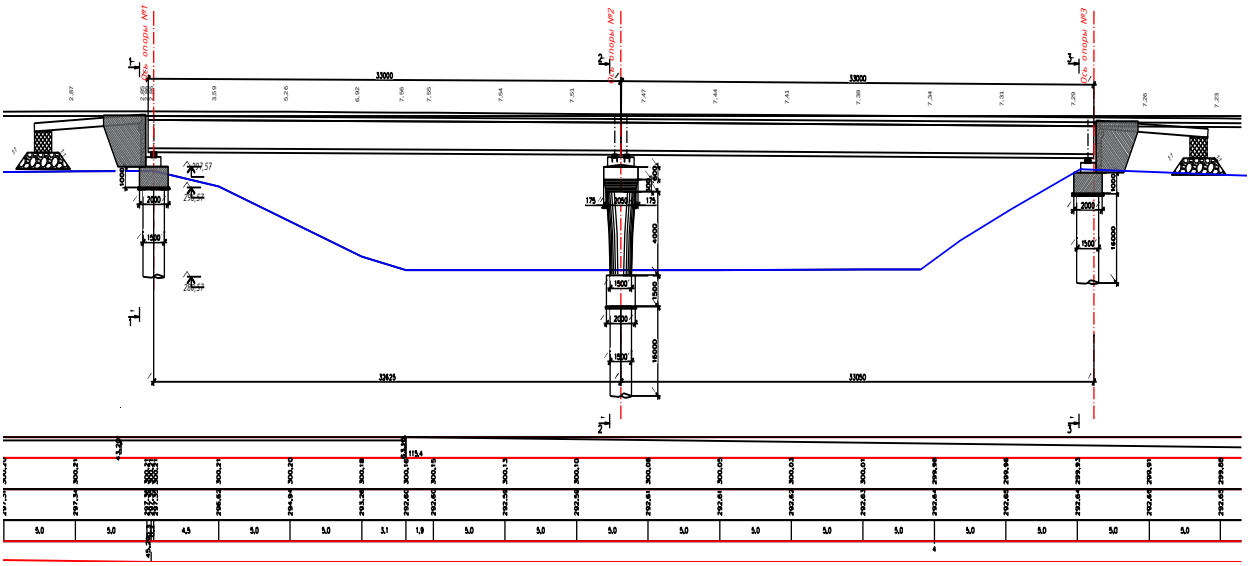

Figure 1 - **Schematic of the road bridge**

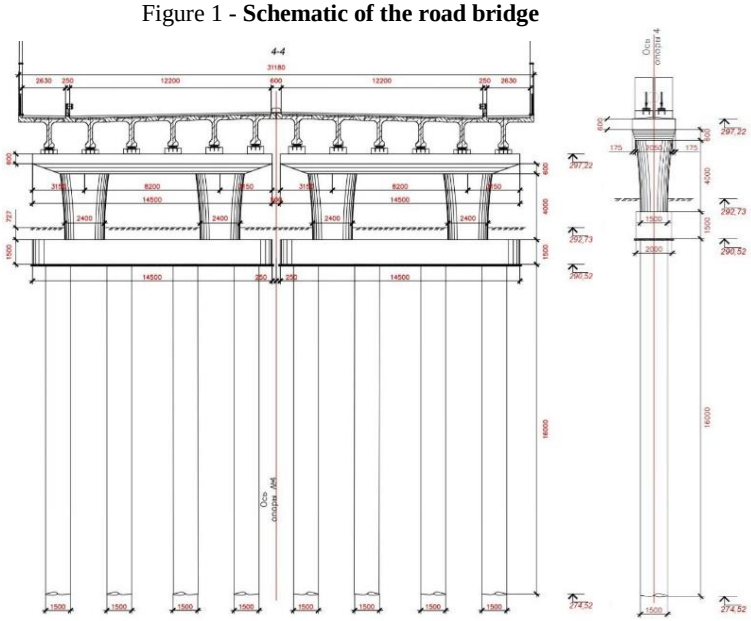

Figure 2 - **Schematic drawing of piers**

During the design process of the bridge crossing, a decision was made to use simple seismic isolation at this site, where each span has a movable support at one end. In this case, the bridge supports operate independently, and the non-uniformity of the acceleration field along the length of the bridge can be ignored.

The following options for connecting the support and spans are possible:

– a rigid support part on one span and a seismic isolating support part on the other;

– seismic isolating supporting parts on both spans resting on the support.

The considered methods of connecting spans lead to the simplest design schemes of support, shown in Fig. 3. The schemes have two degrees of freedom.

a) b)

Figure 3. - **Calculated schemes of the support at different connection of spans with supports: a - seismic isolating + rigid support part; b - seismic isolating + movable part**

Research methods.

For each of the above options, the amplitude-frequency responses are determined, which include the rigidity coefficient ***"c"*** and the inelastic resistance coefficient ***"γ"*** in the element connecting the span to the support. For this purpose, a standard method was used, widely described in literary sources [16]. Following it, amplitude-frequency responses (AFR) are determined by selecting the damping rigidity of the elements on the grid so that the relative displacements are minimal. The algorithm proposed in [14] was used to determine displacements.

Equation of motion for hysteretic damping according to E.S. Sorokin has the following form:

$$\boldsymbol{M\ddot{q} + B_c\tilde{q} + Rq = P}sin\,\omega\, t \quad , \tag{1}$$

where $\boldsymbol{B_c}$ is the hysteretic damping matrix; $\boldsymbol{M}$ is the matrix of inertia of the system; $\boldsymbol{R}$ is the stiffness matrix; $\boldsymbol{P}$ is the vector of impact amplitudes; $\boldsymbol{\omega}$ is the frequency of excitation; $\boldsymbol{q}$ is the vector of displacements of generalized masses; $\boldsymbol{\tilde{q}}$ is a vector complex conjugate to $\boldsymbol{q}$ according to E.S. Sorokin [15].

Matrix $\boldsymbol{B_c}$ is constructed using the E.S. Sorokin generalized hypothesis with the same formulas as the stiffness matrix $\boldsymbol{R}$ when replacing the elasticity modulus of each element $\boldsymbol{E}$ with the product $\boldsymbol{\gamma \cdot E}$, where $\boldsymbol{\gamma}$ is the coefficient of inelastic resistance in the material

When calculating building structures, the Sorokin matrix is often replaced with a matrix of equivalent viscous damping. There are several ways to do this [18]. The most effective method is the distribution of attenuation proportional to the energy of the vibration modes. The following formula is used:

$$\boldsymbol{B_e = B_C \cdot X \cdot K^{-1} \cdot X^{-1}}\ , \tag{2}$$

where $\boldsymbol{X}$ is the matrix of eigenvectors of the undamped system, (matrices $\boldsymbol{M^{-1}R}$); $\boldsymbol{K^2}$ is the diagonal matrix of eigenvalues of matrix $\boldsymbol{M^{-1}R}$.

After approximate replacing of hysteretic damping with equivalent viscous damping, equation (1) takes the following form:

$$\boldsymbol{M\ddot{q} + B_e\dot{q} + Rq = P}\,sin\,\omega\, t \tag{3}$$

The solution to the equation is given in [11] in the following form:

$$\boldsymbol{S}(\omega) = (\omega^2 \cdot \boldsymbol{B_e} \cdot (\boldsymbol{R - A} \cdot \omega^2)^{-1} \cdot \boldsymbol{B_e} + (\boldsymbol{R - A} \cdot \omega^2))^{-1} \cdot \boldsymbol{P}$$

$$\boldsymbol{C}(\omega) = -(\boldsymbol{R - A} \cdot \omega^2)^{-1} \cdot \boldsymbol{B_e} \cdot \omega \cdot \boldsymbol{S}(\omega),$$

As shown in [14], this solution leads to errors in the resonance region, and the authors proposed in [14] the solution in the following form:

$$\boldsymbol{C}(\omega) = (\tfrac{1}{\omega} \cdot (\boldsymbol{A} \cdot \omega^2 - \boldsymbol{R}) \cdot \boldsymbol{B_e}^{-1} \cdot (\boldsymbol{A} \cdot \omega^2 - \boldsymbol{R}) + \boldsymbol{B_e} \cdot \omega)^{-1} \cdot \boldsymbol{P} \tag{4}$$

$$\boldsymbol{S}(\omega) = (\frac{1}{\omega} \cdot \boldsymbol{B_e}^{-1} \cdot (\boldsymbol{A} \cdot \omega^2 - \boldsymbol{R}) \cdot \boldsymbol{C}(\omega) \quad (5)$$

Using formulas (4, 5) by iterating the values of $\boldsymbol{C}$ and $\boldsymbol{\gamma}$ on a grid of their possible values, the sought-for settings for the parameters of rigidity and damping were obtained, minimizing the amplitude of oscillations of the support and the frequency response corresponding to the found values of the parameters.

To simplify the AFC optimization procedure, the original equations were de-dimensionalized. To do this, all equations were divided by the reduced mass of the support. Then the stiffness and inertia matrices take the following form:

For scheme ***a***:

$$\mathbf{M} = \begin{pmatrix} \nu & 0 \\ 0 & \nu_1 \end{pmatrix} \qquad \mathbf{R} = \begin{pmatrix} f + f_1^2 \cdot \nu & -f_1^2 \cdot \nu \\ -f_1^2 \cdot \nu & f_1^2 \cdot \nu \end{pmatrix}; \quad (6)$$

Here $\nu = \frac{m1+m_0}{m_0}$, $f = \frac{k}{k_0}$, $k = \frac{c_0}{m1+m_0}$

For scheme ***b***:

$$\mathbf{M} = \begin{pmatrix} 1 & 0 \\ 0 & \nu_1 \end{pmatrix} \qquad \mathbf{R} = \begin{pmatrix} 1 + f_1^2 \cdot \nu & -f_1^2 \cdot \nu \\ -f_1^2 \cdot \nu & f_1^2 \cdot \nu \end{pmatrix}; \quad (7)$$

Optimization was conducted by setting parameters f_1 and f_2 (rigidity of the insulating supporting parts) and damping parameters γ_1 and γ_2.

During the optimization process (selection of parameters), it was considered that the displacements of spans relative to supports should be limited following the conditions of ensuring the operation of expansion joints. For this purpose, the maximum displacement of the superstructure $\mathbf{u_{lim}}$ under static load was introduced:

$$S_i = m_i \cdot Ag, \quad (10)$$

where A is the acceleration in fractions of the acceleration of gravity g.

Limit static displacement is:

$$u_{lim} = \frac{S_i}{C_i} = \frac{Agm_i}{C_i} = \frac{Ag}{k_i^2}, \quad (11)$$

hence

$$k^2 = \frac{Ag}{u_{lim}}$$

Moving on to dimensionless settings, we obtain the maximum dimensionless rigidity of the insulating supporting parts:

$$f_i^{\,2} \geq \frac{Ag}{u_{lim}k^2} \quad (12)$$

Analysis of results

To perform the necessary calculations, a dynamic calculation of a freestanding support was previously conducted. The period of oscillations T_0 of the support without spans and the displacement $\delta_{1,1}$ of the top of the support under the action of a unit load were determined:

$T_0 = 0.314$ s; $k=20$ s^{-1}; $\delta_{1,1} = 2 \cdot 1.8328 \cdot 10^{-4}$ m/kN.

The reduced mass of the support is determined by maintaining the compliance of the top of the support to ensure the period of its oscillations. The result is:

$$m = \frac{C}{k^2} = \frac{T^2}{\delta_{11} \cdot 4\pi^2} = 27.12 \text{ t} \quad (13)$$

It is crucial that the weight of the spans is significantly greater than the weight of the support.

$\nu_1 = \nu_2 = 1343.8 / 27.12 = 49.26$

With this weight ratio, the dynamic displacements of the support and the load on it are determined solely by the load from the span structure. This is illustrated by the frequency response normalized by the static displacement amplitude of the support without a span (Fig. 4).

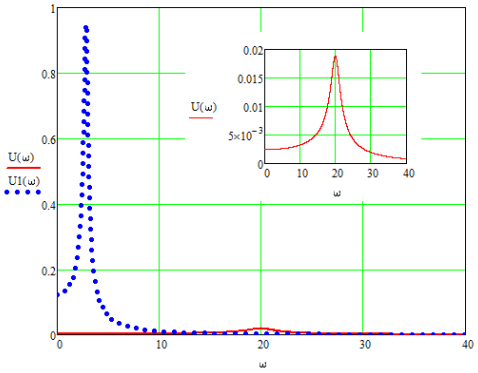

Figure 4.- **Frequency response of vibrations of the top of the support without a superstructure (solid curve) and with a superstructure (dotted curve); displacement in meters**

Consider simple seismic isolation of one span, which, in principle, can be used as a dynamic vibration absorber (DVA). As is known, the critical weight of the DVA is about ν≈2 [7], and considering damping, it is significantly less. This means that the damping effect is not realized in an isolated span. Optimization of the setting in the absence of limitations leads to the transformation of the isolating supporting parts into a Lanchester damper [19], the isolation rigidity is 0, and the damping is greater than the critical one. Unfortunately, in this case, the displacement of the span relative to the support is several meters. **Thus, seismic isolation should be made as flexible as possible, based on acceptable displacements in expansion joints.** Modular expansion joints with rubber expansion pieces can provide up to half a meter of motion. When developing technical solutions for seismic isolation for the bridge in question, the authors proceeded from virtual displacements of the span relative to the support within the range of 6-12 cm.

Despite the obvious approach to seismic isolation for the case under consideration, the issue of setting rigidity and damping in the seismic isolation system remains unclear since they influence the effect of seismic isolation and the displacement of the superstructure, and this influence is not unambiguous.

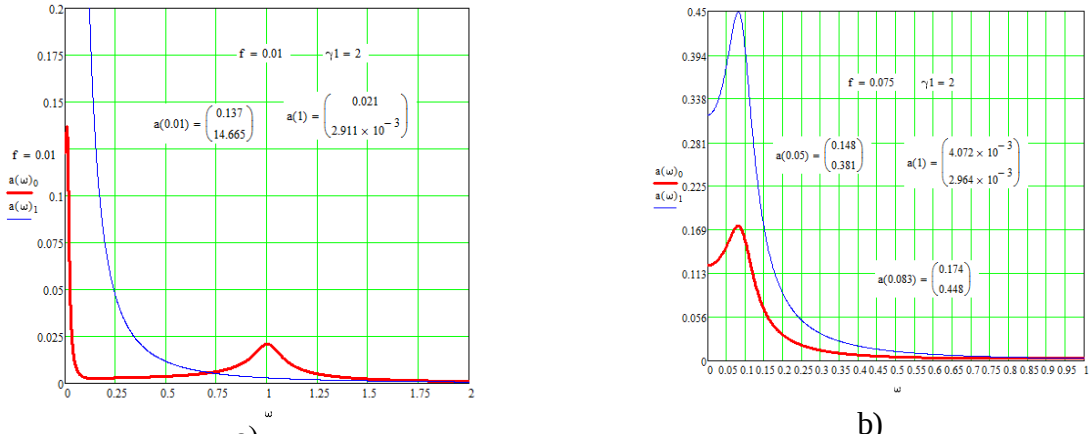

a) b)

Figure 5. – **Frequency response of vibrations of the top of a support with an isolated span when the acceptable compliance of seismic isolation is exceeded: red line – displacement of the top of the support, blue line – displacement of the span**

Figure 5 shows two possible frequency response systems with seismic isolation, which are difficult to implement. In Fig. 5, the rigidity of the insulating supporting parts is given by the following parameters: *a* – f=0.01, *b* – f=0.075. In the first case, the displacement of the span U_{sp} reaches 14 m, which makes the example purely theoretical. In the second case, U_{sp} = 0.448 m, and the displacement of the top of the pier is U_{pier} = 0.174 m. Mutual displacement is Δ = 0.274 m. The expansion joint for such a displacement is quite complex.

Figure 6 shows the frequency response with acceptable seismic isolation rigidity. In Fig. 6a, the minimum rigidity, from our point of view, is set for U_{sp} = 0.377 m, and U_{pier} = 0.207 m; and mutual displacement is Δ=0.207 m. Figure 6,*b* shows the case of maximum isolation rigidity for U_{sp}=0.452 m, and U_{pier}=0.395 m; mutual displacement is Δ=0. 07 m. With a further increase in rigidity, the effect of reducing the seismic load becomes insignificant.

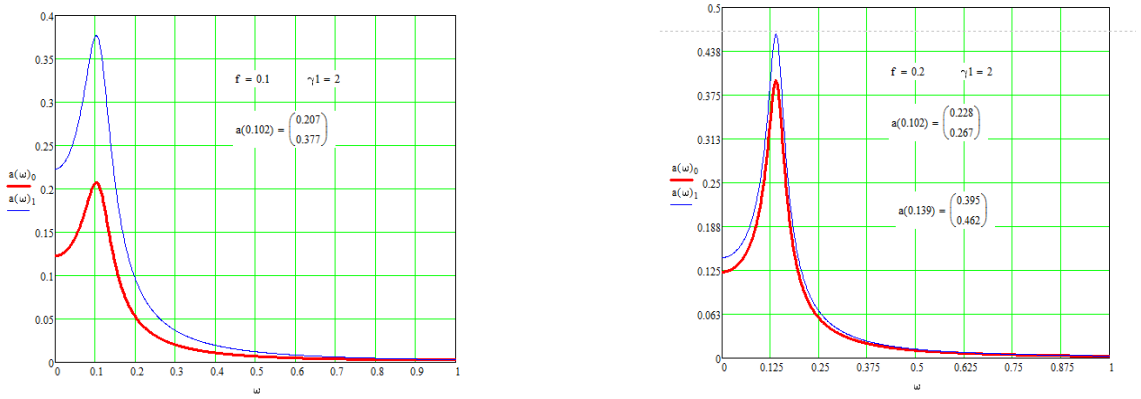

a) b)

Figure 6. – **Frequency response of vibrations of the top of a support with an isolated span structure with acceptable compliance of seismic isolation: red line – displacement of the top of the support, blue line – displacement of the span structure**

The choice of acceptable seismic isolation rigidity for ν>2 significantly depends on damping. At a fixed rigidity, the displacements of the superstructure drop with increasing damping. In all cases, the damping must be significant. Figure 7 shows the dependence of the displacement of the span on damping γ for f=0.15. For acceptable displacements, the value of γ must be greater than 1, i.e. higher than 50% of the critical value.

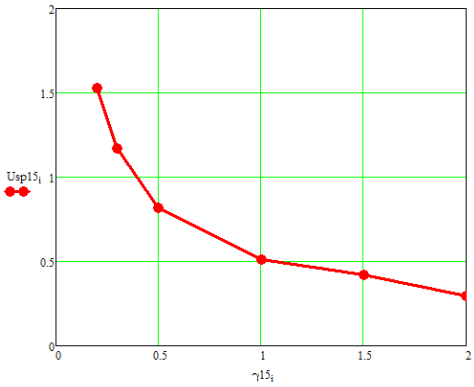

Figure 7. – **Dependence of superstructure displacements on the frequency response on DVA damping**

When calculating a seismic isolation system using the linear-spectral method, considering modal attenuation in the system, the calculated isolation efficiency is quite high.

Conclusion

1. The problem of seismic isolation of a road bridge with light frame supports and heavy reinforced concrete spans is considered. The relative weight of the span structure is very large and does not allow its use as DVA of supports, but seismic isolation of the span structure is quite acceptable.

2. Possible options for installing isolation supporting parts were indicated and the case of simple seismic isolation, when fixed supporting parts are replaced with isolating ones, was considered in detail. The setting of the rigidity and damping of seismic isolation is determined by the acceptable displacements of spans relative to supports. In this case, seismic loads on the support can be reduced by more than 2 times.

3. For any case of an acceptable setting, the damping in the isolation system must be significant and be at least 50% of the critical value. In this case, for a given damping, there is an optimal isolation setting that minimizes the displacement of the span.

References

1. *Zavriev K.S. Nazarov A.G., Aizenberg Ya.M. et al*. Fundamentals of the theory of seismic resistance of buildings and structures. M.: Stroyizdat, 1970. 224 p.
2. *Kartsivadze G.N.* Seismic resistance of artificial road structures during strong earthquakes / M.,Transport, 1974. – 260 p.
3. *Shestoperov G.S.* Seismic resistance of bridges / M., Transport, 1984, 143 p.
4. *Amosov A.A., Sinitsyn S.B.* Fundamentals of the theory of seismic resistance of structures: Textbook. M.: Publishing House ASV, 2001. – 96 p.
5. *Eliseev O.N., Uzdin A.M*. Earthquake-resistant construction. Textbook. SPb.: Publishing house. PVVISU, 1997. 371 p.
6. *Uzdin A.M., Elizarov S.V., Belash T.A.* Earthquake-resistant structures of transport buildings and structures. Teaching aid. Federal State Educational Institution "Training and Methodological Center for Education in Railway Transport". 2012. 500 p.
7. *Uzdin A.M., Sandovich T.A., Al-Nasser-Mohomad Samih Amin*. Fundamentals of the theory of seismic resistance and earthquake-resistant construction of buildings and structures. St. Petersburg: Publishing house. VNIIG, 1993. 175 p.
8. *Kurbatsky E. N., Pestryakova E. A., Zernov I. I.* Seismic resistance of bridges: theory and applications: Textbook / M., ASV Publishing House, 2021, 275 p.
9. *Kuznetsova I.O., Fedotova I.A*. Methodology for calculating metal beam span structures with a solid wall for seismic impacts // Earthquake-resistant construction. 1996. Issue 4. P. 27–35.
10. *Shermukhamedov U., Shaumarov S., Uzdin A.* Use of seismic isolation for seismic protection of railway bridges // *E3S Web of Conferences*, 2021, 264, 02001 https://doi.org/10.1051/e3sconf/202126402001
11. *Shermukhamedov U., Mirzaev I., Karimova A., Askarova D.* Calculation of the stress-strain state of monolithic bridges on the action of real seismic impacts // E3S Web of Conferences, 2023, 401, 05080
12. *Zhgutova, T.V. Khaibin V.* On the issue of using two span structures to dampen seismic vibrations of bridge supports // Earthquake-resistant construction. Safety of structures. 2011, No. 2. P. 64-68.
13. *Grenevich K.M., Kokareva A.V., Uzdin A.M., Nesterova O.P.* Some features of considering damping for calculating harmonic vibrations of linear systems // Earthquake-resistant construction. Safety of structures. 2023. No. 4. P.24-29. DOI 10.37153/2618-9283-2023-4-24-29.
14. *Shermukhamedov U.Z., Kuznetsova I.O.* The influence of the accuracy of adjustment of dynamic vibration dampers on the seismic resistance of bridges // Science and progress of transport. Bulletin of the Dnepropetrovsk National University of Railway Transport. 2012. No. 41, p. 175-180.
15. *Uzdin A., Prokopovich S.* Some principles of generating seismic input for calculating structures // Key Trends in Transportation Innovation, KTTI 2019. E3S Web of Conferences 157, 06021 (2020).
16. *Korenev B.G., Rabinovich I.M.* Handbook on the dynamics of structures / M., Stroyizdat, 1972. 511 p.
17. *Dolgaya A.A., Indeikin A.V., Uzdin A.M.* Theory of dissipative systems. // St. Petersburg, PGUPS, 1999. 99 p.
18. *Belash T.A., Uzdin A.M.* Energy absorption in seismic protection systems of buildings and structures. Monograph. St. Petersburg, PGUPS, 2020, 178 p.
19. Instructions for assessing the seismic resistance of operating bridges on railways and highways networks (on the territory of the Turkmen SSR). RSN-44-88. Ashgabat: Ylym, 1988. 106 p.

ATTENUATION OF SEISMIC SURFACE WAVES AFFECTING THE BUILDING USING VARIOUS BARRIERS

Yuldashev Sh.S.[1], Jumaboyeva Sh.[1], Boytemirov M.B.[1], Tillaboyev Y.K.[1], Abdunazarov A.Sh.[1]
[1]Namangan Engineering-Construction Institute, Namangan, Uzbekistan
E-mail: sh.yuldashev1953@gmail.com,

***Abstract**: In the article, the effect of seismic surface waves on the building was determined using the Plaxis 3D software complex using the Finite Element method. To reduce the effect of seismic surface waves on the building, an open circular trench was designed 10 meters away from the building. The open trench is filled with 3 different materials. The first is GEO FOAM EPS 19, the second is industrial waste car tires and the third is tire particles. The obtained results were comparatively analyzed. Based on the calculations, it was determined that if the elastic modulus of the material inside the open trench is low, and the density is high, the level of seismic surface waves is significantly dampened.*

***Keywords**: Building, seismic surface waves, finite element method, theory of elasticity, trench, seismic barrier, Geo Foam EPS 19, car tire, ground model.*

1. Introduction.

The main purpose of seismic barriers is to protect the area where buildings and structures are located from seismic surface waves. Depending on the propagation characteristics of seismic surface waves, different types and design solutions of seismic barriers can be used. Vertical barriers can also be used to dampen seismic surface waves. Therefore, passive protection can be achieved by filling in open circular trenches.

2. Research materials and methodology

Circular pile foundations for seismic protection were developed by Kalmatron® Corp. (USA). This barrier, according to the developer, ensures the reduction of seismic vibrations by ensuring the uniform operation of the "soil-foundation" system. With such a project, it was possible to reduce the spread of seismic surface waves [1].

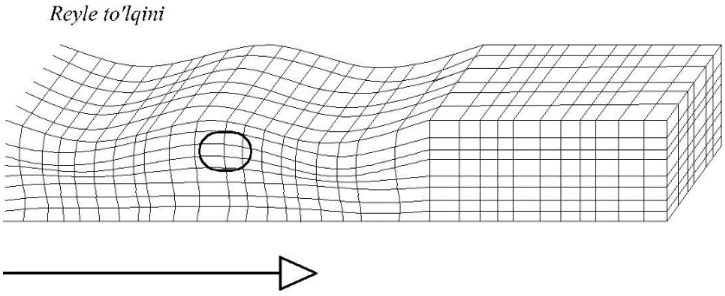

Figure 1. - **Rayleigh surface wave propagation scheme.**

Researcher A. V. Dudchenko [2] analyzed the interaction between Rayleigh surface waves and vertical seismic barriers using an elastic plane and spatial models to optimize the damping properties of vertical seismic barriers. Based on calculations, he determined that the reduction of vibrations in the zone protected from Rayleigh waves depends on the mechanical parameters of the barrier material and its geometric configuration. He accepted the size of the barrier and its attenuation coefficient as objective functions. Two problems are considered: finding the optimal value of the damping coefficient with the limitation of the size of the barrier and finding the minimum size of the barrier with the limitation of the damping coefficient. For both problems, he constructed a solution algorithm using the Kunn-Tucker condition and provided an example of a solution using it [3].

This article deals with the backfilling of an open circular trench to reduce seismic surface waves. Several issues have been considered to reduce the effect of Rayleigh surface waves on building floors.

In the issue under consideration, the effects of the Rayleigh surface wave on the building and the dependence on the ground are determined and compared.

In order to apply the numerical method, a straight parallelepiped with dimensions of 200 *m* length, 100 *m* width, and 50 *m* depth was selected from the area where seismic waves are propagating. In this case, boundary conditions are imposed on the edges of the parallelepiped, which transmit the wave to infinity. The issue also takes into account the influence of underground water at a depth of 25 *m* from the surface of the earth. The building, located on the free surface of the parallelepiped, is 24 *m* long, 24 *m* wide and 27 *m* high, and the ground part is 3 *m* deep. The thickness of the 1st layer of soil is 5 meters, and the thickness of the 2nd layer is 45 meters.

Solving problems of seismic surface wave energy propagation was carried out using the Plaxis 3D software using the finite element method.

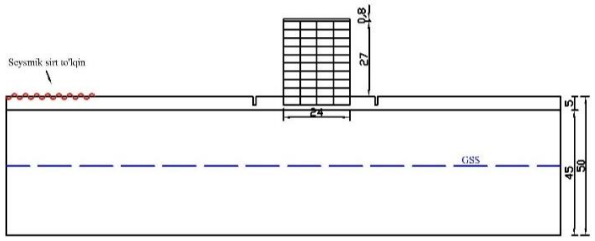

Figure 2. - **Model section**

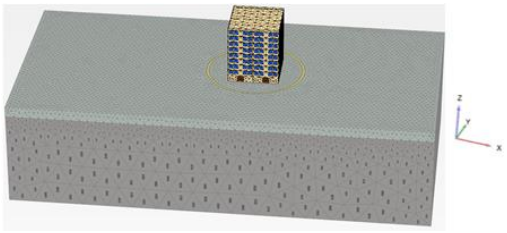

Figure 3. - **Dividing the model into finite elements**

When we replace the infinite half-space with a finite sphere. The following conditions are set at the boundaries, which ensure that the waves tend to infinity [3,7].

$$\left.\begin{aligned}\sigma_x &= a\rho V_p\dot{u}\\ \tau_{yz} &= b\rho V_s\dot{u}\\ \tau_{zy} &= b\rho V_s\dot{w}\end{aligned}\right\} \quad \left.\begin{aligned}\sigma_y &= a\rho V_p\dot{v}\\ \tau_{xz} &= b\rho V_s\dot{w}\\ \tau_{zx} &= b\rho V_s\dot{u}\end{aligned}\right\} \quad \left.\begin{aligned}\sigma_z &= a\rho V_p\dot{w}\\ \tau_{xy} &= b\rho V_s\dot{u}\\ \tau_{yx} &= b\rho V_s\dot{v}\end{aligned}\right\} \tag{1}$$

The research area is divided into 46095 finite elements and 86975 nodes. The shapes of the finite elements are chosen in the form of an irregular tetrahedron. The order of the resulting system of second-order linear differential equations of motion is 260925.

Seismic waves propagated during an earthquake affect the earth's surface through a dynamic load. Here we imagine that the Rayleigh wave moves along the *x-axis*. Taking into account the physical and mechanical properties of the material, we determine the movement of seismic waves in the soil through the displacements of finite element nodes.

A dynamic model of the problem-solving space is presented in Figure 3.

The system of time-dependent motion differential equations of a discrete system created by applying the finite element method to the model under the influence of dynamic load is expressed as follows [3- 6]:

$$[\boldsymbol{M}]\{\ddot{\boldsymbol{u}}(\boldsymbol{t})\} + [\boldsymbol{C}]\{\dot{\boldsymbol{u}}(\boldsymbol{t})\} + [\boldsymbol{K}]\{\boldsymbol{u}(\boldsymbol{t})\} = \{\boldsymbol{F}(\boldsymbol{t})\} \tag{2}$$

The order of this equation is $86975 \times 3 = 260925$

Here $[\boldsymbol{M}]$ – is the mass matrix, $[\boldsymbol{C}]$ – is the damping matrix, $[\boldsymbol{K}]$ – is the singularity matrix, and $\{\boldsymbol{F}(\boldsymbol{t})\}$ is the dynamic load vector. $\{\boldsymbol{u}(\boldsymbol{t})\}$ – displacement, $\{\dot{\boldsymbol{u}}(\boldsymbol{t})\}$ – velocity, and $\{\ddot{\boldsymbol{u}}(\boldsymbol{t})\}$ – acceleration are continuous functions of time. The mass of materials (soil + water + any structure) is taken into account in $[\boldsymbol{M}]$ matrix [3 - 6].

In the numerical representation of the problem of dynamics, the formation of iteration over time is an important factor for the stability and accuracy of the calculation process.

We take Newmark's time iteration coefficients as $\alpha = 0.25$ and $\beta = 0.5$. Properties of the soil are listed in Table 1.

Table 1

Soil properties

Name	Unit of measurement	Designation	Name of the grunt	
			Loam	Pebble
General characteristics of the soil				
Soil model	–	–	Linear elastic	Linear elastic
Soil feature	–	–	Dried	Dried
The specific gravity of the upper layer of the soil under the influence of underground water	kN/m^3	γ_{unsat}	16	19
The specific gravity of the bottom layer of the soil under the influence of underground water	kN/m^3	γ_{sat}	17	20.5
Initial porosity coefficient	–	e_{init}	0.5	0.5
Young's modulus (constant)	kN/m^2	E	50000	90000
Poisson's ratio	–	v	0.35	0.3
Longitudinal wave speed	m/s	V_P	218.4	250.1
Transverse wavelength	m/s	V_S	104.9	133.7
General characteristics of the building				
Model type	–	–	Elastic	
Modulus of elasticity	kN/m^2	E	27500000	
Poisson coefficient	–	v	0.2	
Density	kN/m^3	γ	24	
General characteristics of the barrier				
Geo foam EPS 19				
Model type	–	–	Elastic	
Modulus of elasticity	kN/m^2	E	8800	
Poisson coefficient	–	v	0.1	
Density	kN/m^3	γ	0.184	
Car tire				
Model type	–	–	Elastic	
Modulus of elasticity	kN/m^2	E	1000	
Poisson coefficient	–	v	0.3	
Density	kN/m^3	γ	12	
Tire particles				
Model type	–	–	Elastic	
Modulus of elasticity	kN/m^2	E	1000	
Poisson coefficient	–	v	0.3	
Density	kN/m^3	γ	22	

Solving the system of equations (2) determines the effect of seismic surface waves on the building. Then, to determine the extinction coefficients, problems related to filling material into a circular open trench are solved.

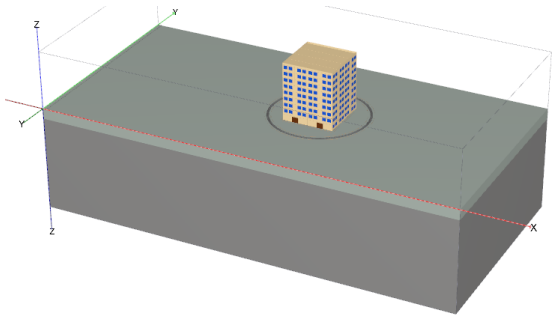

Figure 4. - **Circular open trench model**

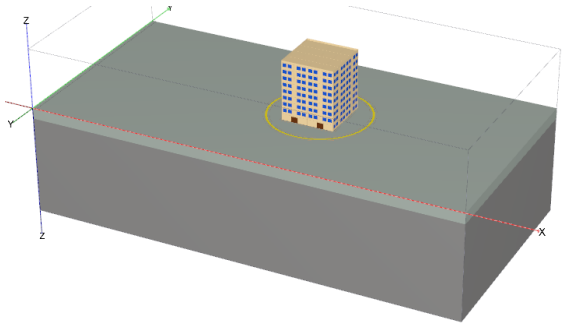

Figure 5. - **Model of a trench filled in.**

Seismic waves propagated during an earthquake affect the earth's surface as a dynamic load. We create the propagation of seismic surface waves by harmonic force. The phase of the harmonic force is 0, the amplitude is 1, the frequency is 10 Hz, and the duration is 5 seconds.

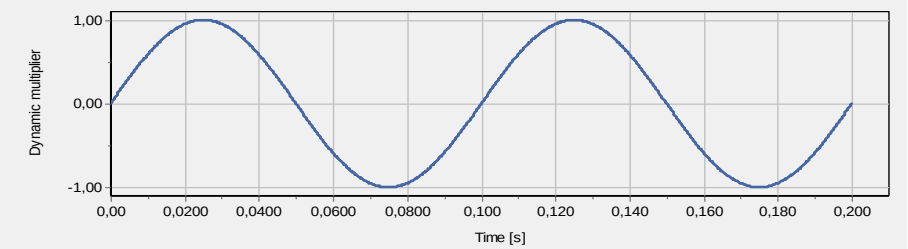

Figure 6. - **Law of harmonic force**

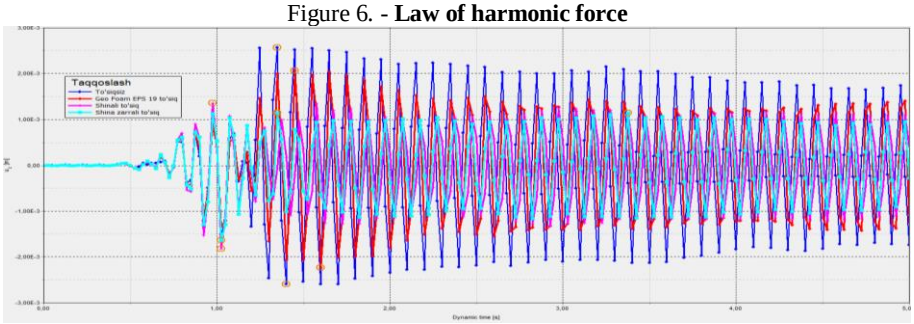

Figure 7. - **Comparison of displacement graphs on the floors of the building**

Table 1

The highest displacement amplitudes in the z-axis when the building is affected by seismic surface waves

Name	No barrier	Barriers					
		Geo Foam EPS 19		Car tire		Tire particles	
	Displacement (mm)	Displacement (mm)	Efficiency	Displacement (mm)	Efficiency	Displacement (mm)	Efficiency
ground floor	2,59	2,23	1,16	1,82	1,42	1,64	1,58
1st floor	2,59	2,17	1,19	1,74	1,49	1,57	1,65
2nd floor	2,26	1,68	1,35	1,32	1,71	1,20	1,88
3rd floor	1,80	1,23	1,46	0,99	1,82	0,91	1,98
4th floor	1,31	0,89	1,47	0,84	1,56	0,81	1,62
5th floor	0,83	0,65	1,28	0,70	1,19	0,66	1,26
6th floor	0,76	0,65	1,17	0,71	1,07	0,70	1,09
7th floor	0,99	0,93	1,06	0,93	1,06	0,89	1,11
8th floor	1,16	1,07	1,08	1,09	1,06	1,02	1,14
9th floor	1,25	1,15	1,09	1,17	1,07	1,10	1,14
roof of the building	1,28	1,16	1,10	1,19	1,08	1,12	1,14

3. Conclusion.

Issues related to the propagation of seismic surface waves in the building were calculated when the seismic barrier was used and when the seismic barrier was not used. When solving the problem, the obtained results were compared. It was found that when using a barrier filled with tire particles, the displacement is 1.58 times in the ground part of the building, 1.65 times on the 1st floor, 1.88 times on the 2nd floor, 1.98 times on the 3rd floor, 1.62 times on the 4th floor, On the 5th floor, it was determined that the level of wave vibration was reduced by 1.26 times and on the floors above by an average of 1.12 times. As a result, it was noted that the effectiveness of the barrier reduces the level of vibration in the building by 1.42 times. based on the obtained results, we can say that using a barrier filled with tire particles can significantly reduce seismic surface waves in the building. It was found that using materials with a low modulus of elasticity and high density when filling an open trench can significantly reduce the level of seismic surface waves in the building.

References

1. *Sergey V. Kuznetsov and Aybek E. Nafasov*. Horizontal Acoustic Barriers for Protection from Seismic Waves // Hindawi Publishing Corporation Advances in Acoustics and Vibration Volume 2011, Article ID 150310, 8 pages doi:10.1155/2011/150310
2. *Дудченко, А. В.* Analysis and optimization of parameters of vertical seismic barriers taking into account energy dissipation // Dissertatsion 2019, 142 pages
3. *Mirsaidov M., Boytemirov M., Yuldashev F.* Estimation of the Vibration Waves Level at Different Distances //Proceedings of FORM 2021: Construction The Formation of Living Environment. – Springer International Publishing, 2022. – pp. 207-215.
4. *Rashidov T. R., Yuldashev, S. S., Karabaeva, M. U., & Boytemirov, M. B.* State Of The Issue Of Protecting The Population, Industrial And Civil Buildings From Traffic Vibrations// mechanical problems. – 2019. – Т. 1. – С. 8-11.
5. *Yuldashev S. S., Boytemirov M.* Influence of the level of the location of the railway canvas on the propagation of waves from train motion //ISJ Theoretical & Applied Science,(05 (85)). – 2020. – Т. 140.
6. *Il'ichev V. A., Yuldashev S. S., Saidov S. M.* Propagation of vibration from trains in relation to track position //Soil Mechanics and Foundation Engineering. – 1999. – Т. 36. – №. 2. – С. 55-56.
7. *Dekhanov U., Tillaboyev Y.* The equation of the driving torque generated by the concave surface rotor blade under the influence of wind pressure // Modern problems of applied mathematics and information technology (MPAMIT2022. (2024)

UPDATING THE CALCULATION OF BUILDINGS FOR SEISMIC IMPACTS IN UZBEKISTAN

Ubaydulloyev M.N.[1], Ubaydulloyev O. M.[1]

[1] *Samarkand State University of Architecture and Construction named after Mirzo Ulugbek, Samarkand, Uzbekistan*
E mail: hodja2002@mail.ru

Abstract. *The paper presents modern approaches and provisions to the calculations of buildings with a special combination of loads, taking into account seismic impacts according to the norms of different countries. Some results of the researches are highlighted, which can be recommended in design practice and for the further scientific work, when creating new regulatory documents in Uzbekistan. Based on the analysis of formulas (2.9-2.11) of Building Codes and Norms QMQ 2.01.03-19, the dependence of the reduction coefficient values on the permissible relative inelastic deformation of elements and the period of natural vibrations of buildings (structures) is analyzed.*

Keywords. *seismic effects, seismic safety of a structure, building calculation, reduction factors, spectral method.*

1. Introduction

The document defining further directions for the development of the construction industry of the Republic of Uzbekistan (RUz) in the field of earthquake-resistant construction, reconstruction, restoration, and strengthening of buildings, structures, and historical monuments of the country, taking into account advanced foreign experience and international standards, while ensuring harmonization

(ensuring mutual compliance) of relevant regulatory documents in Uzbekistan with those of leading countries has been adopted as a Resolution by the Cabinet of Ministers of RUz [1]. At the same time, improvements to the structure and content of Building Codes and Norms (hereinafter referred to as the "QMQ"), enhancements to calculation methods, improvements in the quality and reliability of performed calculations and their assessment for reliability, with a focus on ensuring seismic safety for the population, which is a socio-economic issue have become particularly significant [1-2, 6-11].

2. Materials, methods and object of research

The results of the study [6-8, 23] are focused on analyzing foreign experience in using regulatory documents, related to the facility design in seismic areas, including Eurocodes, international building codes of the United States, United Kingdom standards, Japanese national standards, Chinese national building codes, Korean building regulations, building codes of the Russian Federation and other countries of the Commonwealth of Independent States (CIS) and others, as listed in Appendix №1 to the Decree of the President of Uzbekistan № DP-5963 dated March 13, 2020. The aim is to harmonize QMQ with foreign regulatory documents in order to preserve and maximize the existing benefits of the QMQ, while minimizing its disadvantages. It is also advisable to summarize the experience of certain CIS countries (Russia, Belarus, Kazakhstan, Ukraine, etc.) that have already, to some extent, implemented the "updating" of their standards, taking into consideration Eurocode-8 [6-9, 23].

3. Setting the task

It should also be noted that in the national standards of different countries regarding earthquake-resistant construction, nonlinear effects are taking into account when determining the calculated seismic loads in three directions.

1. The use of reaction spectra for inelastic systems, followed by calculation according to the linear spectral theory (LST), is used in the United States [5, 12-13].

2. The use of elastic system reaction spectra, with the subsequent introduction of a reduction coefficient directly into the LST calculation formulas, is used in Russia, in countries of the Commonwealth of Independent States (CIS), Eurocode 8, the regulations of China, India, Turkey, Algeria and other countries [4, 12-22].

3. Calculation based on the reaction spectra of elastic systems in accordance with LST [2-3], with the subsequent introduction of a reduction coefficient for different structural system elements into the formula for determining the forces in these elements - used in the RUz, when applying the spectral method of calculation for seismic (conditionally static) loads in accordance with clause 2.6b of QMQ 2.01.03-19 [2]. According to paragraphs 2.6 of QMQ, a dynamic method of calculation is implemented for actual or simulated seismic effects, where the forces from a particular combination of loads are determined considering shear forces from seismic impact that are numerically equal to limiting elastic reactions.

The prerequisites and calculation methods used in the spectral method as described in clause 2.6b of QMQ 2.01.03-19 [2] must be reviewed and revised due to a significant shortcoming in the calculation of building (structure) seismic impacts – the lack of equilibrium in the combination of forces in certain sections of structural elements adjacent to nodes in the structural system. This is caused by the location of the reduction factor r in formula (2.8) [2] outside the root term, as well as the use of different coefficients μ and reduction factors for different structural elements with different degrees of responsibility in the transition of the building (structure) from the elastic state to the limit state when calculating the design forces for a specific combination of loads. This makes it difficult to compare the results with those obtained using other standards. To address the issue of the shortcoming of QMQ 2.01.03-19 [2] in the calculation process as per clause 2.6b, it can be accomplished in the simplest manner by incorporating a single reduction factor r into formulas (2.3) and (2.4) of QMQ. This would allow for the differentiation of responsibilities among different components of the structural system. For instance,

this can be achieved by incorporating responsibility factors when selecting the cross-sectional dimensions of components.

4. Results

In accordance with clause 2.21 of QMQ 2.01.03-19 [2], when calculating buildings and structures according to clause 2.6(б) to ensure that the Limit State LS-1 is not exceeded, the calculated forces in the components of the structural system for a specific load combination, including seismic forces are determined by using formula (2.8). When considering the reduction factors r before the root of formula (2.8), a premise is made that the forces in the components are calculated based on the corresponding forces in an elastic system, various reduction factors (attenuation) applied to them, whose values are normalized based on the type of structural system, material, and the importance of the components in terms of the transition of the system to its ultimate state. A different calculation method is associated with considering the reduction factors in formula (2.8) and not in the formulas (2.3-2.4) of the QMQ, leading to the occurrence of unbalanced force combinations in the elements at the junctions to the nodes [6-7, 9]. The values of forces in sections of the considered elements from individual loads determined with a reduction factor $r = \mu = 1{,}0$, assuming elastic deformation of the structure, yields significantly larger the calculated force combinations in sections of the same elements (the worst combinations). Verification of the absence of the Limit State in LS-2 is carried out in the same manner as for an elastic system (at $r = \mu = 1{,}0$), which should not be the case, using the assumption of deformation equality of elastic and non-elastic systems.

Within the same QMQ, different approaches are employed to account for the reduction factor. When calculating the "Spectral Method", various values of the limiting relative nonelastic deformation μ (based on Table 2.11) and reduction factors r are applied for different components of buildings. However, when using the "Dynamic Method", a single value of $[\mu_k]$ (based on Table 2.5) is utilized, and consequently, a single reduction factor r is applied to the entire building (structure) depending on its design, and not for the individual elements.

5. Analysis of the results

In accordance with clause 2.22 of the QMQ 2.01.03-19 standard, the reduction coefficient r is determined using the formulas (2.9-2.11). Previously, its values could be obtained from Figure 2.3 of the QMQ 2.01.03-96 standard, depending on the values of the maximum permissible relative inelastic deformation μ of the elements (as specified in Table 2.11 of the standard):

$$r = 1 - 0{,}07 \cdot \mu \cdot T_1, \tag{2.9}$$

$$r_1 = 0{,}03 + 1{,}95 \cdot T_1, \tag{2.10}$$

$$r = 0{,}85 \cdot \mu^{-0{,}67}. \tag{2.11}$$

By analyzing the given formulas, we found that when solving in a joint decision of formulas (2.9)…(2.11), the obtained values of the natural oscillation periods T_1 do not to correspond with their inflection points $T_{\text{п}}$ as shown in Figure 2.3 of QMQ 2.01.03-96 [3]. In addition, there were no lines in the graph corresponding to the other values of μ in Table 2.11 ($\mu = 3{,}5$; $\mu = 4$; $\mu = 6$; $\mu = 7$; $\mu = 8$), which raises concerns about the accuracy of Figure 2.3 in QMQ 2.01.03-96. Due to these shortcomings, Figure 2.3 has been excluded from QMQ 2.01.03-19.

We attempted to analyze formulas (2.9)-(2.11) by solving them jointly for the values $T_1 = T_{\text{п}}$.

- In the first case (2.9) + (2.10), the formula is derived as follows:

$$T_{\text{п}} = 0{,}97/(1{,}95 + 1{,}07 \cdot \mu). \tag{2.12a}$$

- In the second case (2.10) + (2.11), the following formula is derived:

$$T_{\text{п}} = (0{,}85 \cdot \mu^{-0{,}67} - 0{,}03)/1{,}95. \tag{2.12b}$$

- In the third case (2.9) + (2.11), the formula is derived as follows:

$$T_{\text{п}} = (1 - 0{,}85 \cdot \mu^{-0{,}67})/(1{,}07 \cdot \mu). \quad (2.12c)$$

- In the fourth case, combining formulas (2.9) + (2.10) + (2.11), results in the following formula:

$$T_{\text{п}} = (1{,}7 \cdot \mu^{-0{,}67} - 1{,}03)/(1{,}95 - 1{,}07 \cdot \mu). \quad (2.12d)$$

- In the fifth case, assuming that the dependency graphs of the relationships "$r - T_1$" in Figure 2.3 [3] can be correct, we have selected Formula (2.12d), which corresponds to the inflection points of the periods of oscillation $T_1 = T_{\text{п}}$. We have done this by taking into account two extreme values of μ, namely μ = 2 and μ = 15, in accordance with Figure 2.3, and the reduction factors r calculated using Formula (2.11) for different values of μ and its corresponding values of $\mu^{-0{,}67}$:

$$T_{\text{п}} = (r - 0{,}03)/(0{,}66762 + 2{,}0404 \cdot \mu^{-0{,}67}). \quad (2.12e)$$

For example, when $\mu = 2$: $T_{\text{п}} = (0{,}5342 - 0{,}03)/(0{,}66762 + 2{,}0404 \cdot 0{,}6285) = 0{,}5042/1{,}95 = 0{,}2586$.

This corresponds to the formula (2.10) and the graph shown in Figure 2.3.

At $\mu = 15$: $T_{\text{п}} = (0{,}1385 - 0{,}03)/(0{,}66762 + 2{,}0404 \cdot 0{,}1629) = 0{,}1085/1{,}0 = 0{,}1085$, which corresponds to the graph in Figure 2.3 [3] but does not conform to formula (2.10). In the intermediate sections, the inflection points of $T_{\text{п}}$ deviated from the straight line shown on the graph on the right, due to the nonlinear dependence "$r = \mu$", taking into account $\mu^{-0{,}67}$ values in formula (2.11).

Apparently, the formula (2.10) was selected at only one point at – $\mu = 2$, with a single coefficient of 1,95. However, at $\mu = 15$, this coefficient should be equal to 1,0 in accordance with the graph in Figure 2.3 [3], indicating that it may be variable.

- In the sixth case, the $T_{\text{п}}$ values presented in Figure 2.3 [3] may also be calculated using the formula (2.12f), which is derived from the combined solution of formulas (2.10) and (2.11), with consideration given to the values of μ equal to $\mu = 2$ and $\mu = 15$.

$$T_{\text{п}} = (0{,}85 \cdot \mu^{-0{,}67} - 0{,}03)/[1{,}0 + 0{,}95 \cdot (15 - \mu)/13], \quad (2.12f)$$

where the values of μ are assumed to be in the range $2 \leq \mu \leq 15$, for example, when $\mu = 2$:

$$T_{\text{п}} = (0{,}85 \cdot 2^{-0{,}67} - 0{,}03)/[1{,}0 + 0{,}95 \cdot (15 - 2)/13] = 0{,}5042/1{,}95 = 0{,}2586, \quad (2.12f^*)$$

which corresponds to the formula (2.10) and the graph in Figure 2.3 [3], at $\mu = 15$.

$$T_{\text{п}} = (0{,}85 \cdot 15^{-0{,}67} - 0{,}03)/[1{,}0 + 0{,}95 \cdot (15 - 15)/13] = 0{,}1085/1{,}0 = 0{,}1085. \quad (2.12f^{**})$$

In the intermediate sections, the points of inflection in the $T_{\text{п}}$ curve deviated from the straight-line shown in the graph on the left, due to the nonlinear dependence of "$r = \mu$", when considering the values of $\mu^{-0{,}67}$ in formula (2.11).

- In the seventh case, we also analyzed the option of placing (as shown in the graph) finding their positions from the similarity of triangles, taking into account the two known extreme points $T_{\text{п}2}$ and $T_{\text{п}15}$ on the graphs corresponding to $\mu = 2$ and $\mu = 15$.

$$T_{\text{п}} = T_{\text{п}2} - [(r_2 - r_\mu) \cdot (T_{\text{п}2} - T_{\text{п}15})]/(r_2 - r_{15}). \quad (2.12g)$$

Where the values of $T_{\text{п}}$ and r are taken with indices corresponding to inflection points with the values of $\mu = 2$ and $\mu = 15$, respectively, and r_μ represents the reduction coefficient based on the graph for which the period of fluctuation of $T_{\text{п}}$ is determined. However, even in this case the inflection points of $T_{\text{п}}$ deviated from the straight line to the left due to the nonlinear dependence of "$r = \mu$" when considering the values of $\mu^{-0{,}67}$ in formula (2.11).

- In the eighth case, we also analyzed the placement of intermediate inflection points on the graph of Figure 2.3 [3], finding their position from the proposed modified formula (2.9), to the inflection points on the graphs of Figure 2.3, but assuming that the positions of the inflection points in the original graphs are accurate (this assumption will need to be verified).

$$r = 1 + \mu \cdot T_1 \cdot (0{,}033 \cdot \mu - 1). \quad (2.9h)$$

Based on the combined solution of formulas (2.9a) and (2.11), considering the graphs in Figure 2.3 [3], formula (2.12h) is derived, which allows us for the calculation of $T_{\text{п}}$ values that are as close as possible to the points of inflection in the graphs depicted in Figure 2.3.

$$T_{\text{п}} = (0{,}85 \cdot \mu^{-0{,}67} - 1)/[\mu \cdot (0{,}033 \cdot \mu - 1)]. \quad (2.12i)$$

6. Discussion

Therefore, the results of the analysis of formulas (2.9-2.11) indicate that it is necessary to bring the formulas and inform the developers of computer calculation programs about the modifications made to QMQ. It should be borne in mind that formula (2.11) has been most widely used for more than 28 years, and therefore, it is essential to clarify the location of inflection points as they are crucial in determining r for rigid buildings. Only after that, it will be possible to refine formulas (2.9) and (2.10) in order to ensure accurate calculations of buildings and structures, particularly those with short periods of fluctuation in the first form at ($T_1 \leq T_{\text{п}}$).

7. Conclusions

In light of the above, it is essential to address the identified shortcomings in QMQ 2.01.03-19 [2] with a view to enhancing the reliability (seismic safety and durability) and performance of buildings and structures designed for construction in seismically active areas. The underlying assumptions and calculation methodologies incorporated in the spectral analysis need to be reviewed and adjusted. Many of the shortcomings of QMQ 2.01.03-19 cannot be corrected when the reduction factor r in formula (2.8) is positioned outside the root expression, as well as different coefficients μ and reduction coefficients are taken into account for different elements that have different degrees of responsibility for the transition of a building (structure) to the limit state.

References

1. Resolution by the Cabinet of Ministers of the Republic of Uzbekistan, dated 06.10.2022. No.577. On measures to simplify requirements for the construction industry and systematization of regulations in the field of technical regulation (https://lex.uz/ru/docs/-6230882).
2. *QMQ 2.01.03-19*. Construction in seismic areas / Ministry of construction of the Republic of Uzbekistan. Tashkent. 2019. 110 p.
3. *QMQ 2.01.03-96*. Construction in seismic areas / The State committee of architecture and construction of the Republic of Uzbekistan. Toshkent. 1996. 175 p.
4. BS EN 1998-1. Eurocode 8: Design provisions for earthquake resistance of structures. Part 1: General rules, Seismic actions and rules for buildings. / European committee for standardization: Brussels, Belgium, 2004.
5. *ACI 318-19*: Building code requirements for structural concrete and commentary / Farmington Hills, Michigan, USA. American concrete institute. 628 p. DOI: 10.14359/51716937.
6. *Ubaydulloyev M.N., Ubaydulloyev O., Ubaydulloyeva N., Nasrullayev L.* Design of buildings (structures) taking into account seismic loads according to QMQ 2.01.03-19 // Bulletin of the international association of experts on earthquake-resistant construction. 2022, Vol 2(14), pp. 69-74. DOI:10.38054/iaeee-202223.
7. *Ubaydulloyev M.N.* On the issue of harmonization of regulatory documents of the Republic of Uzbekistan in the field of earthquake-resistant construction with regulatory documents of leading foreign countries. In: Innovative technologies in construction. Tashkent. Uzbekistan. 2023, vol.1, pp. 91-93. https://doi.org/10.5281/zenodo.8136052 .
8. *Khakimov S.A.* New constructive systems of housing and civil buildings and problems of updating seismic norms. In: Collection of materials of the Russian national conference on earthquake-resistant construction and seismic zoning. 2019. https://doi.org/10.37153/2687-0045-2019-13-195-205
9. *Khakimov Sh.A.* Problems of updating seismic norms in the conditions of application of new structural systems of residential and civil buildings // Earthquake engineering. Construction safety. 2022, vol. 2, pp. 29-42. https://doi.org/10.37153/2618-9283-2022-2-29-42
10. *Kondratiev V., Nishonov N., Akhmedov M., Abirov R.* Assessment of possible damages of residential buildings in the Fergana Valley of Uzbekistan. In: E3S web of conferences. EDP sciences. 2023, vol. 405. https://doi.org/10.1051/e3sconf/202340504020

11. *Umarov S., Akramov K., Abobakirova Z., Mirzababayeva S.* Comparison of current and expired norms for the development of methods for checking and monitoring the seismic resistance of buildings. In: E3S web of conferences EDP Sciences. 2024, vol. 474, https://doi.org/10.1051/e3sconf/202447401020

12. *Rodrigues R.A., Mazzilli C.E.N., Bittencourt T.N.* Comparative analysis of normative provisions for seismic design and detailing of reinforced concrete structures // Revista ibracon de estruturas e materiais, 2019, vol. 12(5), pp. 1220-1247. https://doi.org/10.1590/s1983-41952019000500013

13. *Hampshire De.C., Santos S., Zanaica L., Bucur C., De Souza Lima S.* Comparative study of codes for seismic Design of structures. In: Mathematical modelling in civil engineering. 2023, vol. 9, No 1, pp. 1-12. https://doi.org/10.2478/mmce-2013-0001.

14. *Latifi R., Hadzima-Nyarko M.* A comparison of structural analyses procedures for earthquake-resistant design of buildings. In: Earthquake and Structures. 2021, vol. 20, No 5, pp. 531-542. https://doi.org/10.12989/eas.2021.20.5.531

15. *Izhar T., Bano S., Mumtaz N.* Comparative study on analysis and design of reinforced concrete building under Seismic forces for different codal guidelines // International journal of trend in scientific research and development. 2019, vol.3, No 4, pp. 536-551. https://doi.org/10.31142/ijtsrd23819.

16. *Kurbatsky E., Mondrus V., Titov E., Yemelyanova G., Pestryakova E.* Outdated provisions of the norms of the Russian Federation governing construction in seismic areas // Scientific journal Academia. Architecture and construction. 2024, No1, pp. 159-165. https://doi.org/10.22337/2077-9038-2024-1-159-165

17. *Čada P., Máca J.* Comparison of methods used for seismic analysis of structures. In: Acta polytechnica CTU proceedings. 2017, No 13, pp. 20-28. https://doi.org/10.14311/app.2017.13.0020

18. *Wang M., Yang Z., Gao L.* Modification of Chinese-code formula for equivalent lateral force method // Earthquake and structures. 2021, vol. 21, No 2, pp. 137-145. https://doi.org/10.12989/eas.2021.21.2.137

19. *Adhikari D., Adhikari S., Thapa D.A.* Comparative Study on Seismic Analysis of National Building Code of Nepal, India, Bangladesh and China. In: OALib, 2021, vol. 09, No 06, pp. 1-11. https://doi.org/10.4236/oalib.1108933

20. *Büyüksaraç A., Işık E., Bektaş Ö.A.* Comparative evaluation of earthquake code change on seismic parameter and structural analysis; A case of Turkey // Arabian journal for science and engineering. 2022, vol. 47, No 10, pp. 12301-12321. https://doi.org/10.1007/s13369-022-07099-4

21. *Chandak N.R.* Response spectrum analysis of reinforced concrete buildings // Journal of the institution of engineers (India): Series A. 2012, vol. 93, No 2, pp. 121-128. https://doi.org/10.1007/s40030-012-0012-9

22. *Bilgin H., Hadzima-Nyarko M., Isik E., Ozmen H.B., Harirchian E.A.* Comparative study on the seismic provisions of different codes for RC buildings // Structural engineering and mechanics, 2022, vol. 83, No 2, pp. 195-206. https em.2022.83.2.195://doi.org/10.12989/s

23. *Kryucina O.A, Gardeners I.E.* Harmonization with European Union standards: issues, problems, solutions // Photonics Russia. 2020, vol. 14, No 1, pp. 56-65. https://doi.org/10.22184/1993-7296.fros.2020.14.1.56.65

КОЛЕБАНИЯ ТРУБОПРОВОДА, КОНТАКТИРУЮЩЕГО СО СЛОЕМ ГРУНТА, МОДЕЛИРУЕМОГО ЗЕРНИСТОЙ СРЕДОЙ

Мардонов Б.[1], Нишонов Н.А.[1], Рахманов А.[2]

Институт механики и сейсмостойкости сооружений им. М.Т. Уразбаева, Ташкент, Узбекистан
Наманганский инженерно-технологический институт, Наманган, Узбекистан
E mail: nematilla81@mail.ru

Аннотация: *Использована модель зернистой среды для моделирования состояния окружающего трубопровод слоя грунтовой среды. Задача рассмотрена в оссесимметричной постановке. Рассмотрен случай упрощения постановки задачи, когда сдвиговые движения зернистого слоя, окружающего трубопровод происходят при наличии продольной деформации частиц среды в слое. При этом отсуствует резонансное явление в процессе колебаний трубопровода, окруженного слоем зернистой среды. Показано, что рост давления, связанного с силой веса, создает сжатое состояние слоя около трубопровода, это обстоятельство указывает на возможность гашения резонансной амплитуды колебаний трубопровода, уложенного в слое грунта с гранулами.*

Ключевые слова: *трубопровод, слой грунта, зернистая среда, сдвиговые движения, давление грунта, гашение резонансной амплитуды колебаний*

1. Введение

Подземные трубопроводы играют жизненно важную роль в повседневной жизни. Сейсмостойкость систем трубопроводов является очень важной темой исследований из-за ее огромного влияния во время и после землетрясения. Большая часть повреждений трубопроводов в результате землетрясений, о которых сообщалось на сегодняшний день, связана с остаточной деформацией грунта, но также существуют неоспоримые доказательства того, что распространение волн может быть разрушительным [1 – 2]. В работе [3] проанализировано влияние реальных записей нескольких землетрясений на напряженно-деформированное состояние (НДС) полимерных трубопроводов при различных граничных условиях.

Так же систематически сообщалось о разрушениях из-за локального выпучивания подземных стальных трубопроводов. В таких случаях сильно локализованные искривления, связанные с формами локального выпучивания, могут вызвать разрыв стенки и утечку содержимого или ускорить усталостное повреждение. В работе [4] изучено выпучивание подземных трубопроводов под действием продольной сжимающей силы и в работе [5] выявлены возможные эффекты выпучивания подземных трубопроводов, расположенных в мелкодисперсном грунте, при динамическом нагружении. А в работе [6] делается попытка дать численными средствами обоснованный ответ на вопрос, может ли подземный стальной газопровод испытать выпучивание оболочечного типа при колебаниях грунта, вызванных землетрясением. Основное внимание ограничено неблагоприятными, но встречающихся в природе случаями, когда трубопровод пересекает грунтовые образования с неоднородными состояниями и возбуждение грунта возникает в виде плоских SV-волн. Контактное состояние может быть сильно неоднородным как по длине, так и по глубине трубопровода: в пределах большой зоны деформации грунта происходит значительное проскальзывание и потеря контакта, а на удалении от нее преобладают идеальные условия сцепления.

Грунт для трубопровода является не только внешней нагрузкой, но и средой, в которой развиваются деформации линейного сооружения. Внутренние усилия в трубопроводе нелинейно зависят от сопротивления окружающего его массива грунта. В [7] на основе модели упругого тела представлено решение задачи сдвига трубопровода, уложенного в полупространстве. Проведены сравнения результатов теоретических расчетов с известными экспериментальными данными. Путем правильного выбора динамических характеристик модель сопротивления грунта при действии на трубопровод осевой силы может быть с требуемой точностью использована для теоретического анализа работы окружающей трубопровод грунтовой средой. В работах [8–9] такой подход использован для описания теоретических методов определения динамических параметров колебаний жесткой плиты (круглого и квадратичного сечения). Структурное

разрушение грунта при сдвиговых деформациях наблюдались в проведенных экспериментах [10, 11].

Hindy и Novak [12] исследовали аналитически упругие трубопроводы как на однородных участках, так и на участках, состоящих из двух различных сред в горизонтальном направлении. Установлено, что при распространении объемных волн вдоль трубопровода пиковые осевые и изгибные напряжения возникают вблизи границы двух сред и больше, чем в однородном случае. Прогнозы также показали, что изгибающие напряжения, вызванные S-волнами, намного меньше, чем осевые напряжения, вызванные P-волнами.

Крупномасштабное трехмерное моделирование методом конечных элементов динамической реакции взаимодействующей системы грунт – труба в идеале было бы наиболее строгим подходом, которому можно было бы следовать; однако ему мешает связанная с этим трудность надежной интерпретации результатов, экстремальная вычислительная нагрузка и высокий уровень неопределенности вовлеченных параметров модели. Кроме того, было замечено, что учет трехмерных волновых эффектов в реакции участка не всегда обеспечивает более высокую точность по сравнению с двухмерным или даже одномерным анализом [13].

Теоретические и экспериментальные исследования, а также полевые данные показали, что при нестационарной деформации грунта подземные стальные сварные газопроводы не должны подвергаться разрыву при растяжении, а также что другие возможные виды разрушения, такие как выпучивание и овализация секций, не нарушают их целостность и работоспособность [14].

Поверхностное давление под действием динамического нагружения на заглубленные сооружения можно значительно снизить при соответствующем использовании так называемого амортизирующего уплотнения, когда энергопоглащающие материалы помещают в виде плит непосредственно над сооружением или в виде сплошных наружных оболочек вокруг него. Обычно используемые материалы имеют гранулированный состав или ячеистую структуру. Это вспененные пластики и резины, бетон с небольшой плотностью.

В работе [15] были проведены испытания разных материалов и изучены их энергопоглащающие свойства. В ней же сделан обзор по другим опубликованным работам, из анализа которых сделан вывод, что вспененные или ячеистые материалы обладают упругопластичными характеристиками. В [16] испытания были проведены для исследования реакции жесткого, горизонтально ориентированного стального цилиндра, который имел амортизирующее уплотнение из ячеистого бетона низкой прочности. Цилиндр был заглублен в хорошо уплотненный песок и подвержен статическим и динамическим избыточным давлениям, вызванным небольшим генератором взрывной нагрузки. Установлено, что амортизирующее уплотнение снижает пиковые деформации.

В работах [17, 18] расчеты уплотнения внесены в качестве рекомендаций по расчету подземных сооружений, приняв, что отношение глубины сооружение к его диаметру должно быть достаточно большим, чтобы образовался свод из грунта над слоем из ячеистого материала. При условии, что сохраняется целостность грунтового свода он сделал вывод от том, что пиковое давление на сооружение будет равно пределу текучести амортизирующего уплотнения. Получена расчётная формула для требуемой толщины уплотнения. Проведены также теоретические исследования влияния уплотнения по всему периметру цилиндра при толщине уплотнения, равной половине диаметра цилиндра.

2. Постановка задачи.

Для описания теоретической модели механической системы грунтового слоя состоящего из очень большего числа хаотически упакованных одинаковых абсолютно твердых сферических частиц, используем модель зернистой среды, предложенной в работах [19, 20]. Обозначим через $\varepsilon = \varepsilon_{11} + \varepsilon_{22} + \varepsilon_{33}$ - относительное изменение объема, $\gamma_{ij} = \varepsilon_{ij} - \frac{1}{3}\varepsilon\delta_{ij}$ - компоненты девиатора

тензора деформаций, где $\delta_{ij}=1$ при $i=j$, $\delta_{ij}=0$, при $i\neq j$, $\varepsilon_{ij}=\frac{1}{2}(\frac{\partial u_i}{\partial x_j}+\frac{\partial u_i}{\partial x_i})$ - компоненты тензора деформаций, (i,j=1, 2, 3), где $u_i(x_1, x_2, x_3, t)$ – компоненты вектора перемещения в декартовых координатах.

Компоненты тензора напряжений σ_{ij} выражаются через среднее давление p и компоненты девиатора тензора напряжений τ_{ij} по формулам

$$\sigma_{ij}=\tau_{ij}-p\delta_{ij}, \tag{1}$$

$p=-\frac{\sigma_{11}+\sigma_{22}+\sigma_{33}}{3}$ - среднее статическое давление.

Зависимости между компонентами тензора напряжения и тензора деформации определяются по уравнению состояния зернистой среды, которое определяется видом зависимости объемной деформации от компонентов девиатора тензора деформации. Следую работе [5] такую зависимость представляем в виде квадратичной форме

$$\varepsilon=\mu\sum_{i=1}^{3}\sum_{j=1}^{3}\gamma_{ij}^2. \tag{2}$$

Тогда из уравнения состояния определяем зависимости компонентов девиатора тензора напряжений от соответствующих компонентов девиатора тензора деформаций

$$\tau_{ij}=2\mu p\gamma_{ij}. \tag{3}$$

Здесь μ – безразмерный параметр, характеризующий степень сжатия (при μ<0) и разрежения (при μ>0) среды при сдвиговых деформациях. Таким образом, в отличие упругой среды, где уравнение состояние определяются через постоянные Ламе λ и G для зернистой среды достаточно задавать безразмерный параметр μ.

Используем модель зернистой среды для моделирования состояния окружающего трубопровода слоя грунтовой среды. Считаем зернистая среда весомой и заполняет цилиндрический слой радиусом R. Задачу считаем осесимметричной, установим начало координат в правом торце цилиндра и направим ось $0z$ вдоль оси цилиндра, ось $0r$ перпендикулярная к ней. Составляющие вектора перемещения вдоль координатных осей $0r$ и $0z$ соответственно обозначим через $u(r,z)$ и $w(r,z)$. Компоненты тензора деформации ε_{ij}, объемная деформация ε, а также девиатора тензора деформации γ_{ij} выражаются формулами

$$\varepsilon_{11}=\varepsilon_r=\frac{\partial u}{\partial r},\ \varepsilon_{22}=\varepsilon_\theta=\frac{u}{r},\ \varepsilon_{33}=\varepsilon_z=\frac{\partial w}{\partial z},$$

$$\gamma_{11}=\gamma_r=\varepsilon_r-\frac{1}{3}\varepsilon=\frac{1}{3}(2\varepsilon_r-\varepsilon_\theta-\varepsilon_z),\quad \gamma_{22}=\gamma_\theta=\varepsilon_\theta-\frac{1}{3}\varepsilon=\frac{1}{3}(2\varepsilon_\theta-\varepsilon_r-\varepsilon_z),$$

$$\gamma_{33}=\gamma_z=\varepsilon_\theta-\frac{1}{3}\varepsilon=\frac{1}{3}(2\varepsilon_z-\varepsilon_r-\varepsilon_\theta),\ \gamma_{13}=\gamma_{rz}=\frac{\partial w}{\partial r}+\frac{\partial u}{\partial z}. \tag{4}$$

Зависимость объемной деформации от компонентов девиатора деформации и компоненты тензора напряжений σ_{ij} соответственно вычисляются по формулам (1) и (3)

$$\sigma_{ij}=-p\delta_{ij}+2p\mu\gamma_{ij}=-p(1+\tfrac{2}{3}\mu\varepsilon)\delta_{ij}+2\mu p\varepsilon_{ij},\qquad \tau_{ij}=2\mu p\gamma_{ij}. \tag{5}$$

Компоненты тензора напряжений удовлетворяют уравнениям движения

$$\frac{\partial\sigma_r}{\partial r}+\frac{\partial\sigma_{rz}}{\partial z}+\frac{\sigma_r-\sigma_\theta}{r}+\rho g=\rho\frac{\partial^2 u}{\partial t^2}, \tag{6}$$

$$\frac{\partial\sigma_{rz}}{\partial r}+\frac{\partial\sigma_z}{\partial z}+\frac{\sigma_{rz}}{r}=\rho\frac{\partial^2 w}{\partial t^2}, \tag{7}$$

Здесь ρ – плотность зернистой среды.

Поставляя в уравнениях (6) и (7) выражения напряжений с учетом зависимостей (5) можно получить три уравнения, которые совместно с зависимостью (4) составляют нелинейную систему

для определения перемещений $u(r,z,t)$, $w(r,z,t)$ и давления $p(r,z,t)$. В общем случае решения соответствующих краевых задач для этих уравнений требует привлечения численных методов.

Исходя из физических соображения, можно сформулировать упрощенные постановки задач, где удается получить точные или приближенные их решения. Рассмотрим сдвиговые движения зернистого слоя окружающего трубопровода под действием на трубопровод осевое усилие $P(t)$. Считаем, что движение слоя происходит при наличии продольной деформации частиц среды в слое не зависящей от переменной z, т.е.

$$\varepsilon_z = \frac{\partial w}{\partial z} = 0, \ \frac{\partial u}{\partial z} = 0.$$

Таким образом, радиальное и продольное смещения не зависят от переменной z. Движение частиц зернистой среды считаем чисто сдвиговым. Тогда компоненты тензора напряжения будут равны

$$\sigma_{11} = \sigma_{22} = \sigma_{33} = -p, \ \sigma_{12} =, \sigma_{23} = 0, \sigma_{13} = \sigma_{rz} = 2\mu p\gamma_{rz} = 2\mu p\frac{\partial W}{\partial r}, \qquad (8)$$

Объемная деформация слоя согласно (2) определяется по формуле

$$\varepsilon = \mu\left(\frac{\partial \mathrm{W}}{\partial \mathrm{r}}\right)^2. \qquad (9)$$

В случае окружающего трубопровода цилиндрического слоя радиуса R и толщиной $h=R-a$ распределение давления с учетов веса зернистой среды по толщине слоя представим в виде

$$p = p_0 + \rho g(R-r),$$

где $p_0 -$ действующее давление на внешнюю границу слоя, ρ-плотность зернистой среды, a – внешний радиус трубопровода, давления p_0 можно вычислить по формуле $p_0 = \rho_c g(H-R+a)$, $\rho_c -$плотность окружающего зернистой среды слоя грунта, H – глубина заложения трубопровода

Уравнеие сдвигового движения частиц зернистой среды записывается в виде

$$\frac{\partial \sigma_{rz}}{\partial r} + \frac{\sigma_{rz}}{r} = \rho\frac{\partial^2 W}{\partial t^2} \qquad (10)$$

Вводя безразменые перменные $\xi=r/R$, $\bar{t} = t\sqrt{2g/R}$, $\bar{a} = a/R$, $U = W(\xi,\bar{t})/R$, $\xi_0 = 1+\bar{p}_0$, $\bar{p}_0 = \rho_c h_c/\rho R$, $h_c=H-R+a$ – расстояние от свободной поверхности до верхней границы слоя зернистой среды, уравнение (10) с учетом зависимости (8) записываем в виде

$$\mu\frac{\partial}{\partial\xi}[(\xi_0-\xi)\frac{\partial U}{\partial\xi}] + \mu\frac{\xi_0-\xi}{\xi}\frac{\partial U}{\partial\xi} = \frac{\partial^2 U}{\partial\bar{t}^2}. \qquad (11)$$

Функция $U = U(\xi,\bar{t})$ удовлетворяет нулевым начальным и граничным условиям

$$U = U_0(\bar{t}) \ \text{ при } \xi = \bar{1}, \ \ \mathrm{U}= 0 \text{ при } \xi = \bar{a}. \qquad (12)$$

При этом перемещение трубопровода $W_0=W(a,t)$ удовлетворяет уравнению движения

$$m\ddot{W}_0 = -S\sigma_{rz}(a,t) + P(t), \qquad (13)$$

где m, S масса и площадь боковой поверхности трубопровода.

Вводя новую переменную по формуле $z = \sqrt{(\xi_0-\xi)}$ уравнение (11) приводим к виду

$$\mu\frac{\partial^2 U}{\partial z^2} + \mu\left[\frac{1}{z} - \frac{2z}{\xi_0-z^2}\right]\frac{\partial U}{\partial z} = \frac{\partial^2 U}{\partial\bar{t}^2}.$$

Вводя функцию по формуле $v = U(\xi,\bar{t}) - U_0(\bar{t})\frac{z^2-\bar{p}_0}{1-\bar{a}}$,

сведем грания̆ные условия для функции $v(\xi,\bar{t})$ к однородному виду

$$v = 0 \ \text{ при } z_0 = \sqrt{p_0} \ \text{ и } z_1 = \sqrt{1+p_0-\bar{a}}\,. \qquad (14)$$

Функция $v(z)$ удовлетворяет неоднородному уравнению

$$\mu\frac{\partial^2 v}{\partial z^2} + \mu\left[\frac{1}{z} - \frac{2z}{\xi_0-z^2}\right]\frac{\partial v}{\partial z} = \frac{\partial^2 v}{\partial\bar{t}^2} + U_0(\bar{t})F_0(z) - \ddot{U}_0(\bar{t})F_1(z). \qquad (15)$$

Здесь $F_0(z,\bar{t}) = \frac{2\mu}{1-\bar{a}} + \mu\frac{2}{1-\bar{a}}[1-\frac{2z^2}{\xi_0-z^2}]$, $F_1 = \frac{z^2-\bar{p}_0}{1-\bar{a}}$.

Решение уравнения (15), удовлетворяющее условиям (14), можно получить численно. Здесь используется метод Бубнова -Галеркина. Рассмотрим случай действия гармонической силы

$$P = P_0 \sin(\bar{\omega}\bar{t}).$$

где $\bar{\omega} = \omega\sqrt{R/g}$, (ω, P_0 – частота и амплитуда действующей силы).

Полагая $W_0 = A\sin(\bar{\omega}\bar{t})$, $v = v_0(z)\sin(\bar{\omega}\bar{t})$ уравнение (15) приведем к виду

$$\mu\frac{d^2v_0}{\partial z^2} + \mu\left[\frac{1}{z} - \frac{2z}{\xi_0 - z^2}\right]\frac{dv_0}{dz} + \bar{\omega}^2 v_0 = A[F_0(z) + \bar{\omega}^2 F_1(z)]. \quad (16)$$

Решение уравнения (16) находим по методу Бубнова, согласно которому введем функцию $u(z)$, удовлетворяющую уравнению

$$\frac{d^2u}{\partial z^2} + \frac{1}{z}\frac{du}{dz} + \beta^2 u = 0,$$

и условиям (14). Решение последнего уравнения представим в виде

$$u = A_1 F(\beta z), \quad (17)$$

$$F(\beta z) = J_0(\beta z)N_0(\beta z_0) - J_0(\beta z_0)N_0(\beta z).$$

Здесь U_1искомый коэффициент, β корень уравнение

$$J_0(\beta z_1)N_0(\beta z_0) - J_0(\beta z_0)N_0(\beta z_1) = 0\ ,$$

$J_0(s)\ \ N_0(s)$ – функции Бесселя нулевого порядка.

Поставляя (17) в уравнение (16), получаем

$$A_1[(\bar{\omega}^2 - \mu\beta^2)F(\beta z) - \frac{2z\beta\mu}{\xi_0 - z^2}F'(\beta z)] = A[F_0(z) + \bar{\omega}^2 F_1(z). \quad (18)$$

Следую методу Бубнова, умножаем равенство (8) на функцию $u(z)$ и интегрирую в интервале $z_0 < z < z_1$, устанавливаем связь между A и A_1

$$A_1 = cA,$$

$$c = \frac{\int_{z_0}^{z_1}[F_0(z) + \bar{\omega}^2 F_1(z)]F(\beta z)dz}{\int_{z_0}^{z_1}[(\bar{\omega}^2 - \mu\beta^2)F(\beta z) - \frac{2z\mu\beta c\beta F\prime(\beta z)}{\xi_0 - z^2}]F(\beta z)dz}.$$

Касательное напряжение представим в виде

$$\sigma_{rz} = \tau_0(z)\sin(\bar{\omega}\bar{t}).$$

Согласно (8) функция $\tau_0(z)$ определяется формуле

$$\tau_0(z) = -\mu R\rho g z A c[\beta F'(\beta z) + 2z/(1 - \bar{a})]/a.$$

Поставляя выражение σ_{rz} в уравнение (13), получим формулу для амплитуды колебания трубопровода

$$A = \frac{a\bar{P}}{c\mu z_1[\beta F\prime(\beta z) + 2z/(1-\bar{a})] + \alpha\bar{\omega}^2}\ ,$$

где $\bar{P} = \frac{P_0}{\rho g R S}$, $\alpha = \frac{\rho_T L S_T}{\rho R S}$, $S_T = \pi(a_0^2 - a_1^2)$, ρ_T −плотность материала трубы, L и a_1 − длина и внутренний радиус трубопровода.

3. Результаты и их анализ

Расчеты проводились для следующих значений геометрических и физических параметров: a=0.2 м, a_1=0.18 м, L=10 м, H=2м, $P_0=10^4$Н, ρ_c=1800 кг/м^3, ρ=2500 кг/м^3, ρ_T =7800 кг/м^3.

На рисунках 1 и 2 представлены графики зависимости амплитуды колебания трубопровода (рис.1) касательного напряжения (рис.2) от безразмерной частоты $\bar{\omega} = \omega\sqrt{R/g}$ при различных значениях параметра μ и толщины слоя зернистой среды h(м).

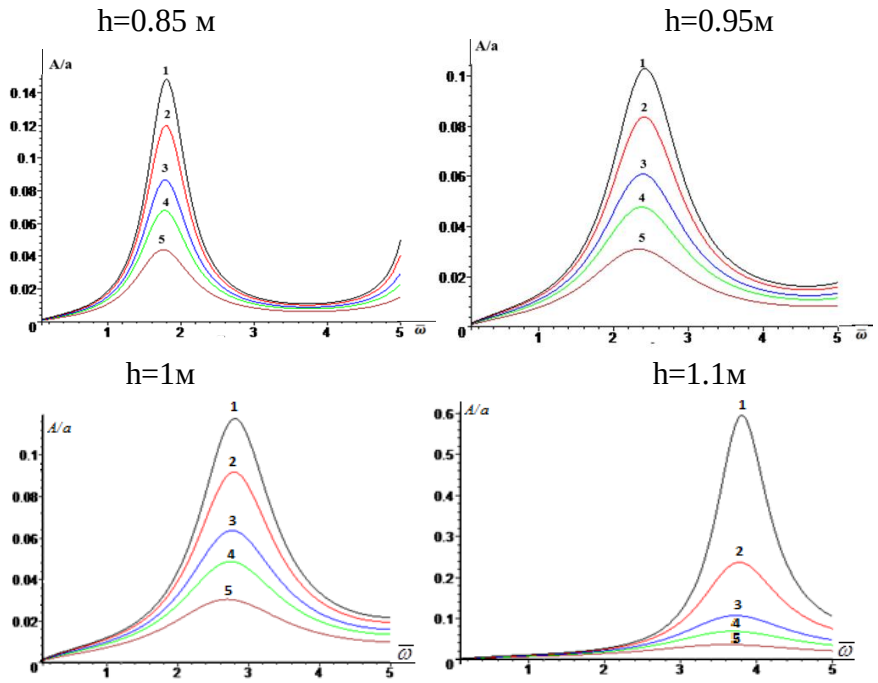

Рисунок 1. – **Зависимости амплитуды колебания трубопровода от безразмерной частоты $\overline{\omega} = \omega\sqrt{R/g}$ при различных значениях параметра μ и толщины слоя зернистой среды h(м): 1– μ= –1; 2 – μ= –1.2; 3 – μ= –1.5; 4– μ= –2; 5– μ= –3.5**

Из рис. 2 заметим, что амплитуда касательного напряжения имеет при тех указанных частотах пиковые значения, которые для толщины слоя h<1м снижается и далее с ростом толщины она увеличивается.

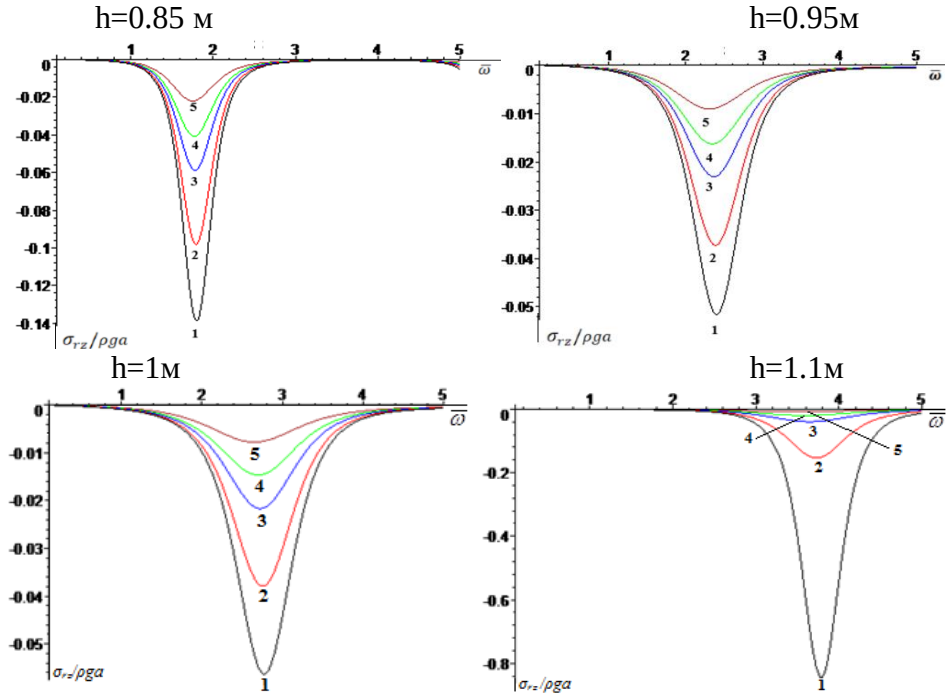

Рисунок 2. – **Зависимости амплитуды колебания касательного напряжения (отнесённого к величине $\sigma_{rz}/\rho ga$) от безразмерной частоты $\overline{\omega} = \omega\sqrt{R/g}$ при различных значениях параметра μ и толщины слоя зернистой среды h(м): 1– μ= –1; 2 – μ= –1.2; 3 – μ= –1.5; 4– μ= –2; 5– μ= –3.5**

Из анализа кривых представленных на рис.1 и 2 следует, что для выбранных параметров задачи и диапазона изменения безразмерной частоты трубопровод имеет резонансную частоту,

которая с ростом толщины слоя зернистой среды перемещается в зону высоких частот. При этом увеличение толщины слоя сначала приводит к снижению и далее с ростом ее растет амплитуды колебаний. Эта закономерность указывает на возможность выбора толщина слоя зернистой среды для снижения амплитуды колебаний трубопровода.

Литература

1. *O'Rourke M.J.* Wave propagation damage to continuous pipe. In: Proceedings of the technical council on lifeline earthquake engineering conference (TCLEE), Oakland, CA, June 28-July 1., Reston, VA: American Society of Civil Engineers; 2009.
2. *Esposito S., Giovinazzi S., Elefante L., Iervolino I.* Performance of the L' Aquila (central Italy) gas distribution network in the 2009 (Mw 6.3) earthquake, 2013, Vol. 11, pp. 2447–2466. http://dx.doi.org/10.1007/s10518-013-9478-8
3. *Nishonov N., Bekmirzaev D., An E., Urazmukhamedova Z., Turajonov K.* Behaviour and Calculation of Polymer Pipelines under Real Earthquake Records // IOP Conference Series: Materials Science and Engineering, 2020, Vol. 869(5). doi:10.1088/1757-899X/869/5/052076.
4. *Mardonov B., Mirzaev, I., Nishonov N.A., An E.V., Kosimov E.A.* Upheaval buckling of underground pipelines of complex configuration located in liquefied soils // E3S Web of Conferences «Modern Materials Science: Topical Issues, Achievements and Innovations (ISCMMSTIAI-2023)» 2023. Vol. 401, 02041. https://doi.org/10.1051/e3sconf/202340102041CONMECHYDRO 2023.
5. *An E.V., Rashidov T.R.* Seismodynamics of underground pipelines interacting with water-saturated fine-grained soil // Mechanics of Solids, 2015. Vol. 50. Issue 3. Pp. 305 – 317.
6. *Psyrras N., Kwon O., Gerasimidis S., Sextos A.* Can a buried gas pipeline experience local buckling during earthquake ground shaking? // Soil Dynamics and Earthquake Engineering. 2019. Vol.116. Pp. 511–529.
7. *Mardonov B.M.,Mirzaev I.,Hojmetov G.H., An E.V.* Theoretical values of the interaction parameters of the underground pipeline with the soil // AIP Conference Proceedings. 2022. Vol.2637, 030009. https://doi.org/10.1063/5.0119270.
8. *Jianbo Dai, Li Wang, Chengtao Hu, Guidi Zhang.* Experimental Study on Seismic Response of Buried Oil and Gas Pipeline Soil Layers under Lateral Multipoint Excitation // Hindawi Journal "Shock and Vibration". 2021, P. 11. Article ID 9887140
9. *Castiglia M., Fierro T., Santucci de Magistris.* Pipeline performances under earthquake-induced soil liquefaction: state of the art on real observations, model tests, and numerical simulations // Shock and Vibration. 2020, P. 20. Article ID 8874200
10. *Toprak S., Taskin F., Koc A.C.* Prediction of earthquake damage to urban water distribution systems: a case study for Denizli Turkey // Bull Eng Geol Environ 68:499–510. 2009.
11. *O'Rourke T.D., Jeon S.S., Toprak S., Cubrinovski M., Hughes M., Ballegooy S. Van, Bouziou D.* Earthquake Response of Underground Pipeline Networks in Christchurch, NZ // Earthq. Spectra 30. 2014. URL: https://doi:10.1193/030413EQS062M.
12. *Hindy A., Novak M.* Earthquake response of underground pipelines. Earthq Eng Struct Dyn, 1979, Vol. 7, Pp. 451–76.
13. *Makra K., Chavez-Garcia F.J.* Site effects in 3D basins using 1D and 2D models: an evaluation of the differences based on simulations of the seismic response of Euroseistest. Bull Earthq Eng, 2016, Vol. 14, Pp. 1177–1194. https://doi.org/10.1007/s10518-015-9862-7
14. *Psyrras N.K., Sextos A.G.* Safety of buried steel natural gas pipelines under earthquake-induced ground shaking: a review. Soil Dyn Earthq Eng, 2017, Vol. 106, Pp. 254–77.
15. *Hoff G.C.* Shock-absorbing materials. US Army Waterways Experiment station, Tech. Rep., 1967, Pp. 6–763
16. *Foster D.C.* Elastic Response of Shock-Isolated Cylinders in a Dense, Dry Sand. US Waterways Experiment Station, Tech. Rep., 1969. Pp.69-6.
17. *Allgood J.R.* Summary of soil-structure interaction, US Naval Civil Engineering Lab., Tech. Rep., 1972, p. 771.
18. *Kawabata T., Ling H.I, Mohri Y., Shoda D.* The behavior of buried flexible pipe under high fill sand design implications, Journal of Geotechnical and Geoenviromental Engineering, ASCE, 2006. Vol.132(10), Pp. 1354-1359.
19. *Вайсман А.М., Гольдштик М.А.* Деформирование зернистой среды // ДАН СССР, 1980, т.252, №1, С.61-64.
20. *Бердичевский В.Л.* Вариационные принципы МСС, М., Наука, 1983, 420 с.

СЕЙСМИЧЕСКИЕ КОЛЕБАНИЯ ПОДЗЕМНЫХ ТРУБОПРОВОДОВ С УЧЕТОМ ВЯЗКОУПРУГОГО ВЗАИМОДЕЙСТВИЯ

Маткаримов А.Х.[1]

[1]*Ташкентский государственнний транспортный университет, Ташкент, Узбекистан*
E mail:abdurashidmatkarimov1952@gmail.com

Аннотация: *Решена система уравнений движения линейного подземного трубопровода, выведенная на основе вариационного принципа Гамильтона–Остроградского при пространственном сейсмическом нагружении с учетом вязкоупругого взаимодействия труб с окружающей средой.*

Ключевые слова: *Подземный трубопровод, сейсмическое нагружение, вязкоупругое взаимодействие.*

1. Введение

Одним из основных факторов, обеспечивающих надежность работы подземных трубопроводов, является выполнение прочностного расчета трубопровода, отражающего действительные условия его работы, что достигается за счет выбора физических и математических моделей. Современное состояние вычислительных средств позволяет более полно учесть многочисленные факторы и с большей степенью достоверности определить фактическое напряженно-деформированное состояние подземного трубопровода.

2. Материалы, методы и объект исследования.

Решена система уравнений движения линейного подземного трубопровода, выведенная на основе вариационного принципа Гамильтона–Остроградского при пространственном сейсмическом нагружении с учетом вязкоупругого взаимодействия труб с окружающей средой. Для изучения сейсмических колебаний используется математическая модель сейсмодинамики подземных сооружений при пространственном нагружении [11-14] на основе сейсмодинамической теории подземных сооружений Т.Р. Рашидова [1] привлечением прикладной теории стержней, предложенной В.З. Власовым [4], Г.Ю. Джанелидзе [5] и обобщенной В.К. Кабуловым [6] для случая перемещения точек стержня при совместном действии продольных, поперечных и крутильных сил. Построена вычислительная схема решения задачи динамического расчета подземных сооружений на основе метода конечных разностей, получены разрешающие уравнения задачи с учетом граничных и начальных условий [13-14]. При этом использованы центральные конечно-разностные соотношения метода конечных разностей с точностью второго порядка с дробными шагами [7,8].

3. Постановка задачи.

При совместных продольных, поперечных и крутильных колебаниях стержня законы распределения перемещений, деформаций и напряжений в сечениях стержня сложны, поэтому теория колебания стержней строится на основании ряда статических и кинематических гипотез относительно закона распределения перемещений, деформаций и напряжений в сечениях стержней [4-6]. Прямолинейный подземный трубопровод аппроксимируется как стержень, взаимодействующий с окружающим грунтом, ось ox (ox_1) направлена по длине стержня, оси oy (ox_2) и oz (ox_3) совмещены с главными центральными осями поперечного сечения. Абсолютные перемещения центра тяжести обозначены через $u,\ \upsilon, w$; углы наклона касательных к упругой линии при чистом изгибе через $\alpha_1,\ \alpha_2$; угол закручивания – через θ. Тогда с учетом кинематических и статических гипотез [6] устанавливается однозначная зависимость между функциями $u_1(x,y,z,t),\ u_2(x,y,z,t),\ u_3(x,y,z,t)$ и $u(x,t),\ \upsilon(x,t),\ w(x,t)$.

$$u_1(x,\ r,\ \gamma,t)=u(x,t)-\alpha_1(x,t)r\cos\gamma-\alpha_2(x,t)r\sin\gamma+\varphi(r,\gamma)\nu(x,t)+$$
$$+a_1(r,\gamma)\beta_1(x,t)+a_2(r,\gamma)\beta_2(x,t),$$

$$u_2(x,\, r,\, \gamma,t)=\upsilon(x,t)-\theta(x,t)r\sin\gamma,\; u_3(x,\, r,\, \gamma,t)=w(x,t)+\theta(x,t)r\cos\gamma.$$

Путем введения вектора девятого порядка

$$Y=\{u,\upsilon,w,\alpha_1,\alpha_2,\theta,\nu,\beta_1\beta_2\} \tag{1}$$

И подставляя векторные выражения вариации кинетической, потенциальной энергий и работы внешних сил в вариационный принцип Гамильтона-Остроградского

$$\int_t(\delta T-\delta П+\delta A)dt=\delta\int_t(T-П+A)dt=0;$$

получено [11,15]:

$$\int_t\int_x\left\{-A\frac{\partial^2Y}{\partial t^2}+B\frac{\partial^2Y}{\partial x^2}+C\frac{\partial Y}{\partial x}+D_{\Pi}Y+D_{\text{A}}(Y-Y_0)+F\right\}E\,\delta Y\,dx\,dt+$$

$$+\int_t\left\{-\overline{B}\frac{\partial Y}{\partial x}-\overline{C}_{\Pi}Y+\overline{C}_{\text{A}}(Y-Y_0)+P^{zp}\right\}E\,\delta Y\,dt\Big|_x+\int_x A\frac{\partial Y}{\partial t}E\delta Y\,dx\Big|_t=0\,, \tag{2}$$

здесь $A,B,C,D_{П},D_{A},\overline{B},\overline{C},E$ -матрицы, F,P^{zp} -векторы девятого порядка.

Таким образом

$$-A\frac{\partial^2Y}{\partial t^2}+B\frac{\partial^2Y}{\partial x^2}+C\frac{\partial Y}{\partial x}+D_{\Pi}Y+D_{\text{A}}(Y-Y_0)+F=0, \tag{3}$$

$$\left[-\overline{B}\frac{\partial Y}{\partial x}-\overline{C}_{\Pi}Y+\overline{C}_{\text{A}}(Y-Y_0)+P^{zp}\right]\delta Y\Big|_x=0, \tag{4}$$

$$A\frac{\partial Y}{\partial t}E\delta Y\Big|_t=0. \tag{5}$$

При вязкоупругом взаимодействии трубы с окружающим грунтом для сил взаимодействия по принципу Вольтерра принято [2,7]

$$P^b(x,t)=D_A^*(Y-Y_0)=D_A\left[(Y-Y_0)-\int_0^t R(t-\eta)[Y(x,\eta)-Y_0(x,\eta)]d\eta\right], \tag{6}$$

и из (3)-(5) получены

$$-A\frac{\partial^2Y}{\partial t^2}+B\frac{\partial^2Y}{\partial x^2}+C\frac{\partial Y}{\partial x}+D_{\Pi}Y+D_{\text{A}}(Y-Y_0)-D_A\int_0^t R(t-\eta)[Y(x,\eta)-Y_0(x,\eta)]d\eta+F=0,$$

$$\left[-\overline{B}\frac{\partial Y}{\partial x}+\overline{C}_{\Pi}Y+\overline{C}_{\text{A}}(Y-Y_0)-\overline{C}_{\text{A}}\int_0^t\overline{R}(t-\eta)\left[Y(x,\eta)-Y_0(x,\eta)\right]d\eta+P^{zp}\right]\delta Y\Big|_x=0,$$

$$A\frac{\partial Y}{\partial t}E\delta Y\Big|_t=0. \tag{7}$$

Для ядра релаксации принято слабосингулярное трехпараметрическое ядро [2,7]

$$R(t)=\overline{A}_be^{-\overline{\beta}t}t^{\alpha-1},\;\; 0<\alpha<1,\;\; [\overline{\beta}]=cek^{-1},\;\; [\overline{A}_b]=cek^{-\alpha}; \tag{8}$$

Трехпараметрическое ядро (8) имеет слабую особенность типа Абеля. Для устранения этой особенности в подинтегральном выражении (7) произведена замена переменных для фиксированных $t_n=(n-1)\tau$ по методике Ф.Б. Бадалова [9], после этого интеграл вычислен по квадратурной формуле:

$$-A\frac{\partial^2 Y}{\partial t^2}+B\frac{\partial^2 Y}{\partial x^2}+C\frac{\partial Y}{\partial x}+D_n Y+$$

$$+D_A\left[\left(Y-Y_0\right)-\frac{A_b}{\alpha}\sum_{k=1}^{n}B_k^b e^{-\beta t_k}\left[Y\left(x,t_n-t_k\right)-Y_0\left(x,t_n-t_k\right)\right]\right]+F=0,$$

$$\left\{-\overline{B}\frac{\partial Y}{\partial x}+\overline{C}_{\Pi}Y+\overline{C}_A\left[\left(Y-Y_0\right)-\right.\right.$$

$$\left.\left.-\frac{A_b}{\alpha}\sum_{k=1}^{n}B_k^b e^{-\beta t_k}\left[Y\left(x,t_n-t_k\right)-Y_0\left(x,t_n-t_k\right)\right]\right]+P^{zp}\right\}\delta Y\big|_x=0,$$

$$A\frac{\partial Y}{\partial t}E\delta Y\Big|_t=0. \qquad (9)$$

При построении вычислительной схемы для системы дифференциальных уравнений с граничными и начальными условиями (9) применены центральные конечно-разностные соотношения метода конечных разностей с точностью второго порядка с дробными шагами [7,8]:

$$\frac{\partial Y}{\partial t}\approx\frac{1}{\tau}\left(Y_{i,j+\frac{1}{2}}-Y_{i,j-\frac{1}{2}}\right)+o\left(\tau^2\right),\ \frac{\partial^2 Y}{\partial t^2}\approx\frac{1}{\tau^2}\left(Y_{i,j+1}-2Y_{i,j}+Y_{i,j-1}\right)+o\left(\tau^2\right),$$

$$\frac{\partial Y}{\partial x}\approx\frac{1}{h}\left(Y_{i+\frac{1}{2},j}-Y_{i-\frac{1}{2},j}\right)+o\left(h^2\right),\ \frac{\partial^2 Y}{\partial x^2}\approx\frac{1}{h^2}\left(Y_{i+1,j}-2Y_{i,j}+Y_{i-1,j}\right)+o\left(h^2\right), \qquad (10)$$

где $t=j\tau,\ x=ih$.

На шаг по времени ставится ограничение $0<\tau<h^2/4$, это соответствует условию $\tau=rh_{\min}^2,\ r\le 1/2$, другое ограничение $c_{\max}\tau<\frac{1}{n}h_{\min}^2,\ n\ge 2$ также удовлетворяет условию устойчивости Куранта.

При разработке машинного алгоритма дробные шаги сетки создают своеобразные затруднения. Поэтому дробные шаги сетки преобразованы в целые шаги сетки и, используя (10) аппроксимированы слагаемые дифференциальных выражений системы (9), начальных условий (5), граничных условий (4), для этого принимают при i=0 аппроксимацию шагом вперед и при i=N аппроксимацию шагом назад.

Таким образом, получается задача Коши для конечно-разностных уравнений сейсмического колебания подземного трубопровода при пространственном нагружении с учетом вязкоупругого взаимодействия с окружающим грунтом:

При $i=1,\ j=0$;

$$Y_{1,1}=\frac{1}{2}\left(\tilde{\tilde{B}}Y_{1,0}^0+\tilde{\tilde{C}}Y_{2,0}^0-\tilde{D}_A B_0^b e^{-\beta t_0}Y_{1,0}+\tilde{\tilde{F}}_{1,0}-2\tau\ A^{-1}\ \dot{Y}_{i,0}^0\right), \qquad (11)$$

при $i=i,\ j=0$;

$$Y_{i,1}=\frac{1}{2}\left(\tilde{A}Y_{i-1,0}+\tilde{B}Y_{i,0}+\tilde{C}Y_{i+1,0}-\tilde{D}_A B_0^b e^{-\beta t_0}Y_{i,0}+\tilde{F}_{i,0}\right)+\tau\ A^{-1}\ \dot{Y}_{i,0}^0, \qquad (12)$$

при $i=N-1,\ j=0$;

$$Y_{N-1,1}=\frac{1}{2}\left(\tilde{\tilde{A}}Y^0_{N-2,0}+\tilde{\tilde{B}}Y^0_{N-1,0}-\tilde{D}_A B^b_0 e^{-\beta t_0}Y_{N-1,0}+\tilde{\tilde{F}}_{N-1,0}\right)+\tau\, A^{-1}\,\dot{Y}^0_{N-i,0}\ , \tag{13}$$

при $i=1,\ j=1$;

$$Y_{1,2}=\tilde{\tilde{B}}Y_{1,1}+\tilde{\tilde{C}}Y_{2,1}-\tilde{D}_A\sum_{k=1}^{2}B^b_{k-1}e^{-\beta t_{k-1}}Y_{1,2-k}+\tilde{\tilde{F}}_{1,1}-Y^0_{1,0}\ , \tag{14}$$

при $i=i,\ j=1$;

$$Y_{i,2}=\tilde{\tilde{A}}Y_{i-1,1}+\tilde{\tilde{B}}Y_{i,1}-\tilde{D}_A\sum_{k=1}^{2}B^b_{k-1}e^{-\beta t_{k-1}}Y_{i,2-k}+\tilde{\tilde{F}}_{i,1}-Y^0_{i,0}\,, \tag{15}$$

при $i=N-1,\ j=1$;

$$Y_{N-1,2}=\tilde{A}Y_{N-2,1}+\tilde{B}Y_{N-1,1}+\tilde{C}Y_{N,1}-\tilde{D}_A\sum_{k=1}^{2}B^b_{k-1}e^{-\beta t_{k-1}}Y_{N-1,2-k}+\tilde{\tilde{F}}_{N-1,1}-Y^0_{N-1,0}\,, \tag{16}$$

при $i=1,\ j\geq 2$;

$$Y_{1,j+1}=\tilde{\tilde{B}}Y_{1,j}+\tilde{\tilde{C}}Y_{2,j}-\tilde{D}_A\sum_{k=1}^{j+1}B^b_{k-1}e^{-\beta t_{k-1}}Y_{1,j+1-k}+\tilde{\tilde{F}}_{1,j}-Y_{1,j-1}\ , \tag{17}$$

при $i=i,\ j\geq 2$;

$$Y_{i,j+1}=\tilde{A}Y_{i-1,j}+\tilde{B}Y_{i,j}+\tilde{C}Y_{i+1,j}-\tilde{D}_A\sum_{k=1}^{j+1}B^b_{k-1}e^{-\beta t_{k-1}}Y_{i,j+1-k}+\tilde{F}_{i,j}-Y_{i,j-1}, \tag{18}$$

при $i=N-1\ j\geq 2$;

$$Y_{N-1,j+1}=\tilde{\tilde{A}}Y_{N-2,j}+\tilde{\tilde{B}}Y_{N-1,j}-\tilde{D}_A\sum_{k=1}^{j+1}B^b_{k-1}e^{-\beta t_{k-1}}Y_{N-1,j+1-k}+\tilde{\tilde{F}}_{N-1,j}-Y_{N-1,j-1}. \tag{19}$$

4. Результаты

Для анализа влияния вязкоупругости взаимодействия подземных трубопроводов с окружающим грунтом на НДС подземных трубопроводов составлена программа расчета по формулам (11) - (19), которые соответствуют задаче Коши для разностных уравнений сейсмических колебаний подземного трубопровода при пространственном нагружении с учетом вязкоупругого взаимодействия с окружающим грунтом, и служат алгоритмом вычисления вектора Y в матричной форме.

Для описания процессов вязкоупругости приняты слабосингулярные ядра Ржаницына-Колтунова по (8). Т.Р. Рашидовым, Г.Х. Хожметовым [3] на основе экспериментальных работ по изучению вязкоупругих свойств взаимодействия различных труб с различными грунтами, например, для грунтов из суглинка, песка и гравия, определены параметры слабосингулярного ядра для суглинка -A=0.134, α=0.2, β =0.25, для песка -A=0.0748, α =0.2, β =0.048, для гравия -A=0.0815, α =0.2, β =0.25. Сейсмическое воздействие принято в виде импульса постоянной величины - u_0=0.007 м, На основе этих данных проведен анализ численных результатов влияния параметров вязкоупругости взаимодействия стальной трубы с грунтами из суглинка, песка и гравия.

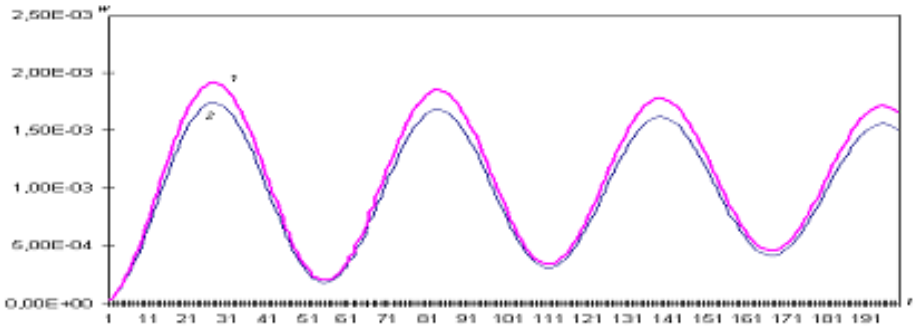

Рисунок 1. - **Влияние вязкости на прогиб w (A=0.134, β=0.25, α=0.2).**

Анализ численных результатов показывает, что вязкость взаимодействия приводит к уменьшению максимальных значений перемещения u, прогиба w, угла наклона α_2, угла сдвига β_2, продольной силы N, поперечной силы Q, моментов M_y, M_a. В рассмотренных примерах разница в результатах упругих и вязкоупругих решений составляет 10% -15%.

5. Заключение

Используя результаты работы можно рационально подбирать размеры сечения труб и обеспечить сейсмостойкость подземных трубопроводов.

Литература

1. Рашидов Т.Р. Динамическая теория сейсмостойкости сложных систем подземных сооружений. - Ташкент: Фан, 1973. -179 с.
2. Ильюшин А.А., Победря Б.Е. Основы математической теории термовязкоупругости. - Москва: Наука, 1970. – 280 с.
3. Рашидов Т. Р., Хожметов Г.Х., Мардонов Б.М. Колебания сооружений, взаимодействующих с грунтом. – Т.: Фан, 1975. -176 с.
4. Власов В.З. Тонкостенные упругие стержни. - Москва: Физматгиз, 1959, -568 с.
5. Джанелидзе Г.Ю. К теории тонких стержней // ПММ. – Москва, 1949. -т.XIII, вып. 6. –с. 397-408.
6. Кабулов В.К. Алгоритмизация в теории упругости и деформационной теории пластичности. – Т.: Фан, 1966. -394 с.
7. Колтунов М.А. Ползучесть и релаксация. – Москва: Высшая школа, 1979. -272 с.
8. Годунов С.К., Рябенький В.С. Разностные схемы (Введение в теорию). - Москва: Наука, 1977. – 440 с.
9. Самарский А.А., Гулин А.В. Численные методы. – Москва: Наука, 1989. – 432 с.
10. Бадалов Ф. Б. Методы решения интегральных и интегро-дифференциальных уравнений наследственной теории вязкоупругости. - Ташкент: Мехнат, 1987. -272 с.
11. Рашидов Т.Р., Юлдашев Т., Маткаримов А.Х. Модели сейсмодинамики подземных сооружений при пространственном нагружении // Вестник ТашИИТ. - Ташкент, 2006. - № 1. - с. 66-74.
12. Юлдашев Т., Маткаримов А.Х. Уравнения сейсмодинамики подземных сооружений при пространственном нагружении в цилиндрической системе координат// Вестник ТашИИТ. - Ташкент, 2006. - № 2. - с.36-43.
13. Маткаримов А.Х., Хайдаров А.Х., Абдусатторов А. Моделирование подземных трубопроводов при пространственном нагружении с учетом вязкоупругого взаимодействия // Вестник ТашИИТ. –Ташкент, 2012. -№ 3/4.-с. 12-14.
14. Маткаримов А.Х., Хайдаров А.Х. Алгоритм решения уравнений подземного трубопровода при динамическом нагружении // Вестник ТашИИТ, 2013, №1/2, с.28-30.
15. Abdurashid Matkarimov, Mukhiddin Khudjaev. Vibrations of the underground pipeline in the vertical plane considering the rotational inertia and transversal shear. E3S Web Conf.Volume 363, 2022. XV International Scientific Conference on Precision Agriculture and Agricultural Machinery Industry “State and Prospects for the Development of Agribusiness - INTERAGROMASH 2022” https://doi.org/10.1051/e3sconf/202236301047

МЕТОДИКА РАСЧЕТА ТРАНСПОРТНЫХ ТОННЕЛЕЙ НА СЕЙСМИЧЕСКИЕ ВОЗДЕЙСТВИЯ

Миралимов М.Х.[1], Каршибоев А.И.[1], Анваров Б.Ф.[1], Ерполатов И.Б.[1]
[1]*Ташкентский государственный транспортный университет, Ташкент, Узбекистан*
E mail: mirzakhid_miralimov@yahoo.com

Аннотация: *В настоящей статье на основе метода конечных элементов с моделью деформирования «обделка-горный массив» приведена методика расчета конструкций автотранспортных тоннелей глубокого заложения на воздействия сейсмических волн сжатия (растяжения) и сдвига. Последовательный анализ, происходящих при этом физических процессов, позволяет в достаточно полной мере определить основные закономерности взаимодействия обделки тоннелей совместно с вмещающим грунтовым массивом, а также разработать рекомендации по конструированию элементов с учетом всех особенностей работы тоннелей в горных условиях.*

Ключевые слова: *Тоннель, массив, грунтовый массив, обделка, конечный элемент.*

1. Введение

В последние десятилетия наблюдается интенсивное развитие транспортного тоннелестроения, обусловленное расширением сети магистральных дорог, увеличением объемов пассажирских и грузовых перевозок, дальнейшим совершенствованием транспортной инфраструктуры.

В настоящее время в Европе эксплуатируются более 10 тыс. км транспортных тоннелей, причем только за последние 15 лет их протяженность увеличилась на 2 тыс. км. Аналогичная картина характерна и для стран юго-восточной Азии, где с 1990 г. построено 2350 км тоннелей, Северной и Южной Америки. Сегодня в мире реализуются около 650 проектов крупных тоннельных сооружений, причем годовые капиталовложения достигли уровня (без Японии) 40 млрд. долл. США [1, 2].

Среди крупнейших горных автодорожных тоннелей, построенных за последние годы, можно выделить тоннель Лаердал длиной 24,5 км в Норвегии, дна параллельных тоннеля длиной по 19,6 км через Тюрингский лес в Германии, два параллельных тоннеля Хида длиной по 10,75 км между г.г. Нагоей и Тоями в Японии. Наиболее крупные подводные автодорожные тоннели построены под Токийской бухтой в Японии (два параллельных тоннеля длиной по 10 км и диаметром 14,14 м), под р. Эльбой в Германии (длиной 3,1 км, диаметром 14,2 м), тоннель Бэмлафиорд в Норвегии длиной 7,9 км, тоннель Вестершельде длиной 6,6 км и диаметром 11,33 м в Нидерландах. К крупнейшим городским тоннелям можно отнести подземную сеть Central Artery в г. Бостоне (США) общей протяженностью 11,3 км, два тоннеля на автомагистрали А86 в г. Париже (Франция) длиной 10 и 7,5 км и диаметром 11,75 м, железнодорожные тоннели между аэропортами в г. Нью-Йорке (США) [3].

В нашей стране за последние годы построены горные автодорожные тоннели на перевале Камчик и Резак общей длиной 1,8 км, а также протяженный железнодорожный тоннель на линии а также «Ангрен – Поп» длиной 19,2 км [4].

На следующие годы намечается строительство нового автодорожного тоннеля длиной более 6 км. Территория в Узбекистане и районы, в которых расположены и проектируются транспортные магистрали, характеризуются повышенной сейсмической активностью.

Следует подчеркнуть, что в основном горные тоннели относятся к тоннельным сооружениям глубокого заложения, глубина которых превышает диаметр обделки не менее чем в 3 раза.

В связи с этим методы, предназначенные для расчета обделок тоннелей мелкого заложения (глубина заложения тоннеля превосходит наибольший размер его поперечного сечения менее, чем в 3 раза), не приемными в таких случая.

При прохождении в горном массиве сейсмических волн сжатия-растяжения и сдвига, распространяющихся от очага землетрясения, в каждом элементе грунта, помимо естественного

напряженного состояния, формируются сейсмические напряжения. В местах контакта грунта с контуром обделки тоннеля (или другим препятствием) при прохождении плоской сейсмической волны возникает концентрация сейсмических напряжений, являющихся дополнительной сейсмической контактной нагрузкой. Важной задачей является оценка напряженного состояния обделки автодорожного тоннеля от действия длинной волны сжатия-растяжения и волны сдвига, задаваемыми напряжениями на бесконечности. Последовательный анализ, происходящих при этом физических процессов, позволяет в достаточно полной мере определить основные закономерности взаимодействия обделки тоннелей совместно с вмещающим грунтовым массивом, а также разработать рекомендации по конструированию элементов с учетом всех особенностей работы тоннелей в горных условиях.

Разработка метода математического моделирования и численное исследование напряженно-деформированного состояния горного массива и элементов тоннелей с учетом особенностей сейсмических контактных нагрузок является в настоящее время актуальной задачей.

2. Материалы, существующие методы и объект исследования.

История развития методов решения задач механики подземных сооружений насчитывающая уже более столетия, начиная с простейших схем равновесия жестких клиньев, которыми аппроксимировалась обделка сводов [5], включает ряд характерных этапов. При этом существенно различными темпами развивались решения двух основных подходов к расчету тоннельных обделок. Первый подход — это имеющий значительно более давнюю предысторию, объектом непосредственного исследования является конструкция обделки, которая представляется в пространстве в виде цилиндрической, призматической оболочки, а в плоскости в виде стержневой аппроксимации. Во втором подходе рассматривается совместность перемещений обделок тоннелей с окружающим массивом и решается контактная задача теории упругости или пластичности [5, 6].

Интересные результаты по расчету на сейсмостойкость тоннелей глубокого заложения получены Н. С. Булычевым [5] и др. на основе рассмотрения квазистатических задач теории упругости для среды, ослабленной неподкрепленными или подкрепленными отверстиями, испытывающей не бесконечности двухосное сжатие или чистый сдвиг, моделирующие соответственно действию длинных (более, чем в 3 раза превосходящих размеры отверстий) продольных и поперечных волн произвольного направления.

Исследования, проведенные Ш. И. Айталиевым, Ж. К. Масановым и других учёных [6-9] также посвящены изучению квазистатической работы тоннельной обделки при сейсмических воздействиях с учетом анизотропии массива и дифракции волн.

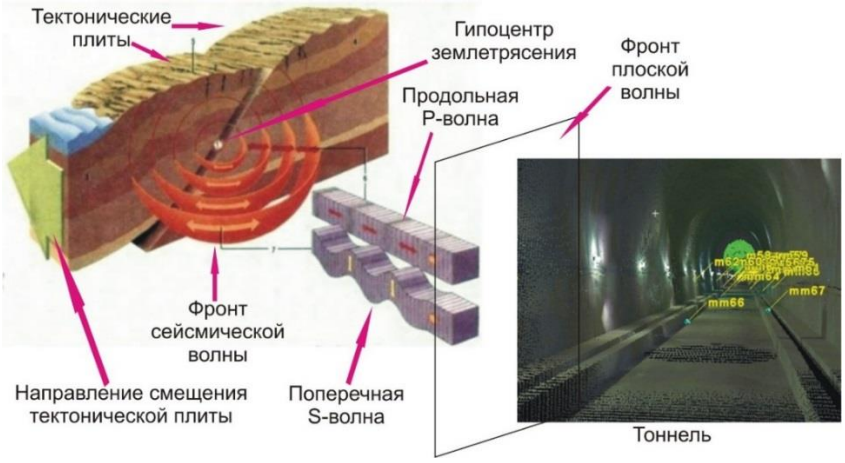

Рисунок 1. **Воздействия сейсмической волны на подземные сооружения**

В развитии динамических методов расчета подземных сооружений, взаимодействующих с грунтом большую роль, сыграли труды Рашидова Т. Р. и А. А. Ишанходжаева [11]. Тоннель может испытывать три вида деформации при сейсмическом воздействии: продольные деформации (сжатия и растяжения), изгибные деформации и деформации сдвига. Поведения тоннелей зависят от параметров землетрясения, характера деформаций массива грунта около тоннеля и особенностей конструкции тоннельной обделки.

В зависимости от соотношения жёсткости тоннельной обделки и массива грунта тоннель будет либо деформироваться вместе с массивом грунта, либо сопротивляться деформациям (рис.1). Проведенные исследования свидетельствуют, что в местах контакта грунта с контуром обделки тоннеля (или другим препятствием) при прохождении плоской сейсмической волны возникает концентрация сейсмических напряжений, являющихся дополнительной сейсмической контактной нагрузкой [8, 9].

3. Постановка задачи и метод решения

При постановке задачи расчета автодорожного тоннеля на сейсмические воздействия будем исходит от следующего:

- рассматриваются плоские контактные задачи теории упругости для сооружения, подкрепляющего вырез в упругой среде и работающего в условиях совместности перемещений при следующих граничных условиях: сейсмические волны предполагаются упругими, гармоническими с плоским фронтом распространения, либо нестандартными, с незначительным отличием (по форме) реального импульса от синусоидального.

- плоский фронт волны является простейшим и широко используется для изучения распространения упругих волн в горных породах и массивах. В этой связи более сложные формы волнового поля представляют математически в виде суперпозиций плоских волн, распространяющихся в разных направлениях.

- грунтовый массив принимают сплошным, линейно деформируемым, однородным, характеризующимся модулем деформации E_0 и коэффициентом Пуассона v_0.

Обделку рассматриваем в условиях плоской деформации, т.е. в предположении, что длина тоннеля превосходит его поперечные размеры не менее чем в 5 раз и сейсмические волны распространяются в плоскости его поперечного сечения. Эти допущения относятся к тоннельным сооружениям, глубина которых превышает диаметр обделки не менее чем в 2 раза. Условимся, чтобы длина сейсмических волн сдвига превосходила диаметр тоннеля не менее чем в 3 раза (например, для скального грунта с модулем деформации $E_0 = 1 \cdot 104$ МПа, объемной массой $\rho_0 = 2.5$ т/м^3 и коэффициентом Пуассона $v_0 = 0.25$ при преобладающем периодом колебаний $T_0 = 0.4$ с, длина упругой волны сдвига составляет 482 м).

Рассмотрим напряженное состояние обделки автодорожного тоннеля глубокого заложения, возникающее под действием сейсмических волн (рис. 2).

При этом действия сейсмических волн сжатия-растяжения и сдвига - эти нормальные ($\sigma_{x'}^{(\omega)}$ и $\sigma_{y'}^{(\omega)}$) и касательные ($\tau_{x'y'}^{(\omega)}$) напряжения, возникающие в массиве на бесконечности по произвольным взаимно-перпендикулярным направлениям x' и y', следует определять на формулам

$$\sigma_{x'}^{(\omega)} = \pm \frac{1}{2\pi} k_c \gamma c_1 T_0; \quad (1)$$

$$\sigma_{y'}^{(\omega)} = \frac{v_0}{1-v_0} \sigma_{x'}^{(\omega)} \quad (2)$$

$$\tau_{x'y'}^{(\omega)} = \pm \frac{1}{2\pi} k_c \gamma c_2 T_0 \quad (3)$$

где c_1 - скорость распространения продольных (сжатия-растяжения) волн, м/с; c_2 - скорость распространения поперечных (сдвиги) волн, м/с; T_0 - преобладающий период колебаний частиц

породы, с; ν_0 - коэффициент Пуассона грунта; k_{c1} - коэффициент сейсмичности, A - условное сейсмическое ускорение частиц породы в долях ускорения свободного падения, принимает значение 0,1, 0,2, 0,4 соответственно для расчетной сейсмичности 7, 8, 9 баллов; $K_1=0,25$ - коэффициент учитывающий допускаемые повреждения обделок тоннелей [7, 10].

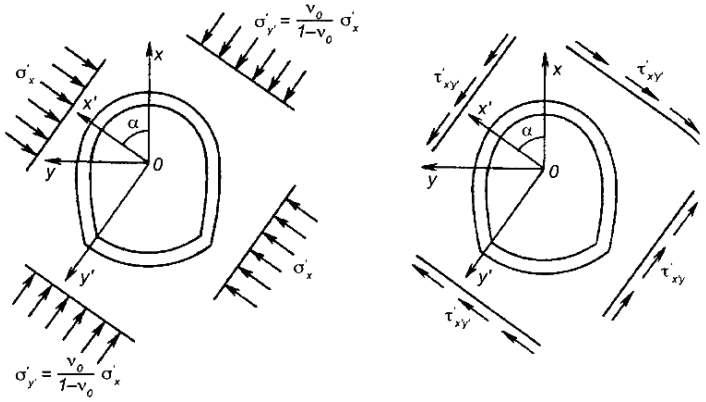

Рисунок 2. - **Расчетная схема к определению напряженного состояния обделки от продольных и поперечных сейсмических волн.**

При расположении тоннеля глубокого заложения в однородных по сейсмической жесткости скальных грунтах при наличии экспериментальных данных возможно уменьшение коэффициента сейсмичности до 0,5 k_c при глубине заложения тоннеля в 100 м и более. Решение данной контактной задачи теории упругости сводится к решению краевой задачи теории упругости, характеризующих соответственно напряженное состояние среды (грунтового массива) и конструкции (тоннельной обделки).

Предположим, что под действием этих сил деформации малы и для них справедливы следующие основные уравнения [8, 10-14]:

1. Уравнения равновесия (Статические уравнения)

$$\frac{\partial \sigma_x}{\partial x}+\frac{\partial \tau_{xy}}{\partial y}+\bar{X}=0,\quad \frac{\partial \tau_{yx}}{\partial x}+\frac{\partial \sigma_y}{\partial y}+\bar{Y}=0 \qquad (4)$$

$$\tau_{xy}=\tau_{yx}=\tau$$

где X *и* Y - объемные силы. Или в матричной форме

$$A\vec{\sigma}+\vec{P}=0$$

где $$A=\begin{bmatrix}\frac{\partial}{\partial x} & 0 & \frac{\partial}{\partial y}\\ 0 & \frac{\partial}{\partial y} & \frac{\partial}{\partial x}\end{bmatrix},\ \vec{\sigma}=[\sigma_x\sigma_y\tau],\ \vec{P}=[\bar{X}\ \ \bar{Y}]$$

2. Зависимости между деформациями и перемещениями (Геометрические уравнения)

$$\varepsilon_x=\frac{\partial u}{\partial x},\quad \varepsilon_y=\frac{\partial v}{\partial y},\quad \gamma_{xy}=\frac{\partial v}{\partial x}+\frac{\partial u}{\partial y}, \qquad (5)$$

или $$\vec{\varepsilon}=A^T\vec{U},\quad \text{где}\quad \vec{\varepsilon}=[\varepsilon_x\ \ \varepsilon_y]^T,\quad \vec{U}=[u\ \ v]^T$$

3. Физические уравнения (Закон Гука)

$$\varepsilon_x=\frac{1}{E}(\sigma_x-\nu\sigma_y),\quad \varepsilon_y=\frac{1}{E}(\sigma_y-\nu\sigma_x),\quad \gamma_{xy}=\frac{\tau_{xy}}{G} \qquad (6)$$

или $\vec{\varepsilon} = B\vec{\sigma}$

где $A = \begin{bmatrix} \frac{\partial}{\partial x} & 0 & \frac{\partial}{\partial y} \\ 0 & \frac{\partial}{\partial y} & \frac{\partial}{\partial x} \end{bmatrix}$, $\vec{\sigma} = [\sigma_x \sigma_y \tau_{xy}]$, $\vec{P} = [\bar{X} \quad \bar{Y}]$

где $B = \frac{1}{E}\begin{bmatrix} 1 & -\nu & 0 \\ -\nu & 1 & 0 \\ 0 & 0 & 2(1+\nu) \end{bmatrix}$

Тогда для уравнения теории упругости с краевыми (граничными) условиями можно записать [11]:

$$\begin{aligned} A\vec{\sigma} + \vec{P} &= 0 \\ \vec{\varepsilon} &= A^T\vec{U} \\ \vec{\varepsilon} &= B\vec{\sigma} \end{aligned} \tag{7}$$

Кинематические граничные условия на контуре C_u

$$\vec{U} = \vec{U}_u \tag{8}$$

Статические граничные условия на контуре C_σ

$$A_c\vec{\sigma} = \vec{P}_\sigma \tag{9}$$

Здесь $\vec{U}_u, \vec{P}_\sigma$ - вектор заданных перемещений на контуре - C_u и вектор заданных усилий на - C_σ, A_c - матрица направляющих косинусов.

Для решения полученных уравнений принять метод конечных элементов [11, 12-14].

4. Результаты расчета и их анализ

Рассмотрим транспортный тоннель с однополосным движением, расположенный в горном районе в трещиноватых гранитах (рисунок 3, а). В расчетном участке порода, вмещающая тоннель – граниты и сильновыветрелые порфиры с поверхности. По разработанной методике будем оценивать несущую способность обделки с учетом зоны региональной трещиноватости, которая может оказать значительное влияние на тоннель, то есть введением коэффициента шероховатости равной 0,35.

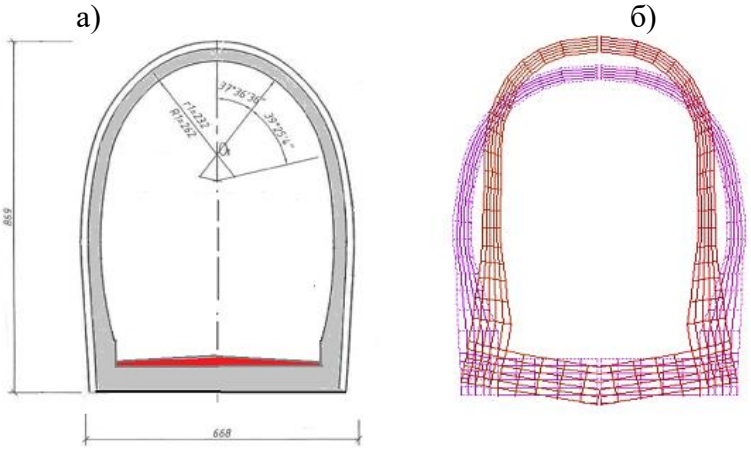

Рисунок 3. - **Схемы обделки тоннеля: а) исходная конструкция, б) днформирование конструкции**

Расчеты показали, что воздействие сейсмической волны существенно влияет на напряженно-деформированное состояние “грунт-обделка”. На рисунок 3,б приведена картина деформирования конструкции обделки тоннеля.

На рисунке 4-5 приведены, распределения горизонтальных и вертикальных изохром перемещений.

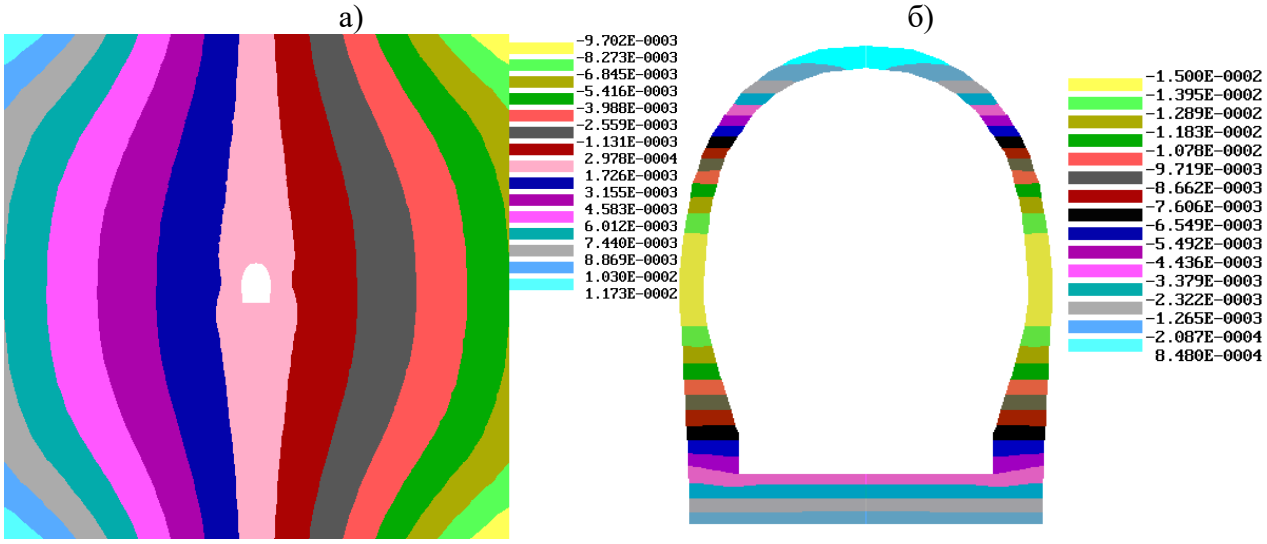

Рисунок 4. - **Изохромы горизонтальных перемещений: а) в системе “грунт- обделка”, б) в тоннельной обделке**

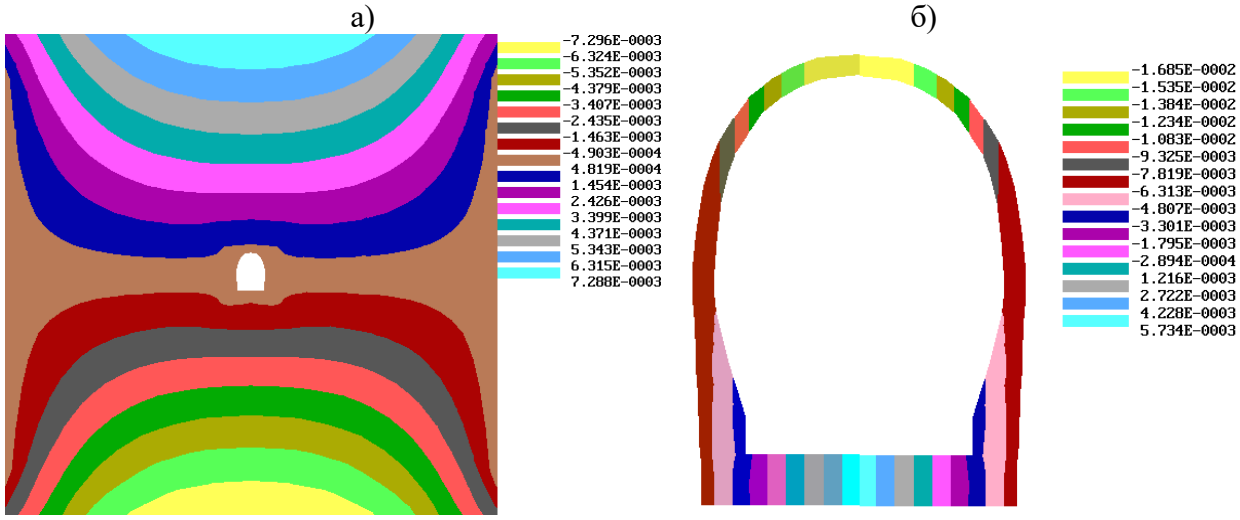

Рисунок 5. - **Изохромы вертикальных перемещений, (м):а) в системе “грунт- обделка”, б) в тоннельной обделке**

На рис.6 изохорами напряжений в системе «грунт-обделка». Из результатов видно, что концентрацию напряжений создаёт тоннельная обделка, как инородное включение в горном массиве. А на рис. 7 приведены, возможная область предельного состояния в системе «грунт-обделка» и векторное поле главных напряжений в тоннельной обделке. Анализ этих данных показывает, что область предельного состояния может увеличиться по окружности тоннеля в случае увеличения внешней сейсмической нагрузки.

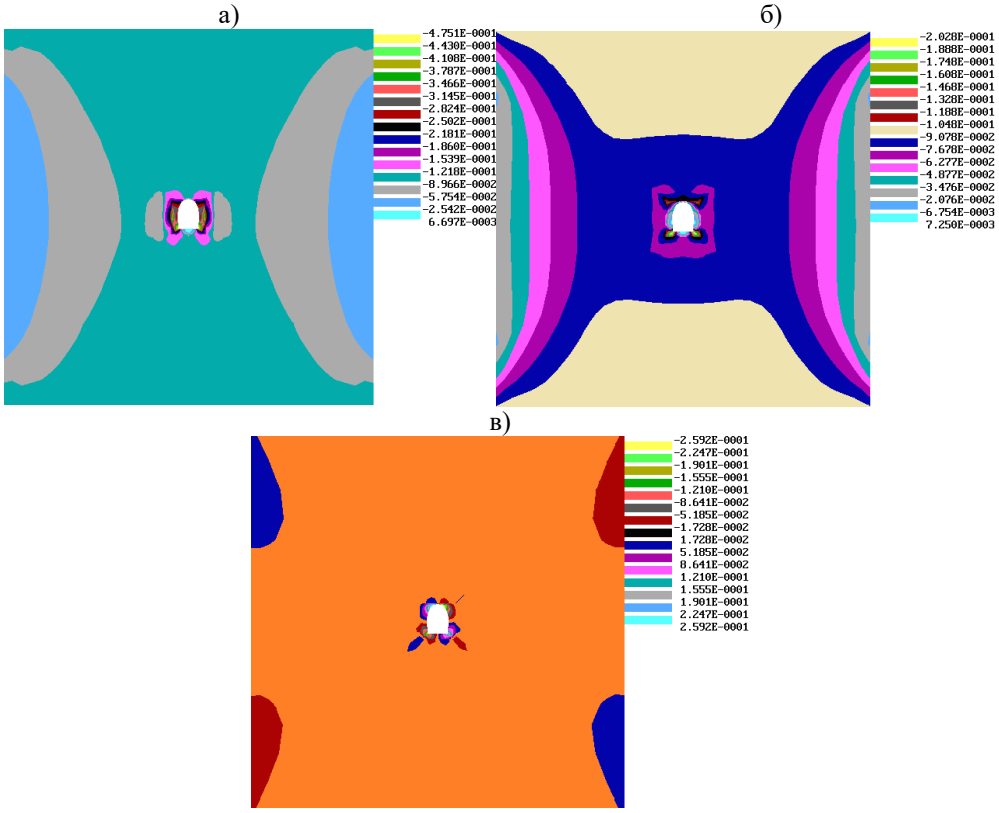

Рисунок 6. - **Изохромы напряжений системы «грунт-обделка», (МПа): а) горизонтальных, б) вертикальных, в) касательных**

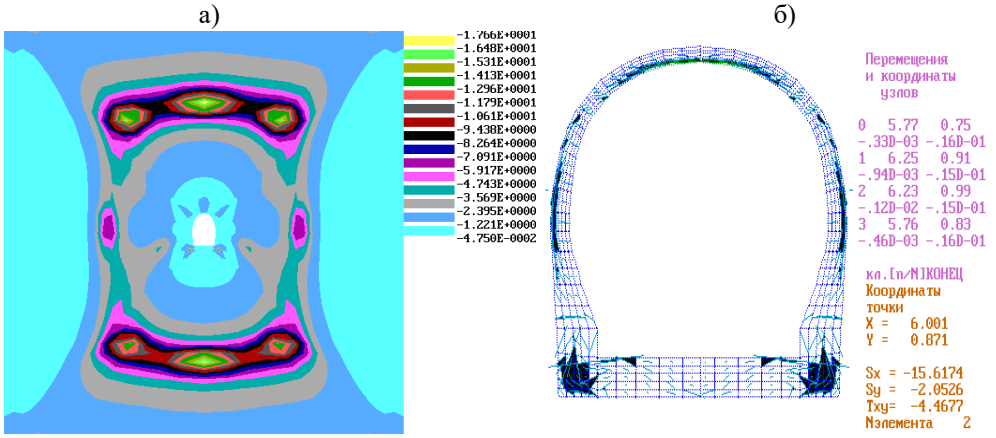

Рисунок 7. - **Возможная область: а) предельного состояния в системе «грунт-обделка», б) векторного поля напряжений**

Выявлено, что максимальные напряжения возникают в соединении стенки и лотковой части тоннельной конструкции. В середине лотковой части обделки напряжения существенно ниже относительно других сечений, так как лоток имеет повышенную жесткость с толщиной в пределах 1,0-1,2 м. Верхняя часть свода и наружная сторона стенки испытывают растягивающие напряжения, но они ниже нормативных значений.

На рисунок 8 показаны распределения главных максимальных и минимальных напряжений в сечениях обделки. В железобетонной конструкции высокие сжимающие напряжения возникли в основном в местах соединения различных элементов обделки между собой (свод-стена, стена-лоток). Максимальные значения сжимающего напряжения равнялось 9,348 МПа, которая далеко не дошла до предельного значения бетона на сжатие равной 14,8 МПа. Это связано с

присутствием в сжатой зоне продольных арматур. Растягивающие напряжения в арматурах частей бетона были самыми максимальными и их значения не превысили 3,40 МПа.

а) б)

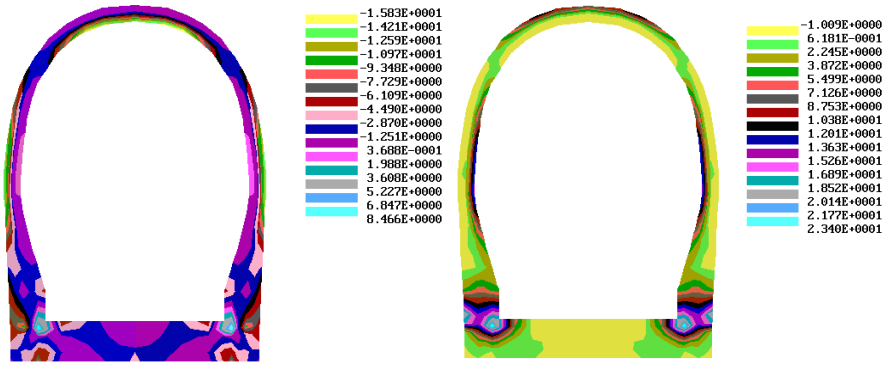

Рисунок 8. - **Изохромы главных максимальных и минимальных напряжений в тоннельной конструкции, (МПа)**

На рисунок 9 приведены полученные из расчета значения распределения напряжений за обделкой в грунте. Из этих рисунков можно увидеть места концентрации напряжений вокруг обделки тоннеля.

а) б)

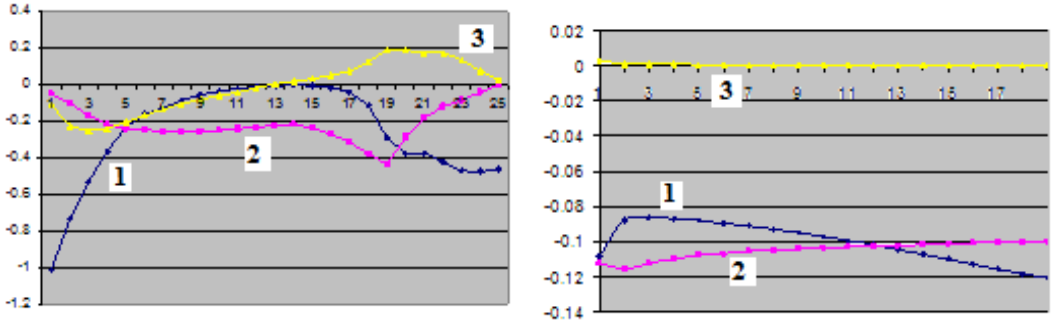

в)

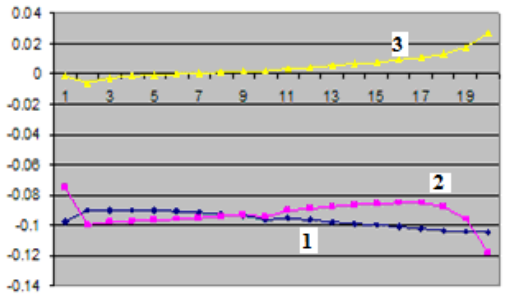

Рисунок. 9. - **Распределения напряжений, (МПа): а) вокруг тоннельной обделки, б) за тоннельной обделкой по оси X, в) за тоннельной обделкой по оси У, 1- горизонтальные напряжения, 2 - вертикальные напряжения, 3 - касательные напряжения**

5. Заключение

На основе метода конечных элементов с моделью деформирования «обделка-горный массив» разработана методика расчета конструкций автотранспортных тоннелей глубокого заложения на воздействия сейсмических волн сжатия (растяжения) и сдвига. Рассмотрен транспортный тоннель с однополосным движением, расположенный в горном районе в трещиноватых гранитах. Проанализированы основные закономерности взаимодействия обделки тоннелей совместно с вмещающим грунтовым массивом, для дальнейшей разработки рекомендаций по конструированию обделок с учетом особенностей работы тоннелей в горных условиях. Важнейшим достоинством предложенного метода расчета заключается в наглядном

просмотре и прослеживании характера деформирование железобетонной конструкции обделки в каждом ее сечении.

Литература

1. *Гарбер В. А.* Научные основы проектирования тоннельных конструкций с учетом технологии их сооружения. НИЦ "Тоннели и Метрополитены". АО "ЦНИИС", 1996, часть 1, с. 169, часть 2, с.22012.
2. *Иманалиев Т.Б.* Перспективные тоннели//Вестник КГУСТА. Вып. 3 (22). Бишкек: КГУСТА, 2008. – С. 78-83
3. Меркин В. Е., Маковский Л. В. Аварийные ситуации при строительстве и эксплуатации транспортных тоннелей и метрополитенов. Журнал «Подземной пространство мира», 1996, №1-2, с. 57-60
4. *Меликулов А. Д., Тоштемиров У. Т.* Современные технологии тоннелестроения на службе развития международных связей Узбекистана вдоль древнего великого шелкового пути. Материалы конференции “Перспективы развития строительных технологий”, ТГТУ, г. Ташкент, 2014, с.151-154
5. *Булычев Н. С.* Механика подземных сооружений, М.: Недра, 1994, с. 381
6. *Булычев Н. С., Фотиева Н. Н.* Оценка устойчивости породы, окружающей горные выработки. Шахтное строительство, 1977, №3, с.15-21
7. *Дорман И. Я.* Сейсмостойкость транспортных тоннелей. М.: Строийиздат, 2000, с. 307
8. *Давыдов С.С.* Новый метод расчета обделки подземных сооружений. Вестник ВИА, 1935, т. 2
9. *Шапошников Н.Н.* Расчет круговых тоннельных обделок на упругом основании, характеризуемом двумя коэффициентами постели. Труды МИИТ, вып. 155, М.: Трансжелдориздат, 1961.
10. *Миралимов М. Х., Ишанходжаев А. А., Болтаев И., Маджидов Н.* Разработка пакета программ по расчету транспортных сооружений методом конечных элементов. Вестник ТАДИ, №3-4, 2013. Ташкент, с.56-69
11. Рашидов Т. Р., Ишанходжаев А. А. Сейсмостойкость тоннельных конструкций метрополитена мелкого заложения. Ташкент, Фан, 1994, с.133
12. *Daniel Suchora.* "Hands on Applied Finite Element Analysis: Applications with ANSYS", AIAA Journal, Vol.54, No. 3, 2016, pp. 1150-1151
13. Seismic Design Aids for Nonlinear Analysis of Reinforced Concrete Structures. Taylor & Francis Group, London, 2010, p. 217
14. *Hartl H., Handel C.* 3D finite element modeling of reinforced concrete structures //Graz Univ. of Technol.: Inst. Of Structural Concrete. - Austria, 2000.- pp.1-10

МАТЕМАТИЧЕСКОЕ МОДЕЛИРОВАНИЕ ЗАДАЧИ ВЗАИМОДЕЙСТВИЯ ЗДАНИЙ И СООРУЖЕНИЙ С ОСНОВАНИЕМ ПРИ СЕЙСМИЧЕСКИХ ВОЗДЕЙСТВИЯХ

Низомов Д.Н.[1]

[1]Институт геологии, сейсмостойкого строительства и сейсмологии НАН Таджикистана
E-mail: nizomov-jn@mail.ru

Аннотация: *Рассматриваются вопросы математического моделирования задачи взаимодействия сооружения с упругим основанием. Разработанные алгоритмы и компьютерные программы позволяют исследовать взаимодействия зданий и сооружений на основе двух упрощённых моделей, а также модели контактной задачи теории упругости. Первые две задачи решаются исходя из дифференциальных уравнений движения, а контактная задача реализуется на основе граничных интегральных уравнений.*

Ключевые слова: *взаимодействие, численное решение, сплайн- аппроксимация, акселерограмма, полупространство, моделирование, граничные уравнения.*

1. Введение

Сооружение и основание образуют связанную динамическую систему, в которой параметры сооружения влияет на характеристики сейсмического воздействия, наблюдаемого в уровне основания здания, и поэтому физические свойства грунта основания оказывает влияние на реакции сооружения. Динамическое взаимодействие сооружения с грунтом основания является одним из основных задач в теории сейсмостойкости зданий и сооружений. Математическое моделирование и исследование напряженно-деформированного состояния взаимодействия сооружений с основанием является актуальной проблемой. Реакция сооружения на сейсмические воздействия зависит от взаимодействия между взаимосвязанных элементов системы «грунт-фундамент-сооружение». В работе исследуются задачи взаимодействия зданий и сооружений с

основанием, которые соответственно приводят к решению систем дифференциальных и граничных интегральных уравнений. Различные аспекты задачи о взаимодействия сооружения с основанием рассмотрены в работах [1-4].

2. Математическое моделирование на основе дифференциальных уравнений

Рассмотрим динамическую модель здания, которая представляет собой систему с конечным числом степеней свободы. При этом предполагается, что на глубине h от земной поверхности расположены коренные породы, куда прикладывается сейсмическое воздействие в виде заданной акселерограммы землетрясения (рис.1).. Система дифференциальных уравнений сейсмических колебаний каркасного здания можно представить в матричной форме

$$\mathbf{M}\ddot{\mathbf{W}} + \mathbf{C}\dot{\mathbf{W}} + \mathbf{K}\mathbf{W} = -\mathbf{M}\mathbf{I}\ddot{w}_0(t), \qquad (1)$$

где $\mathbf{M}, \mathbf{C}, \mathbf{K}$ – матрицы масс, затухания и жесткости, $\ddot{\mathbf{W}}, \dot{\mathbf{W}}, \mathbf{W}$ – векторы ускорений, скоростей и перемещений, $\ddot{w}_0(t)$ – заданная функция акселерограммы землетрясения,

$$\mathbf{M} = diag(m_1\ m_2\ m_3 \cdots m_n), \quad \mathbf{C} = diag(c_1\ c_2\ c_3 \cdots c_n),$$

$$\mathbf{K} = \begin{bmatrix} k_1 + k_2 & -k_2 & & & 0 \\ -k_2 & k_2 + k_3 & -k_3 & & \\ & \cdots & & & \\ & -k_{n-1} & k_{n-1} + k_n & -k_3 & \\ 0 & & & -k_n & k_n \end{bmatrix}, \ddot{\mathbf{W}} = \begin{Bmatrix} \ddot{w}_1 \\ \ddot{w}_2 \\ \cdots \\ \ddot{w}_n \end{Bmatrix}, \dot{\mathbf{W}} = \begin{Bmatrix} \dot{w}_1 \\ \dot{w}_2 \\ \cdots \\ \dot{w}_n \end{Bmatrix}, \mathbf{I} = \begin{Bmatrix} 1 \\ 1 \\ \cdots \\ 1 \end{Bmatrix}.$$

3. Численное моделирование.

Применив методы сплайн аппроксимации [5-7], векторы скоростей и ускорений, соответствующие моменту времени t_n, представляются в виде

$$\ddot{\mathbf{W}}_n = \frac{\alpha_1}{\tau_n^2}\left(\mathbf{W}_n - \mathbf{W}_{n-1}\right) - \frac{\alpha_2}{\tau_n}\dot{\mathbf{W}}_{n-1} - \alpha_3\ddot{\mathbf{W}}_{n-1}, \qquad (2)$$

$$\dot{\mathbf{W}}_n = \frac{\beta_1}{\tau_n}\left(\mathbf{W}_n - \mathbf{W}_{n-1}\right) - \beta_2\dot{\mathbf{W}}_{n-1} - \tau_n\beta_3\ddot{\mathbf{W}}_{n-1}, \qquad (3)$$

$$n = 1, 2, \ldots, N.$$

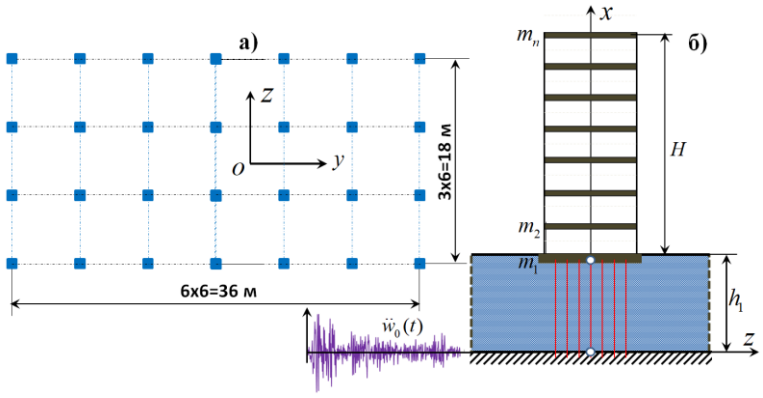

Рисунок 1. - **Модель взаимодействия сооружения с основанием**

Здесь: $\mathbf{W}_{n-1}, \dot{\mathbf{W}}_{n-1}, \ddot{\mathbf{W}}_{n-1}$ – векторы перемещений, скоростей и ускорений, соответствующие моменту времени t_{n-1}, $\mathbf{W}_n, \dot{\mathbf{W}}_n, \ddot{\mathbf{W}}_n$ – то же, соответствующие моменту времени t_n, τ_n – шаг интегрирования на отрезке времени $[t_{n-1}, t_n]$, α_j, β_j – коэффициенты, которые зависят от способа

аппроксимации. Например, если на отрезке $[t_{n-1},\ t_n]$ первую и вторую производные искомой функции последовательно аппроксимировать многочленом первой степени [7], то эти коэффициенты будут равны

$$\alpha_1 = \alpha_2 = 4, \quad \alpha_3 = 1; \quad \beta_1 = 2, \quad \beta_2 = 1, \quad \beta_3 = 0,$$

а при аппроксимации $w(t)$ на отрезке $[t_{n-1},\ t_n]$ кубической параболой

$$\alpha_1 = \alpha_2 = 6, \quad \alpha_3 = 2; \quad \beta_1 = 3, \quad \beta_2 = 2, \quad \beta_3 = 0,5.$$

Внося (2) и (3) в (1) получим систему алгебраических уравнений

$$\left(\frac{\alpha_1}{\tau_n^2}\mathbf{M} + \frac{\beta_1}{\tau_n}\mathbf{C} + \mathbf{K}\right)\mathbf{W}_n = -\mathbf{M}\mathbf{I}\ddot{w}_{0,n}(t) +$$

$$+\mathbf{M}\left(\frac{\alpha_1}{\tau_n^2}\mathbf{W}_{n-1} + \frac{\alpha_2}{\tau_n}\dot{\mathbf{W}}_{n-1} + \alpha_3\ddot{\mathbf{W}}_{n-1}\right) + \mathbf{C}\left(\frac{\beta_1}{\tau_n}\mathbf{W}_{n-1} + \beta_2\dot{\mathbf{W}}_{n-1} + \tau_n\beta_3\ddot{\mathbf{W}}_{n-1}\right), \tag{4}$$

$$n = 1, 2, \ldots, N\ .$$

Введем обозначения:

$$\mathbf{A}_{n-1} = \frac{\alpha_1}{\tau_n^2}\mathbf{W}_{n-1} + \frac{\alpha_2}{\tau_n}\dot{\mathbf{W}}_{n-1} + \alpha_3\ddot{\mathbf{W}}_{n-1}, \tag{5}$$

$$\mathbf{V}_{n-1} = \frac{\beta_1}{\tau_n}\mathbf{W}_{n-1} + \beta_2\dot{\mathbf{W}}_{n-1} + \tau_n\beta_3\ddot{\mathbf{W}}_{n-1}, \tag{6}$$

$$\mathbf{R} = \frac{\alpha_1}{\tau_n^2}\mathbf{M} + \frac{\beta_1}{\tau_n}\mathbf{C} + \mathbf{K}, \tag{7}$$

и уравнение (4) представим в виде

$$\mathbf{R}\mathbf{W}_n = -\mathbf{M}\mathbf{I}\ddot{w}_{0,n}(t) + \mathbf{M}\mathbf{A}_{n-1} + \mathbf{C}\mathbf{V}_{n-1}, \tag{8}$$

где R – матрица обобщенной жесткости, A_{n-1}, V_{n-1} – векторы ускорений и скоростей, соответствующие моменту времени t_{n-1}. Уравнение (8) можно представить в окончательном виде

$$\mathbf{R}\mathbf{W}_n = \mathbf{F}_n, \tag{9}$$

$$\mathbf{F}_n = -\mathbf{M}\mathbf{I}\ddot{w}_{0,n} + \mathbf{M}\mathbf{A}_{n-1} + \mathbf{C}\mathbf{V}_{n-1}, \tag{10}$$

где F_n – вектор обобщенной динамической нагрузки, который состоит из суммы трех векторов: сейсмических, инерционных и сил затухания.

В качестве второго варианта рассматривается модель взаимодействия, где полупространство заменяется упругими опорами, которые соответствуют горизонтальному перемещению и повороту фундаментной плиты (рис.2). Здесь предполагается, что фундаментная плита имеет две степени свободы.

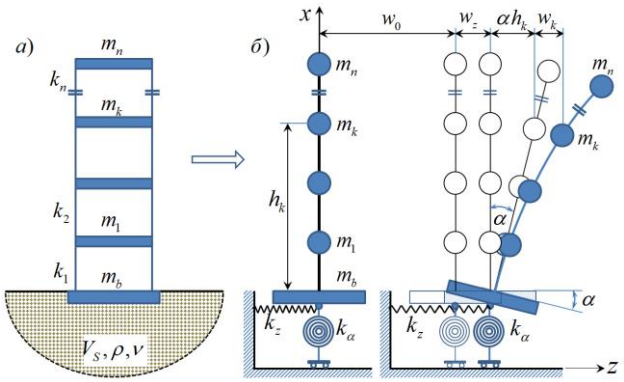

Рисунок 2. - **Упрошенная модель взаимодействия грунта основания со зданием**

В этом случаи блочные матрицы масс и жесткости представляются в виде:

$$\mathbf{M}=\begin{bmatrix}\mathbf{M}_s & \mathbf{M}_{sb}\\ \mathbf{M}_{sb}^{\mathrm{T}} & \mathbf{M}_b\end{bmatrix},\qquad \mathbf{K}=\begin{bmatrix}\mathbf{K}_s & 0\\ 0 & \mathbf{K}_b\end{bmatrix}, \tag{11}$$

где $\mathbf{M}_s$, $\mathbf{K}_s$ – квадратные блоки размера n

$$\mathbf{M}_s=\begin{bmatrix}m_1 & 0 & ... & 0\\ 0 & m_2 & ... & 0\\ & ... & & \\ 0 & ... & & m_n\end{bmatrix},\ \mathbf{K}_s=\begin{bmatrix}r_{11} & r_{12} & ... & 0\\ r_{21} & r_{22} & r_{23} & ... & 0\\ & .... & & & \\ 0 & & r_{n-1n} & r_{nn}\end{bmatrix}=\begin{bmatrix}k_1+k_2 & -k_2 & ... & 0\\ -k_2 & k_2+k_3 & -k_3 & ... & 0\\ & .... & & & \\ 0 & & & -k_n & k_n\end{bmatrix},$$

$\mathbf{M}_b$, $\mathbf{K}_b$ – квадратные блоки 2-го порядка

$$\mathbf{M}_b=\begin{bmatrix}m_b+\sum_{i=1}^{n}m_i & \sum_{i=1}^{n}m_ih_i\\ \sum_{i=1}^{n}m_ih_i & J_b\sum_{i=1}^{n}J_i+\sum_{i=1}^{n}m_ih_i^2\end{bmatrix},\qquad \mathbf{K}_b=\begin{bmatrix}k_z & 0\\ 0 & k_\alpha\end{bmatrix},$$

$\mathbf{M}_{sb}$, $\mathbf{M}_{sb}^{\mathrm{T}}$ – прямоугольные блоки размеров $n\times 2$ и $2\times n$

$$\mathbf{M}_{sb}=\begin{bmatrix}m_1 & m_1h_1\\ m_2 & m_2h_2\\ ... & ...\\ m_n & m_nh_n\end{bmatrix},\quad \mathbf{M}_{sb}^{\mathrm{T}}=\begin{bmatrix}m_1 & m_2 & ... & m_n\\ m_1h_1 & m_2h_2 & ... & m_nh_n\end{bmatrix}.$$

Матрицу затухания можно представить в блочном виде

$$\mathbf{C}=\begin{bmatrix}\mathbf{C}_s & 0\\ 0 & \mathbf{C}_b\end{bmatrix},$$

где матрица C_s принимается по Релею пропорционально матрице масс и жесткостей [8]

$$\mathbf{C}_s=a\mathbf{M}_s+b\mathbf{K}_s \tag{12}$$

a,b – коэффициенты пропорциональности. Квадратная матрица второго порядка C_b представляется в виде

$$\mathbf{C}_b=\begin{bmatrix}c_z & 0\\ 0 & c_\alpha\end{bmatrix}=a_0\mathbf{M}_b+b_0\mathbf{K}_b.$$

Векторы перемещений скоростей и ускорений состоят из $n+2$ элементов

$$\mathbf{W}=\begin{bmatrix}w_1 & w_2 & ... & w_n & w_b & \alpha\end{bmatrix}^{\mathrm{T}},$$

После того как сформированы матрицы масс, жесткостей и затухания, можно приступить к численному решению системы дифференциальных уравнений (1) по выше изложенному алгоритму. На основе изложенных алгоритмов разработаны компьютерные программы на языке Фортран и проведены численные эксперименты при различных воздействиях.

4. Пример 1.

Рассматривается 9-этажное каркасное здание размерами в плане 36×18 м, сеткой колонн 6×6 м, высота этажа $h=3$м (рис.1,а). Сечение колонн – 0,5×0,5 м, сечение ригелей – 0,3×0,45 м, толщина плит – 0,2 м. Общая масса суперструктуры составляет 564,35 тс^2/м: $m_2=m_3=\ldots=m_9=51,79$ тс^2/м, $m_{10}=42,12$ тс^2/м. Предполагается, что фундамент здания опирается на 28-ми буронабивных сваях круглого сечения *d*=0,5, которые опираются на плотный

грунт или скальное основание, достигая проектной глубины (рис.1,б). Буронабивные сваи с армированным каркасом предают нагрузку не только на тот слой грунта, на который опираются, но и по всей боковой поверхности.

На рис.3 показаны полученные графики изменения горизонтальных перемещений массы m_1 и m_{10} во времени от сейсмического воздействия в виде заданной акселерограммы El Centro на уроне коренных пород, расположенных на глубине h_1=20 м от земной поверхности (рис.1,б). Результаты получены при шаге интегрирования τ_n=0,001 с на отрезке времени 8 секунд, хотя продолжительность акселерограммы более 30 секунд. На отрезок времени от нуля до восьми секунд приходится пиковые значения ускорения землетрясений. При этом максимальное перемещение массы m_{10} получается более 20-ти сантиметр.

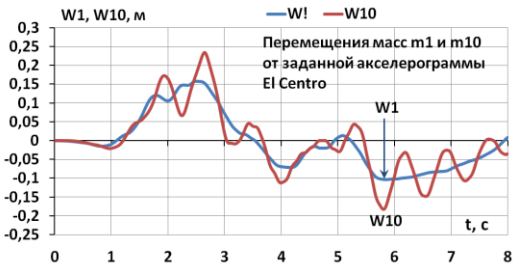

Рисунок 3. - **Графики колебания массы m_1 и m_{10} здания**

5. Вывод.

Предлагаются математические модели, которые описывают упрощенные модели задачи взаимодействия сооружения с основанием. В результате проведенных аппроксимаций по времени получены системы алгебраических уравнений, которые на каждом шаге по времени решаются итерационным методом Зейделя. Разработанные алгоритмы и компьютерные программы могут быть использованы на стадии вариантного проектирования зданий и сооружений, взаимодействующих с основанием.

6. Математическое моделирование на основе граничных интегральных уравнений

Пусть тело сооружения, которое занимает область V+Ω, где Ω=Ω$_0$+Ω$_1$, имеет контактную поверхность Ω$_0$ с полупространством (рис.4). Предполагается, что породный массив полупространства является изотропным и линейно-упругим с модулем сдвига G_0 и коэффициентом Пуассона ν_0 и находится в начальном напряженном состоянии σ_{ij}^0. Также предполагается, что в теле полупространство имеется полость с граничной поверхностью Ω$_2$.

Из рассмотрения сооружения и исходя из теоремы взаимности работ [9] можно записать интегральное уравнение [7]

$$c_{ij}w_j(\xi)+\int\limits_{\Omega_0+\Omega_1} p_{ij}^*(\xi,x)w_j(x)d\Omega(x)-\int\limits_{\Omega_0} w_{ij}^*(\xi,x)p_j(x)d\Omega(x)=$$

$$=\int\limits_{\Omega_1} w_{ij}^*(\xi,x)p_j^0(x)d\Omega(x)+\int\limits_V w_{ij}^*(\xi,y)\bar{Q}_j(y)dV(y), \qquad (13)$$

где $p_j^0(x)$ – заданная нагрузка на поверхности Ω_1; $p_j(x)$ – напряжения на контактной поверхности; $\bar{Q}_j(y)$ – объемная сила. Неизвестными в (13) являются компоненты перемещения на поверхности Ω=Ω$_0$+Ω$_1$ и компоненты напряжений на поверхности Ω$_0$.

Второе граничное уравнение мы получаем из рассмотрения полубесконечного пространства с полостью и с учетом действия контактных напряжений на поверхности полупространства

$$c_{ij}w_j(\xi)+\int_{\Omega_2} p_{ij}^*(\xi,x)w_j(x)d\Omega(x)-\int_{\Omega_0} w_{ij}^*(\xi,x)p_j(x)d\Omega(x)=$$
$$=\int_{\Omega_2} w_{ij}^*(\xi,x)p_j^0(x)d\Omega(x),\quad \xi\in\Omega_2,\quad x\in\Omega_0+\Omega_2,\quad i,j=1,2,3. \qquad (14)$$

где $p_j^0(x)$ – заданная нагрузка на поверхности Ω_2. Неизвестными в (14) являются перемещения на поверхности Ω_2 и напряжения на контактной поверхности Ω_0.

Третье уравнение мы можем получить из (14) если принимать, что $\xi\in\Omega_0$ и $c_{ij}=\delta_{ij}$, тогда будем иметь:

$$w_i(\xi)+\int_{\Omega_2} p_{ij}^*(\xi,x)w_j(x)d\Omega(x)-\int_{\Omega_0} w_{ij}^*(\xi,x)p_j(x)d\Omega(x)=$$
$$=\int_{\Omega_2} w_{ij}^*(\xi,x)p_j(x)d\Omega(x),\quad \xi\in\Omega_0,\quad x\in\Omega_0+\Omega_2, \qquad (15)$$

где неизвестными являются компоненты перемещения на контактной границе Ω_0 и на поверхности Ω_2, а также компоненты напряжений на поверхности Ω_0.

Таким образом, системы из трех граничных уравнений (13)-(15) позволяют сформировать систему разрешающих уравнений задачи взаимодействия сооружения с полу бесконечным пространством, в котором имеется полость с поверхностью Ω_2. Следует отметить, что во всех трех приведенных интегральных уравнениях неизвестными являются перемещения или напряжения на поверхности исследуемого объекта.

7. Численное моделирование.

С целью численного интегрирования, выполняется сплайн-аппроксимация граничных параметров [7]. Например, если контуры Ω_0, Ω_1, и Ω_2 разбиваются соответственно на n_0, n_1 и n_2 постоянных элементов, а область V на m постоянных ячеек, то систему разрешающих алгебраических уравнений, полученную в результате такой аппроксимации, можно представить в матричной форме

$$\begin{bmatrix} \mathbf{A_1^1} & \mathbf{A_1^0} & \mathbf{-B_1^0} & \mathbf{0} \\ \mathbf{0} & \mathbf{0} & \mathbf{-B_2^0} & \mathbf{A_2^2} \\ \mathbf{0} & \mathbf{E_3^0} & \mathbf{-B_3^0} & \mathbf{A_3^2} \end{bmatrix} \begin{Bmatrix} \mathbf{U_1} \\ \mathbf{U_0} \\ \mathbf{P_0} \\ \mathbf{U_2} \end{Bmatrix} = \begin{bmatrix} \mathbf{B_1^1} & \mathbf{D_1^1} & \mathbf{0} \\ \mathbf{0} & \mathbf{0} & \mathbf{B_2^2} \\ \mathbf{0} & \mathbf{0} & \mathbf{B_3^2} \end{bmatrix} \begin{Bmatrix} \mathbf{P^0} \\ \mathbf{Q} \\ \mathbf{P_2} \end{Bmatrix}. \qquad (16)$$

$\mathbf{U_1}=\{\mathbf{W_{1i}}\ \mathbf{W_{2i}}\ \mathbf{W_{3i}}\}^{\mathrm{T}}$, $i=1,2,...,n_1$, $\mathbf{P_0}=\{\mathbf{P_{1i}}\ \mathbf{P_{2i}}\ \mathbf{P_{3i}}\}^{\mathrm{T}}$, $i=n_1+1,...,n_1+n_0$, здесь $\mathbf{E}_3^0$ -- единичная матрица порядка n_0; $\mathbf{W}_{ij}$, $\mathbf{P}_{ij}$ $(i=1,2,3;\ j=1,2,\ldots)$ – векторы, элементы которых соответствуют перемещениям и напряжениям по направлению оси x_i.

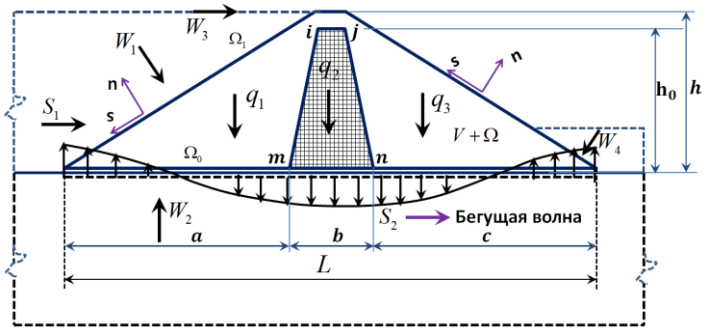

Рисунок 4. - **Нагрузки, действующие на платину**

Три строки в матричном уравнении (16) соответствуют трем интегральным уравнениям (13) – (15); верхний индекс указывает на номер поверхности, где производится интегрирование, а нижний индекс соответствует номеру уравнений в том порядке, как они записаны. Например, $\mathbf{A}_3^2 -$ блочная матрица, элементы у которой соответствуют уравнению (15), при интегрировании по поверхности Ω_2. Каждая из матриц в (16) является блочной матрицей типа

$$\mathbf{A}_{ks} = \begin{bmatrix} a_{11}^{ks} & a_{12}^{ks} & \dots & a_{1N}^{ks} \\ \dots & \dots & \dots & \dots \\ a_{N1}^{ks} & a_{N2}^{ks} & \dots & a_{NN}^{ks} \end{bmatrix}, \quad \mathbf{B}_{ks} = \begin{bmatrix} b_{11}^{ks} & b_{12}^{ks} & \dots & b_{1N}^{ks} \\ \dots & \dots & \dots & \dots \\ b_{N1}^{ks} & b_{N2}^{ks} & \dots & b_{NN}^{ks} \end{bmatrix},$$

$$(k, s = 1, 2, 3),$$

элементы, в которых вычисляются по следующим формулам:

$$a_{ij}^{ks} = \int\limits_{\Delta\Omega_j} p_{ks}^*(i, j) d\Omega_j , \quad b_{ij}^{ks} = \int\limits_{\Delta\Omega_j} w_{ks}^*(i, j) d\Omega_j ,$$

$$d_{ij}^{ks} = \int\limits_{\Delta V_j} w_{ks}^*(i, j) dV_j , \ (k, s = 1, 2, 3),$$

$$i = 1, 2, ..., N , \quad j = 1, 2, ..., M .$$

Векторы заданных напряжений на граничных поверхностях и объемных сил в ячейках тело сооружения записываются так:

$$\mathbf{P}^0 = \{\mathbf{P}_{1i}^0 \ \mathbf{P}_{2i}^0 \ \mathbf{P}_{3i}^0\}^{\mathrm{T}}, \qquad i = 1, 2, ..., n_1 ,$$

$$\mathbf{P}_2 = \{\mathbf{P}_{1i} \ \mathbf{P}_{2i} \ \mathbf{P}_{3i}\}^{\mathrm{T}}, \qquad i = n+1, ..., n+n_2 . \tag{17}$$

$$\mathbf{Q} = \{\mathbf{Q}_{1i} \ \mathbf{Q}_{2i} \ \mathbf{Q}_{3i}\}^{\mathrm{T}}, \qquad i = 1, 2, ..., m .$$

Следует отметить, что при вычислении элементов первой строки матриц в (16) используются фундаментальные решения Кельвина [9], а для двух остальных строках – фундаментальные решения Миндлина [10].

Систему разрешающих уравнений задачи взаимодействия сооружения с полупространством (16) можно записать в стандартном виде

$$\mathbf{[A]\{X\} = \{B\}}, \tag{18}$$

$$\mathbf{\{X\} = \{U_1 \ U_0 \ P_0 \ U_2\}}^{\mathrm{T}},$$

где матрица **[A]** являет квадратной матрицей $\beta(2n_0 + n_1 + n_2)$ порядка, где $\beta = 3$ и 2 соответственно для трех – и двумерных задач. Векторы **{X}** и **{B}** в соответствии состоят из $\beta(2n_0 + n_1 + n_2)$ элементов, например, при разбивке: $n_0 = 5$, $n_1 = 8$, $n_2 = 9$ и при $\beta = 2$, матрица **[A]** будет иметь 54 порядок. После решения системы уравнений (18) и определения искомых перемещений и напряжений на граничных поверхностях можно приступить к вычислению тензора деформаций и напряжений и определению напряженно-деформированного состояния системы.

8. Пример 2.

Исследование напряженно-деформированного состояния неоднородной земляной плотины при совместном воздействии различных нагрузок. Численные исследования проведены на примере неоднородной земляной плотины со следующими геометрическими параметрами:

$$a = c = 160 \text{ м}, \ b = 60 \text{ м}, \ h = 87 \text{ м}, \ h_0 = 82 \text{ м}, \ a_1 = c_1 = 172 \text{ м}, \ b_0 = 36 \text{ м};$$

и упругими параметрами грунта основания, упорных призм и ядра:

$$\mu_0 = 57{,}69 \text{ МПа } (5769 \text{ тс/м}^2), \ \nu_0 = 0{,}3; \ \mu_1 = \mu_3 = 38{,}46 \text{ МПа } (3846 \text{ тс/м}^2); \ \nu_1 = \nu_3 = 0{,}3,$$

$$\gamma_1 = \gamma_3 = 2{,}2 \text{ т/м}^3; \ \mu_2 = 22{,}14 \text{ МПа } (2214 \text{ тс/м}^2); \ \nu_2 = 0{,}4, \ \gamma_2 = 2{,}2 \text{ т/м}^3.$$

Результаты получены при дискретном представлении всей границы на 154 постоянных граничных элементов. На рис.2 показаны графики изменения тангенциальных напряжений вдоль контура ядра плотины при различных воздействиях: q_k+W_1 (кривая 1); $q_k+W_1+W_2$ (кривая 2); $q_k+W_1+W_2+S_1$(кривая 3), где q_k – вес плотины, W_1 – гидростатическое давление, W_2 – фильтрационное противодавление, S_1 – сейсмическое воздействие [11]. Можно увидеть, что действия сейсмической нагрузки приводит к значительному росту напряжений в угловых зонах контура гребни плотины.

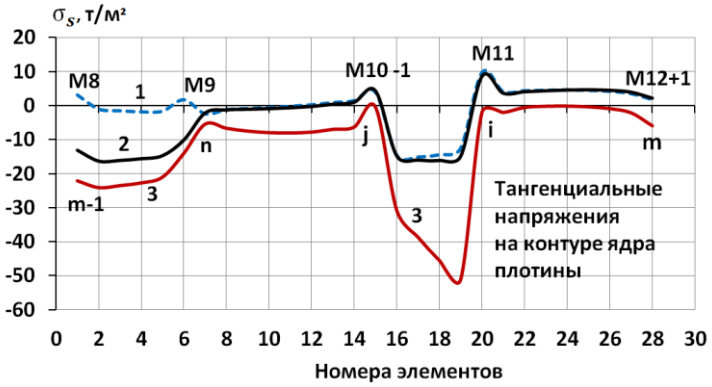

Рисунок 5. - **Графики изменения тангенциальных напряжений на контуре ядра плотины**

9. ВыводыF

Таким образом, разработана математическая модель задачи взаимодействия сооружения с упругим полупространством. Предлагаемый алгоритм расчета является универсальным и позволяет проводить исследования напряженно-деформированного состояния системы как трехмерных, так и двумерных, как статических, так и динамических задач теории упругости. Так как основными неизвестными в разрешающей системе уравнений в случае смешанной задачи являются перемещения и напряжения на граничных поверхностях, то количество неизвестных здесь существенно меньше, чем при решении данной задачи по методам конечных разностей или конечных элементов.

Литература

1. *Баженов В.Г. и др*. Численное моделирование задач взаимодействия сооружений с двухслойным грунтовым основанием при сейсмических воздействиях // Проблемы прочности и пластичности: межвуз. сб. –, - вып. 67, 2005, с.162-167.
2. *Мкртычев О.В., Джинчвелашвили Г.А., Бусалова М.С.* Моделирование взаимодействия сооружения с основанием при расчете на землетрясение // Вестник МГСУ, 2013, №12, с. 34-40.
3. *Kramer, S.L*. Geotechnical Earthquake Engineering, Prentice Hall, Upper Saddle River. New Jersey 1996, 07458- 672c.
4. *Davide Forcellini.* A Novel Framework to Assess Soil Structure Interaction (SSI) Effects with Equivalent Fixed-Based Models. - Department of Civil Engineering, University of Auckland, 20 Symonds St., Auckland 1010, New Zealand.
5. *Низомов Д.Н.* Методы прямого интегрирования дифференциальных уравнений движения дискретных систем Сб. науч. тр. ТТУ: «Строительство и архитектура». Вып. 2 –Душанбе,ТТУ, 1992- с. 39-46.
6. *Низомов Д.Н.* Численное решение динамической задачи мембраны на основе метода граничных элементов при линейной аппроксимации ускорения. Труды ТТУ. Серия: «Стр-во и арх-ра» Вып.3. Душанбе, ТТУ, 1993. с.7-12.
7. *Низомов Д.Н.* Метод граничных уравнений в решении статических и динамических задач- М.: Изд-во Ассоциации строительных вузов (АСВ), 2000.-282с.
8. *Клаф Р., Пензиен Дж*. Динамика сооружений. – М.: Стройиздат, 1979. -320 с.
9. *Новацкий В.* Теория упругости. М.: Мир, 1975, 872с.
10. *Лурье А.И.* Теория упругости. М.: Наука, 1970. - 939с.
11. *Гришин М.М., Розанов Н.П., Белый Л.Д., и др.* Бетонные плотины (на скальных основаниях). М.: Стройиздат, 1975. -352с.

УПРУГОПЛАСТИЧЕСКИЕ ВОЛНЫ В ГРУНТАХ ПРИ ПРОДОЛЬНОМ ДВИЖЕНИИ ПОДЗЕМНОГО ТРУБОПРОВОДА

Рихсиева Б.Б.[1], Салихова З.Р.[1], Хусанов Б.Э.[1]

[1]*Институт механики и сейсмостойкости сооружений им. М.Т.Уразбаева АН РУз, Ташкент, Узбекистан*
E-mail: barnobrkh@gmail.com

Аннотация: *В работе исследуется процесс распространения одномерных цилиндрических волн в грунтах при движении твердого цилиндрического подземного трубопровода в направлении оси симметрии. Получены численные результаты с применением метода конечных разностей при различных граничных условиях, в том числе при движении трубопровода. Определены параметры распространяющихся цилиндрических волн сдвига в грунте при продольном движении подземного трубопровода и границы области пластического деформирования.*

Ключевые слова: *грунтовые среды, подземные трубопроводы, параметры волны, цилиндрическая волна.*

1. Введение

Подземные трубопроводы вовлекаются в движение за счет возникающих сил (напряжений) на их внешней поверхности, взаимодействующей с грунтом. Величины этих напряжений и движения самого трубопровода определяются процессом, возникающим в грунте вокруг трубопровода.

В [1–3] подробно выявлены основные силы, воздействующие на подземные трубопроводы при землетрясениях. Рассмотрены методы для определения характеристики реакции грунта на движение подземного трубопровода. Сопоставлены результаты различных испытаний взаимодействия с трубопроводом. В [4] исследована работоспособность подземных трубопроводов, подверженных постоянному ударному нагружению при проскальзывании с грунтом. Для трубопроводов, имеющих бесконечную и конечную длину, показано влияние граничных условий на деформацию трубопровода. В [5], используя конечно-элементную модель из балочных элементов для трубопровода и нелинейных пружин для грунта, исследована способность рассматриваемой модельной системы «трубопровод-грунт» противостоять обратному смещению разлома. Вопросам безопасности подземных стальных трубопроводов природного газа посвящена работа [6]. Образование выпучивания магистральных газопроводов при землетрясениях исследовано в [7].

Для обеспечения прочности и безаварийной работы подземных трубопроводов, особенно при сейсмических воздействиях, основную роль сыграет процесс, происходящий в окруженном грунте. Поэтому исследования процесс деформирования грунта вокруг подземного трубопровода имеет научное и практическое значение. Изменение механических характеристик грунтов при его деформировании изучено на основе экспериментов в [1, 8]. Методы определения механических характеристик грунтов при динамических (сейсмических) нагрузках и изменение деформационных характеристик грунта при взаимодействии с трубопроводом рассмотрены в [8, 9]. Надежность и прочность системы подземных трубопроводов, как отмечается в [8, 10–11], прежде всего, зависят от сил взаимодействия, возникающих при относительном движении трубопровода и окружающего грунта. При этом, одним из важных моментов является напряженное состояние и динамическое поведение грунта вокруг подземного трубопровода. Развитием исследования динамических процессов и напряженно-деформированного состояния в грунтах является применение нелинейных уравнений состояний. Наиболее общими и широко применяемыми нелинейными уравнениями состояния являются упругопластические законы деформирования [11–12]. В настоящей работе с использованием этих законов деформирования исследуется нестационарное поведение грунта с учетом пластических свойств вокруг подземного трубопровода при продольном движении трубопровода, что является продолжением работы [6,8,10–11].

2. Постановка задачи

Предположим, что в безграничной недеформированной грунтовой среде имеется достаточно протяженный и жестко закрепленный подземный трубопровод с внешним радиусом $r = r_0$.

Пусть в начальный момент времени подземный трубопровод начинает поступательное движение по направлению оси симметрии, при этом деформацией трубопровода пренебрегаем, т.е. считаем его абсолютно недеформируемым. В этом случае в грунте начинают распространяться сдвиговые цилиндрические волны, параметры этих волн являются осесимметричными относительно оси трубопровода и они зависят только от радиальной координаты и времени, т.е. задача является одномерной.

Уравнение движения грунта при отсутствии массовых сил в эйлеровом представлении имеет следую вид:

$$\rho \frac{dv_z}{dt} = \frac{\partial \tau_{zr}}{\partial r} + \frac{\tau_{zr}}{r}, \tag{1}$$

где r – радиальная координата; $v_z = v_z(r,t)$ – скорость частиц грунта по цилиндрической координате z, $\tau_{zr} = \tau_{zr}(r,t)$ – сдвиговое напряжение грунта. Для решения уравнения (1), где неизвестными являются $v_z = v_z(r,t)$ и $\tau_{zr} = \tau_{zr}(r,t)$, добавим соотношение Коши в виде

$$\dot{\varepsilon}_{zr} = \frac{d\varepsilon_{zr}}{dt} = \frac{\partial v_z}{\partial r}. \tag{2}$$

Чтобы получить замкнутую систему уравнений, в (1) – (2) необходимо добавить уравнение состояния. Уравнение состояния грунта принимаем в виде упругопластического закона деформирования:

при $|\tau_{zr}| < \tau_s$ $\qquad \dot{\tau}_{zr} = G\dot{\varepsilon}_{zr}$, (3)

при $|\tau_{zr}| \geq \tau_s$ $\qquad \tau_{zr} = \tau_s$. (4)

где τ_s – предельное значение касательного напряжения при пластическом деформировании.

Для решения этой системы уравнения принимаем следующие начальные условия:

При $t = 0, \quad r > r_0$:

$$v_z(r,0) = 0, \quad \tau_{zr}(r,0) = 0, \quad \varepsilon_{zr}(r,0) = 0; \tag{5}$$

граничные условия: при $r = r_0 \quad t \geq 0$:

$$v_z(r_0,t) = v_0(t) \text{ или } u_z(r_0,t) = u_0(t) \text{ или } \tau_{zr}(r_0,t) = \tau_0(t). \tag{6}$$

где $u_0(t)$ и $v_0(t)$ – перемещение и скорость подземного трубопровода в направлении оси протяженности (Oz).

Таким образом, система уравнений (1)-(4) с начальными (5) и граничными (6) условиями является замкнутой, определяет процесс распространение сдвиговой волны и напряженно-деформированное состояние грунта при продольном движении жесткого подземного трубопровода.

3. Численные результаты задачи и их анализ

Воспользуемся конечно-разностной схемой [6, 13-14] и численно решим поставленную задачу. Безграничный грунт считаем ограниченным радиусом $r = R$, что является областью искомых решений. Учитывая скорость распространения сдвиговых волн c_S, численное решение

рассматриваемой задачи получим до момента времени, когда фронт передней волны достигает границу $r = R$, т.е. получим численное решение до момента времени $t \le (R - r_0)/c_s$.

Рассмотрим вариант задания касательного напряжения на границе $r = r_0 = 0.1$ м по гармоническому закону

$$\tau_0(t) = \tau_{\max} \sin(\omega t). \qquad (7)$$

Исходные данные точно такие, как в [6, 11], а $\tau_{\max} = 5$ МПа, $\omega = 50\pi$ рад/с $\tau_s = 2$ МПа, $G_1 = G/100$. На рис.1–4 приведены изменения касательного напряжения τ_{zr} (рис.1), сдвиговой деформации ε_{zr} (рис.2), скорости частиц v_z (рис.3) и смещения частиц u_z (рис.4) по времени в фиксированных сечениях $r = 0.105$, 0.15, 0.2, 0.3, 0.4 и 0.6 м, соответствующих кривым *1–6*.

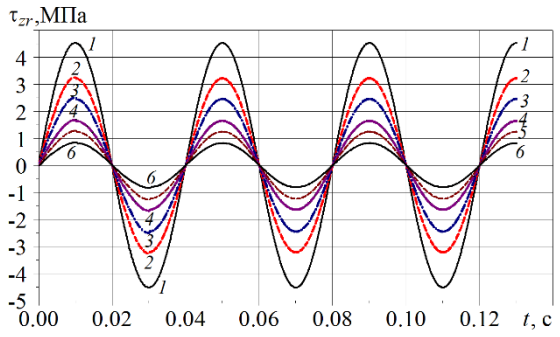

Рисунок 1. - **Изменение касательного напряжения τ_{zr} грунта по времени**

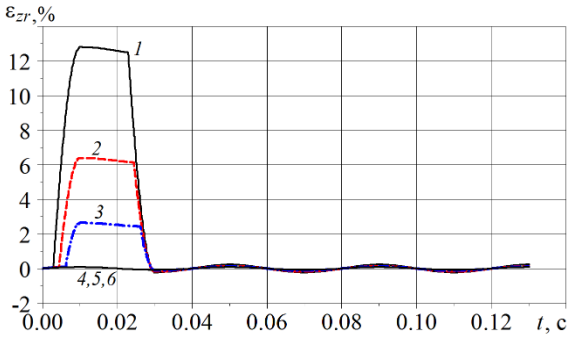

Рисунок 2. – **Изменение сдвиговой деформации ε_{zr} грунта по времени**

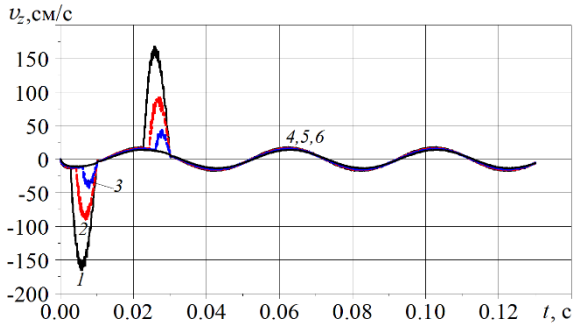

Рисунок 3. – **Изменение скорости частиц грунта v_z по времени**

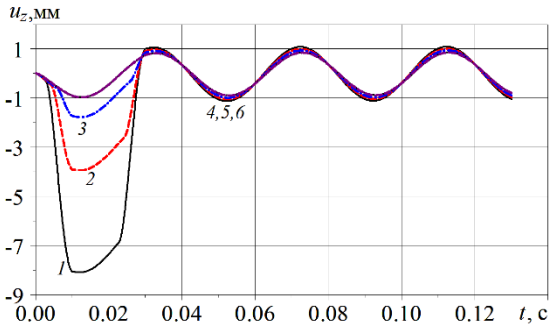

Рисунок 4. – **Изменение продольных смещений u_z грунта по времени**

Зависимость касательного напряжения τ_{zr} от деформации сдвига ε_{zr}, полученная в расчетах в тех же сечениях *1–6*, что и на рис.1–4, приведена на рис.5. Из полученной диаграммы “касательное напряжение – деформация сдвига” можно сделать вывод, что грунт за пределами расстояния r =0.3 м (кривые *4*, *5* и *6*) не испытывает пластическое деформирование, т.е. зона пластического деформирования грунта при продольном движении подземного трубопровода ограничена сечением до r =0.3 м или двукратного размера радиуса трубопровода. Согласованность диаграммы τ_{zr} (ε_{zr}) (рис.5) с кривыми касательного напряжения τ_{zr} (t) (рис.1) и сдвиговой деформации $\varepsilon_{zr}(t)$ (рис.2) подтверждает правильность применения уравнения состояния (3) – (4) с упрочнением.

Рассмотрим теперь результаты расчетов для уменьшенного начального значения τ_s=1 МПа. На рис. 6–9 приведены изменения касательного напряжения τ_{zr} (рис. 6), деформации сдвига ε_{zr} (рис. 7), скорости частиц v_z (рис. 8) и смещения частиц u_z (рис. 9) по времени в фиксированных сечениях грунта. Обозначения кривых на рис. 6–9 прежние, т.е. кривые *1–6* соответствуют значениям параметров в сечениях r=0.105, 0.15, 0.2, 0.3, 0.4 и 0.6 м грунта.

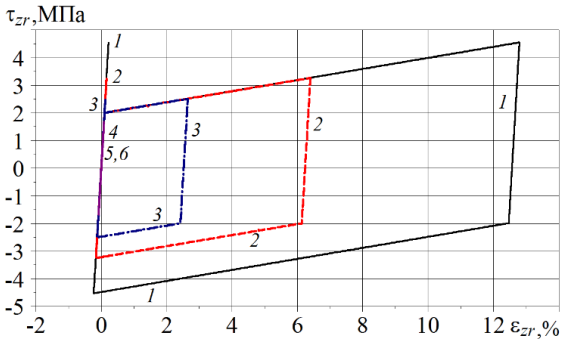

Рисунок 5. – **Диаграмма касательное напряжение – деформация сдвига**

Из рис. 6 видно, что при задании на границе касательного напряжения их значение не зависит от начального τ_s вблизи приложения нагрузок. За счет уплотнения грунта в пластическом деформировании $\tau_{zr}\ (t)$ со временем она практически совпадает с рис.1.

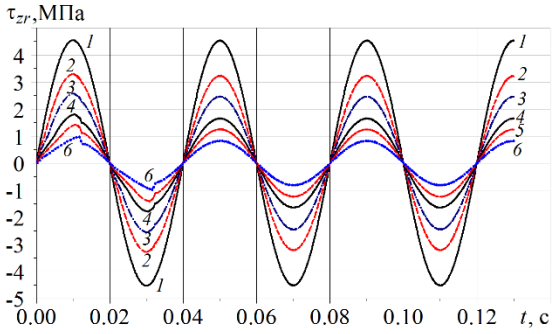

Рисунок 6. – **Изменение касательного напряжения τ_{zr} грунта по времени**

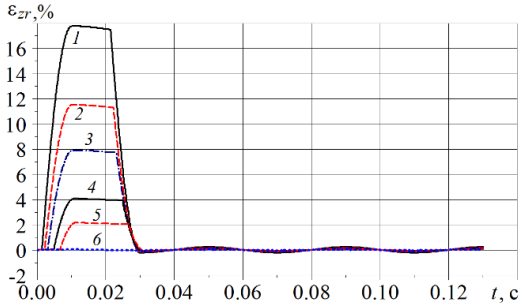

Рисунок 7. – **Изменение сдвиговой деформации ε_{zr} грунта по времени**

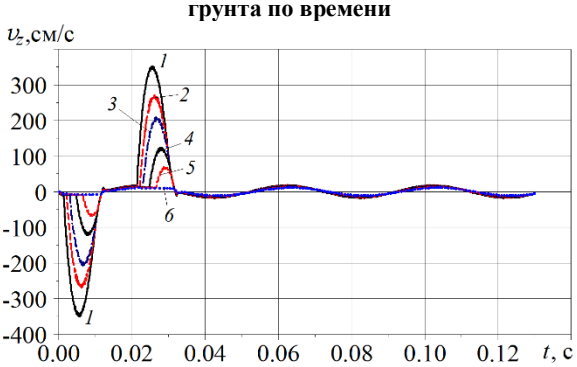

Рисунок 8. – **Изменение скорости частиц грунта v_z по времени**

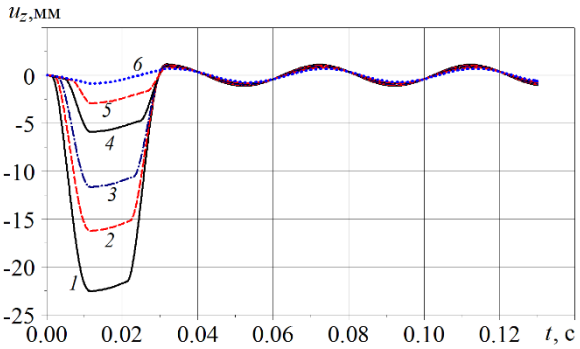

Рисунок 9. – **Изменение продольных смещений u_z грунта по времени**

На рис. 10–12 приведены эпюры максимальных касательных напряжений τ_{zr} (рис. 10), сдвиговой деформации ε_{zr} (рис. 11) и смещений частиц u_z (рис. 12) по радиальной координате грунта для начального значения τ_s=2 МПа (кривые *1*) и τ_s=1 МПа (кривые *2*) упругопластического деформирования грунта. Прямыми вертикальными линиями *1* и *2* на рис. 10–12 обозначены границы радиальных сечений грунта, отделяющие зоны упругого и упругопластического деформирования грунтов. Например, при τ_s=2 МПа в грунте до радиального сечения r =0.245 м в некоторые моменты рассматриваемого процесса происходит упругопластическая деформация, а за границами вертикальной линии *1*, т.е. за пределом r=0.245 м, отсутствуют остаточные деформации, т.е. происходит только упругое деформирование. С уменьшением значения τ_s на 1 МПа эта граница (вертикальная линия *2*) увеличивается и достигает r=0.58 м.

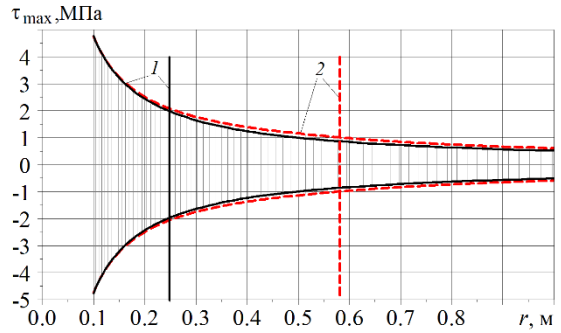

Рисунок 10. – **Распределение максимальных напряжений τ_{zr} по радиусу**

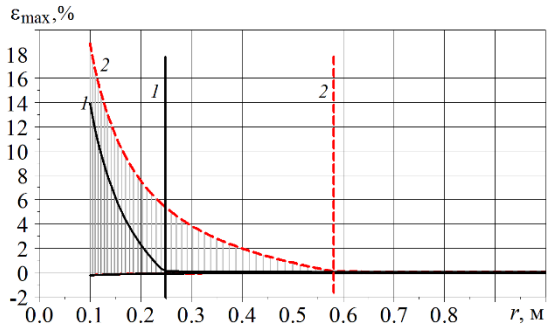

Рисунок 11. – **Распределение максимальных значений деформации ε_{zr} сдвига по радиальному сечению грунта**

При задании на границе касательного напряжения начальное значение τ_s практически не влияет на распределения касательного напряжения $\tau_{zr}(r)$, но значения τ_s существенно влияют на максимальные сдвиговые деформации ε_{zr} и смещения частиц u_z грунта. Уменьшение начального значения τ_s увеличивает не только зону пластического деформирования, но и деформацию ε_{zr} и смещение грунта u_z в области пластического деформирования.

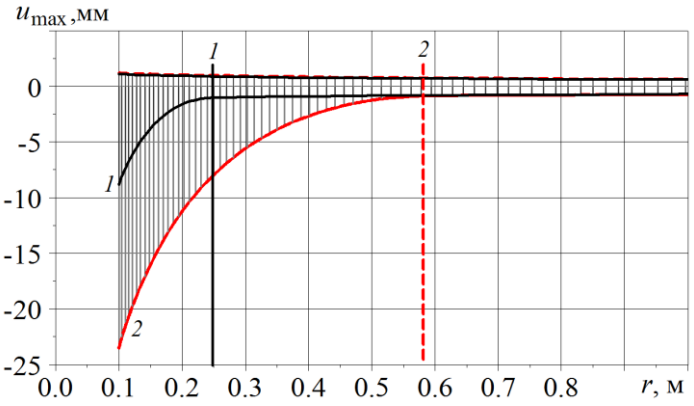

Рисунок 12. – **Распределение максимальных значений смещений u_z по радиусу**

В целом, из рис. 10–12 можно определить толщину грунта (можно рассчитать приконтактный слой), где происходит пластическое деформирование. Как видно из рис. 11–12, при задании на поверхности контакта подземного трубопровода с грунтом за пределами области пластического деформирования сдвиговая деформация ε_{zr} и продольное смещение u_z грунта стабилизируются и не зависят от значения и способа задаваемой касательной нагрузки.

4. Заключение

Численно решением упругопластической задачи установлены существование приконтактного слоя грунта, возможность определения толщины этого слоя, т.е. границы пластического и упругого деформирования грунтов.

Выявлено влияние задания граничных условий на параметры волны, максимальные значения касательного напряжения и сдвиговой деформации, а также на границу области пластического деформирования.

Решением теоретической задачи показана возможность рассчитать приконтактный слой грунта, где происходит пластическое деформирование за пределом которой поведение грунта не зависят от значения и способа задаваемой касательной нагрузки на поверхности контакта трубопровода с грунтом.

Литература

1. *Султанов К.С*. Волновая теория сейсмостойкости подземных сооружений / «ФАН» Ташкент, 2016, 392 с.
2. *Israilov M.S.* Solution of the External Pochhammer–Chree Problem and Bending Seismic Vibrations of the Pipeline in Infinite Elastic Continuum // Mechanics of Solids. 2023, vol.58, pp.26–37.
3. *Sultanov K.* Contact interaction of an underground pipeline with soil under dynamic impacts // Facta Universitatis, Series: Mechanical Engineering, [S.l.], mar. 2024. ISSN 2335-0164. Date accessed: 31 mar. 2024.
4. *O'Rourke T.D., Jung J.K., Argyrou C.* Underground pipeline response to earthquake-induced ground deformation // Soil Dynamics and Earthquake Engineering. 2016, vol.91, pp.272–283.
5. *Vazouras P., Dakoulas P., Karamanos S.A*. Pipe–soil interaction and pipeline performance under strike–slip fault movements // Soil Dynamics and Earthquake Engineering. 2015, vol.72, pp.48–65.
6. *Rikhsieva B., Khusanov B.* Simulation of soil behavior under longitudinal motion of underground pipeline in one-dimensional statement // E3S Web of Conferences. 2023. vol.383, pp.04091.
7. *Psyrras N.K., Sextos A.G.* Safety of buried steel natural gas pipelines under earthquake induced ground shaking: A review // Soil Dynamics and Earthquake Engineering. 2018, vol.106, pp. 254–277.
8. *Sultanov K.S., Vatin N.I.* Wave Theory of Seismic Resistance of Underground Pipelines // Applied Sciences. 2021, vol.11, pp.1–28.
9. *Fares R., Santisi d'Avila M.P., Deschamps A.* Soil-structure interaction analysis using a 1DT-3C wave propagation model // Soil Dynamics and Earthquake Engineering. 2019, vol.120, pp.200–213.
10. *Khusanov B., Rikhsieva B., Salikhova Z*. Longitudinal wave propagation in an extended cylindrical body with external Coulomb friction // E3S Web of Conferences. 2023, vol.402, pp.10015.
11. *Rikhsieva B., Khusanov B.* The influence of plastic properties of the surroundings on the interaction process of the "cylindrical body – External medium" system // AIP Conference Proceedings. 2023, vol.2768, Iss.1, pp.020020
12. *Zhuravkov M., Lyu Y., Starovoitov E.* Mathematical Models of Plasticity Theory. In: Mechanics of Solid Deformable Body / "Springer" Singapore, 2023, pp.149–197.
13. *Wilkins M.L.* Computer Simulation of Dynamic Phenomena / "Springer-Verlag" Berlin, 2010, 246 p.
14. *Rikhsieva B., Khusanov B.* Accuracy and stability of a finite difference scheme for two-dimensional problems of soil dynamics. // E3S Web of Conferences. 2023, vol.420, pp.03012

ЧИСЛЕННЫЙ РАСЧЕТ ГРУНТОВОЙ ПЛОТИНЫ С УЧЕТОМ УПРУГО-ПЛАСТИЧЕСКОГО ДЕФОРМИРОВАНИЯ ГРУНТА ПРИ СЕЙСМИЧЕСКИХ ВОЗДЕЙСТВИЯХ.

Султанов К.С.[1], Умархонов С.И.[1]

[1]Институт механики и сейсмостойкости сооружений, Ташкент, Узбекистан

E-mail: umarkhonov@gmail.com

Аннотация: *В данной статье решено напряженно-деформированное состояние грунтовой плотины под действием сейсмических сил с учетом упругопластического деформирования грунта. Одним из численных методов, используемых при решении динамической задачи, является метод конечных разностей. В качестве грунтовой плотины было исследовано Ахангаранское водохранилище в Ангренском районе. Его высота – 100 м, а максимальный объём воды – 260 млн.м^3. Основание предполагается абсолютно жестким. Приводятся результаты изменения напряжений, перемещений и деформаций во времени в характерных точках грунтовой плотины при действии сейсмических сил, которые приложены к её основанию.*

Ключевые слова: *грунтовая плотина, деформирование, сейсмические воздействия, численное решение, метод конечных разностей, динамическое поведение.*

1. Введение

Грунтовые плотины играют очень важную роль в обеспечении населения питьевой водой и электроэнергией, а также в сельском хозяйстве. Во всем мире построено и строится множество грунтовых плотин. Грунтовые плотины, расположенные в сейсмических регионах, очень опасны, а их постоянный контроль и определение напряженно-деформированного состояния является важной задачей. Грунтовые плотины настолько уникальны, что их напряженно-деформированное состояние невозможно рассчитать практически. Численные методы обычно используются для расчета динамического состояния крупных сооружений. Одним из численных методов, использованных в данной научной статье, является метод конечных разностей.

За последние годы проведен ряд организационных работ по обеспечению стабильной безопасности гидротехнических сооружений Узбекистана. С помощью современных передовых цифровых технологий большое внимание уделяется обеспечению экологической, экономической, энергетической и сейсмической безопасности населения, зданий, в том числе водохозяйственных сооружений.

Мировой опыт показывает, что экономически выгоднее и эффективнее вовремя предотвратить подобные события, чем устранять последствия, связанные с наводнениями или другими авариями на гидротехнических сооружениях. Организация мониторинга и прогнозирования возможных чрезвычайных ситуаций, реализация защитных инженерно-технических мероприятий в целях повышения устойчивости и прочности гидротехнических сооружений имеют приоритетное значение. Гарантированное водоснабжение сельского хозяйства республики во многом зависит от их мощности и стабильной работы. Поэтому вопрос надежной и безопасной эксплуатации гидротехнических сооружений является актуальной проблемой.

Износ и разрушение плотин и других сооружений представляют серьезную угрозу для населения и объектов, расположенных в развитых районах ниже по течению от плотин и рек. Надежность и безопасность плотин зависит от многих факторов, возникающих при их строительстве и эксплуатации. Прочность и безопасность плотин зависит от напряженно-деформированного состояния, вызванного различными воздействиями на тело плотины. Определение и прогнозирование изменений напряженно-деформированного состояния тела плотины позволяет получить полную информацию о прочности и надежности плотины. Задачи определения динамического состояния и прочности грунтовых плотин решались с использованием численных методов [1-21].

При обеспечении прочности плотины и изучении ее напряженно-деформированного состояния возникает ряд вопросов, связанных с её реальной геометрией, неоднородностью тела плотины и конструктивной структуры, определением реальных физико-механических свойств грунта [22]. Надежное определение напряженно-деформированного состояния плотин зависит от методов оценки их технического состояния, используемых математических моделей, уравнений состояния грунтов и методов их решения.

2. Постановка и решение задачи.

Рассмотрим грунтовые плотины, которые имеют твердое основание. Дамбу, которая имеет очень большую длину по сравнению с шириной и высотой, можно рассматривать как плоско деформированную структуру. Во время действия динамических сил, направленных на основание грунтовых плотин частицы среды плотины начинают движение. Динамическое уравнение движения грунтовой плотины имеет следующий вид:

$$\begin{aligned} \rho \frac{d\upsilon_x}{dt} &= \frac{\partial S_{xx}}{\partial x} + \frac{\partial P}{\partial x} + \frac{\partial \tau_{xy}}{\partial y}, \\ \rho \frac{d\upsilon_y}{dt} &= \frac{\partial S_{yy}}{\partial y} + \frac{\partial P}{\partial y} + \frac{\partial \tau_{xy}}{\partial x} - \rho g, \end{aligned} \tag{1}$$

где S_{xx}, S_{yy}, τ_{xy} - компоненты напряжения девиатора; P – давление; υ_x, υ_y - скорости частиц в направлениях x и y; ρ – плотность среды.

Полные напряжения определяются по следующим формулам:

$$\sigma_{xx} = S_{xx} + \mathrm{P}, \qquad \sigma_{yy} = S_{yy} + \mathrm{P}, \qquad \sigma_{zz} = S_{zz} + \mathrm{P}. \tag{2}$$

Принято решение, что модель деформирования плотины будет представлена в виде нелинейных уравнений

$$\dot{P} = -\left(\lambda + \frac{2}{3}\mu\right)\frac{\dot{V}}{V}, \tag{3}$$

$$\frac{dS_{xx}}{dt} + \lambda S_{xx} = 2G\left(\frac{d\varepsilon_{xx}}{dt} - \frac{dV}{3Vdt}\right),$$

$$\frac{dS_{yy}}{dt} + \lambda S_{yy} = 2G\left(\frac{d\varepsilon_{yy}}{dt} - \frac{dV}{3Vdt}\right), \tag{4}$$

$$\frac{dS_{zz}}{dt} + \lambda S_{zz} = 2G\left(\frac{d\varepsilon_{zz}}{dt} - \frac{dV}{3Vdt}\right),$$

$$\frac{d\tau_{xy}}{dt} + \lambda \tau_{xy} = 2G\frac{d\tau_{xy}}{dt}.$$

Связь между пределом прочности и давлением в обобщенном условии Мизеса имеет вид

$$S_{xx}^2 + S_{yy}^2 + S_{zz}^2 + 2\tau_{xy}^2 \le \frac{2}{3}\left[Y(P)\right]^2, \tag{5}$$

$$Y(P) = Y_0 + \frac{\mu P}{1 + \mu P/(Y_{PL} - Y_0)}, \tag{6}$$

$$\lambda = \frac{3W}{2Y^2}H(W), \quad H(W) = \begin{cases} 1, & \text{at } W \ge 0 \\ 0, & \text{at } W < 0 \end{cases}, \tag{7}$$

$$W = 2\mu\left\{\sum_{j=x,y,z} S_{jj}\left(\frac{d\varepsilon_{jj}}{dt} - \frac{1}{3}\frac{dV}{Vdt}\right) + \tau_{xy}\frac{d\varepsilon_{xy}}{dt}\right\}.$$

С помощью системы уравнений (1)-(7) необходимо ввести соотношения, которые связывают компоненты скоростей деформации с массовыми скоростями и уравнение неразрывности грунта

$$\frac{d\varepsilon_{xx}}{dt} = \frac{\partial U_x}{\partial x}, \quad \frac{d\varepsilon_{yy}}{dt} = \frac{\partial U_y}{\partial y}, \quad \frac{d\varepsilon_{xy}}{dt} = \frac{1}{2}\left(\frac{\partial U_y}{\partial x} + \frac{\partial U_x}{\partial y}\right), \tag{8}$$

$$\frac{dV}{dt} - V\cdot\left(\frac{\partial U_x}{\partial x} + \frac{\partial U_y}{\partial y}\right) = 0. \tag{9}$$

В соответствии с этим, система дифференциальных уравнений (1)-(9) представляет собой замкнутую систему, которая описывает динамическое поведение и напряженно-деформированное состояние грунтовых плотин. На гребне и склонах плотины, как правило, напряжения равны нулю. Начальные условия приняты равными нулю.

Геометрические размеры Ахангаранской грунтовой плотины: высота – 100 м, ширина – выше 12 м, ширина – ниже 412 м, ширина центрального ядра – 70 и 8 м.

Физико-механические параметры грунтовой плотины приняты следующими:

Для призмы: плотность – 2250 кг/м^3, модуль эластичности – $E_{плотина}$=60 МПа, коэффициент Пуассона – $\nu_{плотина}$=0.3; Для ядра: плотность – 1960 кг/м^3; модуль эластичности – $E_{ядро}$=30 МПа, коэффициент Пуассона – $\nu_{ядро}$=0.3.

3. Метод решения.

Разностный метод позволяет решить поставленную задачу, используя схему, предложенную М.Уилкинсом [23], которая представляет собой четырехугольную сетку.

Схема Уилкинса обладает преимуществом, которое заключается в том, процесс счета происходит с шагом времени. Выбор осуществляется автоматически из условия стабильности и точности. Он может изменяться каждый раз [23].

$$\frac{\partial \upsilon_x(x,y)}{\partial x} = \lim_{A\to 0} \frac{\int_C \upsilon_x(x,y)\cdot(\vec{n}\cdot\vec{i})ds}{\iint_A dxdy}, \qquad \frac{\partial \upsilon_x(x,y)}{\partial y} = \lim_{A\to 0} \frac{\int_C \upsilon_x(x,y)\cdot(\vec{n}\cdot\vec{j})ds}{\iint_A dxdy}, \tag{10}$$

где A – площадь четырехугольной сетки; c - граница площади A; S – длина дуги; $\vec{n}$ – вектор нормали; $\vec{t}$ – вектор касательной; $\vec{i}, \vec{j}$ – направляющие единичные векторы x, y:

$$\vec{n} = \vec{i}\frac{dx}{dn} + \vec{j}\frac{dy}{dn} = \vec{i}\frac{dy}{ds} - \vec{j}\frac{dx}{ds}.$$

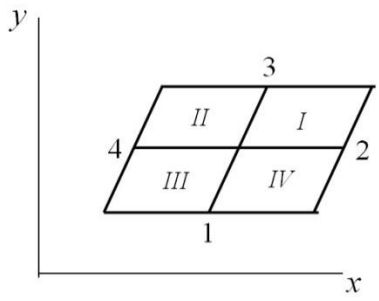

Рисунок 1. - **Ячейки для вычисления частных производных в центре ячеек**

Применяя эти формулы к четырехугольнику *1,2,3,4* с площадью *A* (рис.1) для функции F, определенной в точках *1,2,3,4*, получаем:

$$\int F(\vec{n}\cdot\vec{i})ds = \int (Fdy/ds)ds = F_{23}(y_3 - y_2) + F_{34}(y_4 - y_3) + F_{12}(y_2 - y_1) \tag{11}$$

где $F_{ij} = (F_i + F_j)/2, \ \ (i, j = 1,2,3,4)$, или из рис.1 получим

$$\frac{\partial F}{\partial x} = \frac{(F_2 - F_4)(y_3 - y_1) - (y_2 - y_4)(F_3 - F_1)}{2A}. \tag{12}$$

Аналогично находим

$$\frac{\partial F}{\partial y} = -\frac{(F_2 - F_4)(x_3 - x_1) - (x_2 - x_4)(F_3 - F_1)}{2A}. \tag{13}$$

Полученные таким образом величины дают производные некоторой непрерывной функции *F(x,y); ∂F/∂x* и *∂F/∂xy* в центре четырехугольника. Используя (12)–(13), мы можем написать выражения для $\partial\upsilon_x/\partial x$, $\partial\upsilon_y/\partial x$, $\partial\upsilon_x/\partial y$, $\partial\upsilon_y/\partial y$ в заданной точке пространства в данный момент времени.

Для вычисления ускорения значение функции *F* из (10) определяется в центре прямоугольника, где площадью интегрирования теперь будет служить площадь *1,2,3,4,* указанная на рис.1. Соответствующие конечно-разностные уравнения примут вид [23]:

$$\int_C F(\vec{n}\cdot\vec{i})ds = -[F_I(y_2 - y_3) + F_{II}(y_3 - y_4) + F_{III}(y_4 - y_1) + F_{IV}(y_1 - y_2)],$$
$$\int_C F(\vec{n}\cdot\vec{j})ds = [F_I(x_2 - x_3) + F_{II}(x_3 - x_4) + F_{III}(x_4 - x_1) + F_{IV}(x_1 - x_2)]. \tag{14}$$

В качестве площади *1,2,3,4* берется среднее из площадей четырехугольников A_I A_{II} A_{III} A_{IV} (рис.1).

Таким образом, частные производные по координатам в уравнениях (1), (8) определяются из приведенных соотношений (12)–(14). Разностные соотношения по времени определяются центральным разностным уравнением

$$\frac{\upsilon_x^{n+1/2}-\upsilon_x^{n-1/2}}{\Delta t^n}=\left(\frac{d\upsilon_x}{dt}\right)^n,\ x^{n+1}=x^n+\upsilon_x^{n+1/2}\cdot\Delta t^{n+1/2}, \tag{15}$$

где значения скоростей (υ_x и υ_y) вычисляются при приращении времени на полшага, а значения координат (x и y) – при изменении времени на полный шаг, что приводит ко второму порядку точности аппроксимации [23].

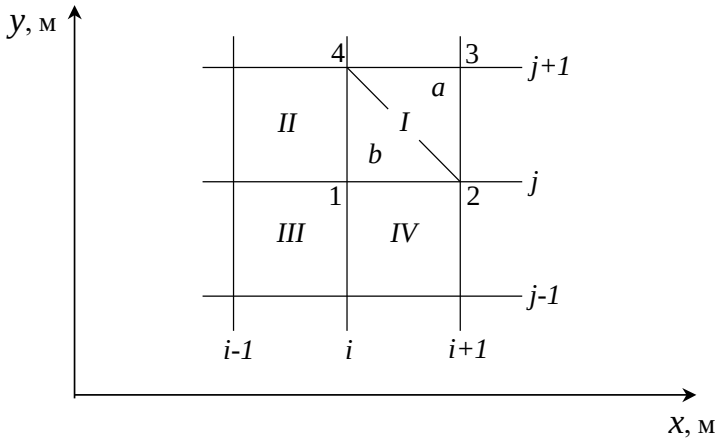

Рисунок 2. - **Четырехугольные сетки**

Пусть в области Ω, занятой средой, построены четырехугольные лагранжевые сетки *i-j*, которые движутся вместе со средой. Центры и вершины четырехугольников показаны на рис.2. Вводим следующие обозначения:

$I=i+1/2,\ j+1/2;\ II=i-1/2,\ j+1/2;\ III=i-1/2,\ j-1/2;\ IV=i+1/2,\ j-1/2;$

$1=i,\ j;\ 2=i+1,\ j;\ 3=i+1,\ j+1;\ 4=i,\ j+1.$

Плоская масса, соответствующая каждому четырехугольнику в начальный момент, определяется путем умножения начальной плотности на площадь тела. Тогда масса в t^0 для четырехугольника I вычисляется по формуле [23]

$$M_I=\left(\frac{\rho_0}{V_0}\right)_I\left(A_a^0+A_b^0\right), \tag{16}$$

где A_a, A_b – соответственно площади треугольников a и b, которые определяются из соотношений

$$\left(A_a\right)_I^n=\left[x_2^n\left(y_3^n-y_4^n\right)+x_3^n\left(y_4^n-y_2^n\right)+x_4^n\left(y_2^n-y_3^n\right)\right]/2,$$

$$\left(A_b\right)_I^n=\left[x_2^n\left(y_4^n-y_1^n\right)+x_4^n\left(y_1^n-y_2^n\right)+x_1^n\left(y_2^n-y_4^n\right)\right]/2, \tag{17}$$

$$A_I^n=\left(A_a\right)_I^n+\left(A_b\right)_I^n. \tag{18}$$

Из условия сохранения массы имеем

$$V_I^n=\frac{\rho_0 A_I^n}{M_1}. \tag{19}$$

Аналогично вычисляются массы M_{II}, M_{III} и M_{IV} .

Пусть в некоторый момент $t=t^n$ известны величины $\upsilon_x^{n-1/2}, \upsilon_y^{n-1/2}, x^n, y^n$ во всех узлах сетки и величины $\sigma_{xx}^n, \sigma_{yy}^n, \sigma_{zz}^n, \tau_{xy}^n, P^n, V^n$ в центрах четырехугольников, образующих сетку.

Получим формулы для определения этих величин внутри и на границе области Ω в момент времени $t=t^{n+1}=t+\Delta t^n$, где Δt^n – шаг по времени.

Запишем уравнения движения (1) с помощью (14), которые центрируются в точке i, j (рис.2):

$$\left(\upsilon_x\right)_{i,j}^{n+1/2}=\left(\upsilon_x\right)_{i,j}^{n-1/2}-\Delta t^n\left(\varphi\left(\sigma_{xx},y\right)_{i,j}^n-\varphi\left(\tau_{xy},x\right)_{i,j}^n\right),$$
$$\left(\upsilon_y\right)_{i,j}^{n+1/2}=\left(\upsilon_y\right)_{i,j}^{n-1/2}+\Delta t^n\left(\varphi\left(\sigma_{yy},y\right)_{i,j}^n-\varphi\left(\tau_{xy},x\right)_{i,j}^n\right), \qquad (20)$$

где

$$\varphi\left(\sigma_x,x\right)_{i,j}^n=\left[\begin{array}{l}\sigma_I^n\left(x_{i+1,j}^n-x_{i,j+1}^n\right)+\sigma_{II}^n\left(x_{i,j+1}^n-x_{i-1,j}^n\right)+\\+\sigma_{III}^n\left(x_{i-1,j}^n-x_{i,j-1}^n\right)+\sigma_{IV}^n\left(x_{i,j-1}^n-x_{i+1,j}^n\right)\end{array}\right]/\left(2\psi_{i,j}^n\right),$$
$$\psi_{i,j}^n=\left[\left(\rho_0A^n/V^n\right)_I+\left(\rho_0A^n/V^n\right)_{II}+\left(\rho_0A^n/V^n\right)_{III}+\left(\rho_0A^n/V^n\right)_{IV}\right]/4. \qquad (21)$$

После нахождения всех величин $\upsilon_x^{n+1/2},\upsilon_y^{n+1/2}$ определяем новое положение координат:

$$x_{i,j}^{n+1}=x_{i,j}^{n-1}+\left(\upsilon_x^{n+1/2}\right)_{i,j}\cdot\Delta t^{n+1/2},\qquad y_{i,j}^{n+1}=y_{i,j}^{n-1}+\left(\upsilon_y^{n+1/2}\right)_{i,j}\cdot\Delta t^{n+1/2}. \qquad (22)$$

Далее, по определенным значениям скорости и координаты, с применением конечно-разностных уравнений (12),(13) запишем расчетные формулы для скоростей деформации в центре ячейки I (рис.2) [23]:

$$\left(\dot\varepsilon_{xx}\right)_I^{n+1/2}=\left[\phi\left(\upsilon_x,y\right)\right]_I^{n+1/2},\ \left(\dot\varepsilon_{yy}\right)_I^{n+1/2}=\left[\phi\left(\upsilon_y,x\right)\right]_I^{n+1/2},\ 2\left(\dot\varepsilon_{xy}\right)_I^{n+1/2}=\left[\phi\left(\upsilon_y,y\right)-\phi\left(\upsilon_x,x\right)\right]_I^{n+1/2}, \qquad (23)$$

где
$$\phi\left(\upsilon,x\right)_I^{n+1/2}=\frac{\left[\left(\upsilon_2-\upsilon_4\right)\left(x_3-x_1\right)-\left(x_2-x_4\right)\left(\upsilon_3-\upsilon_1\right)\right]_I^{n+1/2}}{2A_I^{n+1/2}},$$

$$A_I^{n+1/2}=\frac{\left(A_I^{n+1}+A_I^n\right)}{2},\quad x^{n+1/2}=\frac{\left(x^{n+1}+x^n\right)}{2},\quad y^{n+1/2}=\frac{\left(y^{n+1}+y^n\right)}{2},$$

$$V_I^{n+1/2}=\frac{\left(V_I^{n+1}+V_I^n\right)}{2},\ \left(\frac{\dot V}{V}\right)_I^{n+1/2}\cdot\Delta t^{n+1/2}=\left(\frac{\Delta V}{V}\right)_I^{n+1/2}=\frac{V_I^{n+1}-V_I^n}{V_I^{n+1/2}}.$$

Здесь величины $A_I^{n+1/2}$ и $V_I^{n+1/2}$ вычисляются по уравнениям (16)–(19).

Приращения деформации находим с помощью формулы

$$\left(\Delta\varepsilon_{xx}\right)_I^{n+1/2}=\left(\dot\varepsilon_{xx}\right)_I^{n+1/2}\cdot\Delta t^{n+1/2},\qquad \left(\Delta\varepsilon_{yy}\right)_I^{n+1/2}=\left(\dot\varepsilon_{yy}\right)_I^{n+1/2}\cdot\Delta t^{n+1/2},$$
$$\left(\Delta\dot\varepsilon_{zz}\right)_I^{n+1/2}=\left(\dot\varepsilon_{zz}\right)_I^{n+1/2}\cdot\Delta t^{n+1/2},\qquad \left(\Delta\varepsilon_{xy}\right)_I^{n+1/2}=\left(\dot\varepsilon_{xy}\right)_I^{n+1/2}\cdot\Delta t^{n+1/2}. \qquad (24)$$

С помощью найденных значений скоростей (23) и приращений деформации (24), вычислим величины соответствующих компонент напряжений ($\sigma_{xx}^{n+1},\sigma_{yy}^{n+1},\sigma_{zz}^{n+1},\tau_{xy}^{n+1}$) в центре ячейки I по конкретным принимаемым уравнениям состояния (2)-(4).

Полные напряжения определяются по следующим формулам:

$$\left(\sigma_{xx}\right)_I^{n+1}=\left(S_{xx}\right)_I^{n+1}-\left(P\right)_I^{n+1},\ \left(\sigma_{yy}\right)_I^{n+1}=\left(S_{yy}\right)_I^{n+1}-\left(P\right)_I^{n+1},\ \left(\sigma_{zz}\right)_I^{n+1}=\left(S_{zz}\right)_I^{n+1}-\left(P\right)_I^{n+1} \qquad (25)$$

Аналогично вычисляются величины (23)-(25) и напряжения в центрах ячейки II, III, IV и т.д.

Таким образом, для момента времени $t=t^{n+1}$ вычислены все необходимые параметры задачи: $\upsilon_x^{n+1/2},\upsilon_y^{n+1/2}$, x^{n+1},y^{n+1} на узловых точках внутри сетки, $\sigma_{xx}^{n+1},\sigma_{yy}^{n+1},\sigma_{zz}^{n+1},\tau_{xy}^{n+1},\rho^{n+1}$ - в центрах сетки и можем продолжить проделанную процедуру (алгоритм) вычислений (18) – (25).

4. Результаты.

Рассмотрим численные результаты расчетов, полученные с помощью программы, основанной на методе конечных разностей по схеме Уилкинса. В основном, динамические задачи решены с учетом упругой и упругопластической деформации неоднородной грунтовой плотины под действием горизонтального сейсмического воздействия. Результаты представлены графически.

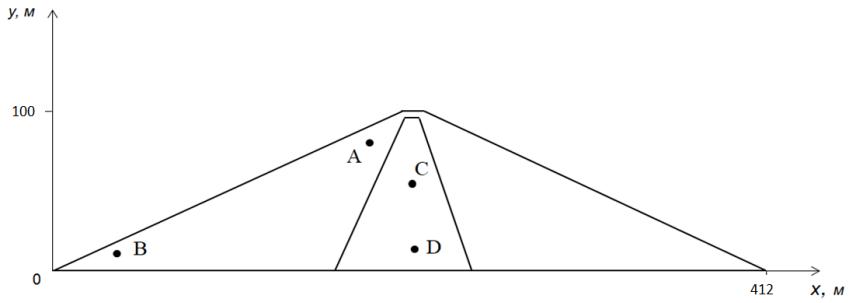

Рисунок 3. – **Поперечное сечение грунтовой плотины**

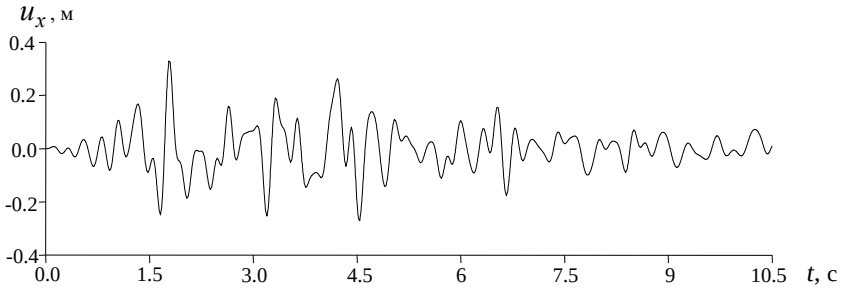

Рисунок 4. – **Сейсмическое воздействие**

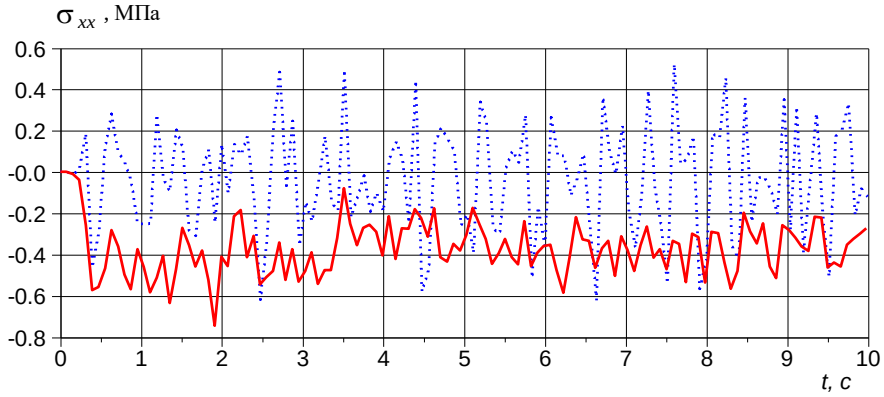

Рисунок 5. - **Изменение горизонтального напряжения по времени в точке С**

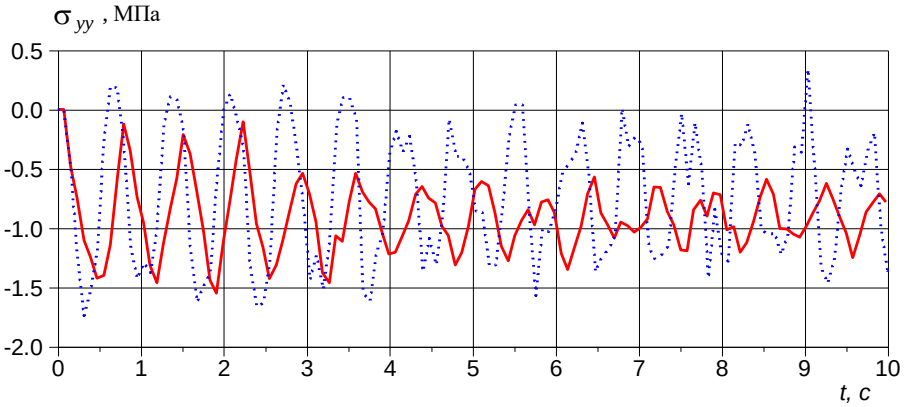

Рисунок 6. - **Изменение вертикального напряжения по времени в точке С**

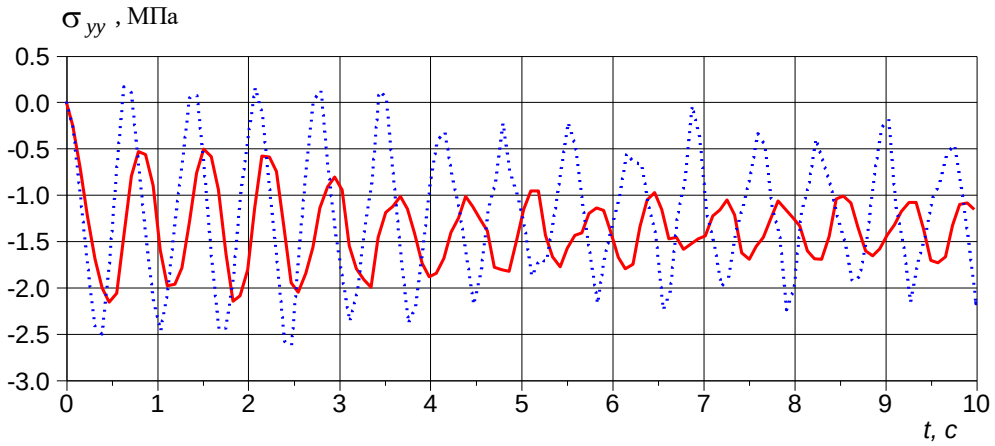

Рисунок 7. - **Изменение горизонтального напряжения по времени в точке Д**

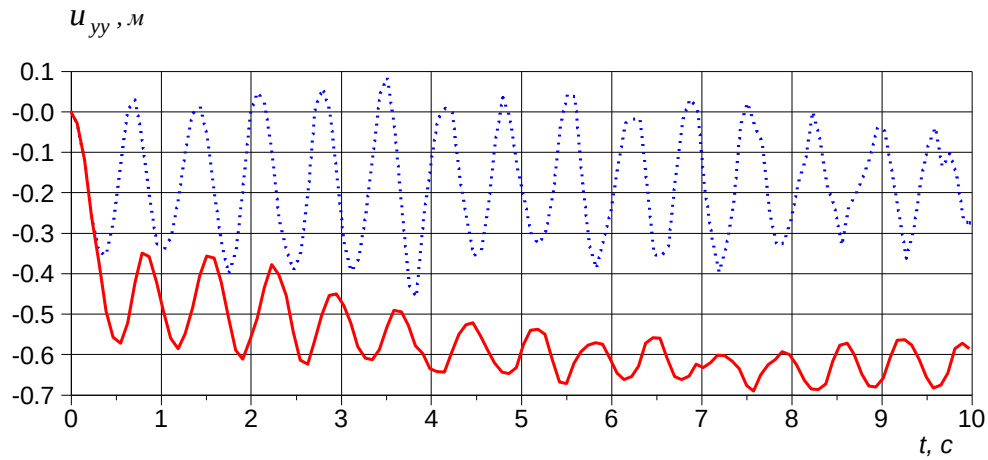

Рисунок 8. - **Изменение вертикального напряжения по времени в точке А**

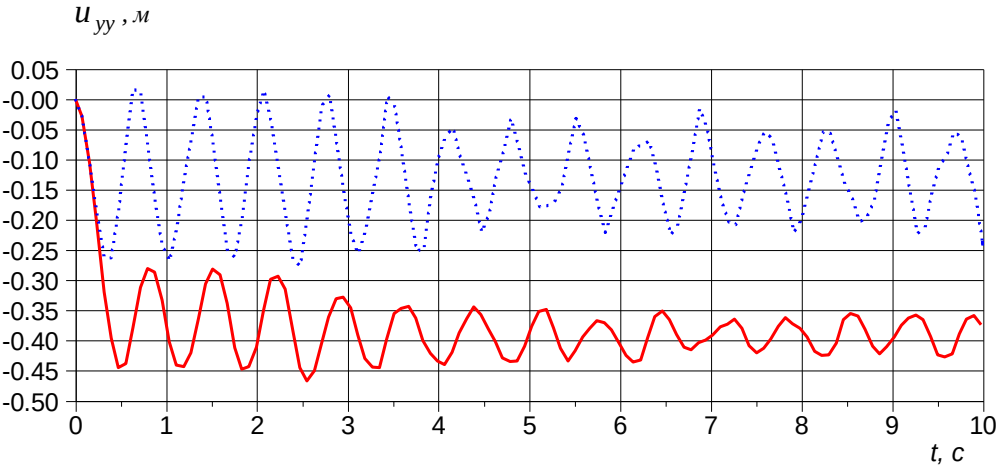

Рисунок 9. - **Изменение вертикального смещения по времени в точке С**

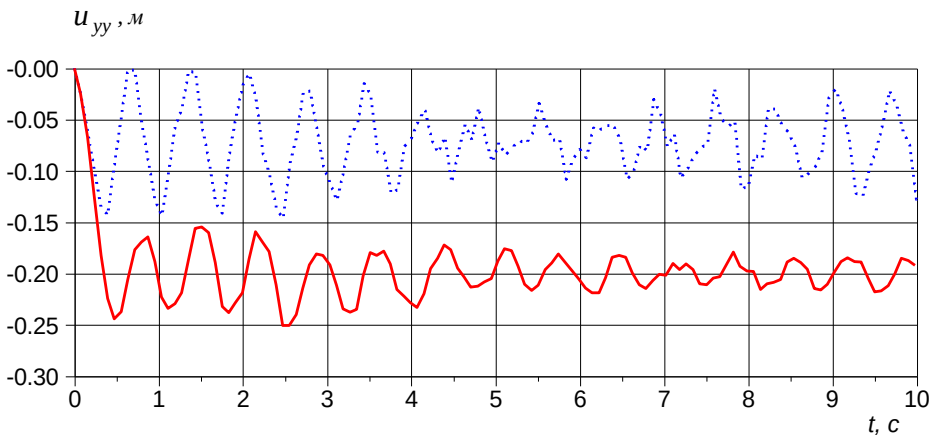

Рисунок 10. - **Изменение вертикального смещения по времени в точке Д**

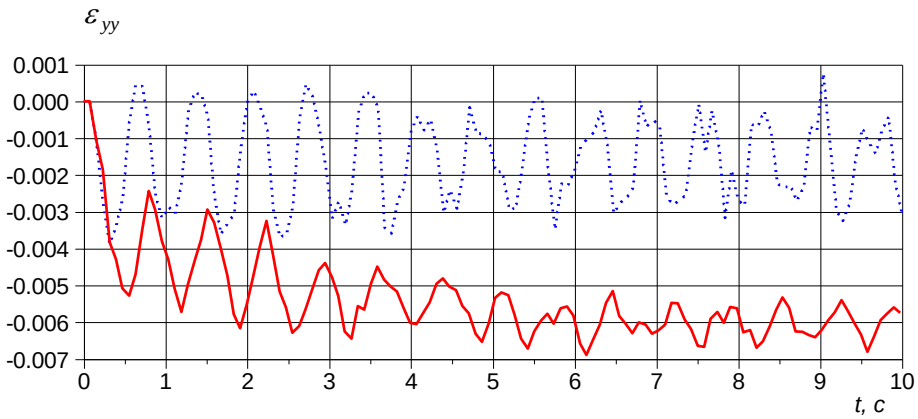

Рисунок 11. - **Изменение вертикальной деформации по времени в точке С**

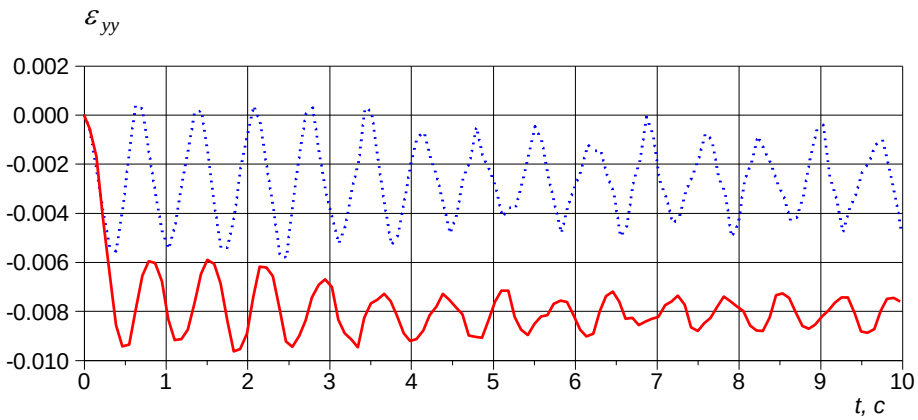

Рисунок 12. - **Изменение вертикальной деформации по времени в точке Д**

5. Анализ результатов

Получены результаты решения динамической задачи для Ахангаранской грунтовой плотины при сейсмических воздействиях в характерных точках плотины А, В, С, Д (рис.5-12). На этих рисунках сплошная линия означает результаты с учетом упруго-пластического деформирования грунта, а пунктирные линии с учетом упругого деформирования грунта. На рисунке 5 показано сравнение результатов, изменение горизонтальных напряжений по времени в точке С с учетом упругого и упругопластического деформирования грунта. Из этого графика видно, что значение горизонтального напряжения на упругопластической стадии имеет отрицательные значения, это означает, что с учетом упругопластического деформирования

грунта в этой точке образуется сжатие. На рисунке 6 показано изменение вертикального напряжения в точке С по времени. Здесь можно сказать, что значение вертикального напряжения уменьшается по времени с учетом упрупластического деформирования грунта и имеет отрицательные значения. Изменение горизонтального напряжения в точке Д по времени показано на рисунке 7. Здесь значение напряжения уменьшается по времени с учетом упрупластического деформирования грунта. На рисунках 8-10 показано изменение вертикального смещения в точках А, С, Д по времени. Из этих рисунков видно, что значение напряжения увеличивается с отрицательным знаком на упругопластической стадии. Изменение вертикальной деформации в точках С и Д по времени показано на рисунках 11-12. Здесь значение деформации увеличивается с отрицательным знаком на упругопластической стадии за счет остаточных деформаций.

6. Заключение

1. Приведены основные соотношения задачи определения напряженно-деформированного состояния грунтовых плотин при динамических воздействиях в плоской постановке. На основе метода конечных разностей приведена методика решения применительно к поставленной двумерной задаче динамики твердых деформируемых тел.

2. Получены численные результаты по определению напряженно-деформированного состояния грунтовых плотин под действием сейсмических сил с учетом веса грунта.

3. Определено напряженно-деформированное состояние Ахангаранской грунтовой плотины при сейсмических воздействиях с учетом упругой и упругопластической деформации грунта. Получены численные результаты изменения по времени напряжений, смещений и деформаций в характерных точках плотины.

Литература

1. *Li B., Zhang Q., Yang S., Tian Y., Li Z.* Identification of failure modes and paths of reservoir dams under explosion loads // Reliability Engineering and System Safety. 2023, 229. https://doi.org/10.1016/j.ress.2022.108892.
2. *Li C., Song Z., Liu S.* Dynamic response of high earth-rock dam on site with easily liquefied and deep overburden under near fault ground motion // Zhendong Yu Chongji/Journal of Vibration and Shock. 2023, 42(17). https://doi.org/10.13465/j.cnki.jvs.2023.17.029
3. *Yang X., Yu T., Jin W., Zhu X.* Three dimensional nonlinear seismic response analysis of Lianghekou super high core rockfill dam // Tumu Yu Huanjing Gongcheng Xuebao/Journal of Civil and Environmental Engineering. 2023, 45(3). https://doi.org/10.11835/j.issn.2096-6717.2021.094
4. *Vo T.T., Nguyen V.T.* An Approach of Seepage Analysis Through Earth Dams Considering the Uncertainties of Soil Hydraulic Conductivity. Lecture Notes in Civil Engineering. 2023, 268. https://doi.org/10.1007/978-981-19-3303-5_93
5. *Hu H., Gan G., Cui L., Xia T., Wang L., Han X.* Nonparametric Representation for Seismic Fragility Assessment of Earth Dams with Spatially Variable Soil Properties // International Journal of Geomechanics. 2023, 23(8). https://doi.org/10.1061/ijgnai.gmeng-7266
6. *Kalateh F., Kheiry M.* A Review of Stochastic Analysis of the Seepage Through Earth Dams with a Focus on the Application of Monte Carlo Simulation // In Archives of Computational Methods in Engineering. 2024, Vol. 31, Issue 1. https://doi.org/10.1007/s11831-023-09972-3
7. *Ohashi R., Nishimura S., Kaneshige M.,Shibata T., Shuku T.* Seismic Response Analysis of Earth Dam with Geostatistical Method and 3-D Survey // Lecture Notes in Civil Engineering. 2023, 288 LNCE. https://doi.org/10.1007/978-3-031-12851-6_46
8. *Nishimura S., Shibata T., Shuku T.* Seismic response analysis of an earth dam by using geostatistical methods and 3-D measurement // In Smart Geotechnics for Smart Societies. 2023, https://doi.org/10.1201/9781003299127-174
9. Juraev, D., & Matkarimov, P. (2023). Stress-strain state and strength of earth dams under static loads. *E3S Web of Conferences*, *365*. https://doi.org/10.1051/e3sconf/202336503008
10. *Sultanov K.* Contact interaction of an underground pipeline with soil under dynamic impacts // Facta Universitatis, Series: Mechanical Engineering, [S.l.], mar. 2024. ISSN 2335-0164. Available at: <http://casopisi.junis.ni.ac.rs/index.php/FUMechEng/article/view/12383>. Date accessed: 31 mar. 2024.
11. *Haghdoost M., Lakzian E., Norouzi R., Abraham J., Sajjadi S. M., Ahadiyan, J.* Numerical simulation using the finite element method to investigate the effect of internal cutoff walls on seepage and hydraulic gradients in homogeneous earth dams // Modeling Earth Systems and Environment. 2023, 9(4). https://doi.org/10.1007/s40808-023-01755-w

12. *Doan N.P., Nguyen B.P., Park S.S.* Seismic deformation analysis of earth dams subject to liquefaction using UBCSAND2 model // Soil Dynamics and Earthquake Engineering. 2023, 172. https://doi.org/10.1016/j.soildyn.2023.108003
13. *Nardo A., Cascone E., Biondi G., Di Filippo G., Casablanca O.* Influence of Vertical Ground Motion on the Seismic Performance of an Earth Dam // Springer Series in Geomechanics and Geoengineering. 2023, https://doi.org/10.1007/978-3-031-34761-0_82
14. *Mirsaidov M., Sultanov T., Yarashov J., Kayumov A.* Strength of earth dams considering the elastic-plastic properties of soils // E3S Web of Conferences. 2023, 365. https://doi.org/10.1051/e3sconf/202336503001
15. *Sultanov K., Umarkhonov S.* Dynamic behavior of earth dams under short-term semi-harmonic loads // E3S Web of Conferences. 2023, 420, 07014. https://doi.org/10.1051/e3sconf/202342007014
16. *Belazouz L., Bouzelha K., Hammoum H., Amiri O., Khelil N.* Reliability Analysis of the Slope Stability of Homogeneous Earth Dam under Seismic Loading // Periodica Polytechnica Civil Engineering. 2024, 68(1). https://doi.org/10.3311/PPci.22537
17. *Cui C.Y.* Seismic behavior and reinforcement mechanisms of earth dam and liquefiable foundation system by shaking table tests and numerical simulation // Soil Dynamics and Earthquake Engineering. 2023, 173. https://doi.org/10.1016/j.soildyn.2023.108083
18. *Sultanov K., Umarkhonov S., Normatov S.* Calculation of earth dam strain under seismic impacts // AIP Conference Proceedings. 2022, 2637, 030008. https://doi.org/10.1063/5.0118430
19. *Loginov P.V., Salikhova Z.R., Sultanov K.S.* Experimental and Theoretical Method for Determining Mechanical Characteristics of Soils under Dynamic Loads // Mechanics of Solids. 2019, vol. 54, No 6. P. 915–928.
20. *Wilkins M.L.* Computer Simulation of Dynamic Phenomena / Springer, Berlin, 2010, 246 p.

ИСПОЛЬЗОВАНИЕ РЕЗУЛЬТАТОВ ВЕРОЯТНОСТНОЙ СЕЙСМИЧЕСКОЙ ОПАСНОСТИ ДЛЯ ОЦЕНКИ ОБЕСПЕЧЕНИЯ ЗАДАННОГО УРОВНЯ СЕЙСМОСТОЙКОСТИ ДЕЙСТВУЮЩИМИ НОРМАМИ СЕЙСМОСТОЙКОГО СТРОИТЕЛЬСТВА

Аминзода П.
Институт геологии, сейсмостойкого строительства и сейсмологии НАНТ, г. Душанбе, Таджикистан
Email: igees_asrt@mail.ru

Аннотация: *Последствия разрушительных землетрясений в Турции, происшедших в начале февраля 2023г. и последовавших за ними землетрясений в Морокко, Китае, Японии, Тайване и др. странах, еще раз показали, что ни одни из действующих в мире норм сейсмостойкости не являются в полной мере совершенны. В связи с чем особую актуальность приобретает вопрос – насколько действующими нормами сейсмостойкого строительства обеспечивается заданный уровень сейсмостойкости. В настоящее время, с разработкой в Таджикистане карт вероятностной сейсмической опасности появился инструмент оценки обеспеченности заданного уровня сейсмостойкости зданий и сооружений, регламентируемого действующими нормами сейсмостойкого строительства СНиП РТ 22-07-2018 «Сейсмостойкое строительство».*

Ключевые слова: *вероятностная оценка сейсмической опасности, расчетная сейсмическая нагрузка, пиковое ускорение грунта, расчетный спектр реакции, нормируемый спектр реакции, синтезированная акселерограмма.*

Анализ катастрофических последствий разрушительных землетрясений в Турции, происшедших в начале февраля 2023г. и последовавших за ними землетрясений в Морокко, Китае, Японии, Тайване и др. странах, еще раз показали, что одной из причин разрушения сотен зданий, повлекших за собой гибели десятков тысяч людей, является, помимо других причин, необеспеченность их заданной сейсмостойкости в соответствии с расчетной сейсмической опасностью территории.

Расчетная сейсмическая опасность представляется в нормативных документах по сейсмостойкому строительству в виде списка населенных пунктов с указанием максимальных ускорений грунта и карт сейсмического районирования/зонирования и служит основой для определения расчетных сейсмических нагрузок.

При анализе причин катастрофических последствий турецких землетрясений 2023г. было обращено внимание, что большинство разрушенных зданий было возведено в соответствии с

нормами сейсмостойкости 2007г., опирающееся на сейсмическое зонирование территории Турции, выполненное по результатам детерминистской оценки сейсмической опасности. В тоже время, действующие нормы сейсмостойкого строительства Турции 2018г. опираются на новую вероятностную карту сейсмической опасности территории страны для периода повторяемости землетрясения 475 лет, значительно отличающейся от предыдущей, включенной в сейсмические нормы 2007г. Согласно опубликованных литературных, применение новой вероятностной карты сейсмической опасности, привело к значительному (до двух раз) увеличению расчетных сейсмических нагрузок [1 - 3].

Данное обстоятельство явилось основанием для проведения оценки обеспечения заданного уровня сейсмостойкости зданий и сооружений действующими нормами сейсмостойкого строительства СНиП РТ 22-07-2018 «Сейсмостойкое строительство», в которых представлена детерминистская карта сейсмической опасности территории Таджикистана 1978г. в баллах интенсивности в соответствии со шкалой MSK-64 (рис.1) [4].

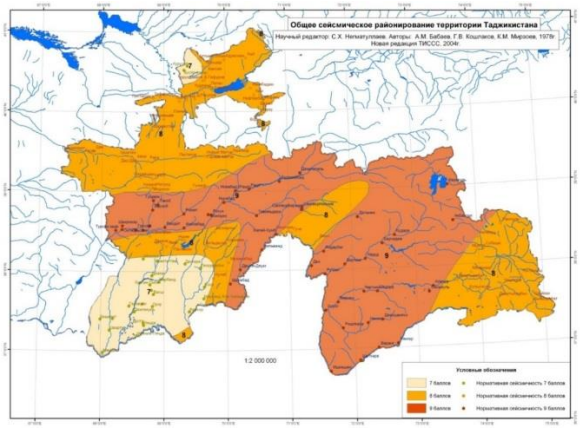

Рис.1. **Действующая карта сейсмической опасности территории Таджикистана**

Как видно по карте вся территория Таджикистана относится к сейсмически опасной и на ней прогнозируется возникновение землетрясений с интенсивностью 7, 8 и 9 баллов, для которых расчетные ускорения, соответственно, составляют 0.1, 0.2 и 0.4g.

Определение при проектировании зданий и сооружений расчетных сейсмических нагрузок по спектральному методу, в соответствии со СНиП РТ 22-07-2018 применяемым в большинстве случаев, базируется на следующих положениях [4]:

Расчетная сейсмическая нагрузка S_{ik} в выбранном направлении, приложенная к точке k и соответствующая i-му тону собственных колебаний, определяется по формуле:

$$S_{ik} = K_1 K_2 K_3 S_{0ik} , \quad (1)$$

где: S_{0ik} - значение сейсмической нагрузки для i-го тона собственных колебаний, определяемое в предположении упругого деформирования конструкций по формуле:

$$S_{oik} = Q_k A \beta_i K_\psi \eta_{ik}, \quad (2)$$

K_1 - коэффициент, учитывающий степень ответственности;

K_2 - коэффициент редукции, учитывающий конструктивные решения;

K_3 - коэффициент, учитывающий высоту зданий и сооружений, определяемый по формуле:

$$K_3 = 1 + 0.05 (n - 5), \quad (3)$$

где n - количество этажей здания (кроме этажей, расположенных ниже планировочной отметки, цокольных и мансардных), при этом $1.0 \le K_3 \le 1.5$; Q_k - вес здания или сооружения, отнесенный к точке k, определяемый с учетом расчетных нагрузок на конструкции; A - коэффициент сейсмичности, значения которого следует принимать равным 0.1, 0.2, 0.4, 0.6, соответственно, при расчетной сейсмичности 7, 8, 9 и более 9 баллов; β_i - коэффициент динамичности, соответствующий i-му тону собственных колебаний, принимаемый согласно ниже приведенных графиков (рис.2);

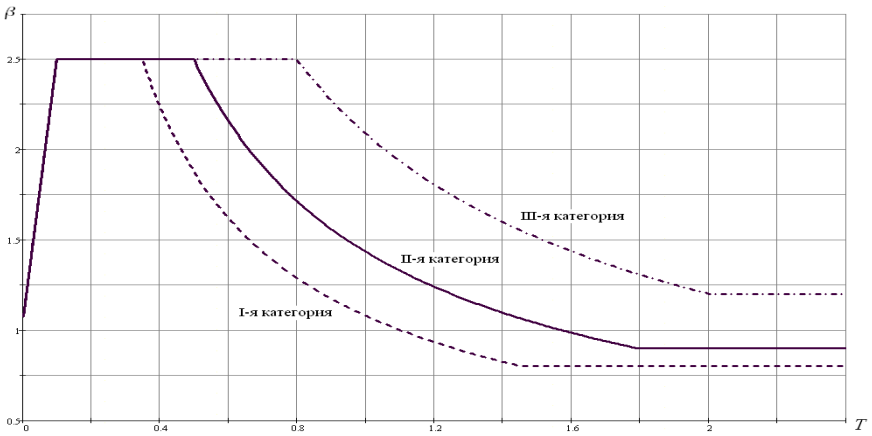

Рис.2. **График коэффициента динамичности β**

K_ψ - коэффициент, учитывающий способность здания и сооружения к рассеиванию энергии;
η_{ik} - коэффициент формы колебаний, зависящий от формы деформации здания или сооружения при его собственных колебаниях по *i*-му тону и от места расположения нагрузки.

К настоящему времени Институтом геологии, сейсмостойкого строительства и сейсмологии НАНТ по специальной методике с применением вычислительного комплекса CRISIS 2015 подготовлен комплект карт вероятностной сейсмической опасности для территории Таджикистана в единицах пиковых ускорений грунта PGA для периодов повторяемости землетрясений 475, 975, 2475 и 4975лет для трех типов грунтовых условий, характеризующихся скоростью распространения поперечных сейсмических волн в верхней 30-метровой грунтовой толще – Vs,30 (рис.3) [5].

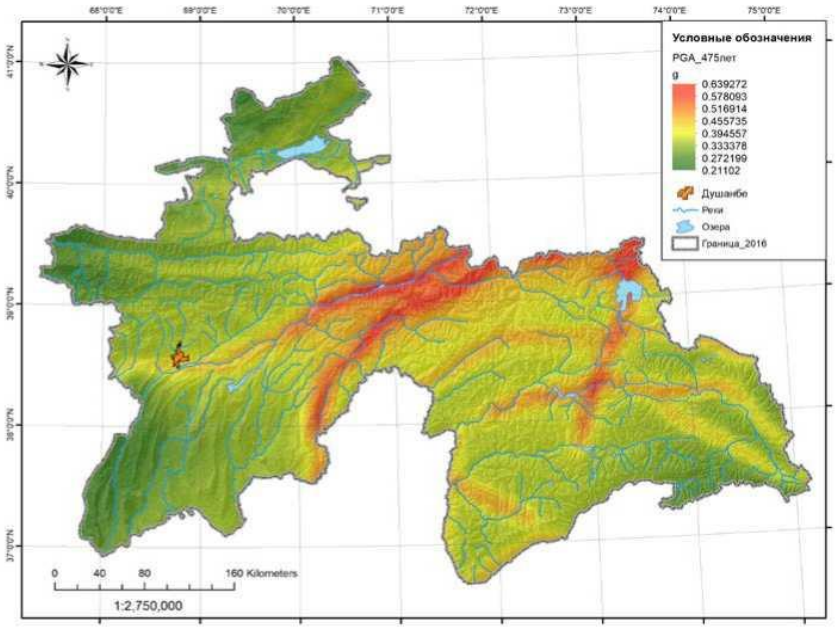

Рис.3. **Пример карты вероятностной сейсмической опасности в PGA для грунтов 1-й категории по сейсмическим свойствам для периода повторяемости землетрясений 475 лет**

Следует особо отметить, что при построении карт для каждой расчетной точки помимо вычисления пиковых ускорений грунта, строятся также расчетные спектры реакции для трех типов грунтовых условий (рис.4).

При применении в практических расчетах вышеприведенных спектров реакции рекомендуется исходить из положений регламентирующего документа Федерального агентства по управлению кризисными ситуациями, согласно которому при землетрясении с периодом повторяемости 475 лет в здании/сооружении допускаются повреждения 0-1-й степени, а при землетрясении с периодом повторяемости 2475 лет – 3-й степени [6].

Очевидно, что с учетом отмеченного, расчетная сейсмическая нагрузка может быть определена по следующей формуле:

$$S_{ik} = Q_k \, R_s(Ti) \, \eta_{ik}, \qquad (4)$$

где $R_s(T_i)$ - значение спектра расчетных реакций в ускорениях в долях g на периоде T_i.

При этом, исходя из условия, что полученные расчетные спектры реакций (рис.3) служат исходными данными для генерирования набора трехкомпонентных синтезированных акселерограмм расчетное сейсмическое воздействие при расчете по спектральному методу также следует задавать в виде трехкомпонентного воздействия без взаимоисключения по направлениям.

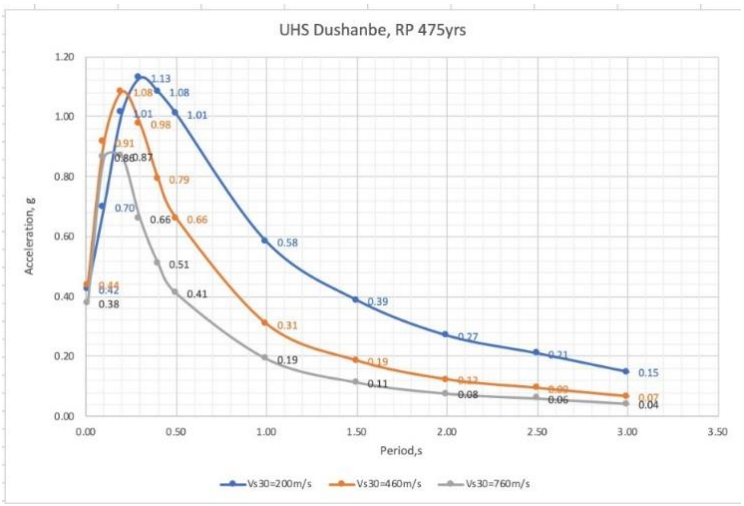

Рис.4. **Пример построенных расчетных спектров реакций**

Данный подход был применен путем проведения расчетных исследований при оценке сейсмостойкости более 30-ти строящихся и возведенных в г. Душанбе высотных зданий. Расчетные исследования включали выполнение конструктивных расчетов с применением программно-вычислительного комплекса ЛИРА-САПР 2022 как на заданные расчетные спектры реакций, так и на расчетные сейсмические нагрузки, определенные в соответствии с действующими нормами (рис.5-7).

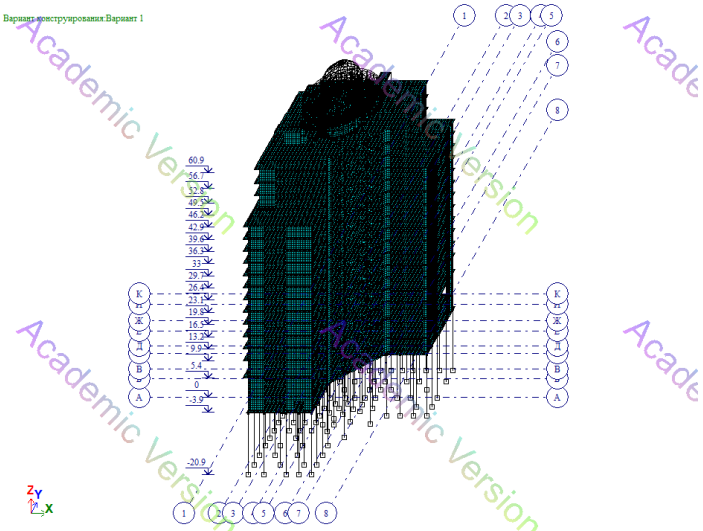

Рис.5. **Пространственная расчетная модель одного из исследованных зданий**

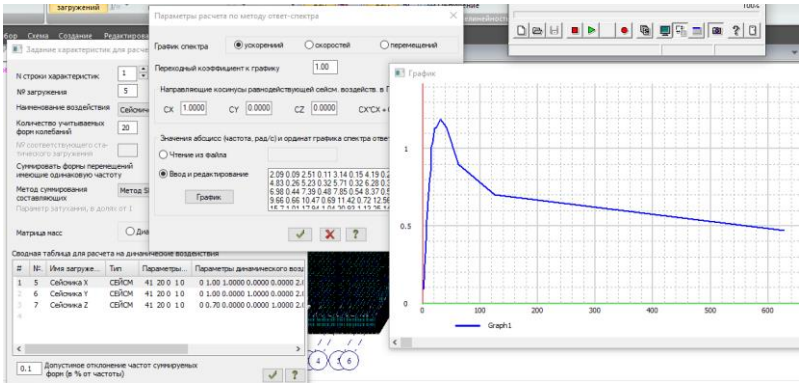

Рис.6. **Расчетное сейсмическое воздействие в виде заданного расчетного спектра**

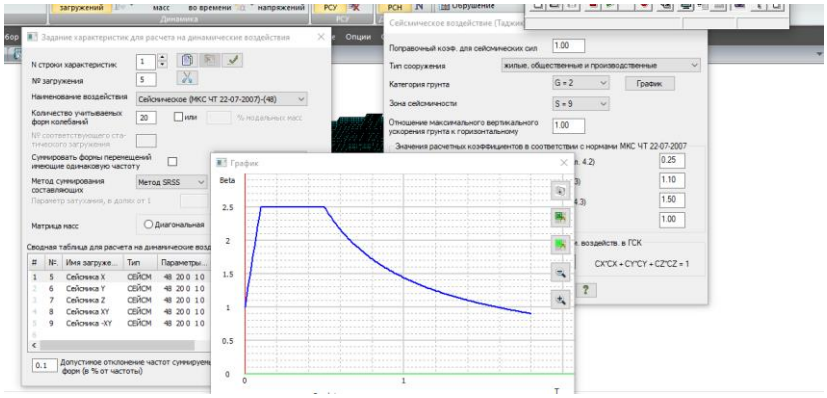

Рис.7. **Расчетное сейсмическое воздействие согласно действующих норм СНиП РТ 22-07-2018**

Согласно результатов проведенных исследований, расчетные значения армирования несущих железобетонных конструкций, являющихся интегральным показателем напряженно-деформированного состояния конструкций, полученных при расчете на расчетные спектры реакции по данным вероятностной сейсмической опасности до 1.5-3 раз ниже по сравнению с результатами нормативных расчетом.

Данное обстоятельство позволяет сделать вывод о достаточной консервативности действующих на территории Таджикистана норм сейсмостойкости СНиП РТ 22-07-2018 и возможности оптимизации уровня расчетных сейсмических нагрузок при включении в новую редакцию норм карт вероятностной сейсмической опасности.

Очевидно, вышеуказанный подход может быть применен также при разработке межгосударственных норм сейсмостойкости.

Литература

1. *Aksoylu C., Mobark A., Arslan M.H., Erkan İ.H.* A comparative study on ASCE 7-16, TBEC-2018 and TEC-2007 for reinforced concrete buildings. Revista de la Construcción. 19(2):282-305.
2. *Koçer M., Uzun M., Çöğürcü M. T.* (2021). Comparison of TSC-2018 and TSC-2007 regulations for Konya in terms of equivalent earthquake load method. Konya Journal of Engineering Sciences. v. 9, n. 3, 535-550. (Elektronik).
3. *İnal F., Can H.* (2022). Comparison of a 9-story reinforced concrete structure using the equivalent seismic load method according to the TSC 2007 and TSC 2019. 5th Advanced Engineering Days, 107-110.
4. СНиП РТ 22-07-2018 «Сейсмостойкое строительство». Душанбе, Издательство: ГУП «НИИСА» «Издательский центр», 2018 - 49с.
5. Научно-технический отчет «Создание новой карты сейсмической опасности территории Таджикистана». №ГР РБ 0116TJ00576. Фонды ИГССС НАНТ, Душанбе, 2020.
6. NEHRP. Recommended seismic provisions for new buildings and other structures (FEMA P-2082-2), Washington, D.C. 2020.

Section B - Engineering seismology and seismic risk
Секция В – Инженерная сейсмология и сейсмический риск

THE MANIFESTATION OF ABNORMAL VARIATIONS OF THE GEOMAGNETIC FIELD IN UZBEKISTAN (TASHKENT SEISMICALLY ACTIVE REGION)

Abdullabekov K.N.[1], Maksudov S.Kh.[1], Yusupov V.R.[1]
[1]*Institute of Seismology, Tashkent, Uzbekistan*
E-mail: valijon.yusupov@mail.ru

Abstract. *The results of long-term geomagnetic research in Uzbekistan are presented. The results are presented on the territory of the Tashkent geodynamic polygon. Local anomalous variations of the geomagnetic field associated with strong earthquakes, the activity of a natural underground gas storage facility and a large reservoir have been identified.*

Numerous local variations of the geomagnetic field have also been identified, the nature of which has not yet been established. These variations have different forms, intensity and time of manifestation. In order to determine their nature, the peculiarities of the manifestation of variations according to magnetic observatories, at the points of the century course, in the territories of seismically active regions of the globe have been studied. The analysis of the results showed the absence of a scientifically based conclusion on the mechanisms of manifestation of this type of anomalous variations of the geomagnetic field. Their frequent manifestation does not contribute to the identification of abnormal variations caused by the processes of preparation of strong earthquakes.

Keywords: *magnetic field, anomalous variation, amplitude, geodynamic polygon, Earth's crust, mantle, fault.*

1. Introduction

Since the middle of the 20th century, geomagnetic research to identify geodynamic processes and search for precursors of strong earthquakes has been widely carried out in most seismically active regions of the globe.

The territory of Uzbekistan, like the whole of Central Asia, is a seismically active region. Therefore, earthquake forecasting is important in all respects, primarily for society.

Research on the problem of earthquake forecasting in Uzbekistan was started after the strong Tashkent earthquake of April 26, 1966 (M=5.3). In the first 2-3 years, special geodynamic polygons were organized – Tashkent, Ferghana and Kyzylkum. Seismometric, geomagnetic, deformometric, hydrogeochemical and other studies began to be organized in the territories of these polygons. Work on the search for geomagnetic precursors of earthquakes in Uzbekistan has been underway since 1968. on specially organized geodynamic polygons and in epicentral zones of strong earthquakes that have occurred. Geomagnetic studies were also carried out on the territories of man–made objects - natural underground gas storage facilities, large reservoirs and exploited oil and gas fields using repeated route, area and stationary regime measurements. Absolute proton magnetometers were used. Over the more than 50-year period of geomagnetic research, more than 1,100 points have been laid with a total length of route, area surveys of about 7,750 km. About 25 stationary magnetic stations were involved. As a result, a wide amplitude-time spectrum of local variations of various nature was revealed, associated with:

1) the processes of preparation and occurrence of strong ($M \geq 5$) earthquakes;

2) the activities of man–made facilities - underground natural gas storage facilities, large reservoirs and exploited oil and gas fields;

3) processes occurring at various depths in the Earth's crust and upper mantle.

This work is devoted to a detailed analysis of local anomalous variations of the geomagnetic field of the third type.

2. The methodology

Geomagnetic research was organized by launching stationary magnetic stations and laying profiles of repeated magnetic measurements. For more than 55 years of research, in some years the number of stationary magnetic stations was more than 35 and the length of profile measurements was more than 2,300 km with 540 points. This article presents the results of long-term geomagnetic studies on the territory of the Tashkent geodynamic polygon. During the period of geomagnetic studies

conducted on the territory of the landfill, local anomalous variations of the geomagnetic field were revealed due to the strong earthquakes that occurred, the activity of man–made objects - natural underground gas storage facilities, large reservoirs. The results obtained – identified precursors of earthquakes, anomalous variations of a man-made nature are given in our publications [1-7].

With the accumulation of geomagnetic research data at stationary magnetic stations and points of repeated observation profiles, numerous local anomalous variations of the geomagnetic field were revealed, which were not associated with the processes of preparing strong earthquakes, the activities of man-made objects.

3. The results of the research

During the initial phase of research, the identified local anomalous variations in the geomagnetic field were initially overlooked. They appeared at single observation points or at several points of a small area. Long-term observations in the territories of geodynamic polygons showed the manifestation of longer (3-7 years) abnormal variations.

It is noteworthy that these anomalous variations coincided temporally with significant seismic events, such as a strong seismic event, a series of minor earthquakes, or an uptick in background seismic activity.

The results of research on the identification of anomalous variations of the geomagnetic field of a local and regional nature on the territory of the Tashkent geodynamic polygon of Uzbekistan are summarized below for the entire period (1968-2019).

In 1968, three profiles with a total length of 300 km were laid on the territory of the landfill, with 52 measuring points (Fig.1). Two profiles have a north–easterly direction, coinciding with the location of the regional Karzhantau fault. The third profile crosses the Karzhantau fault zone and two profiles in a northwesterly direction.

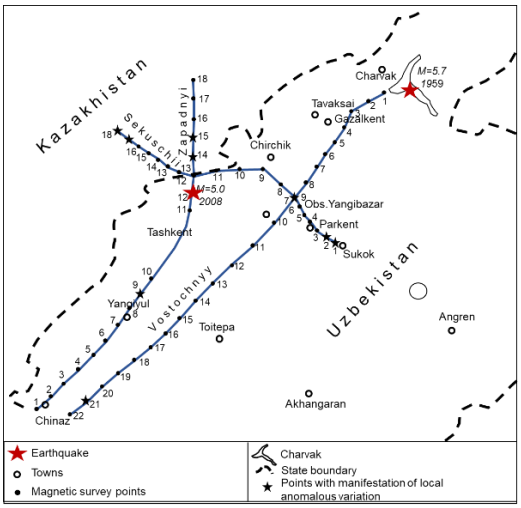

Figure 1. - **Schematic map of the Tashkent geodynamic polygon.**

Figure 2 shows local anomalies of the geomagnetic field at the route points of the Tashkent geodynamic polygon. Abnormal variations appeared on 8 points out of 52 (marked with asterisks). As you can see, the changes have different forms, intensity, time of manifestation and duration. These changes differ even at neighboring points (Sec 1 and 2, 14a and 15), the distance between which does not exceed 5 km. At some points (zap.9; sec. 1 and 2), against the background of a slow change, cove-shaped, sinusoidal, zigzag anomalous changes of a medium-term nature appear. These changes are manifested in different sections of the Tashkent geodynamic polygon. Figure 2 shows for example the points (secant 17 and 18), where there are no significant changes during the research.

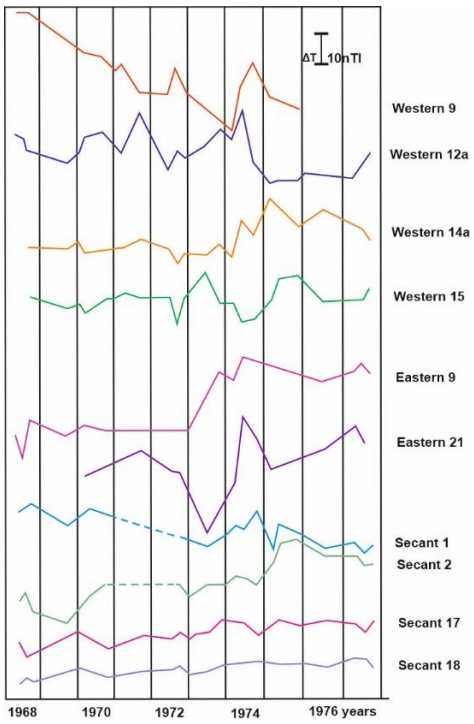

Figure 2. **- Local variations of the geomagnetic field at the points of the Tashkent geodynamic polygon caused by near-surface sources.**

Figure 3 shows an example of detecting local anomalous variations at two stationary stations of the Tashkent geodynamic polygon. The stations are located at a distance of 500 meters from each other. The local anomaly has an arcuate shape of a positive sign [8].

Here at station 1, the anomaly has an intensity of about 2.5 nTl, and at the station 2 - 4.5 nTl. The duration of the anomaly in both stations is the same and is about 17 days. The anomaly was isolated relative to the Yangibazar Magnetic Observatory, located at a distance of 40 km.

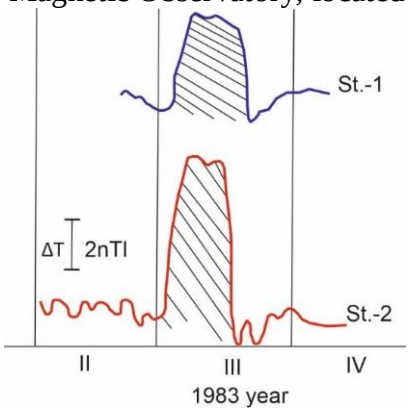

Figure 3. **- Local changes recorded by two stations located at a distance of 500 m from each other on the territory of the Tashkent geodynamic polygon.**

Now about the results of detecting long-period regional changes in the geomagnetic field. The changes in the geomagnetic field at the points of repeated surveys relative to the Yangibazar magnetic observatory for the period 1989-1992 are presented. It should be noted that during this period, no noticeable or strong earthquakes occurred at the Tashkent landfill and in the adjacent territories, and no activation of the seismic background was noticed. During the period under review, a bay-shaped anomaly of a negative sign with a duration of about 3 years appeared at most points of the landfill. The anomaly manifested itself at 30 of the 40 points located mainly along the regional Karzhantau fault. The length of the anomaly is 150 km. The profile is divided into three sections. The northeastern section covers the area of the Charvak reservoir. Further, the profile of geomagnetic research stretches in a southwesterly direction. The anomaly in the first section manifested itself at 9 of the 13 points located in the water area of the Charvak reservoir. In the second section of the profile, the anomaly

appeared on 10 out of 14 points and on the third segment of the profile on 11 out of 13 points. Figure 4 shows the changes in the average values of ΔT at points along the marked sections of the profile. What are the features of the manifestation of this regional anomaly: - firstly, the amplitude and duration of the anomaly decreases in time in a southwesterly direction. If the amplitude of the anomaly on the territory of the Charvak reservoir is 7 nTl with a duration of about 3 years (curve "a", Figure 4), then in the second segment these parameters have a value of 5 NT and about 2 years (curve "b", Figure 4). In the third section – 4 nTl and 1 year, respectively (curve "b", Figure 4); - secondly, at a distance of about 150 km, the amplitude of the anomaly decreases by only 3 nTl. Therefore, it can be assumed that the anomaly manifested itself at a greater extent than the length of the profile at the polygon. Judging by the attenuation of the intensity of the anomaly in the south-westerly direction, the "focus" of the source of the anomaly is located in the north-easterly direction from the Tashkent landfill.

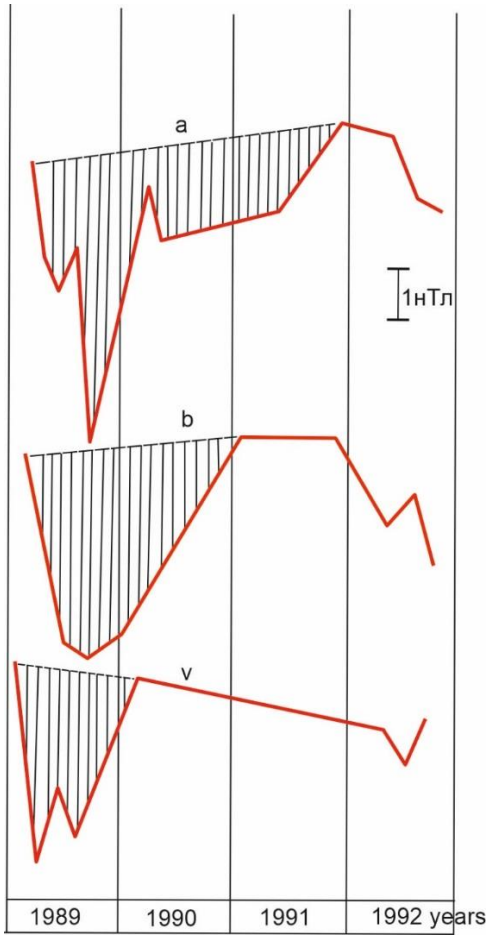

a – the first segment of the profile; b – the second segment of the profile; v – the third segment of the profile.

Figure 4. **- The manifestation of a bay-shaped regional anomalous variation of the geomagnetic field at the points of the Tashkent geodynamic polygon.**

This regional anomaly on the territory of the Tashkent geodynamic polygon is manifested for the first time since 1968. The selectivity of the manifestation of this regional anomaly at the points of repeated surveys suggests that the boundary of the area of manifestation of the anomaly has a complex configuration on the plan.

The first points of repeated geomagnetic observations in the water area of the large Charvak reservoir were laid 26 points in December 1973. In 1976, their number increased to 35 [8].

In a detailed analysis of the dynamics and morphology of the local field change in the reservoir area for 1974-1979, the points were divided into three groups. By the nature of the change, the points were combined into zones (Figure 5).

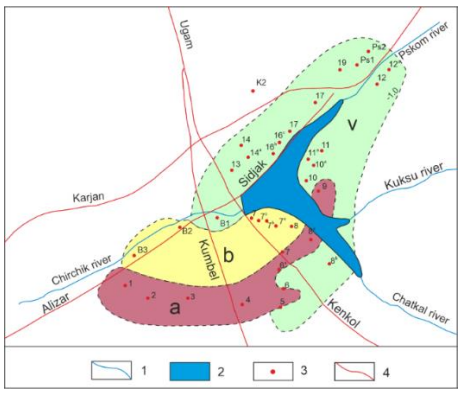

1 - rivers; 2 - Charvak reservoir; 3 - points of repeated magnetic observations; 4 - faults; "a" - zones of heterogeneous changes in the geomagnetic field.

Figure 5. - **The division of the territory in the area of the Charvak reservoir according to the nature of the change in the geomagnetic field.**

Zone "a" occupies the southern part of the study area. Zone "b" covers the southern and southwestern parts. The rest of the research area is occupied by zone "b". It can be seen that the zones have a complex configuration. Figure 6 shows the change in the averaged values of ΔT for three zones.

In zone "a", along with the quasi-sinusoidal change, a slow trend component is clearly manifested. The value of the trend component is about 5.5 nTl over a 6-year research period.

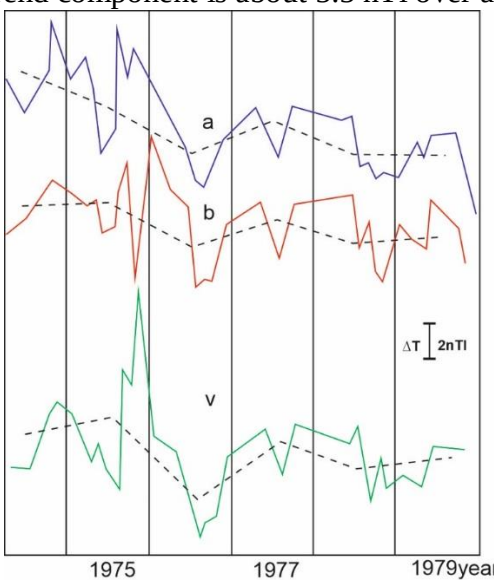

____ change in monthly averages ΔT; ---- change in average annual values ΔT;

Figure 6. - **Dynamics of local changes in the magnetic field in the area of the Charvak reservoir.**

The morphology of the high-frequency part of the field change in zone "b" differs slightly from the morphology in the other two zones. Here, a slight trend change was observed in 1974-1976 and then it disappears (see the curve of average annual values – dotted line).

The sinusoidal change is most intense in the "b" zone. The trend component here is the same as in zone "b". The quasi-sinusoidal anomalous change in all three zones manifested itself in 1974-1976 with a minimum value in the second half of 1976. Further, until 1979, the average annual value of the field varies slightly.

The following are the results of geomagnetic studies on the territory of the Tashkent geodynamic polygon for the period 2004-2019. The measurements were carried out at points located in the area of the regional Karzhantau fault. The profile also covers the epicentral zone of the Tavaksay earthquake of 1977, the water area of the Charvak reservoir (Figure 7). Measurements of the geomagnetic field were carried out at 29 points. It should be noted that according to the nature of the change in the magnetic field, the points were divided into three zones. Common to all points is the absence of any drastic changes in ΔT. The first zone includes 14 points (Figure 7).

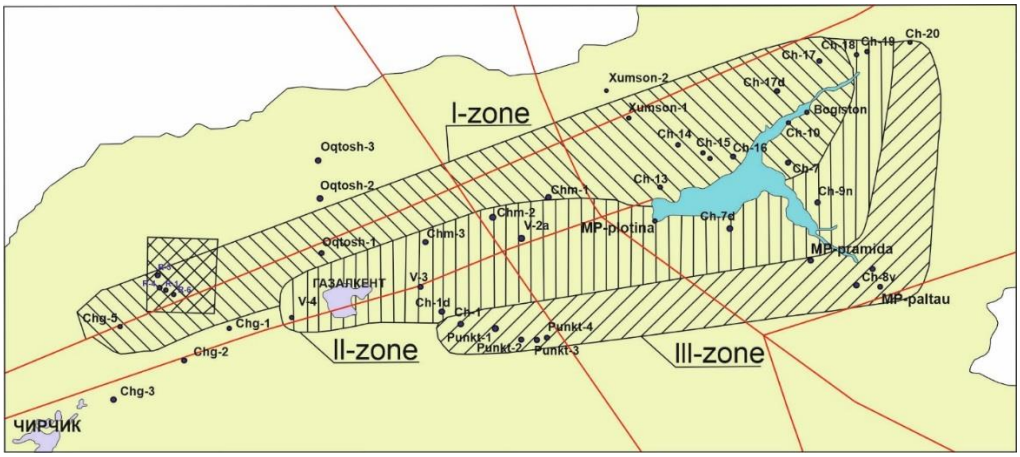

Figure 7. - **Selected zones by the nature of the ΔT change**

In this zone, the magnetic field is slowly decreasing. Figure 8 (1 - zone) shows a decrease in the average value of ΔT by 14 points.As can be seen, the decrease is monotonous and the decrease gradient averages about 0.7 nTl /year.

The second zone includes 9 points. Here (2nd zone Figure 8) the average value of ΔT almost does not change until 2016 and since 2017 there has been a slight decrease in ΔT.

The third zone includes 7 points (3 - zone, Figure 8). The zone covers the south and southeastern parts of the study area. The average ΔT value remains unchanged until 2008.Over the period 2009-2011, the field changes slightly in a bay-like shape, with a return to the initial level at the end of 2011. Starting in 2012, the field begins to decrease monotonously. During this period, the decrease gradient is on the order of 1.9 nTl/year.

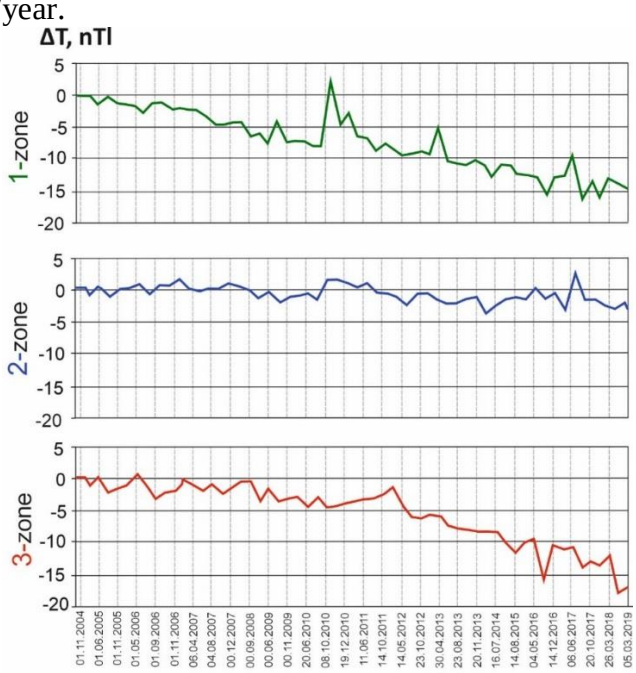

Figure 8. - **Change in the average values of ΔT in the selected zones.**

In all three zones, during 2016-2019, the change acquires the same character and a slow decrease in ΔT is observed. Therefore, the field change during this period is considered separately. It should be noted that in 2016, additional re-filming points were laid and the total number of points increased to 48. The layout of the points is shown in Figure 9. In this case, the points were divided into two zones by the nature of the field change (Figure 9). The first zone included 34 points. The zone stretches from southwest to northeast. The change in the average ΔT value for the zone is shown in the figure (curve 1, Figure 10). As you can see, the change in this zone is negative. During the period V.2016- VI.2017, the field does not change, during VI-2017-VIII.2017, the field decreased by almost 5 nTl and remains at this level until VI.2019.

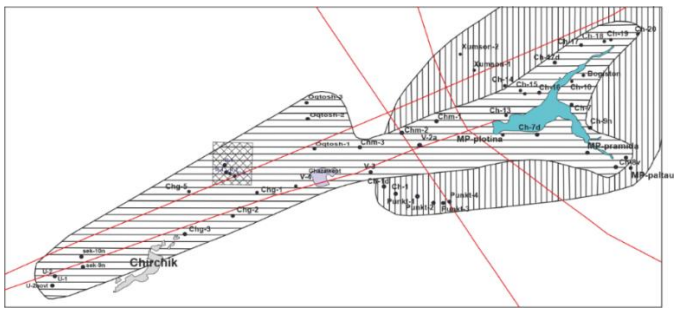

Figure 9. - **Selected zones according to the nature of the ΔT change.**

The second zone (curve 2, Figure 10) occupies the northeastern part of the study area. It covers the northeastern part of the first zone from the north, east and south.

Here, the average value of the field is 2.2 nTl when the value changes over the study period from 0 to 5 nTl .

So, starting from 1973 to 2019, studies conducted on the territory of the Tashkent landfill revealed local anomalous changes in the geomagnetic field of various nature, intensity, duration and size of the area of manifestation. This is the first time that such a massive nature and convincing registration of local variations of the geomagnetic field has been carried out in the world practice of geomagnetic research.

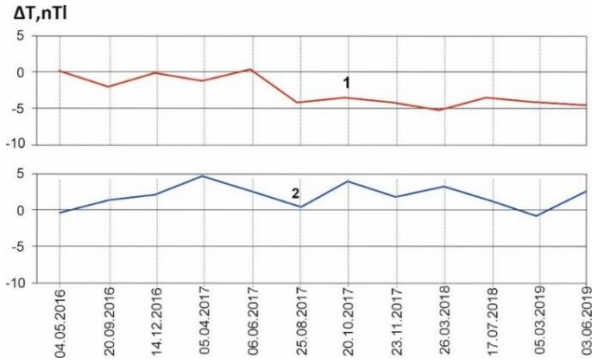

Figure 10. - **The change in the average values of DT in the selected zones.**

The registered local variations have different intensity, form of manifestation, duration and size in area. A detailed analysis of the area and time of manifestation of local anomalies showed the absence of any connection between them and the geological–tectonic, hydrogeological, geomorphological features of the studied territories. They are also not associated with the geophysical features of the earth's crust, the seismic regime or individual strong earthquakes that occurred in the region.

4. Discussion of the results

As a result of more than 55 years of geomagnetic research in the territories of geodynamic polygons of Uzbekistan, local anomalous changes in the geomagnetic field were revealed due to the processes of preparing strong (M≥5) earthquakes, the operation of underground natural gas storage facilities, large reservoirs. Numerous local anomalous changes have also been identified due to processes occurring at various depths of the Earth's crust, possibly also within the upper mantle. This is evidenced by the above results.

What published data are available today on the study of local anomalous variations of the geomagnetic field over the past 50-60 years?

Even at the initial stage of geomagnetic research on the secular course of the Earth's magnetic field, V.P. Orlov and V.S. Sokolov in the mid-1960s revealed an intense manifestation of a local anomaly in the Khabu-Rabat region (Tajikistan) [9]. The anomaly manifested itself only in one point of the age-old course. Later, special studies at this point showed that the field change was caused by the loss of the primary thermally stable magnetization of igneous (diabases, porphyrites) rocks and the occurrence of a weaker secondary magnetization in them [10].

K.N. Abdullabekov analyzed data from the global network of magnetic observatories. Anomalous changes in the vertical component of the magnetic field have been identified at some observatories. In his opinion, the sources of these regional anomalies may be in the Earth's crust and upper mantle [1].

I.G. Zolotov analyzed the change in the average annual values of the elements of the geomagnetic field for three observatories - Alibag, Abinger – Hartland and Tso-Ze [11]. He found that against the background of a smooth low-frequency change, high-frequency irregular fluctuations are observed. The frequency of the low–frequency part of the secular course at the Alibag and Abinger - Hartland observatories is in the range of 80-150 years, and at the Tso–Ze observatory - about 40 years. The high-frequency part of the secular course at all three observatories is a complex curve with significantly shorter periods. Nothing is said about the nature of the latter.

Since 1982, the scientific station of the Institute of High Temperatures of the Russian Academy of Sciences has organized routine observations of the geomagnetic field at five stations on the territory of the Bishkek Geodynamic polygon (Kyrgyzstan) [12]. In 1985, a sixth station was added. From 1988 to 1991, four more stations were added to the existing stations. At the Aksu reference station, the measurement discreteness was 20 seconds, at the other stations – 20 minutes. In 1992, 11 repeat observation points were included in the geomagnetic monitoring network. The frequency of measurements at these points was 3-5 days. One of the conclusions from the long period of observations is that there are always minor and significant variations of the geomagnetic field in the time series. Moreover, the nature of the variation is also different at different points of the network. It is assumed that the differences in the course of variation may be related to: the location of a particular station relative to the source of the deformation process; the difference in physical, including magnetic properties of rocks; with different geological and geoelectric structure of the section under a single station; with the presence of current systems of various nature in the area of observation points that are not related to geodynamic processes [13].

As can be seen, the data on the study of local anomalous variations of the geomagnetic field are very insignificant and statements about the nature of these anomalies are also at the level of assumptions.

5. Conclusion

So, local anomalous variations appear with linear dimensions from the first units to 100 kilometers or more. Consequently, the sources of these anomalies seem to be located at different depths in the Earth's crust and upper mantle. It should be assumed that the larger the area of the anomaly manifestation, the deeper the source of the anomaly should be located.

The forms of manifestation of local anomalies in most cases are bay-shaped, sinusoidal, and trending. The bay-shaped and trending shapes have both positive and negative signs. Their intensity can range from 2-3 to 25 nTl or more. In the case of manifestation in the form of a trend, the gradient of change ranges from 0.5-1.0 to 3 or more nTl / year.

As the results of long-term observations on the territory of the Tashkent geodynamic polygon, in particular in the area of the Charvak reservoir, show, the form of manifestation, the size of the area, and the intensity of anomalies do not remain constant. They all change over time. In this regard, they cannot be associated with the geological, tectonic, and geophysical features of the studied territories.

The smallest local anomalies in linear dimensions, which appeared at single points of repeated surveys and at some stationary observation stations in Uzbekistan, are anomalous variations registered for the first time at a sufficiently large number of magnetic points. The linear size of the manifestation of these anomalies is 3-5 km. All the above-mentioned anomalies were detected due to frequent and long-term measurements of the geomagnetic field at the points of repeated surveys.

At this stage of research, an urgent task is to determine the nature of the identified local anomalous variations. This will allow the identification of local anomalies caused by the processes of preparation of strong earthquakes. To solve this problem, it is proposed to organize a complex of long-term geophysical (seismological, geomagnetic, electrical, pulsed electromagnetic, etc.) studies.

6. Acknowledgements

The authors express their gratitude to Professor A.I. Tuychiev for participating in the discussion. This research was conducted with the financial support of the State Basic Research Development Program (2022-2023) of the Committee for the Coordination of Science and Technology Development under the Ministry of Innovation of the Republic of Uzbekistan.

References

1. *Abdullabekov K.N., Maksudov S.H.* Variations of the geomagnetic field of seismically active areas, FAN Publishing House, Tashkent, 1975. 128 p.
2. Electric and magnetic precursors of earthquakes. Edited by *V.P. Golovkov.* FAN Publishing House, 1983, 135 p.
3. *Abdullabekov K.N., Berdaliev E.B. Maksudov S.H. Tuichiev A.I.* The first results of geomagnetic studies in the area of the Shurtan gas field. // Uzbek Geological Journal, 1994, No.2, pp.16-18.
4. *Abdullabekov K.N., Shapiro V.A.* Observations of variations of the geomagnetic field during the Gazli earthquake on May 17, 1976. Geomagnetism and Aeronomy. Volume XIII, No. 1, 1978, pp.177-179.
5. *Abdullabekov K.N.* Electromagnetic phenomenon in the earth's Crust. A.A. Balkema, Rotterdam, Netherlands, 1991, 169 p.
6. *Tuichiev A.I.* Anomalous changes in the geomagnetic field caused by seismogeodynamic, technogenic processes in the territory of Uzbekistan // Geology and mineral resources. 2007 No.3. pp.52-54.
7. *Abdullabekov K.N., Maksudov S.H., Tuichiev A.I.* Results of long-term studies of anomalous variations of the geomagnetic field caused by seismogeodynamic and technogenic processes. Geology and Mineral Resources, 2016. No. 4, pp.56-60.
8. *Berdaliev E.* Local changes in the geomagnetic field and their connection with seismotectonic processes in the Earth's crust. Dissertation for the academic degree. PhD in Physics.- mat. of Sciences. IZMIRAN USSR. 1980.- 127s.
9. *Orlov V.P., Sokolov V.P.* The age-old course of the geomagnetic field and its anomalies. In the collection "The present and the past of the Earth's magnetic field". M., Publishing house "Nauka". 1965. pp. 27-34.
10. *Barsukov O.M.* et al. About the nature of one of the anomalies of the secular course of the Earth's magnetic field. Physics of the Earth, 1968. No. 9. pp.85-87.
11. *Zolotov I.G.* On the division of the secular course into smooth and random parts. Abstracts of the VIII-conference on the permanent geomagnetic field, rock magnetism and paleomagnetism. M., 1970. pp. 23-26.
12. *Mukhamadeeva V.A., Vorontsova E.V., Lazareva E.A.,* Historical aspects of geomagnetic observations at the Bishkek geodynamic polygon. Abstracts of the sixth International Symposium "Problems of geodynamics and geoecology of intracontinental orogens". Bishkek. 2014. pp.207-211.
13. *Volykhin A.M., Bragin V.D., Zubovich A.V.,* etc. The manifestation of geodynamic processes in geophysical fields. M. Nauka. 1993. 158p.
14. *Yusupov V.R.* Anomalies of geomagnetic field related to natural and technogenic events in Charvak area. Geodesy and Geodynamics 9 (2018) pp.367-361
15. *Yusupov V.R., Isroilov Kh.B.* The results of electrometric studies of earthquake Precursors in Uzbekistan International Journal of Geology, Earth & Environmental Sciences ISSN: 2277-2020 pp.74-82
16. *Abdullabekov K.N., Yusupov V.R.,* Some Results of the Study of Variations of Electromagnetic Fields Caused by Different-Rank Seismogeodynamic Processes and the Mode of Operation of Man-Made Objects International Journal of Magnetics and Electromagnetism (England) ISSN: 2631-5068. 2020y pp.2-9
17. *Yusupov V.R., Shukurov Z.F., Yadigarov E.M.* Analysis of the geomagnetic field and vertical movement near the intersection of Karjantau and Tavaksay faults in Uzbekistan Geodesy and Geodynamics 12 (2021) pp.102-109
18. *S. Kh. Maksudov, K. N. Abdullabekov, A.I.Tuichiev, Yusupov V.R.* Geomagnetic Field Variations Caused by the Processes Occurring at Different Depths in the Earth's Crust and Upper Mantle. Physics of the Solid Earth, 2021, Vol. 57, No. 3 pp.295–308
19. *K.N.Abdullabekov, Yusupov V.R.* Models (form) of long-, medium- and short-term earthquake precursors Geodesy and Geodynamics 13 2022 https://doi.org/10.1016/j.geog.2022.07.002 pp. 609-618
20. *K.N.Abdullabekov, Maksudov S.Kh., Yusupov V.R*. Results of Geomagnetic Studies on the Problem of Forecasting Strong Earthquakes in Uzbekistan // International Journal of Geosciences Vol.14 No.5, May 2023 pp. 437-449 https://www.scirp.org/journal/paperinformation.aspx?paperid=125377
21. *Khairul Adib Yusof, Mardina Abdullah, Nurul Shazana Abdul Hamid, Suaidi Ahadi and Essam Ghamry* Statistical significance of geomagnetic diurnal variation anomalies prior to worldwide Journal of Society and Space November 2021 DOI: 10.17576/geo-2021-1704-25
22. *Boris S. Svetov, Sergej D. Karinskij, Yurij I. Kuksa and Vladimir I. Odintsov Magnetotelluric* monitoring of geodynamic processes ANNALI DI GEOFISICA, VOL. XL, N. 2, March 1997 pp.435-443
23. *Hitoshi Mizutani and Tsuneo Ishido* A New Interpretation of Magnetic Field Variation Associated with the Matsushiro Earthquakes J. Geomag. Geoelect r., 28, 179-188, 1976
24. By Panayiotis VAROTSOS,t~ *Nikos SARLIS, and Efthimios SKORD* Magnetic field variations associated with SES Proc. Japan Acad., 77, Ser. B (2001) pp 87-92

25. *Thomas Forbriger, Rudolf Widmer-Schnidrig, Erhard Wielandt, Mark Hayman, Nicholas Ackerley* Magnetic field background variations can limit the resolution of seismic broad-band sensors Geophys. J. Int. (2010) 183, 303–312

26. *D. Enescu.* Geomagnetic anomalies – possible earthquake precursors – linked with 2004 significant seismic activity in vrancea (Romania) Rom. Journ. Phys., Vol. 50, Nos. 9–10, P. 1213–1221, Bucharest, 2005

27. J. *Marvin* Herndon Geodynamic basis of heat transport in the Earth CURRENT SCIENCE, VOL. 101, NO. 11, 10 DECEMBER 2011

28. *Igor I. Rokityansky, Valeriia I. Babak and Artem V. Tereshyn* Seismic Waves - Probing Earth System Low-Frequency Electromagnetic Signals Observed before Strong Earthquakes DOI: http://dx.doi.org/10.5772/intechopen.88522 pp.1-16

29. *V.D. Russov, V.Yu. Maxymchuk, R. Ilic, V.M. Pavlovych, R.Jasmin, V.G. Bakhmutov, O. S., V.M. Vaschenko, J. Skvar'c, L. Hanzic, J.Vaupotičc, M.E. Beglaryan, E.P. Linnik, S.I. Kosenko, D.N. Saranuk, V.P. Smolyar, A.A.* Gudyma The peculiarities of cross-correlation between two secondary precursors | radon and magnetic field variations, induced by stress transfer changes physics/0605244v3 12 Aug 2012 pp-1-27

30. *I. I. Rokityansky, T. A. Klymkovych, V. I. Babak & A. Isac* (2012) Annual and diurnal variations of induction vectors in relation to geodynamic processes, Geomatics, Natural Hazards and Risk, 3:3, 239-249, DOI: 10.1080/19475705.2011.601432

31. *Strachimir Chterev Mavrodiev, Lazo Pekevski* Geomagnetic Earthquake Precursors Improvement Formulation on the basis of SKO (Skopje) and PAG (Intermagnet) Geomagnetic Data https://doi.org/10.48550/arXiv.1212.2627

32. *Nepeina, K.; Bataleva, E.; Alexandrov, P.* Electromagnetic Monitoring of Modern Geodynamic Processes: An Approach for Micro-Inhomogeneous Rock through Effective Parameters. Appl. Sci. 2023, 13, 8063. https://doi.org/10.3390/ app13148063

33. *Mihai, A.; Toader, V.-E.; Moldovan, I.-A.; Radulian, M.* Exploring the Relationship between Geomagnetic Variations and Seismic Energy Release in Proximity to the Vrancea Seismic Zone. Atmosphere 2023, 14, 1005. https://doi.org/ 10.3390/atmos14061005

34. *Elena Bataleva* On the question of the relationship of variations in geophysical fields, lunar-solar tidal effects and seismic events E3S Web of Conferences 127, 0 (2019) //doi.org/10.1051/e3sconf /201912702019

35. *Nicholas V.* Sarlis Statistical Significance of Earth's Electric and Magnetic Field Variations Preceding Earthquakes in Greece and Japan Revisited // Entropy 2018, 20, 561; doi:10.3390/e20080561

36. *Gautam Rawat, Vishal Chauhan & S. Dhamodharan* (2016) Fractal dimension variability in ULF magnetic field with reference to local earthquakes at MPGO, Ghuttu, Geomatics, Natural Hazards and Risk, 7:6, 1937-1947, DOI: 10.1080/19475705.2015.1137242

37. *Vikulin A.V., Dolgaya A.A., Vikulina S.A. 2014.* Geodynamic waves and gravity. Geodynamics & Tectonophysics 5 (1), 291–303. doi:10.5800/GT-2014-5-1-0128.

38. *Ken'ichi Yamazaki*. Temporal variations in magnetic signals generated by the piezomagnetic effect for dislocation sources in a uniform medium / Geophys. J. Int. (2016) 206, 130–141 doi: 10.1093/gji/ggw12

39. *Mioara Mandeaa, Isabelle Panetb, Vincent Lesurd, Olivier de Vironc, Michel Diamentc, and Jean-Louis Le Mouël.* Recent changes of the Earth's core derived from satellite observations of magnetic and gravity fields PNAS November 20, 2012 vol. 109 no. 47 19129–19133 https://doi.org/10.1073/pnas.120734610

40. *G. Duma1 and Y. Ruzhin* Diurnal changes of earthquake activity and geomagnetic Sq-variations / Natural Hazards and Earth System Sciences (2003) 3: 171–177

41. *Ludmila F.* Model of the singular current source—The indicator of geodynamic processes in Japan in 2009-2011 // Natural Science 5 (2013) 38-45

42. *Xiuyi Yao, Zhisheng Feng, Yuntian Teng, Yunhui Wang, Qiuyue Zheng* / Geomagnetic Variations Associated with Strong Earthquakes in Yunnan Area Open Journal of Earthquake Research, 2017, 6, 228-237 DOI: 10.4236/ojer.2017.64015

43. *Igor I. Rokityansky, Valeriia I. Babak, Artem V. Tereshyn, Masashi Hayakawa.* Variations of Geomagnetic Response Functions before the 2011 Tohoku Earthquake **Open** Journal of Earthquake Research, 2019, 8, 70-84 DOI: 10.4236/ojer.2019.82005

44. *Schirninger C.; Eichelberger, H.U.; Magnes W.; Boudjada M.Y.; Schwingenschuh K.; Pollinger A.; Biagi, P.F.; Solovieva M.; Wang J.; Cheng B.; et al.* Satellite Measured Ionospheric Magnetic Field Variations over Natural Hazards Sites. Remote Sens. 2021, 13, 2360. https:// doi.org/10.3390/rs13122360

45. *Alina Grigorian, Aleksey Baranov* Local Variations of the Geomagnetic Field Components as Possible Precursors of the Paravan and Spitak Earthquakes Research Square pp. 1-27 DOI: https://doi.org/10.21203/rs.3.rs-2068511/v1

46. *Rahman Piriyev* Electromagnetic earthquake precursory signatures in the ULF RANGE: perspectives of the studies Geodynamics JGD. 2021; Volume 1(30)2021, Number 1(30) 48-57

IMPLEMENTATION OF SEISMIC MONITORING FOR THE EXAMPLE OF THE GISSARAK DAM.

Alimov B.G.[1], Kurbanov T.S.[1], Artikov F.R.[1], Islamov H.A.[1]
[1]*Institute of Seismology, Tashkent, Uzbekistan*
E-mail: sadokat.anvarova@mail.ru

Abstract. *Implementation and analysis of comprehensive monitoring of the seismic situation of reservoirs on the territory of the Republic of Uzbekistan, in order to improve the quality of the obtained seismic data to study incoming seismic information about seismological processes in order to ensure the seismic safety of infrastructure facilities.*
Keywords: *Seismic monitoring, hydraulic structures safety, seismometer, accelerometer.*

1. Introduction

The Gissarak reservoir is located in Central Uzbekistan on the territory of the Kashkadarya region. According to its structural position, this territory belongs to the region of transition from the Tien Shan epiplatform orogen to the Turanian platform. The seismicity of the territory is directly related to the tectonics of the region and manifests itself along the faults of the earth's crust, activated at the present stage of geological development. The areas of dynamic influence of active faults are combined according to the data of R.N. Ibragimov into seismogenic zones [1].

2. Methodology and Instrumentation.

Seismic monitoring at hydraulic structures. Today, the world has made great progress in the field of seismic monitoring of dams [2–5]. The high cost of seismic monitoring systems for large strategic dams, using available modern technologies for recording and transmitting data to remote control centers, is justified by the enormous value attached to these dams [6–9].

The data processing equipment supplied to the processing center included two servers equipped with advanced software for data collection, analysis and archiving. Data acquisition software is capable of automatically downloading data from remote locations upon startup and on demand. This software is also capable of remotely configuring, monitoring and synchronizing devices, as well as monitoring health status [10,11].

Seismic monitoring has provided seismology scientists with invaluable information about the structure's response to seismic activity based on time-lapse observations and early warnings. Using this information, facility personnel can perform rapid deployments and inspections to meet the need for safe and cost-effective operation of facilities [12–14].

One possible arrangement of instruments is shown in Figure 1. This is given as an example only, but the actual number and arrangement can be made after a careful assessment of the needs depending on the type and importance of the dam and the seismic region in which it is located [15,16].

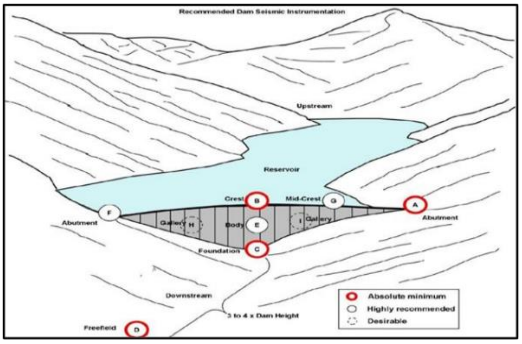

Figure 1. - **Layout of seismic instruments on the dam [15,16].**

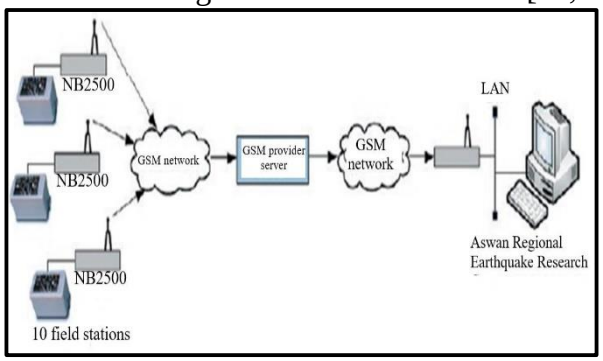

Figure 2. - **Seismic data transmission diagram [17**].

Since there is no Internet access or reliable land lines to transmit data from remote locations inside the dam and outside the two dams, the Global Mobile Telecommunications System (GSM) is used to transmit data in real time [17]. Mobile Telecommunications Systems are a proven technology for both temporary and permanent networked seismic telemetry communications (Fig. 2).

Practice of using monitoring systems. The main goal of the entire project was the organization of a seismometric monitoring system for the main hydraulic structures and the organization of seismological monitoring of natural and man-made earthquakes on the territory of hydroelectric power stations and reservoirs. [18–20] (Fig. 3,4,5). In April 2022, firm «Geobitas», in accordance with Agreement No. 1 dated October 15, 2021, installed equipment for seismological observations at four reservoirs. The systems were installed on: Charvak, Gissarak, Andijan and Tupalang reservoirs.

Equipment required for seismic monitoring (Fig 3):

1) Solar panel
2) Charge controller
3) Battery
4) Digital seismometer «Appatit-V»
5) Media converter
6) GPS antenna
7) Chassis with media converters
8) Ethernet Switch
9) Personal computer
10) Protective box

The main objectives of the network are the continuous recording of data on ground movement at the locations of seismological stations and the transmission of recorded data on ground movement at observation points via communication channels to the data collection point.

A seismic monitoring system has been implemented at the Gissarak reservoir (Fig 4):

1) Solar panel-4 pcs
2) Charge controller-4 pcs
3) Battery pcs-4 pcs
4) Digital seismometer from «Appatit-V» -4 pcs
5) Media converter -4 pcs
6) GPS antenna -4 pcs
7) Chassis with media converters-4 pcs
8) Ethernet Switch -4 pcs
9) Personal computer -1 pcs
10) Protective box -4 pcs

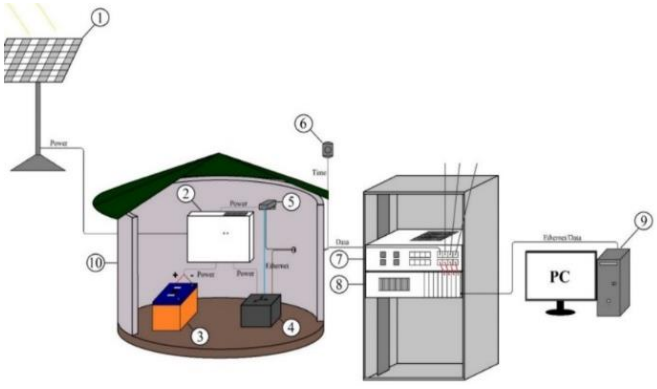

Figure 3. - **Seismological system diagram with a list of equipment.**

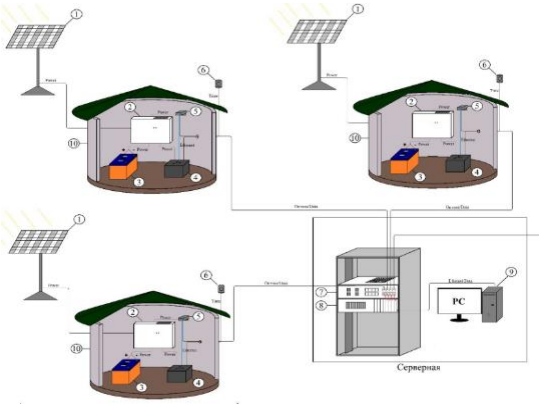

Figure 4. - **Schematic diagram of the seismological system.**

General layout of seismometers at the Gissarak Dam (Fig 5)

Figure 5. - **Layout of the seismological system at the Gissarak dam.**

The seismological equipment installed on the reservoirs is a Russian broadband electromechanical velocimeter with a built-in MEMS accelerometer called «Apatit-V». (Fig. 6)

Figure 6. - **Equipment layout and placement.**

View vibration spectra for 4 stations (low and high frequencies). Using the example of the Gissarak reservoir (Fig. 7)

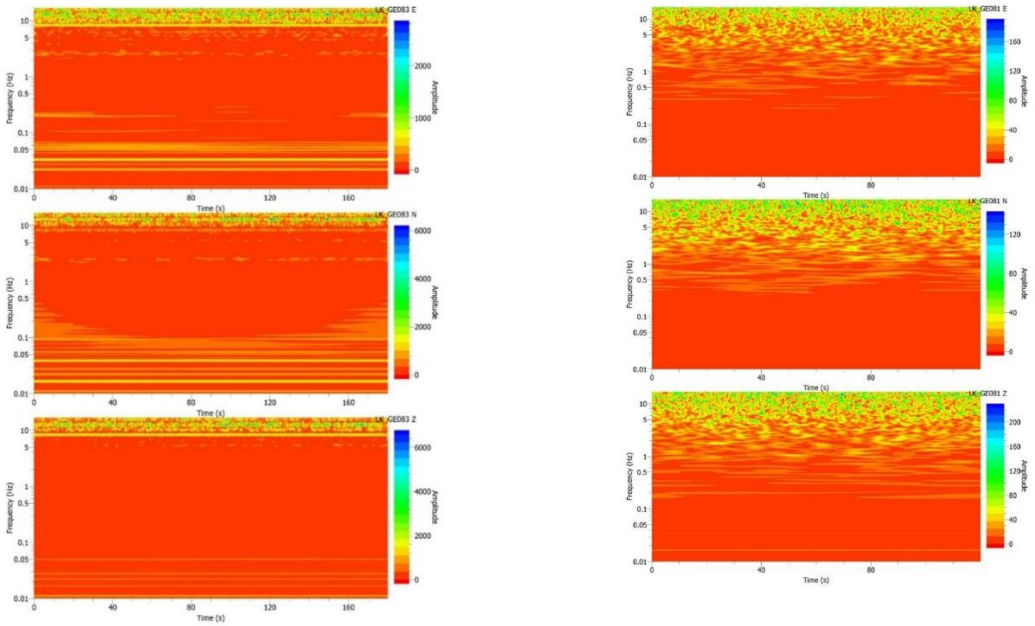

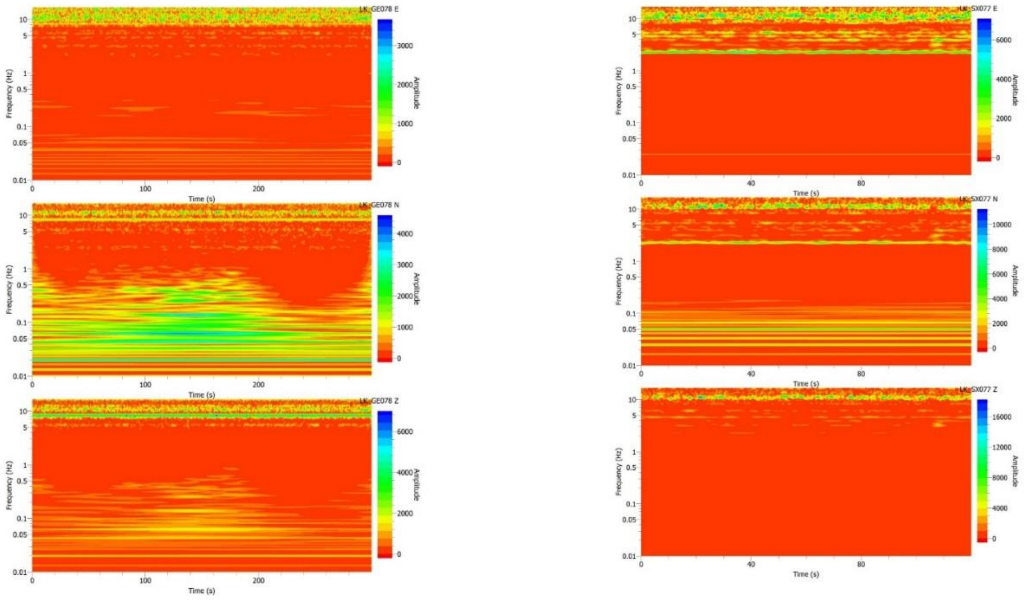

Figure 7. - **Results of vibration spectra data from 4 stations. Frequency =0.01-10 (Hz). Color amplitude=0-16000 (C)**

The study used a damage detection module consisting of two different detection algorithms that were developed for long-term monitoring of structures (Fig. 8)

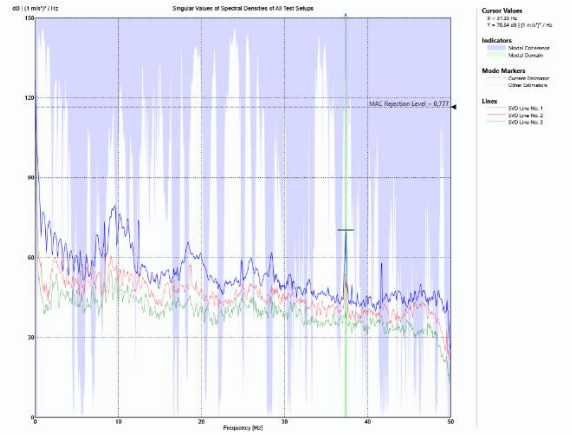

F(max)=37,3 Hz

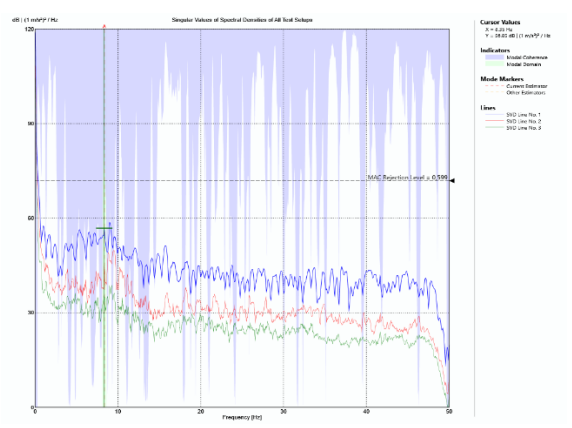

F(max)=8,3 Hz

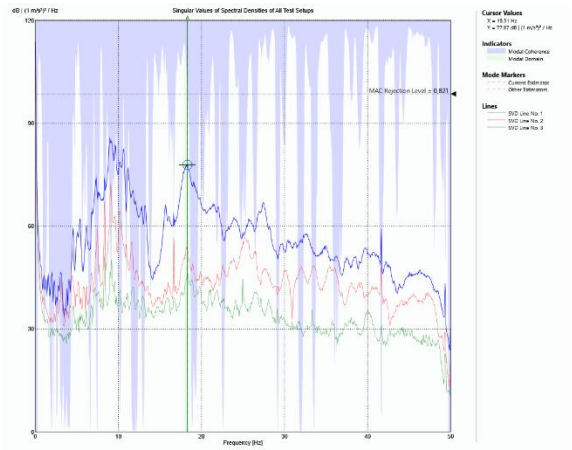

F(max)=18,3 Hz

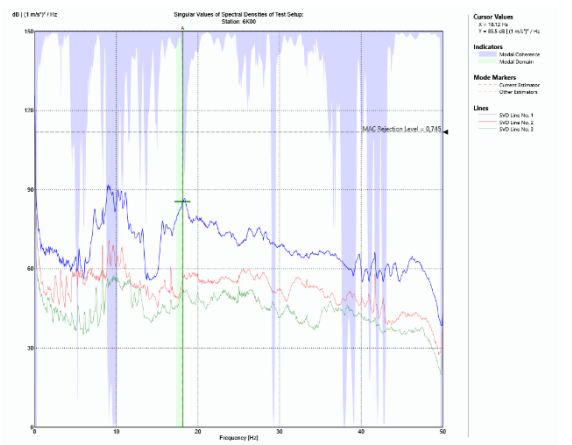

F(max)=18,1 Hz

Figure 8. - **Resonant frequencies, judging by the analysis, range from F(max)=8.35-37.35 Hz.**

3. Results

Seismic equipment of dams and reservoir sites is currently accepted not only for research work, but mainly for understanding the significant seismic hazards faced by existing dams in seismic areas. With the advent of digital seismic equipment, it can now be an integral part of dam safety monitoring efforts. Digital earthquake data can be collected by site personnel and remote-control centers using computers. When installing digital devices with a modem and communications, remote access is provided. Seismic instrument recordings taken from dam sites also help in the safe design of new dams in seismically active regions. Increasing awareness of the importance of seismic instruments for dams has led to their installation in large numbers at large hydroelectric facilities. Currently, there are many seismic equipment manufacturers available in the world. The degree of progress of firms in the production of seismometers, software development and data transmission. Seismic instruments are expensive to install, operate and maintain, but this clearly justifies their use in dams and makes their installation highly recommended.

4. Discussion

Through seismic measurements and dynamic analysis of dams, it is possible to discover the reasons why earth and concrete dams consistently performed better than expected by design or analysis when shaken by earthquakes. These reasons may be:

—increasing damping, reducing the seismic impact on the dam;

—increasing the tensile strength of concrete under dynamic loading, which increases the elasticity of the object

— creation of a system that provides seismometric observations of the operation of a structure during the period of seismic activity;

— observations of the condition of the structure under seismic impacts are carried out to assess the possibility of the development of dangerous deformations and other signs;

—instrumental determination of the dynamic characteristics of the structure.

References

1. *Ibragimov R.N.* Seismogenic zones of the Middle Tien Shan. Tashkent: Fan, 1978, 144 p.
2. Water Technologies (n.d.). *Aswan High Dam, River Nile, Sudan,* Egypt. Retrieved on 12th June 2020 https://www.water-technology.net/projects/aswan-high-dam-nile-sudan-egypt/
3. *McKenna, E. (n.d.). Aswan High Dam. Encyclopedia Britannica.* Retrieved on 12th June 2020 https://www.britannica.com/topic/Aswan-High-Dam
4. *REFTEK* (2013). Strong Motion Structural Monitoring Technology is used on the Aswan Dams. May 2013. Retrieved on 12th June 2020. https://reftek.com/ref-teks-strong-motion-structural-monitoring-technology-used-aswan-dams/
5. USCOLD (2000). Observed Performance of Dams during Earthquakes. Vol. II, October 2000, pp.15- 20.
6. USBR (1987). Concrete Dams Instrumentation Manual. Page12.
7. *Mihailov, V. and Dojcinovsky, D.* Strong Motion Instrumentation of Dams in Macedonia-Some Experience and Results. 13th World Conference on Earthquake Engineering Vancouver, B.C., Canada, August 1-6, 2004, Paper No. 475
8. National Research Council. Earthquake Engineering for Concrete Dams: Design, Performance, and Research Needs. Panel on Earthquake Engineering for Concrete Dams, Committee on Earthquake Engineering. National Academy Press Report pp.33-35. Washington, D.C. 1990
9. FEREC (n.d.). Instrumentation and Monitoring. Chapter 9, pp.20, 31.
10. Wikipedia (2012). Seismometer. Retrieved on 10th June 2020 https://en.m.wikipedia.org/wiki/Seismometer
11. *Dewey, J. and Byerlym, P.* The Early History of Seismometry to 1900. USGS. Last modification on January 2004. Retrieved on 10th June 2020.
12. *Bartholomew, C. L. and Haverland, M. L.* USBR Concrete Dams Instrumentation Manual. USBR, October 1987, pp.121- 125. https://www.usbr.gov/tsc/techreferences/mands/mands-pdfs/CDamInst.pdf
13. *Evangelidis, C.* Seismic monitoring of Large Dams. Alliance for Disaster Risk Reduction (ALTER). Retrieved on 10th June 2020
14. GeoSig (n.d.). Seismic Instrumentation and Monitoring of Dams. Switzerland. Retrieved on 10th June 2020 https://www.geosig.com/Dams-pg38.aspx
15. USACE (1995). Instrumentation of embankment Dams and Levees. Manual No. 1110-2-1908, 30 June 1995. Chapter 4, pp.19-21. Washington, DC.
16. Nile Alley. Aswan High Dam. Retrieved on 12th June 2020. http://www.nilecruised.com/aswan-high-dam/

17. *Ibragimov A.Kh., Alimukhamedov I.M., Rakhmatullaev Kh.L.* Assessment of seismic stability of buildings Nakamura's method. Second European Conference on Earthquake engineering and seismology. Istambul, Turkey, 2014.
18. Water Technologies (n.d.). Aswan High Dam, River Nile, Sudan, Egypt. Retrieved on 12th June 2020 https://www.water-technology.net/projects/aswan-high-dam-nile-sudan-egypt/
19. *Nasrat Adamo, Nadhir Al-Ansari, Varoujan Sissakian , Jan Laue, Sven Knutsson* «Dam Safety: Use of Seismic Monitoring Instrumentation in Dams» Journal of Earth Sciences and Geotechnical Engineering, Vol.11, No.1, 2020, 203-247
20. Rock-earth dams https://leg.co.ua/arhiv/generaciya/kamenno-zemlyanye-plotiny/Page-29.html

ASSESSMENT OF SEISMIC IMPACT CHANGE THROUGH ENGINEERING-TECHNICAL REINFORCEMENT OF LOESS SOILS

Bozorov J.Sh.[1], Oripov N.K.[1], Yadigarov E.M.[1], Xusomiddinov A.S.[1]
[1]*Institute of Seismology, Tashkent, Uzbekistan*
E-mail: j.bozorov1968@gmail.com

Abstract: *The article presents changes in physical-mechanical and seismic properties of loess soils through engineering-technical preparation. An analysis of results of engineering-geological, seismological and instrumental field research is presented in this research work as well. In addition, a 3D model of the construction site was created using Plaxis 3D software. Changes in acceleration, velocity and displacement values in the 3D models created for the pre- and post-engineering conditions have been evaluated.*
Keywords. *Earthquake, peak acceleration, seismic intensity, deep soil mixing, loess soils.*

1. Introduction.

The works [1-5] state that in the territory of Uzbekistan and adjacent regions, both in historical period and at the present stage, earthquakes of magnitude M≥7 and the intensity of shaking on the MSK-64 scale at the epicenter of I_0=9-10 points have occurred several times, and, therefore, the works studied problems of ensuring seismic safety of the territory of the Republic and the relevance thereof. Moreover, an increase of seismic intensity on the earth surface is very important due to seismic intensity increment as a result of earthquakes in the areas where loess soils are scattered [6-8]. Based on the above, an extent of effects of artificial strengthening of loess soils using the Deep Soil Mixing Method to the seismicity level of construction sites is described herewith.

2. Methotology.

The Deep Soil Mixing Method (DSM) had been used for artificial strengthening of loess soils [9-10]. Deep Soil Mixing (DSM) is used throughout the world. In the United States, Great Britain, Germany, France, Japan, China, Russia, Turkey and other developed countries of the world it is used for improving physical and mechanical properties of soils, using cement and lime mixtures mixed with local soils spread on construction sites as a method to improve Load-Bearing Capacity of soils. This method (DSM) of mixing soil with cement slurry is much more effective compared to other methods used for increasing soil strength [11]. The method not only reduces project costs, but also eliminates delays during construction. Mixing soil with cement slurry is also more environmentally friendly since it reduces carbon dioxide emissions in more extent than other methods of improving soil quality (Figure 1). It should be noted that there is no need for on-site mining of existing materials, and there will be very little waste removal. The soil present at the construction site is used as a construction material and does not require transportation of expensive and bulky construction materials at the construction site. This allows to reduce the movement of vehicles. Technology of deep soil mixing with cement mixtures. Deep soil mixing is a soil conditioning method that improves properties of loose, dispersed soils by mechanically mixing them with a cement binder. Mixing minerals such as cement, lime or bentonite with soil leads to strengthening soil properties [11].

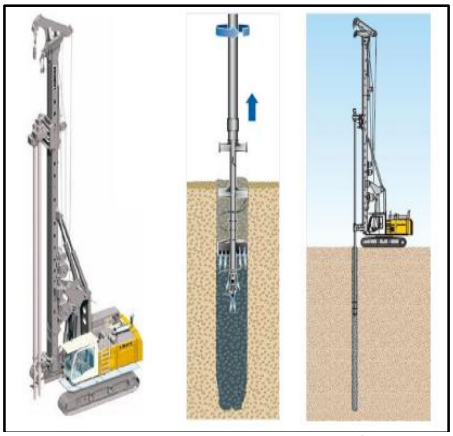

Figure 1. - **The Production Flow Diagram according to the technology of Deep Soil Mixing with cement slurry**

3. Results.

The researches were conducted in a construction area of "16-story residential buildings" located at the intersection of Turkestan and Movarounnahr streets, Kokand City, Fergana Region. Quaternary deposits are scattered in the research area. “Golodnostep” complexes (apQIIIgl) of Upper Quaternary deposits formed by alluvial-proluvial way are scattered as well. In the construction area there are loess soils, clays and sandy soils in a form of a small layer, pebble stone down to 25-meter deep. As a result of engineering-geological studies, the soils in the field were divided into 4 engineering-geological elements. Engineer geological element 1 – Sandy Loam. Engineer geological element 2 – Loam Soil. Engineer geological element 3 – Gravel. Engineer geological element 4 – Pebble Stone. Physico-mechanical properties of each element were defined.

Seismological survey and engineer-geological field research were also carried out on the construction site. Seismological surveys were performed using MASW method and the following results were obtained (Table 1).

Table 1.

Values of engineering-geological and seismic properties of soils before the engineering preparation

Tracking Point	Vs30, m/sec	ρ30, g/cm ^{3}	(Vsi·ri)	Plug Soil (660*1.9)	dI, score
Profile - average	300	1,75	525	1254	+0,64

Table 2.

Improving strength of soil in a construction site with the method of Deep Soil Mixing

Indicators of soil properties	Units	Natural state
Soil Density,	(ρ), g/cm ^{3}	1,55-2,05 1,75
Soil Skeletal Density,	(ρ_d), g/cm ^{3}	1,50-1,60 1,55
Humidity,	(W), %	13,5-27,2 20,5
Porosity,	(n), %	42,4-50,0 43,2
Transverse Wave Velocity,	(V_s), m/s	260-350 300
Seismic Impedance,	($Vs_i \cdot r_i$)	495
Seismic Intensity Increment	($\triangle$I), score	+0,64

Deep Soil Mixing (DSM) provides a fast, cost-effective and environmentally friendly method of densifying and dynamically strengthening soils and improves soil deformation properties. The system is designed to improve condition of soft soils by mixing a cement binder with clay, peat, or bottom layers. The technology is designed for consolidation of subsiding soils on a large area and is the most economical method suitable for any type of soil. Some 154 DSM piles with a length of 19 m and a diameter of 1 m were placed on a field of 620 m^2 under a 16-story residential building located at the intersection of Turkestan and Movaraunnahr streets, Kokand City, Fergana Region. Engineer-

geological, seismological and instrumental field research was carried out in the pit where DSM piles were placed and the following results were obtained (Tables 2, 4, 5).

In the construction site, seismometric measurements of microseisms were performed to determine soil parameters according to the Nakamura Method [12-13].

The method of estimating the seismic intensity increment allows to estimate the H/V spectral ratio (horizontal and vertical oscillations, Nakamura method, 1991). [14-15]. The Seismic Intensity Increase Estimation Method, i.e. data processing using JSesame software based on synchronous recording of natural noise at two or more points and subsequent comparison of amplitude-spectral properties of microseismic noise allows to estimate the H/V spectral ratio (horizontal and vertical oscillations, Nakamura Method, 1991) [14-15].

Noises caused by man-made and other factors during processing were cut from the time series (Fig. 2). The coefficient of liquefaction of soils under cyclic influence was calculated (Table 3).

$$K_g = \frac{A^2}{F_0} \tag{1}$$

here, A - amplification factor, F_0 - dominant frequency of grunts.

The following ratio is used to determine an increase in intensity of seismic vibrations:

$$\Delta I = \lg 2\left(\frac{A_i}{A_n}\right) \tag{2}$$

here, A*i* - H/V value at measurement point, H/V value at An-base point

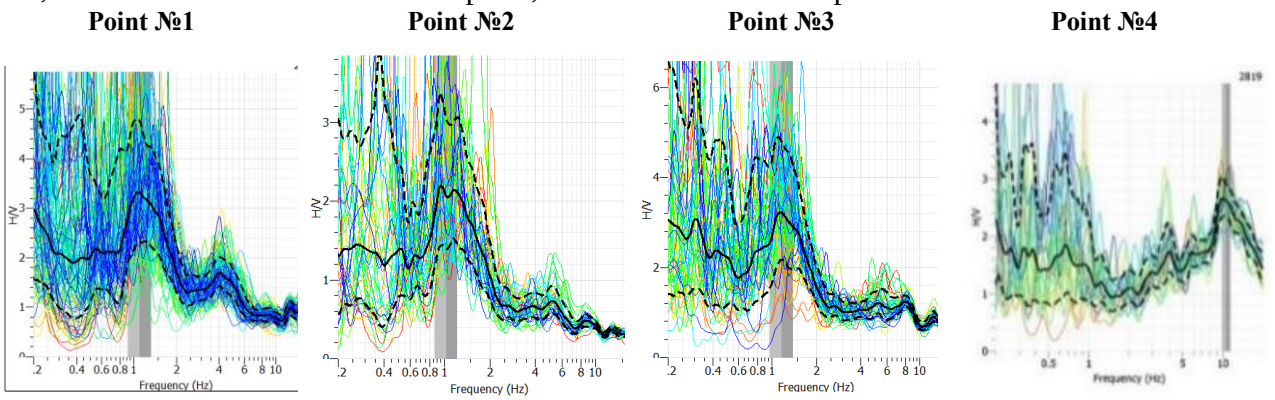

Figure 2. - **Calculated HVSR spectra for tracking points**

Table 3.

Calculation parameters of soils according to HVSR Method

No	HVSR	Fo	Kg	dI
1	4	1,5	10,6	-0,54
2	5,2	0,7	38,6	-0,11
3	8	1,1	14,5	-0,81
4	2	1,03	3,88	-0,43

Table 4.

Results of field seismological research after engineering-geological preparation

Tracking Point	Vs_{30}	ρ_{30}	Plug Soil (660*1.9)	$dI_{s,j,}$
Profile 1	350	2,3	1254	+0,32
Profile 2	506	2,46	1254	0,005
Profile 3	550	2,40	1254	-0,03
Profile - average	470	2,39	1254	0,09

Table 5.

Values of engineering-geological and seismic properties of soils after engineering preparation

Indicators of soil properties	Units	After preparation
Soil Density,	(ρ), g/cm 3	2,30-2,46 2,40
Soil Skeletal Density,	(ρ_d), g/cm 3	1,65-1,75 1,70
Humidity,	(W), %	10,5-20,2 15,5
Porosity,	(n), %	34,4-39,5 36
Transverse Wave Velocity,	(V_s), m/s	350-550 470
Seismic Impedance,	($Vs_i \cdot r_i$)	1,124
Seismic Intensity Increment	($\triangle$I), score	0,09

4. Analysis.

Thus, we can see that, according to the results of seismological field research, the average transverse waves velocity in the field before engineering-geological preparation was V_s =300 m/sec, and the seismic impedance was $Vs_i \cdot \rho_i$=495 ha, and, after engineering preparation the average transverse waves velocity in the field changed to V_s =470 m/sec, and the impedance - to $Vs_i \cdot \rho_i$=1124.

According to the results of instrumental studies, the results for soil scattered on the construction site before and after engineering preparation were analyzed. Before the preparation, it was determined that the soils were located in the third category of soils in terms of seismic properties. After engineering training, the grunts moved to the second category. The dominant frequency of soils in the construction site varies in the range of 0,7-1,5 Hz. The Seismic Instability Factor does not exceed the value of 38,6.

Evaluation of seismic impact and seismic effect change in construction sites with scattered subsiding soils by preparing DSM piles using FEM (Finite Elements Method) in spatial space. In this case, numerical methods cannot be directly applied to solve the problem of propagation of seismic waves in an infinite half-space. To perform this task, we replace the infinite half-space with a finite parallelepiped in the area of our interest [18].

At the same time, boundary conditions of the following form are imposed, with the continuation of the parallelepiped representing the effect of the abandoned part on the faces of the abandoned sides, i.e., passing the waves incident on the boundary without returning them.

$$\left.\begin{aligned}\sigma_x &= a\rho V_p \dot{u}\\ \tau_{yz} &= b\rho V_s \dot{u}\\ \tau_{zy} &= b\rho V_s \dot{w}\end{aligned}\right\} \quad \left.\begin{aligned}\sigma_y &= a\rho V_p \dot{v}\\ \tau_{xz} &= b\rho V_s \dot{w}\\ \tau_{zx} &= b\rho V_s \dot{u}\end{aligned}\right\} \quad \left.\begin{aligned}\sigma_z &= a\rho V_p \dot{w}\\ \tau_{xy} &= b\rho V_s \dot{u}\\ \tau_{yx} &= b\rho V_s \dot{v}\end{aligned}\right\} \qquad (3)$$

Here, σ and τ are normal and shearing stresses; $\dot{u}$ and $\dot{v}$ - projections of the velocities of the boundary points on the axes; V_P and V_S are Velocity of **P** and **S** waves; α and β are dimensionless parameters; ρ is the density of the material.

Geometric relations can be formulated as follows:

$$\varepsilon = Lu \qquad (4)$$

L^T is the transposition of the differential operator, which is defined as follows:

$$\mathrm{L^T} = \begin{bmatrix} \frac{\partial}{\partial \mathrm{x}} & 0 & 0 & \frac{\partial}{\partial \mathrm{y}} & 0 & \frac{\partial}{\partial \mathrm{z}} \\ 0 & \frac{\partial}{\partial \mathrm{y}} & 0 & \frac{\partial}{\partial \mathrm{x}} & \frac{\partial}{\partial \mathrm{z}} & 0 \\ 0 & 0 & \frac{\partial}{\partial \mathrm{z}} & 0 & \frac{\partial}{\partial \mathrm{y}} & \frac{\partial}{\partial \mathrm{x}} \end{bmatrix} \qquad (5)$$

We determine the displacement, velocity and acceleration of the nodes formed in soils considering physical and mechanical properties of the material [19].

The system of master equations depending on the time of movement of the system under an influence of dynamic load is as follows:

$$[M]\{\ddot{u}\} + [C]\{\dot{u}\} + [K]\{u\} = \{F\}, \quad (6)$$

where the order of the system of differential equations is 39,039, [M] is the Mass Matrix, $\{u\}-$ is a displacement vector, $[C]\ -$ is the Damping Matrix, which also considers the boundary conditions, $[K]-$is Matrix Hardness, and $\{F\}-$ is the Load Vector. Displacement $\{u\}$, velocity$\{\dot{u}\}$ and acceleration$\{\ddot{u}\}$ may change over time.

For digital implementation of the problem, we use a software complex Plaxis 3D [18-19], which contains possible variants of the physical equations for the material.

The [M] matrix takes into account the mass of materials (soil + water + any structures). Stability and accuracy of iteration over time is an important factor in formulation of numerical calculation of a dynamic process. Newmark's Numerical Iteration Scheme is applied. X=14, Y=11, Z=0.

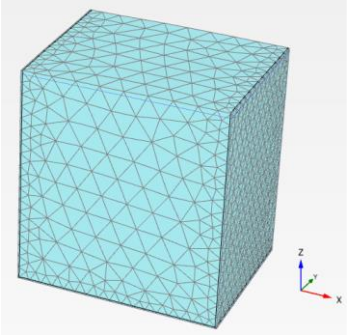

Figure 3. - **5535-finite element 3D model of the site in pre- and post-engineering preparation states**

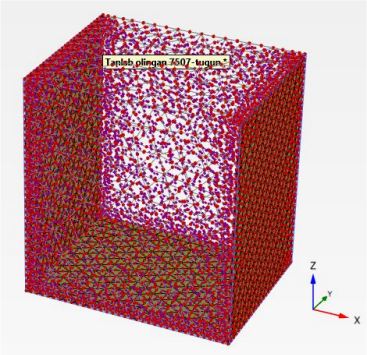

Figure 4. - **A 3D model of the selected model divided into 13247 nodes**

Table 6

Results of indicators of engineering-geological and seismic properties before and after engineering preparation

Indicators of soil properties	In natural state, before engineering preparation	After engineering preparation
Soil Density, (ρ), g/cm^3	1,55÷2,05 1,75	2,05-2,20 2,10
Soil Skeletal Density (ρ_d), g/cm^3	1,50÷1,60 1,55	1,65-1,75 1,70
Humidity (W), %	13,5÷27,2 20,5	10,5-20,2 15,5
Porosity (n), %	42,4÷50,0 43,2	34,4-39,5 36
Transverse Wave Velocity (V_s), m/s	260÷350 300	450-650 550
Longitudinal Wave Velocity(Vp), m/s	510÷850 600	850-1200 960
Seismic Impedance ($Vs_i \cdot r_i$)	525	1155
Seismic Intensity Increment (ΔI)	+0,64	0,074
Modulus of Elasticity. E (MPa)	4,1	13,1
Poisson's Ratio, μ	0,33	0,25
Inner Friction Angle, φ	25	32
Binding power. C, (kPa)	7	20
Groundwater Level, h	5,2	5
Dimensions of the building	20m x 26,1m	20m x 26,1m

As a result of applying the FEM, a continuous mechanical system is replaced by a discrete system. The studied area is divided into 13,247 nodes and 5,535 finite elements. The number of generated second-order linear differential equations is 39,741. Shapes of the finite elements are chosen as irregular tetrahedrons. At the next stage of solving the problem, the parameters of the soil before and after engineering preparation are inputted in the application (Table 6).

After inputting soil parameters, real accelerogram recorded as a result of earthquake in that area is entered as seismic effect for both selected models of the same size. The accelerogram is shown in Figure 3 below. The accelerogram coordinates (x=37.85; y=72.18) were recorded as a result of an earthquake of magnitude M=5.7, the depth of the earthquake epicenter N=112 km, which occurred on 16.06.2020 at 01:30, local time.

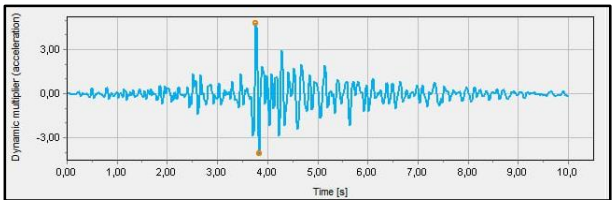

Figure 5. - **Real accelerogram inputted in Plaxis 3D software**

After performing calculations using the Plaxis 3D software set, we would be able to determine the values of velocity, acceleration and displacement at any time of the seismic impact at any nodes. Below are the results of the seismic effect when it reaches its maximum value.

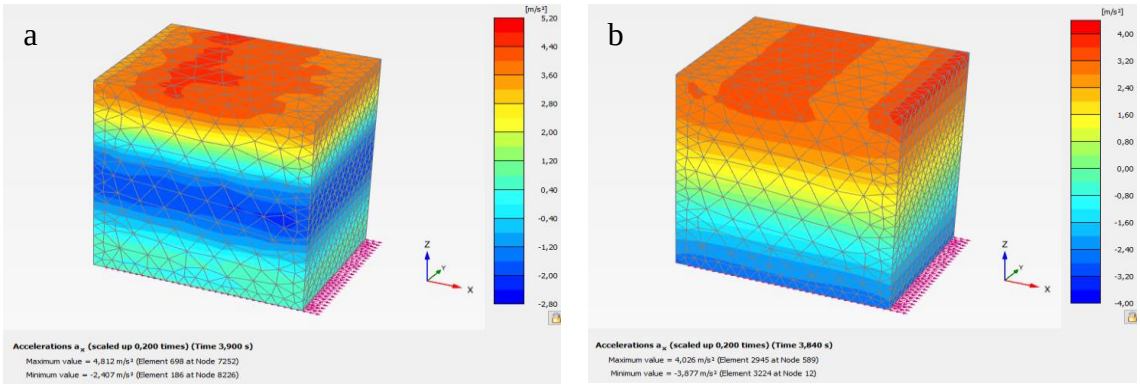

Figure 6. - **3D model of accelerations at all nodes along the X-axis for *t=3* sec**
a) in a natural state b) in a state after engineering preparation

In natural state, the greatest acceleration value of $a_x = 417{,}4\ cm/s^2$ is reached on 7507th node *at t=3 sec*, and after engineering preparation, on the same 7507th node *at t=3* the highest acceleration value *of* $a_x = 329{,}9\ cm/s^2$ is reached. As it can be seen from above, we can say that the elimination of sedimentation and seismic properties of soils using the deep soil mixing method provides attenuation of seismic waves caused by earthquakes to buildings and structures, because accelerations $\triangle a_x = 88{,}1\ cm/s^2$ are reduced, percentage accelerations per node are decreased by *20,96* %.

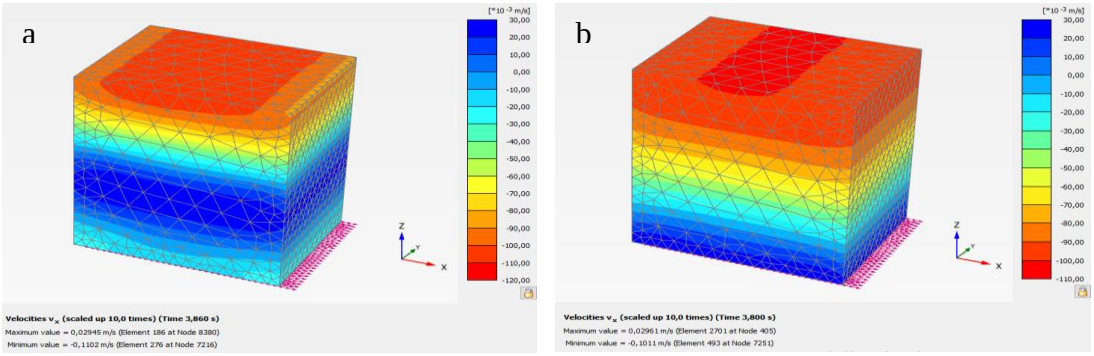

Figure 7. - **a) in a natural state b) A 3D model of velocities in a state after engineering preparation at all nodes along the X-axis at *t=3* sec**

The figure above shows how a seismic effect affects a selected node for the entire 10 second period as acceleration example. So, time values when maximum and minimum times of the given accelerogram are reached, without breaking the law, correspond to the acceleration values.

In natural state, the highest velocity is reached at a value of $v_{x1} = 10,8$ *cm/s* on 7,507th node with natural coordinates (x=14, y=11, z=0) at $t=3$ sec, and in the post-engineering preparation state, at the node with coordinates (x=15, y=10, z=0) at $t=3$ sec, the highest velocity is reached at the value of $v_{x2}=9,6$ *cm/s*. It can be seen that the velocities in nodes after engineering preparation were decreased by $\Delta v_x = 1,2$ *cm/s* , and in percentage by *11,2 %*

Changes in the highest values of displacement over time were analyzed at 7,011th node at $t=3$ sec along the X axis in natural and post-preparation state. Maximum displacement value in natural state model is $u_{x1}=0,57$ *cm* , and the highest value of displacement in the case of post-engineering preparation reached the value of $u_{x2}=0,46$ *cm*. As it is seen from the above, displacement in nodes after engineering preparation is reduced by $\Delta u_x = 0,11$ *cm*, which is in percentage means a difference of *19,29 %*. The above results are presented in the following table with the values of acceleration, velocity and displacement parameters.

Table 7

In natural state	In Post-Engineering State	Difference	In natural state	In Post-Engineering State	Difference	In natural state	In Post-Engineering State	Difference
Acceleration, a_x (cm/s^2)			Velocity, v_x (*cm/s*)			Displacement, u_x *(cm)*		
a_{x1}	a_{x2}	Δa_x	v_{x1}	v_{x2}	Δv_x	u_{x1}	u_{x2}	Δu_x
417.4	*329.9*	*88.1*	*7.0*	*9.6*	*1.2*	*0.57*	*0.46*	*0.11*

Node accelerations in percentage has decreased by *20.96*%. The velocity is this calculation has decreased by *11.2 %*, and the displacement, in percentage, has decreased by *19.29%*.

5. Discussion.

On the light of above data, we can see that the difference in seismic intensity increment has decreased by Δ I=0.76≈1 points. Nowadays, use of Deep Soil Mixing piles in order to prevent subsidence during operation and to reduce the seismic effect caused by earthquakes in the construction of multi-storey residential buildings in areas with loess soils is becoming popular in construction works. Plaxis 3D complex was used for confirmation of the above-mentioned points and to determine to what extent the Deep Soil Mixing piles serve to reduce the level of seismicity of a construction site. A model of the construction site was created by the software and specific properties were entered for each model. The selected model has been divided into 5,535 elements and 13,247 nodes, and the order of the system of differential equations was 39,741. The difference of the highest and the lowest values of the accelerations before and after post-engineering preparation at the 7,507th node with coordinates (x=14; y=11; z=0) at $t=3$ sec decreased by $a_x = 88.1$ *cm/s*$^{2.}$ Now, the difference between the maximum and minimum velocity values before and after the engineering preparation at this very node at *t=3 sec* decreased by $\Delta v_x = 1.2$ *cm/s*. The displacement values may be somewhat underestimated, since the specific characteristics of accelerometers are not designed to record large periods (of time). Moreover, the greatest displacement at *t=3sec* has made $u_x = 0.57$ *cm*, and, after engineering preparation, at the coordinate node of (x=14; y=11; z=0) at $t=3$ sec the highest displacement value made $u_x = 0.46$ *cm*. It can be seen that displacements in nodes (elements) after engineering preparation has decreased by $\Delta u_x = 0.11$ *cm*.

This work was funded by grants from the Academy of Sciences of the Republic of Uzbekistan, "Development of scientific foundations for assessing various levels of seismic risk and reducing earthquake losses in seismically active areas" and the Agency for Innovation Development, #ALM202311142839 "Creation of a simulation digital model of the city of Tashkent allowing to assess the level of economic damage from strong earthquakes" and #AL5822012294 "Development of technology for predicting the risk of strong earthquakes", #AL5822012298"Create an electronic database on seismological soil characteristics to replace Table 1.1 in the regulatory document. seismological part of KMK “Construction of seismic areas”", as well as the project "Regionally

coordinated assessment of earthquake and flood risks and selective analysis of landslide scenarios to strengthen financial resilience and accelerate risk reduction in Central Asia", funded by the EU Program "Strengthening Financial Resilience" and Accelerating Risk Reduction" (SFRARR) funded by the European Union and implemented by the World Bank. We sincerely thank all the project team members, in particular Sergey Tyagunov, Paola Ceresa, Antonella Peresan, Gabriele Coccia, Denis Sandron and Stefano Parolai, and the World Bank specialists, in particular Stuart Alexander Fraser and Madina Nizamitdin, for their constructive contributions to the project. We are grateful for the suggestions and feedback from the editor and the two reviewers, which substantially improved the manuscript.

References

1. *Artikov T.U., Ibragimov R.S., Ibragimova T.L., Kuchkarov K.I., & Mirzaev M.A.* (2018). Quantitative assessment of seismic hazard for the territory of Uzbekistan according to the estimated maximum ground oscillation rates and their spectral amplitudes. Geodynamics & Tec- Tonophysics, 9(4), 1173–1188. doi:10.5800/GT-2018-9-4-0389
2. *Ibragimov, R. S., Ibragimova, T. L., Mirzaev, M. A., & Rebetsky, Yu. L. (2023).* the probability of a strong (m≥6.0) earthquake in the south Fergana seismic activity zone in the coming years. Geodynamics & Tectonophysics, 14(1). https://doi.org/10.5800/GT-2023-14-1-0688
3. *Sadykov, Yu. M., Atabekov, I. U., & Ibragimov, R. S. (2023).* Seismotectonic Analysis and Development of the Mathematical Model of the Stress–Strain State of the Earth's Crust in the Zone of Collision of the Western Tien Shan with the Pamir Arc. Geotectonics, 57(3), 306-315. https://doi.org/10.1134/S0016852123030068
4. *Artikov, T. U., Ibragimov, R. S., Ibragimova, T. L., Mirzaev, M. A., & Rebetsky, Yu. L.* (2022). Stress State of the Earth's Crust, Seismicity, and Prospects for Long-Term Forecast of Strong Earthquakes in Uzbekistan. Russian Geology and Geophysics, 63(12), 1442-1458. https://doi.org/10.2113/RGG20214408
5. *Atabekov, I. U., Artikov, T. U., Ibragimov, R. S., Ibragimova, T. L., & Mirzaev, M. A.* (2021). Relationship between Strong Earthquakes and Activation of Deep Faults in Central Asia (Uzbekistan): Numerical Simulation of Stress Field Variations. Geotectonics, 55(3), 377-392. https://doi.org/10.1134/S0016852121030031
6. *Khusomiddinov, A., Yodgorov, S., Sadirov, F., Yadigarov, E., Aktamov, B., & Avazov, S.* (2022). Estimation of the Seismic Intensity Increments in Tashkent Region. AIP Conference Proceedings, 2432. https://doi.org/10.1063/5.0089662
7. *Ismailov, V., Khusomiddinov, S., Khusomiddinov, A., Yodgorov, S., Aktamov, B., & Avazov, S.* (2022). Seismic risk assessment of Jizzakh region. 030035. https://doi.org/10.1063/5.0089664
8. *Ismailov, V. A., Yodgorov, S. I., Allayev, S. B., Mamarozikov, T. U., & Avazov, S. B.* (2022). Seismic microzoning of the Tashkent territory based on calculation methods. Soil Dynamics and Earthquake Engineering, 152, 107045. https://doi.org/10.1016/j.soildyn.2021.107045
9. *Korpach A.I., & Lofitsky A.V.* (2015). Vozmojnosti primeneniya tekhnologii glubinnogo peremeshivaniya grunta DSM dlya ograjdeniya kotlovanov (Application potential of the DSM (deep soil mixing) technology for excavation fencing). Geotechnics (Geotekhnika), No. 3, 16-22.
10. *Zekhniev, F., Vnukov, D., & Korpach, A.* (2017). Soil bases improvement by using deep soil mixing technology. pnrpu Construction and Architecture Bulletin, 8(4), 116-125. https://doi.org/10.15593/2224-9826/2017.4.12
11. *Bogdanov O.I., & Korpach A.I.* (2013). Primenenie tekhnologii glubinnogo peremeshivaniya grunta DSM dlya usileniya gruntovykh osnovaniy (Application of DSM deep soil mixing technology for reinforcement of soil foundations.). Innovatsionnie konstruksii i tekhnologii v fundamentostroenii i geotekhnike Innovative Structures and Technologies in Foundation and Geotechnical Engineering), 271–276.
12. *Yang, S., Mavroeidis, G.P., de la Llera, J.C., Poulos, A., Aguirre, P., Rahpeyma, S., Sonnemann, T., & Halldorsson B.* (2019). Empirical site classification of seismological stations in Chile using horizontal-to-vertical spectral ratios determined from recordings of large subduction-zone earthquakes. Soil Dynamics and Earthquake Engineering, 125, 105678. https://doi.org/10.1016/j.soildyn.2019.05.017
13. *Tao, Y., & Rathje, E.* (2020). Taxonomy for evaluating the site-specific applicability of one-dimensional ground response analysis. Soil Dynamics and Earthquake Engineering, 128, 105865. https://doi.org/10.1016/j.soildyn.2019.105865
14. *Zhu, C., Pilz, M., & Cotton, F.* (2020). Evaluation of a novel application of earthquake HVSR in site-specific amplification estimation. Soil Dynamics and Earthquake Engineering, 139, 106301. https://doi.org/10.1016/j.soildyn.2020.106301
15. *Güven, İ. T.* (2022). Seismic vulnerability indices for ground in Derince-Kocaeli (NW Turkey). Environmental Earth Sciences, 81(5), 167. https://doi.org/10.1007/s12665-022-10288-x
16. *Russ, J. C.* (2012). Ground Improvement (K. Kirsch & A. Bell, Eds.). CRC Press. https://doi.org/10.1201/b13678
17. Stroitel'stvo v seysmicheskikh rayonax (Construction in seismic areas). (2019). In Stroitelnye normy i pravila (Construction Standards and Regulations)–Tashkent: "AQATM" Data & Calculation Center under State Committee for Architecture of the Republic of Uzbekistan (p. 121).

18. *Yuldashev Sh.S.* (2018). Vliyanie vysoty raspolojeniya zheleznodorozhnogo polotna na uroven kolebaniya grunta, voznikayushchego pri dvizhenii poyezdov. (Effect of a rail bed location height on the level of soil vibrations generated by train traffic). Nauchnoe Znanie Sovremennosti (Modern Scientific Knowledge), 55–57.
19. Plaxis 3d. (n.d.). Https://Www.Seequent.Com/Products-Solutions/Plaxis/
20. Material Models Manual /PLAXSIS CONNECT Edition (20; p. 256). (n.d.).

2023 TURKEY EARTHQUAKE: DAMAGE ASSESSMENT USING REMOTE SENSING AND DEVELOPMENT OF RAPID ASSESSMENT PROTOCOL

Gilani Amir[1], Miyamoto Kit[1], Takhirov Shakhzod [2]
[1] Miyamoto International, Sacramento, California, USA
[2] Structures Lab and Center for Smart Infrastructure, University of California at Berkeley, Berkeley, California, USA
E-mail: agilani@miyamotointernational.com

Abstract: *The 2023 Turkey earthquake caused 35,000 mid-rise buildings collapse, killed 51,000 people, and 4.1 million people homeless. Following the earthquake, satellite imagery data was reviewed to assess the damaged areas. Next, a ream of structural engineers and disaster risk reduction experts from Miyamoto International were deployed to Turkey for the earthquake response, shelter assessments, recovery strategies and to investigate the damage caused by this earthquake. The team conducted field surveys at earthquake-affected sites such as Pazarcik, Adiyaman, Antakya, Hatay, and many other towns. The NASA-JPL satellite damage assessment shows around 20 to 30 percent of building stocks are collapsed or damaged. This was followed by conducting repairability assessment for the largest municipality in the affected area, Gaziantep for Internally Displaced Population (IDP), by assisting them in returning to repairable buildings. First, the program assisted displaced families by providing information to restore their confidence in the structural safety of buildings. The program identified undamaged structures and rebranded them as habitable through publicly visible "green tagging." 3,500 undamaged structures were assessed, supporting an estimated 90,000 people. A broader community communication campaign was implemented to provide the community with information on the structural safety of assessed structures through in-person events and the distribution of communication materials online. These communication campaigns reached an estimated 200,000 people across Turkey, including more than 5,000 people through in-person events. Second, the program provided technical assistance on cost-efficient, rapidly implementable repairs required to make light and moderately damaged building stock habitable. The program conducted state-of-the-art app-based vulnerability assessment surveys to identify the vulnerability classification and cost-efficient repair method based on locally available materials and labor for each damage type. Bill of Quantities (BOQs) and generated repair cost estimates enabled households to repair their homes rapidly. 3,100 structures were assessed, supporting an estimated 75,000 people.*

Keywords: *2023 Turkey Earthquake, remote sensing, damage assessment, repairability assessment, earthquake aftermath, reconstruction*

1. Introduction

Earthquake reconnaissance is very important for any seismic event and, as such, has been extensively covered by many agencies, engineering companies, and researchers [1-8]. It is absolutely required after each seismic event, so general damage surveys of a region can be rapidly conducted. As a result, information about earthquake impacts can be documented as initial important observations. In the next stage and based on the collected information, the priorities and strategies for repairs and reconstruction can be established.

On February 6, 2023, a series of devasting earthquakes struck southeastern Turkey and the adjoining northern border areas of Syria. The East Anatolian fault zone, which extends further down to Syria, was responsible for the 2023 Turkey earthquake with Mw=7.8 moment magnitude. The earthquake was devastating as it involved the break in the fault that extended for 300 kilometers. The maximum Peak Ground Acceleration (PGA) was more than 0.11g. The PGA map prepared is given in Figure 1 [9].

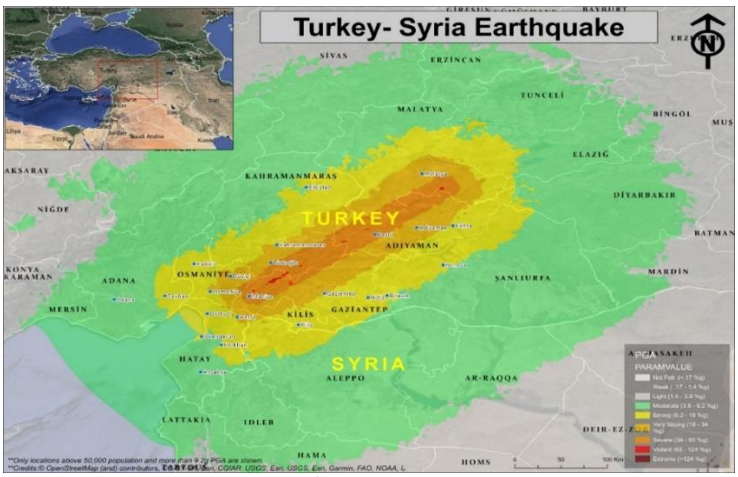

Figure 1. - **PGA map for Mw=7.8 Turkey Earthquake**

The safe return home and repopulation of earthquake-affected cities and towns was a priority for the affected families, local communities, and the Government of Turkey (GoT) [10]. Such approach had been undertaken by the authors in the previously effected areas previously by earthquakes (see for example [11], [12], [13], [14], and [15]) In order to provide rapid and sustainable emergency shelter solutions that accelerate the safe return of Internally Displaced Persons (IDPs) and enable the early recovery of affected communities, the authors led a six-month emergency Shelter and Settlements (S&S) Activity including providing building repairability assessments and guidelines on lightly damaged buildings, as well as public outreach, pedagogical awareness, and communications campaigns on non-damaged and repairable buildings. The scope of the effort consisted of i) conducting damage assessment based on the review of satellite imagery data [16] and ii) performing repairability assessment of light to moderately damaged buildings [17]. Both these topics are relevant to the countries of Central Asia given the simplicity of these areas and construction typologies for residential buildings. It further emphasizes the need for the development and implementation of a response protocol that can be rapidly activated after natural disasters using the available state-of-the-art technologies.

2. Remote Damage Assessment

There were pockets of significant destruction, like Hatay. This was due to the soil and the geographical effect of the earthquake. The NASA-JPL satellite damage assessment showed that about 20 to 30 percent of building stocks collapsed or were damaged. Table 1 presents a summary of the damage. The authors have utilized this technique in the aftermath of previous earthquakes [18].

Table 1

Damage Assessment Summary of Cities in Turkey

Province	Location Name	CITY_AREA	Damage Area	Damage %
Adana	Ceyhan	10.86	0.32	3%
Adiyaman	Adiyaman	23.05	4.05	18%
Adiyaman	Besni	3.5	1.32	38%
Adiyaman	Çelikhan	0.92	0.51	55%
Adiyaman	Gölbaşı	4.37	2.45	56%
Adiyaman	Kâhta	9.13	0.06	1%
Adiyaman	Samsat	1.7	0.02	1%
Adiyaman	Sincik	0.5	0.14	28%
Adiyaman	Tut	0.48	0.24	50%
Elazig	Baskil	0.84	0.23	27%
Gaziantep	Araban	1.51	0.04	3%
Gaziantep	Gazientep	119.31	4.76	4%
Gaziantep	İslahiye	4.68	1.91	41%
Gaziantep	Nizip	7.97	0.03	0%
Gaziantep	Nurdagi	3.33	1.78	53%
Gaziantep	Oğuzeli	2.19	0.02	1%
Gaziantep	Yavuzeli	0.92	0.02	2%
Hatay	Antakya	46	16.7	36%
Hatay	Dörtyol	6.12	0.18	3%
Hatay	Erzin	5.96	0.23	4%

Province	Location Name	CITY_AREA	Damage Area	Damage %
Hatay	Hassa	1.92	0.84	44%
Hatay	İskenderun	10.16	4.1	40%
Hatay	Kırıkhan	7.66	4.36	57%
Hatay	Kumlu	1.66	0.11	7%
Hatay	Payas	19.02	0.82	4%
Kahramanmaras	Andırın	1.43	0.52	36%
Kahramanmaras	Çağlayancerit	0.69	0.28	41%
Kahramanmaras	Ekinözü	1.25	0.84	67%
Kahramanmaras	Elbistan	13.91	7.88	57%
Kahramanmaras	Kahramanmaras	49.42	8.18	17%
Kahramanmaras	Nurhak	2.54	0.72	28%
Kahramanmaras	Pazarcik	2.89	1.64	57%
Kahramanmaras	Türkoğlu	3.47	1.04	30%
Killis	Elbeyli	0.31		0%
Killis	Kilis	13.27	0.64	5%
Killis	Musabeyli	0.54	0.04	7%
Killis	Polateli	0.13		0%
Maltaya	Akçadağ	1.76	0.48	27%
Maltaya	Arguvan	0.47		0%
Maltaya	Battalgazi	0.46	0.14	30%

An example of a damage chart developed based on satellite imagery is presented in Figure 2 [16]. Field assessment validated the accuracy of remote assessment. For example, in Kahramanmaras city, 197 of the 230 collapsed buildings were within the zone identified by satellite imagery [16].

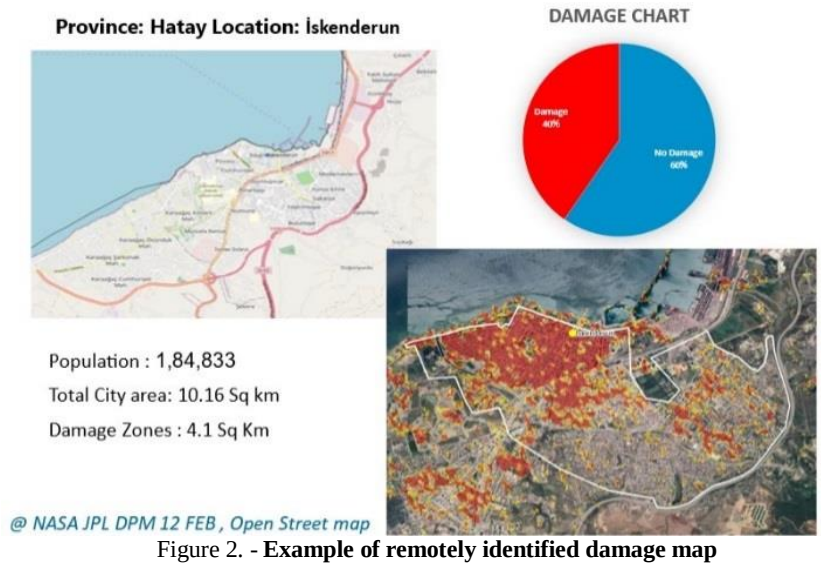

Figure 2. - **Example of remotely identified damage map**

3. Field Assessment

The current version of the Turkish seismic code has many provisions on par with the international best practice. However, buildings of earlier vintage and buildings designed per current code but which lacked proper seismic detailing due to inadequate construction inspection suffered damage. Contributing factors to the damage, in particular, to the reinforced concrete buildings, included the following: see Figure 3.

- Lack of confinement, such as the absence of 125-degree hooks
- Use of round aggregates
- Inadequate shear and axial capacity of columns
- Building irregularity including soft and weak stories
- Building irregularity, including column offset [19]

Poor confinement

Round aggregates

Column failure

Soft or weak story

Column offset

Figure 3. - **Examples of observed damage**

4. Reparability Assessment: Background

The repairs focused on slightly damaged buildings. 0 presents the repair matrix used in this project. Examples of observed damage are presented in Figure 4; Figure 5 presents examples of repairs.

Table 2

Damage and repair matrix

Type	Description of damage	Repair
P1	Minor cracks in structural members	Epoxy repair
P2	Minor spalling of concrete members	Repair with mortar
A3	Hollow block infill wall damage	Wire mesh and mortar
A4	Hollow block infill wall with window damage	Wire mesh and mortar; lintel
B3	Solid block infill wall damage	Wire mesh and mortar
B4	Solid block infill wall with window damage	Wire mesh and mortar; lintel
F1	Minor plaster damage, cracking (<3 mm)	Wire mesh and plaster
F2	Minor plaster damage, partition walls	Wire mesh and plaster
F3	Floor finish damage	Plaster
F4	Ceiling finish damage	Plaster

P1

A3/B3

F2

F4

Figure 4. - **Examples of observed damage**

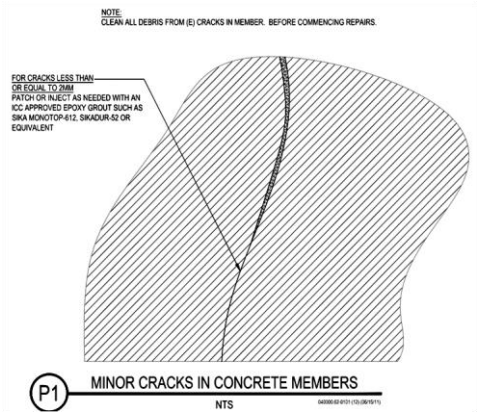

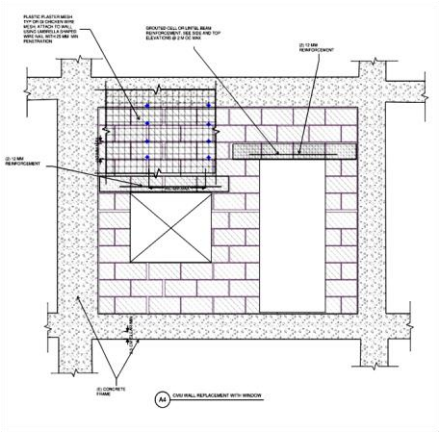

P1 A4/B4

Figure 5. - **Schematics of repairs**

A GIS-based data collection platform was developed [20]. The authors trained a group of local engineers in the use of digital data collection and storage and identifying the different types of damages, as listed in Table 1.

Because the data collection was based on gathering data for the building and the individual units in each building, two sets of data were collected, and a unique QR code was assigned to track the collected data. Examples of screenshots of data collection are presented in Figure 6.

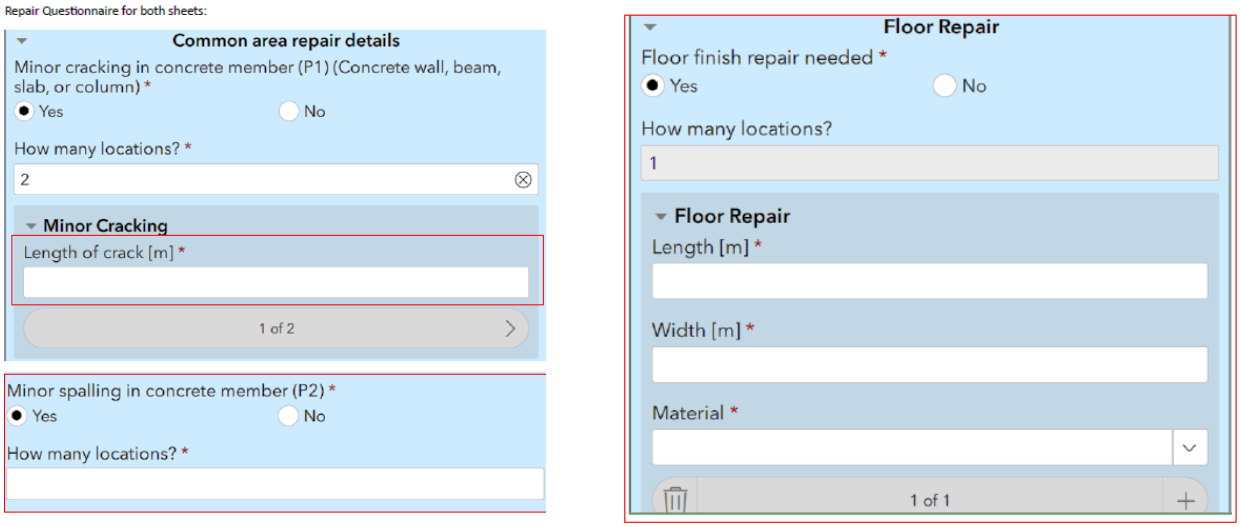

Figure 6. - **GIS-based Data collection template**

A repair logic was developed to allow estimating BoQ for each of the repair types listed in 0. Fifteen (15) quantity items were identified to cover all the possible repairs for the damage matrix. The quantities comprised:

Q01: No of epoxy tubes
Q02: No of bags of mortar
Q03: No. of bags of grout
Q04: Repair length in m
Q05: Cleaning length in m
Q06 Surface preparation area in m^2
Q07: Plaster area in m^2
Q08: Paint area in m^2
Q09: Mesh area in m^2
Q10 Repair area in m^2
Q11 No. of hollow blocks
Q12 No. of solid brick.
Q13 No of damaged block

Q14 No. of nail
Q15 Length of 12-mm reinforcement in m.

5. Reparability Assessment: Findings

The rapid assessment considered both buildings and units in buildings. The overall project consisted of six (6) pools of structures comprising approximately 15,500 surveys. The data was collected electronically using ArcGIS Survey 123 [20], and post-processed in Matlab [21]. Next, for each unit, a web-based folder was generated using Python [22] and data was stored on the server for individual assessment, which can be accessed by individual owners using the unique QR code assigned to their unit. Example data from a pool of units with a sample size of 1600 units is discussed in this section.

BoQ was developed for approximately 2500 units in multi-unit buildings. As seen in Figure 7, the distribution of the number of damages was more uniform for the units, although still most units had four or fewer recorded damages. Figure 8 presents the number of each type of damage as a percentage of all observed damages. As can be seen, similar to the common area damage, types F1 and F2 comprise nearly the entirety (9%) of all recorded damage types. 0 summarizes quantiles for the common unit damage. Note that paint followed by mesh, plaster, and nailing constitute the major repairs.

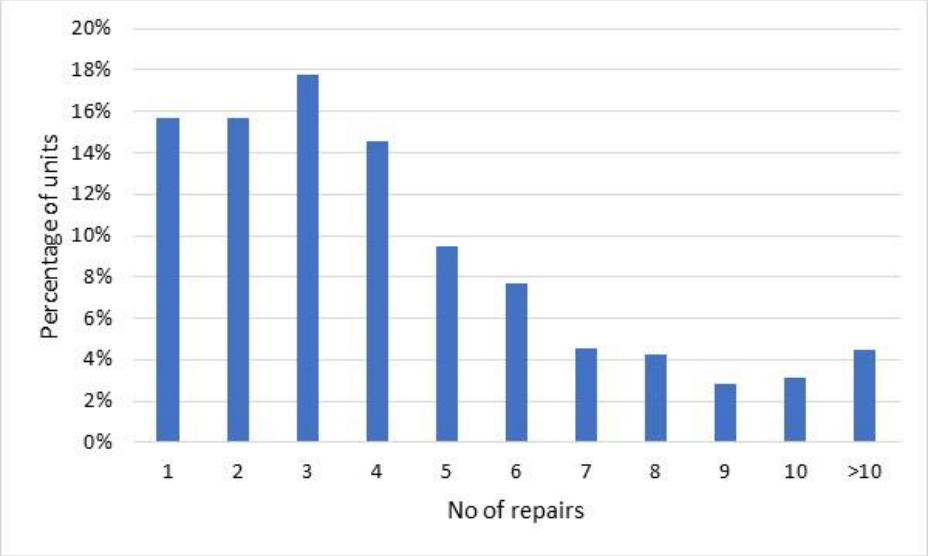

Figure 7. - **Distribution of occurrences of all damage**

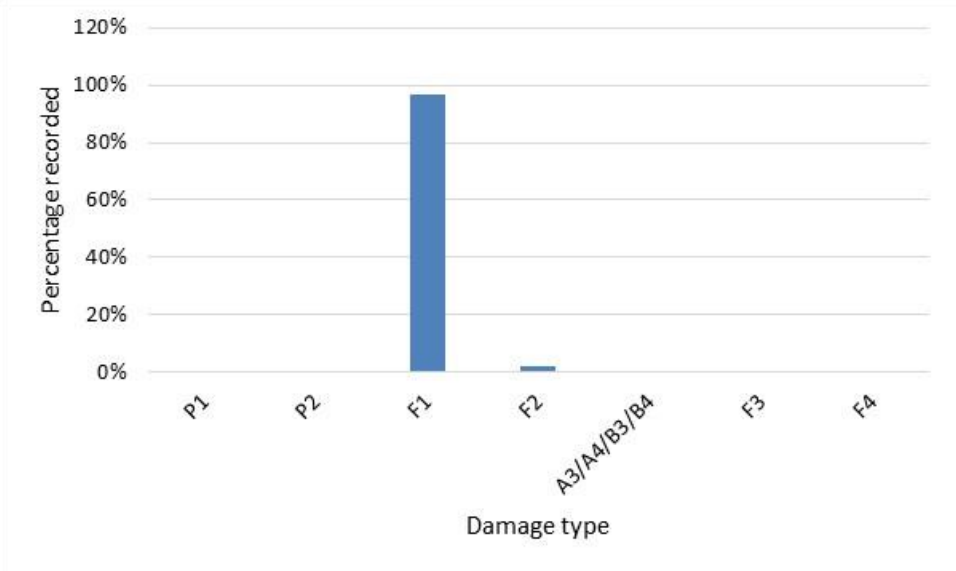

Figure 8. - **Distribution of types of damage**

Table 3

Computed quantities

Item names	Item description	Quantity
Q01	Epoxy tube (EA)	12
Q02	Mortar bags(EA)	664
Q03	Grout bags (EA)	116
Q04	Repair (m)	14
Q05	Clean (m)	14
Q06	Surface prep (m2)	2
Q07	Plaster area (m2)	12798
Q08	Paint area (m2)	115202
Q09	mesh area (m2)	12790
Q10	Repair area (m2)	379
Q11	Hollow blocks (EA)	4426
Q12	Solid brick (EA)	1898
Q13	Damaged block (EA)	8073
Q14	Nail (EA)	11257
Q15	Rebar (m)	64

6. Conclusions

The 2023 earthquake in Turkey resulted in a significant number of casualties, structural damage, and displaced citizens. On-field surveys were conducted, and results were compared with the remotely obtained damaged data. To supplement the structural damage assessment programs undertaken in the aftermath of the earthquake, a repair assessment for the buildings experiencing light (not structural) damage was undertaken with the goal of developing the BoQ for repairs to expedite repair, recovery, and re-occupancy of such buildings with the objective of reducing the IDP in the country. A GIS-based platform was developed to conduct surveys, record data, compute quantities, and provide secure access to the owners to download reports for individual residences. The findings presented here are applicable to the Central Asian countries, given the high seismicity of the region and building typologies. In particular, the following is recommended:

- Ensure the building code follows the international best practice for seismic design,
- Implement a construction quality management, including robust construction inspection,
- Develop a response protocol, including monitoring and damage and repair assessment programs.

7. Acknowledgements

The authors acknowledge the financial and technical support provided by USAID/BHA, HFH, and CRS. The efforts of the teams conducting the surveys and recording the data are acknowledged.

References

1. *Miyamoto, H.K., and Gilani, A.S. (2008).* Recent earthquakes in Indonesia and Japan: observed damage and retrofit solutions. Proceedings of the 14th World Conference on Earthquake Engineering, October 12-17, 2008, Beijing, China.

2. *Miyamoto, H.K., Gilani, A.S., and Wada, A.* (2008). Reconnaissance report of the 2008 Sichuan earthquake, damage survey of buildings and retrofit options. Proceedings of the 14th World Conference on Earthquake Engineering, October 12-17, 2008, Beijing, China.

3. *Miyamoto, H.K., Gilani, A.S., Wada, A.* (2011). Damage mitigation for school buildings in seismically vulnerable regions. International Journal of Disaster Resilience in the Built Environment. Vol. 2, No. 1, pp. 8-29. DOI 10.1108/17595901111108344.

4. *Yashinsky, M., Takhirov, S., Mosalam, K., Hutchinson, T. and Falko Kuester, F.* (2014). From a Distance: Inspection of Bridges in the aftermath of the South Napa Earthquake, Bridge Design & Engineering Magazine, issue 77, pp.52-54.
5. *Mosalam, K.M., Takhirov, S.M., and Park, S.* (2014). Applications of Laser Scanning to Structures in Laboratory Tests and Field Surveys. Journal of Structural Control and Health Monitoring, Volume 21, Issue 1, pages 115–134, January 2014.
6. *Engineering Research Institute (EERI) (2016).* Learning from Earthquakes (LFE) Program web page, available at https://www.eeri.org/projects/learning-from-earthquakes-lfe/.
7. *Hosseini, S., Barker, K., & Ramirez-Marquez, J. E. (2016).* A review of definitions and measures of system resilience. Reliability Engineering and System Safety, 145, 47–61. doi:10.1016/j.ress.2015.08.006.
8. *Tremayne, H., Mieler, Martinelli, M.D., Olshansky, R., Berger, J.* (2017). Development of a framework for resilience reconnaissance. 6th World Conference on Earthquake, 16WCEE 2017, Santiago Chile, January 9th to 13th, 2017.
9. Unites States Geological Survey (2023).
10. Ministry of Interior, Republic of Turkey (2023).
11. *Miyamoto, Sechi, Victor, St Come, Broughton, Gilani, and Singh* (2024) Haiti earthquake 2021: Findings from the repair and damage assessment of 179,800 buildings International Journal of Disaster Risk Reduction.
12. *Kast, Miyamoto, Meguro, and Gilani* (2024) Massive indigenous housing recovery platform in Afghanistan after the 2022 earthquake, World Conference on Earthquake Engineering.
13. *Saini, Miyamoto, Nifuku, das, and Gilani* (2024) Estimation of regional attenuation relationship and development of fragility curves in southern Haiti based on accelerometer observations, World Conference on Earthquake Engineering.
14. *Miyamoto, Gilani, and Wong* (2011) Massive Damage Assessment Program and Repair and Reconstruction Strategy in the Aftermath of the 2010 Haiti Earthquake. Earthquake Spectra.
15. *Miyamoto and Gilani* (2017) Damage assessment and seismic retrofit of traditional and modern midrise buildings in the aftermath of 2015 Nepal earthquake, World Conference on Earthquake Engineering.
16. NASA Jet Propulsion Laboratory (JPL) (2023).
17. Turkey National Shelter Cluster Power Update (2023), 18-Feb-2023.
18. *Selvakumaran, Rolland, Cullen, Davis, Macabuag, Chakra, Karageozian, Gilani, Geiß, Haro, Marinoni* (2024) Improving operational use of post-disaster damage assessment for Urban Search and Rescue by integrated graph-based multimodal remote sensing data analysis, Under review Journal: Progress in Disaster Science
19. *National Information Centre of Earthquake Engineering India* (NICEE) (2017). IITK-BMPTC Earthquake Tips.
20. *ArccGIS Survey 123 https://survey123.arcgis.com/*
21. *MathWorks. Matlab Version R2020a; 2020*
22. *Python https://www.python.org/*

APPLICABILITY OF THE HV METHOD IN SEISMIC MICROZONING

Ibragimov A.Kh.[1], Mamarozikov T.U.[1]
[1]*Institute of Seismology Academy of Sciences of Uzbekistan*
E-mail: timur.mamarozikov@yandex.com

Abstract:. *A comparison of HVSR and MASW methods for seismic microzoning is provided. Seismic intensity increment values are compared using two methods.*
Keywords*: HVSR, MASW, cross-section. velocity.*

1. Introduction

Recently, MASW and the Nakamura Method (HVSR) have been widely used in seismic microzoning surveys of urbanized areas [1,2,3,4]. Seismic surveys often have difficulty selecting locations (less and less soils not covered with asphalt and sidewalks) and insufficient length of non-asphalt areas for geophones. In this regard, the application of the HVSR (Nakamura) method using one three-component seismic station becomes relevant [5,6,7].

2. Methodology and Instrumentation

Both methods MASW and HVSR were used in Bukhara seismic microzoning [8]. According to MASW, velocity sections were obtained, from which the Vs30 was determined. Also, using the Dinver program as part of the Geopsy [9] system, the calculated HVSR spectra were converted into velocity sections, from which the Vs30 was also determined.

Microseism measurements were performed using three-component digital seismometers CMG-6TD with a Guralp EAM recorder, UK. The measurement duration was 30 minutes for each registration point [4,10,11,12,13,14]. The frequency response of the three-component seismometer is linear in the frequency range of 0.03-50 Hz. The bit size of the digitizing unit is -24 bits. Geopsy was used to process the data [15].

Figure 1. - **Broadband three-component CMG-6TD seismometer and EAM recorder**

The microseism processing results were obtained as a plot of the spectrum-frequency ratio and in tabular form (fig 2).

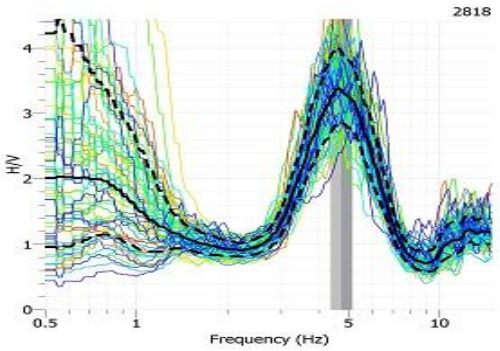

Figure 2. - **HVSR spectrum**

The HVSR spectrum data in tabular form were used in the construction of velocity sections (fig 3) [16, 17]:

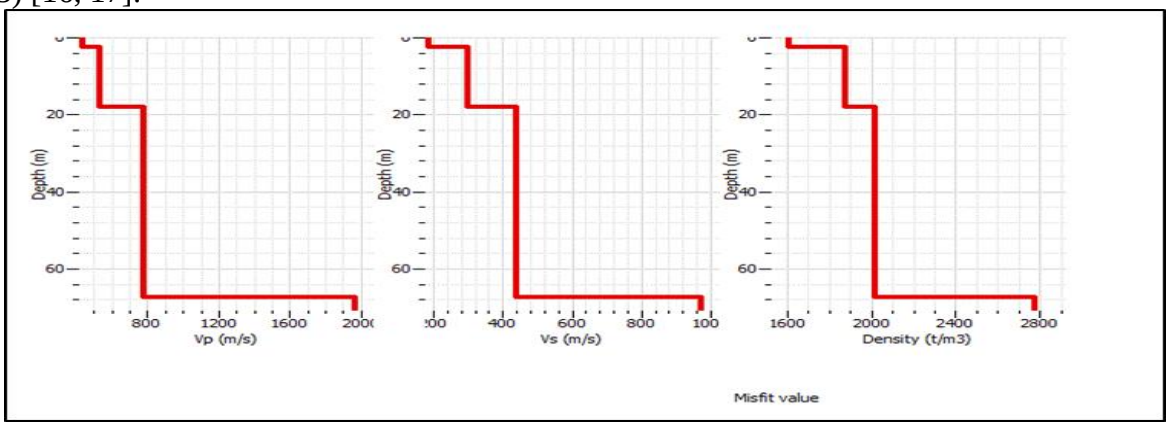

Figure 3. - **Distribution curves with depth Vp, Vs and density for the recording point**

The multi-channel analysis of surface waves (MASW) method is based on the recording and analysis of Rayleigh and Love waves. Rayleigh waves are surface waves moving along a free surface, such as a surface-to-air boundary. Long wave oscillations penetrate deeper, have a higher phase velocity and are more sensitive to the elastic properties of deep-lying layers, while short wave oscillations are more sensitive to near-surface layers, which leads to dispersion of the recorded seismic signal [18, 19, 20].

Geophysical MASW surveys were performed by the 24-channel MAE X820S seismic survey station with 2 m geophone spacing. For registration, 4.5 Hz vertical seismic sensors were used. Excitation and reception were carried out according to the Z-Z scheme, a flank observation system with a maximum and minimum distance from the receiving line of 48 and 2 m, respectively. The accumulation of the signal was selected depending on the distance of the source from the receiving line, as well as the selection of the optimal quality of recording seismic traces taking into account the ratio of the useful signal to external noise at long-distance and ranged from 5 to 10 blows with a sledgehammer weighing 8 kg.

Dispersion analysis is performed by two-dimensional F-K transformation of the recorded seismic signal in the frequency range of propagation of surface waves. This analysis allows us to obtain a dispersion curve - the dependence of phase velocity on frequency.

As a result of the analysis of the obtained seismograms, a dispersion region was built and a dispersion curve of the fundamental mode of Rayleigh wave oscillations was identified (fig 4).

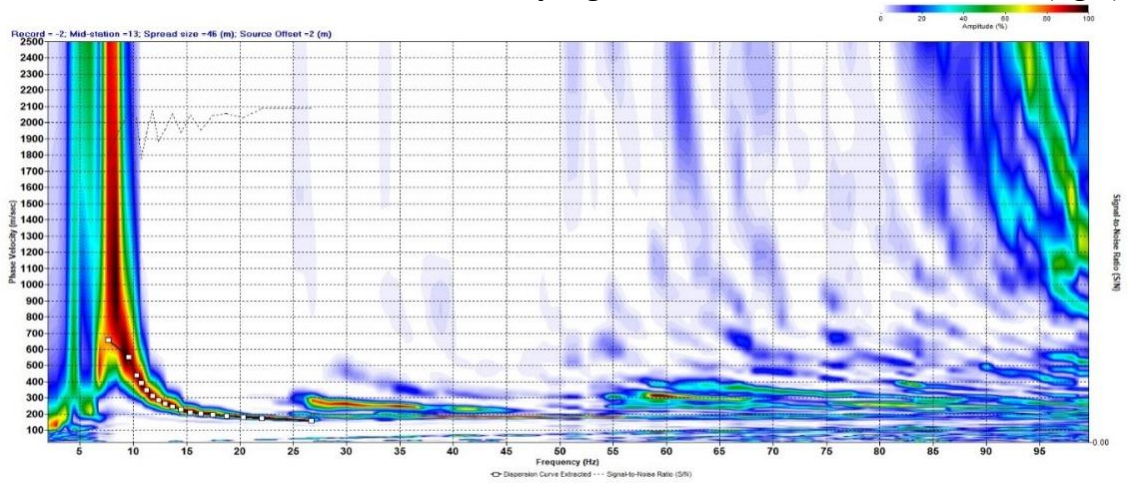

Figure 4. - **Dispersion image with isolated dispersion curve of the fundamental mode of Rayleigh wave oscillations**

According to the obtained dispersion curve, the maximum Rayleigh wavelength is 78 m, which makes it possible to determine that the maximum depth of the studies will be 39 m. As a result of the inversion of the dispersion curve, a profile Vs (z) up to 37.5 m deep was obtained (fig.5)

Figure 5. - **Vs (z) profile by MASW**

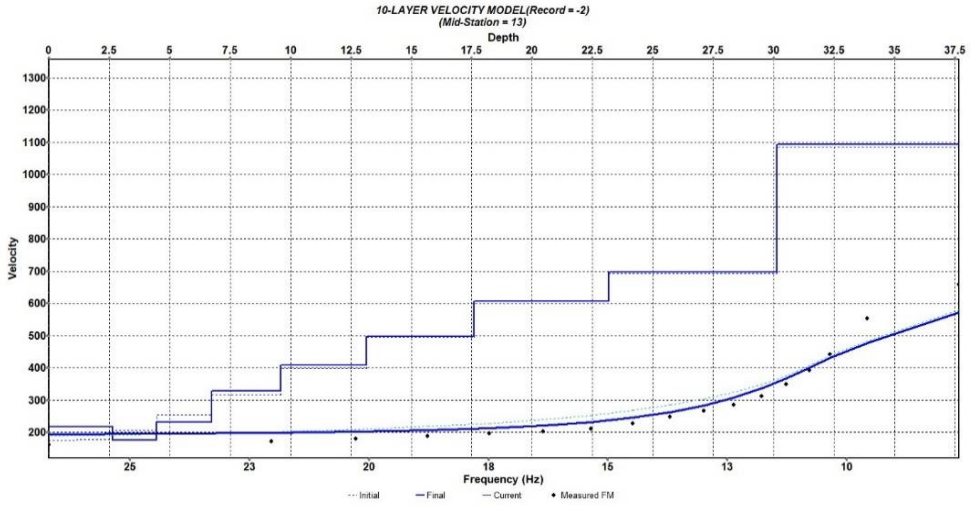

It can be noted on the profile that to a depth of 7 m, there are bulk soils, sandy loams with a shear wave propagation rate of 220 m/s, then along the profile, there is a gradient increase in speed up to 700 m/s, which is associated with sand differences and underlain by pebbles with a speed of Vs - 1100 m/s.

3. Results

Obtained results of shear wave velocity by both methods were used to calculate the Vs30 parameter (table 1), which is used to determine elastic properties of upper soil structure, that gives the most increment of seismic intensity [21].

As can be seen, results obtained by both methods are close with a maximum difference of about 30 m/s. To understand how this difference affects seismic intensity increment, it was calculated by

$$\Delta I = 1{,}67 \lg(\rho_{et}\upsilon_{et}/(\rho_t\upsilon_t)$$

where υ_{et} and υ_t are weighted average values of propagation rates of longitudinal or shear waves for the calculated soil thickness at the reference and investigated area; ρ_{et} and ρ_t - weighted average values of soil densities for the design thickness at the reference and investigated area

The difference in seismic intensity increment calculated by both methods does not exceed 0.073 which is not affected by the resulting seismic intensity.

Cross-plot of data (fig. 6) shows the relationship of data. The relationship between MASW Vs30 and HVSR Vs30 is given by:

Vs30 (MASW) = 1.5368*Vs30 (HVSR) -198.56

Table 1.

Results of MASW and HVSR Vs30 calculation

Vs30 from MASW	Vs30 from HVSR	Difference, m/s	the difference in intensity increment
380,98	356,29	-24,69	-0.048
377,81	408,16	30,35	0.056
329,05	327,80	-1,25	-0.002
345,32	353,60	8,28	0.017
397,09	397,80	0,71	0.001
350,22	328,59	-21,64	-0.046
373,51	350,00	-23,51	-0.047
362,38	340,91	-21,47	-0.044
361,50	328,95	-32,56	-0.068
373,03	402,14	29,11	0.054
361,98	344,43	-17,55	-0.036
379,21	413,22	34,01	0.062
317,06	292,40	-24,66	-0.058
356,60	322,23	-34,36	-0.073
358,79	347,22	-11,57	-0.023
378,46	417,83	39,37	0.071
329,16	301,51	-27,66	-0.063
340,99	346,02	5,03	0.010
380,05	382,17	2,12	0.004
404,69	436,55	31,86	0.054
362,39	327,51	-34,88	-0.073
376,51	395,78	19,27	0.036

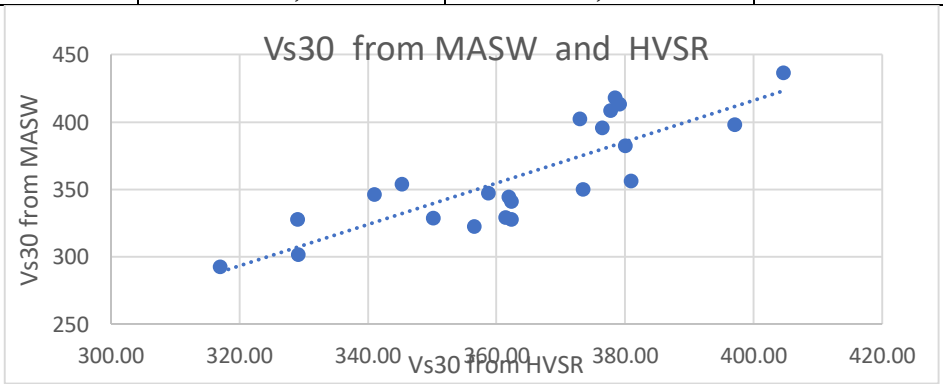

Figure 6. - **Association of MASW and HVSR Vs30**

4. Discussion

As can be seen from Table 1 the maximum difference in the Vs30 value does not exceed 34.88 m/s, which gives a difference in the increase in the intensity of seismic impacts of 0.073 points.

This gives reason to conclude that the Nakamura method is applicable to solving seismic microzoning problems and allows for investigating the elastic properties of soil strata.

This work was funded by grants from the Academy of Sciences of the Republic of Uzbekistan, "Development of scientific foundations for assessing various levels of seismic risk and reducing earthquake losses in seismically active areas" and the Agency for Innovation Development, #ALM202311142839 "Creation of a simulation digital model of the city of Tashkent allowing to assess the level of economic damage from strong earthquakes"

References

1. *Nogoshi, M. and Igarashi, T.* (1971). On the amplitude characteristics of microtremor (Part 2), J. Seismol. Soc. JPN, 24, 26–40.
2. *Nakamura, Y.* (1989) A method for dynamic characteristics estimation of subsurface using microtremor on the ground surface, Quarterly report of Railway Technical Res. Inst. (RTRI), 30, 25–33.
3. *Lunedei, E., & Malishewsky, P.(*2015).A Review and some new issues on the theory of the H/V technique for ambient vibrations. In: A. Ansal (Ed.), Perspectives on European Earthquake Engineering and Seismology, Geotechnical and Earthquake Engineering(Vol. 39, pp. 371—394).Springer, Cham.
4. *D'Amico,V.; Picozzi, M.; Baliva, F.; Albarello, D.* (2008). Ambient noise measurements for preliminary site-effects characterization in the urban area of Florence, Italy. Bull. Seismol. Soc. Am., 98, 1373–1388.
5. *Yutaka Nakamura.* (2019) What Is the Nakamura Method? Seismological Research Letters 90 (4): 1437–1443.
6. *Hiroshi Kawase at al.* (2019) Direct evaluation of S-wave amplification factors from microtremor H/V ratios: Double empirical corrections to "Nakamura" method. Soil Dynamics and Earthquake Engineering. 126 105067. P.p.1-14
7. *S. Molnar at al.* (2022) A review of the microtremor horizontal-to-vertical spectral ratio (MHVSR) method. https://doi.org/10.1007/s10950-021-10062-9 J Seismol (2022) 26:653–685
8. *Rakhmatov A.R., Mamarozikov T.U., Yadigarov E.M., Ibragimov A.Kh.* Integration of methods for determining Vs30 // materials of the international scientific conference "Current problems of ensuring seismic safety of the population and territories", Tashkent, Uzbekistan. pp. 240-245. (in Russian).
9. *Wathelet, M., Chatelain, J.-L., Cornou, C., Di Giulio, G., Guillier, B., Ohrnberger, M. and Savvaidis, A. (*2020). Geopsy: A User-Friendly Open-Source Tool Set for Ambient Vibration Processing. Seismological Research Letters, 91(3), 1878--1889, doi: 10.1785/0220190360.
10. *Sylvette Bonnefoy-Claudet, Fabrice Cotton, Pierre-Yves Bard.* (2006). The nature of noise wavefield and its applications for site effects studies: A literature review. Earth Sci. Rev. 79, 205–227.
11. *Arai, H., Tokimatsu, K.*. (1998). Evaluation of local site effects based on microtremor H/V spectra. Proceeding of the Second International Symposium on the Effects of Surface Geology on Seismic Motion. Yokohama, Japan, pp. 673–680.
12. *Bour, M., Fouissac, D., Dominique, P., Martin, C.* (1998). On the use of microtremor recordings in seismic microzonation. Soil Dynamics and Earthquake Engineering 17 (7–8), 465–474.
13. *Duval, A.-M., Vidal, S., Méneroud, J.-P., Singer, A., De Santis, F., Ramos, C., Romero, G., Rodriguez, R., Pernia, A., Reyes, N., Griman, C.,* (2001). Caracas, Venezuela, site effect determination with microtremor. Pure and Applied Geophysics 158 (12), 2513–2523.
14. *Maresca, R., Castellano, M., De Matteis, R., Saccorotti, G., Vaccariello, P.,* (2003). Local site effects in the town of Benevento (Italy) from noise measurements. Pure and Applied Geophysics 160 (9), 1745–1764
15. *Kuvvet ATAKAN at al.* (2004) The h/v spectral ratio technique: experimental conditions, data processing and empirical reliability assessment. 13th World Conference on Earthquake Engineering. Vancouver, B.C., Canada August 1-6, 2004. Paper No. 2268
16. *Roberts, J.C., Asten, M.W., (*2005). Estimating the shear velocity profile of quaternary silts using microtremor array (SPAC) measurements. Exploration Geophysics 36, 34–40.
17. *Lontsi AM, Sánchez-Sesma FJ, Molina-Villegas JC, Ohrnberger M, Krüger F.* (2015) Full microtremor H/V(z,f) inversion for shallow subsurface characterization. Geophys J Int 2015;202:298–312. http://dx.doi.org/10.1093/gji/ggv132.
18. *Ivanov, J., C. D. Johnson, J. W. Lane, R. D. Miller, and D. Clemens,*(2009) Near-surface evaluation of Ball Mountain Dam, Vermont, using multi-channel analysis of surface waves (MASW) and refraction tomography seismic methods on land-streamer data: 79th Annual International Meeting, SEG, Technical Program Expanded Abstracts, 28, 1454-1458.
19. *Mahvelati, Siavash & Coe, Joseph.* (2017). The Use of Two-Dimensional (2D) Multichannel Analysis of Surface Waves (MASW) Testing to Evaluate the Geometry of an Unknown Bridge Foundation. 10.1061/9780784480441.069.

20. *F. Rehman et al*. (2018) MASW Survey with Fixed Receiver Geometry and CMP Cross-Correlation Technique for Data Processing: A Case Study of Wadi Fatima, Western Saudi Arabia// Open Journal of Geology. – 2018. – V. 8. – №. . – P. 463-473.
21. *Medvedev, S.V.(*1962). Engineering seismology. M.: Stroyizdat,. 284 p. (in Russian).

SEISMIC HAZARD OF THE FERGANA VALLEY TERRITORY

Ibragimov R.S.[1], Ibragimova T.L.[1], Mirzaev M.A.[1], Ashurov S.Kh.[1]
[1]Institute of Seismology named after. G. Mavlyanov, Tashkent, Uzbekistan
E.mail: ibrroma@yandex.ru

Abstract. *The territory of Fergana Valley is characterized by complex tectonic structure and high level of seismic activity. Many earthquakes with magnitude M≥6.5 and intensity of shaking in the epicenter I0=8-9 MSK-64 have occurred here during the historical and instrumental period of observations. Probabilistic analysis of Fergana Valley and its mountainous frame seismic hazard was carried out. Quasi-homogeneous seismological provinces, active crustal faults and seismogenic zones were considered as models of seismic sources. Parameterization of seismic source models was carried out, including determination of seismic potential, parameters of different magnitudes earthquake recurrence, predominant kinematic type of motion in the earthquakes sources. In assessing seismic hazard in terms of macroseismic intensity, five different dependencies obtained for the Central Asian region were used as attenuation laws. The weights to the attenuation dependencies were selected on the basis of the ranking procedure based on the degree of their applicability to the study area. The equations of ground motion for shallow active crust embedded in the CRISIS software package, with the help of which the hazard calculations were performed, were used in the hazard assessment in the engineering parameters of seismic vibrations. Epistemic uncertainties in seismic process parameters and seismic effects were taken into account by constructing a logic tree. For different probabilities P (P=0.90, P=0.95, P=0.98 and P=0.99) of not exceeding the level of seismic impacts within 50 years, maps of detailed seismic zoning of the Fergana Valley have been developed, expressing seismic hazard in points of the macroseismic scale and in values of Peak Ground Acceleration. Hazard curves are given for a number of large cities.*

Keywords*: seismic hazard, active faults, seismic potential, seismic activity, macroseismic intensity, Peak Ground Acceleration, hazard curve, seismic zonation*

1. Introduction

In Uzbekistan, the Andijan, Namangan and Fergana provinces are located in the Fergana Valley, where more than 10 million people live. Here, in addition to residential buildings, a large number of agricultural and industrial enterprises, fuel and energy complex facilities are concentrated, and intensive development of underground minerals is underway.

By its structural position, the mountain frame of the Fergana depression belongs to the orogenic structures of the Western Tien Shan. From the south, the depression is bounded by the Alay, Turkestan and Zeravshan ranges, extending in latitudinal direction. To the northeast of the Fergana depression are the Fergana and Talas ranges, extending from northwest to southeast. The Chatkal and Kuramin ranges extend to the north of the Fergana depression. The main tectonic disturbances associated with shaking in the territory of the Fergana Valley are the South Fergana fault system near latitudinal strike and the same-name flexural-fracture zone of northeastern strike, the system of near meridional Kurshab and Taldysu faults located in the southeastern part of the study area, the North Fergana fault system and the same-name flexural-fracture zone of northeastern strike located in the western part of the study area. Quite perceptible shaking in the Fergana Valley causes earthquakes occurring within the Chatkal-Atoynak and Talaso-Fergana faults. The areas of active dynamic influence of the above mentioned faults were identified by R.N.Ibragimov [1] as the corresponding seismic generating zones. During the historical and instrumental period of observations within these zones many strong earthquakes have occurred, some of which had magnitude M≥6.5 and intensity of shaking in the epicenter I_0=8-9 MSK-64 (Fig.1). These earthquakes killed thousands of people and caused huge damage to the economy of the country. Therefore, the problem of seismic safety for this territory is very urgent.

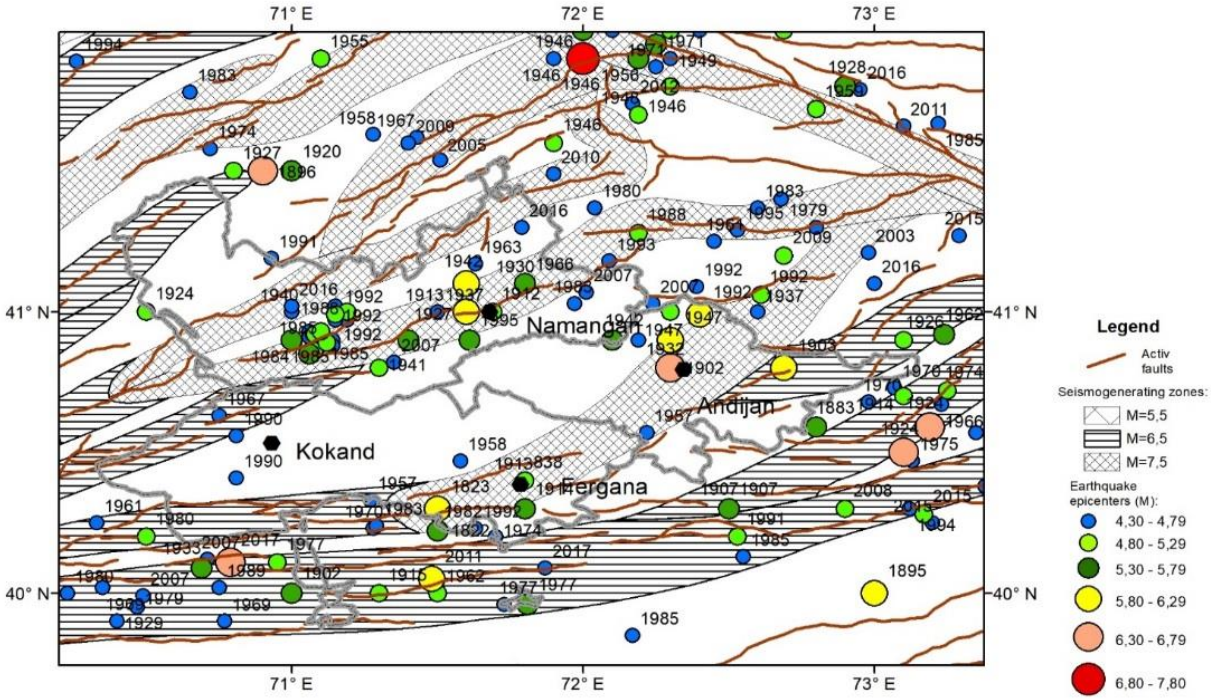

Figure 1. - **Map of the epicenters of noticeable and strong earthquakes in the study area for the historical and instrumental observation period, indicating active faults of the earth's crust according to [10] and seismogenic zones according to [1]**

Many studies have been devoted to various aspects of the problem of assessing the seismic hazard of the study area [1-5, etc.]. In [1-3], hazard assessments of Eastern Uzbekistan were obtained within the framework of deterministic and probabilistic-deterministic approaches [6], without taking into account epistemic and aleatory uncertainties in the parameters of the seismic process and seismic impacts. It is shown in [7] that this can lead to a significant underestimation of the study area seismic hazard. In [4, 5], seismic zonation was carried out using the classical probabilistic approach [8, 9], however, given that the seismic hazard in these studies was assessed for the entire Central Asian region, the areal detail of these constructions is not high enough. In this study, assessments of the seismic hazard of the Fergana Valley territory and its mountainous surroundings were obtained within the framework of a probabilistic approach and with a high degree of detail.

2. Data and analysis methods used

Probabilistic seismic hazard analysis (PSHA) is an analytical method in which the probability of exceeding each fixed level of seismic impacts within a certain period of time is estimated for a location under study. The implementation of PSHA involves the construction of two interconnected models - a model of seismic sources surrounding the studied point, and a seismic effect model that predicts the magnitude of the seismic impact at the studied point from each seismic event occurring within the seismic sources.

To calculate seismic hazard of the territory of the Fergana depression and its mountainous frame, seismic sources of three types were considered: active crustal faults, seismogenic zones representing buffer zones of active faults, and area sources of earthquakes - quasi homogeneous seismological provinces. The set of models reflects two major components of the seismic process - scattered (background) seismicity, which is manifested within area formations (blocks, microplates) and seismicity concentrated within linear structures (active crustal faults, seismogenic zones), to which, as a rule, the strongest earthquakes are confined. Parameterization of seismic source models, along with determination of geometric characteristics of each source in plan and depth, includes estimation of its seismic potential, parameters of earthquake recurrence of different magnitudes and predominant kinematic type of motions in earthquake sources.

3. Source model in the form of active crustal faults

The Active Fault Database of Eurasia (AFEAD) [10] was used to assess the seismic hazard of the study area; for each fault there is information about its morphology and kinematics with quantitative indicators of Late Quaternary displacements. The faults present in the database are differentiated into 4 classes (A, B, C, D) according to the degree of severity (reliability) of manifestation of modern geodynamic activity - attribute CONF.

To estimate the seismic potential of active faults, relationships based on the correlation of the M_{max} value with the geometric characteristics of the tectonic disturbance (fault length L, the length of the maximum possible surface rupture on a given fault l, the rupture width W corresponding to this length, and the area of the maximum surface rupture A= l*W) are usually used. In this study, the estimated value of M_{max} for each active crustal fault was found by averaging with equal weights the estimates of seismic potential from five different relationships obtained in [11-14], in which the value of M_{max} is expressed through the length and area of the rupture. It was assumed that the width of the rupture is half of its length W= l /2. It should be said that the length of the rupture l, which can be formed in the event of an earthquake with maximum magnitude M_{max}, is only a certain percentage of the entire length of the fault L. In our study, the ratio l/L was assumed to be the same as in [15].

When estimating the average annual recurrence of earthquakes of different magnitudes N(M) in the model of active faults, in addition to the geometric characteristics of faults, data on displacement rates (slip rate parameter) are used. We obtained estimates of the N(M) values by averaging over four different relations obtained in [16, 17]. The relationships given in these studies differ from each other by the nature of seismic moment release. Based on the results of analyzing the database of active crustal faults, we considered three different models of seismic sources in the form of active faults, taking into account the confidence classes of their manifestation of modern geodynamic activity (CONF attribute in the AFEAD database). In the first variant, faults with confidence classes A and B were considered. In the second variant, faults of classes A, B and C were considered. Finally, the third option considered faults with confidence classes A, B, C, and D. Figure 2 shows for example the configuration of the active fault model for the third variant. The values of seismic potential M_{max} (in the numerator) and the average annual frequency of earthquakes with magnitude $M \geq 5.0$ (in the denominator) are given in the form of a simple fraction in the same figure. The parameter b - angular coefficient of the earthquake recurrence plot was taken equal to one in each of the three considered fault models, which is close to its regional value.

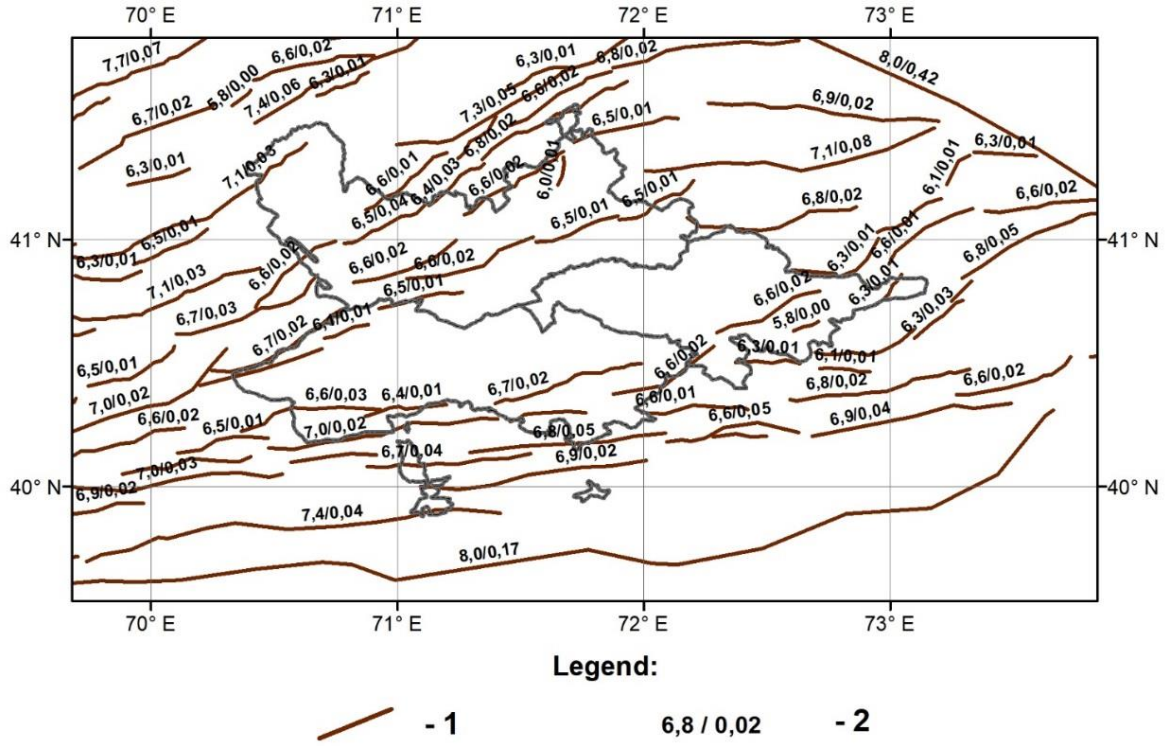

Figure 2. - **Model of seismic sources in the form of active faults of the Earth's crust with confidence class of manifestation of modern geodynamic activity A+B+C+D: 1) geometry of the fault; 2) seismic potential (in the numerator) and seismic activity of the fault, reduced to magnitude M=5.0 (in the denominator)**

Seismological parameterization of area's models sources and seismogenic zones was carried out by the regional earthquake catalog, which includes information on historical and instrumental seismic events. Information about the periods of representativeness of earthquakes of different magnitude levels in the regional catalog, the methods used for its declustering, and the equations of relationship between different types of magnitudes used in PSHA can be found in [2, 7].

4. Source model in the form of seismogenic zones

A seismogenic zone is an area of active dynamic influence of a large fault or a system of closely located and equally directed crustal ruptures, which generate strong earthquakes at the stage of tectonic activation of a region [1]. In plan, seismogenic zones are an overlapping along the strike of a set of pleistoseist areas of strong earthquakes that have occurred and are expected to occur in the future. The contours of seismogenic zones are defined taking into account the spatial position of active faults. Geometric and morphological features of tectonic faults, as well as the age of their emplacement are taken into account. The geometric configuration of the model of seismogenic zones is borrowed from [1]. On the basis of seismotectonic and seismological data in [1], about 10 seismogenic zones with seismic potential Mmax ≥ 6.5 were identified in the studied area.

Estimates of the maximum possible earthquake of seismogenic zones were obtained on the basis of seismological and seismotectonic methods of determining the value of M_{max}, described in detail in [1, 2]. The seismic hazard was calculated at the highest value of M_{max} in the seismogenic zone when it was determined by seismological and seismotectonic methods. For seismic sources located outside seismogenic zones, the value of seismic potential was obtained by adding half a magnitude unit to the magnitude of the maximum observed earthquake in this source. The determination of recurrence parameters for the model of sources in the form of seismogenic zones was carried out as follows. For sources that had a sufficient number of seismic events to reliably construct a recurrence plot, the seismic activity attributed to magnitude M=4.0 and the straight line angular coefficient (parameter b) were taken directly from the plot. For seismic generating zones with a small number of seismic events, a regional value of the b parameter was taken, and seismic activity at a given value of the slope angle of the recurrence plot was calculated from a sample of earthquakes falling directly

within the seismic source. Traditional methods of distribution and summation of seismic activity determination were used. The values of seismic potential and earthquake recurrence parameters for each seismic source in the model of seismogenic zones are shown in Figure 3.

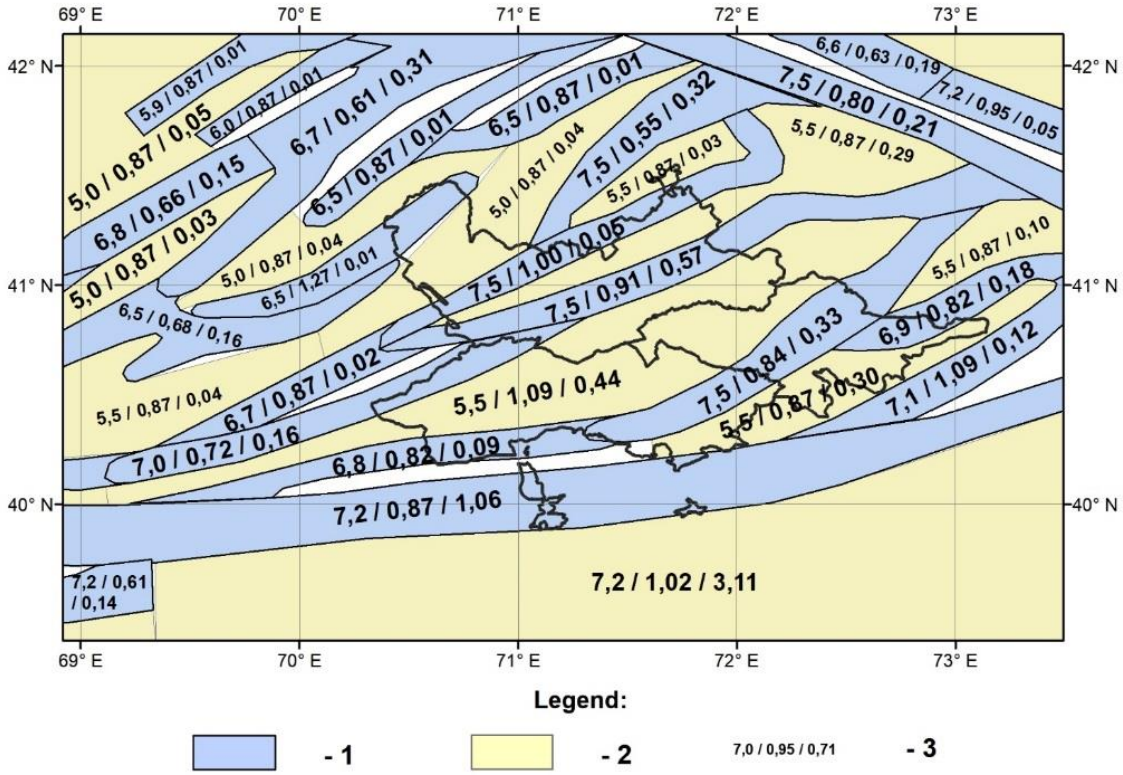

Figure 3. **- Model of seismic sources in the form of seismogenic zones for the study area: 1 - seismogenic zones; 2 - sources located outside the seismogenic zones; 3 - estimates of seismic potential M_{max}, parameter b and seismic activity reduced to magnitude M=4.0.**

5. Area source model.

The contours of the area source model were formed during the development of maps of general seismic zoning of the territory of Uzbekistan OSR-2017 [2]. In general, this model quite clearly reflects the block structure of the Earth's crust. In Eastern Uzbekistan, three megazones were identified: Pritashkent; Talaso-Fergana; Fergana depression and its mountainous frame. In turn, the megazones themselves were also divided into subzones - areas with different seismic activity. In order to adequately assess the seismic hazard of the border areas, we included additional area zones located partially or completely on the territory of neighboring states.

The value obtained by adding 0.3-0.5M magnitude units to the magnitude of the maximum observed earthquake in this source was used as an estimate of the seismic potential of area sources. The rule for finding the recurrence parameters for the area source model was the same as for the seismogenic zone model. The configuration of the area source model with their seismic potential and recurrence parameters is shown in Figure 4.

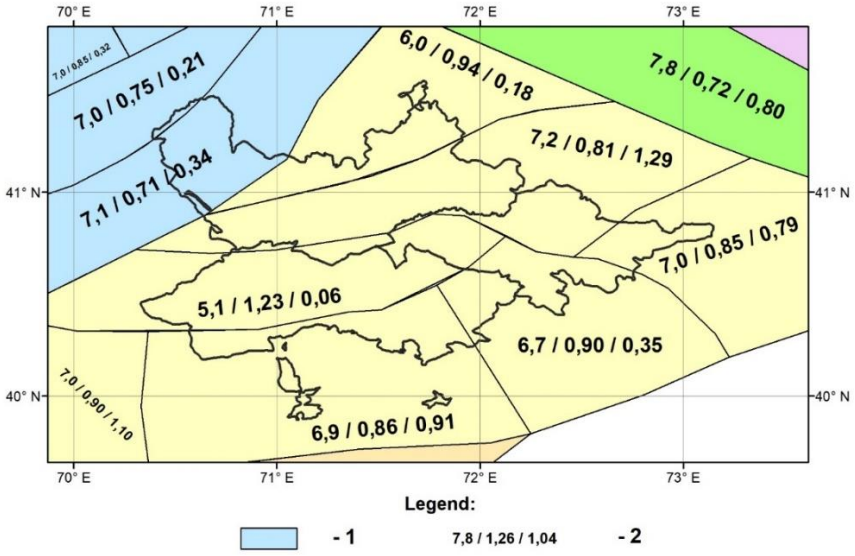

Figure 4. - **Model of area sources: 1 - source contours; 2 - estimates of seismic potential Mmax, parameter b and seismic activity reduced to magnitude M=4.0**

According to the studies conducted in [18, 19], the predominant kinematic type of motion in earthquake sources in the study area is heave. Therefore, it is this type that we used in the predicted ground motion equations (GMPE).

6. Attenuation of seismic intensity with distance

To assess the seismic hazard of the Fergana depression territory and its mountainous surroundings in terms of macroseismic intensity, several equations of attenuation of seismic intensity with distance were selected. Along with the dependence of N.V. Shebalin [20], obtained from the world data:

$$I = 1.5M - 3.5\lg R + 3 \tag{1}$$

three author's dependences established on the basis of the analysis of isoseist patterns of strong earthquakes that occurred in the territory of Central Asia [21] were considered:

- Blake-Shebalin type dependence:

$$I = 1.32M - 3.01 \cdot \lg R + 3.55, \qquad \sigma = 0.7 \tag{2}$$

- Kovesligethy type dependency:

$$I = 1.33M - 2.37 \cdot \lg R - 0.00205R + 2.24 \tag{3}$$

- dependence, in which the attenuation coefficient depends on the depth of earthquake origin [21]:

$$I = 1.475M - 2.646\lg H + 1.905 - 0.498M \lg\left(\frac{R}{H}\right) + 1.159\lg H \lg\left(\frac{R}{H}\right) - 1.401\lg\left(\frac{R}{H}\right), \tag{4}$$

$$\sigma = 0.6$$

The dependence D.Bindi[22] obtained somewhat earlier for the same seismically active region was also involved in the analysis:

$$I = 0.898M + 1.215 - 1.809\lg\left(\frac{R}{H}\right) - 0.0034(R - H), \qquad \sigma = 0.73 \tag{5}$$

In all the above attenuation dependences related to the macroseismic intensity, the hypocentral distance Rhyp is used as the distance R, and the magnitude M is used as magnitude MS.

We ranked the above mentioned attenuation models by two different methods - LH [23] and LLH [24]. The result of ranking the models by the LH method is to assign it to one of the four classes A, B, C and D as its fit to the real data deteriorates. The LLH method allows to give weights to each of the considered attenuation models. The results of the attenuation models (1) - (5) ranking are summarized in Table 1.

Table 1.

Ranking results of different attenuation models by LH and LLH methods

	Dependency number				
	1	2	3	4	5
Dependency class according to the criterion LH	A	B	A	A	D
Weights to dependencies by criterion LLH	0.200	0.200	0.213	0.221	0.166

7. Predicted ground motion equations

The strong motion network, including about 20 stations, has been operating in the territory of Uzbekistan since 2018. At the same time, the data accumulated to date are insufficient to construct regional attenuation laws with distance values of Peak Ground Accelerations and their spectral amplitudes. Therefore, at this stage of the study, the ground motion equations (GMPE) embedded in the CRISIS software package [25] were used as attenuation laws when assessing the seismic hazard of the study area in the engineering indicators of seismic effects. When selecting the ground motion equations for each seismic source, we relied on studies [26], in which the Earth's crust is typified on the basis of geological, geophysical and seismological data. According to these studies, there are mainly two types of crust on the territory of Uzbekistan. Shallow active crust, which is distributed in the eastern and central part of the study area, and stable shallow crust of non-cratonic type, which is located in the west, within the Turan Platform. Dependences [27-29] were used with equal weights for the shallow active crust to which the study area belongs.

Seismic hazard calculations were performed using the CRISIS software package. The grid spacing for the calculation was 0.1^0x0.1^0.

Epistemic uncertainties in the selection of seismic sources were taken into account by constructing a logic tree. The following weights (w) were assigned to each of the considered models:

- model of area sources - w=1/3;
- model of seismogenic zones - w=1/3;
- model of active faults with confidence class A and B- w=1/12;
- model of active faults with confidence classes A, B and C - w=1/6;
- active fault model with confidence class A, B, C and D- w=1/12.

Thus, the total weight of models of active faults of the Earth's crust with different confidence groups was w=1/3, i.e. was the same as for models of area sources and seismogenic zones. At the same time, the models of active faults with confidence classes A, B, and C, as moderately conservative, were given more weight than the other two.

8. Research results

Fig 5 and 6 show seismic zoning maps of Fergana Valley and its mountainous frame territory in points of the macroseismic scale and in values of Peak Ground Accelerations (PGA, g). Constructions are made for probabilities P=0.90, P=0.95, P=0.98 and P=0.99 of not exceeding the level of seismic impacts within 50 years. Since the laws of attenuation of seismic intensity with distance are developed for average ground conditions, which for the territory of Uzbekistan are soils of II category on seismic properties, then the above maps refer exactly to this ground category. Maps of the studied territory seismic hazard in values of Peak Ground Accelerations were constructed for each of the three categories of soil, spread on the studied territory. Differentiation of ground conditions was carried out through the VS30 parameter, which characterizes the velocity of transverse seismic waves in the upper 30 m of the ground stratum. In Figure 6, for example, these maps, as well as maps in the values of macroseismic intensity, are given for soils of II category of seismic properties (V_{S30}=450 m/s).

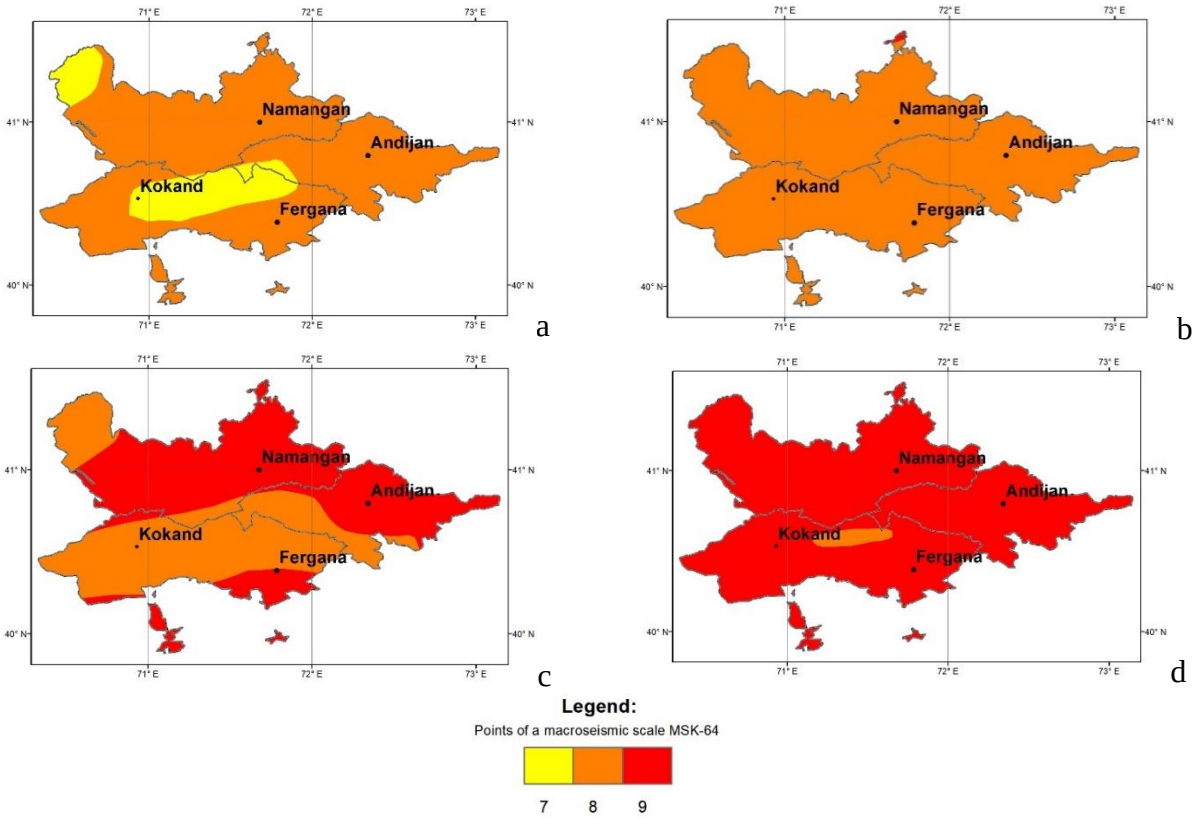

Figure. 5 - **Maps of the Fergana Valley seismic zoning in points of the macroseismic scale MSK -64 for various probabilities of not exceeding the level of seismic impacts within 50 years: a) P=0.90; b) P=0.95; c) P=0.98; d) P=0.99**

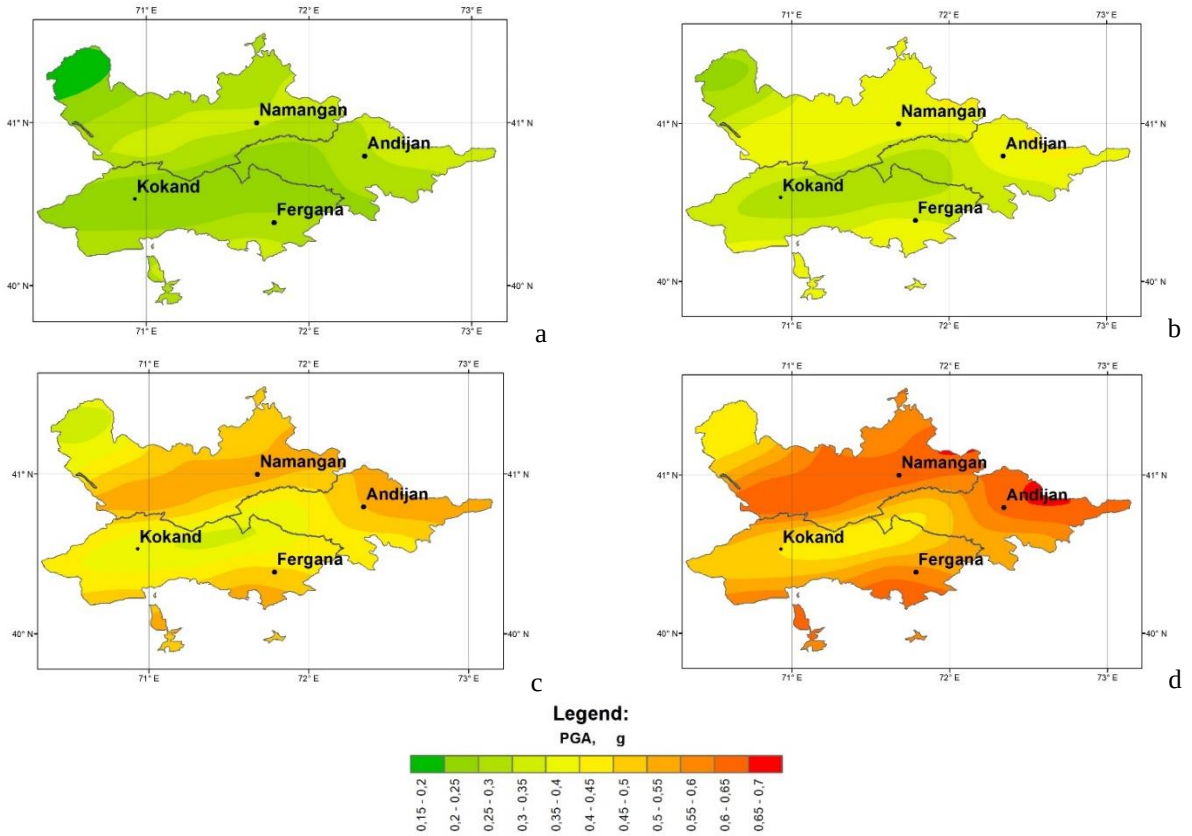

Figure. 6 - **Map of the Fergana Valley seismic zoning in the values of Peak Ground Accelerations (PGA, g) on soils of category II according to seismic properties (V_{S30} = 450 m/s) for various probabilities of not exceeding the level of seismic impacts within 50 yeas: a) P=0.90; b) P=0.95; c) P=0.98; d) P=0.99**

Figure 7 shows hazard curves in macroseismic intensity values for four large cities in the Fergana Valley - Namangan, Andijan, Fergana and Kokand. On the abscissa axis is the value of

seismic impact in MSK-64 scale points, and on the ordinate axis is the probability of its exceedance within 50 years. Horizontal lines in the figure show the periods of repetition of seismic impacts corresponding to different probabilities of exceeding the impact level.

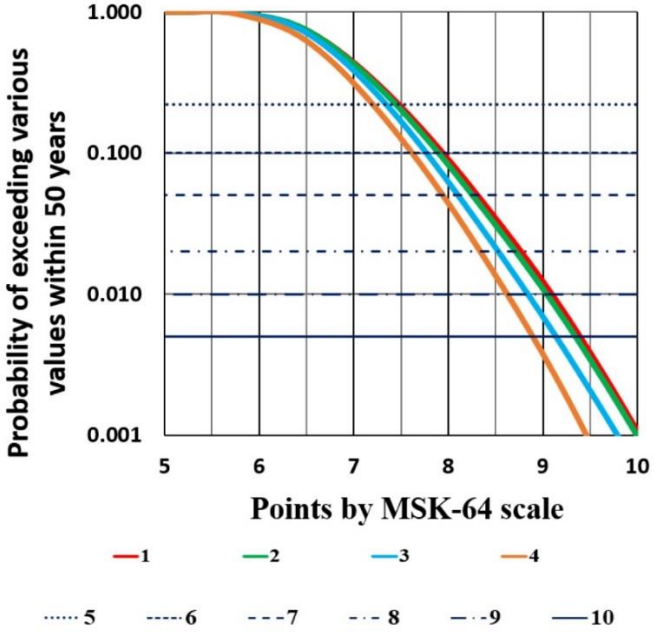

Figure 7. - **Hazard curves in macroseismic intensity indices for some large cities of the Fergana Valley: 1 - Namangan; 2 - Andijan; 3 - Fergana; 4 - Kokand. 5 - 10 periods of recurrence of shaking, corresponding to different probabilities of exceeding the level of seismic impacts within 50 years: 5 - 200 years; 5 - 4750 years; 5 - 975 years; 5 - 2470 years; 5 - 4975 years; 5 - 10000 years.**

Similar hazard curves for the same cities in values of Peak Ground accelerations are shown in Figure 8. The constructions are also made for soil conditions of II category on seismic properties.

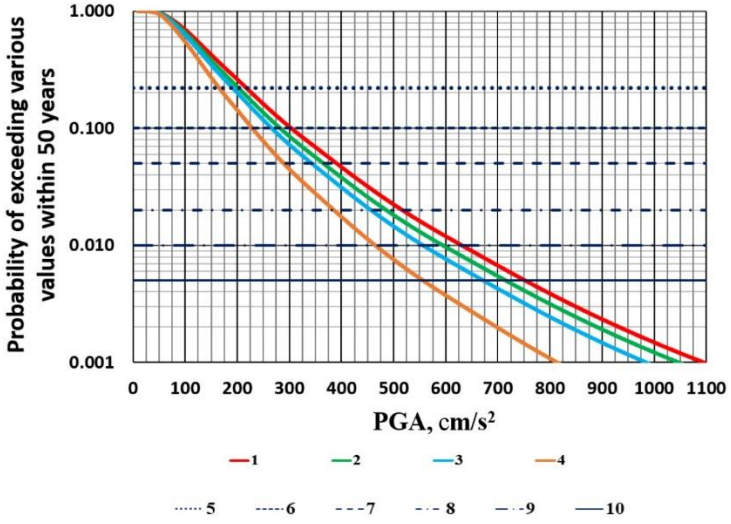

Figure 8. - **Hazard curves in values of Peak Ground Accelerations for some large cities of Fergana Valley: 1 - Namangan; 2 - Andijan; 3 - Fergana; 4 - Kokand. 5 - 10 periods of repetition of shaking, corresponding to different probabilities of exceeding the level of seismic impacts within 50 years: 5 - 200 years; 5 - 4750 years; 5 - 975 years; 5 - 2470 years; 5 - 4975 years; 5 - 10000 years**

9. Conclusion

The main results of the conducted research are summarized as follows.

The territory of Fergana valley is characterized by complex tectonic structure and high level of seismic activity. During the historical and instrumental period of observations there are a lot of strong and destructive earthquakes with magnitude M≥6.5 and intensity of shaking in the epicenter I0=8-9 MSK-64. Five alternative models of seismic sources have been developed to assess seismic hazard

of the Fergana depression and its mountainous frame: the model of area sources, the model of seismogenic zones and three models of active crustal faults with different degrees of reliability of manifestation of modern geodynamic activity in the latest and modern period of time. Seismological parameterization of the constructed models of seismic sources was carried out, including determination of seismic potential, parameters of earthquake recurrence of different magnitudes, predominant kinematic type of movement in the sources for each source.

Taking into account the weights given to each seismotectonic model, probabilistic maps of of the Fergana Valley territory detailed seismic zoning have been developed, expressing seismic hazard in points of the macroseismic scale and in values of maximum Peak Ground accelerations. The developed maps are well enough structured and reflect the modern structural plan and seismicity distribution of the study area. In the process of their construction, epistemic and aleatory uncertainties in the parameters of the seismic process and seismic effects were taken into account. These maps can be used for antiseismic measures and, first of all, for seismic-resistant construction of facilities and structures with different categories of responsibility, located in different ground conditions.

References

1. *Ibragimov R.N., Nurmatov U.O., Ibragimov O.R.* Seismotectonic method for assessing seismic hazard and issues of seismic zoning. - On Sat. Seismic zoning and earthquake forecast in Uzbekistan. – K.N.Abdullabekov (chief editor) – Tashkent: State Enterprise “Institute of HYDROINGEO”, 2002. P. 59-74.
2. *Artikov TU, Ibragimov RS, Ibragimova TL, Mirzaev MA* Complex of general seismic zoning maps OSR-2017 of Uzbekistan // Geodesy and Geodynamics . 2020. 11(4). PP . 273-294/ DOI : 10.1016/ j . geog.2020.03.004
3. Quantitative assessment of seismic hazard for the territory of Uzbekistan according to the estimated maximum *Artikov T.U., Ibragimov R.S., Ibragimova T.L., Kuchkarov K.I., Mirzaev M.A.* ground oscillation rates and their spectral amplitudes. *Geodynamics & Tectonophysics*. 2018;9(4):1173-1188. (In Russ.) https://doi.org/10.5800/GT-2018-9-4-0389
4. *Poggi V., Silacheva N., Ischuk A., Ibragimov R., Ismailov V., Abdrakhmatov K., Kobuliev Z., Karayev J., Parolai S., Bazzurro P.* Development of an improved PSHA model for Central Asia // Proceedings of the Third European Conference on Earthquake Engineering and Seismology (3ECEES) September 4 - September 9 2022, Bucharest, Romania. PP. 3900-3905
5. *Ullah Sh., Bindi D., Pilz M., Danciu L., Weatherill G., Zuccolo E., Ischuk A., Mikhailova N., Abdrakhmatov K., Parolai S.* Probabilistic seismic hazard assessment for Central Asia // Annals of geophysics. Special Issue. 2015. 58. 1. S0103. doi:10.4401/ag-6687.
6. *Riznichenko YU . IN* . Favorites works . Problems of seismology. – M.: Publishing house. Academy of Sciences of the USSR, 1985. 407 p .
7. *Ibragimov RS, Ibragimova TL, Mirzaev MA, Ashurov SH* Comparison of seismic hazard assessments obtained within the probabilistic and probabilistic-deterministic approaches for the territory of Uzbekistan // Seismic Instruments. 2022. 58(S1):21-35. doi: 10.3103/S0747923922070040
8. *Cornell CA* Engineering seismic risk analysis // Bulletin of the Seismological Society of America. 1968. V. 58. PP. 1583-1606.
9. *McGuire, R. K.* Seismic Hazard and Risk Analysis. - EERI Publications: Earthquake Engineering Research Institute, Oakland, California, 2004. 240 pp.
10. *Zelenin, E., Bachmanov, D., Garipova, S., Trifonov, V., Kozhurin, A.,* 2022 The Active Faults of Eurasia Database (AFEAD): the ontology and design behind the continental-scale dataset. Earth System Science Data 14(10), 4489–4503. https://doi.org/10.5194/essd-14-4489-2022.
11. *Hanks TC,* Bakun WH M-logA observations for recent large earthquakes // Bulletin of the Seismological Society of America. 2008. 98. N. 1. PP. 490–494. doi: 10.1785/0120070174
12. *Leonard M.* Earthquake Fault Scaling: Self-Consistent Relating of Rupture Length, Width, Average Displacement, and Moment Release // Bulletin of the Seismological Society of America , 2010. 100 (5A): 1971 - 1988. doi: 10.1785/0120090189
13. *Leonard M.* Self-consistent earthquake fault-scaling relations: update and extension to stable continental strike-slip faults // Bulletin of the Seismological Society of America . 2014. 104:1971–1988
14. *Wells DL, Coppersmith KJ* New empirical relationships among magnitude, rupture length, rupture width, rupture area and surface displacement // Bulletin of the Seismological Society of America. 1994. 84. No. 4.PP. 974-1002.
15. *Nowroozi A.* Empirical relations between magnitude and fault parameters for earthquake in Iran // Bulletin of Seismological Society of America. 1985. Vol.75. N. 5. RR . 1327-1338.
16. *Anderson, JG,* Luco, JE Consequences of slip rate constants on earthquake occurrence relations // Bulletin of the Seismological Society of America. 1983. 73. PP. 471–496.
17. *Youngs, RR, Coppersmith, KJ* Implications of fault slip rates and earthquake recurrence models to probabilistic seismic hazard estimates // Bulletin of the Seismological Society of America. 1985. 75. 939–964.

18. *Ibragimova T.L., Ibragimov R.S., Mirzaev M.A., Rebetsky Yu.L.* The current stress of Earth's crust in the territory of Uzbekistan according to focal earthquake mechanisms // Geodynamics & Tectonophysics. 2021. 12 (3), 435–454. doi:10.5800/GT-2021-12-3-0532.
19. *Rebetsky, Yu.L., Ibragimova, TL, Ibragimov, RS, Mirzaev MA* Stress State of Uzbekistan's Seismically Active Areas // Seismic Instruments. 2020. V. 56. P. 679–700, https://doi.org/10.3103/S0747923920060079.
20. *Shebalin NV* Macroseismic Data as Information on Source Parameters of Large Earthquakes // Physics of the Earth and Planetary Interiors. 1972. 6 (4). PP. 316–323. https://doi.org/10.1016/0031-9201(72)90016-7.
21. *Artikov TU, Ibragimov RS, Ibragimova TL, Mirzaev MA* Models of the macroseismic field earthquakes and their influence on seismic hazard assessment values for Central Asia // Geodynamics & Tectonophysics. 2020. 11(3):606-623. (In Russ.) https://doi.org/10.5800/GT-2020-11-3-0494 .
22. *Bindi D., Parolai S., Oth A., Abdrahmatov K., Muraliev A., Zschau J.* Intensity prediction equations for Central Asia // Geophysical Journal International. 2011. N.187. PP. 327-337. Doi: 10.1111/j.1365-246X.2011.05142.x.
23. *Scherbaum F., Cotton F., Smit P.* On the use of response spectral-reference data for the selection of ground-motion models for seismic hazard analysis: The case of rock motion," Bulletin of the Seismological Society of America. 2004. 94(6). PP. 341-348.
24. *Scherbaum F., Delavaud E., Riggelsen, C*. Model Selection in Seismic Hazard Analysis: An Information-Theoretical Perspective // Bulletin of the Seismological Society of America. 2009. 99. pp. 3234-3247.
25. *Ordaz M., Aguilar A., Arboleda J.* CRISIS2007. Program for Computing Seismic Hazard. Institute of Engineering UNAM, Mexico, 2007. URL: www.iingen.unam.mx [Access date: March 2016].
26. *Chen Y.S., Weatherill G., Pagani M., Cotton F. A* transparent and data-driven global tectonic regionalization model for seismic hazard assessment // Geophys. J. Int. 2018. V. 213, Iss. 2.PP. 1263–1280. https://doi.org/10.1093/gji/ggy005
27. *Abrahamson, Silva, and Kamai.* Summary of the ASK14 Ground Motion Relation for Active Crustal Regions // Earthquake Spectra. 2014. V. 30. N. 3.
28. *Campbell KW, Bozorgnia Y. NGA-West2* Ground Motion Model for the Average Horizontal Components of PGA, PGV, and 5% Damped Linear Acceleration Response Spectra // Earthquake Spectra. 2014. V. 30. N. 3. PP. 1087 – 1115.
29. *Chiou B.S.-J. and Youngs RR* Update of the Chiou and Youngs NGA model for the average horizontal component of peak ground motion and response spectra // Earthquake Spectra. 2014. 30(3):1117-1153.

SEISMIC RISK ASSESSMENT OF RESIDENTIAL BUILDINGS IN THE CITY OF JIZZAKH IN TERMS OF ECONOMIC INDICATORS

Ismailov V.A.[1], Aktamov B.U.[1], Yodgorov Sh.I.[1], Avazov Sh.B.[1], Islamova N.F.[1]
[1]*Institute of Seismology, Tashkent, Uzbekistan*
E-mail: b.u.aktamov@gmail.com

Abstract. *The probability of seismic risk level of the study area in 475 years using the 95% peak acceleration map was developed to assess the socio-economic loss probability of residential buildings. The small size of the study area under the influence of earthquakes makes it possible to develop programs for preparing for strong earthquakes in order to reduce the damage levels of buildings.*

Keywords. *Earthquake, seismic risk, seismic hazard, seismic impact, seismic vulnerability, peak acceleration, seismic intensity.*

1. Introduction

At of January 1, 2022, the permanent population of Jizzakh was 185,200 people. The city of Jizzakh and its neighboring regions were hit by a powerful earthquake. Assessment of losses caused by strong earthquakes and reducing the consequences of earthquakes are important in the field of seismic safety. Special attention is paid to the assessment of different levels of seismic risks in determining the extent of economic losses caused by an earthquake in the protection of the areas where the population and buildings are located from seismic risk.

The city of Jizzakh is located directly in the seismically active area of Southern Fergana and is considered seismically active.

Notable and strong earthquakes recorded near the city of Jizzakh from the historical period to the present day have been invisible. The greatest seismic impact of these earthquakes was observed in the following seismic events: the historic Ural-Tyubin earthquakes of 1897 with M=6.6 and M=6.7, respectively, occurred in the South Fergana seismically active area. The first of them happened at a distance of about 60 km from Jizzakh, and the second - much closer to the city, about 25-30 km South-East of the city of Jizzakh.

It allows to ensure the sustainable development of the population and regions and to assess possible losses that may occur in residential buildings under the influence of an earthquake, as well as to implement measures to reduce economic losses within the specified periods.

2. Literature analysis and methodology.

Seismic risk assessment scientific research has been developed since the 70-90s of the last century. The main reason for this is related to the 1971 San Fernando (USA) earthquake with a magnitude of M=6.5. After this earthquake, many insurance companies failed to cover the economic losses. During this period, dedicated research centers were established in the USA and methods of forecasting seismic risk were first developed. In this regard, R.V. Whitman, D.C. Friedman, I.M. Idriss, C.S. Oliveira, H.C. Shah and other scientists conducted several scientific studies [1;2].

The scientific-methodological and practical aspects of seismic risk assessment, i.e. seismic risk, seismic impact and seismic vulnerability levels of buildings, are discussed by M.Lu, N.Mert, K.Hasegawa, H.Hayashi, M.I.Carreno, G.Gruntal, J.Zschau, V.I Osipov, S.K. Shoigu, V.A. Larionov, G.L. Koff, V.G. Alkaz, M.A. Shakhramanyan, V.B. Zaalishvili, E.N. Chernykh, Yu.K. Chernov, Khusomiddinov S., Sh.I.Yodgorov, Sh.B.Avazov and others to carry out several scientific research works [9;22].

Despite the fact that a lot of important scientific and practical results have been obtained in the past period, there are a number of problems in this area at present. Studies on the assessment of seismic risk in direct economic indicators have not been fully analyzed, and scientific methodological bases have not been developed sufficiently. One of them is determining the seismic risk based on deterministic and probabilistic approaches in seismic risk assessment.

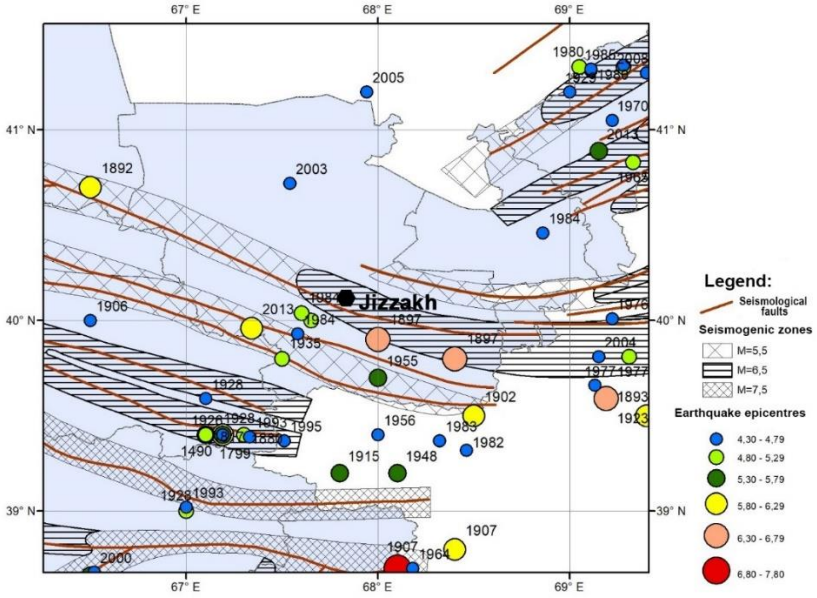

Figure 1. - **Map of epicenters of historical earthquakes**

The city of Jizzakh is located in the Central part of the Republic of Uzbekistan. The seismicity of the area is directly related to the tectonic condition of the region. The strong earthquakes that occurred in and around the city of Jizzakh are related to the geodynamic condition of the seismically active area of Southern Ferghana. Due to the dynamic influence of the regional fault system in the study area, in the west of Jizzakh, the South Fergana fault system changes its direction to the North-West and passes to the Bessapan and North Nurota fault systems. South of the city of Jizzakh, it passes into the North-Kuljuktov-Turkestan and South-Auminzatov-Aktov seismically active regions and is connected with the corresponding deep earth faults of the earth's crust. South of the latitudinal faults, there are two deep fault systems: South Tien-Shan and Gissaro-Kokshaal, which are distinguished by their very high seismic status. Seismic effects of earthquakes occurring on their borders are largely invisible in macroseismic effects in the city of Jizzakh. Northeast of Jizzakh city, Pskom-Tashkent and Angren are located in the seismically active regions, and strong earthquakes

due to the Karjantov and Angren fault systems also cause significant earthquakes in the study area [17].

20-25 km southwest of the city of Jizzakh, South Fergana seismic active area, 2013 M=6.2 Marjonbulok earthquake, North Kuljuktov-Turkestan seismic active area approximately 40-50 km south of Jizzakh, and 2017 Bakhmal earthquake approximately 45 kilometers from the city occurred at a distance (Fig. 1) [12;17].

The study allows to determine the amplitude-frequency characteristics of the ground layer, taking into account the seismic condition of the area, and, accordingly, the characteristics of vibrations on the free surface of the field or at internal points of the medium, modified by the layered medium. [17;18;19].

It allows to carry out calculations in the assessment of seismic risk and to determine the initial seismic impact based on the synthetic accelerogram and to create seismogrunt models of the soil layer. The real accelerograms of three earthquakes and their mechanism and the law of propagation of seismic waves for the research area are selected in accordance with the seismological conditions of the territory of the Republic of Uzbekistan.

The peak acceleration values of the surface waves for the points obtained from the peak acceleration profiles were 0.41g and 0.02g. The isolines of different levels of peak accelerations were summed and an initial seismicity of 0.231g was taken as the basis for the seismic zoning map [4;7].

According to the maximum acceleration levels of vibrations in the ground layers in the studied area, it was divided into the following intermediate limit values: from 0.100 to 0.380.

Various methods of calculation and interpretation have been used in seismic risk assessment, which allow to evaluate individual elements of risk, percentage of damages or a set of different elements represented by any economic indicators [3;5;6]. To a large extent, this is determined by the completeness of preliminary data on seismic risk at different levels and one or another aspect of the determined seismic effects. A peak acceleration map (PGA) of the Jizzakh city area was developed (Figure 2).

Spatial location of residential buildings built in the research area, the number of distribution of peak accelerations of different intensities from 0.1g to 0.4g are presented in statistical figures. Seismic risk assessment was carried out based on deterministic probabilistic approaches.

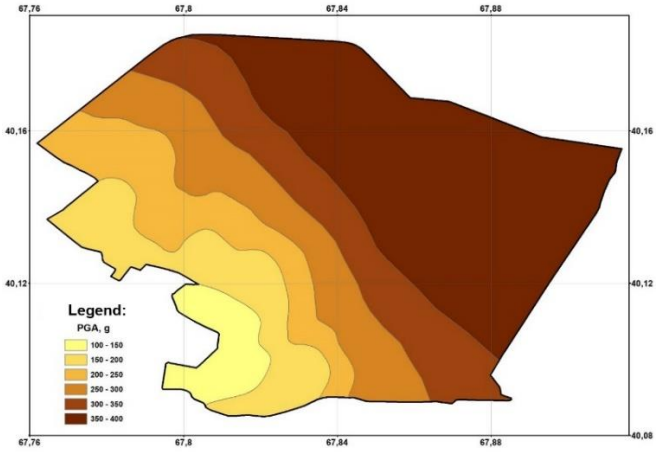

Figure 2. - **Peak acceleration map of Jizzakh city area (PGA)**

Thus, the above vulnerability functions for different types of buildings were used to calculate the average level of vulnerability of buildings in administrative districts (Figure 3).

Buildings built from local building materials (guvalak, pakhsa and raw brick); buildings made of baked bricks; reinforced concrete (panel, large panel, monolithic and reinforced concrete) buildings [8;9;10].

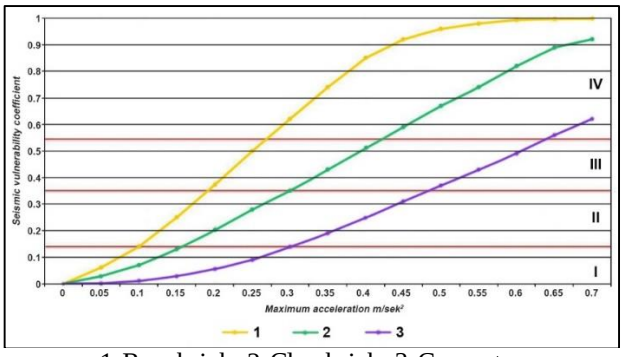

1-Raw brick; 2-Clay brick; 3-Concrete.

Figure 3. - **Vulnerability function for residential buildings using different types of building materials.**

The vulnerability functions presented above are used to calculate the average vulnerability level for different buildings within the administrative districts.

The conducted studies show that residential buildings in the area of Jizzakh city are characterized by different vulnerability functions, respectively. It was found that the main part of existing residential buildings in the territory of Jizzakh are individual residential buildings built from local materials (clay brick, concrete, raw brick) [11;13].

It should be noted that the average level of vulnerability of buildings and structures is calculated based on the calculated values of seismic vulnerability for buildings under seismic influence. The amount of seismic vulnerability of buildings and structures is determined as follows:

$$MVR = \frac{\sum_{i=1}^{n} N_i \cdot MVR_i}{\sum_{i=1}^{n} N_i} \quad (1)$$

Here, MVR-vulnerability indicator of buildings and structures; MVR corresponding to the average values of the selected type of buildings; Number of buildings of the same type with N-seismic vulnerability. This indicator (MVR) serves to quantitatively compare the seismic vulnerability of residential buildings in the urban area, and its functional role in relative indicators is significant [20;23;25].

One of the most important stages of seismic risk assessment is the classification of buildings according to the degree of response to a certain seismic impact.

3. Discussion.

The most important element of seismic risk was assessed by the average damage condition of buildings with different construction materials according to the level of seismic exposure. The peak acceleration (PGA) in the range of probability of occurrence of strong earthquakes at peak accelerations (PGA) with intensity from 0.1g to 0.4g in the area of Jizzakh city under different levels of seismic effects was calculated in useful area and economic indicators in the assessment of seismic risk due to earthquakes (Table 1).

Table 1.

PGA	Amount of buildings	Type of buildings			Construction site	Cadastre price	Loss of useful area, (thousand, m2)	Economic loss, (billion, soums)
		Concrete	Raw brick	Clay brick				
400	6686	46	151	6489	628,79	429,14	524,04	351,67
350	4041	24	75	3942	403,63	266,09	293,85	191,28
300	2847	33	80	2734	267,47	184,08	164,53	111,28
250	1894	23	82	1789	174,61	114,87	84,61	54,08
200	3238	32	96	3110	275,15	184,95	98,96	64,93
150	1545	14	59	1472	126,15	80,23	30,45	18,95

In the economic assessment of seismic risk, it is determined by calculating the actual cost and damage level of residential buildings according to the cadastral passport. The results of this study

were evaluated based on the level of damage to buildings and the cost of economic damages [14;15;16].

The level of seismic damage of buildings is evaluated in the following indicators:

0. No damage 0 %

1. Damage at the level of current repair, restoration costs up to 15% of the book value of the building.

2. Damage at the level of capital repair, restoration costs up to 35% of the book value of the building.

3. Restoration, restoration costs of the building up to 55% of the book value. It should be noted that the issue of restoration of the building will be decided by a special commission.

4. The building should be demolished when the damage is higher than 55% [16;21].

4. Results.

A systematic analysis of the database for the territory of Jizzakh and a map of cadastral prices of residential buildings located at different levels of seismic intensity were developed. Using the Maskur map, a map of seismic risk assessment in terms of direct economic losses was developed (Fig. 4,5).

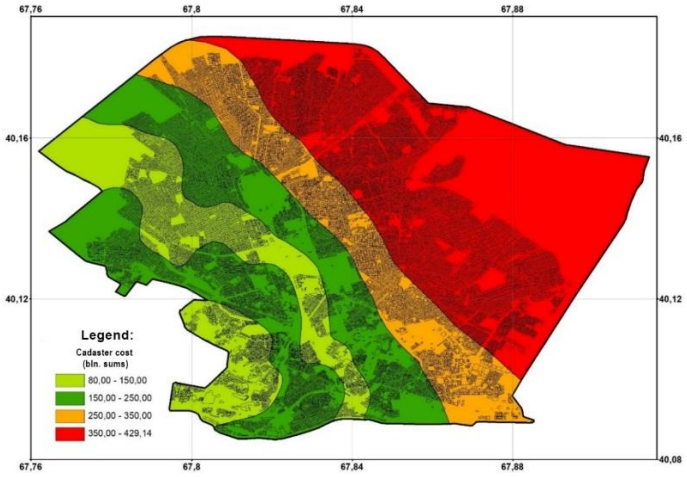

Figure 4. - **Map of the distribution of residential buildings of different seismic intensity by actual cadastral prices.**

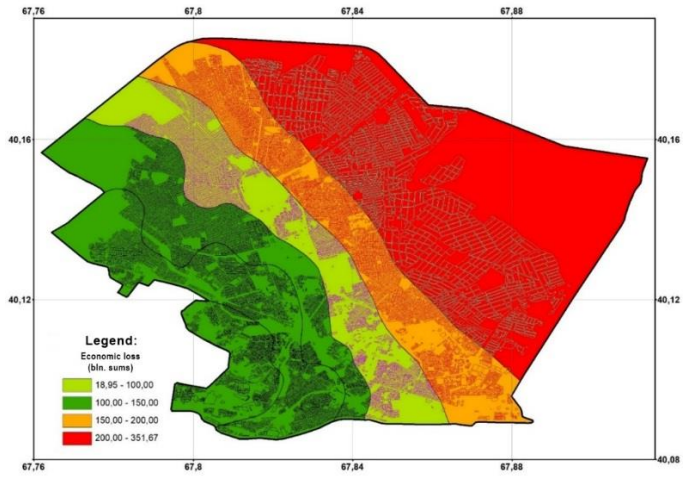

Figure 5. - **Seismic risk assessment map of residential buildings located in the city of Jizzakh in terms of direct economic losses.**

The damage level of 20,251 residential buildings in Jizzakh city was assessed according to the seismicity effect level at peak accelerations (PGA) of 0.15g to 0.4g. Also, the amount of damage caused to buildings by construction materials of buildings located at different levels of seismic intensity was calculated in percentages (Table 2).

Table 2.

Type of buildings	Seismic damage levels	Damage to buildings in seismic intensity %					
		0.15 PGA	0.2 PGA	0.25 PGA	0.3 PGA	0.35 PGA	0.4 PGA
A (Raw brick)	0	-	-	-	-	-	-
	1	74	-	-	-	-	-
	2	26	62	50	-	-	-
	3	-	38	50	37	26	14
	4	-	-	-	63	74	86
B (Clay brick)	0	87	-	-	-	-	-
	1	13	80	72	65	-	-
	2	-	20	28	35	76	48
	3	-	-	-	-	44	52
	4	-	-	-	-	-	-
C (Concrete)	0	96	93	91	87	-	-
	1	4	7	9	13	81	74
	2	-	-	-	-	19	26
	3	-	-	-	-	-	-
	4	-	-	-	-	-	-

Limited values of the amount of damage caused by the types of construction materials of buildings at different levels of seismic intensity in the territory of the city of Jizzakh were estimated as a percentage. As can be seen from the above data, the most vulnerable to seismic effects are A-type buildings, which are made of local construction materials such as guvalak, raw brick, and thatch. According to the analysis of the data, it was observed that the greatest damage to this type of buildings was observed in the regions with seismic effects of 0.2g and more seismic intensity [9;22].

5. Conclusion.

Systematic electronic database for 20,251 real estate objects on the scale of Jizzakh city as of February 1, 2024. Structured data of structural type of residential buildings, location coordinates and real price according to the cadastre were divided according to seismic risk levels for structural types of each building. This database was created for the rapid quantitative assessment of direct losses due to seismic effects by structural types of buildings and structures in all settlements of the city of Jizzakh, as a basis for the development of pre-preparation measures and loss reduction programs for possible socio-economic losses in the area. is done.

According to the economic index of damage expressed on the basis of one indicator, the seismic risk map for the territory of Jizzakh city (cadastral data) estimated the total amount of economic damage at 792.19 billion soums.

This work was funded by grants from the Academy of Sciences of the Republic of Uzbekistan, "Development of scientific foundations for assessing various levels of seismic risk and reducing earthquake losses in seismically active areas" and the Agency for Innovation Development, #ALM202311142839 "Creation of a simulation digital model of the city of Tashkent allowing to assess the level of economic damage from strong earthquakes" and #AL5822012294 "Development of technology for predicting the risk of strong earthquakes", #AL5822012298"Create an electronic database on seismological soil characteristics to replace Table 1.1 in the regulatory document. seismological part of KMK “Construction of seismic areas”", as well as the project "Regionally coordinated assessment of earthquake and flood risks and selective analysis of landslide scenarios to strengthen financial resilience and accelerate risk reduction in Central Asia", funded by the EU Program "Strengthening Financial Resilience" and Accelerating Risk Reduction" (SFRARR) funded by the European Union and implemented by the World Bank. We sincerely thank all the project team members, in particular Sergey Tyagunov, Paola Ceresa, Antonella Peresan, Gabriele Coccia, Denis Sandron and Stefano Parolai, and the World Bank specialists, in particular Stuart Alexander Fraser and Madina Nizamitdin, for their constructive contributions to the project. We are grateful for the

suggestions and feedback from the editor and the two reviewers, which substantially improved the manuscript.

References

1. *Frolova, N. I., Malaeva, N. S., Ruzhich, V. v., Berzhinskaya, L. P., Levina, E. A., Suchshev, S. P., Larionov, V. I., & Ugarov, A. N.* (2022). Assessing the Social and Economic Indicators of Seismic Risk Using the Town of Angarsk as an Example. Izvestiya, Atmospheric and Oceanic Physics, 58(8), 881–907. https://doi.org/10.1134/S0001433822080011
2. *Frolova, N. I., Suchshev, S. P., Ugarov, A. N., & Malaeva, N. S.* (2023). Updated indicators of seismic risk for the territory of the Irkutsk region and the Republic of Buryatia. Russian Journal of Seismology, 5(1), 26–50. https://doi.org/10.35540/2686-7907.2023.1.02
3. *Colajanni, P., & D'Anna, J.* (2024). Seismic risk assessment of residential buildings by the Heuristic vulnerability model: influence of fragility curve models and inventory scale. Bulletin of Earthquake Engineering, 22(3), 877–910. https://doi.org/10.1007/s10518-023-01801-z
4. *Acevedo, A. B., Yepes-Estrada, C., González, D., Silva, V., Mora, M., Arcila, M., & Posada, G.* (2020). Seismic risk assessment for the residential buildings of the major three cities in Colombia: Bogotá, Medellín, and Cali. Earthquake Spectra, 36(1_suppl), 298–320. https://doi.org/10.1177/8755293020942537
5. *Lovon, H., Tarque, N., Silva, V., & Yepes-Estrada, C.* (2018). Development of Fragility Curves for Confined Masonry Buildings in Lima, Peru. Earthquake Spectra, 34(3), 1339–1361. https://doi.org/10.1193/090517EQS174M
6. *Calderon, A., & Silva, V.* (2019). Probabilistic seismic vulnerability and loss assessment of the residential building stock in Costa Rica. Bulletin of Earthquake Engineering, 17(3), 1257–1284. https://doi.org/10.1007/s10518-018-0499-1
7. *Martins, L., Silva, V., Crowley, H., & Cavalieri, F.* (2021). Vulnerability modellers toolkit, an open-source platform for vulnerability analysis. Bulletin of Earthquake Engineering, 19(13), 5691–5709. https://doi.org/10.1007/s10518-021-01187-w
8. *Cherif, S., Chourak, M., Abed, M., & Douiri, A.* (2018). Potential Seismic Damage Assessment of Residential Buildings in Imzouren City (Northern Morocco). Buildings, 8(12), 179. https://doi.org/10.3390/buildings8120179
9. *Ismailov, V., Khusomiddinov, S., Khusomiddinov, A., Yodgorov, S., Aktamov, B., & Avazov, S.* (2022). Seismic risk assessment of Jizzakh region. 030035. https://doi.org/10.1063/5.0089664
10. *Aroquipa, H., & Hurtado, A.* (2022). Seismic resilience assessment of buildings: A simplified methodological approach through conventional seismic risk assessment. International Journal of Disaster Risk Reduction, 77, 103047. https://doi.org/10.1016/j.ijdrr.2022.103047
11. *Koohfallah, K., Raissi Dehkordi, M., D'Ayala, D., Ghodrati Amiri, G., Eghbali, M., & Samadian, D.* (2024). Seismic resilience of typical steel school building and retrofitting options based on FEMA P-58 under mainshock-aftershock effects. Journal of Building Engineering, 86, 108636. https://doi.org/10.1016/j.jobe.2024.108636
12. *Moradi, S., Khan, M. M., Hossain, N. U. I., Shamsuddoha, M., & Gorod, A.* (2023). Modeling and assessing seismic resilience leveraging systems dynamic approach: A case study of society 5.0. International Journal of Critical Infrastructure Protection, 43, 100639. https://doi.org/10.1016/j.ijcip.2023.100639
13. *Vona, M., Manganelli, B., Tataranna, S., & Anelli, A.* (2018). An Optimized Procedure to Estimate the Economic Seismic Losses of Existing Reinforced Concrete Buildings due to Seismic Damage. Buildings, 8(10), 144. https://doi.org/10.3390/buildings8100144
14. *Vicente, R., Ferreira, T., & Maio, R.* (2014). Seismic Risk at the Urban Scale: Assessment, Mapping and Planning. Procedia Economics and Finance, 18, 71–80. https://doi.org/10.1016/S2212-5671(14)00915-0
15. *Feliciano, D., Arroyo, O., Cabrera, T., Contreras, D., Valcárcel Torres, J. A., & Gómez Zapata, J. C.* (2023). Seismic risk scenarios for the residential buildings in the Sabana Centro province in Colombia. Natural Hazards and Earth System Sciences, 23(5), 1863–1890. https://doi.org/10.5194/nhess-23-1863-2023
16. *Abarca, A., & Monteiro, R.* (2019). Towards Large Scale Seismic Risk Assessment in Algeria: Case Study to the City of Blida. IOP Conference Series: Materials Science and Engineering, 603(5), 052065. https://doi.org/10.1088/1757-899X/603/5/052065
17. *Artikov, T. U., Ibragimov, R. S., Ibragimova, T. L., & Mirzaev, M. A.* (2020). Models of the macroseismic field earthquakes and their influence on seismic hazard assessment values for Central Asia. Geodynamics & Tectonophysics, 11(3), 606–623. https://doi.org/10.5800/GT-2020-11-3-0494
18. *Bhochhibhoya, S., & Maharjan, R.* (2022). Integrated seismic risk assessment in Nepal. Natural Hazards and Earth System Sciences, 22(10), 3211–3230. https://doi.org/10.5194/nhess-22-3211-2022
19. *Vicente, R., Ferreira, T., & Maio, R.* (2014). Seismic Risk at the Urban Scale: Assessment, Mapping and Planning. Procedia Economics and Finance, 18, 71–80. https://doi.org/10.1016/S2212-5671(14)00915-0
20. *Saputra, A., Rahardianto, T., Revindo, M. D., Delikostidis, I., Hadmoko, D. S., Sartohadi, J., & Gomez, C.* (2017). Seismic vulnerability assessment of residential buildings using logistic regression and geographic information system (GIS) in Pleret Sub District (Yogyakarta, Indonesia). Geoenvironmental Disasters, 4(1), 11. https://doi.org/10.1186/s40677-017-0075-z

21. *Elizabeth Philip, S., & Helen Santhi, M.* (2020). Peak Ground Acceleration Analysis using Past Earthquake Data. Journal of Physics: Conference Series, 1716(1), 012013. https://doi.org/10.1088/1742-6596/1716/1/012013
22. *Ismailov, V. A., Yodgorov, S. I., Khusomiddinov, A. S., Yadigarov, E. M., Botirovich, A. S., & Aktamov, B. U.* (2023). New classification of soils by seismic properties for the building code in Uzbekistan. Geomechanics and Geoengineering, 1–21. https://doi.org/10.1080/17486025.2023.2296975
23. G., S. T., & S., V. K. (n.d.). Evaluation of Peak Ground Acceleration and Response Spectra Considering the Local Site Effects. In Geotechnical Applications for Earthquake Engineering (pp. 1–17). IGI Global. https://doi.org/10.4018/978-1-4666-0915-0.ch001
24. *Fadel Miguel, L. F., Riera, J. D., Ontiveros-Pérez, S. P., & Miguel, L. F. F.* (2022). Probabilistic Assessment of the Seismic Peak Ground Acceleration (PGA) at seven Colombian Cities. Revista Sul-Americana de Engenharia Estrutural, 19(3), 1–10. https://doi.org/10.5335/rsaee.v19i3.13909
25. *Adeel, M. B., Nizamani, Z. A., Aaqib, M., Khan, S., Rehman, J. U., Bhusal, B., & Park, D.* (2023). Estimation of V S30 using shallow depth time-averaged shear wave velocity of Rawalpindi–Islamabad, Pakistan. Geomatics, Natural Hazards and Risk, 14(1), 1–21. https://doi.org/10.1080/19475705.2022.2161953

EVALUATION OF RESONANCE RISK AND STRENGTH OF A HIGH-RISE BUILDING USING THE MICROTREMOR METHOD

Ismailov V.[1], Oripov N.[1, 2], Yanbukhtin I.[2], Bozorov J.[1]
[1]*Institute of Seismology named after G. Mavlyanov, Tashkent, Uzbekistan*
[2]*Center for Advanced Technologies, Tashkent, Uzbekistan*
E-mail: vakhit.mbm@gmail.com

Abstract: *Currently, microtremor analysis is an effective method for assessing the dynamic characteristics of buildings and the level of damage that may occur during an earthquake. The study was conducted in one of the high-rise buildings located in the center of the city of Tashkent and in the area where it is located. Measurements on the free surface and on the assigned floors of the building took 25-30 minutes. The HVSR method was used to determine the dominant frequency of the free surface, and the FSR method was used to determine the natural frequency of the building. The analysis showed that the natural frequency of the building significantly exceeds the value of the natural frequency of the terrain where it is located. This, in turn, is characterized as a low level of resonance.*

Keywords: *microtremor, HVSR, FSR, resonance, vulnerability index.*

1. Introduction

One of the parameters that cause significant damage to buildings and structures are their dynamic and seismic characteristics such as natural frequency, resonance value [1,2] and building vulnerability index [3-5]. These parameters can be obtained by recording ambient noise. In this study, a 26-story apartment building was investigated using the microtremor method to obtain the building safety performance. The main advantages of microtremor analysis are simplicity, efficiency and speed, which provide a reliable, accurate and stable assessment of building vibration modes from low-amplitude excitation.

The eigenfrequency value on soil is determined by processing microtremor data using the HVSR (Horizontal to Vertical Fourier Spectral Ratio) [3,6,7]. And the natural frequency value of the building is determined using FSR (Floor Spectral Ratio) method and the analysis spectrum is obtained from each floor to get the natural frequency value of the building [8-10]. The building resonance value is determined based on the spectrum for each component (NS and EW). Resonance can be used to determine the level of possibility of a building experiencing resonance during an earthquake. Resonance risk occurs if the dominant periods of the ground and buildings are close to each other. The value of the amplification and natural frequency in soil and buildings can get the value of soil vulnerability analysis, building vulnerability analysis and building resonance [1].

2. Methods

2.1. Microtremor measurements

Microseismic is avibration of the Earth. The weak vibration can beoriginated from the human activity, ocean waves, wind,traffic and others. Source of microtremor ormiscroseismic can be divided into natural and artificialsources. Examples natural microseismic can come fromrain, wind, running water, or ocean waves, while sourcesof artificial microseismic generally come from industrialand

human activities, including the sound of machines,cars, people walking, and so on. The amplitude of themicroseismic is so small that it is difficult for humans todetect it, but with the development of technology,instruments that can detect these waves are created,which are commonly called seismometers [11].

Microtremor has based on ambient noise recordings to determine dynamical characteristic parameters of building [12]. Many researchers reviewed, introduced and applied of ambient noise analysis for both purposes. Nakamura et al. [3,4] and Sato et al. [5] identified damaged building using vulnerability index of structure estimated from transfer function parameters.

Microtremors were recorded in different parts of -2F, -1F, 1F, 3F, 6F, 9F, 12F, 15F, 18F, 21F, 24F and roof floors of a T1 business class residential complex. Free-field measurements were also taken close to the building and at a sufficient distance to avoid its influence. To improve the quality of microtremor recording and reduce interference, measurements were performed only at night. Measurements were performed at a total of 60 points and took 48 hours. Ambient noise measurements were made using a CMG-6TD seismometer (Guralp, UK). Each sensor provided vibration recording over a wide frequency range from 0.03 to 100 Hz.

Microtremor was recorded three directions (EW, NS, Z) with 1/100 second sampling rate. The recording length was 30 minutes, because frequencies below 1 Hz were not of interest.

2.2. Horizontal to Vertical Spectral Ratio (HVSR)

Microtremor measurements can be utilized to determine the soil predominant frequency. For this purpose, the microtremor HVRS method that proposed by Nakamura [2,5] was used. Then, power spectra of ground motion should be calculated for two horizontal directions (EW and NS) and also for vertical direction (V). Finally, to determine the site frequency, the spectral ratio of the combined horizontal (H) to vertical (V) component of ground motion must be calculated. The frequency of the peak amplitude in the spectral ratio graph is the predominant (natural) frequency of the site. By comparing the fundamental frequency obtained from the microtremor H/V spectral ratio with the function received from the seismic log, the researchers concluded that the H/V microtremor spectral ratio provides a reliable estimate of sediment frequency [13].

The following formula is the basis for calculating the horizontal to vertical microtremor spectrum ratio (HVSR) and is expressed as follows:

$$HVSR = \frac{\sqrt{[(S_{north-south})^2+(S_{east-west})^2]}}{S_{vertical}} \quad (1)$$

To obtain reliable HVSR curve results, quality control is required based on the SESAME 2004 standard. There are three reliable criteria for HVSR curves, including [14]:

1. $f_0 > 10/Iw$
2. $nc(f_0) > 200$, $nc = Iw.\ nw.\ f_0$,
3. $\sigma A(f) < 2$ to $0.5f_0 < f < 2f_0$ if $f_0 > 0.5$ Hz, or

$\sigma A(f) < 3$ to $0.5f_0 < f < 2f_0$ if $f_0 < 0.5$ Hz

where Iw is the window length, nw is the number of windows selected to obtain the average H/V curve, nc is the number of significant cycles, σA is the standard deviation of A H/V (f), and f_0 is the peak frequency in the H/V curve.

Data processing to obtain the HVSR on the free field was performed in the following way: recorded times series were visually inspected to identify possible erroneous measurement and stronger transient noise. Each record was then split into 20-30 s-long windows tapered with 5% cosine function. A Fast Fourier Transform (FFT) was calculated for each window in each seismometer component. The Fourier spectra were smoothed using Konno and Ohmachi [7] with 40 smoothing constants. HVSR was computed as the geometric average of both horizontal component spectra divided by the vertical spectrum for each window. This analysis was used GEOPSY software.

2.3. Floor Spectral Ratio (FSR)

The use of HVSR is not recommended when determining transfer function parameters in buildings, this is because only in a few cases it gets good results. This inaccuracy is because it cannot be assumed that the horizontal and vertical spectra have a fixed value at ground level, so there is no reason to use them in the assessment of building structures. If this is still implemented in buildings, it will likely be very dangerous in cases of very strong soil amplification, because the analysis results are not close to the actual situation. In this case, the HVSR may give an incorrect assessment or building response because it is identified as a spurious transfer function parameter [2].

The floor spectra ratio (FSR) method is a method for determining the natural and resonant frequencies of buildings that describe the characteristics of buildings against earthquakes [6,15]. In the FSR method, other building characteristics that can be obtained besides the natural frequency are the building resonance index and the building vulnerability index. The natural frequency building value is determined from the spectrum analysis of each building floor to the ground below it. The data calculation process is carried out to determine the natural frequency value of the building using equation (2) [1].

$$f_0(FSR) = \frac{f_b NS}{f_t NS} = \frac{f_b EW}{f_t EW} \quad (2)$$

Equation (2) is FSR analysis equations where f_b is the value of the building frequency, f_t is the value of the ground frequency, and NS-EW is the respective components of the data.

Resonance can be used to determine the level of possibility of a building experiencing resonance during an earthquake [1]. There are several classifications:

1. Low resonance (R>25%)
2. Medium resonance (15% <R< 25%)
3. High resonance (R<15%)

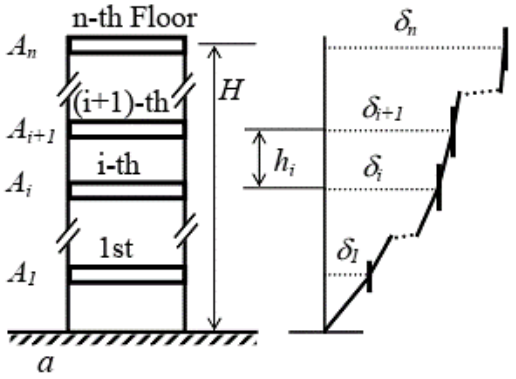

Figure 1. - **Schematic model of *n-th* floor structures and its mode shape. *δj* is the horizontal displacement, *hi* is the height, *Ai* is amplification factor of *i-th* story column, *H* is the height of the *n-th* floor structure, and a is the horizontal acceleration of foundation ground**

The building resonance index (R) is determined based on the spectrum of each component (NS and EW) which is calculated based on the following equation:

$$R = \left|\frac{f_b - f_t}{f_t}\right| \times 100\% \quad (3)$$

here f_b is the natural frequency of the building, and f_t is the natural frequency of the ground.

2.4. Vulnerability index

The vulnerability of buildings is one of the most important parameters for evaluation potential damages in urban area caused earthquake. Nakamura et al. and Sato et al. showed that the vulnerability index can be used to describe the building strength in bearing the earthquake shakings. It is considered that the vulnerability of structures against earthquake disasters can be estimated by the drift angle, related to the input earthquake acceleration a in cm/s^2. Here, α is a portion which effects this structure among whole earthquake motion a:

$$\alpha = e \times a, \quad (4)$$

where e shows the efficiency of earthquake motion working for this structure.
A deformation performance and the degree of earthquake motion amplification can be estimated from the dynamic characteristics of structures. Here, the primary natural frequency of the structure that seems to have influence on earthquake damage is considered. Displacement δ_i of ith floor is estimated from this primary natural frequency F and amplitude A_i of ith floor as follows (Fig. 1):

.

$$\delta_j = A_i \times \alpha/(2\pi F_s)^2. \quad (5)$$

Therefore, the drift angle γ_i of ith floor is shown as:

$$\begin{aligned} \gamma_i &= \delta_{i+1} - \delta_i/h \\ &= \Delta A_i \times \alpha/(2\pi F)^2/h_i \\ &= e \times K_{bi} \times a, \end{aligned} \quad (6)$$

where

$$K_{bi} = \Delta A_i/(2\pi F)^2/h_i \times 10{,}000, \quad (7)$$

$$\Delta A_i = A_{i+1} - A_i, \quad (8)$$

ΔA_i shows the difference of amplification of the ith floor, h_i is the height of ith floor in meter, and F is the predominant frequency of structure.

Thus, the drift angle γ_i for each floor is estimate from vulnerability index K_{bi} multiplied by the maximum acceleration on the surface ground a in cm/s^2 and the efficiency e of earthquake motion. Here, ${}_{av}K_b$ value is derived as averaged K_{bi} for each structure for the discussion as follows:

$${}_{av}K_b = \frac{A}{(2\pi F)^2 \times H} \times 10{,}000, \quad (9)$$

where A – shows the amplitude of the top floor and H – is the total height of structure in meter.

In addition, when ${}_{av}K_b$ is substituted for K_{bi} in Eq. (6), averaged drift angle γ_{av} will be calculated. K_{bi} and ${}_{av}K_b$ are expressed in unit of 10^{-6}, 10,000 in Eqs. (7) and (9) is multiplied for adjustment.

3. Analysis of results

3.1. Ground natural frequency

Ground natural frequency obtained from HVSR analysis is the average frequency of each vertical and horizontal spectrum. The obtained spectral ratio for the site of where the T1 building is located is shown in Figure 2. Based on this figure, the natural frequency of the site is 0.64 Hz.

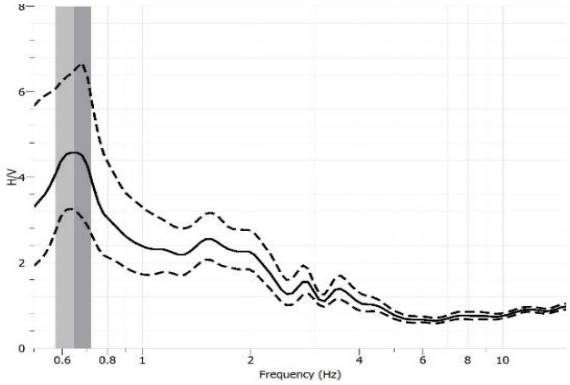

Figure 2. - **Spectral ratio (H/V) for site of where the T1 building is located, natural frequency 0.64 Hz**

3.2. Floor Spectral Ratio Analysis

FSR (Floor Spectral Ratio) analysis was conducted to determine the natural frequency of building (Fig. 3). The FSR analysis was calculated by dividing the dominant frequencies of the building floors determined from the spectrum analysis by the free surface frequency. The EW component values of all floors ranged from 0.97-4.8 Hz, and the NS component values ranged from 1-4.95 Hz. The average natural frequency of each component was ±2.5 Hz.

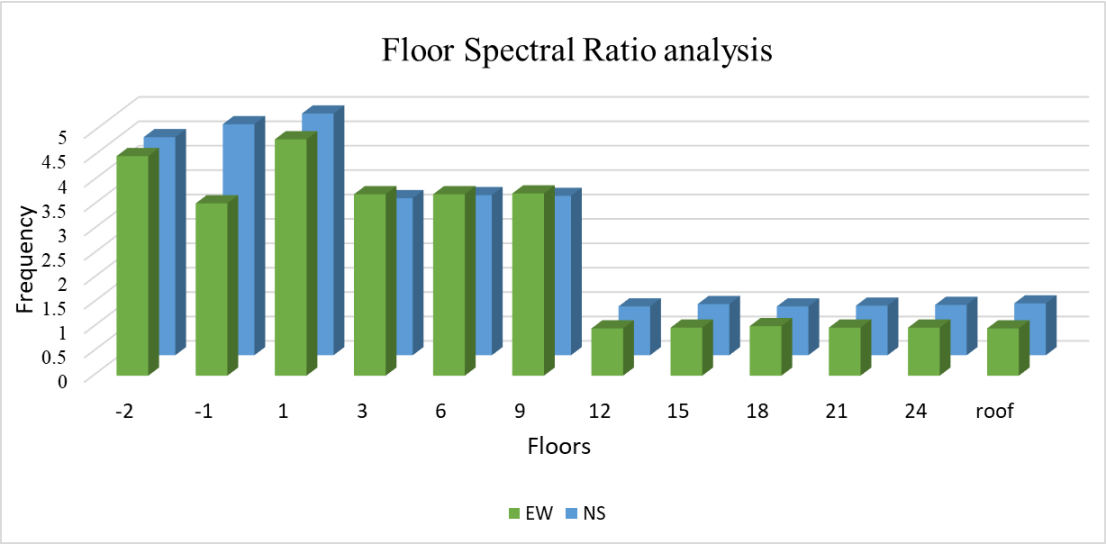

Figure 3. - **Diagram of natural frequency variation by floors based on FSR analysis**

3.3. Ground and Building resonance

The magnitude of building to site resonance ranged from 51% to 617% for the EW component and 59% to 674% for the NS component (Fig. 4). The average resonance value is ±290%. Based on the above classification [1], the obtained resonance value is categorized as low resonance because the natural frequency of the building is much higher than the value of the natural frequency of the site. For the horizontal components, resonance values up to the 9th floor differed by values greater than >100%, and from the 12th floor and above, values differed by values below <100%. This significantly reduces the probability of resonance phenomenon.

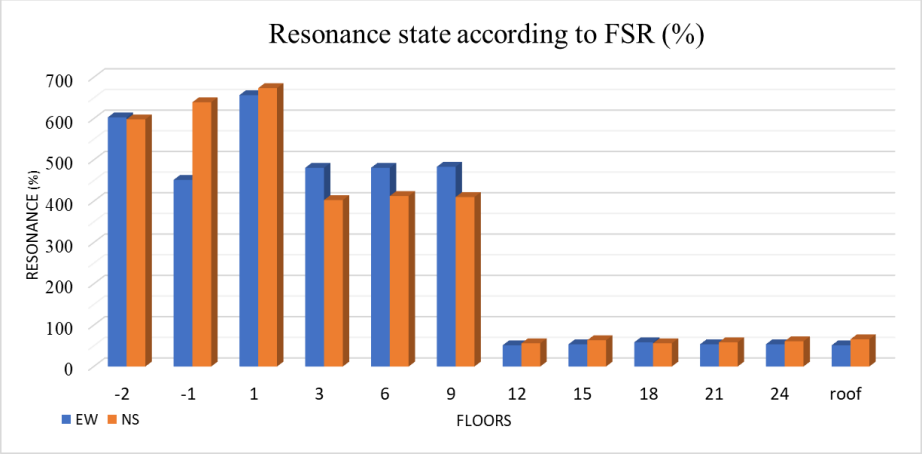

Figure 4. - **Diagram of resonance variation by floor**

4. Building vulnerability index

The building vulnerability index (Kb) shows the level of damage that occurs to the building in the event of an earthquake. The greater the vulnerability value of a building, the greater the potential damage that will occur [5,16-17].

Based on the processing results, the vulnerability index values of building T1 changed from 0.42 to 9.45 for the EW component and from 0.43 to 7.12 for the NS component. The lowest vulnerability index was observed on the 9th floor and the highest on the roof (Fig. 5). This indicates that the building is very resistant to earthquakes.

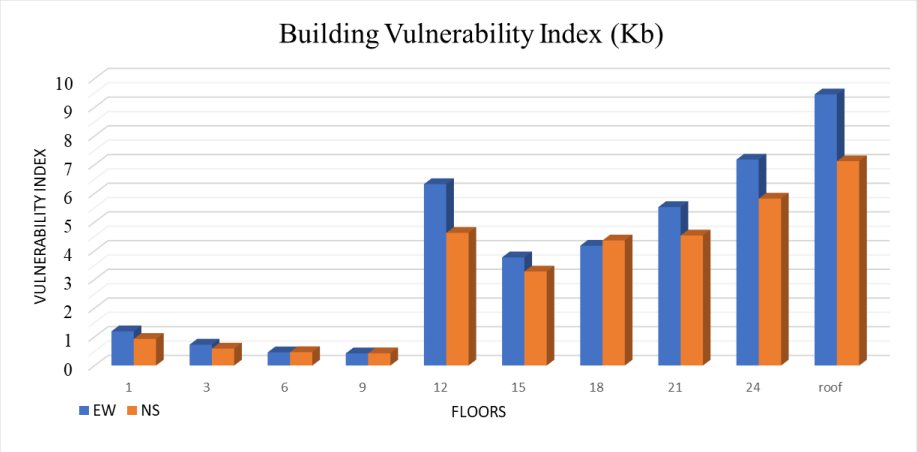

Figure 5. - **Diagram of change of vulnerability index by floors**

5. Conclusions

Based on the results of calculations and analysis, the soil on which building T1 is located is found to have a frequency of 0.64 Hz by HVSR method. The FSR analysis showed that the natural frequency of the building was determined to be 0.97 Hz – 4.8 Hz in the EW component and 1 Hz – 4.95 Hz in the NS component. It should be said that above the 9th floor there was a sharp decrease in the natural frequency of the building. This indicates that the building was divided into two parts.

The magnitude of the building and ground resonance varied between 51% – 617% in the EW component and between 59% – 674% in the NS component. The mean value of the component resonance was ±290%. In turn, this figure is categorized as low resonance because the natural frequency of the building is much higher than the value of the natural frequency of the ground.

The vulnerability index ranged from 0.42 to 9.45 for the EW component and from 0.43 to 7.12 for the NS component. The vulnerability index values decreased from the 1st floor to the 9th floor and increased sharply from the 9th floor above. In general, the values showed a result below <10. The vulnerability index value of the building shows that the building is of low category (safe).

This work was funded by grants from the Academy of Sciences of the Republic of Uzbekistan, "Development of scientific foundations for assessing various levels of seismic risk and reducing earthquake losses in seismically active areas" and the Agency for Innovation Development, #ALM202311142839 "Creation of a simulation digital model of the city of Tashkent allowing to assess the level of economic damage from strong earthquakes".

References

1. *Gosar A. (2010)* Site effects and soil-structure resonance study in the Kobarid basin (NW Slovenia) using microtremors. Natural Hazards and Earth System Science 10(4), 761-772. DOI:10.5194/nhess-10-761-2010
2. *Herak M.* (2011) Overview of recent ambient noise measurements in Croatia in free-field and in buildings Geofizika 28(1).
3. *Nakamura Y, Gurler E.D., Saita J., Rovelli A., Donati S.* (2000) Vulnerability investigation of roman colosseum using Microtremor. Prepared for 12th WCEE in Auckland, NZ 2660/6/A
4. *Nakamura Y., Saita J., Sato T.,* Increasing Seismic Safety by Combining Engineering Technologies and Seismological Data, edited by Mucciarelli M., Herak M., Cassidy J. (2009) NATO Science for Peace and Security Series C: Environmental Security, 281-292. DOI:10.1007/978-1-4020-9196-4
5. *Sato T., Nakamura Y., Saita J.* (2008) The change of dynamic characteristics using microtremor. The 14th WCEE, Beijing, China
6. *Gallipoli M.R., Mucciarelli M., Castro R.R., Monachesi G., Contri P.* (2004) Structure, soil-structure response and effects of damage based on observations of horizontalto-vertical spectral ratios of microtremors. Soil Dynamics and Earthquake Engineering 24(6):487-495. DOI:10.1016/j.soildyn.2003.11.009
7. *Konno K. & Ohmachi T.* (1998) Ground-Motion Characteristics Estimated from Spectral Ratio between Horizontal and Vertical Components of Microtremor. Bulletin of the Seismological Society of America vol.88, No.1, pp 228-241.
8. *Gosar A.* (2007) Microtremor HVSR study for assessing site effects in the Bovec basin (NW Slovenia) related to 1998 Mw5.6 and 2004 Mw5.2 earthquakes.

9. *Prakosa P.T., Ibad M.I., Kafi M.S., Burhanudin M.A., Rahmania A.* (2015) Earthquake Microzonation and Strength Building Evaluation at Gelora Bung Tomo Stadium Surabaya Using Micro-Tremor Method. 7th International Conference on Physics and Its Applications 2014 (ICOPIA 2014) 1: 14-20.

10. *Sungkono S., Warnana D.D., Triwulan, Utama W.* (2011) Evaluation of Buildings Strength from Microtremor Analyses. IRE Transactions on Engineering Management 1(4):6-12

11. *Okada H.* (2003) The microtremor survey method. Society of Exploration Geophysicists with the cooperation of Society of Exploration Geophysicists of Japan and Australian Society of Exploration Geophysicists

12. *Hadianfard M.A., Rabiee R., Sarshad A.* (2017). Assessment of Vulnerability and Dynamic Characteristics of a Historical Building Using Microtremor Measurements. International Journal of Civil Engineering, 15(2), 175-183. https://doi.org/10.1007/s40999-016-0086-2

13. *Mokhberi M.* (2015) Vulnerability evaluation of the urban area using the H/V spectral ratio of microtremors. International Journal of Disaster Risk Reduction 13(1), pp. 369-374. DOI:10.1016/j.ijdrr.2015.06.012

14. SESAME, Guidelines for The Implementation of the H/V Spectral Ratio Technique on Ambient Vibrations Measurements, Processing and Interpretation, (2004) Available: http://sesame-fp5.obs.ujfgrenoble.fr/Delivrables/Del-D23HVUser Guidelines.pdf

15. *Satriyo A., Suryanto W., Anggono T., Al Kamali M.L., Yufi H.S*. (2023) Study Characteristics of a Multipurpose Reactor Building G.A. Siwabessy using Floor Spectral Ratio. E3S Web of Conferences. Volume 468, 2023. ICST UGM 2023. https://doi.org/10.1051/e3sconf/202346809003

16. *Sarkowi M., Wibowo R.C., Sunanda Yogi I.B., Yusuf M., Boka Y.S.* (2022) Microtremor analysis to evaluate BMKG region III building, Bali, Indonesia. IJES Vol. 14, No. 2, 2022, 104-111. DOI: 10.30495/ijes.2022.1942485.1659

17. *Irie Y., Nakamura K.* (2000) Dynamic characteristics of a R/C building of five stories based on microtremor measurements and earthquake observations. In: Proceeding of 12th WCEE, Wellington, pp 500-508

18. *Bekler T., Demirci A., Ekinci Y.L., Büyüksaraç A.* (2019) Analysis of local site conditions through geophysical parameters at a city under earthquake threat: Çanakkale, NW Turkey. Journal of Applied Geophysics 163(4) 31-39 DOI:10.1016/j.jappgeo.2019.02.009

19. *Hosseini K.A., Hosseini M., Jafari M.K., Hosseinioon S.* (2009) Recognition of Vulnerable Urban Fabrics in Earthquake Zones: A Case Study of the Tehran Metropolitan Area, JSEE, Winter, Vol. 10, No. 4.

20. *Oynakov E., Ivanov R., Aleksandrova I., Milkov J., Popova M.* (2023) Evaluation of the Nakamura Vulnerability Index of a Cast-in-Situ Reinforced-Concrete Building from Ambient Noise Records. Environmental Protection and Disaster Risks (pp.66-76). DOI:10.1007/978-3-031-26754-3_6

ON THE ISSUE OF SEISMIC RISK IN THE TERRITORY OF BATKEN, KYRGYZSTAN

Kamchybekov M.P.[1], Yegemberdiyeva K.A.[1], Murataliev N.M.[1]

[1]Institute of Seismology NAS KR, Bishkek, Kyrgyzstan

E-mail: kis@mail.kg

Abstract: *The territory of Batken oblas tis one of the seismically active regions of Kyrgyzstan, which has a high seismic potential, which is confirmed with the data on strong earthquakes of the historical past.*

For seismic risk tasks in Batken city, the work was carried out to determine the types of buildings based on a visual inspection of residential buildings. The results of the performed typification served as the initial data for calculating vulnerability and assessing seismic risk. The predominant type on the EMS-98 scale are wood lodges (WL) of the "synch" type (wooden frame structure), accounting for 43% of the housing stock. Unreinforced masonry buildings (URML) are also typical. They make up 29%. One-story adobe buildings are in third place, i.e. 18%. Charts of victims at different times and in different areas of the city were compiled. It should be noted that urban areas are highly vulnerable, since prefabricated houses and reinforced masonry buildings constitute a small percentage, making up 10% of the total housing stock. The work provides a seismic risk map for the territory of Batken city, where areas with the corresponding level of destruction are marked.

Determining the seismic risk for a given city is not only of interest for predicting the economic impacts of future earthquakes, but may also have implications for risk mitigation. Seismic loss results can be used to develop retrofit plans for various types of structural designs with a view to improve their seismic performance.

Key words*: seismic hazard, seismic risk, vulnerability, seismic losses.*

1. Introduction

Over the past few decades, damage from natural disasters has increased dramatically throughout the world. There are many reasons for the increase in seismic losses, and these certainly include the growth of the world population, the emergence and development of new megacities, many of which are located in areas of increased seismic hazard, high vulnerability and risk/

The territory of Batken oblast is one of the seismically active regions of Kyrgyzstan, which has a high seismic potential, which is confirmed with data on strong earthquakes of the historical past,

the South Fergana Fault passing through this area – the main tectonic element that determines its high seismogenicity [7],

Scientists first separated the concepts of "seismic risk" and "seismic hazard" in 1972 at the Sixth European Congress on Seismic Engineering [1,2]. As is known, seismic hazard is understood as the frequency of occurrence of certain earthquake intensities, and risk is the negative consequences for humans and the environment from the effects of seismic vibrations.

The seismic impact on certain areas depends on many factors, such as the terrain and slope of the area, engineering-geological, hydrogeological conditions and tectonic structure. These factors have a great influence on the vulnerability of buildings and engineering infrastructure, and taking them into account on the intensity of seismic manifestations is the most important and pressing issue of assessing seismic hazard and seismic risk.

Irrational use of land in large settlements significantly contributes to the vulnerability of urban structures and increases seismic risks for buildings, the population and the territory as a whole. The seismic vulnerability of a structure is its susceptibility to damage from ground shaking of a given intensity. The purpose of vulnerability assessment is to obtain the probability of a given level of damage to a given type of building as a result of seismic impacts [3-6].

The various scales that currently exist are necessary to assess the consequences of seismic impacts and how a construction project will behave during an earthquake, i.e. rank buildings and structures according to seismic resistance and degree of destruction. They help in defining methodologies for predicting losses and seismic risk. In this work, we used the European modernized EMS-98 scale [17].

The European modernized EMS-98 scale distinguishes structural vulnerability into 6 classes: from high – class A, to low – class F. Masonry buildings correspond mainly to vulnerability class A, up to reinforced concrete buildings, metal buildings – classes from D to F.

In order to divide residential buildings into appropriate classes in urban areas, their certification is performed. In turn, these classes can be divided into subclasses depending on their physical and mechanical characteristics, such as the main load-bearing system, architectural components, construction materials, service life of the structure, etc. The certification of buildings and structures includes the following points: dividing the city territory under study into zones or sections; classification of objects within each zone or area; determining the number of objects of each class in each zone or area; determination of the vulnerability function of objects of each class.

In Batken city, the work has been carried out to determine the types of buildings based on a visual inspection of residential buildings. Residential buildings in the city are represented mainly with one-story adobe houses of the "synch" type (wooden frame structure), which, according to the EMS-98 scale, are relatively earthquake-resistant, some are made of brick, as well as four-story brick and large-panel residential buildings. The design of the synch house consists of strengthening the corners of the walls with wooden posts with clay filling of the walls. Multi-storey residential buildings are located in the city center, while the private sector covers the rest of the urban area. In the structure of urban development, the share of adobe non-earthquake-resistant houses makes up the majority.

2. Results

The results of the performed typification served as the initial data for calculating vulnerability and assessing seismic risk. In the housing stock of Batken city, brick buildings have a small percentage; for the most part, the rest of the residential buildings in the city are "synch" type houses. An analysis of the seismic resistance of buildings according to EMS-98 classifications showed that the share of earthquake-resistant buildings in the city's housing stock is of a small percentage.

Figure 1 shows the territory of Batken city divided into separate sectors. The division was made as follows: multi-storey residential buildings were taken into one sector, areas with well-built private houses were collected into other sectors, areas of new buildings with sparse residential buildings and dense buildings were also included in separate areas.

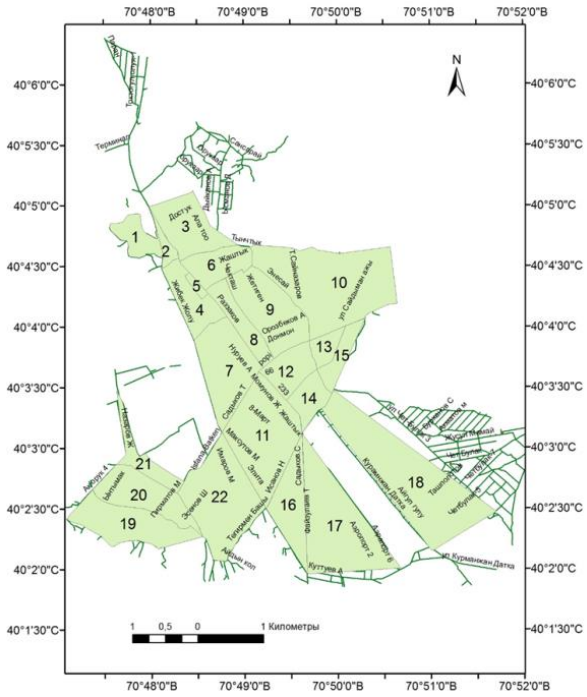

Figure 1**. - Division of the territory of Batken city into sectors.**

Figure 2 shows the number of buildings for each of the available typologies. As can be seen, the predominant typology on EMS-98 scale are wood lodges (WL) of the "synch" type, constituting 43% of the housing stock and located mainly in geo-units 7, 11 and 18. Unreinforced masonry buildings (URML) are also typical. They make up 29% and are mostly located in sectors 7, 11 and 22. And finally, one-story adobe buildings are in the third place – 18%, and are most concentrated in geo-units 7, 11 and 22. It should be assumed that the urban area is highly vulnerable, since prefabricated houses and reinforced masonry buildings make up only a small percentage, i.e. 10% of the total housing stock. In order to calculate and build the following graphs, the [8-16,18] technique was used.

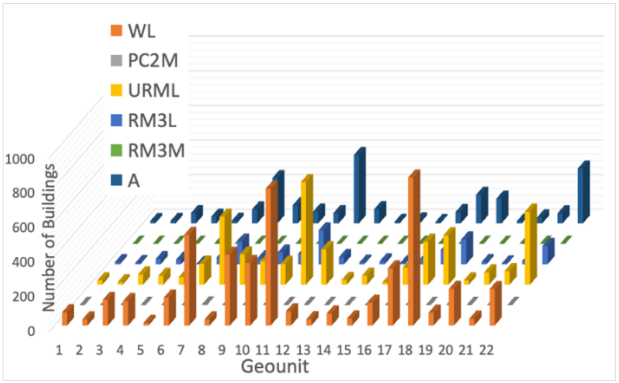

Figure 2. **- Distribution of buildings in Batken by building typology for each geocell**.

During seismic shocks, the population receives various injuries and damage from the debris of destroyed buildings and structures. The intensity of destruction depends on the probability of buildings receiving the appropriate degree of damage [2].

During destructive earthquakes, depending on the type and the corresponding degree of damage to the building, human losses also occur, such as general, sanitary and irrevocable. And, thus, there is a possibility that people will receive a corresponding degree of damage, provided that such a degree of damage to the building has occurred [1,5].

Figure 3 shows the distribution of population of Batken city by sector. The population of Batken city is distributed mainly in sectors or geo-units 7, 11, 18 and 22, which are also geo-units with higher vulnerability [18].

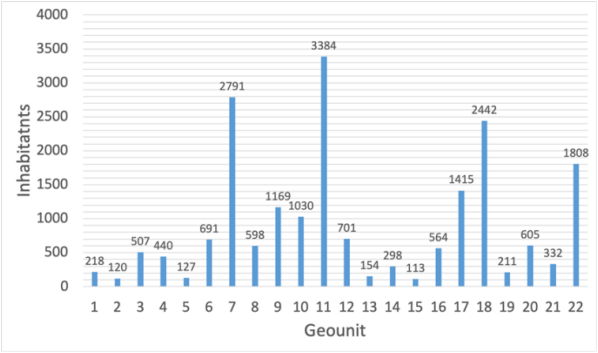

Figure 3. - **Population distribution in each geo-unit or sector.**

When predicting damage to people in a residential building, the distribution function of people in the building during the time of day is taken into account. For residential buildings, it can be assumed that during sleep this function is equal to 1, during working hours – 0.75, while people are traveling to their place of work – 0.60 and 0.70 when traveling from work [5].

With the value of peak ground acceleration PGA=0.53g, using the methodology [18], based on theoretical conclusions and calculations [8-16], we obtain results on the number of victims at different times of the day in different sectors (Figure 4-7):

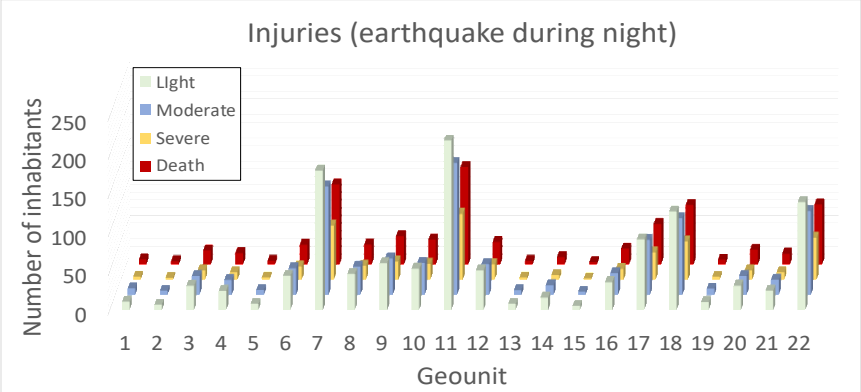

Figure 4. - **The number of victims at night.**

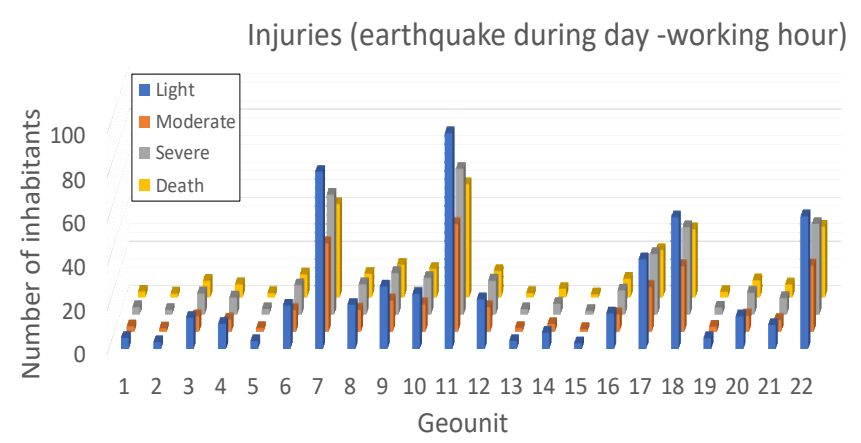

Figure 5. - **The number of victims during daytime working hours**.

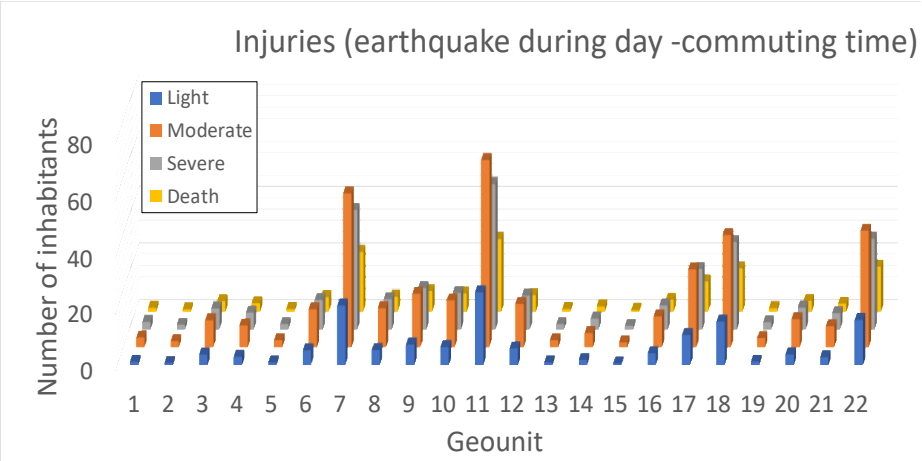

Figure 6. - **The number of victims on the way to and from work.**

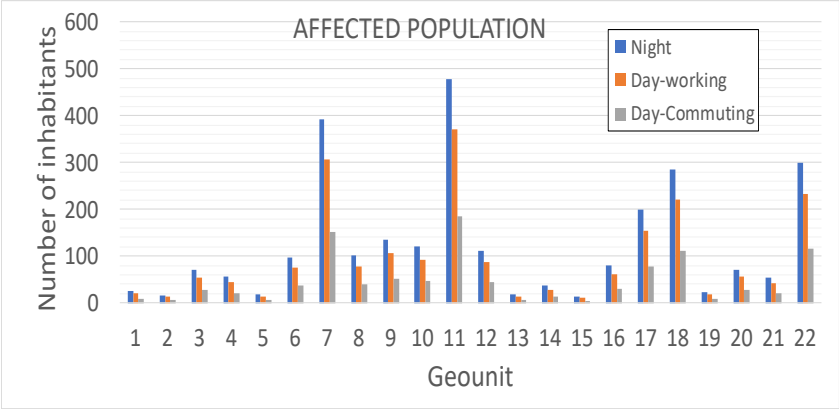

Figure 7. - **The number of victims at night, during daytime working hours and on the way to and from work.**

As can be seen from the figures above, the largest number of victims both during the day, at night, and during working hours, on the way to and from work, occurs in sectors 7, 11, 18 and 22. Geounits 7, 11, 18 and 22 are the territories with the largest number affected population.

The consequences of a predicted earthquake given the initial data and this seismic risk model are presented in Figure 8.

In sectors 7, 11, 18, 22 – synch residential buildings, non-seismic resistant, in sections 5, 6, 8 houses, mainly adobe, old construction, which are more than 50 years old, will be subject to greater destruction under seismic impacts compared to other areas of the territory of the city. All these areas are located in the 8-point zone according to the seismic microzoning map of the city with the groundwater level from 8 to 1 meter to the north according to the map of groundwater depths.

According to the results of seismic risk assessment, these sectors are found to have a large percentage of seismic risk – 35%.

Since in sectors 6,9,12,13,16,21 there are also partially old adobe houses, they increase the seismic risk of these areas up to 30%. In sectors 14, 17 there are also structures of adobe houses and the percentage of seismic risk is 25%. Sectors 2, 15 will have a 20% risk of destruction from seismic impacts. In sectors 1,3,4,10,19,20 of the city there are also adobe houses, which contribute 15% risk of destruction in this seismic risk assessment.

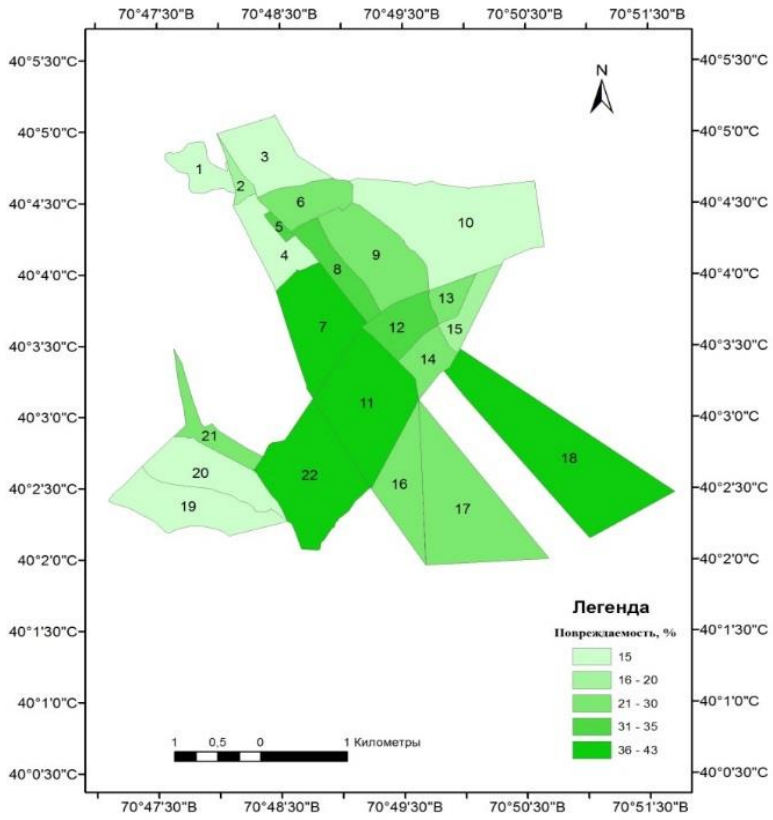

Figure 8. - **Seismic risk map of the territory of Batken city.**

3. Conclusions

Determining the seismic risk for a given region is not only of interest for predicting the economic consequences of future earthquakes, but may also have implications for risk mitigation. Loss assessments that predict damage to the built (man-made) environment can be particularly important for government emergency response and disaster planning. In addition, the results of seismic damage assessment can be used to reduce seismic risk by adjusting seismic standards when designing new buildings and structures, attracting additional funds to ensure the seismic resistance of buildings and structures, while quantitatively comparing them with potential losses that can subsequently be avoided. In addition, seismic loss results can be used to develop retrofit plans for various types of structural schemes to improve their seismic performance.

References

1. *Aleksandrov A.A., Larionov V.I., Sushchev S.P., Frolova N.I., Gumerov A.K.* Methods for analyzing seismic risk for the population and urbanized areas // Bulletin of MSTU named after N.E. Bauman. Natural Sciences Series – 2015. No. 2. - pp. 110-124.
2. *Akatiev V.A., Metelkin E.V., Nigmetov G.M.* Methods and tools for assessing and reducing seismic risk. Review // Technosphere Security. - 2016. No.5. – pp. 75-86.
3. *Aptikaev F.F., Gitis V.G., Koff G.L., Frolova N.I.* Seismic hazard and seismic risk assessment. M.: Testing, Certification and Metrology Center. – 1997. – pp. 53.
4. *Larionov V.I., Sushchev S.P., Akatiev V.A.* Vulnerability of engineering structures during earthquakes // Encyclopedia of Safety: Construction, Industry and Ecology. T. 3: Seismic resistance and thermal protection of structures / Edited by V.A. Kotliarevskii. - M.: ASV Publishing House, 2010. - pp. 165–184.
5. *Larionov V.I., Nigmetov G.M., Sushchev S.P., Ugarov A.N., Frolova N.I.* Assessment of vulnerability and seismic risk using GIS technologies from the occurrence of instability of the soil foundations of buildings during earthquakes / / Earthquake-resistant construction. 1999. - No. 2(22). pp. 23-28.
6. *Kamchybekov M.P. Egemberdieva K.A. Murataliev N.M.* Seismic risk of the territory of Batken city // Bulletin of the Institute of Seismology of the National Academy of Sciences of the Kyrgyz Republic. #1(23), 2024 – pp. 30-38.

7. *Kamchybekov M.P. Egemberdieva K.A. Murataliev N.M.* On the question of the macroseismic investigation of consequences of the Isfara-Batken earthquake, january 31, 1977 // Bulletin of the Institute of Seismology of the National Academy of Sciences of the Kyrgyz Republic. #2(22), 2023 – pp. 23-28.
8. *Calvi G.M., Pinho R., Magenes G., Bommer J.J.,* Restrepo-Vélez L.F and Crowley H. Development of seismic vulnerability assessment methodologies over the past 30 years. // ISET Journal of Earthquake Technology, Paper No. 472, Vol. 43, No. 3. – 2006. - pp. 75-104.
9. FEMA 273 (1996). NEHRP guidelines for the seismic rehabilitation of buildings. Federal Emergency Management Agency, Washington DC, USA
10. FEMA 440 (2005). Improvement of nonlinear static seismic analysis procedures. Federal Emergency Management Agency, Washington DC, USA
11. Federal Emergency Management Agency (FEMA). 2017. Hazus Estimated Annualized Earthquake Losses for the United States, Federal Emergency Management Agency Publication (April): P-366.
12. https://www.fema.gov/media-library-data/1497362829336 7831a863fd9c5490379b28409d541efe/FEMAP-366_2017.pdf
13. Federal Emergency Management Agency (FEMA). 2019. Hazus Earthquake Model, FEMA Standard Operating Procedure for Hazus Earthquake Data Preparation and Scenario Analysis. Federal Emergency Management Agency (May).
14. *Fajfar P.* (1996). Design spectra for the new generation of codes. Proceedings of the 11th World Conference on Earthquake Engineering, Acapulco; paper No. 2127
15. *Cattari S, Degli Abbati S, Ferretti D, Lagomarsino S, Ottonelli D, Tralli A* (2014) Damage assessment of fortresses after the 2012 Emilia earthquake (Italy). Bull Earthq Eng. 12(5):2333–2365 doi:10.1007/s10518-013-9520-x
16. *Gencturk, B. Elnashai, A.S. and Song, J. et al., (*2007). Fragility Relationships for populations of buildings based on inelastic response. Department of Civil and Environmental Engineering, University of Illinois at Urbana-Champaign. 194 p (http://mae.cee.illinois.edu/publications/reports/Report07-18.pdf)
17. *Grunthal, G.* European Macroseismic Scale 1998. Cahiers du Centre Européen de Géodynamique et de Séismologie 1998; Vol.15, pp.1-99.
18. *Molina S., Lang, D.H. and Lindholm, C.D*. (2010). SELENA - An open-source-tool for seismic risk and loss assessment using a logic tree computation procedure. Computers and Geosciences, 36, 257-269. http://dx.doi.org/10.1016/j.cageo.2009.07.006.

CLUSTERING THE DISTRIBUTION OF EARTHQUAKES NEAR RESERVOIRS

Khamidov L.A.[1], Anvarova S.G.[1], Ganieva B.R.[1]

[1]*Institute of Seismology named after G.A. Mavlyanov, Tashkent, Uzbekistan*

E-mail: sadokat.anvarova@mail.ru

Abstract. *The work determined the spatiotemporal distribution of background and extra-background seismic processes in tectonic faults of the earth's crust in areas near the Charvak, Andijan, Akhangaran and Karkidon reservoirs of Uzbekistan. In the clusters allocated for the reservoir zones, in each cycle there is a period of seismic activation, a peak of seismic activation, a period of decline in seismic activation and a period of seismic quiescence. The manifestations of changes in weak seismicity in different seismically active zones and geological structures in the local territory of the zones of influence of large reservoirs in Eastern Uzbekistan are considered. This will create the possibility of simultaneous tracking of seismic cycles of different periods across clusters in fault zones, combining them with variations in the hydrological regime of operation of reservoirs. It will also make it possible to assess the level of seismicity caused by these reservoirs in the area under consideration at a given time interval.*

Keywords: *catalogue, reservoir, cluster, earthquakes, magnitude*

1. Introduction

In the near zones of large reservoirs in Uzbekistan, earthquake epicenters are distributed extremely unevenly over the surface of the earth's crust. In some parts, called seismic zones, earthquakes occur frequently and very strong earthquakes can occur there. But in most of these areas earthquakes do not occur, or occur with weak strength. Such areas are called conditionally and can be called aseismic. Seismic zones, as a rule, are located along narrow extended belts. As a rule, the focus of attention of seismologists is on strong earthquakes, but within the framework of the study of technogenic seismicity, studies of weak earthquakes are also of great interest [1]. Unlike strong earthquakes, weak earthquakes occur more often and carry quite extensive information about the tectonic processes occurring in the focal zones of the strongest earthquakes.

Therefore, the main goal of the research is to present the structure of weak seismicity in Eastern Uzbekistan, where the Charvak, Andijan, Akhangaran and Karkidon reservoirs are operated.

Considering the manifestations of changes in weak seismicity of various seismically active zones or geological structures in local territories of the near zones of large reservoirs in Uzbekistan, it turned out that they can be caused both by changes in the local stress fields constantly operating in them, and by the formation and occurrence of the deformation influence of exploited man-made objects [2 ,3,4]. Consequently, the possibility of identifying weak seismic processes in tectonic faults of the earth's crust in zones of influence of reservoirs and studying the features of its manifestation is relevant when studying seismicity caused by reservoirs.

2. Methodology

The local catalog we compiled for each object was taken as the initial database. They are quite homogeneous for weak earthquakes and allow both the determination of the displacement of the earth's crust caused by the reservoir and the statistical analysis of seismic data [5, 6]. These studies were carried out by clustering the distribution of earthquakes in zones of tectonic faults in the zones of influence of the considered reservoirs and by numerical methods for modeling the process of water loading and unloading of reservoirs, solving boundary value problems of mathematical physics [4,6,7]. An analysis of works devoted to the study of seismic manifestations in the territories of the Andijan, Charvak, Akhangaran and Karkidon reservoirs of Eastern Uzbekistan indicates the absence of a single local catalog for the study areas. In this regard, based on available literature data, we formed our own database for the period 2011-2023, which includes more than 2300 seismic events. To compile the local catalog, the following platforms were used: the earthquake catalog of the Republican Center for Seismic Forecasting Monitoring under the Ministry of Emergency Situations of the Republic of Uzbekistan [8], the Experimental Methodological Expedition of the National Nuclear Center of the Republic of Kazakhstan [9], the Unified Geophysical Service of the Russian Academy of Sciences of Russia [10], the Data Center "United Research Institutes" seismology" IRIS [11].

Information about the studied reservoirs of Eastern Uzbekistan, for which catalogs of local earthquakes have been compiled, is shown from the website of the Ministry of Water Resources of the Republic of Uzbekistan (https://suvchi.gov.uz/ru) in Table 1.

Table 1

Information about the studied reservoirs of Eastern Uzbekistan, for which catalogs of local earthquakes have been compiled

№	Name of reservoirs	Year of entry, year	Volume, million m^3	Dam		Seismicity, in points
				Height, m	Length, m	
Eastern Uzbekistan						
1	Andijan	1970	1900	121	850	8-9
2	Charvak	1978	2006	168	764	8-9
3	Akhangaran	1989	198,0	100	1933	8
4	Karkidon	1967	218,4	70,3	420,2	8

The results of seismic monitoring for all of these observation systems are summarized in the form of a separate catalog of earthquakes, which indicates the date and time of the earthquake, the location of the epicenter, the depth of the source, the magnitude or energy class, the distance from the reservoir site to the epicenter, as well as some other parameters of the earthquake.

When compiling the catalog of local earthquakes, only those data on earthquakes were included that exactly corresponded in all respects to at least three of the four seismometric sources listed above. Based on these data and earthquake catalogs, we have compiled a local catalog of earthquakes for the zones of influence of reservoirs in Eastern Uzbekistan. The local catalog of earthquakes in the zone of influence of the reservoirs of Eastern Uzbekistan was prepared in the EXEL environment and laid entirely in the Arc.Gis environment and is available in the IS fund of the Academy of Sciences of the Republic of Uzbekistan. Empirical formulas for the recurrence of earthquakes within active tectonic faults in the zones of influence of reservoirs in Eastern Uzbekistan have been determined (Table 2).

Table 2

Empirical formulas for the recurrence of earthquakes within active structures in the zones of influence of reservoirs in Eastern Uzbekistan

№	Reservoirs	Empirical formulas	Reliability of approximation
1	Andijan	lgN = -0,9384M + 5,3716	R^2 = 0,9912
2	Charvak	lgN = -0,9692M + 4,9882	R^2 = 0,9819
3	Akhangaran	lgN = -0,9548M + 4,9511	R^2 = 0,9514
4	Karkidon	lgN= -0,9681M + 5,4796	R^2 = 0,966

Accordingly, based on the values of the coefficients, it can be noted that the frequency of earthquakes in the above-mentioned zones may have a fractal dimension. The distribution of earthquakes for the period under study for each object shows the density of the sources closer to the zones of active tectonic structures. Therefore, the spatio-temporal distribution of earthquakes in the reservoir zones of Eastern Uzbekistan has been constructed. The method proposed by F.Waldhauser and W.L.Ellsworth was used [12]. To further analyze the characteristics of earthquakes, as in previous studies [2,5,6], we used the nearest neighbours method to conduct cluster analysis [13]. In this method, the similarity is determined by the square, Euclidean distance. The best results can be obtained according to [14,15], when the threshold value $d=d_0^2$ of the square of the Euclidean distance $(x_2-x_1)^2+(y_2-y_1)^2$ is taken equal to $1xM^2$ to $1,2xM^2$ km (M-magnitude). After clustering, earthquakes are divided by the number of compactions of epicenters as clusters, taking into account the fact that earthquakes are distributed non-uniformly in time.

3. Results and discussion

The spatiotemporal distribution of clusters across the zone of influence of the Andijan reservoir is shown in Figure 1a. When comparing with tectonic structures, we used clippings from the tectonic map of Uzbekistan and adjacent territories, developed by the Laboratory of Neotectonics and Geodynamics of the Geological Institute of the Russian Academy of Sciences (clipping in Figure 1b) [16].

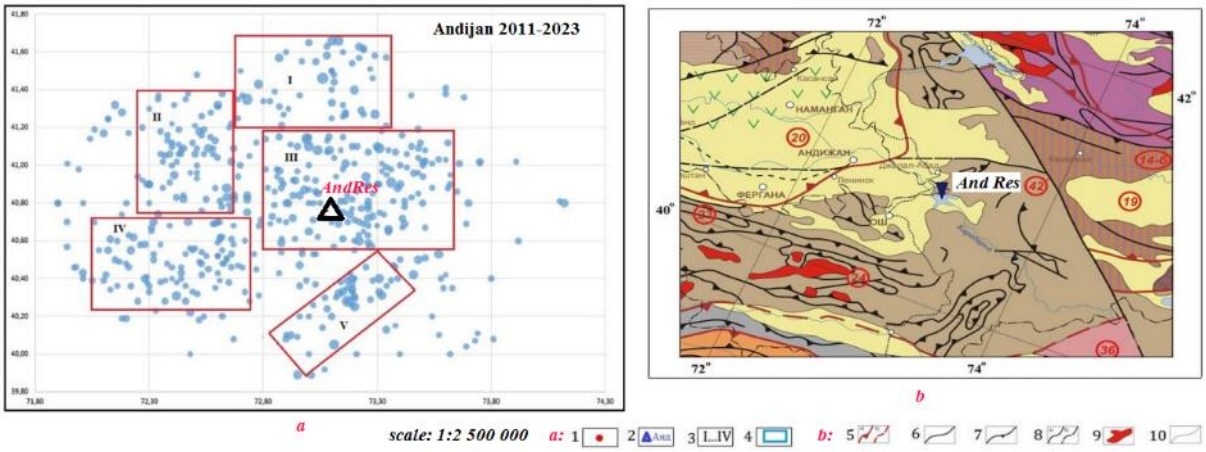

Legend: **a:** 1 - epicenters of earthquakes with M≥2.5 for the period 2011-2023; 2- location of the reservoir; 3-clusters identified by the nearest neighbors method [15]; 4- dedicated clusters; **b:** 5- sutures; 6- shifts; 7- thrusts; 8- major faults; 9- granitoids; 10- boundaries between structural elements

Figure 1 - **Spatio-temporal distribution of earthquakes by clusters in the Andijan reservoir zone and comparison with the structures in the cutout of the map "Tectonic map of Uzbekistan and adjacent territories [16]"**

The spatiotemporal distribution of clusters across the zone of influence of the Charvak reservoir is shown in Figure 2a.

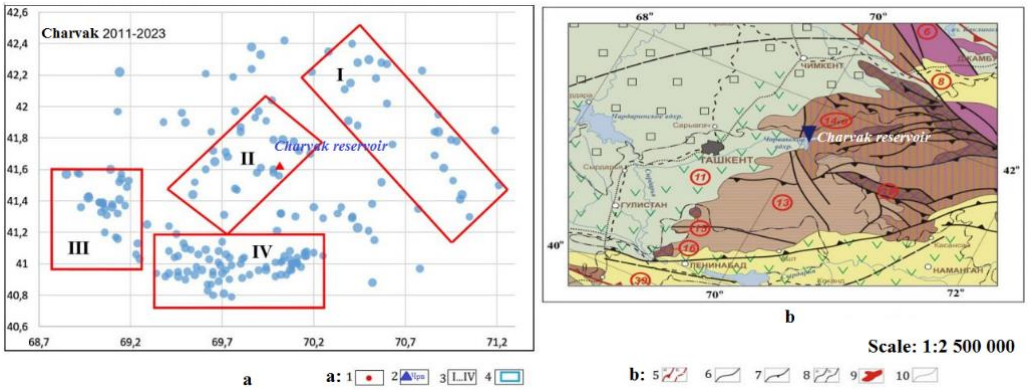

Legend: the same as in Fig. 1

Figure 2 – **Spatio-temporal distribution of earthquakes by clusters in the Charvak reservoir zone and comparison with structures in the map cutout from [16]**

The spatiotemporal distribution of clusters across the zone of influence of the Akhangaran reservoir is shown in Figure 3a.

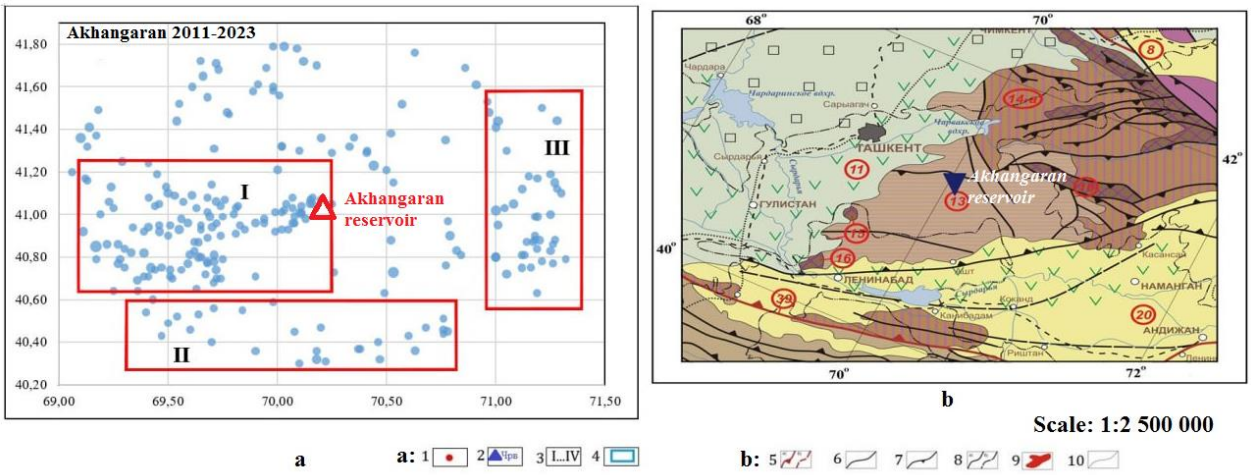

Legend: the same as in Fig. 1

Figure 3. - **Spatio-temporal distribution of earthquakes by clusters in the area of the Akhangaran reservoir and comparison with the structures in the cutout of the map "Tectonic map of Uzbekistan and adjacent territories [16]"**

The spatiotemporal distribution of clusters across the zone of influence of the Karkidon reservoir is shown in Figure 4a.

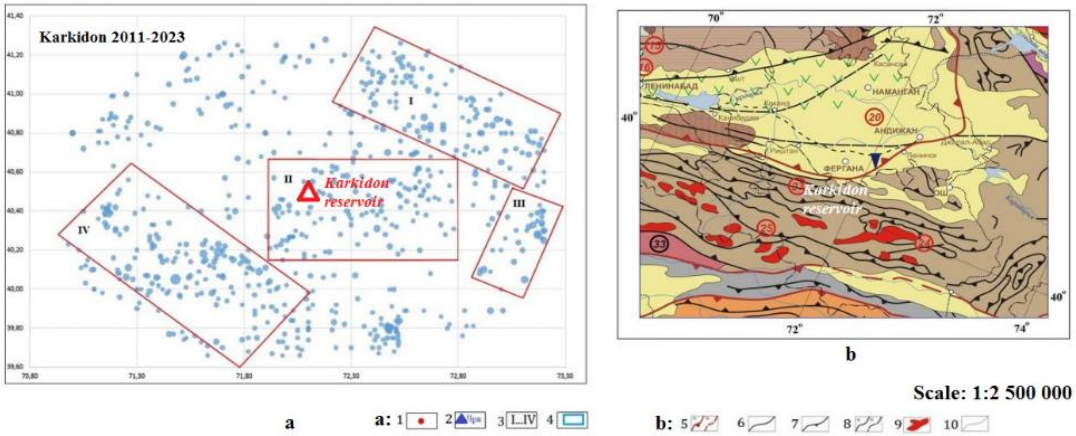

Legend: the same as in Fig. 1

Figure 4 - **Spatio-temporal distribution of earthquakes by clusters in the Karkidon reservoir zone and comparison with structures in the cutout of the map "Tectonic map of Uzbekistan and adjacent territories [19]"**

The sequence of earthquakes in the zone of the Andijan, Charvak, Akhangaran and Karkidon reservoirs is considered from the perspective of the geodynamics of the Chatkal-Kurama and Fergana valleys of the Western Tien Shan orogen.

Examples of the sequence of earthquakes [17,18] with $M \geq 2.5$ or $M \geq 3$ in the area of the Andijan, Charvak, Akhangaran and Karkidon reservoirs are shown by cluster in Figures 5,6,7,8 below.

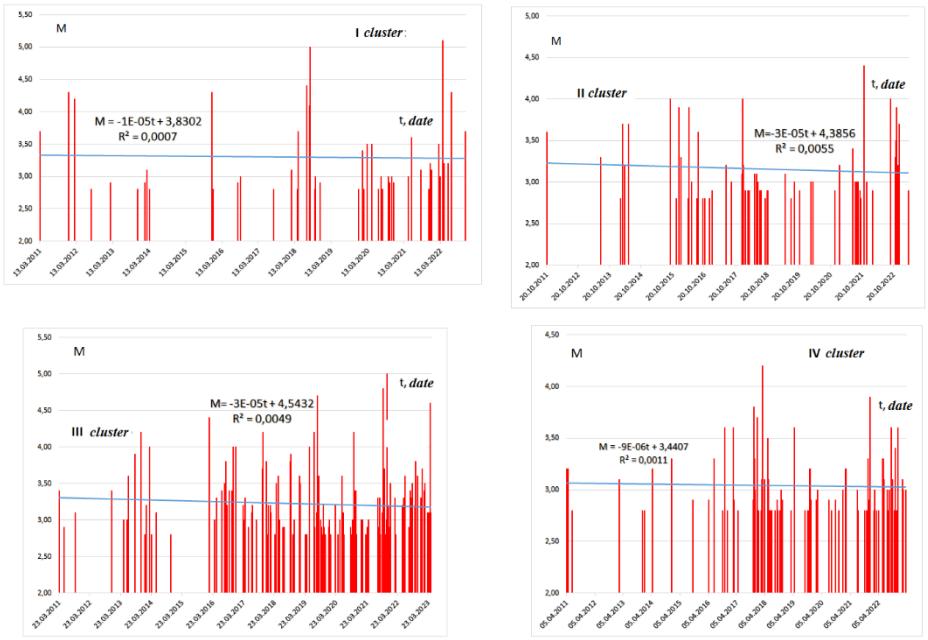

Figure 5 - **Sequence of occurrence of earthquakes with M≥2.5 in the Andijan reservoir area for each cluster**

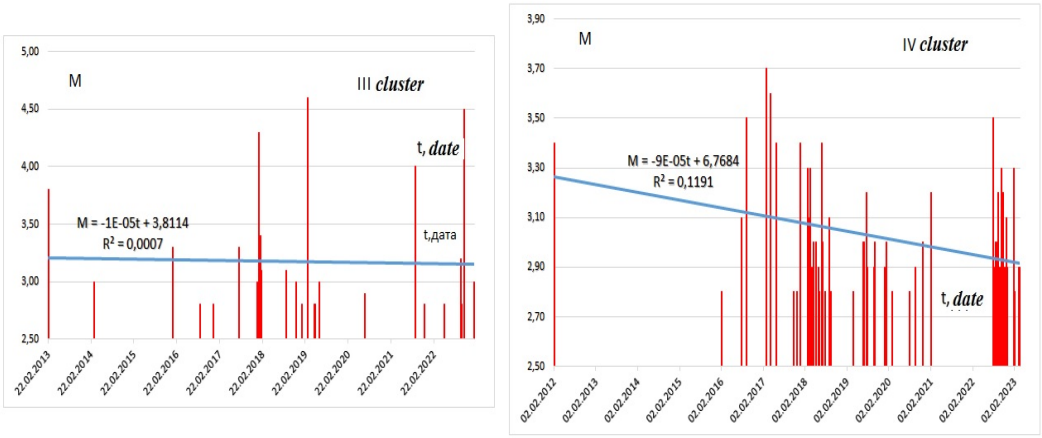

Figure 6 - **Sequence of occurrence of earthquakes with M≥2.5 in the Charvak reservoir zone for each cluster**

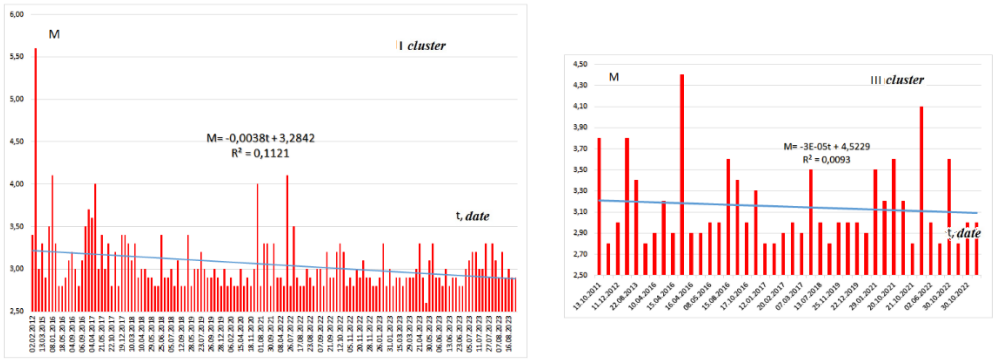

Figure 7 - **Sequence of occurrence of earthquakes with M≥2.5 in the Akhangaran reservoir zone for each cluster**

According to Pradeep Talwani, in most cases of reservoir-induced seismicity, the seismicity follows flooding, large changes in the reservoir level, or its filling at a later time above the highest water level reached at that time [19]. This is classified as initial seismicity. This “initial seismicity” is explained by the coupled response of the reservoir to initial filling or changes in water level. It is characterized by an increase in seismicity above pre-flood levels, a major event, general stabilization,

and a lack of seismicity in the zone of influence of the reservoir. It is characterized by widespread seismicity on the periphery, migrating outward in one or several directions of nearby faults. Over time, the number and strength of earthquakes decrease, and seismicity returns to the background level that was before the reservoir was flooded [2,19]. Preliminary results of two-dimensional (similar to E.A. Roeloffs [20]) calculations suggest that this "long-term seismicity" depends on the frequency and amplitude of changes in lake level, reservoir size and foundation properties.

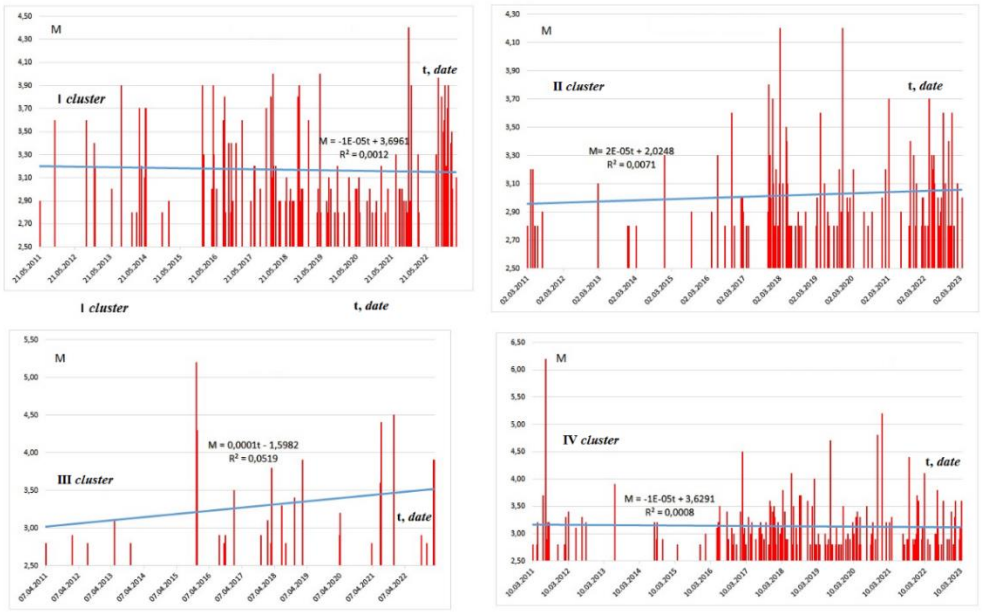

Figure 8 - **Sequence of occurrence of earthquakes with M≥2.5 in the Karkidon reservoir zone for each cluster**

Changes in force show delays relative to changes in lake level. Longer-term changes in water level (1 year) are more likely to cause deeper and stronger earthquakes than short-term changes in water level [7,20]. Earthquakes occur in reservoirs where lake level changes are comparable to or account for most of the shallowest water depth. Seismicity is likely to be more widespread and deeper in a larger reservoir than in a smaller one [21]. Induced seismicity is observed both in faults beneath the deepest part of the reservoir and in surrounding areas. It manifests itself as outside the background or additional seismicity in relation to the seismicity that existed before the operation of the object. The location of seismicity is determined by the nature of the faults below and near the reservoirs.

4. Conclusions

As can be seen from Figures 5,6,7 and 8, after an earthquake with a certain large energy class for each cluster, periods of seismic calm occur. It is expressed by lower energy classes or the absence of earthquakes in the studied area of each cluster.

Based on the sequences of occurrence of earthquakes with K≥8 within the zones of the identified clusters in the zones of the Andijan, Charvak, Akhangaran and Karkidon reservoirs, it can be noted that it increases the density of earthquakes in zones of close tectonic structures (Figures 1,2.3,4).

Consequently, in the sequence of occurrence of weak earthquakes in the zones of influence of the Andijan, Charvak, Akhangaran and Karkidon reservoirs located near tectonic faults, a local loading or unloading regime is observed.

In the clusters allocated for the zones of the Andijan, Charvak, Akhangaran and Karkidon reservoirs, in each cycle a period of seismic activation, a peak of seismic activation, a period of decline in seismic activation and a period of seismic quiescence can be observed.

5. Acknowledgements

The authors express their deep gratitude to the Presidium of the Academy of Sciences of the Republic of Uzbekistan and the leadership of the Institute of Seismology named after G. O. Mavlonov for organizing the financial support of these studies from the budget. In addition, the authors express

their gratitude to the editors and reviewers who actively worked in preparing the article for publication.

References

1. *Saltykov V.A., Kravchenko N.M.* Parameters of Kamchatka seismicity in 2008 // Geodynamics & Tectonophysics. 2010. Vol. 1. № 2. P. 186–196. https://doi.org/10.5800/GT-2010-1-2-0014
2. *LKhamidov, F. Artikov, Kh.Khamidov, B.Ganieva and S.Anvarova* Seismicity caused by the hydrological regime of large reservoirs.// CONMECHYDRO – 2022.- J. E3S Web of Conferences 365, 03043 (2023).-P.1-11. https://doi.org/10.1051/e3sconf/202336503043
3. 3.. *El Hariri, M., R. A. Abercrombie, C. A. Rowe, and A. F. do Nascimento* (2010). The role of fluids in triggering earthquakes: Observations from reservoir induced seismicity in Brazil, Geophys. J. Int. 181, no. 3, P.1566–1574, doi: 10.1111/j.1365-246X.2010.04554.x.
4. *Khamidov L.A.* Stress relief during earthquakes occurring in faults around reservoirs in Southern Uzbekistan (in Russian) // Reports of the Academy of Sciences of the Republic of Uzbekistan, No. 4, 2023 - Tashkent. S.103.109. https://academy.uz/uz/journals/maruzalar
5. *Khamidov L.A., Adilov K.A.* Determination of the displacement of the earth's crust caused by a reservoir (in Russian) // International scientific and practical conference "Rakhmatulin Readings", May 26-27, 2023, Tashkent, National University named after A.R. Beruni. -WITH. 34-35.
6. *Anvarova S.G., Ganieva B.R., Artikov F.R.* Local catalog of earthquakes in the near zone of large reservoirs in Central and Southern Uzbekistan (in Russian) // Tr. XXIV-Ural Youth Scientific School in Geophysics - UMSHG-2023, Perm, March 22-24, 2023.-Perm.-Russia.-2023.-P.3-7.
7. *Anvarova S.G., Khamidov L.A.* Sequence of manifestation of earthquakes with M≥3 in the zone of influence of the Akhangaran reservoir of Uzbekistan (in Russian) // XXV Ural Youth Scientific School in Geophysics." Collection of scientific materials. Ekaterinburg, March 25-29, 2024. pp. 9-13.
8. Catalog of earthquakes from 2018 to 2023 of the Republican Center for Seismic Forecasting Monitoring (RCSM) under the Ministry of Emergency Situations of the Republic of Uzbekistan: URL: https://rcsm.fvv.uz/ru/catalog_col .
9. Catalog of earthquakes of the Experimental Methodological Expedition of the National Nuclear Center of the Republic of Kazakhstan (electronic resource) – URL: http://www.kndc.kz/index.php/ru/sejsmicheskie-byulleteni/interactive-bulletin.
10. Catalog of earthquakes of the Unified Geophysical Service of the Russian Academy of Sciences of Russia (in Russian) - (electronic resource) (электронный ресурс) – URL: http://ceme.gsras.ru/ceme/ssd_news.html.
11. Catalog of earthquakes of the data center "United Research Institutes of Seismology" IRIS (electronic resource) – URL: http://ds.iris.edu/wilber3/find_event.
12. F. *Waldhauser, W.L. Ellsworth, A* double-difference earthquake location algorithm: method and application to the Northern Hayward Fault // California, Bull. Seism. Soc. Am. 90 (6) (2000) 1353-1368.
13. *J.W.Han, K. Micheline, J. Pei.* Cluster analysis Data Mining, (Third ed.)// 2012, pp. 443-495.
14. *L.Zhang, J.Li, G.Wei, W.Liao, Q.Wang, Ch.Xiang* Analysis of the relationship between water level fluctuation and seismicity in the Three Gorges Reservoir (China) // Geodesy and Geodynamics.- vol.8.- (2017) P.96-102.
15. *J.W.Han, K. Micheline, J. Pei.* Cluster analysis Data Mining, (Third ed.)// 2012, pp. 443-495.
16. Tectonic map of Uzbekistan and adjacent territories // Geological Institute of the Russian Academy of Sciences, lab. Neotectonics and modern geodynamics. Moscow. (in Russian) - 2004.
17. *Kasahara K.* Mechanics of earthquakes (in Russian). – M.: Mir, – M.: Мир,1985.- 264 с.
18. *Muratalieva Zh.Z., Omuralieva A.M.* Monitoring the dynamics of seismicity within the Kemino-Chilik zone, generating earthquakes with M≥8 (in Russian). // Russian Seismological Journal. - 2020. - Vol. 2, No. 4. - P. 51–62. DOI: https://doi.org/10.35540/2686-7907.2020.4.05
19. *Pradeep Talwani (Talwani P.)* On the Nature of Reservoir-induced Seismicity// Pure and applied geophysics, Birkhäuser Vergal, Basel, 150 (1997) 473–492.
20. *Roeloffs E. A. (1988),* Fault Stability Changes Induced Beneath a Reser6oir with Cyclic Variations in Water Le6el, J. Geophys. Res. 93, 2107–2124.
21. *Simpson D.W., and Negmatullaev S. K.* (1981), Induced Seismicity at Nurek // Reser6oir, Bull.Seismol. Soc. Am. 71, 1561–1586.

SPECIAL INSPECTIONS AND TESTING FOR CONCRETE BUILDING CONSTRUCTION IN HIGH SEISMIC AREAS

Taniwangsa W. [1], Chavez J.W.[1]
[1]*Structural Engineer, California, USA*
E-mail: wtaniwangsa@gmail.com

Abstract: *Special Inspection and Testing are enforced in the current Code in high seismic areas. The enforcement of this extra step is to achieve the objective of seismic design that is to protect lives and properties during large seismic events. Combination of good structural concept, design with complete details, good quality control during construction are means to achieve resilient structures. This paper presents the importance of the Special Inspection and Testing roles applicable to the construction of reinforced concrete building structures based on USA Codes.*

Keywords: *Seismic Design, Resilient, Special Inspection and Testing, Reinforced Concrete Buildings.*

1. Introduction

Inspection and Testing are one very important part of both Quality Assurance and Quality Control programs. Inspection is a subsystem of Quality Assurance system and of a Contractor Quality Control System. Inspection may also be part of the Authority Having Jurisdiction (AHJ) to enforce legal Codes and other Regulations. Both Quality Assurance and Quality Control refer to tools or terms that can be implemented to achieve a good quality project in accordance with the construction documents and specifications.

There may be different types of inspection during construction such as:

- Regular Building Inspections –including but not limited to the inspections for footing and foundation, fire and smoke-resistant penetration, and energy inspections, etc.
- Electrical, Plumbing & Mechanical Inspections.
- Special Inspection and Testing for building construction in high seismic areas – Detail discussion shown in section 4.

Inspection includes visual observations, field measurements, laboratory testing and assembly and evaluation of the test data. An Inspection and Test Report is a document signed by a certified inspector and used to demonstrate and provide evidence of the verified attributes plus the results of the inspection/test activity performed.

Inspection and testing are used to confirm that the inspected product and process meets the criteria established and adheres to the approved plans and local building codes. Testing services are performed by Testing Laboratories that are independent commercial organizations that provide testing services and inspection personnel. All Inspection organizations/Agencies and Testing Laboratories should be accredited and approved by the Authority Having Jurisdiction (AHJ).

The information derived from the inspection and testing process, when properly evaluated and with conclusions and decisions implemented, will result in improvement of the quality of the product or process. The intended quality is achieved only by implementation of an adequate quality assurance program. Quality Control should have strong active support from top management and active concern and participation of everyone involved in the construction process.

2. Model Codes and Building Codes in USA

In the USA, a new building design or a retrofit building project needs to follow the valid Building Code at the jurisdiction where the project is located. This Local Building Code is based on an International Building Code (IBC).

The IBC comprises of a series of Model Codes, which are separate documents applicable for buildings, residential structures, electrical, mechanical, and other disciplines nation-wide. The IBC is developed by the International Code Council (ICC). The latest version of this code is from 2021, and this Model Code is updated every three years.

The IBC is not enforceable until it is adopted and/or amended by an AHJ such as a State, County and/or City. Then it becomes the Building Code for that State, County or City. It is used to specify the minimum standards that govern the design and construction of buildings and non-building structures in a given jurisdiction.

For example, the 2022 California Building Code (2022 CBC), which modifies some provisions the 2021 IBC and adds new ones is the enforceable Code for California. The CBC is considered one of the stringent codes in the USA. Cities and Counties within California adopted CBC with or without their own Amendments and enforced the adopted Code under their own jurisdictions (AHJ). The AHJs are responsible for enforcing the Building Code in issues that include:

- Permitting – checks on Design Teams
- Inspection – checks on Contractor

Aside from the model codes, there are also Standards such as the ASCE 7-16, "Minimum Design Loads and Associated Criteria for Buildings and Other Structures", and other referenced Standards such as ASCE 41, AISC 360 and AISC 341, ACI 318, etc. The Code relies on these Standards that are sets of technical definitions, specifications, and guidelines. A Code tells you what you need to do, and a Standard tells you how to do it.

When submitting a building project to the building officials in a high–seismic area for a permit, the Construction Documents (sets of drawings, set of calculations, specifications), Statement of Special Inspections and other data are required with each application. The construction documents shall be prepared by a Registered Design Professional (RDP).

3. Seismic-Resistant Design Principles

Design and construction are closely related. To have a good quality construction it is necessary first to have a superior design with buildable details. This section summarizes the current seismic design philosophies, then and now, and provides lessons or samples of earthquake damage during past earthquakes.

a. Seismic Design Philosophy

Historically, the general philosophy of seismic-resistant design for structures other than essential facilities has been well established and proposed as follows:

- To prevent non-structural damage in frequent minor ground shaking.
- To prevent structural damage and minimize non-structural damage in occasional moderate ground shaking.
- To avoid collapse or serious damage in rare major ground shaking.

The implementation of this philosophy presents in many cases serious problems particularly regarding quantifying the different types of damage (structural and non-structural) and quantifying what constitutes frequent minor, occasional moderate, and rare major earthquake ground shaking.

b. Earthquake damages can be categorized into two groups:

A. Earthquake Direct Effects:

- Ground failures or instabilities due to ground failures:

a. Surface faulting: surface or fault rupture

b. Vibration of soil or effects of seismic waves that may cause:

Ground cracking/splitting, Liquefaction, Differential settlement, Lateral spreading, and Landslides.

- Vibrations transmitted from the ground to the structure (direct ground shaking vibration).

B. Earthquake Indirect Effects or Consequential Phenomena such as:

- Tsunami, Seiches, Flood, and Fire.

The seismic effect or damage that it is usually the main concern to the structural engineer, and which is extensively considered by the code seismic-resistant design provisions, is the vibration of the structure in response to ground shaking at its foundation. Although damage due to other effects may exceed those due to vibration, procedures for considering these effects and for coping with them may be outside the scope of the structural engineering discipline and so they are usually not included or they are just slightly considered in seismic-resistant codes. Nonetheless, the structural engineer should be aware of the different seismic hazards and should advise the client of potential damage involved in locating structures at certain sites. Thus, the first step in the design procedure of a future

structure should be the evaluation of the suitability of the site selected with proper consideration for the potential of any one of the above types of damages.

c. Lesson Learned from Past Earthquakes

Field inspection and analyses of the performance of structures during past earthquake have shown that building design which blindly follows the seismic code regulations does not guarantee always safety against collapse or serious damage. The reasons for this can be summarized as follows:

1. There are large uncertainties involved in estimating the design earthquake shaking demands and predicting the response of the real three-dimensional soil-foundation-building system.
2. The performance of the building system depends on its state when the earthquake strikes - thus construction and maintenance, which includes repair, retrofitting and/or modifications, must also be considered in addition to the design aspects.
3. Design and construction of a structure are intimately related and the achievement of good workmanship depends, to a large degree, on the simplicity of the detailing of the members, their connections and supports. For example, in the case of a reinforced concrete structures, although it is possible to detail complex reinforcement on paper and even mimic them in laboratory specimens such design details in the field may not be economically feasible. A design is only effective if it can be constructed and maintained.

Samples of damage in various types of buildings both due to deficiencies in seismic design and poor workmanship during construction, and damages due to ground failures are shown below.

Examples of Damage of Masonry Structures due to direct ground shaking vibration.

Photo 1: **View of downtown Managua City, Nicaragua, after the 1972 Managua Earthquake. The debris is from the complete collapse of unreinforced masonry and adobe buildings.**

Photo 2: **The second story 8-in. unreinforced solid brick masonry walls of this commercial building in Coalinga collapsed during the 1983 Coalinga Earthquake because of inadequate tying at the floor, roof, and transverse walls.**

Photo_3a and Photo_3b: **Overview and detail of supporting column and walls at the top corner of a Commercial Building during the 2014 South Napa Earthquake. Note the remaining epoxy anchors between the diaphragm and brick walls.**

Example of Damage to Reinforced Concrete structures due to direct ground shaking vibration.

Photo_4: **Close-up of the failure of one of the shear walls in a building showing incipient types of failure at the construction joints due to poor workmanship at the joints. The failure of this particular wall did not occur at the construction joint, and it was attributed to lack of adequate axial-flexural capacity. Note the lack of any extra reinforcement at the edge of the shear walls.**

Photo_5: **Failure of Column due to inadequate shear reinforcement. These photos are taken from different earthquake events. Collapse of heavily loaded columns may cause collapse of the building. These structures were built with the original earthquake-resistant philosophy that was collapse prevention.**

Photo_6: **Collapse of an upscale apartment building during the 2023 Pazarcik earthquake. The earthquake struck before dawn. The staggering death toll was the consequence of a structural system that prioritized growth over safety.**

Photo_7: **Building Collapse during the 1971 Sylmar Earthquake. Death toll and number of injured are very high when collapse of building happen.**

Examples of Earthquake damages due to Ground failure.

Photo_8: **Collapse of Apartment Buildings due to soil liquefaction during the 1964 Niigata earthquake.**

Photo_9: **Surface rupture due to Ground shaking during the 2004 Parkfield earthquake.**

d. Current Performance-Based Seismic-Resistant Design Philosophy

Current design codes are based on satisfying conformance to prescriptive criteria in materials, configuration, detailing, strength, and stiffness with the goal of achieving certain levels of performance, such as that the structure should have less than 10% chance of collapse given the occurrence of the Maximum Considered Earthquake. However, the current design trend is to orient the design to be performance-based, where the design process is reversed by defining the end goal as the starting point. This implies identifying optimal solutions to multiple, and sometimes compelling objectives on safety, economy, serviceability, sustainability and robustness.

In both, a prescriptive or based-performance design of building structures, there are certain guidelines that can be followed in selecting an adequate building configuration structural layout, structural system, structural material, and non-structural components:

- Building (superstructure and non-structural components) should be light and unnecessary masses/weights should be avoided.
- Building superstructure should be simple, preferable symmetric, and regular in plan and elevation to prevent significant torsional forces. Large height-width ratio and large plan area should also be avoided.
- Building and its superstructure should have a uniform and continuous distribution of mass, stiffness, strength and ductility, avoiding formation of soft stories. Buildings include basement, lots of time they have “plaza” on top of basement and the “tower/superstructure” continue above the “plaza.

- Building superstructures should have preferable shorter spans and the use of long cantilevers should be avoided.
- Non-structural components could either be separated or integrated to the main structure. In the first case, it is preferable that the non-structural components be well separated from the main structure to avoid interaction between them. In the latter case, it is desirable that the structure should have sufficient lateral stiffness to avoid significant damage under minor and moderate earthquake shaking. It should also have toughness with stable hysteric behavior (that is, stability of strength, stiffness, and deformability) under the repeated reversal of deformations which could be induced by severe earthquake ground motion. The stiffer the structure, the less sensitive it will be to the effects of the interacting non-structural components, and the tougher it is, the less sensitive it will be affected by sudden failure of the interacting non-structural elements.
- Building superstructure should be detailed so that inelastic deformations can be constrained (controlled) to develop in desired regions and according to a desirable hierarchy.
- Building superstructure should have the largest possible number of defense lines, that is, it should be composed of different tough structural subsystems which interact or are interconnected by very tough structural elements (structural fuses) whose inelastic behavior would permit the whole structure to find its way out from a critical stage of dynamic response.
- Building superstructure should be provided with **balanced stiffness and strength** between its members, connections and supports.
- The stiffness and strength of the entire building should be compatible with the stiffness and strength of the soil foundation.

4. Special Inspection and Testing

a. Development and History of Special Inspection in the USA

Historically, Special Inspections and Testing started with the Uniform Building Code (UBC), which included requirements for special inspection of certain types of construction since 1937. Special inspection requirements have not always been vigorously or uniformly enforced. These requirements were conceived at a time when testing of construction materials was more prevalent and necessary due to variations in materials quality and when the labor force was less costly. Subsequently, the quality of construction materials has become more consistent while the cost of labor has risen dramatically, both in absolute terms and as a percentage of the total construction cost. The result has been a reduction in the testing of construction materials and more emphasis on inspection of the labor portion of the work.

These trends, along with periodic earthquakes in California highlighting the need for better quality control of construction, and the emergence of the International Building Code (IBC) as the national model building code have resulted in placing more attention on the special inspection requirements within the last thirty years or so. This has pushed the interest in conducting special inspection, particularly among engineers who see special inspection as an extension of their construction phase services.

b. What are Special Inspections and Testing for Seismic-Resistant Structures

Special inspection is the inspection of a construction activity requiring unique expertise or where additional assurance of quality is deemed necessary. Concrete placement, masonry construction, structural welding and high strength bolting are common special inspection items.

The requirement for special inspection, called Statement of Special Inspection needs to be submitted as part of Permit Submittal by the Register Design Professional (RDP) and it becomes part of the design documents and building permits.

There are two levels of Special Inspections: Continuous Special Inspection and Periodic Special Inspection.

Continuous Special Inspection. It is the inspection of construction or work that requires special inspection in accordance with the statement of special inspections and, due to the nature of the work, is inspected by an approved special inspector who is continuously present in the area when and where the construction or work is being performed.
Periodic Special Inspection. It is the inspection of construction or work that requires special inspection in accordance with the statement of special inspections and, due to the nature of the work, is inspected by an approved special inspector who is intermittently present in the area when and where the construction or work has been or is being performed.

c. Duties and Qualifications of Personnel for Special Inspection and Testing

i. Building Officials Duties

The building official is the authorized person to enforce the provisions of the code. The building official has the authority to render interpretations of the code and to adopt policies and procedures in order to clarify the application of its provisions.

The building official makes the required inspections, or the building official shall have the authority to accept reports (in written) of inspection by approved agencies or individuals. The building official is authorized to provide expert opinion as deemed necessary to report on unusual technical issues that arise, subject to the approval of the appointing authority.

ii. Owner or Representative Responsibility

The owner of the construction project or the engineer or architect of record, acting as the owner's agent, is the person that employs the special inspector(s). Contractors may not employ the special inspector(s) since this would constitute a conflict of interest and is not in accordance with the intent of special inspection as an independent evaluation.

iii. Special Inspectors Qualifications

A special inspector is a specially qualified person with both inspection and practical experience in the construction operation requiring special inspection. The individual must submit his qualifications to the local building official for approval. Approval is sometimes done on a case-by-case basis or is granted to local testing agencies who employ inspectors with the particular expertise. In many cases the approval is informal, based on previous experience with firms and individuals.

The International Code Council (ICC) has a certification program that includes many of the common special inspections. Also, the International Accreditation Service (IAS) has an accreditation program for special inspection agencies. Engineers may be qualified as Special Inspectors; however, an engineering degree or license does not automatically qualify a person as a special inspector.

iv. Special Inspectors Duties

The special inspector observes the work for conformance with the approved design drawings, specifications and workmanship provisions of the building code, brings discrepancies to the immediate attention of the contractor and to the design authority and the building official if not corrected. Periodic and final inspection reports are required to be submitted to the building official and engineer or architect of record.

The special inspector is considered an extension of the building official by virtue of the code requirements for inspections by the building official and special inspection. The AHJ formalizes the relationship with special inspectors in this regard, and they are called "deputy inspectors".

v. Contractor responsibility.

Each contractor responsible for the construction of a main wind- or seismic force resisting system, designated seismic system or a wind- or seismic force-resisting component listed in the statement of special inspections shall submit a written statement of responsibility to the building official and the owner or the owner's authorized agent prior to the commencement of work on the

system or component. The contractor's statement of responsibility shall contain acknowledgement of awareness of the special requirements contained in the statement of special inspections.

5. Structural Observations

Where required by the provisions, the owner or the owner's authorized agent shall employ a registered design professional to perform structural observations. The structural observer shall visually observe representative locations of structural systems, details and load paths for general conformance to the approved construction documents. Structural observation does not include or waive the responsibility for other type of required inspections by the Code. Prior to the commencement of observations, the structural observer shall submit to the budding official a written statement identifying the frequency and extent of structural observations. At the conclusion of the work included in the permit, the structural observer shall submit to the building official a written statement that the site visits have been made and identify any reported deficiencies that, to the best of the structural observer's knowledge.

Structural observations shall be provided for those structures where one or more of the following conditions exist:

1. The structure is classified as *Risk Category III or* IV (Essential buildings).
2. The structure is a *high-rise building.*
3. The structure is assigned to *Seismic Design Category* E (high seismic area) and it is greater than two stories above the grade plane.
4. Such observation is required by the *registered design professional* responsible for the structural design.
5. Such observation is specifically required by the building official.

6. Code Requirements for Inspection and Testing for Concrete Construction

The 2022 CBC requires the following Special Inspections and Tests for Concrete construction:

1. Inspect reinforcement, including prestressing tendons, and verify placement.
2. Reinforcing bar welding per AWS D1.4.
3. Inspect anchors Cast-in-place.
4. Inspect Post-installed anchors in hardened concrete.
5. Verify use of required mix design.
6. Make cylinders for concrete strength, perform slump test, air content test, take temperature of concrete before placement.
7. Inspect concrete and shotcrete placement for proper application techniques.
8. Concrete curing per ACI 318 section 26.5.
9. Inspect prestressed concrete for: Prestressing forces and grouting of bonded tendon.
10. Inspect erection of precast concrete members.
11. Inspection of PC diaphragm connections.
12. Inspect installation tolerances of PC diaphragm connections.
13. Verify in-situ concrete strength prior to stressing of tendons and prior removal of shores, and forms.
14. Inspect formwork for shape, location and dimensions of the concrete being formed.

Table 1705.3 of 2022 CBC shown the required Special Inspections and Tests of Concrete construction, including the level of Special Inspections and Reference Standards, as shown below.

2022 CBC – TABLE 1705.3 REQUIRED SPECIAL INSPECTIONS AND TESTS OF CONCRETE CONSTRUCTION				
TYPE	**Continuous Special Inspection**	**Periodic Special Inspection**	**Reference Standard**	**IBC Reference**
1. Inspect reinforcement, including prestressing tendons, and verify placement	--	X	ACI318: Ch. 20, 25.2, 25.3, 26.6.1-26.6.3	--
2. Reinforcing bar welding:				
a. Verify weldability of reinforcing bars other than ASTMA706	--	X	AWSD1.4; ACI 318: 26.6.4	
b. Inspect single-pass fillet welds, maximum 5/16"	--	X		--
c. Inspect all other welds.	X	--		
3. Inspect anchors cast in concrete.	--	X	ACI 318: 17.8.2	--
4. Inspect anchors post-installed in hardened concrete members (see footnote b)				--
a. Adhesive anchors installed in horizontally or upwardly inclined orientations to resist sustained tension loads.	X	--	ACI 318: 17.8.2.4	--
b. Mechanical and adhesive anchors not defined in 4.a.	--	X	ACI 318: 17.8.2	--
5. Verify use of required design mix	--	X	ACI 318: Ch. 19, 26.4.3, 26.4.4	1904.1, 1904.2
6. Prior to concrete placement, fabricate specimens for strength tests, perform slump and air content tests, and determine the temperature of the concrete.	X	--	ASTM C31 ASTMC172 ACI 318: 26.5, 26.12	--
7. Inspect concrete and shotcrete placement for proper application techniques.	X	--	ACI 318: 26.5	--
8. Verify maintenance of specified curing temperature and techniques.	--	X	ACI 318: 26.5.3-26.5.5	--
9. Inspect prestressed concrete for:				
a. Application of prestressing forces; and	X	--	ACI 318: 26.10	--
b. Grouting of bonded prestressing tendons.	X	--		
10. Inspect erection of precast concrete members.	--	X	ACI 318: 26.9	--
11. For precast concrete diaphragm connections or reinforcement at joints classified as moderate or high deformability elements (MDE or HDE) in structures assigned to Seismic Design Category C, D, E or F, inspect such connections and reinforcement in the field for:			ACI 318: 26.13.1.3	
a. Installation of the embedded parts	X	--	ACI 550.5	--
b. Completion of the continuity of reinforcement across joints.	X	--		--
c. Completion of connections in the field.	X	--		--
12. Inspect installation tolerances of precast concrete diaphragm connections for compliance with ACI 550.5.	--	X	ACI 318: 26.13.1.3	--
13. Verify in-situ concrete strength, prior to stressing of tendons in post-tensioned concrete and prior to removal of shores and forms from beams and structural slabs.	--	X	ACI318: 26.11.2	--
14. Inspect formwork for shape, location and dimensions of the concrete member being formed.	--	X	ACI 318: 26.11.1.2(b)	_
For SI: 1 inch = 25.4 mm.				
a. Where applicable, see Section 1705.13: Special Inspections for Seismic Resistance.				
b. Specific requirements for special inspection shall be included in the research report for the anchor issued by an approved source in accordance with 17.8.2 in ACI 318, or other qualification procedures. Where specific requirements are not provided, special inspection requirements shall be specified by the registered design professional and shall be approved by the building official prior to the commencement of the work. c. OSHPD 1R, 2 & 5 Installation of all adhesive anchors In horizontal and upwardly inclined positions shall be performed by an ACI/CRSI Certified Adhesive Anchor Installer, except where the factored design tension on the anchors is less than 100 pounds and those anchors are dearly noted on the approved construction documents or where the anchors are shear dowels across cold joints in slabs on grade where the slab is not part of the lateral force-resisting system.				

7. Discussions

Special Inspection and Testing are important tools that are used to control and improve the construction quality of building structures and manufactured products. It is expected that this practice, which is extensively applied in the USA, may be applied also to other rapidly developing region, like Central Asia. These tools and good planning will be useful to help the growth of the countries'

infrastructure and the construction industry by developing and implementing resilient structures, which may be simple, but yet robust and easier to implement.

8. Conclusions

While this practice is based on design practice in the USA, the same principles can be applied in other developing regions such as in Central Asia region, and particularly in Uzbekistan.

9. Acknowledgements

The authors express gratitude to Dr. Takhirov for the opportunity to present this important topic of Special Inspection and Testing for Reinforces Concrete building structures in high seismic areas.

References

1. *American Welding Society.* Structural Welding Code (ANSI/AWS D1.4-2020).
2. *American Society of Civil Engineers.* Minimum Design Loads and Associated Criteria for Buildings and Other Structures (ASCE/SEI 7-16) // Structural Engineering Institute.
3. *American Society of Civil Engineers.* Seismic Evaluation and Retrofit of Existing Buildings (ASCE/SEI 41-17) // Structural Engineering Institute.
4. *American Concrete Institute.* Specification for Tolerances for Concrete Construction and Materials (ACI 117-10) and Commentary (ACI-117R-10) // Report by ACI Committee 117.
5. *American Concrete Institute.* Building Code Requirements for Structural Concrete (ACI 318-19) and Commentary (ACI-318R-19) // Report by ACI Committee 318.
6. *American Concrete Institute.* Code Requirements for the Design of Precast Concrete Diaphragms for Earthquake Motions (ACI 550.5-18) and Commentary (ACI-550.5R-18) // Report by ACI Committee 550.5.
7. *ASTM International.* Standard Practice for Making and Curing Concrete Test Specimens in the Field (ASTM C31).
8. *ASTM International.* Standard Practice for Sampling Freshly Mixed Concrete (ASTM C172).
9. *Concrete Reinforcing Steel Institute.* Manual of Standard Practice, 30th Edition
10. *Chronicle Books. San Francisco.* The Quake of '89 As Seen by the News Staff of San Francisco Chronicle // Chronicle Books, San Francisco.
11. *Earthquake Engineering Research Institute.* Northridge Earthquake January 17, 1994 – Preliminary Reconnaissance Report, Report No.94-01 // Earthquake Engineering Research Institute with support from the National Science Foundation.
12. *Earthquake Engineering Research Institute.* The Hyogo-Ken Nanbu Earthquake January 17, 1995 – Preliminary Reconnaissance Report, Report No.94-04 // Earthquake Engineering Research Institute with support from the National Science Foundation and Federal Emergency Management Agency.
13. *International Code Council*. 2021 International Building Code – A Member of International Code Family, Chapters 1 and 17 // International Code Council.
14. *International Code Council*. 2021 International Existing Building Code – A Member of International Code Family // International Code Council.
15. *International Code Council*. 2022 California Building Code – California Code of Regulations, Title 24, Part 2, Vol. 1 of 2, Section 104 // California Building Standards Commission.
16. *International Code Council*. 2022 California Building Code – California Code of Regulations, Title 24, Part 2, Vol. 2 of 2, Chapter 17 // California Building Standards Commission.
17. *International Code Council*. 2022 California Existing Building Code – California Code of Regulations, Title 24, Part 10 // California Building Standards Commission.
18. *International Conference of Building Officials*. 1997 Uniform Building Code (1997 UBC).
19. *Pacific Earthquake Engineering Research Center*. PEER Preliminary Notes and Observations on the August 24, 2014, South Napa Earthquake, Report No. 2014-13 // Headquarter, University of California, Berkeley.
20. *Prentice-Hall International Series in Civil Engineering Mechanics,* Dynamic of Structures 4th Edition, 2011 // Anil K. Chopra, Pearson.
21. *The Masonry Society.* Building Code Requirements and Specification for Masonry Structures, TMS 402/602-16 // Reported by TMS Committee 402/602.
22. *The Masonry Society.* Performance of Masonry Structures in The Northridge, California Earthquake of January 17, 1994 // Reconnaissance Team – The Masonry Society.

TESTING OF AN MICROCOMPUTER-BASED STATION IN MICROTREMOR SURVEYS

Yanbukhtin I.R.[1], Mamarozikov T.U.[2], Zakirov A.Sh.[1], Musaev. U.T.[1]

[1]*Center for Advanced Technologies under Ministry of Higher education, science and innovations;*
[2]*Institute of Seismology, Tashkent, Uzbekistan*
E-mail: Ilyas9348702@gmail.com

Abstract. *Testing of an accelerometer and geophones used microcomputer based microtremor recording station with widely used sensors as TROMINO and Guralp. Testing was carried out using HVSR method. Results showed applicability of use such type of recording stations.*

Keywords: *microtremor, microcomputer, accelerometer, geophones, H/V.*

1. Introduction

Construction is one of the drivers of national economic growth. In recent years, our country has experienced a construction boom. The expansion of construction is associated with such factors as population growth, increasing welfare and purchasing power of citizens. In turn, the growth of construction contributes to the creation of new architectural solutions and improvement of infrastructure. In our republic, there is a certain gap in the system of maintenance and seismic monitoring of large national economic facilities. To eliminate such gaps, the state began to pay great attention and financial support to ensuring the security of strategic facilities and, first of all, the population. In order to introduce a system of continuous instrumental seismological monitoring on reservoirs located in the seismically active zone of the country, and ensure the implementation of Presidential Decree No. PP-4794 of July 30, 2020 “On measures to radically improve the system for ensuring seismic safety of the population and territory of the Republic of Uzbekistan”, the Cabinet of Ministers The Republic of Uzbekistan signed the resolution “On the implementation of a system of continuous instrumental seismological observations of water bodies located in seismically active zones of the Republic” on December 17, 2020. In this regard, the issue of seismic protection, as well as the development of effective methods for assessing the seismic resistance of buildings, as well as seismic monitoring, is becoming very relevant for our country. The goal of the research carried out within the framework of the project IL-5221091401 is to create a hardware and software complex for assessing the deficiency of seismic resistance of buildings and structures. As part of the project, for the first time in Uzbekistan, a hardware and software complex using RASBERRY PI will be created and applied to assess the seismic resistance of buildings and structures, consisting of a station with motion sensors and installed software for their operation.

2. Materials and methods

One of the methods for assessment of the seismic resistance of buildings and structures is modal analysis of structures motion [1-6] and microtremor analysis [7, 8]. For this purpose, microcomputer-based motion detection equipment was constructed. This equipment includes 3-axial digital accelerometer ADXL 355 and 3-axis geophones as a seismometer. As an ADC ADS1256 was used.

To compare the work and the data obtained, TROMINO, Guralp 6TD, Guralp 5TDE devices were used

TROMINO is a small (1 dm3, < 1 kg) universal device equipped with a 3-axis velocimeter (with adjustable dynamic range), 3-axis accelerometer, GPS receiver, built-in radio transmitter/receiver (for synchronization between different devices), radio synchronization system (for MASW studies, etc.). TROMINO operates in the range of 0.1-1024 Hz and is powered only by 2 AA batteries (1.5 V) [9].

Güralp 5TDE is a digital accelerometer with a built-in data acquisition module based on Linux, providing remote monitoring and control with unprecedented flexibility. Combining a 5TC strong motion meter, a DM24 ADC, and an integrated data acquisition module (EAM), the 5TDE is a low-noise sensor with built-in and external storage. Featuring a web-based user interface and multi-protocol communications over serial and Ethernet connections, the optional Wi-Fi module provides 802.11b/g connectivity [10].

Güralp 6TD is a digital broadband force feedback velocimeter, the 6TD has zero mechanical non-linearity (overall measured linearity exceeds 90 dB) [11].

Testing was carried out in the back of the Advanced Technology Center, testing duration was 1 hour. The devices were arranged in a row and oriented to the cardinal points.

3. Results

As a result, hourly recordings from the instruments were obtained and the spectra of the recordings of each of the instruments were calculated (Figure 1)

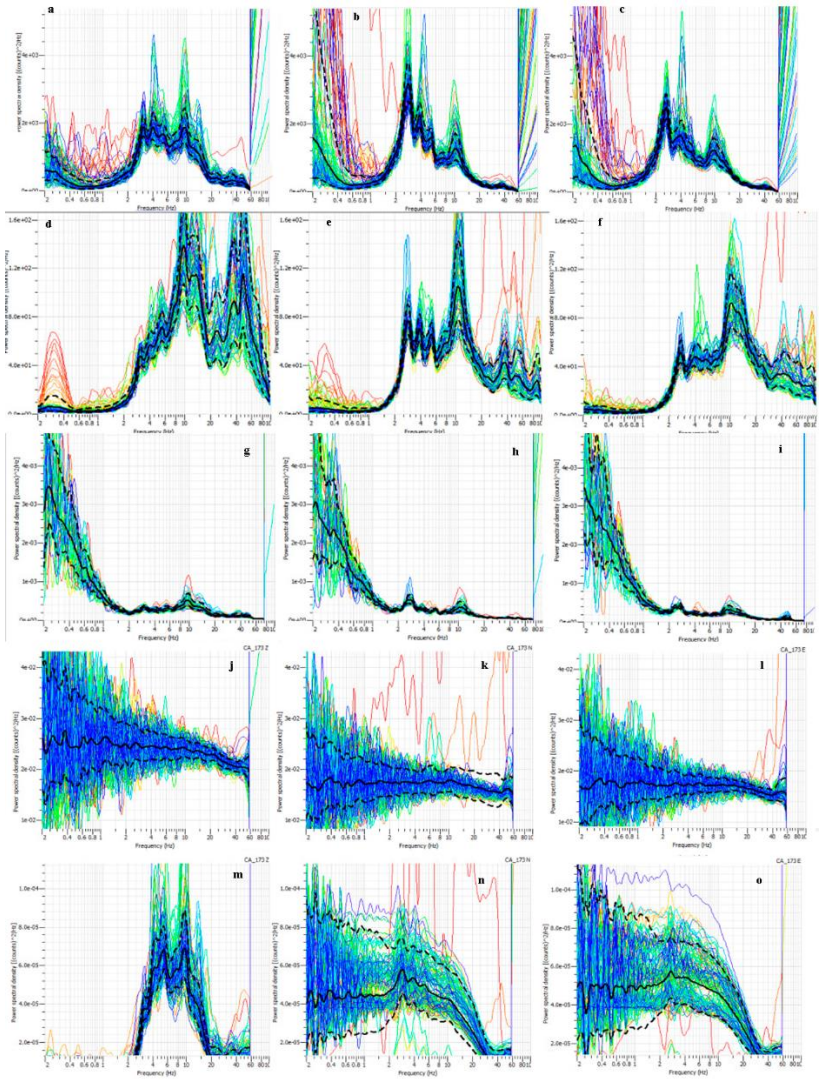

Figure 1. - **Spectra of recordings:** a-c - z,y,x components of Guralp 6TD; d-f - z,y,x components Guralp 5TDE; g-i - z,y,x components of TROMINO; j-l - z,y,x accelerometer components, m-o - z,y,x components of the velocimeter

As can be seen from Figure 1, all devices recorded vibrations in the frequency range 2-40 Hz. The Guralp devices are distinguished by the greatest sensitivity; the dynamic range of the TROMINO and velocimeter data is similar and is lower than the Guralp. The shape of the frequency response of all recordings is similar for all devices except the accelerometer of the device, which is due to the low sensitivity of the accelerometer

Based on the data obtained, an H/V analysis was performed, based on an analysis of the spectral relationships of the vertical and horizontal components, which makes it possible to isolate the resonant characteristics of the structure under study and determine the transfer coefficient during vibrations at resonant frequencies [12,13,14,15,16,17,18,19,20].

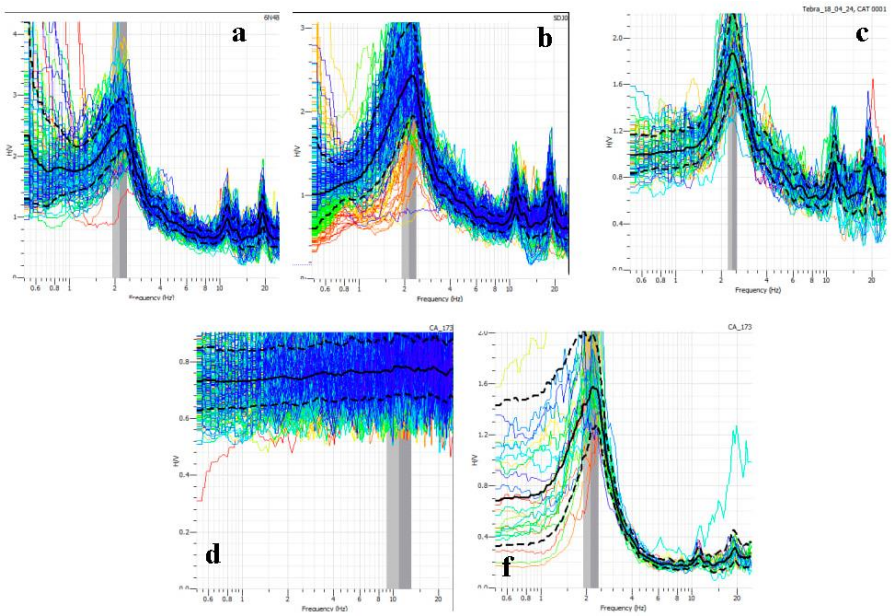

Figure 2. - **H/V analysis results: a- Guralp 6TD; b – Guralp 5TDE; c – TROMINO; d – accelerometer; f – velocimeter**

4. Discussion

As a result of the analysis, it is clear that the results obtained using the velometer repeat the results of the Guralp and TROMINO devices, having similar peaks at frequencies of 2, 10 and 20 Hz, which is due to the structure of the rear Center of Advanced Technologies. The sensitivity of the accelerometer did not allow us to register vibrations on the first floor of the building, which is why there is a straight line on the H/V graph. Stronger motions which appear in higher floor can be registered on accelerometer.

5. Conclusion

As a result of the work, a prototype of a device was built for recording microseisms in values of vibration velocity and acceleration. The results were tested and compared with devices used to solve the problem of recording microtremor.

References

1. *Andersen P., Brincker R., Ventura C., Cantieni R*. (2008) Mode Estimation of Civil Structures Subject to Ambient and Harmonic Excitation Proceedings of the 26th International Modal Analysis Conference (IMAC) Orlando, Florida USA.
2. *Christelle Salameh, Bertrand Guillier, Jacques Harb, Cécile Cornou, Pierre-Yves Bard, Christophe Voisin.* Seismic response of Beirut (Lebanon) buildings: instrumental results from ambient vibrations. Bull Earthquake Eng (2016). doi:10.1007/s10518-016-9920-9, pp 1-26.
3. *Benedettini F., Morassi A.,* (2011) Dynamic testing, structural identification and damage detection on Dogna's bridge. Proceedings of the 8th International Conference on Structural Dynamics, EURODYN 2011, Leuven, Belgium.
4. *Soler-Llorens, Juan Luis & Galiana-Merino, Juan & Benabdeloued, Boualem Youcef Nassim & Rosa-Cintas, Sergio & Zamora, Javier & Giner-Caturla, Jose.* (2019). Design and Implementation of an Arduino-Based Plug-and-Play Acquisition System for Seismic Noise Measurements. Electronics. 8. 1035. 10.3390/electronics8091035
5. *Soler-Llorens, Juan Luis & Galiana-Merino, Juan & Giner-Caturla, José & Rosa-Cintas, Sergio & Benabdeloued, Boualem Youcef Nassim.* (2019). Geophonino-W: A Wireless Multichannel Seismic Noise Recorder System for Array Measurements. Sensors. 19. 4087. 10.3390/s19194087.
6. *Ventura C. E., Brincker R., Dascotte E., Andersen P.* (2001) FEM Updating of the Heritage Court Building Structure Proceedings of the 19th International Modal Analysis Conference (IMAC), Kissimmee, Florida, pp.324-330.
7. *Sylvette Bonnefoy-Claudet, Fabrice Cotton, Pierre-Yves Bard.* (2006). The nature of noise wavefield and its applications for site effects studies: A literature review. Earth Sci. Rev. 79, 205–227.
8. *Arai, H., Tokimatsu, K.*. (1998). Evaluation of local site effects based on microtremor H/V spectra. Proceeding of the Second International Symposium on the Effects of Surface Geology on Seismic Motion. Yokohama, Japan, pp. 673–680.
9. Tromino, accessed 24.04.2024 https://moho.world/en/tromino/

10. Gurlp 5TDE datasheet, accessed 24.04.2024 https://www.guralp.com/documents/DAS-050-0006-2.pdf
11. Gurlp 6TD datasheet, accessed 24.04.2024 https://www.guralp.com/documents/DAS-T60-0002.pdf
12. *Nogoshi, M. and Igarashi, T.* (1971). On the amplitude characteristics of microtremor (Part 2), J. Seismol. Soc. JPN, 24, 26–40.
13. Nakamura, Y. (1989) A method for dynamic characteristics estimation of subsurface using microtremor on the ground surface, Quarterly report of Railway Technical Res. Inst. (RTRI), 30, 25–33.
14. *Lunedei, E., & Malishewsky, P.*(2015).A Review and some new issues on the theory of the H/V technique for ambient vibrations. In: A. Ansal (Ed.), Perspectives on European Earthquake Engineering and Seismology, Geotechnical and Earthquake Engineering(Vol. 39, pp. 371—394).Springer, Cham.
15. *D'Amico,V.; Picozzi, M.; Baliva, F.; Albarello, D.* (2008). Ambient noise measurements for preliminary site-effects characterization in the urban area of Florence, Italy. Bull. Seismol. Soc. Am., 98, 1373–1388.
16. *Yutaka Nakamura.* (2019) What Is the Nakamura Method? Seismological Research Letters 90 (4): 1437–1443.
17. *Hiroshi Kawase at al.* (2019) Direct evaluation of S-wave amplification factors from microtremor H/V ratios: Double empirical corrections to "Nakamura" method. Soil Dynamics and Earthquake Engineering. 126 105067. P.p.1-14
18. *S. Molnar at al.* (2022) A review of the microtremor horizontal to vertical spectral ratio (MHVSR) method. https://doi.org/10.1007/s10950-021-10062-9 J Seismol (2022) 26:653–685
19. *Wathelet, M., Chatelain, J.-L., Cornou, C., Di Giulio, G., Guillier, B., Ohrnberger, M. and Savvaidis, A.* (2020). Geopsy: A User-Friendly Open-Source Tool Set for Ambient Vibration Processing. Seismological Research Letters, 91(3), 1878--1889, doi: 10.1785/0220190360.
20. *Sylvette Bonnefoy-Claudet, Fabrice Cotton, Pierre-Yves Bard.* (2006). The nature of noise wavefield and its applications for site effects studies: A literature review. Earth Sci. Rev. 79, 205–227.

UTILIZING VARIATIONS IN ELECTROMAGNETIC FIELDS OF ALTERABLE NATURES AS PREDICTORS OF STRONG EARTHQUAKE

Yusupov V.R.[1]
[1]*Institute of Seismology, Tashkent, Uzbekistan*
E-mail: valijon.yusupov@mail.ru

Abstract. *The article presents a joint analysis of the results of ground-based and satellite observations of an alternating electromagnetic field at the time of their behavior immediately before a strong earthquake. So, before the earthquake itself, several magnetometric anomalous effects (peculiar anomalies) were observed, and during the earthquake itself, the behavior of electromagnetic fields changed significantly. The operation of stationary magnetic research stations in the territories of geodynamic polygons of Uzbekistan was at different levels and varied depending on various factors.*

Keywords: *earthquakes, precursor, geodynamic polygon, forecast, magnetic field.*

1. Introduction

Research on the very problem of earthquake forecasting in the world has been especially intensified since the second half of the last century, since along with theoretical research it became possible to additionally conduct high-level laboratory, ground-based and satellite experiments [1-14]. Thanks to them, various anomalous changes in geophysical fields were detected both in the lithosphere itself and in other terrestrial shells (in the atmosphere and ionosphere) during the preparation of the earthquakes themselves. Variations in geophysical fields associated with the preparation and occurrence of earthquakes can be conditionally divided into factors causing earthquakes [15-16], earthquake indicators [17-18] and earthquake precursors [19].

The problem of identifying geomagnetic indicators of seismic tectonic processes has long attracted the attention of geophysicists around the world. Some scientists believe that this problem can be solved, and there is a catalog of geomagnetic signatures associated with dozens of predicted earthquakes (Abdullabekov and Maksudov 1975, Sadovsky 1981, Ogata et al. 1996, Wiss 1997, Gaffet et al. 2003). The opposite opinion is that there is still no accurate way to predict earthquakes (Solonenko 1987, Geller et al. 1997). Thus, the problem of earthquake forecasting is far from its final solution. The main problem is that anomalous geodynamic effects are complicated by a wide range of physico–geological processes unrelated to stresses in the Earth's crust [20-21].

Despite numerous attempts to identify anomalous geomagnetic variations associated with geodynamic processes and earthquakes (for example, Moore 1964, Abdullabekov, Maksudov 1975,

1987, Johnston 1978, Finkelstein 1983, Shapiro, Abdullabekov, 1982, Finkelstein, Maslatov 1984, Akishev et al. 1986, Fraser-Smith 1990, Hayakawa 1993, Appelbaum, Finkelstein 1998, Hattori 2002, Gaffet et al. 2003, Gokhberg and Shalimov 2008, Sobisevich and Sobisevich 2010, Moskovskaya 2011, Yamazaki 2011) only a few have achieved success. This circumstance is due to the unclear nature of anomalous changes in geomagnetic variations and an insufficiently developed methodology for detecting anomalies caused by geodynamics relative to other unrelated factors. In a study (Finkelstein and Maslatov 1984), a method was proposed to exclude a short-term anomalous geomagnetic field from the total function.

In this case, here we propose to discuss the behavior of anomalous geomagnetic variations over longer periods (from several days to several months) and their online use for monitoring geodynamic processes. It is well known that abnormal geomagnetic variations are a complex function of various factors. Literature analysis (Wait 1951, Jacobs et al. 1964, Pudovkin et al. 1973, Bezuglaya and Akhverdyan 1973, Vanian et al. 1967, Fitterman 1978, 1979, Forbringer et al. 2010, Solomatin and Tikhonov 2011) and personal observation experience allowed us to conclude that the observed general geomagnetic variation can be represented as the sum of many (numerous) factors. Each factor has a separate origin and can create a wide range of magnetic anomalies (Finkelstein 1987) [21].

2. Materials and methods

Experiments were carried out with the methods of repeated route and area magnetic surveys within a network of stationary magnetometric stations located in specific geodynamic polygons. The first experiments by the method of repeated route surveys were started in 1968 at the Tashkent Geodynamic test site together with the Institute of Terrestrial Magnetism, Ionosphere and Radio Wave Propagation of the Academy of Sciences of the Former USSR (IZMIRAN). Three routes were laid along and across the seismogenic zones. The distance between the points was 5 km . The total length of the routes at this training ground is about 330 kilometers. The modulus of the total vector T was measured using an absolute proton magnetometer PM-5. The measurements were taken to the baseline of the T-variometer of the Yangibazar magnetic Observatory [2-5]. Since the 1970s, the volume of experimental work has gradually increased. In addition to IZMIRAN, the Institute of Earth Physics (Moscow), the Institute of Geophysics (Yekaterinburg), the Institute of High Temperatures (Moscow) and others began to take part in the experiments [2-5]. Measurements began to be carried out with more high-precision instruments: TMP, TM-5, MPP, MV-01 PMP, G-816, GSM-19T and others. Measurements were carried out synchronously at ordinary and stationary stations. The volume of experimental work gradually increased. Experiments began to be carried out in man-made facilities (underground gas storage, high-altitude reservoirs, areas of gas and oil fields, epicenters of strong earthquakes, etc.). Measurements at stationary stations were carried out with a frequency of 10-20 minutes around the clock, at points of repeated area surveys - every 15 days, at points of repeated route surveys 3-4 measurement cycles per year. The total length of the repeated route surveys was larger than 7,750 kilometres, the number of repeated measurement points reached approximately 1,110, the number of stationary stations ranged from 15–25, and in certain years, this number even reached 37.

Many achievements in the field of studying the Earth's crust have become possible only thanks to the development of experimental techniques and methods for analyzing the results obtained. Outstanding achievements in the field of experimental technology include the creation of an automatic standard magnetic observatory with telemetry devices, the development of highly sensitive magnetometers, the creation of integrating computing systems to work in combination with the development of computational methods for analyzing magnetic data. A recently developed method for measuring the vertical gradient of the magnetic field has great potential, and the successful development of this method is facilitated by a sharp increase in the sensitivity of magnetometers used for magnetic surveys. This system significantly increases the resolution, eliminates time corrections and, using the Laplace and Euler equations, makes it possible to distinguish the sources of anomalies located inside the base and at closer distances from the earth's surface. Including the beginning of the

use of magnetometric methods for earthquake prediction. Currently, more than 150 magnetic observatories around the world are conducting magnetic observations.

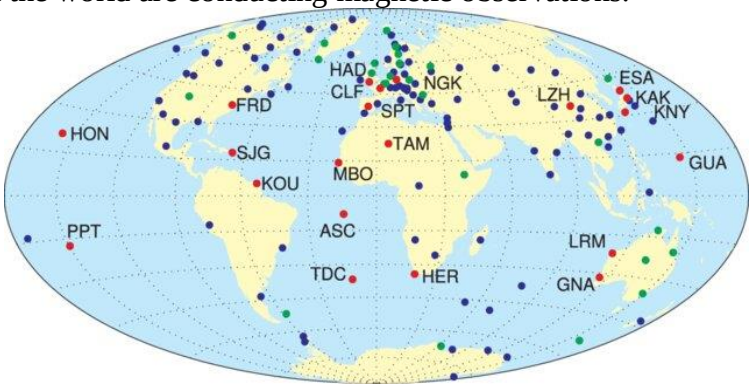

Figure 1. - **Diagram of stationary stations from INTERMAGNET.**

One of the main tasks of magnetic observatories is to provide homogeneous and highly accurate (in an absolute sense) data on the Earth's magnetic field for the longest possible time interval. The traditional scheme of conducting magnetic observations is the continuous recording of field changes using variometers and periodic absolute measurements (Parkinson, 1986; Jankowski & Sucksdorff, 1996). The same scheme has been adopted as a standard for the Intermagnet network of magnetic observatories (INTERMAGNET Manual, 1999). Absolute measurements occupy a special place and their role is becoming increasingly important [22-23].

A technique for detecting geomagnetic variations caused by dangerous geodynamic processes at depth has been developed. This methodology was tested using data from three Japanese observatories in the network of the international INTERMAGNET project (www.intermagnet.org 2011). The abnormal behavior of the geomagnetic field was discovered during the period of the strongest Tohoku-Oki earthquake on March 11, 2011. A theoretical assessment of the possible mechanisms of these anomalous geomagnetic variations was considered. In Japan, the possibility of abnormal geomagnetic variations near the epicenter of an earthquake and their rapid monitoring (online or with a one-day delay) has been demonstrated. The main tool of the developed methodology is the determination of the geodynamic magnetic effect using a differential function [21].

However, in early studies (Pudovkin 1973, Abdullabekov and Maksutov 1975), the days of magnetic storms observed before strong earthquakes were mistaken for harbingers of earthquakes. Since in most of these works the method of eliminating the above-mentioned factors (noise) is ignored, the results were obtained without the correct formulation of the problem, and therefore it was difficult to achieve the goal and to believe their assessment.

3. Research results

Geomagnetic variations. The concept of the "background" level of geomagnetic variations is a key concept in the formulation of the above-mentioned problems. Therefore, it is important to define what we mean by this. Based on the experience of measuring geomagnetic variations at mid-latitudes covering an area of about (9-16) × 104 km2, we can assume that normal fields exist if, during a quiet night near two separated observation points, the data agree with a certain accuracy for several months (Jacobs et al., 1964, Finkelstein 1983). This means that the differential function of variations between the observation points will be an almost constant horizontal line.

In Fig. 2, 3, for this event, one can notice the presence of the highest wavelet coefficients for the first three levels of decomposition in connection with the geomagnetic storm. Sharp changes in the vertical component of the geomagnetic field are emphasized by the highest amplitudes of the wavelet coefficients. On the other hand, smooth oscillations caused by the magnetosphere in calm conditions represent a very small amplitude of the wavelet coefficients. In the work of Mendes et al. (2005), it was found that "when a geomagnetic storm is in the development stage (periods of disturbance), the wavelet coefficients are significantly large" especially during the initial and main

phases. The initial phase and maximum height of the tsunami near MMB occurred after the main phase [24].

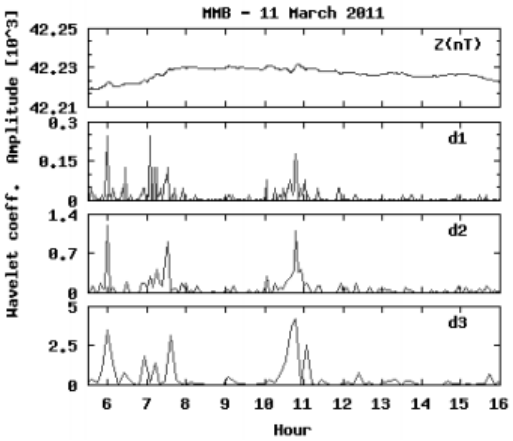

Figure 2. - **Geomagnetic field dataset for Memanbetsu Station. The panels show from top to bottom the Z component of the geomagnetic field and the amplitudes of the wavelet coefficients at levels 1, 2 and 3 for March 11, 2011 [24].**

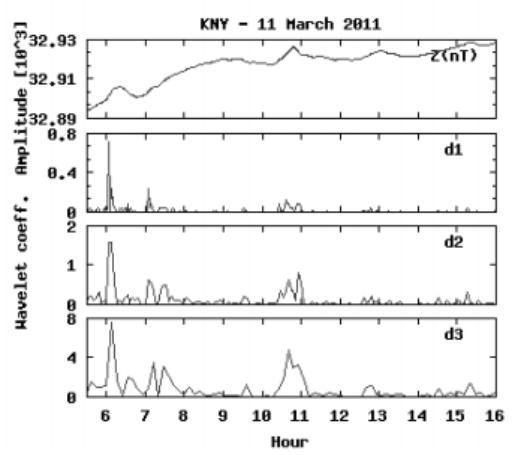

Figure 3. - **Geomagnetic field dataset for Kanoya Station (KNY). The panels show from top to bottom the Z component of the geomagnetic field and the amplitudes of the wavelet coefficients at levels 1, 2 and 3 for March 11,2011[24].**

The results are encouraging. In the next step, we will present a further study using more events and more stations to conduct a complete analysis. The first stage of interpretation of the results suggests that the discrete wavelet transform can be used to characterize the effects of Tsunamis on the geomagnetic field, but needs further study.

Currently, quite diverse and interesting articles are being published based on terrestrial and satellite data on terrestrial and electromagnetic radiation observed during the preparation for an earthquake. These phenomena can be detected both on a laboratory and geological scale. Currently, in some seismically active countries of the world, a network has been organized to collect a large number of electromagnetic radiation data generated in preparation for an earthquake. Constant monitoring of the frequency spectrum of electromagnetic radiation from the earth can be very useful from the point of view of forecasting large earthquakes $M \geq 5$ within the country [25].

Here we have considered several anomalies, abnormal effects when electromagnetic fields changed during an earthquake. Here are some examples of predicted earthquakes in the world:

China. A successful earthquake prediction was made in 1975 in Haicheng, Liaoning Province, in Northeast China. The area around Haicheng was under the close attention of seismologists for several years before 1975, as some signs indicated that a strong earthquake could occur here in the near future. Instruments were installed to record the slopes of the Earth's surface, fluctuations in the magnetic field and changes in the electrical resistance of soils. Instrumental observations clearly indicated the changes taking place in the bowels of the Earth.

In 1976, three earthquakes were predicted in China: on May 29 in Yunnan Province, on August 16 in Sichuan Province, on November 7 on the border of these two provinces of Sichuan and Yunnan.

For many months before each earthquake, seismologists issued a long-term forecast based on the study of seismicity, repeated leveling and magnetic anomalies. The operational forecast for these three earthquakes was made within a few hours to several days before the earthquake, mainly based on data on an increase in the number of weak tremors. Security measures were taken, and in one case, a mass evacuation of the population was carried out four days before the earthquake.

USA. In the USA, an earthquake was successfully predicted, which took place in 1974 in California near Hollister, at the place where the Calaveras fault closes with the San Andreas fault. This area is one of the most instrument-rich and most studied seismic zones in the world. Magnetometer data revealed a change in the Earth's magnetic field, and tilt meters showed that the Earth's surface is shifting. A day after the changes were established, an earthquake with a magnitude of 5.2 occurred.

Japan. Comprehensive research on earthquake forecasting in Japan has been conducted since 1964. In Japan, devastating earthquakes occur almost every year, and the possibility of successful forecasts is of great public interest. Identification of a number of objectively instrumentally recorded earthquake precursors, several successful operational forecasts were made, which allowed people to be removed from buildings that were soon destroyed by earthquakes. Any parameter of the geophysical field that changes before an earthquake, so that it can predict the possibility of an earthquake with a careful study of the nature of its changes in physical or chemical fields, is called a harbinger of an event. Recently, the world has been paying more and more attention to geophysical, geomagnetic, geoelectric and electromagnetic precursors. A number of geomagnetic data from three stations obtained through an INTERMAGNET located at a distance of less than 500 km before the earthquake in Japan on September 5 has been identified. Then, using the method of characteristic curves, the influence of the daily course of the geomagnetic field is eliminated. After that, by studying anomalies that become more distinct after the implementation of the method, all cases are compared with the seismic activity of the region. Among the various magnetic components of the Earth's geomagnetic field, the horizontal components are more suitable than others for predicting the proposed process, mainly due to the large variations of the geomagnetic field in the vertical direction, and due to the presence of a geomagnetic gradient.

Uzbekistan. To date, repeated route and area surveys of the magnetic field at the Tashkent, Ferghana, Kyzylkum landfills, a network of stationary magnetometric stations, repeated surveys at man-made facilities (Charvak, Poltoratskoye underground gas storage facility, areas of gas and oil fields), epicenter surveys in the epicenters of strong earthquakes that occurred (Gazli in 1976 and 1984, Isfara- Batken 1977, Tavaksai 1977, Nazarbayev 1980, Chimion 1982, Papal 1984 and others.

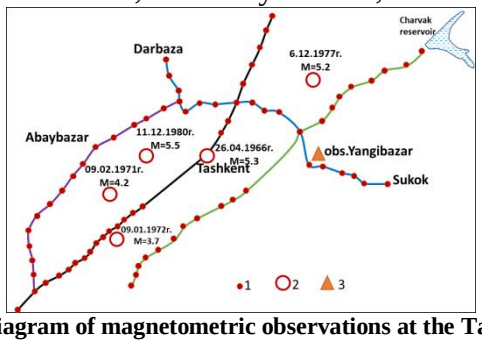

Figure 4. - **is a diagram of magnetometric observations at the Tashkent test site.**
1-magnetic observation points, 2-earthquake epicenters, 3-Yangibazar Observatory.

At the Tashkent test site, three routes - Western, Eastern, Abaybazar-Chinaz, are laid along the Karzhantau seismogenic zone. The fourth Secant route is laid perpendicular to the strike of the seismogenic zone. The distance between the observation points is 5 kilometers. In cases of abnormal changes, the distances between points increase to 2.5 kilometers. Since 1968, 3-4 cycles of repeated route measurements have been carried out. In the early years, measurements at ordinary points were brought to the baseline of the T-variometer of the Yangibazar magnetic observatory. Since 1974, measurements at ordinary points have been carried out using proton magnetometers synchronously with the Yangibazar Observatory. During the research period, several long-term and medium-term

anomalous changes in the magnetic field associated with earthquakes were detected at the landfill (Figure 4).

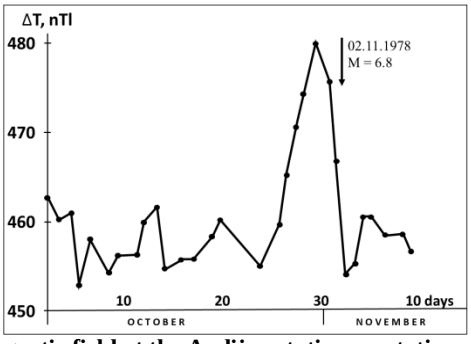

Figure 5. - **Abnormal changes in the magnetic field at the Andijan stationary station associated with the Alai earthquake on November 2, 1978 with a magnitude of M=6.8, which occurred at a distance of 130 km from the station [27]**

Thus, an abnormal change was also detected at the stationary Chimion station, i.e. the ratio of cove-like variations at Chimion station relative to Yangibazar station. According to repeated route observations at the Tashkent, Ferghana and Kyzylkums polygons, long-term anomalous magnetic field changes associated with the Abaybazar on February 9, 1971 with a magnitude of M =4.2, and the Khalkabad on January 9, 1971 (M=3.7, H=5 km) were identified. Isfara-Batken earthquake on January 31, 1977 (M=5.75), Alai earthquake on November 2, 1978 with M=6.8 and others.

For example, abnormal changes in the magnetic field associated with the Tavaksai earthquake on December 6, 1977 with a magnitude of M = 5.2 along the Secant and Eastern routes of the Tashkent landfill. Figure 6 shows long-term and medium-term anomalous changes in the magnetic field at point 9 of the Secant route of the Tashkent landfill associated with the Tavaksai earthquake on December 6, 1977 with a magnitude of M=5.2 [13, p.105]. The time of the long-term harbinger is 7 years, the medium-term one is 2 years.

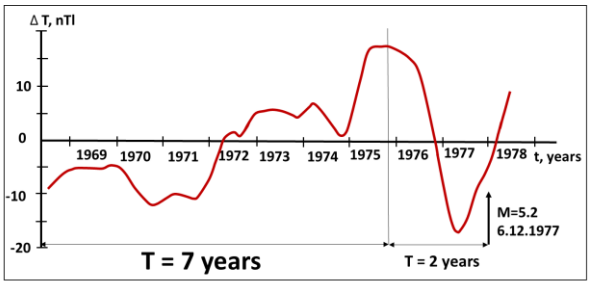

Figure 6. - **is a graph of long-term and medium-term changes in the magnetic field at point Sec -9 associated with the Tavaksai earthquake on December 6, 1977 with a magnitude of M= 5.2 [27].**

According to repeated route observations at the Tashkent, Ferghana and Kyzylkum ranges, long-term abnormal changes in the magnetic field are associated with an earthquake. In Uzbekistan, scientists have received many results related to earthquakes. Table 1 shows the magnetometric anomalies.

The developed improved monitoring system for the complex of geophysical earthquake precursors in Uzbekistan is based on the accumulated 50-60 years of experience in the territories of seismically active regions, geodynamic polygons of Uzbekistan. The routes of repeated magnetic surveys were laid and the first measurements were carried out on them. The routes were laid taking into account the geological and tectonic situation, seismogenic zones and operating stationary stations on the territory of Uzbekistan.

Measurements at the route points and at the stationary point were carried out synchronously with the Yangibazar Observatory.

The representativeness of stationary magnetic research stations in the territories of geodynamic polygons of Uzbekistan was at different levels and varied depending on various factors, such as:

- on the level of seismic activity of the geodynamic polygon territory;
- depending on the number of available magnetic stations;

- from the organization and conduct of special geomagnetic studies in the territories of man–made facilities - natural underground gas storage facilities, large reservoirs and exploited oil and gas fields.

Table 1.

A list of long-term, medium-term, short-term anomalous changes in the magnetic field, modern movements of the Earth's crust and other precursors.

№	Earthquake	Magnitude M	Intensity of abnormal changes	Duration of abnormal changes. in years	Note
1.	Abaybazar on February 9, 1971.	4.2	-15 +23 nTl	2.6	The anomaly appeared at 15 points of the Western route
2.	Alai earthquake on November 1, 1978.	6.8	-15 +4 nTl	5	The anomaly appeared at 5 repeated points of the Eastern route.
3.	Niigata earthquake 1964	7.5	0 + 16 mm	21	Modern movements of the Earth's crust
4.	Abaybazar earthquake of February 9, 1971	4.2	10 nTl	2.6	Anomalous changes in the magnetic field over time at certain points along the western route.
5.	Chimion earthquake on May 6, 1982	5.8	0.2+1,5 nTl	0.5	Medium-term anomalous changes in the ratio of the amplitudes of bay-like variations at stations
6.	Marjanbulak earthquake on May 26, 2013.	6.2	0 +15 nTl	1.5	The anomaly is local. highlighted at point 7a of the Western Route
7	Przheval earthquake of 1970	6.8	0 + 40 mm	3	Vertical displacement of one of the characteristic reference points of the Almaty polygon.

The largest number of magnetic stations involved occurred in the period 1980 - 1990. At that time, the number of stations was 36, of which there were 12 at the Tashkent test site, 11 at Ferghana, 6 at Kyzylkum, and 7 in Central and Southern Uzbekistan.

The number of stationary stations for 2023 at the Tashkent landfill is -4, Ferghana -5, Kyzylkum -3, Central and Southern Uzbekistan – 3. The total number for the marked period is -15 (Figure 7).

Currently, there are 3 stations operating on the territory of the Tashkent geodynamic polygon. These are the Yangibazar Observatory, the Nazarbayev and Khumsan stations. All two stations are located in the Karzhantau fault zone. The distance between these stations is about 50 km. Relative to the Yangibazar Observatory, the Nazarbayev station is located at a distance of 40 km to the northwest. Khumsan Station is 50 km northeast of Yangibazar.

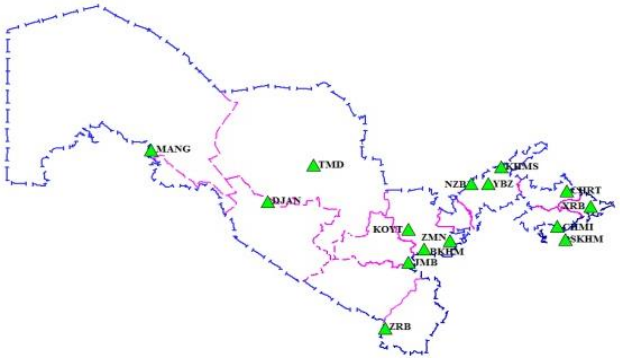

Figure 7. - **The layout of stationary magnetometric stations in Uzbekistan.**

The territory of the Tashkent landfill is characterized by an abundance of faults in the north–western, northern, north–eastern and sub-latitude directions. Although the Poltoratsko – Syrdarya seismotectonic zone is the most seismically active, the Tuyabuguz earthquake of May 25 (M=5.6) in 2013 indicates the potentially seismic activity of other seismogenic zones of the territory of the Tashkent geodynamic polygon. In this regard, the territory of the landfill should be covered with a network of magnetic stations more or less evenly. This will make it possible to control the entire territory of the landfill. To do this, it is proposed, in addition to the existing two stations, to organize stationary magnetic stations near the settlements of Nurafshan (Toitepa). Akhangaran, Angren,

Syrdarya, Gulistan, Pakhtakor. There will be 10 stations in total, including the Yangibazar Observatory. With an area of 10,000 km2 of the Tashkent geodynamic polygon, an average of 1,000 km2 falls on each station. A control point should be installed near each station, at a distance of 0.5 - 1.0 km, where it will be necessary to carry out a control measurement during the next measurement cycle at the points of repeated measurements of the geomagnetic field. This is necessary to control the operation of this stationary magnetic station.

Based on the analysis of general literature data obtained by scientists from leading countries of the world (Russia, Japan, China, USA, etc.), catalogs of earthquake precursors on geomagnetism, modern movements of the Earth's crust, pulsed electromagnetic radiation of the Earth's crust and other geospheres, long-term, medium-term, short-term precursors of seismic danger associated with various stages of earthquake preparation are identified;

The results of repeated route and area surveys of the magnetic field at the Tashkent, Ferghana, Kyzylkum landfills, on a network of stationary magnetometric stations, the results of repeated surveys at man-made facilities (East Ferghana, Charvak, Poltoratskoye underground gas storage, areas of gas and oil fields), epicenter surveys in the epicenters of strong earthquakes (Gazli 1976 and 1984 years, Isfara - Batken 1977, Tavaksai 1977, Nazarbayev 1980, Chimion 1982, Papal 1984 and others), as well as the age-old course of the geomagnetic field of the world network of geomagnetic observatories for more than a century.

4. Discussion of the results.

As can be seen from the analysis of data from long-term magnetometric studies of earthquake precursors at landfills in Uzbekistan, as well as numerous results obtained in a number of other countries, the problem of earthquake forecasting is an extremely complex and multifactorial task. Along with the specific questions regarding each method individually, there are also general problems. The authors tried to find common spatial and temporal features of the manifestation of magnetometric precursors depending on the magnitude of earthquakes.

5. Conclusions

Over the past decade, research on earthquake prediction has revived again, and experiments are currently being conducted around the world to predict them. When considering the data from these experiments, a number of issues related to the assessment of the forecast are important: a detailed specification of the experiment, the measure of success used and the choice of an appropriate reference model.

Here we have reviewed each of them, paying special attention to the analysis of long-term earthquake forecasts.

The analysis of the materials showed that the precursors have different shapes, configurations and signs of the amplitudes of the curves of the studied fields. There is no single harbinger form. Many curves have bay-shaped shapes of positive and negative signs. There are (observed) stepwise, wave-oscillatory and other forms of anomalous curves of the recorded field. The variety of forms of manifestation primarily depends on the geological and tectonic structure of the regions and the variety of different processes in the Earth's crust.

A large number of regular seismic observations are currently being carried out. These stations track the coordinates of the epicenter, the magnitude of the earthquake and register the arrival of seismic waves. This is all observed after the occurrence of the earthquake itself. Currently, electromagnetic field variations are being observed by more than 200 magnetic observatories around the world, which conduct only magnetic observations. Stationary magnetic observations are very few in comparison with purely seismic registrations, about 1000 times. By increasing the number of magnetometric stationary stations and improving the quality of their operation, we increase the probability of predicting (forecasting) possible earthquakes in the studied area.

Reliable prediction of possible earthquakes in a seismically active territory is possible as a result of a comprehensive interpretation of all types of geophysical, geochemical, hydrogeological, and geological fields, based on the study of criteria for their behavior over a long period of time in the

History of the Earth as a cosmic body and the influence of factors of extraterrestrial origin. Earthquake on May 9, 1966. (strength of 7 points) was predicted by Y.S.Shmanenko from the very close location of the Moon relative to the focus of the Tashkent earthquake on April 26, 1966.

6. Acknowledgements

The authors express their gratitude to academician K.N.Abdullabekov and Professor S.H. Maksudov for participating in the discussion. This research was conducted with the financial support of the State Basic Research Development Program (2022) of the Committee for the Coordination of Science and Technology Development under the Ministry of Innovation of the Republic of Uzbekistan.

References

1. *Biagi, P.F.* (1999) Seismic Effects on LF Radiowaves. In: Hayakawa, M., Ed., At mospheric and Ionospheric Electromagnetic Phenomena Associated with Earthquakes, TERRAPUB, Tokyo, 535-542.
2. *Biagi, P.F., Magippinto, T., Schiavulli, L., Ligonzo, T. and Ermini, A*. (2013) European Network for Collecting VLF/LF Radio Signals (D5.1a). DPC-INGV-S3 Project. Short Term Earthquake Prediction and Preparation.
3. *Hayakawa, M., Molchanov, O.A., Ondoh, T. and Kawai, E.* (1996) The PrecursorySignature Effect of the Kobe Earthquake on Subionospheric VLF Signals. Journal of Communications Research Laboratory, 43, 169-180. https://doi.org/10.1109/ELMAGC.1997.617080
4. *Hayakawa, M., Ohta, K., Maekawa, S., Yamauchi, T., Ida, Y., Gotoh, T., Yonaiguchi, N., Sasaki, H. and Nakamura, T.* (2006) Electromagnetic Precursors to the 2004 Mid Niigata Prefecture Earthquake. Physics and Chemistry of the Earth, 31, 356-364. https://doi.org/10.1016/j.pce.2006.02.023
5. *Hayakawa, M.* (2018) Earthquake Precursor Studies in Japan. In: Ouzounov, D., Pulinets, S., Hattori, K. and Taylor, P., Eds., Pre-Earthquake Processes: A Multidisciplinary Approach to Earthquake Prediction Studies, Geophysical Monograph 234, John Wiley & Sons, Inc., Hoboken, 7-18. https://doi.org/10.1002/9781119156949.ch2
6. *Hattori, K., Takahashi, I., Yoshino, C., Isezaki, N., Iwasaki, H., Harada, M., Kawabata, K., Kopytenko, E., Kopytenko, Y., Maltsev, P., Korepanov, V., Molchanov, O., Hayakawa, M., Noda, Y., Nagao, T. and Uyeda, S.* (2004) ULF Geomagnetic Field Measurements in Japan and Some Recent Results Associated with Iwateken Nairiku Hokubu Earthquake in 1998. Physics and Chemistry of the Earth, 29, 481-494. https://doi.org/10.1016/j.pce.2003.09.019
7. *Freund, F.T., Takeuchi, A. and Lau, B.W.S. (*2006) Electric Currents Streaming Out of Stressed Igneous Rocks—A Step towards Understanding Pre-Earthquake Low Frequency EM Emissions. Physics and Chemistry of the Earth, 31, 389-396. https://doi.org/10.1016/j.pce.2006.02.027
8. *Nils Olsen, Hermann Luhr, Christopher C. Finlay, Terence J. Sabaka, Ingo Michaelis, Jan Rauberg and Lars Tøffner-Clausen.* The CHAOS-4 geomagnetic field model // Geophysical Journal International (2014) 197, 815–827·doi: 10.1093/gji/ggu033
9. *Varotsos, P., Sarlis, N., Skordas, E. and Lazaridou, M.* (2006) Additional Evidence on Some Relationship between Seismic Electric Signals (SES) and Earthquake Focal Mechanism. Tectonophysics, 412, 279-288. https://doi.org/10.1016/j.tecto.2005.10.037
10. *Bleier, T., Dunson, C., Maniscalco, M., Bryant, N., Bambery, R. and Freund, F.* (2009) Investigation of ULF Magnetic Pulsations, Air Conductivity Changes, and Infrared Signatures Associated with the 30 October Alum Rock M5.4 Earthquake. Natural Hazards and Earth System Sciences, 9, 585-603. https://doi.org/10.5194/nhess-9-585-2009
11. *Eftaxias, K., Athanasopoulou, L., Balasis, G., Kalimeri, M., Nikolopoulos, S., Contoyiannis, Y., Kopanas, J., Antonopoulos, G. and Nomicos, C.* (2009) Unfolding theProcedure of Characterizing Recorded Ultralow Frequency, kHZ and MHz Electromagnetic Anomalies Prior to the L'Aquila Earthquake as Pre-Seismic Ones-Part1. Natural Hazards and Earth System Sciences, 9, 1953-1971.https://doi.org/10.5194/nhess-9-1953-2009http://www.nat-hazards-earth-syst-sci.net/9/1953/2009
12. *Contadakis, M.E., Biagi, P.F. and Hayakawa, M.* (Eds.) (2009) Ground and SatelliteBased Observations during the Time of the Abruzzo Earthquake. Natural Hazardsand Earth System Sciences, No. 102, 151. http://www.nat-hazards-earth-syst-sci.net/specialissue102.html
13. *Ouzounov, D., Pulinets, S., Romanov, A., Romanov, A., Tsybulya, K., Davidenko,D., Kafatos, M. and Taylor, P.* (2011) Atmosphere-Ionosphere Response to the M9Tohoku Earthquake Revealed by Multi-Instrument Space-Borne and Ground Observations: Preliminary Results. Earthquake Science, 24, 557-564.https://doi.org/10.1007/s11589-011-0817-z
14. *Tramutoli, V., Aliano, C., Corrado, R., Filizzola, C., Genzano, N., Lisi, M., Martinelli, G. and Pergola, N.* (2013) On the Possible Origin of Thermal Infrared Radiation(TIR) Anomalies in Earthquake-Prone Areas Observed Using Robust SatelliteTechniques (RST). Chemical Geology, 339, 157-168.https://doi.org/10.1016/j.chemgeo.2012.10.042

15. *Kiladze, R., Kachakhidze, N., Kereselidze, Z., Kachakhidze, M., Ramishvili, G. andKukhianidze, V.* (2005) Atmospheric Pressure as an Earthquake Initiative Factor onthe Example of Five Earthquakes in the Georgia. Bulletin of Georgian Academy, 171,278-281.

16. *Kachakhidze, M., Kiladze, R., Kachakhidze, N., Ramishvili, G. and Kukhianidze, V*.(2010) Connection of Large Earthquakes Occurring Moment with the Movement ofthe Sun and the Moon and with the Earth Crust Tectonic Stress Character. NaturalHazards and Earth System Sciences, 10, 1629-1633.https://doi.org/10.5194/nhess-10-1629-2010http://www.nat-hazards-earth-syst-sci.net/10/1629/2010

17. *Kachakhidze, M., Kachakhidze, N., Kiladze, R., Kukhianidze, V. and Ramishvili, G.(*2003) Relatively Small Earthquakes of Javakheti Highland as the Precursors ofLarge Earthquakes Occurring in the Caucasus. Natural Hazards and Earth SystemSciences, 3, 165-170. https://doi.org/10.5194/nhess-3-165-2003

18. *Kachakhidze, N., Kachakhidze, M., Kereselidze, Z. and Ramishvili, G.* (2009) Specific Variations of the Atmospheric Electric Field Potential Gradient as a PossiblePrecursor of Caucasus Earthquakes. Natural Hazards and Earth System Sciences, 9,1221-1226. https://doi.org/10.5194/nhess-9-1221-2009

19. *Kachakhidze, M.K., Kachakhidze, N.K. and Kaladze, T.D.* (2015) A Model of theGeneration of Electromagnetic Emissions Detected Prior to Earthquakes. Physicsand Chemistry of the Earth, 85-86, 78-81. https://doi.org/10.1016/j.pce.2015.02.010

20. *Mjachkin, V.I.* (1978) Earthquake Preparation Processes. Nauka, Moscow, 230.

21. *M Finkelstein, C Price and L Eppelbaum.* Is the geodynamic process in preparation of strong earthquakes reflected in the geomagnetic field? 2012 Journal of Geophysics and Engineering 9 (2012) 585–594DOI: 10.1088/1742-2132/9/5/585

22. *Jankowski J., Sucksdorff C.* IAGA Guide for magnetic measurements and observatory practice. Warsaw, 1996, 235 p.3.

23. *Parkinson W.* Introduction to geomagnetism. Moscow: Mir, 1986, 527 p.

24. *Virginia Klausner, Odim Mendes, Margarete O. Domingues. Japanese tsumani* 2011 effects on the geomagnetic field: Preliminary results. Twelfth International Congress of the Brazilian Geophysical Society, held in Rio de Janeiro, Brazil, August 15-18, 2011. pp.2-5

25. *Kachakhidze, M., Kachakhidze-Murphy, N., Khvitia, B. and Ramishvili, G.* (2019) Large Earthquake Prediction Methods. Open Journal of Earthquake Research, 8, 239-254. https://doi.org/10.4236/ojer.2019.84014

26. *Xiaocan Liu, Katsumi Hattori, Peng Han, Huaran CHen, Yoshino CHie, and Xudong Zhao*.Possible Anomalous Changes in Solar Quiet Daily Geomagnetic Variation (Sq) Related to the 2011 off the Pacific coast of Tohoku Earthquake (Mw 9.0) Pure Appl. Geophys. 177 (2020), 333–346

27. *K.N.Abdullabekov, Yusupov V.R.* Models (form) of long-, medium- and short-term earthquake precursors Geodesy and Geodynamics 13 2022 https://doi.org/10.1016/j.geog.2022.07.002 pp. 609-618

28. *Yusupov V.R., Shukurov Z.F., Yadigarov E.M*. Analysis of the geomagnetic field and vertical movement near the intersection of Karjantau and Tavaksay faults in Uzbekistan Geodesy and Geodynamics 12 (2021) pp.102-109 https://www.sciencedirect.com/science/article/pii/S1674984721000148

29. *MaksudovS. Kh., Abdullabekov K. N., Tuichiev A.I., Yusupov V.R.* Geomagnetic Field Variations Caused by the Processes Occurring at Different Depths in the Earth's Crust and Upper Mantle. Physics of the Solid Earth, 2021, Vol. 57, No. 3 pp.295–308 https://ui.adsabs.harvard.edu/abs/2021IzPSE..57..295M/abstract

30. *Yusupov Valijon, Soloviev Anatoly, Sidorov Roman*. Studying diurnal and secular variations of the Earth's magnetic field using data from Yangibazar magnetic observatory (Uzbekistan) // RUSSIAN JOURNAL OF EARTH SCIENCES Volume 22 № 6 pp. 2-14 https://doi.org/10.2205/2022ES000815

ГЕОДИНАМИЧЕСКАЯ ОБСТАНОВКА ЗЕМНОЙ КОРЫ ЗАПАДНО-ТЯНЬ-ШАНЬСКОЙ МИКРОПЛИТЫ

Атабеков И.У.[1], Садыков Ю. М.[1]
[1]*Институт сейсмологии АН РУз, Ташкент, Узбекистан*
E-mail: atabekovi@mail.ru

Аннотация: *В представленной работе тектоническая обстановка земной коры Западно-Тянь-Шаньской микроплиты проанализирована с помощью математической модели. На основу модели легли современная карта активных разломов и современные движения микроплиты, созданная по многочисленным источникам. В результате определены возможные места опасных землетрясений.*

Ключевые слова: *тектоническое движение, микроплиты, уравнения Стокса, схематическая карта.*

1. Введение

Современное тектоническое движение изучаются инструментальными наблюдениями, спутниковой геодезией, реконструкцией механизмов очагов землетрясений, по материалам трещинообразовании земной поверхности, сейсмодислокацией сильных современных и исторических, в том числе, палео землетрясений. Математическое моделирование таких движений с учетом результатов полученных вышеназванными инструментами и верифицированное на их данных играет немаловажное значение для тектонического прогнозирования опасных мест сильных землетрясений.

2. Материалы, методы и объект исследования

Современная структура Западно-Тянь-Шаньской микроплиты (ЗТШМПл) сформировалась в результате внутриконтинентального коллизионного горообразования в условиях взаимодействия Евразийской, Индийской и Аравийской плит. В пределах ЗТШМПл выделяется следующая система тектонических блоков 2-го ранга: Чаткало-Курама, Таласо-Фергана, Южный Тянь-Шань и Ферганская впадина [1]. Учитывая взаимосвязи новейших, молодых и современных движений с неотектонической структурой Средней Азии по данным источников [2, 3, 4, 5] построена схематическая карта активных разломов ЗТШМПл (рис. 1).

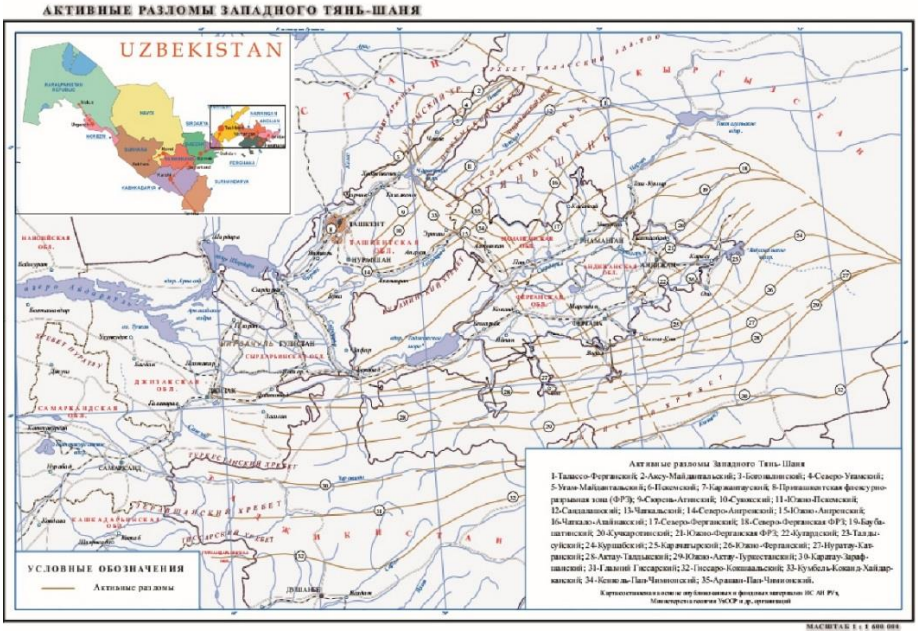

Рисунок 1. - **Схематическая карта активных разломов Западно-Тянь-Шанской микроплиты**

На карте отражены активные разломы, флексурно-разрывные зоны, палеозойские дислокации, поверхностные трещинообразования, а также изосейсты сильных землетрясений. Эта карта стала основой для создания математической модели напряженного состояния земной коры ЗТШМПл [6]. Поскольку такое обилие разломов трудно учесть в модели, было решено поэтапно усложнять задачу, с включением сначала самых глубинных разломов. За

ограничивающую границу приняли Таласо-Ферганский, Аксу–Майдантальский, Богоналинский, Гисаро-Кокшальский разломы. В качестве внутренних разломов сначала взяли Северо-Ферганский и Южно-Ферганский, а затем и их зоны динамического влияния. Поскольку тектонический характер современных движений более подходит на ползучее движение, в качестве определяющего уравнения приняты уравнения Стокса для вязкой несжимаемой жидкости с вязкостью 10^{-20}-10^{-22} пуаз. Трехмерные уравнения усреднены с учетом рельефа и границы Мохо ЗТШМПл. Усреднение проводится на определенную глубину. Поскольку в энергетическом смысле выделенной сейсмической энергии глубины 15 -20 км на несколько порядков превышает другие глубины по всей Центральной Азии, было решено ограничится анализом напряженного состояния на этом уровне. При усреднении фоновое напряжение включается дополнительно в правую часть уравнения Стокса. Усреднение уравнения несжимаемости при этом позволяет получить вертикальную скорость перемещения на поверхности Земли. В результате усреднения получаются уравнения для определения горизонтальных движений, что очень важно для тектоники. Определяя главные горизонтальные напряжения и их направления из решения задачи, принимая за третью компоненту литологическое напряжение можно провести геодинамический анализ на принятых глубинах.

Как известно, решения уравнений в частных производных всецело определяются их граничными условиями. В качестве граничных условий приняты горизонтальные скорости, определенные с помощью GPS [7] (рис. 2).

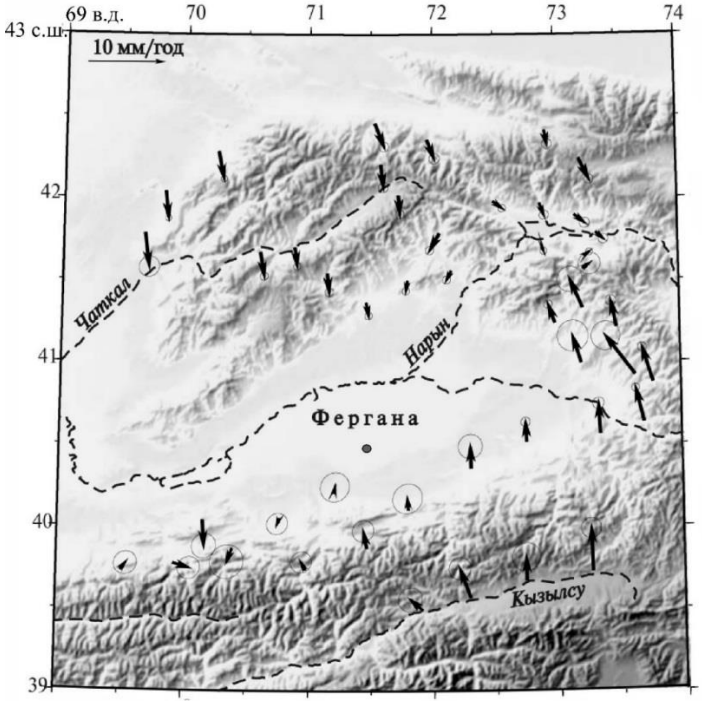

Рисунок 2. - **Скорости перемещений, построенные по данным GPS в [7]**

Использование материалов GPS требует большой осторожности, поскольку они показывают движения поверхности Земли. Инструментально отмечено [2], что перемещения к северу пунктов, расположенных на Памире, в Северо-Западном Куньлуне и в Тариме, происходят с близкими скоростями 15-20 мм/год. Это свидетельствует о том, что в настоящее время Памир и Тибет перемещаются в сторону Тянь-Шаня совместно. На фронте этого сближения Тарим пододвигается под Тянь-Шань. По данным [7] выделяются несколько районов отличающихся ориентацией векторов перемещения. В первую очередь группа пунктов, расположенных в пределах Таласо-Ферганского блока. Первая группа направлена на ЮЮЗ и все они расположены к северо-востоку от Таласо-Ферганского сдвига. К юго-западу от сдвига, в пределах того же Таласо-Ферганского блока все вектора согласно ориентированы на северо-запад. Обе группы векторов подчеркивают современную геодинамическую

обстановку в зоне Таласо-Ферганского правостороннего сдвига. Группа пунктов наблюдения, расположенных в пределах Чаткало-Кураминского блока ориентированы в южном направлении, что также свидетельствует в пользу выталкивания Чаткало-Кураминского блока на запад от Таласо-Ферганского сдвига на фоне меридионального сжатия. Группа пунктов наблюдений, расположенных в пределах южной части Ферганской впадины и Алайской долины ориентированы субмеридионально. Противоположную, южную, ориентацию показывает группа пунктов наблюдений, расположенных в долине между саями Лайляк и Исфара. Характерно, что по величине перемещений пункты наблюдений, расположенные в равнинных частях (Ферганская впадина, Нарынская впадина) уступают пунктам расположенных в горных областях. В целом данная схема подтверждает субмеридиональную ориентацию сжимающих напряжений, действующих в пределах Западного Тянь-Шаня и связанных вероятно с давлением Памирского выступа на Южный Тянь-Шань.

3. Анализ результатов моделирования

По результатам численного решения уравнения Стокса построено поле скоростей перемещения, и они сгруппированы по средним направлениям (рис. 3).

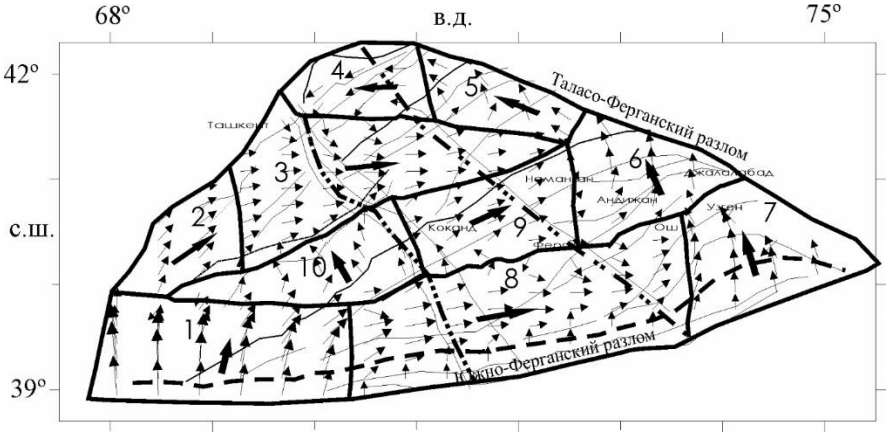

Рисунок 3. - **Поле скоростей сгруппированные по средним направлениям движения по результатам математической модели**

Результаты показывают, что территория Ферганской впадины вращается против часовой стрелки вокруг точки с координатами (39°8′ с.ш., 69°9′ в.д.) со скоростью угла вращения 4 нанорадиан/год. Вертикальные скорости вполне согласуются с установленными инструментальными данными. Тектонические блоки 2-го ранга разделились на блоки 3-ранга с характерным средним направлением движения. Сопоставление этого рисунка с комплексом геолого-геофизических материалов позволяет нам утверждать, что эти участки соответствуют реальным блокам верхней части земной коры ЗТШМПл. Результаты численного решения также сопоставлены с очагами землетрясений по каталогу УНТЦ с 1902 по 2023 с магнитудой M≥3.0. Многие очаги располагаются по границам выделенных блоков. По этим результатам следует, что наибольшей сейсмической активностью отличается южная внешняя граница ЗТШМПл, соответствующая Гиссаро-Коокшальскому разлому, зоне взаимодействия Памирской дуги и Южно-Тянь-Шаньского блока 2-го ранга. Усовершенствование модели с привлечением зон динамического влияния Северо-Ферганского и Южно-Ферганского разломов слегка изменяет поле скоростей перемещения.

В качестве узлов напряженности приняты участки, где пересекаются разнонаправленные векторы скоростей. Сопоставление их с областями ожидаемой сейсмической активизации по комплексу прогностических параметров [8] дало удовлетворительное совпадение. По полученным напряжениям с добавлением литостатического давления для рассматриваемых глубин построена геодинамическая обстановка региона (рис. 4) по методу Андерсона, согласно которому сравниваются отношение вертикального напряжения σ_{ver} к горизонтальным наибольшим σ_1 и наименьшим σ_2 напряжениям. Этот метод предложен еще в 1951 году Андерсеном (Anderson) и использовался при построении карты напряжений по

всему миру [9, 10, 11]. В этих работах выделяются три различных случая. При первом случае преобладает вертикальное напряжение $\sigma_1=\sigma_{ver}$, когда гравитация вызывает нормальные разломы, создавая горизонтальную деформацию растяжения. Во втором случае где $\sigma_2=\sigma_{ver}$, при котором разница между двумя горизонтальными напряжениями создает сдвиговую деформацию. Третий случай это когда оба горизонтальных напряжения превышают вертикальное напряжение $\sigma_3=\sigma_{ver}$, при котором деформация сжатия компенсируются за счет надвига или взброса. В отличие от подходов Zoback и Heidbach [9, 10, 11] мы используем правило знаков напряжений, принятое в классической механике, т.е. считается, что сжимающие напряжения отрицательны, а растягивающие – положительны. В силу этого главные напряжения σ_1 являются минимальными сжимающими, а σ_3 – максимальными сжимающими. Вследствие этого случай 1 и случай 3 в нашем примере поменяются местами.

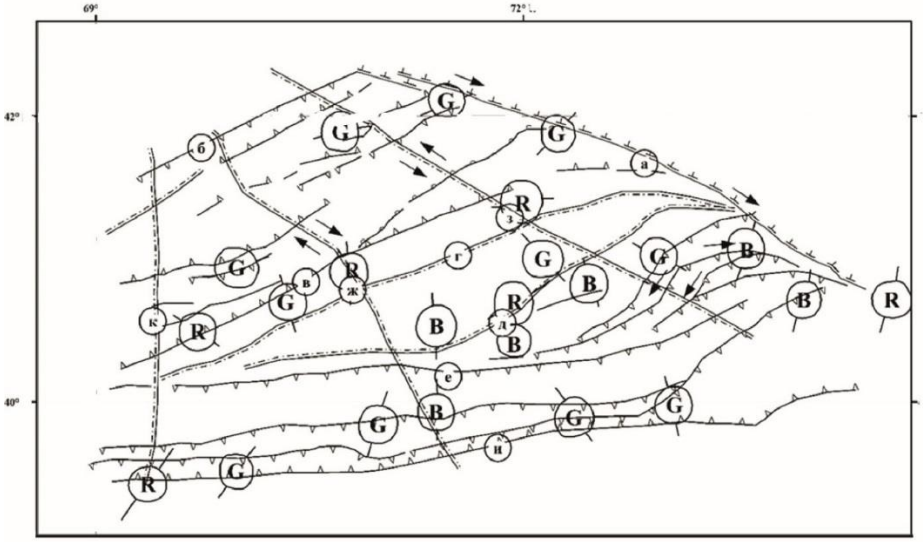

Рисунок 4. - **Геодинамическая обстановка Западно-Тянь-Шаньской микроплиты построенная по численной модели: G- взброс, B-сдвиг, R-сброс.**

4. Заключение

- Создана карта современных движений Западно-Тянь-Шаньской микроплиты с учетом активных разломов.

-Построена математическая модель напряженного состояния микроплиты по уравнениям Стокса, которые усреднены с использованием рельефа и границы Мохо.

-По результатам математической модели дана геодинамическая обстановка земной коры микроплиты.

Литература

1. *Садыков Ю.М., Нурматов У.А.* Сейсмотектоника Западного Тянь-Шаня // Проблемы сейсмологии. 2021, №2, стр.61–73.
2. *Буртман В.С.* Геодинамика Памир-Пенджабского синтаксиса // Геотектоника, 2013, №1, стр. 36-58
3. *Ярмухамедов А.Р., Якубов Д.Х., Саттаров А.С.* Современная геодинамика Восточного Узбекистана / Ташкент, ФАН, 1979, 112 с.
4. *Ибрагимов Р.Н.* Сейсмогенные зоны Среднего Тянь-Шаня / Ташкент, ФАН, 1978, 144с.
5. *Ходжаев А.К.* Палеосейсмогеология Чаткало-Кураминского региона / Ташкент, ФАН, 1985, 132 с.
6. *Атабеков И.У., Садыков Ю.М.* Напряженное состояние земной коры Западного Тянь-Шаня в Центральной Азии (Узбекистан): Математическое моделирование // Геотектоника. 2022, №3, стр. 50-65. https://doi.org/10.31857/S0016853X22030031.
7. *Зубович А.В.* Данные спутниковой геодезии о современных движениях земной коры. В кн. Современная геодинамика областей внутриконтинентального коллизионного горообразования (Центральная Азия) / Часть III.5, Москва, Научный Мир, 2005б стр.201-218.
8. *Артиков Т.У., Ибрагимов Р.С., Ибрагимова Т.Л., Мирзаев М.А., Ребецкий Ю.Л.* Напряженное состояние земной коры, сейсмичность и перспективы долгосрочного прогноза сильных землетрясений на территории Узбекистана // Геология и геофизика. 2022, Т.7, №12, стр. 1733–1753.

9. *Zoback M.L.* First and Second Modern Pattern of Stresses in the Lithosphere: The World stress Map project. // Journal of Geophysical Research, 1992, vol.97, No. B8, pp. 11,707-11,728
10. *Zoback M. L., Zoback M.* Lithosphere Stress and Deformation. // Treatise on Geophysics. 2007, pp.255–271. https://doi.org/10.1016/b978-0-444-53802-4.00115-9
11. *Heidbach O., Rajabi M., Cui X. , Fuchs K. , Müller B., Reinecker J., Reiter K., Tingay M., Wenzel F., Xie F. , Ziegler M.O., Zoback M.L., Zoback M.* The World Stress Map database release 2016: Crustal stress pattern across scales // Tectonophysics. 2018. vol. 744, pp.484-498. https://doi.org/10.1016/j.tecto.2018.07.007

ПОСЛЕДСТВИЯ ЗЕМЛЕТРЯСЕНИЯ В ГОРОДЕ ИСКЕНДЕРУН

Ахмедов М.А.[1]
[1]*Институт механики и сейсмостойкости сооружений, Ташкент, Узбекистан*
E-mail: gulora@yandex.ru

Аннотация: *6 февраля 2023 г. в восточной части Турции произошло катастрофическое землетрясение с магнитудой отдельных толчков 7,8 и 7,5, очаги которых находились в Восточно-Анатолийском разломе. Это привело к гибели десятков тысяч людей. В 11 из 17 пострадавших провинций Турции погибло 50 783 человека, 297 пропали без вести и 107 204 получили ранения. В Хатае, одной из 11 провинций, где землетрясение нанесло наибольший ущерб, погибли 23 065 человек, и ещё 30763 человек получили ранения. Обрушилось 13 517 зданий, 8 162 требовали сноса и 67 346 были сильно повреждены. В представленном докладе изложены последствия землетрясения в г. Искендерун.*

Ключевые слова: *землетрясение, ущерб, вторичное воздействие, риск.*

1. Введение

Город в провинции Хатай на юге Турции, г. Искендерун расположен на побережье одноименного залива на берегу Средиземного моря (рис. 1). Количество жителей в Искендеруне сегодня — 331 697 человек, плотность населения — 446,4/км².

Рисунок 1. - **Искендерун на карте провинции Хатай в Турции [1]**

Сегодня Искендерун — один из крупнейших городов провинции Хатай, является крупным турецким портом в Восточном Средиземноморье. Также Искендерун крупный центр черной металлургии и с развитой индустрии переработки продуктов сельского хозяйства. Во многом бесперебойное функционирование этих отраслей обеспечивает устойчивое развитие целого региона. Изучение крупного катастрофического землетрясения, произошедшего в Турции находится в поле зрения как сейсмологов, так и специалистов по сейсмостойкому строительству [1-3]. В данной работе мы попытаемся понять суть произошедшего и какие уроки могут быть излечены из этого события.

2. Последствия прямого воздействия землетрясения

В результате прямого воздействия катастрофического землетрясения 6 февраля 2023 в Искендеруне произошло обрушение 534 зданий, 337 из которых требовали сноса и 4622 получили серьезные повреждения [4], в том числе были разрушены современные здания последних лет постройки (рис. 2) [5], исторические постройки (Собор Благовещения (рис. 3) [5]). По меньшей мере 3109 человек погибли в городе и более 12 000 получили ранения [6].

Рисунок 2. - **Здание в Искендеруне, построенное в 2019 году: до. и после землетрясения. Фото: bbc.com[5]**

Рисунок 3. - **Разрушенная католическая церковь после землетрясения [5]**

Рисунок 4. - **Фото: Umit Bektas / Reuters [5].**

3. Последствия вторичных воздействий землетрясения

Вторичные воздействия, вызванные сейсмическим воздействием также имели значительное влияние на инфраструктуру.

Турецкий порт Искендерун временно приостановил свою работу из-за полученных, в результате мощного землетрясения обрушения причала порта. В результате опрокинулись контейнеры, что привело к сильному пожару (рис. 5), пламя которого охватило почти всю пристань. Огонь был настолько сильным, что его не могли хотя бы взять под контроль в течении двух дней [7]. Взять огонь под контроль пожарные смогли только 8 февраля [7] и

окончательно потушили его 10 февраля. В общей сложности 3670 контейнеров были уничтожены пожаром в порту [7, 8].

Рисунок 5. – **Горящие контейнеры в порту Искендерун [7].**

Далее, из-за землетрясений, в Искендеруне поднялся уровень моря. Наводнение произошло вдоль береговой линии города, затопив улицы и площади на глубину до 200 м вглубь города [9] (рис. 6). Вода не отступила даже через два дня после землетрясения [9].

Рисунок 6. – **Затопленные набережные Искендеруна[9]**

Ситуация в городе, в котором проживало более 300 тысяч человек, осложнялась крупным пожаром, возникшим на складе временного хранения контейнеров в порту Искендеруна сразу после землетрясения 6-го февраля и затоплением его пригородных районов и сельскохозяйственных угодий (рис. 7).

Рисунок 7. – **Затопленный пригород Искендеруна [9]**

Согласно данным сейсмологических наблюдений, к затоплению Искендеруна привело смещение Аравийской тектонической плиты. Она сдвинулась в сторону Сирии на три метра и опустилась примерно на шесть метров [10].

Искендерун находится в зоне стыка двух тектонических плит – Анатолийской и Аравийской. В результате землетрясений Аравийская платформа сдвинулась на 3 метра относительно Анатолийской, а также оказалась на 6 метров ниже, чем была до нее [10]. Или

Турция сместилась на 3 метра к Юго-Западу в Средиземное море, что привело к изменению прибрежной зоны, какие-то районы поднялись над уровнем моря, какие-то опустились.

Следующим последствием землетрясения было явление разжижения грунтов. С помощью спутника и дистанционного зондирования было обнаружено разжижение грунта вдоль южной части Восточно-Анатолийском разлома от Антакьи до Голбаси. Разжижение наблюдались в прибрежных районах, речных долинах и вблизи них, а также в осушенных озерах или болотах, покрытых отложениями голоцена. Эти последствия были широко распространены в долине Амик и на равнине реки Оронт, к северу от Антакьи (рис. 1). Разжижение также наблюдалось в Самандаге. На озере Гельбаши, провинция Адыяман, произошло боковое распространение вдоль северного, восточного и южного побережья. Часть берега озера также была затоплена. Гельбаши также пострадал в результате разжижения и бокового распространения (рис. 8, 9).

Рисунок 8. – **Пример разжижения и частично наклоненного жилого дома в Гельбаши [9]**

Рисунок 9. – **Оседание грунта на озере Гельбаши в результате бокового распространения [9]**

Разжижение под Искендеруном привело к выбросу песка, которое привело к оседанию грунта под Искендеруном при землетрясении. После землетрясений в городе наблюдались регулярные наводнения. Более раннее наводнение может быть связано с разжижением, в то время как последующие события могут быть вызваны повреждением побережья и водной инфраструктуры. Большие участки побережья и участки пирсов были затоплены. Большие волны от плохой погоды и цунами, возможно, способствовали последствиям, наблюдаемым в Искендеруне, после землетрясения.

Несмотря на то, что эпицентр находился в 90 км от береговой линии, в Средиземном море было зарегистрировано цунами. Небольшие волны цунами были зафиксированы у побережья Кипра. Сила цунами составила 0,17 м, а волны цунами были зафиксированы на уровне 0,12 м в Искендеруне.

Кроме изменения уровня моря и прибрежной зоны в Турции, возможны изменения направление рек, образование небольших разломов и образование на их местах новых озёр. Строительство городов на морском побережье большой риск, из-за изменения уровня моря, землетрясений и цунами.

4. Обсуждение

Теперь, Турции придется переселять население 300 000 города, дальше от морского побережья. Восстановление прибрежной зоны очень затратное и бессмысленно, если учитывать, что дома на первых этажах зданий постепенно могут уйти под воду, затопив подземные парковки и канализационные сети [7, 9].

В результате данного землетрясения в соседней Сирии погибли по крайней мере 8476 человек. От землетрясения пострадали более двух десятков городов, оно затронуло по меньшей мере 15,73 миллиона человек и 4 миллиона зданий. Тысячи людей оказались в ловушке под завалами рухнувших зданий. Многие люди пропали без вести под завалами. Около 1,5 миллионов человек остались без крова. Более 2 миллионов жителей пострадавших провинций были эвакуированы в более безопасные районы.

В чем же причина разрушений? Чем выше этажность, тем больше амплитуда колебаний и вероятность обрушения – этот факт, как правило принимается как императив. Тем не менее, в Искандеруне были разрушены не только многоэтажные постройки (рис. 3, 5).

Отсюда вывод, что грунтовые условия имеют если не первостепенное значение, то во всяком случае очень важное. Так как в соседнем городе Эрзин даже старые сооружения, хорошо пережили землетрясение.

Во всяком случае вопросы о причинах таких катастрофических разрушений и многочисленных жертвах на данном этапе остаются дискуссионными и ждут всеми признанной экспертной оценки.

5. Заключение

На фоне соседнего города Эрзин который практически не пострадал стоит отметить причины данных отличий. Первое и самое важное это выбор места для возведения строений (land use planning). Это имеет первостепенное значение так как именно это во многом стало причиной большинства разрушений. Вторым фактором, повлиявшим на многочисленные жертвы считаем, что это недостаток самих строительных норма принятых в регионе и не должное исполнение уже существующих. Также стоит отметить и вторичное воздействие землетрясений, к которым в целом готовность специальных служб оказалась недостаточной.

Литература

1. *Jiang, Xinyu, Xiaodong Song, Tian Li, Kaixin Wu.* Special Focus/Rapid Communication Moment Magnitudes of Two Large Turkish Earthquakes on February 6, 2023 from Long-Period Coda // Earthquake Science. 2023, vol. 36, No. 2, pp. 169-174. https://doi.org/10.1016/j.eqs.2023.02.008.
2. *Saraçoğlu, Mustafa Halûk, and Ahmet Özkaya*. Investigation of Acceleration on Non-Structural Building Elements under Earthquake Effect // *Turkish Journal of Engineering*. 2023, vol. 7, No. 1, pp. 56-63 https://doi.org/10.31127/tuje.1021866.
3. *Zahradník, Jiří, Fatih Turhan, Efthimios Sokos, František Gallovič*. Asperity-like (Segmented) Structure of the 6 February 2023 Turkish Earthquakes // *EarthArXiv*. 2023
4. 2023 Turkey–Syria earthquakes // https://en.wikipedia.org/wiki/2023_Turkey%E2%80%93Syria_earthquakes
5. Turkey earthquake: Before and after pictures show extent of destruction // https://www.bbc.com/news/world-europe-64544998
6. Authorities seize aid intended for earthquake victims in epicenter area // https://bianet.org/haber/authorities-seize-aid-intended-for-earthquake-victims-in-epicenter-area-274389
7. Как Турция и Сирия справляются с последствиями землетрясения. Фотогалерея // https://www.rbc.ru/photoreport/07/02/2023/63e211e29a79471af84a3d85
8. *Ozalp Mehmet* Will the Turkish earthquakes affect how the country is governed? // https://theconversation.com/will-the-turkish-earthquakes-affect-how-the-country-is-governed-199946.
9. Турецкий город Искендерун начал уходить под воду после землетрясения // https://www.m24.ru/videos/proisshestviya/09022023/549120?utm_source=CopyBuf
10. Тектоническая плита под Турцией опустилась на 6 метров, что привело к затоплениям // https://topcor.ru/31919-tektonicheskaja-plita-pod-turciej-opustilas-na-6-metrov-chto-privelo-k-zatoplenijam.html

МОДЕРНИЗАЦИЯ ИНЖЕНЕРНО-СЕЙСМОМЕТРИЧЕСКОЙ СТАНЦИИ НАБЛЮДЕНИЙ С ПРИМЕНЕНИЕМ КОМПЬЮТЕРНЫХ ТЕХНОЛОГИЙ.

Галиаскаров В.А.[1], Тешабаев З.Р.[1]

[1]Институт механики и сейсмостойкости сооружений имени М.Т. Уразбаева, Ташкент, Узбекистан
E-mail: victor.galiaskarov@gmail.com

***Аннотация*:** *При создании 12-и канального измерительного комплекса было выявлено различие коэффициентов усиления в измерительных каналах. Для изменения коэффициентов усилений в измерительных каналах была осуществлена коррекция путем ввода корректирующих коэффициентов в программу компьютера, что привело к одному значению усиления по напряжению во всех каналах.*

Созданная компьютерная программа для ИССН позволяет растягивать сейсмограммы при просмотре и анализе зарегистрированных землетрясений, что повышает точность при определении амплитудно-частотных характеристик колебаний здания.

***Ключевые слова*:** *инженерно-сейсмометрическая станция, сейсмограмма, коррекция усиления каналов.*

1. Введение

Изучение последствий сильных землетрясений показывают, объекты, возведенные без соблюдения норм сейсмической защиты, подвержены разрушениям, приводящим к человеческим жертвам. Возведения зданий, соответствующих сейсмостойкости, должны строиться согласно расчетам, а построенные здания должны соответствовать строительным нормам, и исследованы с помощью специализированного оборудования.

Анализ результатов инструментальных наблюдений за колебаниями сооружений на различных грунтовых основаниях при землетрясениях, имеет прямое отношение не только к созданию новых нормативных документов, но и оценке методов расчета на сейсмостойкость, усовершенствованию расчетных моделей и схем сооружений [1-3].

Результаты натурных измерений являются исходной информацией для обоснования модели и теоретических предпосылок при расчетах зданий и сооружений. По записям колебания грунтового основания и здания формируются расчетные значения сейсмических воздействий, при этом большое значение имеет амплитудно-частотный спектр внешних нагрузок. Исходя из этого, в институте механики и сейсмостойкости сооружений АН РУз разработан и создан 12-ти канальный измерительный комплекс на основе компьютерной технологии [4].

Регистрирующее устройство с ПК, входящие в состав измерительного комплекса предназначены для регистрации электрических сигналов от 12-и сейсмометров или иных датчиков и их записи на персональный компьютер. Измерительный комплекс обладает возможностями наблюдения на экране дисплея ПК за процессами, происходящими в реальном масштабе времени и позволяет сохранить данные результатов измерений в виде файлов для их дальнейшей обработки.

2. Объект исследования

На базе измерительного комплекса создана Инженерно-сейсмометрическая станция наблюдений (ИССН), расположенная в подвальном помещении здания института, где происходит регистрация и запись колебаний основания здания во время землетрясений (рис.1). Наблюдения за колебаниями здания при землетрясениях осуществляются с помощью двух точек наблюдений, организованных в подвальном помещении (№ 1) и на чердаке здания (№ 2). В точках наблюдений №1 и №2 установлены сейсмодатчики для регистрации записей перемещений (СМ-3) и ускорений (ОСП-2М), которые регистрируют продольные, поперечные и вертикальные колебания по направлениям OX, OY, OZ относительно оси здания (рис.2, Табл.2).

Рисунок 1. - **Расположения ИССН в подвальном помещении, точка №1**

На каждое направление (X, Y, Z) необходимо задействовать по четыре канала. Распределение измерительных каналов по направлениям здания приведены в Табл. 1. Перед эксплуатацией 12-и канальной системы необходимо определить коэффициенты усиления в различных каналах, что связано с разбросом параметров радиодеталей одного номинала, примененных при построении каналов. Каналы, сейсмометры которых ориентированные в одном направлении, должны иметь одинаковые коэффициенты усиления во всем амплитудно-частотном диапазоне, что позволит определить точные значения смещений и ускорений в измерительных точках.

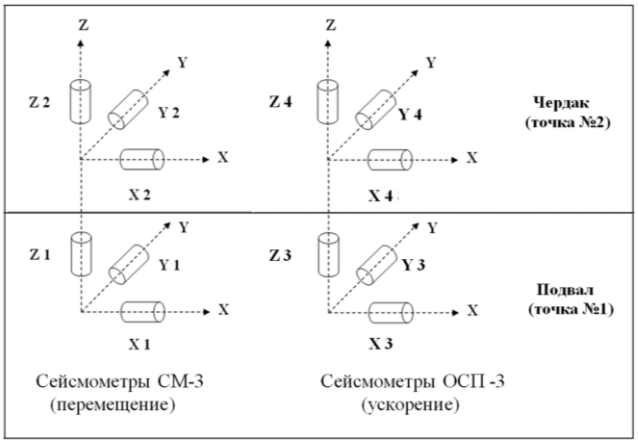

Рисунок 2. - **Расположение сейсмометров в здании института.**

Таблица 1.

№ канала	Сейсмометр	Расположение сейсмометра	Направление перемещения	
1	СМ-3	Подвал	X-1	Продольное
2	СМ-3	Подвал	Y-1	Поперечное
3	СМ-3	Подвал	Z-1	Вертикальное
4	СМ-3	Чердак	X-2	Продольное
5	СМ-3	Чердак	Y-2	Поперечное
6	СМ-3	Чердак	Z-2	Вертикальное
			Направление ускорения	
7	ОСП-3М	Подвал	X-3	Продольное
8	ОСП-3М	Подвал	Y-3	Поперечное
9	ОСП-3М	Подвал	Z-3	Вертикальное
10	ОСП-3М	Чердак	X-4	Продольное
11	ОСП-3М	Чердак	Y-4	Поперечное
12	ОСП-3М	Чердак	Z-4	Вертикальное

3. Постановка задачи

Для определения значений коэффициентов усиления измерительных каналов собрана схема в составе звукового генератора ГЗ-102, двенадцати измерительных каналов и компьютера с программным обеспечением (рис.3). На входы каналов подавался сигнал с генератора амплитудой 30 мВ и частотой 25 Гц. Не меняя величины входного сигнала, устанавливаем делители входного сигнала в каждом канале в положение с одинаковыми показаниями коэффициентов затухания β: 1; 2; 5; 10; 20; 50; 100. На дисплее против каждого канала появляется средняя величина амплитуды Аср в цифровом виде, рассчитанная программой (рис.4) Значения амплитуд сигналов в каждом канале приведены в Табл.2.

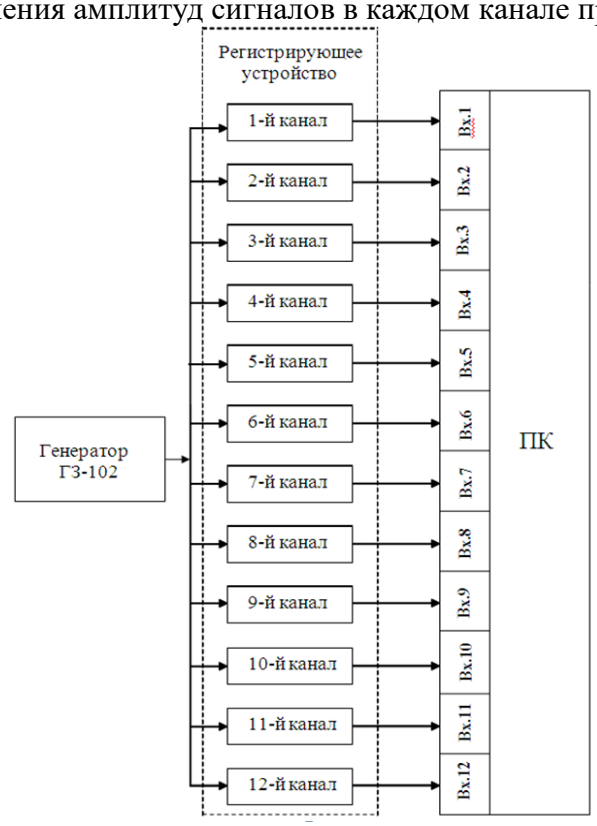

Рисунок 3. - **Проверка 12-и канального регистрирующего устройства звуковым генератором**

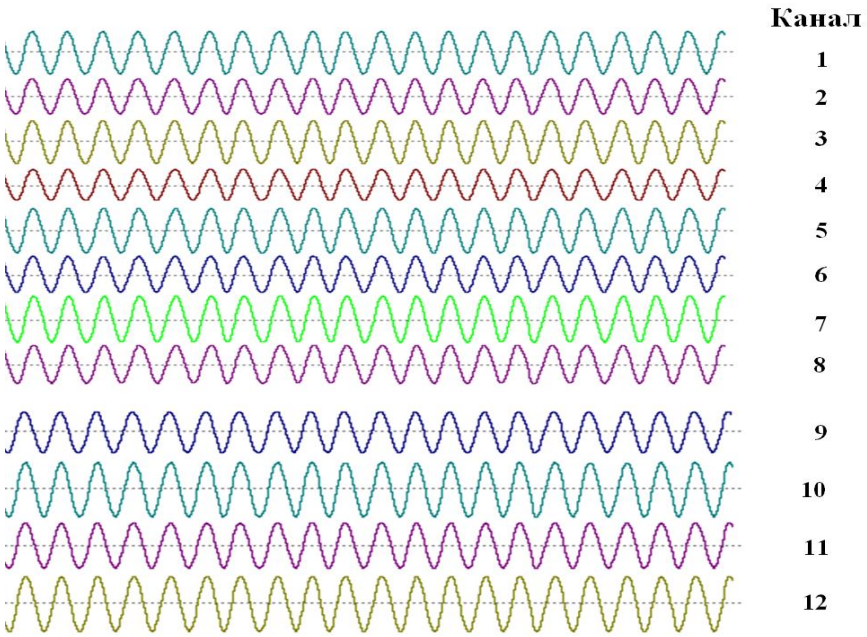

Рисунок 4. - **Сигнал генератора амплитудой 30 мВ и частотой 25 Гц, обработанный регистрирующей системой и показанный на дисплее при β=20 в каждом канале.**

Таблица 2.

Канал (n)	Положение делителя входного сигнала, β						
	1	2	5	10	20	50	100
	Acp, B	Acp, B	Acp, B	Acp, B	Acp, B	Acp, B	Acp, B
1	2.28	1.45	0.72	0.43	0.23	0.11	0.06
2	2.34	1.98	0.98	0.59	0.17	0.15	0.11
3	2.26	1.64	0.81	0.49	0.25	0.12	0.07
4	2.30	1.21	0.59	0.35	0.16	0.14	0.12
5	2.27	1.21	0.59	0.36	0.26	0.15	0.13
5	2.23	1.21	0.60	0.35	0.19	0.09	0.05
7	2.26	1.40	0.69	0.42	0.24	0.11	0.05
8	2.17	1.23	0.60	0.36	0.27	0.21	0.19
9	2.14	1.32	0.65	0.40	0.29	0.23	0.20
10	2.27	1.21	0.59	0.36	0.21	0.15	0.13
11	2.23	1.21	0.60	0.35	0.26	0.09	0.05
12	2.26	1.40	0.69	0.42	0.28	0.11	0.05

Используя данные, приведенные в Табл.2, производится корректировка коэффициентов усилений измерительных каналов. Рассмотрим на примере коррекцию измерительных каналов, расположенных в подвале и на чердаке здания при коэффициенте затухания $\beta = 20$ (Табл.2).

Чтобы выровнять амплитудные характеристики в каналах, необходимо привести усиления всех каналов к единому значению, например, к величине амплитуды первого канала.

Пример, амплитуда второго канала Acp2 = 0.17 В (вольт), амплитуда первого канала Acp1 = 0.23 В. Приведем коррекцию второго канала, т.е. поднимем усиление во втором канале до величины первого канала 0.23 В.

$$K_2 = Acp1 / Acp2,$$

где – K_2- коэффициент отношений средней амплитуды первого канала к средней амплитуде корректируемого (второго) канала; Acp1 - средняя амплитуда первого канала; Acp2 - средняя амплитуда корректируемого второго канала.

Для первого канала коэффициент коррекции равен $K_1 = 0.23 / 0.23 = 1$.

Для второго канала коэффициент коррекции равен $K_2 = 0.23 / 0.17 = 1.35$.

Для коррекции усиления второго канала в программу вводится коэффициент коррекции $K_2 = 1.35$

$$Acp2 * K_2 = 0.17 * 1.35 = 0.23,$$

тем самым, выравнивается усиление второго канала до величины амплитуды первого канала.

Таблица 3.

Канал (n)	Положение делителя входного сигнала, β													
	1		2		5		10		20		50		100	
	Acp	Kn	Acp	Kn	Acp	Kn	Acp	Kn	Acp	Kn	Acp	Kn	Acp	Kn
1	2.28	1	1.45	1	0.72	1	0.43	1	0.23	1	0.11	1	0.06	1
2	2.34	1.03	1.98	1.37	0.98	1.36	0.59	1.37	0.17	1.35	0.15	1.36	0.11	1.83
3	2.26	0.99	1.64	1.13	0.81	1.13	0.49	1.14	0.25	0.92	0.12	1.09	0.07	1.17
4	2.30	1	1.21	1	0.59	1	0.35	1	0.16	1.44	0.14	1	0.12	1
5	2.27	0.99	1.21	1	0.59	1	0.36	1.03	0.26	0.88	0.15	1.07	0.13	1.08
6	2.23	0.97	1.21	1	0.60	1.02	0.35	1	0.19	1.21	0.09	0.64	0.05	0.42
7	2.26	1	1.40	1	0.69	1	0.42	1	0.24	0.96	0.11	1	0.05	1
8	2.17	0.96	1.23	0.88	0.60	0.87	0.36	0.86	0.27	0.85	0.21	1.91	0.19	3.8
9	2.14	0.95	1.32	1.06	0.65	0.94	0.40	0.95	0.29	0.82	0.23	2.09	0.20	4.0
10	2.28	1	1.45	1	0.72	1	0.43	1	0.21	1.10	0.11	1	0.06	1
11	2.34	1.03	1.98	1.37	0.98	1.36	0.59	1.37	0.26	0.88	0.15	1.36	0.11	1.83
12	2.26	1.01	1.64	1.13	0.81	1.13	0.49	1.14	0.28	0.82	0.12	1.09	0.07	1.17

Для третьего канала коэффициент коррекции равен $K_3 = 0.23 / 0.25 = 0.92$. Для четвертого канала коэффициент коррекции равен $K_4 = 0.23 / 0.16 = 1.44$, аналогично проводятся коррекции

для остальных каналов при β = 20.

Результаты проведенных вычислений коэффициентов коррекций для 12 каналов при всех положениях делителей входного сигнала помещены в Табл. 3. Введение коэффициентов коррекций выравнивают амплитудные характеристики усилителей, приводя их к одинаковому усилению во всех каналах. Для этого в программу были внесены коэффициенты коррекции K_n, вычисленные при проверке каналов регистрирующего устройства.

Рисунок 5. - **Амплитуда сигналов в 12 каналах после коррекции (при β =20).**

После коррекции усиления каналов, можно приступить к тарировке 12-и канальной регистрирующей системы.

Для выявления адекватности записи сигнала сейсмометра разработанной регистрирующей системой был использован экспериментальный вибростенд (рис.6), имитирующий колебания объекта при землетрясениях. Измерительный комплекс состоит из 12 сейсмодатчиков, 12-канальной ИССН, компьютера с программным обеспечением и канала с тензометрическим усилителем «ТОПАЗ» [5].

При тарировке каналов регистрирующего устройства подвижная платформа экспериментального стенда совершает движение в горизонтальной плоскости с заданной амплитудой и частотой, имитирующих колебания объекта при землетрясениях.

Регистрирующее устройство предназначено для регистрации электрических сигналов от 12-и сейсмометров или иных датчиков и их записи на персональный компьютер.

Каждый канал регистрирующего устройства состоит из: - делителя ступенчатого снижения величины входного электрического сигнала в 1; 2; 5; 10; 20; 50 и 100 раз.

- усилителя для усиления слабых электрических сигналов;

- аналого-цифрового преобразователя (АЦП), для преобразования аналоговой информации, поступающей с сейсмометрического датчика в цифровой код для ввода в компьютер.

Тензометрический измерительный канал состоит из тензометрического датчика, тензометрического усилителя «ТОПАЗ-4-01» с блоком питания «АГАТ» и аналого-цифрового преобразователя.

Компьютер с программным обеспечением общий для регистрирующего устройства и тензометрического канала.

Рисунок 6. - **Калибровка измерительных каналов ИССН с сейсмометрами на экспериментальном вибростенде.**

4. Результаты

После проведения тарировочных работ, ИССН была введена в эксплуатацию для регистрации в точках наблюдений колебаний здания института при землетрясениях [6].

Для ИССН создана программа регистрации и записи сейсмограмм землетрясений с последующим сохранением в виде файлов по каждому землетрясению. Программа регистрации записала данные сейсмометров, произошедшего землетрясения в Китае 13.05.2020 года с магнитудой 4.3 в эпицентре, зарегистрированная ИССН с силой менее 1 балла.

Также создана программа для просмотра сейсмограмм, позволяющая растягивать сейсмограммы при их просмотре и анализе. На рис.7 приведена сейсмограмма данного землетрясения.

На данной сейсмограмме приведены записи 6 каналов, три канала с сейсмометрами, расположенными на чердаке (при β=10) и три канала с сейсмометрами, расположенных в подвальном помещении (при β=50). Данные коэффициенты затуханий β выставлены предварительно для подбора оптимальных значений при эксплуатации ИССН.

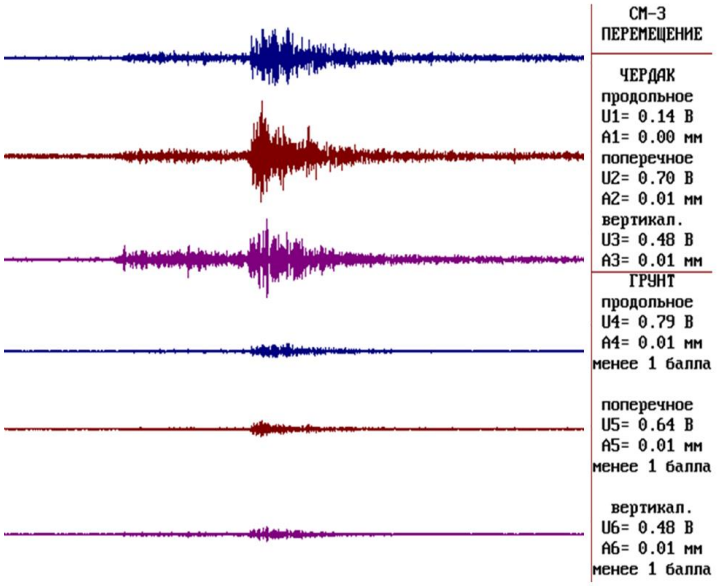

Рисунок 7. - **Сейсмограмма землетрясения, произошедшего в Китае 13.05.2020 г.**

На рис.8 приведен фрагмент сейсмограммы рис.7, растянутой до 12 секунд, что позволило подсчитать периоды колебаний. Интервал между пунктирными вертикальными линиями равен одной секунде [7].

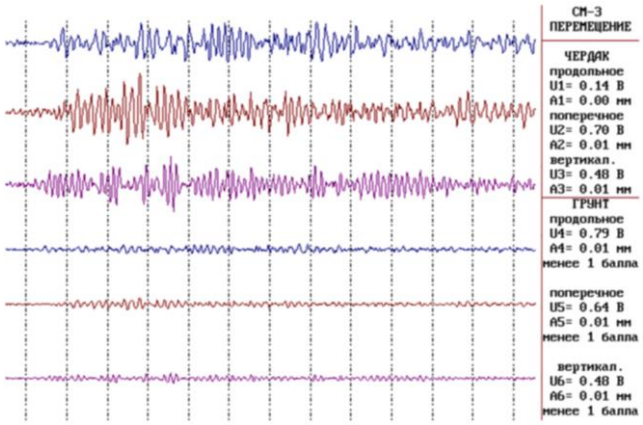

Рисунок 8. - **Фрагмент сейсмограммы рисунка 7 длительностью 12 секунд.**

На рис.8 приведен фрагмент сейсмограммы рис.7, растянутой до 12 секунд, что позволило подсчитать периоды колебаний. Интервал между пунктирными вертикальными линиями равен одной секунде [7].

Например:

в продольном направлении здания период колебаний равен

$$T_{прод} \approx 0.2\ с;$$

в поперечном направлении здания период колебаний равен примерно

$$T_{поп} \approx 0.17\ с;$$

в вертикальном направлении здания период колебаний равен

$$T_{верт} \approx 0.17\ с.$$

5. Заключение

1. Создание 12-и канального измерительного комплекса выявило различие коэффициентов усиления в измерительных каналах, что связано с разбросом параметров комплектующих электронных деталей. Для устранения данного недостатка была осуществлена коррекция каналов путем ввода корректирующих коэффициентов в программу компьютера, что позволило добиться одинакового усиления во всех каналах.

При создании многоканальных измерительных комплексов, при наличии различных коэффициентов усилений в каналах, можно использовать данный метод коррекции каналов с целью получения одинакового усиления во всех каналах.

2. Созданная программа для ИССН, регистрирует и записывает данные, поступающих от сейсмометров, с последующим сохранением в виде файлов по каждому землетрясению.

Программа для просмотра, позволяет растягивать сейсмограмму при анализе землетрясений, что повышает точность определения амплитудно-частотных характеристик колебаний здания для проведения дальнейших расчетов на сейсмостойкость.

Литература

1. Рекомендации по организации и эксплуатации станций инженерно-сейсмометрической службы. Москва, 1984г., 75с.
2. Аппаратура и методика сейсмометрических наблюдений в СССР. М.: Наука, 1974, 242с.
3. Приборы и методы регистрации землетрясений. Сейсмические приборы. М.: Наука, выпуск 19, 1987, 182с.
4. Отчеты о научно-технической работе по уникальным объектам: «Инженерно-сейсмометрические станции наблюдений» ИМ и СС АН РУз, Ташкент, ежегодные отчеты НИР с 2005 по 2022 годы.
5. *Мехеда В.А.* Тензометрический метод измерения деформаций. Самара,изд.СГАУ,2011,55с.
6. Руководство по сбору, обработке и использованию инженерно-сейсмометрической информации. М.:ЦНИИСК им. В.А. Кучеренко Госстроя СССР, 1980, 50с.
7. *Галиаскаров В.А., Тешабаев З.Р.* Экспериментальные исследования колебаний сооружений при землетрясениях. Сборник материалов Республиканской научно-практической конференции по теме «Перспективы подготовки кадров в сфере сейсмостойкости зданий и сооружений». Ташкентский архитектурно – строительный университет. Ташкент, 23-24 декабря 2023 г., с.212-217.

ОЦЕНКА СЕЙСМИЧЕСКОГО РИСКА ДЛЯ ФЕРГАНСКОЙ ОБЛАСТИ

Ёдгоров Ш.И.[1], Актамов Б.У.[1], Авазов Ш.Б.[1], Тешаева Р.Б.[1]
[1]Институт сейсмологии им.Г.А. Мавлянова АН РУз, Ташкент, Узбекистан
E-mail: shuhrat.2016avazov@gmail.com

Аннотация. *В мировой практике большое значение имеют вопросы оценки потерь от сильных землетрясений и уменьшения последствий землетрясений в области сейсмической безопасности. В целях защиты населения и территорий, расположенных в сейсмоактивных районах, особое внимание уделяется оценке масштабов экономических потерь от землетрясений, в частности, оценке различных уровней сейсмических рисков. В статье представлены оценки сейсмического риска Ферганской области, на основе сценарного землетрясения с использованием программы «INTensity MAP v3.02» и «SeismicRiskAssessment 3». В результате чего были определены последствия повреждения существующих конструктивн ых категорий жилых зданий при сценарном землетрясении, а также экономические потери в 15 районах и 4 городах Ферганской области.*

Ключевые слова: *сейсмический интенсивность, землетрясение, грунт, сейсмический риск, экономический ущерб, геонформационные системы.*

1. Введение.

В мировом масштабе вопросы прогнозирования последствий сильных землетрясений на территории регионов и снижения их ущерба являются наиболее значимыми. Обеспечение стабильного развития государств, расположенных в сейсмоопасных зонах связано с экономическим ущербом, нанесенного землетрясением. В частности, проведение комплексных исследований с целью оценки сейсмического риска и прогноза его на определенный период дает возможность разработать превентивные мероприятия по снижению последствий сильных землетрясений. В настоящее время имеется принципиальная возможность долгосрочной прогнозной оценки последствий сильного землетрясения. В частности, возможен прогноз сейсмической опасности в определенных территорий и реакции зданий и сооружений на сейсмические воздействия, и, следовательно, прогноз состояния урбанизированной территории после землетрясения. На основе такого прогноза, в свою очередь, возможна разработка мер по смягчению последствий землетрясения, а также обоснование планировочных решений при освоении новых сейсмоопасных территорий. Оценка и районирование сейсмического риска территорий областей в этом аспекте весьма актуальная задача.

При рассмотрении сейсмического риска территории Ферганской области Республики Узбекистана учтён положительный опыт Узбекистана (Ismailov, V. A. et al 2023, Ismailov, V. A. et al 2022, Yodgorov Sh.I. 2022, Исмаилов В.А. ва бошқ. 2020, Исмаилов В.А. и др. 2021), а также существующих передовых методологий оценки и картирования, применяемый в других странах, в частности Германии (Wieland M. et al 2015), Италии, России (Осипов В.И. и др. 2015), Молдовы, Армении и др. Необходимо отметить работу Италянских (Bragato, P. L. et al 2020, Ibragimov R.S. et al 2022, Peresan A. et al 2023, Petrovic B. et al 2022, Poggi V. et al 2021), Китайских (Xin D. et al 2021), а также Непалских (Bhochhibhoya S. and Maharjan, R. 2022) специалистов которые занимается снижения риска землетрясений.

Территория Ферганской области Республики расположена в сейсмически активных зонах и в полной мере подвержена ощутимым сейсмическим воздействиям. По историческим и инструментальным данным на территории республики зафиксированы землетрясения, вызывавшие сотрясения с 8 и 9 баллов по шкале MSK-64. Следовательно, для этих территорий высока вероятность повторения подобных событий и в будущем. Это свидетельствует о вероятности возникновения экономических, социальных и экологических последствий (Нурматов У.А. и Юсупджанова У.А. 2023, Нурматов У.А. и др.2023)

2. Методы исследования.

Для разработки карты сейсмического риска территории Ферганской области Республики Узбекистан созданы несколько база данных на основе ГИС платформ, которые позволяют систематизировать и оценивать региональное распределение информаций о сейсмической

опасности, количестве здании и их конструктивных типах, коэффициенте сейсмической уязвимости зданий и застроенных территории, кадастровой стоимости зданий и т.д.

Теоретические основы оценки сейсмического риска рассмотрены многими исследователями. На основе учета всех факторов (сейсмическая опасность, уязвимость застройки, сейсмический риск) разработана методика оценки и прогноза сейсмического риска. Согласно общепринятой концепции, сейсмический риск определяется как суперпозиция сейсмической опасности и уязвимости различных элементов риска (люди, инженерные сооружения гражданского и промышленного назначения, линии жизнеобеспечения, другие составляющие инфраструктуры, экономическая и коммерческая деятельность и т. д.). Концепция оценки сейсмического риска состоит из трех блоков задач: источник, воздействие и последствие, а каждый блок - из ряда элементов риска, оценка которых в совокупности позволяет реально определить возможный экономический ущерб от землетрясения (Rebetsky Yu. L. et al 2020).

Алгоритм анализа сейсмического риска использует возможности ГИС, послойно комбинируя данные о пространственном распределении сейсмической опасности, уязвимости застройки, а также ценностей, т.е. кадастровой стоимости зданий подверженных риску повреждения и потерь. Анализ сейсмической уязвимости проводится с использованием программы «GESI_Program», которая основана на методике оценки сейсмического повреждения зданий. При этом существующая застройка на территории области собрана и классифицирована по конструктивным типам здании. Выделены 3 типа зданий: здания, построенные с использованием местных глинистых материалов; кирпичные здания и железобетонные здания (рис.1.).

Уязвимость зданий — свойство строительного сооружения, реагирует на сейсмические воздействия. Это ключевая характеристика надежности и безопасности сооружения, поскольку реальные последствия воздействия напрямую зависят от нее. Ущербы, причиняемые строительным сооружениям землетрясениями, описываются (квалифицируются) степенью конструктивных повреждений.

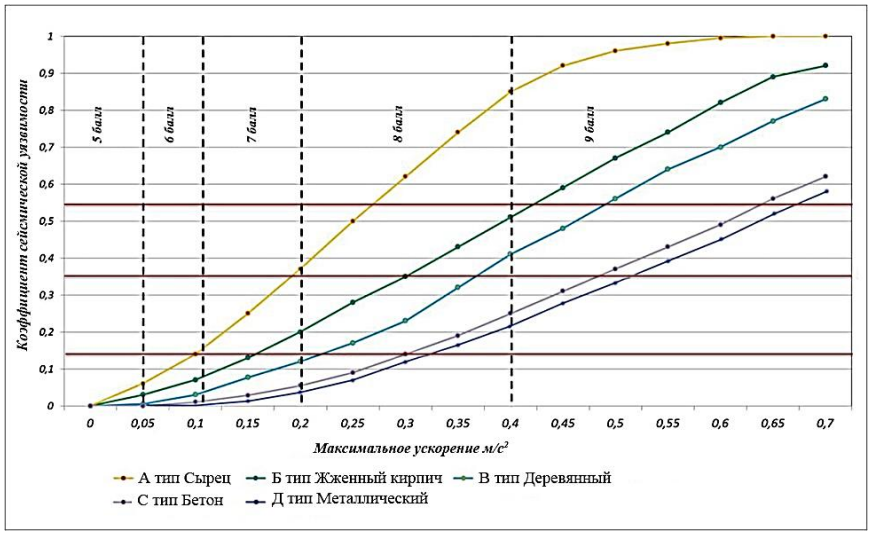

Рисунок 1. - **Функция уязвимости для различных типов зданий построенные с из местных материалов** («кирпич-сырец», жженый кирпич и железобетон)

3. Результаты.

При оценке сейсмической уязвимости каждого здания использованы кадастровые материалы Госкомземгеодезкадастр РУз. Анализ конструктивных типов зданий на территории области показывает, что основную часть составляют здания со стенами из сырцового кирпича (местные материалы)- 634376 шт. Кроме того, на территории области распространены здания, построенные из гуваляка, пахсы, которые также отнесены как сырцовой кирпич. Здания из

жженого кирпича составляют 35608 шт. Очень немного зданий, построенных железобетона 178 шт. зданий.

Для выбора сценарного землетрясения использована программа “INTensity MAP v3.0”. Программа «INTensity MAP v3.02» (рис. 2), разработана специалистами Института сейсмологии АН РУз в области оценки сейсмической опасности (№ DGU 09237). Основной целью программы является оценка сейсмического эффекта при заданных параметрах землетрясений для средных грунтовых условий.

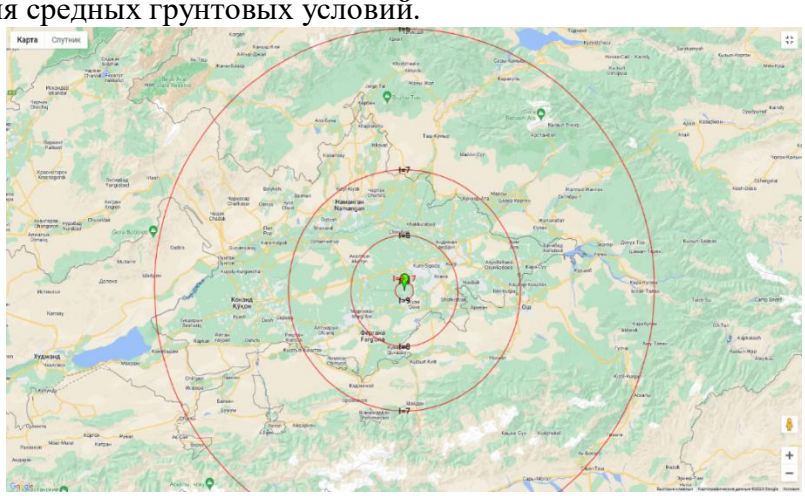

Рисунок 2. - **Карта изосейст при заданных параметрах для сценарного землетрясении по программе “INTensity MAP v3.0”для Ферганской области (X=72.007, У=40.591, M=7, H=15 км)**

Для выбора места эпицентра сценарного землетрясения использовали карту общего сейсмического районирования и сейсмогенных зон территории Республики (Исмаилов В.А. и др.2023, Ибрагимов Р.С. и др. 2022). В формировании поля сейсмических движений поверхности земли наряду с очаговыми факторами, путями распространения волн в поглощающей и рассеивающей геологической среде важную роль играют локальные грунтовые условия, которые в ряде случаев являлись основной причиной повреждения зданий и сооружений. Реакция рыхлой грунтовой толщи на сейсмические колебания определяется как физико-механическими и сейсмическими свойствами грунта и геометрией грунтовых слоев, так и интенсивностью воздействий. Получить распределение абсолютных величин сейсмической интенсивности от сценарного события (на территории исследований) следует путем сложения значений сейсмической интенсивности от сценарного события для средних грунтов, полученной путем расчетов по закону затухания, и слоя приращений интенсивности с учетом грунтовых условий. Для оценки сейсмической интенсивности использовали данные расчета изосейстов сценарного землетрясения и категория грунта, определяемые по строительным нормам. При расчетах сейсмического риска применяются различные способы вычисления и толкования, позволяющие получить оценки, как отдельных элементов риска, так и набора разных элементов, выраженных в процентном отношении потерь или каких-либо экономических терминах. В значительной степени это определяется полнотой и детальностью исходной информации о различных элементах риска.

В данной работе мы акцентируем внимание на одном, но важнейшем элементе риска - средней повреждаемости строений в случае заданного сейсмического воздействия. Именно этот элемент сейсмического риска вносит максимальный прямой вклад в экономический ущерб и является угрозой для здоровья или жизни людей. В связи с тем, что в Ферганском области расположены сейсмогенные зоны с различной магнитудой (Нурматов У.А. и Юсупджанова У.А. 2023, Atabekov, I. U. et al 2021) и вероятность возникновения сильных землетрясений с интенсивностью 7, 8 и 9 баллов велика (Artikov T. U. et al 2015, Artikov T. U. et al 2016, Artikov T. U. et al 2018, Artikov T. U. et al 2018, Artikov T. U. et al 2020, Artikov T. U. et al 2020, Artikov T. U. et al 2021, Ibragimova, T. et al 2021, Ibragimova, T. et al 2023), нами рассчитан сейсмический риск в случае воздействия 6, 7, 8 и 9 балльных землетрясений. Ущерб при сейсмических воздействиях можно оценивать прямым способом, т.е. оценка реальной

стоимости затрат на восстановления здания и на основании качественных оценок повреждаемости. В данной работе ущерб, связанный с повреждением зданий оценен в зависимости от затрат на ремонтные работы.

4. Заключения.

Для оперативной оценки последствий сильных землетрясения или прогнозирования возможного сейсмического риска при сценарном землетрясения на территории Самаркандской области использовали нами разработанную компьютерная программа «SeismicRiskAssessment 3», которая основана на ГИС технологии. Данная программа является логическим продолжением “INTensity MAP v3.0”. Если программа “INTensity MAP v3.0” позволяет построить карту изосейст при заданных параметрах землетрясения. На основе выделенных зон «SeismicRiskAssessment 3» производится расчет последствии землетрясении в экономических показателях. Экономический ущерб при этом сценарном землетрясении составляет 3893 млрд. сумов (рисунок 3 и 4).

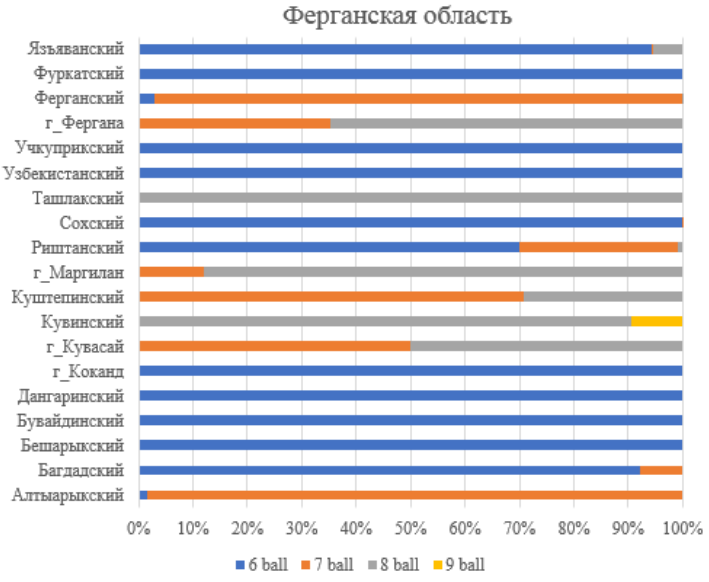

Рисунок 3. - **Распределение жилых домов по регионам на основе различной сейсмичности.**

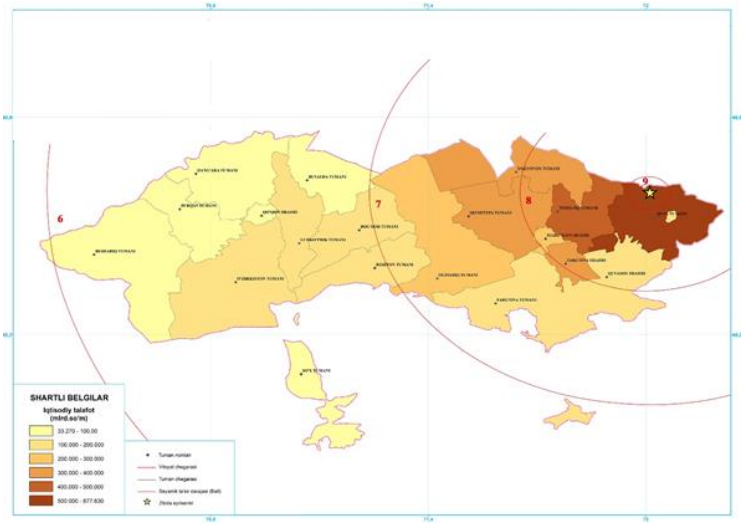

Рисунок 4. - **Карта сейсмического риска при сценарном землетрясении Ферганской области.**

Эта работа финансировалась за счет грантов Академии наук Республики Узбекистан “Разработка научных основ для оценки различных уровней сейсмического риска и снижения потерь от землетрясений в сейсмически активных районах” и Агентства по инновационному развитию, #ALM202311142839 “Создание симуляционной цифровой модели города

Ташкента, позволяющей для оценки уровня экономического ущерба от сильных землетрясений" и #AL5822012294 "Разработка технологии прогнозирования риска сильных землетрясений", #AL5822012298 "Создать электронную базу данных по сейсмологическим характеристикам грунта для замены таблицы 1.1 в нормативном документе. Сейсмологическая часть КМК" Строительство сейсмических зон".

Литература

1. *Artikov, T. U., Ibragimov, R. S., Ibragimova, T. L., Mirzaev, M. A., & Artikov, M. T.* (2015). Revealing the seismicity increase in interrelationships in various seismic zones in Uzbekistan as a case study. Geodesy and Geodynamics, 6(5), 351–360. https://doi.org/10.1016/j.geog.2015.03.007
2. *Artikov, T. U., Ibragimov, R. S., Ibragimova, T. L., & Mirzaev, M. A.* (2016). Study of modern seismic zoning maps' accuracy (case for Eastern Uzbekistan). Geodesy and Geodynamics, 7(6), 416–424.
3. *Artikov, T. U., Ibragimov, R. S., Ibragimova, T. L., & Mirzaev, M. A.* (2018). Identification of expected seismic activity areas by forecasting complex seismic-mode parameters in Uzbekistan. Geodesy and Geodynamics, 9(2), 121–130. https://doi.org/10.1016/j.geog.2017.11.005
4. *Artikov, T. U., Ibragimov, R. S., Ibragimova, T. L., Kuchkarov, K. I., & Mirzaev, M. A.* (2018). Quantitative assessment of seismic hazard for the territory of Uzbekistan according to the estimated maximum ground oscillation rates and their spectral amplitudes. Geodynamics & Tectonophysics, 9(4), 1173–1188.
5. *Artikov, T. U., Ibragimov, R. S., Ibragimova, T. L., & Mirzaev, M. A*. (2020). Complex of general seismic zoning maps OSR-2017 of Uzbekistan. Geodesy and Geodynamics, 11(4), 273–292.
6. *Artikov, T. U., Ibragimov, R. S., Ibragimova, T. L., & Mirzaev, M. A.* (2020). Models of the macroseismic field earthquakes and their influence on seismic hazard assessment values for Central Asia. Geodynamics & Tectonophysics, 11(3), 606–623. https://doi.org/10.5800/GT-2020-11-3-0494
7. *Artikov, T. U., Ibragimov, R. S., Ibragimova, T. L., Mirzaev, M. A., & Rebetsky, Y. L.* (2021). Methods and results of long-term strong earthquakes forecast in the Uzbekistan territory. IOP Conference Series: Earth and Environmental Science, 929(1), 012028. https://doi.org/10.1088/1755-1315/929/1/012028
8. *Atabekov, I. U., Artikov, T. U., Ibragimov, R. S., Ibragimova, T. L., & Mirzaev, M. A.* (2021). Relationship between Strong Earthquakes and Activation of Deep Faults in Central Asia (Uzbekistan): Numerical Simulation of Stress Field Variations. Geotectonics, 55(3), 377–392. https://doi.org/10.1134/S0016852121030031
9. *Bhochhibhoya, S. , & Maharjan, R.* (2022). Integrated seismic risk assessment in Nepal. Natural Hazards and Earth System Sciences 22, nhess-, 3211–3230.
10. *Bragato, P. L., Barnaba, C., Scaini, C., & Sugan, M.* (2020). Time-invariance and geographical divide of earthquake mortality in Italy since 1800. Annals of Geophysics, 63(6). https://doi.org/10.4401/ag-8406
11. *Bragato, P. L., Barnaba, C., Scaini, C., & Sugan, M.* (2020). Time-invariance and geographical divide of earthquake mortality in Italy since 1800. Annals of Geophysics, 63(6). https://doi.org/10.4401/ag-8406
12. *Ibragimova, T. L., Ibragimov, R. S., Mirzaev, M. A., & Rebetsky, Yu. L.* (2021). The current stress of earth's crust in the territory of uzbekistan according to focal earthquake mechanisms. Geodynamics & Tectonophysics, 12(3), 435–454. https://doi.org/10.5800/GT-2021-12-3-0532
13. *Ibragimov, R. S., Ibragimova, T. L., Mirzaev, M. A., & Rebetsky, Yu. L.* (2023). THE PROBABILITY OF A STRONG (M≥6.0) EARTHQUAKE IN THE SOUTH FERGANA SEISMIC ACTIVITY ZONE IN THE COMING YEARS. Geodynamics & Tectonophysics, 14(1). https://doi.org/10.5800/GT-2023-14-1-0688
14. *Ismailov, V. A., Yodgorov, S. I., Khusomiddinov, A. S., Yadigarov, E. M., Botirovich, A. S., & Aktamov, B. U.* (2023). New classification of soils by seismic properties for the building code in Uzbekistan. Geomechanics and Geoengineering, 1–21. https://doi.org/10.1080/17486025.2023.2296975
15. *Ismailov, V., Khusomiddinov, S., Khusomiddinov, A., Yodgorov, S., Aktamov, B., & Avazov, S.* (2022). Seismic risk assessment of Jizzakh region. 030035. https://doi.org/10.1063/5.0089664
16. *Peresan, A., Scaini, C., & Barnaba, C.* (2023). Crowd-Sourced Buildings Data Collection and Remote Training: New Opportunities to Engage Students in Seismic Risk Reduction. Earth Science, Systems and Society, 3. https://doi.org/10.3389/esss.2023.10088
17. *Petrovic, B., Scaini, C., & Parolai, S.* (2022). Applying the damage assessment for rapid response approach to the august 24 M6 event of the seismic sequence in central Italy (2016). Frontiers in Earth Science, 10. https://doi.org/10.3389/feart.2022.932110
18. *Poggi, V., Scaini, C., Moratto, L., Peressi, G., Comelli, P., Bragato, P. L., & Parolai, S.* (2021). Rapid Damage Scenario Assessment for Earthquake Emergency Management. Seismological Research Letters, 92(4), 2513–2530. https://doi.org/10.1785/0220200245
19. *Rebetsky, Yu. L., Ibragimova, T. L., Ibragimov, R. S., & Mirzaev, M. A.* (2020). Stress State of Uzbekistan's Seismically Active Areas. Seismic Instruments, 56(6), 679–700. https://doi.org/10.3103/S0747923920060079
20. *Wieland, M., Pittore, M., Parolai, S., Begaliev, U., Yasunov, P., Tyagunov, S., Moldobekov, B., Saidiy, S., Ilyasov, I., & Abakanov, T.* (2015). A Multiscale Exposure Model for Seismic Risk Assessment in Central Asia. Seismological Research Letters, 86(1), 210–222. https://doi.org/10.1785/0220140130

21. *Xin, D., Daniell, J. E., Tsang, H.-H., & Wenzel, F.* (2021). Residential building stock modelling for mainland China targeted for seismic risk assessment. Natural Hazards and Earth System Sciences, 21(10), 3031–3056.
22. *Ибрагимов Р.С., Ибрагимова Т.Л., Мирзаев М.А., & Ашуров С.Х.* (2022). Сопоставление оценок сейсмической опасности, получаемых в рамках вероятностного и вероятностно-детерминистического подходов, для территории Узбекистана. Вопросы инженерной сейсмологии, 49(4).
23. *Yodgorov Sh.I.* (2018). Geoinformational basis of estimation of the modern status of geoecological factor of seismic risk for the territory of Bukhara. International Journal of Geology, Earth and Environmental Sciences. - India, 8(№2), 36–43.
24. *Исмаилов В.А., Ёдгоров Ш.И., & Актамов Б.У.* (2020). Қишлоқ ҳудудларда қурилган биноларнинг кучли зилзилаларда шикастланишини баҳолаш (Жиззах вилояти мисолида). Тошкент Архитектура Қурилиш Институти ДИЗАЙН, , 2-сон.
25. *Исмаилов В.А, Ибрагимов Р.С., Нурматов У.А., Ибрагимов А.Х., Ёдигоров Ш.И., Т.Л.Ибрагимова, Ю.М.Садиков, Э.М.Ядигаров, А.С.Хусомиддинов, М.А.Мирзаев, Б.У.Ахтамов, Ш.Б.Авазов, Т.У.Мамаразиков, Ж.Ш.Бозоров, А.Мансуров, Р.Б.Тешаева, С.Ашуров, Ф.Ф.Рузимбаев, Э.Юлдашев, & Х.А.Исламов.* (2023). Детальное сейсмическое районирование и микрорайонирование территории крупных городов Ферганской долины. Ташкент: ИС АН РУз, 2023, 280 с.
26. *Исмаилов В.А., Артиков Т.У., Нурматов У.А., Ибрагимов Р.С., & Ёдгоров Ш.И.* (2021). Современное состояние вопроса оценки сейсмической опасности и сейсмического риска на территории Узбекистана. Журнал “Геология и Минеральные Ресурсы,” №2, 97–103.
27. *Ларионов В.И, Сущее С.П, Фролова Н.И., Угаров А.Н., Кожаринов С.В., & Барская Т.В.* (2015). Геоэкология. Инженерная геология. Гидрогеология. Геокриология (№1).
28. *Нурматов У.А., & Юсупджанова У.А.* (2023). О кратковременной изменчивости напряженного состояния Южно-Ферганской сейсмогенной зоны. Проблемы сейсмологии. Проблемы Сейсмологии, 2, 29–37.
29. *Нурматов У.А., & Юсупджанова У.А.* (2023). Прогноз землетрясений, оценка сейсмической опасности и сейсмического риска в Центральной Азии. XI Казахстанско-Китайский Международный Симпозиум, 209–214.
30. *Нурматов У.А., Садыков Ю.М., & Юсупджанова У.А.* (2023). Геодинамические блоки западного Тянь-Шаня и прилегающих территорий. Материалы Международной Конференции “Актуальные Проблемы Обеспечения Сейсмической Безопасности Населения и Территорий”. - Ташкент, ИС АН РУз, 218–226.

ОЦЕНКА СЕЙСМИЧЕСКОЙ ОПАСНОСТИ ТЕРРИТОРИИ ГОРОДА ТАШКЕНТА КАК ОСНОВА РАЗРАБОТКИ СИМУЛЯЦИОННОГО МОДЕЛИРОВАНИЯ ПОСЛЕДСТВИЙ СИЛЬНЫХ ЗЕМЛЕТРЯСЕНИЙ

Исмаилов В.А.[1], Ибрагимов Р.С.[1], Ёдгоров Ш.И.[1], Нурматов У.А.[1], Актамов Б.У.[1]
Институт сейсмологии им.Г.А. Мавлянова, Ташкент, Узбекистан
E-mail:vakhit.mbm@mail.ru

Аннотация. *В мировом масштабе сегодня большое значение приобретают вопросы прогнозирования потерь в результате сильных землетрясений и снижения их последствий. Для обеспечения устойчивого развития стран с высоким сейсмическим риском оценка экономических потерь в регионах, пострадавших от землетрясений, должна проводиться в рамках научно обоснованных рекомендаций. В связи с этим оценка сейсмического риска путем комплексных исследований и своевременного прогнозирования позволит принять меры по снижению последствий землетрясений. В этой статье рассмотрены вопросы оценки сейсмической опасности территории города с учетом грунтовых условий для разработки симуляционного моделирования последствий сильного сценарного землетрясения.*

Ключевые слова: *сейсмическая опасность, землетрясение, магнитуда землетрясения, сейсмическое воздействие, грунтовые условия, сейсмические волны, экономический ущерб, геонформационные системы.*

1. Введение.

Территория города Ташкента находится в зоне повышенного сейсмического потенциала, где риск возникновения землетрясений магнитудой M≤6,5 высокое. По данным инструментальной базы на территории города зафиксированы сильные землетрясения в 1868, 1886, 1924 и 1966, 2008 годов с магнитудой от 5,0 до 6.0 и сейсмической интенсивности 7, 8-9 баллов. Также в 1980 году произошло землетрясение в Назарбеке силой 8 баллов с магнитудой M = 5,3. Периодическое возникновения сильных землетрясений связаны с наличием в пределах города регионального Каржантауского разлома, который имеет активизацию [1-4].

Проблема защиты населения и территорий, уменьшение ущерба от природных катастрофических процессов и, в частности, от землетрясения является общенациональной

Государственной задачей. После приобретения независимости Республики особое внимание уделяется решению этой проблемы. В целях развития сферы сейсмологии, обеспечение сейсмостойкости сооружении и сейсмической безопасности на основе мировых стандартов Президентом Республики Узбекистан принят Постановление от 17.04.2024 года №УП-161 «О мерах по повышению сейсмостойкости зданий и сооружений и совершенствованию деятельности по мониторингу сейсмической опасности». В данном постоновлении особое внимание уделено совершенствованию научных разработок в области обеспечения сейсмической безопасности территории республики. Согласно 8 пункта 1-приложения этого постановления Институту сейсмологии и другим организациям поставлено задача “Создание цифровых симуляционных моделей, позволяющих оценить уровень поврежденности регионов под воздействием сильных землетрясений для управления снижением сейсмической риска в сейсмически активных зонах (на примере города Ташкента)” [5-11].

Для создание цифровых симуляционных моделей территорий основой является сейсмологические данные. Сейсмологические данные входить: сейсмотектоническая обстановка района; оценка сейсмической опастности; инженерно-геологические характеристики грунтов; сейсморазведочные работы; инструментально-сейсмометрические методы на основе регистрации микросейсм и другие.

2. Методика оценки сейсмической опасности.

При оценке сейсмической опасности используются в основном два подхода: детерминистский и вероятностный.

Детерминистский подход основан на учете максимального потенциала сейсмического источника, определяемого его геолого-тектоническими особенностями. Как правило этот подход выполняется в двух случаев возникновения землетрясения: 1) при наличии очага с максимальной возможной магнитуды от основной сейсмогенной зоны на минимальном расстоянии до исследуемой территории и 2) когда, из-за рассеянности очагов землетрясении, фоновой сейсмичности непосредственно под объектом исследования принимается как основной сейсмический источник. Такой подход, в последние годы, при оценке сейсмического риска получил новое называние «неодетерминистское» или «сценарное землетрясение».

В процессе оценки сейсмической опасности от сценарного события можно выделить ряд условий, в значительной степени влияющих как на характер пространственного распределения уровня сейсмической опасности, так и на его фактические численные значения [5-7]:

1. Параметры сейсмического события, к которым относятся: магнитуда, глубина очага, координаты эпицентра и гипоцентральное расстояние.
2. Закон затухания сейсмической интенсивности. Например, для Узбекистана на основе статистического анализа записей сейсмических колебаний и макросейсмических данных Т.У.Артиковым и Р.С.Ибрагимовым получены эмпирические уравнения затухания сейсмических колебаний как макросейсмических баллах, так и пиковых ускорениях.

Вероятностный подход оценивает вероятность возникновения расчетного сейсмического воздействия на участке от различных сейсмических источников. При вероятностной оценке сейсмического воздействия на сооружения и здания учитываются, в основном, три фактора: сила воздействия, спектральный состав колебаний и вероятность превышения расчетных значений в течение заданного периода времени. При оценке силы воздействия используются такие параметры, как интенсивность сотрясений земной поверхности (в значениях ускорений, скоростей или смещений) и закон затухания сейсмических колебаний для данного региона.

В формировании поля сейсмических движений на поверхности земли наряду с очаговыми факторами, определяющими путь распространения сейсмических волн в поглощающей и рассеивающей геологической среде, важную роль играют локальные грунтовые условия, которые в ряде случаев являлись основной причиной повреждения зданий и сооружений. Реакция рыхлой грунтовой толщи на сейсмические колебания определяется как

физико-механическими и сейсмическими свойствами грунта и геометрией залегания грунтовых слоев, так и интенсивностью воздействий.

3. Обсуждение результатов.

Сейсмотектоническая обстановка и оценка сейсмической опастности города Ташкента. Изучение сейсмической опасности Ташкента и сопредельных с ним областей за два последних десятилетия проводились в рамках национальных программ по уменьшению последствий сильных землетрясений и ряда крупных международных проектов. [2,3]. Эти исследования осуществлялись на основе различных методологических подходов, с использованием различных сейсмологических данных и сейсмотектонической основы, на базе различных программных средств, позволяющих определять количественные характеристики сейсмической опасности. Реализация этих проектов позволила с одной стороны, оценить преимущества и недостатки применявшихся подходов, с другой – наметить дальнейшие пути исследований по улучшению методологии создания карт общего сейсмического районирования в будущем. На основе проведенных исследований можно сделать следующие выводы относительно сейсмической опасности города Ташкента. Город Ташкент расположен непосредственно в пределах Пскемско-Ташкентской сейсмогенной зоны, сейсмический потенциал которой по сейсмологическим и сейсмотектоническим данным оценивается значением M_{max} =6.5 - 7.0 (рис.1)

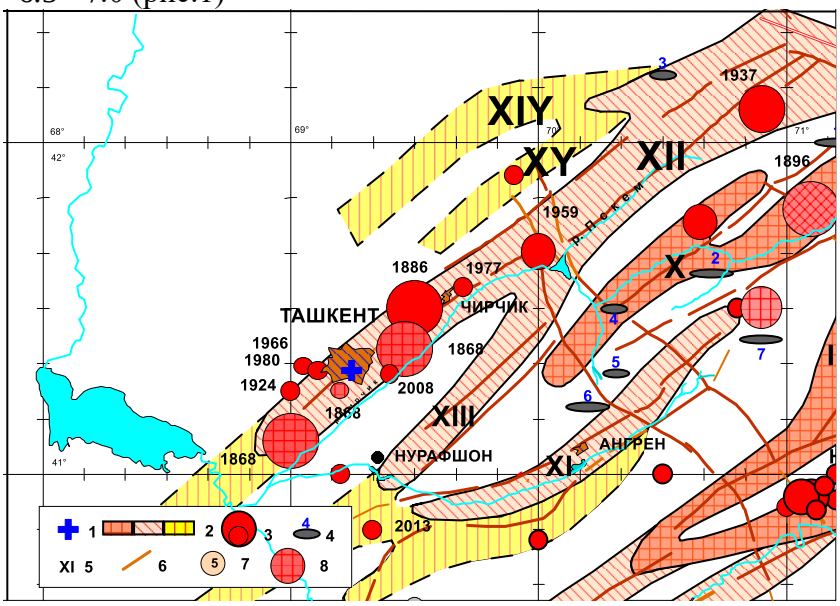

Рисунок 1. - **Сейсмогенные зоны Приташкентского района и эпицентры сильных землетрясений.**

Активные разломы. Для оценки сейсмической опасности территории г.Ташкенти и сопредельных территорий интерес представляют наиболее крупные структуро-контролируюшие разломы, с которыми связаны современные и прошлые землетрясения, оставившие в земной поверхности следы виде сейсмодислокации. Эти активизированные герцинские разломы на протяжении новейшего этапа являются наиболее подвижными и проницаемыми участками земной коры и характеризуются изменчивостью полей тектонических напряжений во времени. Активизированные разломы, выявленные по геологическим и геофизическим и геоморфологическим данным представлены, взбросами, надвигами, взбросо-надвигами, взбросо-сдвигами, флексурно-разрывными зонами. Они отличаются протяженностью, шириной, глубиной проникновения, простиранием, формой проявления и т.д. Реальную угрозу на строящихся объектов в г. Ташкенте и сопредельных территориях представляют следующие разломы земной коры и связанные с ними очаги землетрясений (рис.2).

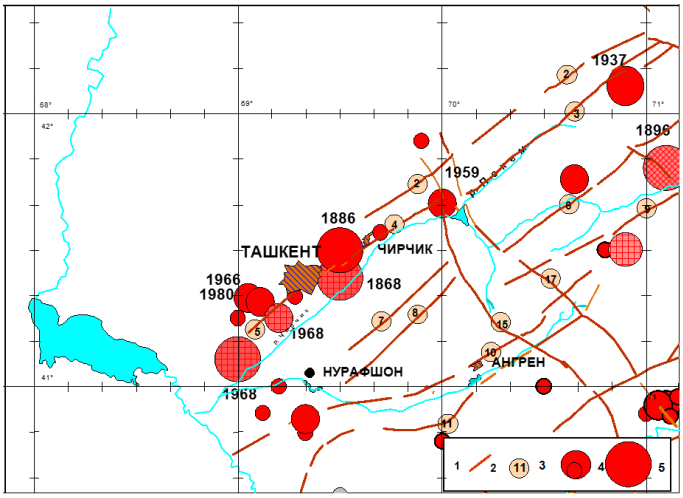

1-активные разломы; 2-номер разлома: (2-Аксу-Майдантал-богоналинский; 3-Пскемский; 4-каржантауский4 5-Приташкентская флексурно-разрывная зона; 6-Южно-Пскемский; 7-Сюрен Атинский; 8-Сукокский; 9-Чаткальский; 10-Северо-Ангренский; 11-Южно-Ангренский; 15-Кумбель-Коканд-Хайдарканский; 17 Арашанский); эпицентры землетрясений: 3- с M≥5.0 и M≥5.5; 5-с M≥6.0.

Рисунок 2. - **Активные разломы Приташкентского района и эпицентры сильных (с M≥ 5.0) землетрясений по [Новый каталог, 1977].**

Оценка сейсмической опасности для средних грунтовых условий. По утвержденной в 2019 году Министерством строительства РУз карте общего сейсмического районирования территории Узбекистана (ОСР-2017), построенной в рамках вероятностно-детерминистического подхода, сейсмичность города Ташкента на грунтах второй категории по сейсмическим свойствам составляет I=8 баллов по шкале MSK-64 [4-12].

Результаты проведенного вероятностного анализа сейсмической опасности территории города Ташкента сведены в таблицы 1-2 приведенные ниже.

Таблица. 1.

Значения интенсивности сейсмических воздействий (в баллах макросейсмической шкалы MSK-64) на грунтах II категории по сейсмическим свойствам для города Ташкента при различных вероятностях P не превышения уровня сейсмических воздействий в течение 50 лет

P	0.9	0.95	0.98	0.99
T, годы	475	975	2475	4975
I, баллы	8(7.67)	8 (8.08)	8 (8.48)	9 (8.83)

Таблица. 2.

Значения максимальных ускорений колебаний грунта (PGA, g) города Ташкента для различных вероятностей P не превышения уровня сейсмических воздействий в течение 50 лет на грунтах I, II и III категории по сейсмическим свойствам

Категория грунта	Значения максимальных ускорений a_{max}, g			
	P=0,9	P=0,95	P=0,98	P=0,99
I категория	0.208	0.274	0.379	0.463
II категория	0.262	0.350	0.466	0.579
III категория	0.336	0.421	0.563	0.678

Для различных вероятностей P не превышения уровня сейсмических воздействий в течение 50 лет получены спектры реакции грунтов различных категорий по сейсмическим свойствам.

*Оценка грунтовых условий***.** На исследуемом площадки были выполнены сейсморазведочные работы по методу MASW [1-6,7]. Сейсморазведка, благодаря большой глубинности и высокой детальности исследований является ведущим методом геофизических исследований земной коры. Для оценка грунтовых условий территории Ташкента проведены сейсмологические работ в 728 точках. При этом созданы инженерно-сейсмологические модели грунтовых условий для каждой точки. Модели имели информацию о скорости распространения поперечных волн в 30 метровой толщи (Vs30), плотность грунтов и их средние значения для 30 м. толщи, мощность различных грунтовых слоев и состояние грунтов.

На основании обработанных данных составлена карта скорости поперечных волн для 30м толщи (Vs30) (рис.3) [9,10,11].

Оценку приращений сейсмической интенсивности по МСЖ проводят путем сравнения значений сейсмических жёсткостей изучаемых и референтных грунтов по формуле:

$$\Delta I_{C.Ж.} = 1.67 \lg\left(\rho_0 V_0 / \rho_i V_i\right),$$

где ΔIс.ж. – приращение за счёт различия сейсмической жесткости грунтов на изучаемом участке и участке со средними грунтовыми условиями, $\rho_0 V_0$, $\rho_i V_i$ –сейсмические жесткости референтной и изучаемой грунтовой толщи по поперечным волнам. Значение V_0, ρ_0, Vi, ρ_i определяются в верхней 30-ти метровой толще и вычисляются по формулам [8,9-13].

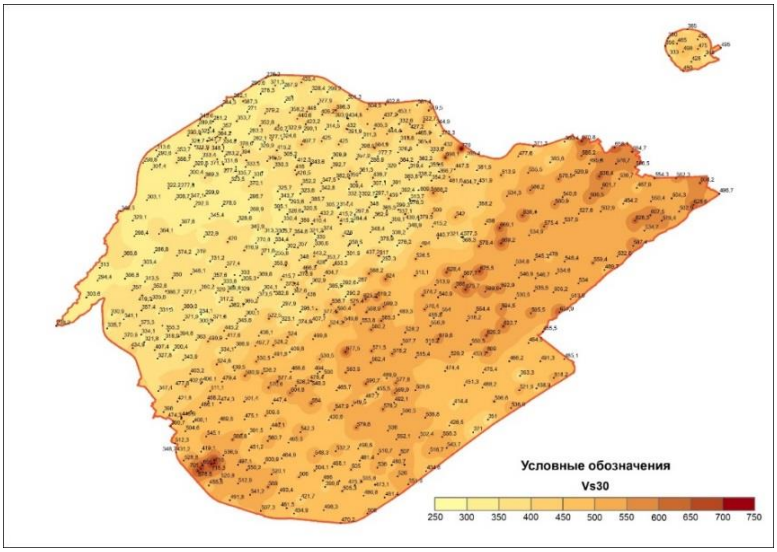

Рисунок 3. - **Карта распределения Vs30**

На рис.4 представлена карта приращение сейсмической интенсивности, которая позволяет оценивать влияние грунтовқх условий на сейсмическую опасность.

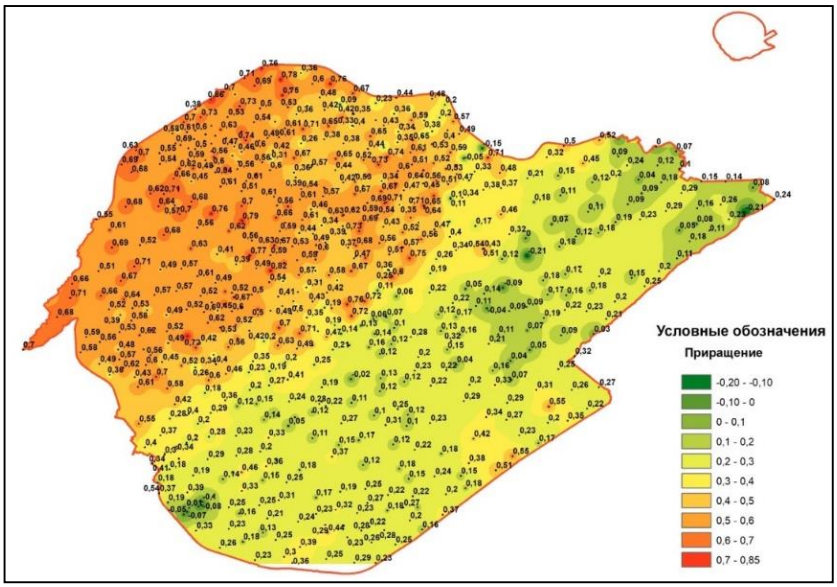

Рисунок 4. - **Карта приращений сейсмической интенсивности по методу сейсмических жесткостей г. Ташкент.**

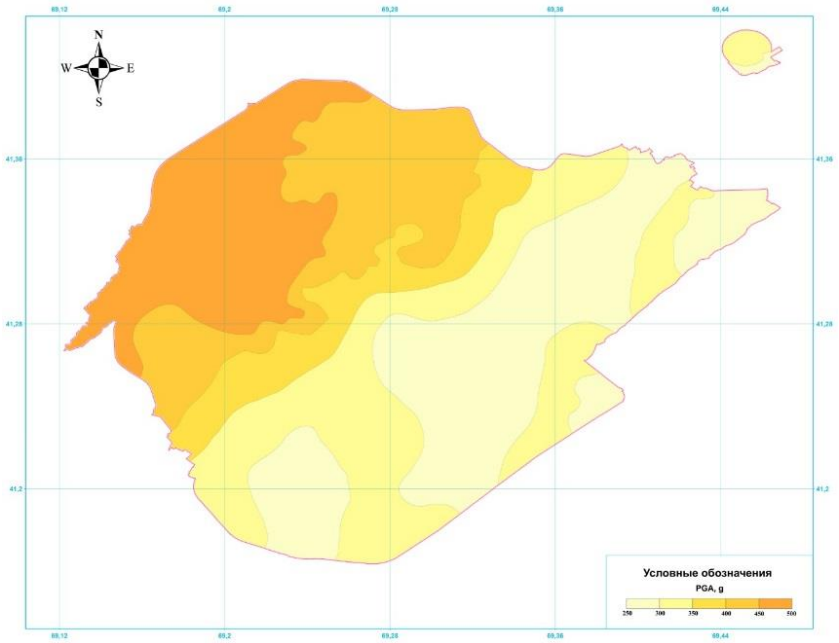

Рисунок 5. - **Карта сейсмического микрорайонирования территории города Тошкент по значениям пикового ускорения (PGA)**

Для симуляционного моделирования не малое значение имеет параметры процесс колебания грунтовых толщ при сценарном землетрясении. Для оценки изменении параметров сейсмических колебаний в пространстве при заданных величинах сейсмического ускорения методом конечных элементов рассчитана значение сейсмического ускорения в каждой модели (728 моделей). На основании этих данных составлены карта (рис.5).

4. Заключение.

Территория г. Ташкент приурочен к Ташкентско-Пскемской сейсмогенной зоне, которая обусловлена Пскемской, Каржантауской и Приташкентской флексурно-разрывной зоной. Сейсмический потенциал зоны оценивается M≤6.5 и интенсивностью I=8 баллов.

На территории Ташкента выделены 4 инженерно-геологических района по геолого-структурному признаку и 18 инженерно-геологических участков по типу инженерно-геологического разреза до глубины 30 м. Каждому инженерно-геологическому участку дана оценка приращения сейсмической интенсивности.

Определения сейсмических жесткости грунтовых толщ на глубину 30м и в некоторых пунктах и более метров в 728 точках, установления соотношении спектров горизонтальных колебаний к вертикальным при регистрации микросейсм в 728 точках. Обобщенные результаты оценки показывают изменение приращения сейсмической интенсивности в пределах от -0,22 до + 0,89 баллов.

Разработана карта оценки изменения параметров сейсмических колебаний на территории г.Ташкент по значениям пикового ускорения (PGA). На исследуемой территории по значениям максимального ускорения колебания грунтовых толщ выделены следующие предельные значения: 0,23g-0.55g, что является основой для разработки симуляционного моделирования.

Эта работа финансировалась за счет грантов Академии наук Республики Узбекистан “Разработка научных основ для оценки различных уровней сейсмического риска и снижения потерь от землетрясений в сейсмически активных районах” и Агентства по инновационному развитию, #ALM202311142839 “Создание симуляционной цифровой модели города Ташкента, позволяющей для оценки уровня экономического ущерба от сильных землетрясений” и #AL5822012294 “Разработка технологии прогнозирования риска сильных землетрясений”, #AL5822012298 “Создать электронную базу данных по сейсмологическим

характеристикам грунта для замены таблицы 1.1 в нормативном документе. Сейсмологическая часть КМК" Строительство сейсмических зон".

Литература

1. *Artikov, T. U., Ibragimov, R. S., Ibragimova, T. L., Mirzaev, M. A., & Rebetsky, Yu. L.* (2022). Stress State of the Earth's Crust, Seismicity, and Prospects for Long-Term Forecast of Strong Earthquakes in Uzbekistan. Russian Geology and Geophysics, 63(12), 1442-1458. https://doi.org/10.2113/RGG20214408
2. *Atabekov, I. U., Artikov, T. U., Ibragimov, R. S., Ibragimova, T. L., & Mirzaev, M. A.* (2021). Relationship between Strong Earthquakes and Activation of Deep Faults in Central Asia (Uzbekistan): Numerical Simulation of Stress Field Variations. Geotectonics, 55(3), 377-392. https://doi.org/10.1134/S0016852121030031
3. *Ibragimov, R. S., Ibragimova, T. L., Mirzaev, M. A., & Rebetsky, Yu. L.* (2023). THE PROBABILITY OF A STRONG (M≥6.0) EARTHQUAKE IN THE SOUTH FERGANA SEISMIC ACTIVITY ZONE IN THE COMING YEARS. Geodynamics & Tectonophysics, 14(1). https://doi.org/10.5800/GT-2023-14-1-0688
5. *Artikov T.U., Ibragimov R.S., Ibragimova T.L., Kuchkarov K.I., & Mirzaev M.A.* (2018). Quantitative assessment of seismic hazard for the territory of Uzbekistan according to the estimated maximum ground oscillation rates and their spectral amplitudes. Geodynamics & Tec- Tonophysics, 9(4), 1173–1188. doi:10.5800/GT-2018-9-4-0389
6. *Ismailov, V., Khusomiddinov, S., Khusomiddinov, A., Yodgorov, S., Aktamov, B., & Avazov, S.* (2022). Seismic risk assessment of Jizzakh region. 030035. https://doi.org/10.1063/5.0089664
7. *Ismailov, V. A., Yodgorov, S. I., Allayev, S. B., Mamarozikov, T. U., & Avazov, S. B.* (2022). Seismic microzoning of the Tashkent territory based on calculation methods. Soil Dynamics and Earthquake Engineering, 152, 107045. https://doi.org/10.1016/j.soildyn.2021.107045
8. *Khusomiddinov, A., Yodgorov, S., Sadirov, F., Yadigarov, E., Aktamov, B., & Avazov, S.* (2022). Estimation of the Seismic Intensity Increments in Tashkent Region. AIP Conference Proceedings, 2432. https://doi.org/10.1063/5.0089662
9. *Bindi D, Mayfiled M, Parolai S, Tyagunov S, Begaliev UT, Abdrakhmatov K, Moldobekov B, Zschau J* (2011) Towards an improved seismic risk scenario for Bishkek, Kyrgyz Republic. Soil Dyn Earthq Eng. doi:10.1016/j.soildyn.2010.08.009
10. *Parolai S, Orunbayev S, Bindi D, Strollo A, Usupayev S, Picozzi M et al* (2010) Site assessment in Bishkek (Kyrgyzstan) using earthquake and noise recording data. Bull Seismol Soc Am. doi:10.1785/0120100044
11. *Tyagunov S, Gruenthal G, Wahlstrom R, Stempniewski L, Zschau J* (2006) Seismic risk mapping for Germ Nat. Hazard Earth Syst Sci 6: pp. 573–586
12. *Tyagunov S., Ismailov V., Ibragimov R.* Engineering-seismological aspects of earthquake scenario preparation: experience of the IDNDR-RADIUS project implementation in Tashkent, Uzbekistan // Proceeding of In-ternational Workshop «Recent earthquakes and disaster prevention manage-ment». - Ankara. 1999. pp. 21-28.
13. *Artikov T.U., Ibragimov R.S., Ibragimova T.L., Mirzaev M.A.* Models of the macroseismic field earthquakes and their influence on seismic hazard assessment values for Central Asia. Geodynamics & Tectonophysics. 2020;11(3):606-623. (In Russ.) https://doi.org/10.5800/GT-2020-11-3-0494
14. *Frolova, N. I., Malaeva, N. S., Ruzhich, V. v., Berzhinskaya, L. P., Levina, E. A., Suchshev, S. P., Larionov, V. I., & Ugarov, A. N.* (2022). Assessing the Social and Economic Indicators of Seismic Risk Using the Town of Angarsk as an Example. Izvestiya, Atmospheric and Oceanic Physics, 58(8), 881–907. https://doi.org/10.1134/S0001433822080011

ОЦЕНКА СЕЙСМИЧЕСКОЙ ОПАСНОСТИ В ГОРОДЕ САМАРКАНДЕ

Кондратьев В.А.[1], Кузьмина Е.Н.[2]

[1]Самаркандский государственный архитектурно-строительный университет, Самарканд, Узбекистан
[2]Тульский государственный университет, Тула, Россия
E-mail: vkondratev1958@mail.ru

Аннотация: *Приведены основные результаты исследований, имевших целью оценку сейсмической опасности территории г. Самарканда, что является первым из основных и неотъемлемым этапом комплексных исследований по оценке и управлению сейсмическим риском. На основе оценки роли составляющих и влияющих факторов, выполненной с использованием результатов нескольких альтернативных методов (приращения сейсмической балльности, инженерно-геологического районирования, результатов электроразведочных исследований, оценки сейсмической интенсивности по методу сейсмической жесткости, результатов исследований слабых землетрясений, расчетного метода сейсмического микрорайонирования, данных обследования последствий землетрясений) и GIS-технологий, разработана векторизованная карта сейсмического микрорайонирования, которая использовалась на последующих этапах исследований.*

Ключевые слова: *землетрясения, сейсмическая опасность, историческая сейсмичность, тектоника, инженерная геология, микросейсморайонирование, GIS-технологии.*

1. Введение

Из всех видов чрезвычайных ситуаций природного характера, наибольшую опасность для населения и народного хозяйства Узбекистана представляют землетрясения. Согласно статистическим данным, сейсмические события с интенсивностью 5 - 6 баллов происходят на территории нашей республики в среднем один раз в год.

Природные и техногенные землетрясения, чрезвычайно опасные сами по себе, в отношении возможных социальных и экономических потерь, зачастую являются причиной, провоцирующей и ряд других катастрофических явлений (наводнения и затопления территорий, сели, оползни, обвалы, снежные лавины и пр.), дополнительно вызывая возникновение, так называемых вторичных поражающих факторов (таких как пожары, вспышки эпидемий, химическое и радиационное заражение территорий и пр.). При этом, отмеченные негативные последствия могут наблюдаться далеко за пределами территории, непосредственно пострадавшей от землетрясения.

Город Самарканд и Самаркандская область в этом отношении не является исключением. Согласно карте общего сейсмического районирования, сейсмичность территории, на которой расположен город, оценивается в 8 баллов. На территории города имеются зоны с неблагоприятными в сейсмическом отношении грунтовыми условиями (повышающими сейсмический эффект), участки с неблагоприятным рельефом, а также участки, где возможны сейсмические повреждения грунтов и оползневые явления. В частности, на территории одной таких зон расположены практически все архитектурные памятники и часть административных зданий городского и областного значения. Результаты предварительно проведённой инвентаризации зданий на территории города. свидетельствовали о довольно высокой степени их сейсмической уязвимости (особенно в частном секторе, возведённых в различные периоды индивидуальными застройщиками).

Всё это указывает на то, что опасность землетрясений, а также всех сопутствующих им чрезвычайных ситуаций для города Самарканда является довольно высокой.

Город Самарканд представляет собой довольно сложный организм, с развитой инфраструктурой и системами жизнеобеспечения. Это второй по величине город нашей Республики, являющийся крупным историко-культурным и современным промышленным, научным и образовательным центром, известным всему миру своими уникальными архитектурными памятниками, привлекающими ежегодно множество туристов.

Отмеченное определило необходимость проведения исследований по оценке и управлению сейсмическим риском для г. Самарканда, с разработкой комплекса превентивных мероприятий и планов управления риском, направленных на максимальное снижение возможных ущербов при землетрясениях различной интенсивности и повышение степени подготовленности города в случае таких землетрясений.

Оценка и управление сейсмическим риском - это многоплановая проблема. В ее решении должны быть задействованы специалисты многих отраслей деятельности: научные работники, специалисты в области планирования и управления, сотрудники управлений по чрезвычайным ситуациям и коммунальных служб и др.

В связи с этим, с точки зрения изучения передового мирового опыта, особый научный и практический интерес представляют исследования, проведённые для крупных городов мира, выполненные с международным участием и привлечением широкого круга специалистов, акцент на которые и был сделан при проведении аналитического обзора.

Первые описания таких работ в специальной литературе датируются началом 70-х годов прошлого столетия, когда такие исследования стали проводиться специалистами США. В частности, одной из первых основополагающих работ в этой области является исследование, связанное с оценкой сейсмического ущерба в Калифорнии, выполненное Советом по Прикладным Технологиям (АТС) США по заказу Федерального Агентства по Чрезвычайным Ситуациям (FEMA) в период 1982 - 1985 гг. Практически все известные последующие работы в области оценки сейсмического риска имеют ссылки на это исследование. С некоторыми модификациями, принципы исследований, предложенные АТС, использовались при выполнении оценок сейсмического риска в различных городах мира.

Одной из первых комплексных работ по оценке сейсмического риска для населенных территорий, проведенных при широком участии международных специалистов, является проект, реализованный для г. Кито (Эквадор).

Уникальным является опыт исследований, реализованных в рамках инициативы ООН RADIUS для 9 крупных городов мира (включая Ташкент), а одной из фундаментальных работ в рассматриваемой области является разработанная специалистами США Методологии Оценки Сейсмического Ущерба - «HAZUS».

Одним из современных исследований в данной области является проект по оценке сейсмического риска для г. Стамбула (Турция).

Заслуживает особого внимание и опят исследований и разработок, накопленный в странах СНГ, - Российской Федерации, Казахстане, Киргизии и Таджикистане.

Начало исследованиям проблемы оценки и управления сейсмическим риском в Узбекистане было положено в ходе выполнения Международных проектов для города Ташкента. Своё дальнейшее развитие эти исследования получили в ходе выполнения ряда Государственных научно-технических программ при финансировании ККРНТ при Кабинете Министров Республики Узбекистан начиная с 2002 года, в частности, 3.Ф.-1.10.2.4, ГНТП–3.7.1.1, ГНТП–8.17, Ф-1.2.2, 79-04, А-5060, ГНТП 28.5, ГНТП 16.3.7, ГНТП 3.7.1.13, И-8-16, ГНТП К-16-007. ГНТП А14-ФА-Ф052 и др.

Результаты проведённого аналитического обзора свидетельствуют о том что, исследования, посвященные проблеме обеспечения сейсмической безопасности, активно ведутся во многих странах мира уже не одно десятилетие, но только в последнее время они получили несколько иные приоритеты. Основной их целью стала не просто оценка сейсмической опасности, и не просто оценка сейсмической уязвимости зданий и сооружений с целью обеспечения и повышения их сейсмостойкости, а комплексный подход к решению этой проблемы с разработкой всего спектра вопросов, направленных на разработку стратегии снижения возможного социально-экономического ущерба и последствий возможных землетрясений, а также других провоцируемых ими чрезвычайных ситуаций.

В отношении рассмотренного в данной статье этапа исследований, имеющего целью оценку сейсмической опасности для территории г. Самарканда, в рамках аналитического обзора был проведен обзор и анализ имеющейся сейсмологической и инженерно - геологической информации, в том числе, по материалам исследований Института сейсмологии АН РУз, Самаркандского филиала DUK «O'ZGASHKLITI», а также другим источникам, опубликованным в открытой печати.

В частности, в [6] приведены результаты исследований эпицентральных зон землетрясений Самаркандского района, выполненные А.А.Мицкевичем.

Большой цикл исследований по сейсмическому микрорайонированию территории Узбекистана был проведён Е.М. Бутовской, особая ценность которых заключалась в оценке количественных параметров сейсмического режима Западного Узбекистана (в частности, восточной части Западного Узбекистана - для районов Самарканда и Гиссара).

Исторические сведения об ощутимых и сильных землетрясениях Западного Узбекистана были собраны и классифицированы И.Б. Яковлевой в монографии «Сейсмичность Западного Узбекистана» [7].

Сейсмичность территории Узбекистана исследовалась М.И. Икрамовым в [8], где также содержатся сведения о проявлении в Самарканде серии Ура-Тюбинских землетрясений.

По сведениям, приведённым в [9], Газлийское землетрясение в Самарканде проявилось с интенсивностью 6 - 7 баллов.

В [10] приведены результаты микросейсмического обследования Исфара-Баткентского землетрясения на территории некоторых городов, включая Самарканд, выполненные С.М. Касымовым, где приводятся данные о проявлении этого землетрясения на территории города.

Изучением тектонического строения Самаркандской впадины занимались А.Д. Архангельский [11], В.А. Николаев [12], С.Н. Кулинников, А.С. Аделунг, А.Г. Бабаев [13], А.Х. Чистяков [14] и др.

Вопросы разработки методов оценки сейсмической активности, включая построение карт сейсмической активности отражены в работах Ю.В. Ризниченко, Горбуновой И.В. [15, 16] и А.И. Захаровой, И.Б. Яковлевой [17, 18] и др.

Ценная информация о структурно–геологических характеристиках района представлена в работах Н.П. Костенко [19] и О.К. Чедия [20].

Оценка инженерно-геологических и, в частности, гидрогеологических условий (в том числе, исследуемого региона), представлена в работах П.И. Бутова, М.А.Шмидта, В.М. Толстунова, А.И. Шевченко, Г.Ф. Тетюхина, Г.А. Мавлянова, А.М. Султанходжаева [21 - 25] и др.

Разработке методики и принципам районирования посвящены исследования И.В. Попова [26], М.В. Чуринова [27], Ф.В. Котлова, Г.С. Золотарева [28] и др.

На основании проведённого анализа было установлено, что имеющейся сейсмологической и инженерно-геологической информации, необходимой для проведения оценок сейсмического риска, достаточно и проведения дополнительных сейсмологических и инженерно-геологических исследований не требуется.

Наиболее подробная информация по результатам исследований, касающихся геологии, тектоники, геоморфологии, гидрогеологии и сейсмичности района, приведена в [29], где также освещаются результаты исследований по инженерной геологии, электроразведке и сейсмометрии, определены сейсмические характеристики грунтов, выделены преобладающие периоды колебаний.

Резюмируя вопрос аналитического обзора исследований, следует отметить, что оценка последствий сильных землетрясений в крупных городах мира в последние годы показывает, что число жертв среди населения и размеры материального ущерба могут быть значительно сокращены, если заблаговременно производится оценка сейсмического риска населенных территорий, подготавливаются и реализуются соответствующие планы управления сейсмическим риском.

Отмеченный передовой мировой опыт проведения исследований, посвященных проблеме оценки и управления сейсмическим риском, и опыт имеющегося в нашей республике, жизненно важно и чрезвычайно актуально распространить для наиболее крупных городов Узбекистана (в качестве первого этапа), а затем (в перспективе) и для других городов и населённых территорий.

Целью исследований, основные результаты которых представлены в данной статье, являлась оценка сейсмической опасности территории г. Самарканда, как первого из основных, и неотъемлемого этапа комплексных исследований по оценке и управлению сейсмическим риском.

Задачами исследования, которые потребовалось решить для достижения поставленной цели, являются : сбор, изучение и классификация сведений об исторической сейсмичности территории, изучение сейсмологических и инженерно-геологических условий на территории города и прилегающей к нему территории, данных о микросейсморайонировании, обработка информации, выбор и определение параметров сценарных землетрясений, с оценкой распространения сейсмического эффекта, а также разработка соответствующих GIS-проектов.

2. Материалы, методы и объект исследования.

Комплексная оценка сейсмического риска, выполняющаяся с целью оценки возможных последствий сильных землетрясений, возможности заблаговременно подготовиться к ним и снизить возможные потери на сейсмоактивных территориях, состоит из нескольких этапов и требует сбора большого количества самой разнообразной информации. Общие принципы выполнения исследований по оценке и управлению сейсмическим риском приведены в [2].

Первым этапом исследований является оценка сейсмической опасности исследуемой территории.

Оценка сейсмической опасности может быть либо детерминированной, основанной на развитии сценарного землетрясения, которое принято наиболее вероятным с учетом повторяемости событий различного масштаба для данного региона, либо с определенным порогом вероятности превышения сейсмических характеристик, вызванных различными возможными сейсмическими событиями. После определения исходной сейсмической опасности в регионе, характеризующейся определенным уровнем сейсмических характеристик на скальных грунтах основания, необходимо учесть влияние грунтовых условий поверхностного слоя, расположенного на твердых породах : мощности и строения слоя рыхлых грунтов; уровня грунтовых вод; плотности и скоростей распространения сейсмических волн.

Вторым этапом является проведение инвентаризации зданий, сооружений и систем жизнеобеспечения, расположенных на исследуемой территории. Инвентаризация осуществляется в соответствии с классификацией зданий и сооружений, учитывающей : конструктивную схему и материал, год постройки, качество строительства, условия эксплуатации. В единые классификационные группы могут быть объединены сооружения, имеющие одинаковую степень уязвимости к сейсмическим воздействиям. Для разработки карты расположения объектов на территории города, можно использовать картографические материалы, спутниковые изображения и технологии GPS-позиционирования.

Третьим этапом является выполнение оценки физического ущерба. На этой стадии исследования, карта сейсмической опасности, учитывающая грунтовые условия на населенной территории, совмещается с картой расположения различных объектов. Для оценки возможных потерь должны быть построены (или использованы) зависимости повреждаемости (уязвимости) зданий и сооружений от величины характеристик сейсмической опасности. Эти зависимости (кривые повреждаемости, вероятностные матрицы повреждаемости) разрабатываются либо на основании инженерного анализа последствий прошедших землетрясений (обычно такой анализ позволяет построить зависимость уровня повреждений конструкций от величины сейсмической интенсивности), либо на основании расчета сейсмостойкости конструкций зданий и сооружений под действием сейсмических нагрузок (расчет по спектральным кривым, расчет на действие сейсмических ускорений или смещений, заданных акселерограммами или сейсмограммами и пр.).

Четвертый этап – оценка возможного числа раненых, погибших и оставшихся без крова людей. Для выполнения этой работы необходимо составить карты распределения населения по зданиям различного назначения в разное время суток, оценить количество людей, оказавшихся в зданиях, получивших повреждения различного уровня тяжести и затем использовать соотношения, связывающие число пострадавших (с разной степенью тяжести) со степенью повреждений зданий и сооружений.

Пятый этап - оценка экономического ущерба от прямых потерь. На этом этапе

оцениваются потери в денежном выражении только от прямого повреждения зданий и сооружений.

На последующих этапах : оцениваются размеры возможного материального и социального ущерба от вторичных поражающих факторов (пожары, затопления, химическое и радиоактивное заражение территорий, эпидемии и пр.); выполняются расчеты необходимых материальных ресурсов для спасения людей и восстановления поврежденных зданий и сооружений; оценивается продолжительность аварийно-спасательных работ и ликвидации последствий землетрясения, исходя из имеющихся ресурсов людей, техники, строительных материалов и пр.; оцениваются возможные экономические потери вследствие прекращения работы взаимозависимых промышленных предприятий, отказов в функционировании систем жизнеобеспечения; разрабатываются оптимальные и резервные схемы движения специального транспорта и строительной техники в случае повреждения отдельных дорожных сооружений и пр.

Для решения поставленных задач используются как специальные, так и общенаучные методы исследований, в частности: методы КСИ (конкретное социологическое исследование), а именно, документальный метод (анализ документов), методы сбора, анализа и оценки сведений (регистрирование единичных событий - анализ документов, сбор данных - выборочная фиксация, обработка и анализ информации - категоризация, описание, систематизация). Использовались и общенаучные методы, а именно, общелогические методы – анализ, синтез и аналогия, теоретические методы – гипотетический и классификация.

Объектами исследования на этапе оценки сейсмической опасности (как первом этапе комплексных исследований по оценке и управлению сейсмическим риском) являются сведения об исторической сейсмичности территории города, структурно-геоморфологических характеристиках региона, геологических и инженерно-геологических процессах и явлениях, литологическом строении, электроразведочных и сейсморазведочных исследованиях, инструментальных исследованиях слабых землетрясений, сейсмическом микрорайонировани.

Объектами комплексных исследований по оценке и управлению сейсмическим риском в целом, являются здания, сооружения и население, как объекты и составляющие элементы риска на рассматриваемой территории.

3. Постановка задачи.

На основе изучения передового мирового опыта проведения исследований по оценке и управлению сейсмическим риском, а также имеющегося отечественного опыта, накопленного в ходе выполнения ряда международных проектов для г. Ташкента и ряда ГНТП, автором (совместно с академиком АН РУЗ д.т.н. профессором Т.Р. Рашидовым) разработаны Концепции обеспечения сейсмической безопасности [2]. Отмеченные Концепции прошли практическую апробацию, неоднократно представлялись на ряде международных конференций в странах ближнего и дальнего зарубежья, где получили одобрение и поддержку.

В соответствии с [2], рассматриваемый первый этап комплексных исследований по оценке и управлению сейсмическим риском должен включать следующие разделы, с параллельной разработкой соответствующих GIS-проектов (методология использования GIS для оценки и управления сейсмическим риском приведена в подготовленной автором специальной монографии [5]) :

Изучение исходной сейсмологической информации

- сбор и обработка информации об исторической сейсмичности территории, сведений об тектонических условиях и сейсмологических исследованиях региона и прилегающей территории. Разработка GIS-карт очаговых зон региона;
- сбор информации и оценка параметров произошедших и возможных землетрясений (спектров колебаний в ближней зоне землетрясений, параметров затухания сейсмической энергии и сотрясений с расстоянием, периодов повторения сотрясений различной интенсивности). Выбор расчетных (8-9-балльных) землетрясений для разработки сценариев;
- разработка GIS-карт интенсивности для каждого из расчетных землетрясений с

учетом затухания (карты изосейст);

Изучение необходимой инженерно-геологической информации

- сбор информации и изучение инженерно-геологических условий исследуемой территории. Разработка GIS-карт грунтовых условий (с отражением данных об уровне грунтовых вод, мощности слоев, изменении грунтов по глубине, наличии массивов галечника и пр.);
- оценка влияния грунтовых условий на сейсмический эффект (коэффициенты усиления, проявления динамической неустойчивости грунтов, зон возможного разжижения, просадок и пр.);

Оценка сейсмического эффекта для расчетных вариантов землетрясений

- разработка GIS-карт сейсмического микрорайонирования (интенсивности в баллах) исследуемой территории с учетом грунтовых условий;
- разработка GIS-карт распределения сейсмического эффекта (проявления динамической неустойчивости грунтов, зон возможного разжижения грунтов, просадок и пр.);

Оценка сейсмической опасности должна обеспечить информацию о ней для определенного места или для большой области, либо детерминированным, либо вероятностным способом. Если используются детерминированные методы оценки, то сейсмическая опасность выражается уровнем значений параметров, характеризующих сотрясения грунта во время землетрясения. Это могут быть значения интенсивности I колебаний (по шкалам MMI, MSK, или используемой в Узбекистане шкале РСТ Уз [4]), уровня максимальных ускорений (PGA - Peak Ground Acceleration), максимальных скоростей грунта (PGV - Peak Ground Velocity), спектральных ускорений (SA - Spectral Acceleration), спектры реакции и т.п. Если же оценка опасности выполняется вероятностными методами, то сейсмическая опасность, H - это вероятность того, что землетрясение с определенным уровнем параметров колебаний грунта (интенсивности, PGA, PGV, SA) произойдет в течение определенного периода в определенной области :

$$H = F(P|H).$$

Результатом оценки сейсмической опасности может быть численная величина параметра сейсмических сотрясений, карта или кривая опасности (hazard curve).

По результатам предварительно проведённой инвентаризации зданий на территории города установлено, что подавляющее большинство зданий существующей застройки относится к типам, для которых уже проводился анализ последствий разрушительных землетрясений. Т.е. кривые и матрицы повреждаемости этих зданий могут быть построены как зависимость степени их повреждения от интенсивности сейсмического воздействия по шкале РСТ Уз [4]. Поэтому, в качестве характеристики сейсмической опасности была выбрана интенсивность сейсмического воздействия и с целью её картирования (для использования на последующих этапах выполнения исследований) поставлена задача разработки векторизованной карты сейсмического районирования территории города.

4. Результаты

По результатам проведённого обзора исследований, касающихся геолого - тектонических условий исследуемой территории, её структурно-геологических характеристик, сейсмичности и инженерно-геологических условий, собрана и классифицирована необходимая исходная информация для проведения оценок сейсмической опасности, в частности:

1. Проведённый анализ данных об исторической сейсмичности территории показывает, что все сильнейшие землетрясения происходили на довольно значительном расстоянии от города, преимущественно на юго-востоке от г. Самарканда.

Наибольшие повреждения городу нанесли Уратюбинское, Каратагское, Бойсунское и Ургутское землетрясения. Отмеченные выше землетрясения, по имеющимся на данный

момент данным, являются наиболее сильными для территории города.

Эти землетрясения, с соответствующими их характеристиками, приняты в качестве вариантов сценарных землетрясений.

Из четырёх отмеченных вариантов, наиболее неблагоприятным вариантом сценарного землетрясения является Уратюбинское землетрясение. На основе анализа записей сейсмограмм [29], а также возможных сильных землетрясений данной территории с магнитудой M = 6,5 (K = 16 - 17), было установлено, что преобладающими периодами функции очага для эпицентральной зоны является T = 0,4; 0,6 сек. Этим периодам соответствуют максимальные амплитуды спектра колебаний A = 5 и 7 мм. Потенциальным из возможных очагов будущих землетрясений определена очаговая зона под Ура-Тюбе с глубиной 10 - 15 км. Из возможных углов падения упругих волн для территории Самарканда [29], принята величина $\alpha = 85^0$;

2. В результате изучения структурно-геоморфологических характеристик региона установлено, что северо-восточный блок, где расположена часть города Самарканда, приподнят относительно юго-западного блока и имеет наклон в юго-западном направлении. Разрывные нарушения, окружающие блоки активизированы в новейшем этапе.

3. В результате обзора исследований, касающихся изучения геологических и инженерно-геологических процессов и явлений установлено, что на территории г. Самарканда имеет широкое развитие выветривание, эрозия, оврагообразование и суффозия.

4. На территории г. Самарканда наибольшее распространение имеют четвертичные отложения, которые представлены сохским, ташкентским, голодностепским и сырдарьинским комплексами. В литологическом отношении они представлены суглинками, песками, дресвой, гравием и галечником.

5. По данным электроразведочных исследований собраны и классифицированы сведения о геологическом строении поверхностных грунтов, их простирании и залегании на территории города в пределах 30 метровой толщи.

6. По данным сейсморазведочных исследований территории города были изучены упругие характеристики грунтов, как по площади, так и по глубине (до 30 м). Изучена карта приращения сейсмической интенсивности для территории города, которая является основой карты сейсмического микрорайонирования.

7. По данным инструментальных исследований слабых землетрясений установлено, что в спектрах смещений выделены два ярко выраженных экстремума. Первый из них наблюдается при T = 0,4 сек, второй – при T = 0,8 сек. Наибольшее количество колебаний от землетрясений приходится на эти периоды.

8. Повышенное значение приращения интенсивности (около «+1» балла) характерно для территории антропогенных отложений, а также территорий, где в составе лессовых пород развиты линзообразные включения дресвы.

9. Изучена карта-схема сейсмического микрорайонирования г. Самарканда в его перспективных границах, согласно которой на территории города выделены 7-ми, 8-ми и 9ти балльные зоны. Участки с сейсмичностью 9 баллов расположены в основном на территории «старого города» и занимают около 20% общей территории города.

10. Проведена обработка отмеченной сейсмологической и инженерно-геологической информации с использованием GIS С-технологий.

В частности, разработана GIS-основа исследуемой территории, проведена идентификация границ территории города и разработана серия карт по оценке сейсмической опасности территории по следующим темам :

- административные границы города;
- реки, каналы;
- водоемы;
- улицы города;
- расположение эпицентров исторических землетрясений;
- карта сглаженной сейсмичности региона;

- карта распределения грунтов на территории города;
- карта уровня грунтовых вод;
- карта микросейсморайонирования территории города (Рис. 1).

Для проведения оценок сейсмической опасности исследуемой территории (и на последующих этапах выполнения исследований) использовалось программное обеспечение GIS ArcView, разработанное ESRI (Environmental System Research Institute, USA), которое было передано исполнителям в ходе выполнения международного проекта для города Ташкента.

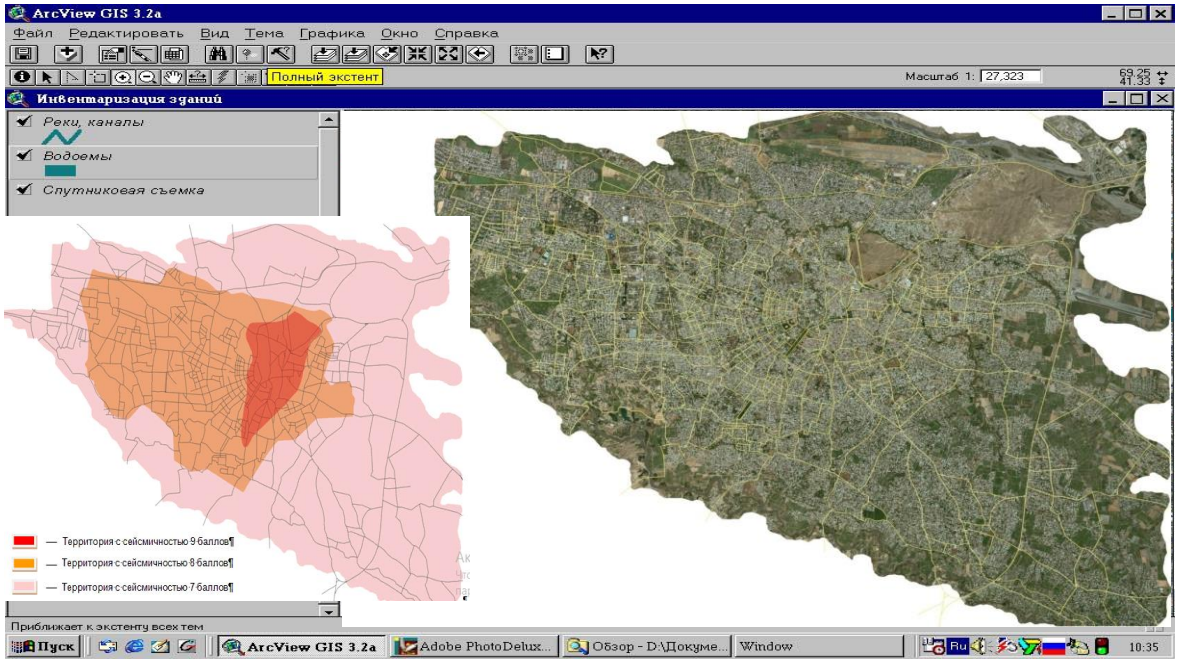

Рисунок 1. - **Процедура создания векторизованной темы по растровому изображению спутниковой съёмки территории города и карта микросейсиорайонирования.**

5. Анализ результатов

Полученные результаты согласуются с положениями КМК [1], согласно которым, сейсмичность территории г. Самарканда оценивается в 7, 8 и 9 баллов, с ожидаемым интервалом повторяемости землетрясений отмеченной интенсивности, соответственно, 150, 500 и 1000 лет.

Достоверность проведённой оценки сейсмической опасности (включая карту сейсмического микрорайонирования исследуемой территории) обеспечена комплексной оценкой роли составляющих и влияющих факторов, оцененных на основе использования результатов нескольких альтернативных методов (оценки приращения сейсмической балльности, инженерно-геологического районирования, результатов электроразведочных исследований, оценки сейсмической интенсивности по методу сейсмической жесткости, результатов исследований слабых землетрясений, расчетного метода сейсмического микрорайонирования, данных обследования последствий землетрясений).

6. Обсуждение

Полученные результаты исследований по оценке сейсмической опасности использовались на последующих этапах комплексных исследований по оценке и управлению сейсмическим риском для г. Самарканда.

Результаты проведённых исследований обеспечат возможность долгосрочного и оперативного планирования действий, снижающих сейсмический риск на территории города. Они могут быть использованы как при решении текущих вопросов управления и эксплуатации городского хозяйства, так и при разработке генеральных планов развития города органами управления и планирования, силовыми структурами, эксплуатационными и кадастровыми

службами и пр. И, кроме того, разработанные в отношении сейсмического риска GIS-проекты, вполне могут послужить основой для разработки соответствующих проектов и для других видов чрезвычайных ситуаций природного и техногенного характера.

Накопленный уникальный практический опыт проведения исследований и разработок, направленный на решение проблемы оценки и управления сейсмическим риском, базирующийся на передовом мировом опыте, жизненно важно и чрезвычайно актуально распространить для наиболее крупных городов Узбекистана (в качестве первого этапа), а затем (в перспективе) и для других городов и населённых территорий.

7. Заключение

В соответствии с целью и задачами исследований на данном этапе проведён аналитический обзор, обработка и классификация сейсмологической и инженерно-геологической информации (сведений об исторической сейсмичности, проявлении сейсмического эффекта от землетрясений на территории города, их характеристиках, анализ исследований по тектонике, геоморфологии, гидрогеологии и сейсмичности района, материалы исследований по инженерной геологии, электроразведке и сейсмометрии территории города, сведений о сейсмических характеристиках грунтов, преобладающих периодах их колебаний; данные о сейсмическом микрорайонировании территории города в его перспективных границах/

Установлено, что все сильнейшие землетрясения происходили на довольно значительном расстоянии от города. Наибольшие повреждения городу нанесли Уратюбинское, Каратагское, Бойсунское и Ургутское землетрясения, которые могут рассматриваться в качестве вариантов сценарных землетрясений. Наибольшее значение интенсивности, проявившееся на территории города при отмеченных землетрясениях, составило 8 баллов. Из 4 отмеченных вариантов, наиболее неблагоприятным вариантом сценарного землетрясения является Уратюбинское землетрясение, для которого установлена очаговая зона, преобладающие периоды функции очага для эпицентральной зоны, максимальные амплитуды спектра колебаний, глубина гипоцентра и возможный угол падения упругих волн для территории города.

Проведена обработка отмеченной сейсмологической и инженерно-геологической информации с использованием GIS-технологий (программный пакет ArcView GIS 3.2a). Разработана серия карт по следующим темам: расположение эпицентров исторических землетрясений; карта сейсмичности региона; административные границы города; реки, каналы; водоемы; улицы; карта распределения грунтов и уровня грунтовых вод на территории города; карта микросейсморайонирования его территории (Рис. 1)

8. Благодарности

Автор выражает искреннюю благодарность сотрудникам и руководству областного и городского хокимиятов, областного УЧС, служб кадастра, управления махаллинскими комитетами г. Самарканда, проявившим заинтересованность в проведении отмеченных исследований в целом, оказавшим их поддержку, в том числе в сборе необходимой исходной информации, а также академику АН РУз д.т.н. профессору Турсунбаю Рашидовичу Рашидову, под общим научным руководством которого проводились данные исследования.

Литература

1. КМК 2.01.03-19. Строительство в сейсмических районах. Минстрой РУз. – Ташкент, 2019. – 107 с.
2. *Рашидов Т.Р., Кондратьев В.А.* Современные концепции оценки и управления сейсмическим риском в Узбекистане. Узбекский журнал «Проблемы механики». № 5. Ташкент: Фан. 2007 г. с. 13 - 21.
3. Разработка научно-практических основ обеспечения сейсмической безопасности для города Самарканда и рекомендаций по снижению ущерба при возможных землетрясениях / Отчет НИР (заключительный) – Самарканд : СамГАСИ, 2011 г.– 340 с.
4. Стандарт Республики Узбекистан РСТ Уз 836-97 «Шкала для определения интенсивности землетрясения в пределах от 6 до 10 баллов». Введён в действие 01.01.1998 г.
5. *Кондратьев В.А.* Методология применения геоинформационных технологий при оценке и управлении

сейсмическим риском. Монография. Академия Министерства по чрезвычайным ситуациям Республики Узбекистан. Ташкент: Академия МЧС Республики Узбекистан. 2024 г. 148 с.
6. *Мицкевич А.А.* Эпицентральная зона землетрясений Самаркандского района. Изд. Комитета по науке РУз, Ташкент, 1937.
7. *Яковлева И.Б.* Анализ и обобщение сейсмологических данных. В кн. «Сейсмичность Западного Узбекистана». «Фан», РУз, 1972.
8. *Икрамов М.И.* О сейсмичности территории Узбекистана. Автореф., канд. диссерт. Самарканд, 1933.
9. *Касымов С.М., Джураев А., Мадатов П.* Карта изосейст Газлийского землетрясения 8 апреля и 15 мая 1977 г. Информ. Сообщение № 184. Изд. «Фан», РУз, 1977.
10. *Касымов С.М.* Результаты микросейсмического обследования Исфара-Баткентского землетрясения 31 января 1977 г. на территории некоторых городов РУз. Информ. Сообщ. № 194, Изд. «Фан», РУз, 1978.
11. *Архангельский А.Д.* Схема тектоники СССР. Бюллетень МОИП. Отд. геол., часть П, вып.4. М., 1933.
12. *Николаев В.А.* О некоторых чертах строения и развития подвижных поясов земной коры. Изв. АН СССР, сер. геол. наук, № 2, 1953.
13. *Бабаев А.Г.* Литология, палеография и нефтегазоносность меловых отложений Западного Узбекистана. Изд. АН РУз, Ташкент, 1959.
14. *Чистяков А.А.* Новейшая тектоника и геоморфология в восточной части бассейна р. Зарафшан. Дисс. канд., МГУ, М., 1958.
15. *Ризниченко Ю.В.* Метод суммирования землетрясений для изучения сейсмической активности. Изв. АН СССР, сер. геофиз. наук, № 7, 1964.
16. *Горбунова И.В.* Построение карт сейсмической активности с постоянной точностью. Труды ИФЗ, вып. 32 (199), М., Изд. «Наука», 1964.
17. *Захарова А.И., Яковлева И.Б.* Исследование сейсмичности с помощью количественных методов. В кн. «Сейсмичность Западного Узбекистана». Изд. «Фан», РУз, 1972.
18. *Яковлева И.Б.* Карта максимально возможных землетрясений Узбекистана по комплексу геолого-геофизических данных. В кн. «Сейсмология Узбекистана», Изд. «Фан», РУз, 1975.
19. *Костенко Н.П.* Развитие складчатых и разрывных деформаций в орогенном рельефе. М., Недра, 1972.
20. *Чедия О.К.* К методике составления карт новейшей тектоники для среднеазиатских гор. Душанбе, 1963.
21. *Бутов П.И.* Гидрогеологические исследования в Самаркандской котловине в 1924-1926 гг. Фонды МГ РУз, Ташкент, 1929.
22. *Шмидт М.А*. Гидрогеологический и геологический очерк западной части Зарафшанской котловины. Материалы по гидрогеологии и инженерной геологии, вып. 5, Изд. Комитета по науке РУз, Ташкент, 1937.
23. *Толстунов В.М.* Гидрогеологический очерк долины р. Зарафшан и Санзар. Фонды Института Средазгидроводхлопок. Ташкент, 1948.
24. *Шевченко А.И.* Гидрогеологическая классификация орошаемых территорий Узбекистана. Изд. АН РУз, Ташкент, 1961.
25. *Тетюхин Г.Ф., Мавлянов Г.А., Султанходжаев А.М.* Гидрогеологические особенности Зарафшанского бассейна. Ташкент, 1975.
26. *Попов И.В.* Инженерная геология СССР, часть 1. Общие основы региональной инженерной геологии. Изд. МГУ, 1961.
27. *Чуринов М.В., Цыпина И.М., Лазарев В.П.* Принципы и методика составления общих карт территории Советского Союза масштаба 1:1500 000 и 1: 2 500 000. «Советская геология», № 11, 1962.
28. *Золотарев Г.С., Пиотровский Т.Ю.* Макеты инженерно- геологических карт горноскладчатых областей для подземного и наземного (городского и дорожного) строительства и рекомендации по их составлению. Изд. МГУ, М., 1973.
29. Заключительный отчет по теме «Разработать комплексную методику сейсмического микросейсморайонирования в различных инженерно-геологических и тектонических условиях территории Узбекистана и применить её для составления карт сейсмического микрорайонирования. Сейсмическое районирование территории г. Самарканда в его перспективных границах. № гос. рег. 77005876. Проблема № 0.74.03. Шифр 02.Д4. Академия наук Узбекской ССР. Институт сейсмологии. Ташкент. 1980. – 97 с.

К ОЦЕНКЕ СЕЙСМИЧЕСКОЙ ОПАСНОСТИ Г.ТАШКЕНТА

Нурматов У.А.[1], Садыков Ю.М. [1], Юсупджанова У.А. [1]

[1]*Институт сейсмологии имени Г. А. Мавлянова, Ташкент, Узбекистан*

E-mail: ulfat.nurmatov@mail.ru

Аннотация. *Статья посвящена изучению сейсмотектонической обстановки г.Ташкента и прилегающих территорий. Рассмотрены вопросы формирования и развития геодинамических структур в новейшем и современном этапе, основных разломов, которые ответственны за современную сейсмичность Приташкентского района. Приводятся информации о современных вертикальных движениях земной коры, о линейных источниках землетрясений и об исторических землетрясениях, возникших как в пределах города, так и прилегающих территориях, которые представляли реальную угрозу города.*

Ключевые слова: *Сейсмическая опасность, активный разлом, сейсмогенная зона, тектонические структуры, эпицентр землетрясения, современные движения.*

1. Введение

Формирование основных структур, определяющие современный геоморфологический облик Приташкентского района, куда входить г. Ташкент и прилегающие территории, приходится на новейший этап геодинамического развития. Современную структуру представляет северо-восточная система положительных и отрицательных элементов различного порядка, разграниченных древними разломами, активизированными в неоген-четвертичный этап геологического развития. Ядерную часть поднятий образуют породы консолидированного фундамента. Они постепенно погружаются под мезозойско-кайнозойских отложений в юго-западном направлении. Разломы, в основном северо-восточной ориентации, различаются историей тектонического развития, глубиной проникновения и особенностями деформирования [Ибрагимов Р.Н., Нурматов У.А. и др. 2002].

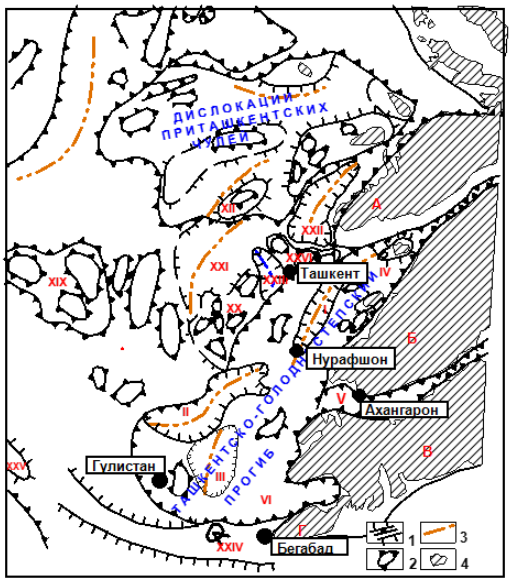

1-границы поднятий и прогибов; 2-локальные антиклинальные складки; 3-оси синклинальных структур; 4-выходы домезозойского фундамента. А, Б, В – мегантиклинали Тянь-Шаня-Каржантауская, Чаткальская, Кураминская, Моголтауская. Ташкентско-Голодностепский прогиб: I – Янгибазарская синклиналь; II-Пахтинская синклиналь; III-Мирзачульская синклиналь.Депресии: IV-Верхне-Чирчикская; V-Ангренская; VI-Мирзараватская; VII-Баламская; XIX-Джаусумкумское поднятие; XX-Янгиюльское поднятие; XXI-Келесская синклиналь; XXII-Беркебашская синклиналь; XXIII-Сарыагачская синклиналь; XXIV-Мехнаткашский вал; XXV-Писталитауское поднятие; XXVI-Майско-полторацкое поднятие.

Рисунок 1. - **Фрагмент схемы тектонического районирования Ташкентско-Голодностепского прогиба и сопредельных территорий [по Таль-Вирский, 1982].**

Одним из крупных структурных комплексов Приташкентского района является Ташкентско-Голодностепская олигоцен антропогеновая впадина, которая имеет сложное тектоническое строение в пределах которой расположен г.Ташкент. По данным О.А.Рыжкова, Р.Н.Ибрагимова, А.А.Юрьева [1961], впадина располагается в зоне сочленения двух крупных

структурных комплексов между Туранской плитой и Чаткало-Кураминской горной системой. Переход в сторону плиты постепенный и имеет ассиметричное строение. Ось ее простирания с северо-востока на юго-запад и в районе Голодной степи поворачивается на северо-запад и сливается с Сырдаринской впадиной. Глубина залегания фундамента здесь по геофизическим данным достигает 3000 м. По поверхности фундамента выделяется большое количество структур более высокого порядка, которые осложнены разрывными нарушениями. Почти все положительные и отрицательные элементы палеозойского фундамента отразились в структуре покрова. Среди них выделяются поднятия Приташкентских чулей, Сырдарьинская, Янгиюльская, Джаусумская и Майско-Полторацкая группы поднятий, Келесский и Чирчикско-Голодностепский прогибы (Рисунок.1). Они в свою очередь также осложнены положительными и отрицательными элементами более низшего порядка, которые отражаются в осадках мезозоя-кайназоя в виде интенсивно развивающейся антиклинальных и синклинальных складок. Наиболее крупные зоны складок находятся на продолжении Чаткало-Кураминских мегантиклиналей и протягиваются к юго-западу через Майско-Пролторацкую, Пскентско-Букинскую группу поднятий. Между ними располагаются Чирчикско-Голодностепский, Нижнеангренский и Мирзарабатский прогибы. Состав палеозойского фундамента по структурно-фациальным чертам сходны с Курамино-Ферганским срединным массивом. В строении рельефа палеозойского фундамента можно отметить следующие особенности. Большинство поднятий и прогибов часто пересечены разрывными нарушениями, смещения их исчисляются сотнями метров. Примечательно, что с удалением от Чаткало-Кураминских горных сооружений эти структуры имеют субширотное простирание, а ближе к горам – северо-восточное. Таким образом все положительные и отрицательные элементы палеозойского фундамента отражаются в современной структуре Приташкентского района (Рисунок. 1) [Ибрагимов, 1978].

2. Результаты сейсмотектонического анализа

Неотектоника. *Полторацко-Сырдаринская антиклинальная зона* (Рисунок.2) представляет собой наиболее крупную по размеру и амплитуде положительную структуру, являющуюся непосредственным продолжением Каржантауского антиклинального поднятия с погружением шарнира в сторону впадины. Она отчетливо выРисуноковывается и по кровле палеогеновых отложений. Строение зоны асимметричное, ее северо-восточный склон более крутой, чем южный.

Полторацко-Сырдаринская антиклинальная зона располагается на приподнятом крыле Приташентской флексурно-разрывной зоны, которая в свою очередь служит южной границей, отделяющей ее от Чирчикско-Голодностепской синклинали. На севере граничить с Келесской синклинальной зоной. Зона состоит из кулисообразно расположенных локальных складок неодинакового строения и в целом куполовидной формы с осложнениями в виде локальных брахиантиклиналей. Простирается в основном с северо-востока на юго-запад.

Наиболее крупная антиклинальная складка – Карачатау с выходом в ее ядре палеозойских пород. Для нее характерно наличие в южном крыле надвига, по которому не только срезаны меловые и неогеновые толщи, но и нарушены террасы р.Чирчик вплоть до голодностепской, местами затронуты даже молодые наносы. По данным Н.П.Васильковского и др. [1940], амплитуда перемещения в кайнозойских отложениях достигает 1000 м.

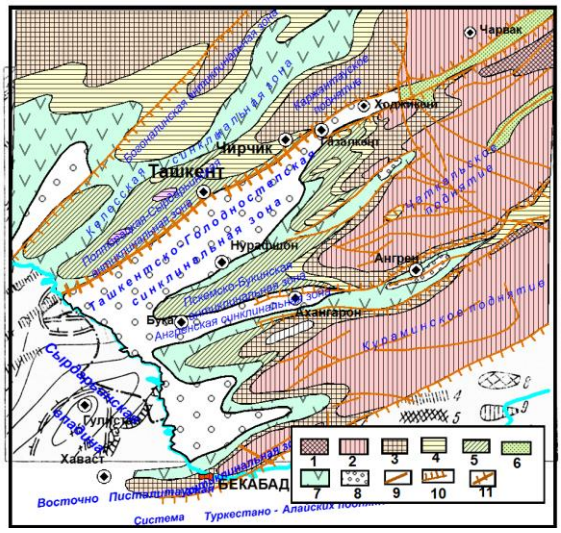

Участки: 1-интесивно поднимающиеся с миоцена; 2- с позднего эоплейстоцена; 3- с раннего неоплейстоцена; 4- со среднего неоплейстоцена; 5-с позднего неоплейстоцена; 6- эоплестоценовые прогибании, вовлеченные в поднятия в раннем неоплейстоцене; 7- ранее и средне неоплейстоценовые прогибаний; 8- голоценовые прогибании; 9- менее активные разломы; 10- наиболее активные разломы; 11- флексурно разрывная зона.

Рисунок.2. **Карта новейших тектонических движений Приташкентского района [Ахмеджанов и др., 1971].**

Крупнейшая синклинальная зона – Чирчикско-Голодностепская представляет собой довольно сложное тектоническое образование. В ее пределах палеозойские породы залегают на глубине не менее 2,5 км. Северо-восточная часть замкнута, а на юго-западе впадина сливается с Ангренской и Мирзараватской синклиналями и раскрывается в сторону Голодной степи. Почти вся площадь покрыта четвертичными образованиями мощностью 200-500 м. В наиболее опущенной части, юго-восточнее Ташкента, мощность кайнозойских моласс превышает 2 км. Характерная особенность зоны – непрерывное прогибание в течение мезозоя-кайнозоя, особенно в олигоцен-антропогеновое время, полнота стратиграфических разрезов и слабое проявление складчатых движений.

Таким образом, Приташкентская флексурно-разрывная зона является наиболее тектонически активной структурой Ташкентского-Голодностепской впадины, с которой связаны эпицентры сильных землетрясений, возникшие в г.Ташкенте и прилегающих территориях.

В пределах г.Ташкента осадочный мезо-кайнозойский чехол города включает от юрских до четвертичных отложений. Верхнемеловые и палеогеновые отложения распространены повсеместно, литологически и по мощностям выдержаны. Метаморфизм палеогеновых пород очень слабый. Мощность палеогена варьирует в пределах 75-145м. На морских отложениях палеогена залегают, красноцветные внизу и буроцветные вверху, неогеновые молассы (конгломераты, мергели, и гипсы). Далее следуют четвертичные отложения, слабо уплотненные, местами загипсованные, каменистые. Мощность пород в прогибах до 60-70м. Среднечетвертичные отложения (ташкентский комплекс) представлены лессовой формацией. Лессы слагают все высокие террассы рек и водоразделы. Лессами сложена большая часть Ташкента. Мощность лессов достигает 50 м (юго-запад города). Позднечетвертичные отложения (голодностепский комплекс) вложены в Ташкетский комплекс. В основании залегают галечники и пески, верхняя часть сложена суглинками и супесями. Мощность пород комплекса 20-30м. Современные отложения (сырдарьинский комплекс) представлены лессами (водоразделы) и галечниками (в речных долинах). Мощность не более 20м. Линейно вытянутые в юго-западном направлении структуры Каржантау, в западной части города, ограничены глубокой Келесской депрессией (субмеридионального простирания). Данная депрессия ограничивает с запада поднятия Чигатайское, Ташкентское и Чирчикское, перемежающиеся Бозсуйским и Ташкентским прогибами. Все структуры северо-восточной ориентации. Наиболее сейсмоопасной структурой в регионе является система Каржантауского и Приташкентской флесурно-разрывной зоны (ФРЗ), с которыми связаны практически все

сильные землетрясения. В районе сел.Кибрай ФРЗ проявляется в виде участка брекчированных неогеновых алевролитов, в районе ВДНХ Узбекистана, в скважинах I и II вскрыта кровля палеогена с разницей абсолютных отметок в 65 м, когда расстояние между скважинами 200м. Это возможно лишь при функционировании ФРЗ. За чертой города происходит затухание вышеназваных линейных складок северо-восточной ориентации. Происходит подъем палеозойского фундамента и в районе г.Янгиюль он на 600-700 м выше, чем в г.Ташкенте. Также наблюдается интенсивный подъем фундамента к северу от города.

Голоценовые (последние 12 тыс.лет истории земли) тектонические движения современного рельефа. В результате исследования новейших и голоценовых тектонических движений были сделаны следующие выводы [Ланге,1971]:

- унаследованный от ранних этапов неотектогенеза общий характер развития тектонических структур осадочного чехла сохраняется и в настоящее время. Наблюдается преобладание северо-восточного направления складок осадочного чехла, осложняющийся развитием наложенных структур широтного и субширотного простирания. (северо-западная часть города);

- линейные складки представлены локальными кулиса образными поднятиями и разделяющими их пологими тектоническими седловинами;

- разрывные нарушения обусловлены напряжениями, возникающими в толще осадочного чехла в процессе формирования его преимущественно складчатой структуры. Кулиса образное расположение локальных поднятий, ограничивающих тектонические седловины, можно рассматривать как признак левых сдвигов по приуроченным к этим седловинам разломам субмеридионального направления;

- деформации осадочного чехла в современном рельефе представляют собой отражение тектонических процессов, протекающих в толще палеозойского фундамента. Развитие этих процессов имеет непрерывно-прерывистый характер;

- ундуляция шарниров линейных структур – тектонических седловин, соответствующих перегибам осей складок осадочного чехла рассматриваются как наиболее вероятные сейсмоопасные зоны.

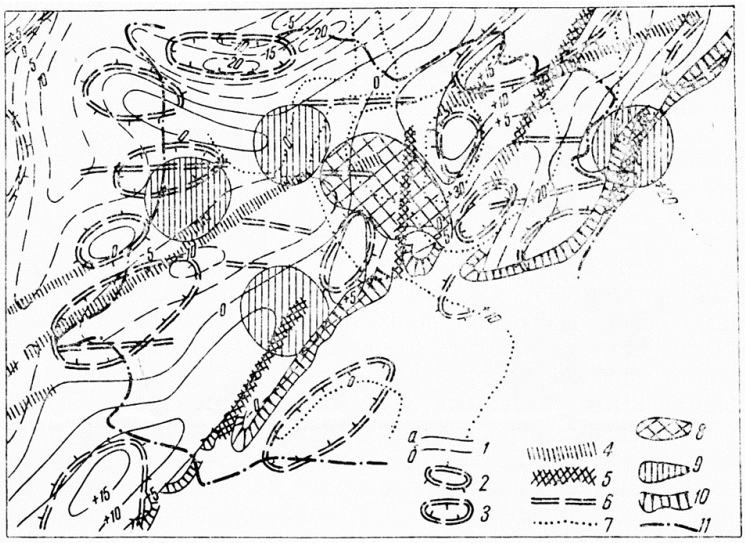

1-линии равных амплитуд деформаций среднеплейстоценовой аккумулятивной равнины, ***м***; 2-участки голоценовых относительных поднятий; 3-участки относительных голоценовых опусканий; 4-зоны вероятных дизъюнктивных нарушений; 5-средне и позднеплейстоценовые «тектонически ослабленные зоны»; 6-предполагаемые направления плейстоцен-голоценовых зон трещиноватости; 7-линии равных амплитуд относительных, ***мм.*** (по данным нивелирования); 8-плейстосейстовая область Ташкентского землетрясения 1966 г.; 9-участки возможных сейсмопроявлений; 10-склон позднеплейстоценовой долины Чирчика; 11-граница города.

Рисунок.3. **Схематическая карта молодых тектонических деформаций территории г.Ташкента [Ланге,1971].**

Современные вертикальные тектонические движения. Исследование особенностей вертикальных движений земной поверхности проведенные в 1962-1965 гг., т.е. до

возникновения Ташкенского землетрясения и 1966 г. после землетрясения показали положительные движения реперов наблюдений по всей территории города. Интенсивность движений в центральной и северо-восточной части города доходило до +20-30 мм. Значения движений северной и западной частях имели значения +10 мм. [Корешков,1973, 1974]. По данным Д.АТашходжаева и соавторов [1999] максимальное значение движений отмечены в северо-восточной части города и доходило до +3 мм. На южной части положительная изолиния имеет северо-западное простирание. Сопредельные территории с севера и с запада подвержены опусканию.

На рис.4 приведена карта СВДЗК по измерениям выполненных в 1992-1993 (I цикл) и 2000-2002 (II цикл) годах [14]. Изолинии движений проведены через 1 мм/год и дополняющей их раскраской: зеленой – зона опускания, коричневой – зона поднятия. Можно видеть, что вся территория города воздымается. Здесь изолинии имеют, в основном, широтные простирания.

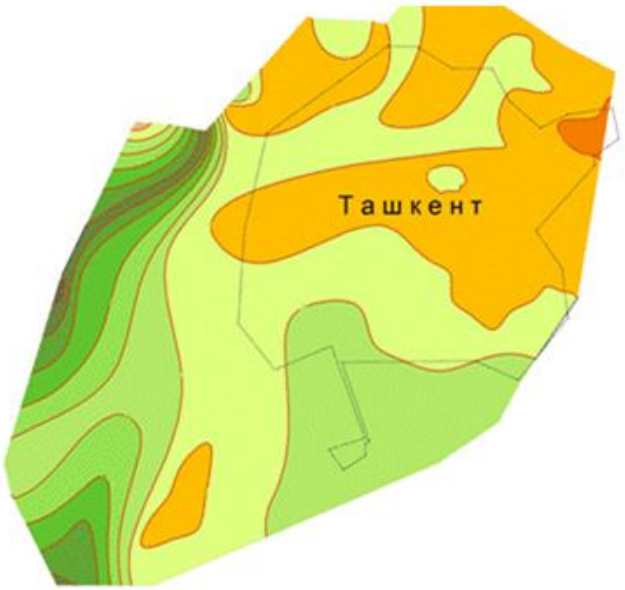

Рисунок 4. - **Карта современных вертикальных движений земной коры на территории г. Ташкента и его окрестностей в 1992-1993 (I цикл) и 2000-2002 (II цикл) годах. [14].**

Активные разломы. Для оценки сейсмической опасности территории г.Ташкенти и сопредельных территорий интерес представляют наиболее крупные структуро-контролируюшие разломы, с которыми связаны современные и прошлые землетрясения, оставившие в земной поверхности следы ввиде сейсмодислокаций. Эти активизированные герцинские разломы на протяжении новейшего этапа являются наиболее подвижными и проницаемыми участками земной коры и характеризуются изменчивостью полей тектонических напряжений во времени. Активизированные разломы, выявленные по геологическим и геофизическим и геоморфологическим данным представлены, взбросами, надвигами, взбросо-надвигами, взбросо-сдвигами, флексурно-разрывными зонами. Они отличаются протяженностью, шириной, глубиной проникновения, простиранием, формой проявления и т.д. Реальную угрозу на строящихся объектов в г. Ташкенте и сопредельных территориях представляют следующие разломы земной коры и связанные с ними очаги землетрясений (Рисунок.5).

Каржантауский разлом (4) представлен крутым надвигом и прослеживается вдоль границы одноименного хребта, который отделяет его от Чирчикской впадины. В районе с. Хумсана он пересекает зону Угамских разломов северо-западного простирания. По нему на правом берегу р. Чирчик палеозойские породы надвинуты на отложения мезо-кайназойя. Вертикальная составляющая превышает 3000 м, падение поверхности смесителя от 40 до 70^0. На местности он проходит в северо-восточном направлении через села Хандайлык, Хумсан, севернее Богустана и далее по правому берегу р. Пском. На участке долины р. Чирчик по

данным М.П.Васильковского [1941] резает местами террасы четвертичных отложений, и амплитуда смешения достигает порядка 1000 м. В юго-западном направлении Каржантауский разлом погружается в мезозойско-кайнозойские отложения в виде флексурно-разрывной зоны. С Каржантауским разломом связано возникновение Бурчмуллинского 1959 г. и Таваксайского 1977 г. землетрясений.

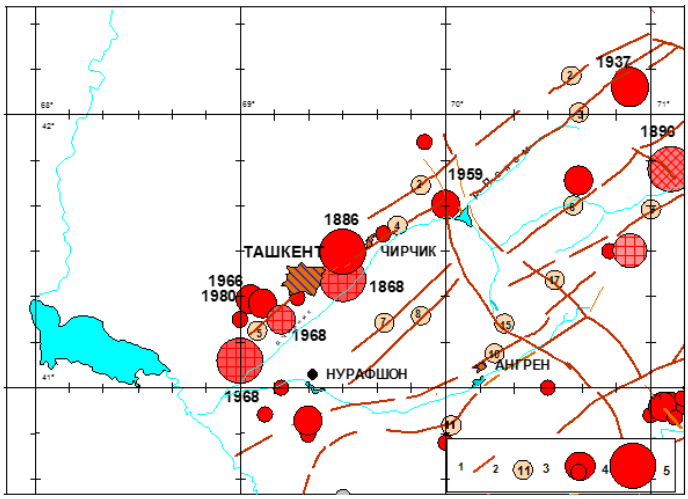

1-активные разломы; 2-номер разлома: (2-Аксу-Майдантал-Богоналинский; 3-Пскемский; 4-Каржантауский4 5-Приташкентская флексурно-разрывная зона; 6-Южно-Пскемский; 7-Сюрен-Атинский; 8-Сукокский; 9-Чаткальский; 10-Северо-Ангренский; 11-Южно-Ангренский; 15-Кумбель-Коканд-Хайдарканский; 17 Арашанский); эпицентры землетрясений: 3- с M≥5.0 и M≥5.5; 5-с M≥6.0.

Рисунок 5. - **Активные разломы Приташкентского района и эпицентры сильных (с M≥ 5.0) землетрясений по [9].**

Приташкентская флексурно-разрывная зона (5) установлена О.А.Рыжковым, Р.Н.Ибрагимовым, А.А.Юрывим [1961] в результате анализа мощности неоген-антропогеновых отложений и по отделенным разрывам на поверхности. Данные бурения и геологической съемки показали, что по отдельным участкам зоны на протяжении новейшего этапа тектонического развития происходили интенсивные, дифференцированные движения больших амплитуд (до 2000-2500 м), зафиксированные отложениями кайнозойских моласс на одном крыле зоны и размывом на другом. Установлены также смешение палеогеновых отложений с разницей в 65 м в районе санатории «Семашко» по данным скважин, пробуренных на расстоянии 200 м друг от друга.

В пределах г.Ташкента геолого-геофизическими исследованиями выделен ряд разломов являющиеся составной частью Приташкентской флексурно-разрывной зоны. К их числу относятся Ташкентско-Алмалыкский, Каракамышский, Чирчикский, Чинабадский и др. разломы.

Зона Нурекатинских разломов (7,8) состоит из, серии параллельных дизъюнктивных нарушений. Наиболее крупные из них Сюрень-Атинский и Сукокский. По ним установлены смещения только за четвертичное время до 800-1100 и. Местами отдельными разломами разорвана даже голодностепская поверхность выравнивания. Амплитуда этих подвижен достигает 50-60 м. Эти разломы ограничивают с севера Паркент-Нурекатинский грабен, выполненный мезозойско-кайнозойскими породами. На юго-западном погружении они прослеживаются геофизическими методами.

Сильные землетрясения. Активизированные разломы Приташкенткого района, выявленные по геологическим и геофизическим и геоморфологическим данным представленные, взбросами, надвигами, взбросо-надвигами, взбросо-сдвигами и флексурно-разрывными зонами в совокупности приняты за геологическую основу всех сейсмогенных зон территории. Г. Ташкент приурочен к центральной части выделенной Ташкентско-Пскемской сейсмогенной зоны. Геологическую основу сейсмогенной зоны представляют Пскемский (3), Каржантауский (4) разломы и Приташкентская флексурно-разрывная зона (5, Рисунок.5). Инструментальные данные, так же исторические и палеосейсмодислокации показывают высокую сейсмическую активность данной сейсмогенной зоны. В ее пределах за прошедши

период возникли 4 землетрясения с M≥6.0, 4 с M≥5.0 и более 5 с M≥4.5 (Рисунок.6)[Ибрагимов и др., 2005]. Обращает внимание, что из четырех землетрясений с M≥6.0 три возникали в ближайших к Ташкенту районах. Ближайшее из них возникло в 1868 г. 4 февраля с M=6.0 на расстоянии 35-40 км от нынешней границы города, а следующее 4 апреля того же года на расстоянии 4-6 г.Ташкента с M=6.0. Исходя из числа возникновения этих землетрясений нельзя исключить, что по всей вероятности, речь идет об одном землетрясении. В этом же году 17 апреля зарегистрировано еще одно землетрясение с M=5.5. Судя по времени возникновения и пространственного положения (на расстоянии около 20 км от второго землетрясения с M=6.0) это землетрясение, по всей вероятности, является афтершоком второго землетрясения.

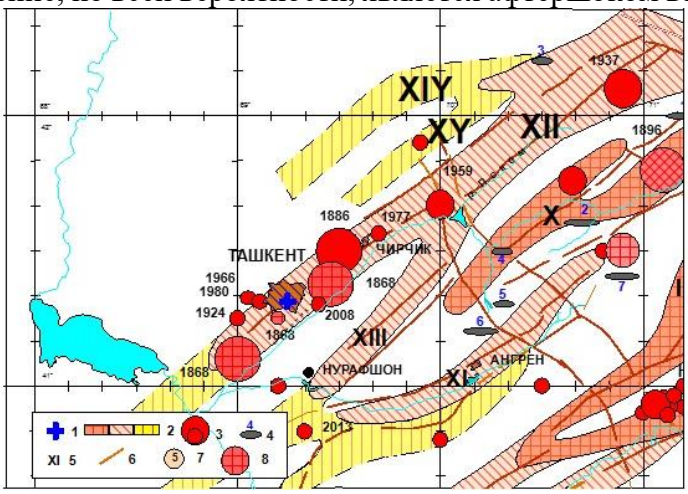

1-площад строительства; 2-сейсмогенные зоны, в пределах которых могут возникать землетрясения с M≤7.5, M≤6.5, M≥5.0 [Ибрагимов и др., 2002]; 3-эпицентры землетрясений с M≥4.5, M≥5.0 и M≥6.0; 4-палеосейсмодислокации и их порядковый номер; 5-номер сейсмогенной зоны (X-Сандалашская, XI-Ангренская, XII-Ташкентско-Пскемская, XIII-Нурекатинская, XIY-Лянгарская, XY-Угам-Каржантауская); 6-активные разломы; 7-порядковый номер разлома; 8-эпицентры исторических землетрясений.

Рисунок.6. - **Сейсмогенные зоны Приташкентского района и эпицентры сильных землетрясений.**

Следующее сильное землетрясение возникло в 1868 г. с M=6.5. Эпицентр землетрясения находился на расстоянии 25 км к северо-востоку от г.Ташкента в зоне Каржантауского разлома. Следующее землетрясение в г.Ташкенте возникло 7.06 1924 г. с M=4.8. Сила землетрясения в Ташкенте опушалась интенсивностью 6-7 баллов. Последующие периоды активизации очаговой области г.Ташкента наблюдался в 1966 г. возникновением Ташкентского землетрясения с M=5.3 и в 1980 г. Назарбекского землетрясения с M=5.3. Последняя активизация Ташкентской очаговой области зарегистрирована в 2 августа 2008 г. с K=12.6, т.е. с M=5.2. Хотя сила землетрясения оценивается почти соизмеримая с Ташкентским 1966 г. эффект от нее не ощущался не так сильно, как в предыдущих случаях. Это может быть связан с тем, что сила последнего землетрясения, может быть, немножко завышена. Кроме зарегистрированных сильных землетрясений, возникших в пределах Приташкентского района выявлен ряд сейсмодислокаций являющиеся последствием возникших в древности сильнейших землетрясений. Ближайшая из них **Палеосейсмоструктура «Карабузук"** отмечено в районе Ангренской сейсмогенной зоны (дислокация №6 на Рисунок.6) [Ходжаев, 1985]. Палеосейсмоструктура приурочена к зоне Кумбельского разлома и вытянута в северо-западном направлении от руч. Таваксай до руч. Карабузук более чем на 8,5 км. Максимальные амплитуды вертикальных перемещений достигают 15м, горизонтальные зафиксированы в верховьях р. Карабузук. Сила землетрясения, которая вызвала такую дислокацию, была оценена равным M=7.2. Расстояния от дислокации до г.Ташкента около 80 км. В случае возникновения землетрясения в сейсмогенной зоне такой силы из-за затухания сейсмической интенсивности с расстоянием эффект в г.Ташкенте не будет превышает 8 баллов.

Сейсмогенные зоны. Приведенные выше разломы земной коры Приташкентского района приняты в качестве линейных источников сейсмичности-сейсмогенных зон. Исходя из приведенных выше результатов г.Ташкент расположен в пределах Ташкентско-Пскемской

сейсмогенной зоны, где возможны возникновение землетрясений с M≤6.5 и с интенсивностью I=8 баллов.

На сейсмическую опасность г.Ташкента могут кроме собственных землетрясений значимое влияние могут оказать события, возникшие в других частях Ташкентско-Пскемской сейсмогенной зоны, а также сильные землетрясения, возникшие в пределах сопредельных сейсмогенных зонах. В пределах Ташкентско-Пскемской сейсмогенной зоны, кроме вышеперечисленных, происходили еще три сильные землетрясения. Это Пскемское 1937 г. с M=6.4, Бричмуллинское 1959 с M=5.7 и Таваксайское с M=5.1. Из-за большого расстояния от эпицентров этих землетрясений до г.Ташкента сейсмический эффект от них в городе ощущалась с интенсивностью меньше 8 баллов.

Кроме землетрясений, возникающих в самой зоне, на г.Ташкент могут влиять землетрясения, возникшие в Нурекатинской сейсмогенной зоне, обусловленной Нурекатинской системой разломов. По сейсмическому потенциалу эта зона, по комплексу геолого-тектонических данных, отнесена к категории зон, где могут возникать землетрясения с M≤6,5[Ибрагимов и др., 2002].

3. Заключение

Таким образом Приташкентская флексурно-разрывная зона и Каржантауский разлом являются наиболее тектонически активными структурами Ташкентского-Голодностепской впадины, в пределах которой расположен г.Ташкент. Эпицентры всех сильных землетрясений, возникшие в г.Ташкенте и прилегающих территориях приурочены к зонам этих разломов. Ташкентско-Пскемская сейсмогенная зона, обусловленная вышеотмеченными разломами, является основным линейным источником сейсмичности данной территории. Сейсмический потенциал сейсмогенной зоны равняется M≤6.5, интенсивность I=8 баллов.

Литература

1. *Ахмеджанов М.А., Борисуноков О.М., Ибрагимов Р.Н.* и др. Основные структуры Приташкентского района. В кн. Ташкентское землетрясение. Ташкент, 1971. С.248-258.
2. *Васильковский Н.Н., Репников М.П.* Сейсмическая характеРисуноктика Северо-восточной части Ташкентского района в связи с его тектоникой. В кн.: Тектоника и сейсмичность северо-восточной части Ташкентского района. УзФАИ, Ташкент,1940.
3. *Васильковский Н.П.* Геологическое строение долины р.Ангрен. Ташкент, Фан.1941.
4. *Ибрагимов и др.* Сейсмотектонический метод оценки сейсмической опасности и вопросы сейсмического районирования. В кн. Сейсмическое районирование и прогноз землетрясений в Узбекистане. Ташкент, Гидроингео, 2002. стр.59-75.
5. *Ибрагимов Р.Н.* Сейсмогенные зоны Среднего Тянь-Шаня. Ташкент: Фан, 1978. -148 с.
6. *Корешков Н.А.* О постановке и некоторых результатах геодезических работ на Ташкентском, Ферганском, Душанбинском геодинамических полигонах. В сб. “Современные движения земной коры”, №5, Тарту, 1973 г.
7. *Корешков Н.А.* О состоянии геодезических работ на Ташкентском, Ферганском и Душанбинском геодинамических полигонах. В сб. “Поиски предвестников землетрясений на прогностических полигонах”, М., 1974 г.
8. *Ланге К.О.* Геоморфология и молодая тектоника Ташкентского сейсмического района. В кн. Ташкентское землетрясение. Ташкент, 1971. С.284-295.
9. Новый каталог сильных землетрясений на территории СССР с древнейших времен до 1975 г. / Под. ред. *Н.В.Кондорской и Н.В.Шебалина.*- М: Наука,1977.-536с.
10. *Рыжков О.А., Ибрагимов Р.Н.* и др. Тектоника Ташкентской Голодностепской предгорной олигоцен-антропогеновой впадины // Узб.геол.журн.-1961.-№5.
11. *Таль-Вирский Б.Б.* Геофизические поля и тектоника Средней Азии. М.: Недра, 1982, 272.
12. *Ташходжаев Д.А.,Юн Л.П., Ярмухамедов А.Р.* О новой карте современных вертикальных движений земной коры Узбекистана по геодезическим данным. Геология и минеральные ресурсы. 1999, №2. С.38-39.
13. *Ходжаев А.К.* Палеосейсмология Чаткало–Кураминского региона.-Ташкент: Фан, 1985.-140 с.
14. *Юн Л.П.* и др. Карта современных вертикальных движений земной коры на территории г. Ташкента и его окрестностей. Geokfrt/3dn.ru/hubl/1-1-0-2.

МЕХАНИЗМЫ ХИМИЧЕСКИХ ИЗМЕНЕНИЙ СОДЕРЖАНИЯ ПОДЗЕМНЫХ ВОД

Расулов А.В.[1], Саттарова Н.А.[1], Хасанова Г.И.[1]

[1]*Институт сейсмологии, Ташкент, Узбекистан*

E-mail: gulhayo.xasanova.89@mail.ru. n.sattorova406@gmail.com

Аннотация. *Выделены теории, обосновывающие природу аномальных изменений химического, газового и изотопного состава подземных вод, наблюдаемых в результате процесса подготовки землетрясений, и изменений состава подземных вод Ташкентского артезианского бассейна, связанных с сейсмическими процессами.*

Ключевые слова: *подземные воды, химический, газовый состав, изотопы, природа аномальных изменений, Ташкентский артезианский бассейн, аномальные изменения.*

1. Введение

Землетрясения – это стихийные бедствия, наносящие большой моральный и материальный ущерб человечеству и экономике. Поэтому вопрос углубления знаний о процессах, вызывающих землетрясения, проведение исследований особенностей признаков сильных землетрясений является важной и актуальной задачей, стоящей перед наукой. В последние годы проблема прогноза землетрясений является одной из важных задач исследователей, при этом основное внимание уделяется изучению проявления детекторов землетрясений в различных гидрогеохимических полях. Инертные и радиоактивные элементы, такие как гелий и радон, были впервые идентифицированы как индикаторы землетрясения во время ташкентского землетрясения 1966 года.

Исследования, проведенные в Ташкентском артезианском бассейне, показали, что изменения химического, газового и изотопного состава подземных вод до и после ташкентского землетрясения выявили гидрогеохимические и радиогидрогеологические аномалии.

Глубины скважин «ИБК», «Назарбек», «Текстиль», «Фазилов», «Ахмад Яссавий», принадлежащих Ташкентскому артезианскому бассейну, составляют 600м, 1400м, 2300м, 1942м. Эти меловые слои в основном состоят из таких минералов, как известняк, песчаник и конгломерат.

Средние значения кислорода и Eh в подзеных водах составляют соответственно: O_2 18,118%, 16,753%, 14,945%, 18,2%, Eh 231,7мВ, 223,64мВ, 230,9мВ, 54,07мВ. Средние значения температур в этой скважине составляют 53,3, 49,97, 36,21, 18,63, 50,56^0 С соответственно (табл. 1).

2. Материалы и методы

Как отмечал Н.Х. Хитаров (1974), термодинамическая ситуация определяет переход многих химических элементов и микроэлементов в грунтовые воды, их растворимость увеличивается с повышением температуры. Физически скорость диффузии ионов увеличивается в результате повышения температуры. Влияние температуры на подземных воды имеет двоякий эффект: во-первых, увеличивается ее растворимость и выход некоторых элементов в водный раствор, во-вторых, многие из них (He, Ar, CO_2 , Hg, O_2 и др.) переводят жидкую фазу из водной в газовую [10].

Таблица 1

Средние значения литологического состава, температуры, кислорода и, Eh артезианского бассейна Ташкента.

Название источников воды	Возраст водных пород	Литологический состав водоносных пород	Температура воды При Т ^{0}C	Средние значения содержания O_{2}, %	Средние значения содержания Eh мВ	O_{2}, %,
Артезианский бассейн Ташкента						
ИБК	K_{2}	Трещинистые известняки, песчаники, конгломераты	53,31	1 8,118	231,7	2,276 -18,2
Назарбек			49.97	16 753	223,64	
Текстиль			36,21	14 945	230,9	
Фазилов			18.63	18,2	54.07	

В результате наблюдений, проведенных на скважинах «ИБК», «Назарбек», «Фозилов», расположенных в Ташкентском артезианском бассейне, установлено, что перед землетрясениями произошел ряд изменений в газовом и химическом составе подземных вод [7].

В скважинах 11 сентября 2021 г. величина M = 4,4 (Казахстан, R=32 км, logR=2,66) от землетрясения первый по показателям кислорода, pH и Eh изменения наблюдаемый. В частности, перед землетрясением в скважинах Назарбек и Фозилов 4 дня назад начал снижаться кислород, а в скважине ИБК 3 дня назад содержание кислорода в скважине также вернулось к фоновому уровню (рис.1-3).Количество ионов водорода начало увеличиваться за 4 дня до землетрясения, достигло максимального значения 9 сентября, концентрация начала снижаться за день до землетрясения, землетрясение произошло 11 сентября. После землетрясения концентрация снижалась до 17 сентября (рис.4.5.6), где увеличение ионов водорода приводит к увеличению кислотности и снижению pH.

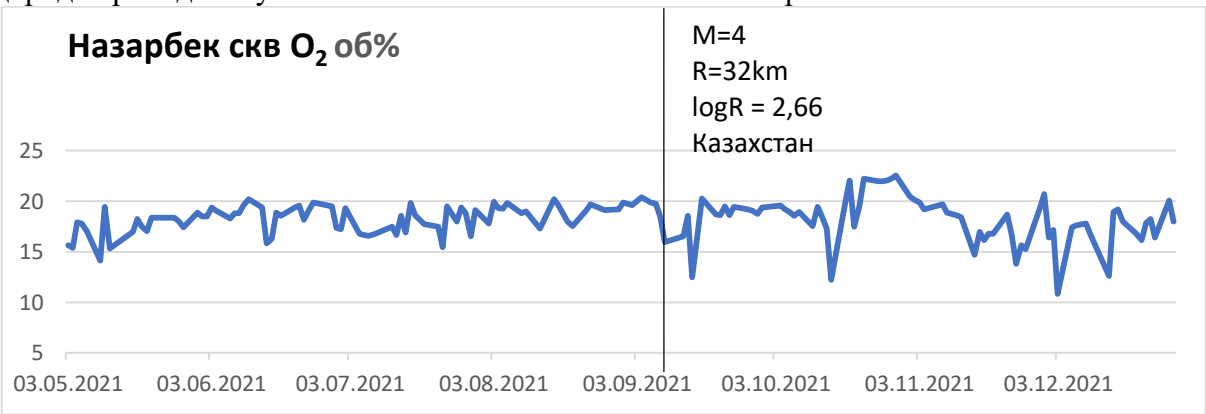

Рисунок 1. **-График изменения кислорода в скважине «Назарбек»**

Рисунок 2. - **График изменения кислорода в скважине «ИБК»**

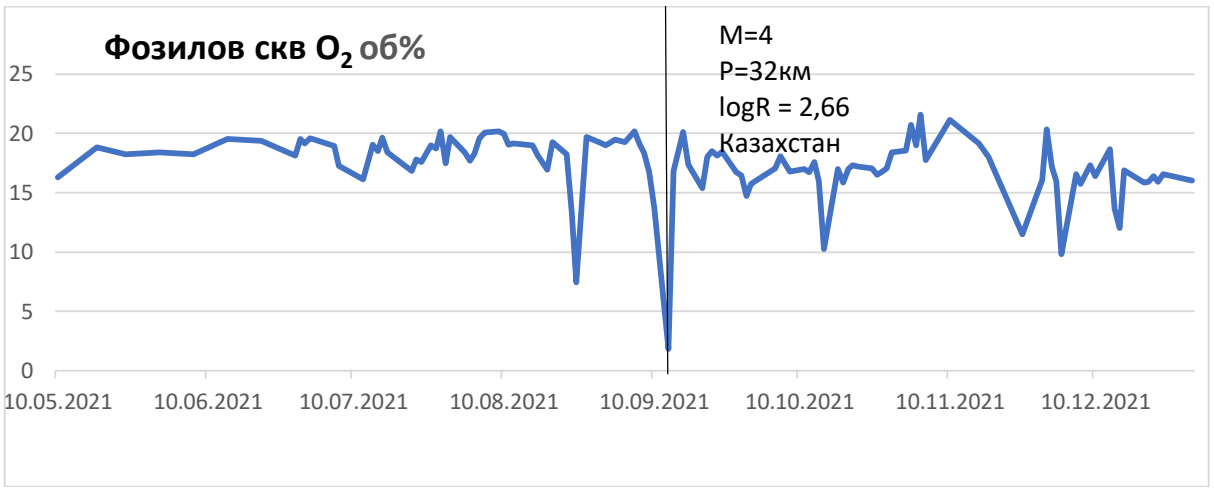

Рисунок 3. **-График изменения кислорода в скважине «Фазилов»**

Рисунок 4. - **График изменения pH в скважине «ИБК»**

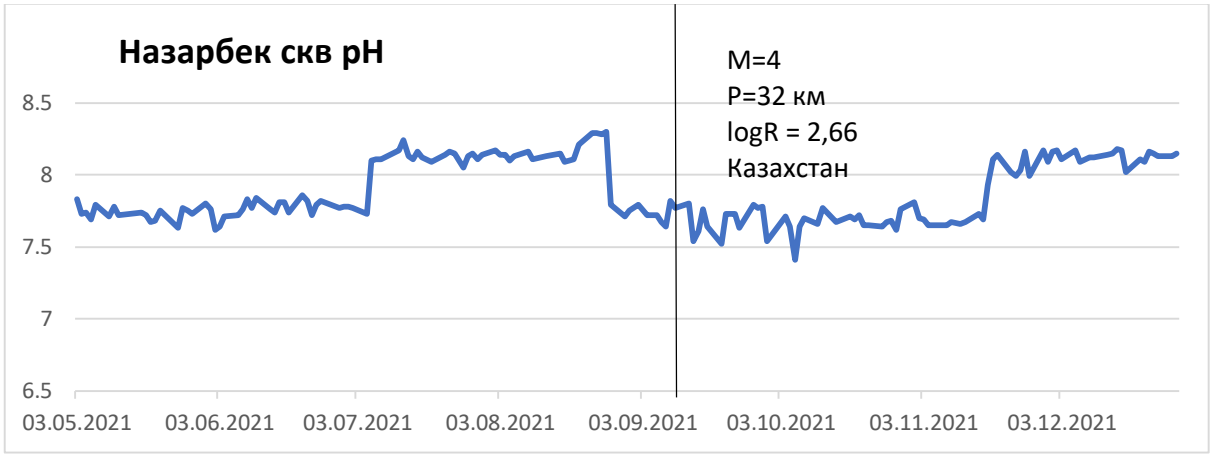

Рисунок 5. - **График изменения pH в скважине Назарбек**

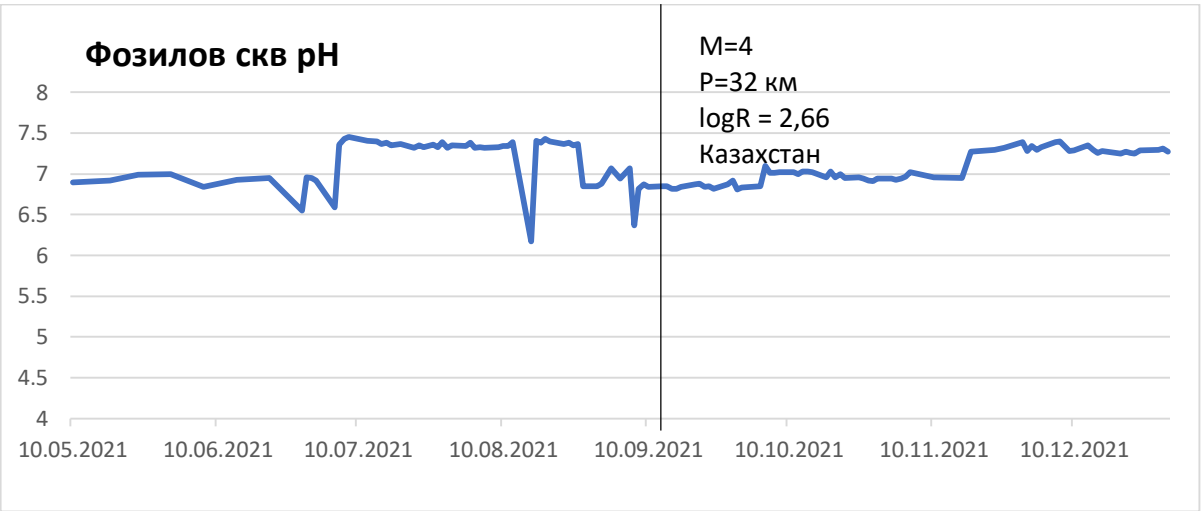

Рисунок 6. - **График изменения показателя pH в скважине «Фозилов».**

Многолетние исследования концентрации ионов водорода в артезианском бассейне Ташкента позволили определить резкое изменение pH в период сейсмической активизации на этом участке. Снижение pH было обнаружено по всей территории за несколько дней, а иногда и за 1-2 месяца до землетрясения. После землетрясения значения pH постепенно увеличиваются и возвращаются к исходному значению через 8-11 месяцев [7].

По результатам многих исследований, небольшие землетрясения небольшой магнитуды, незаметные на Земле, вызывают химические изменения. Микросейсмические явления приводят к значительному снижению pH в подземных вод и нарушениям химических связей в горных породах [6,12]. Он вступает в реакцию с окружающей водой и образует кислые сточные воды. Хотя магнитуда землетрясения невелика, выработанной механической энергии достаточно, чтобы разорвать химические связи. Чем выше магнитуда землетрясения, тем больше количество разорванных ковалентных связей в силикатах и выше кислотность грунтовых вод. Изменения кислотности достаточно велики, чтобы растворить минералы в горных породах и высвободить захваченные элементы, такие как металлы, что позволяет им перемещаться по поверхности Земли. Некоторые из этих элементов, такие как кальций и магний, играют важную роль в связывании углекислого газа в атмосфере и, таким образом, могут влиять на глобальную температуру. Повышение кислотности приводит к растворению минералов карбонатов кальция и магния Изменения кислотности происходят только в результате растрескивания пород на основе кремнезема, таких как гранит.

Химически активные молекулы кислорода и водорода выделяются из силикатных минералов вследствие открытия новых поверхностей перед землетрясениями. Породы, слагающие мантию Земли, в основном состоят из силикатов — различных соединений со структурой кремния и кислорода. Обычные силикаты в мантии включают оливин, гранат и пироксен. Другими основными породами мантии являются оксид магния. Другие элементы мантии включают железо, алюминий, кальций, натрий и калий. Температура мантии сильно варьирует: от 1000° C (1832°F) вблизи границы с мантией до 3700° C (6692°F) вблизи границы с ядром. В мантии температура и давление обычно возрастают с глубиной. Под действием высокой температуры и высокого давления силикаты мантии меняют свою кристаллическую структуру. Брид-гиманитовый силикат составляет 97% мантии [13].

Минеральные поверхности генерируют активированные формы кислорода путем расщепления воды. Экспериментально установлено, что этот процесс приводит к образованию активированного кислорода на границе минерал-вода, который также забирает кислород из минералов [4].

Согласно 1-му закону термодинамики, в природе один вид энергии переходит в другой вид энергии в эквивалентном количестве, то есть механическая сила, возникающая при

движении пластин, может легко разорвать прочные ковалентные связи Si-O в [SiO4]4- тетраэдры [энергия диссоциации: 793,2 ± 16,4 кДж моль-1] силикатных минералов приводит к образованию поверхностно-связанных радикалов (SBR) с неспаренным электроном в кристаллической оболочке, таких как E'-центр (≡Si•), кислородный радикал (≡SiO•) и пероксирадикал (≡SiO•) [1]

3. Процесс образования кислорода

Вновь образовавшиеся поверхности содержат три разных центра: центр E', оксицентр и пероксицентр, эти центры очень активны и вступают в определенные реакции с грунтовыми водами.

$$\equiv Si\text{-}OO\text{-}Si\equiv \rightarrow \equiv SiO\ O\ \bullet + \equiv Si\bullet \quad [9]$$

$$\equiv SiO\bullet + H_2O \rightarrow SiOH + HO_2\bullet \quad [10]$$

$$2HO_2\bullet \rightarrow H_2O_2 + O_2 \quad [11]$$

На основе знаний о поверхностной реакционной способности кварца и его поведении при взаимодействии с водой были проведены исследования с использованием мертвой воды (H_2O^{18}, 97%) с меченым изотопом O^{18} в качестве индикатора для отслеживания источника активированного кислорода (в природном абразивном кварце, содержащем O^{18} (~0,2%) OH, H_2O_2 и O_2 образуются одновременно в реакциях между водой и новообразованными поверхностями. Радикал H, отделившийся от центра E' объединяется с образованием H_2 [3, 4, 5].

$$\equiv Si^{\cdot} + H_2O \rightarrow Si\text{-}OH + H \quad [12]$$

$$2H \rightarrow H_2 \quad [13]$$

В результате этого процесса значение pH минеральных вод снижается, а окружающая среда становится кислой. Для измерения изотопного состава OH использовался метод бензойной кислоты (БА) и проводилась реакция с водой, содержащей изотоп O^{18}. Результаты, полученные бензойнокислотным методом, показали, что количество п-гидроксибензойных кислот с изотопным содержанием O^{18} и O^{16} получено в соотношении 137 и 139. Отсюда можно заключить, что бензойная кислота, богатая O^{18}, была бы получена, если бы активированный кислород выделялся только из воды. Удивительно , но гидроксобензоид, п-C_6H_4COOH (^{18}OH), образующийся при окислении бензойной кислоты новообразованным OH после диссоциации H_2O_2 в реакциях составляет лишь ~27%, п-C_6H_4COOH (^{16}OH) составил (~73%). Высокое содержание O^{16} в H_2O_2 объясняется уравнениями 6 и 7, где атомы кислорода в ≡SiO участвуют в образовании H_2O_2. есть по крайней мере один атом кислорода, который переходит от ≡SiOO к HO_2. Если диссоциация связи в ≡Si–O–O происходит по связи O–O, то только один кислород в HO_2 происходит из ≡Si-O-O и ожидается, что содержание O^{16} в продукте H_2O_2 составит ~ 50%. Действительно, высокое содержание O^{16} в H_2O_2 (>50%) указывает на то, что атомы кислорода в ≡SiO как переходят в H_2O_2, так и образуются в результате диссоциации связи Si–O в HO_2 ≡Si–O–O показывает. O^{18} Из-за быстрого добавления обогащенного O OH C_6H_5COOH в раствор (уравнение 14) H_2O_2 образуется за счет комбинации OH (уравнение 12), образованного из ≡ Центры SiO будут

$$OH + C_6H_5COOH \rightarrow pC_6H_4OHCOOH \quad [14]$$

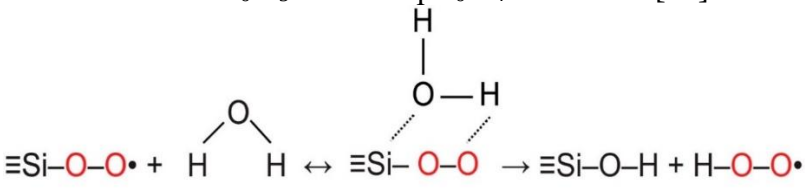

[15]

Предполагаемые пути переноса кислорода при окислении пероксирадикала (≡ Si OO). Атом H воды соединяется с концевым кислородом поверхностного пероксирадикала (≡ Si OO), а атом O воды соединяется с атомом Si ≡ Si OO, поэтому пероксикислородная пара (O–O) представляет собой сохраняется и образуется HO_2 (пергидроксильный радикал). Красные буквы обозначают каменистый кислород из силикатов.

Увеличение кислорода также приводит к усилению окислительно-восстановительного процесса, а также наблюдаются аномалии показателя Eh (рис. 7, 8, 9).

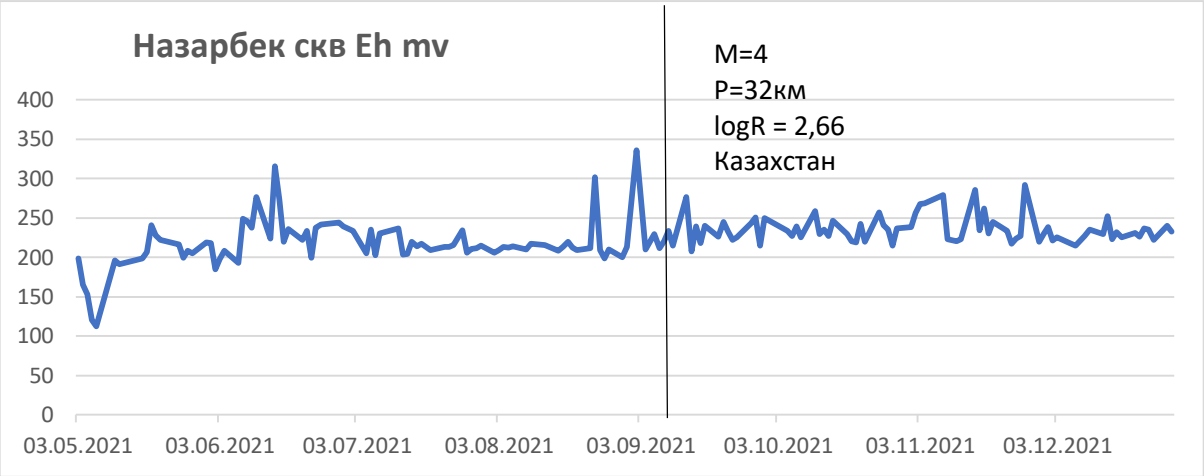

Рисунок 7. **Изменение количества Eh в скважине «Назарбек»**

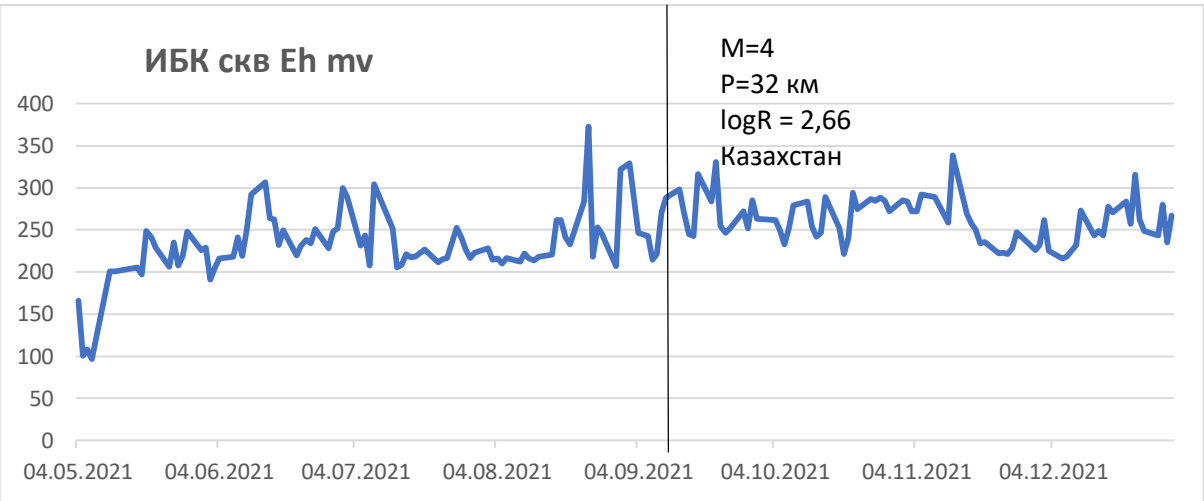

Рисунок 8. **Изменение количества Eh в скважине «ИБК»**

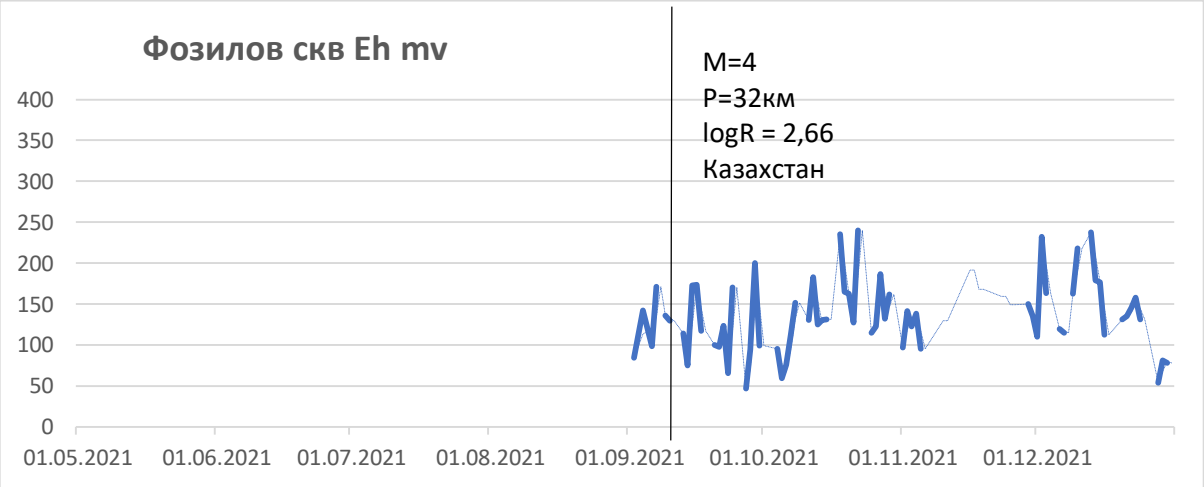

Рисунок 9. **Изменение количества Eh в скважине «Фазилов».**

4. Заключение

По результатам наших наблюдений наблюдается ряд изменений в составе подземных вод при геодинамических процессах, в частности, содержание кислорода сначала уменьшается за счет смыкания старых поверхностей, а затем увеличивается за счет раскрытия новых поверхностей, что приводит к изменяется окислительно-восстановительный потенциал показателя Eh, увеличение ионов водорода повышает кислотность грунтовых вод, т.е. pH показателя падает.

Увеличение кислотности грунтовых вод вызывает растворение таких минералов, как карбонаты кальция и магния. Увеличение содержания углекислого газа в воде наблюдается за счет выделения углекислого газа из карбонатов.

Литература

1. “A mineral-based origin of Earth’s initial hydrogen peroxide and molecular oxygen” Hongping He, Xiao Wu, Jianxi Zhu https://doi.org/10.1073/pnas.2221984120
2. «Изменения химического состава грунтовых вод перед крупными землетрясениями и возможные последствия для животных» *Рэйчел А. Грант 1, Тим Холлидей 2, Вернер П. Бальдерер 3, Фанни Лойенбергер, Мишель Ньюкомер, Гэри Сир и Фридеманн Т. Фройнд*
3. www.mdpi.com/journal/ijerph
4. Микросейсмические явления вызывают значительное падение pH в подземных водах *М. Стиллингс, Р. Дж. Ланн, С. Питарули, З. К. Шиптон, М. Кинали, Р. Лорд, С. Томпсон* Первая публикация: 17 декабря 2020 г. https://doi.org/10.1029/2020GL089885
5. Согласно новому исследованию, крошечные землетрясения делают грунтовые воды кислыми сайт УКРИ
6. Землетрясения могут окислить грунтовые воды *Аарон Сиддер* 10 февраля 2021 г.
7. *А. Н. Султанходжаев, Г. Ю. Азизов, Т. Закиров, И. А. Лунева, Н. Ф. Саидкамалов, С. С. Хусамиддинов* "Гидрогеосейсмологические исследования в Восточной Фергане" ИЗДАТЕЛЬСТВО "ФАН" УЗБЕКСКАЯ ССР ТАШКЕНТ - 1978г.
8. “Oxygen Isotopes in Mantle and Crustal Magmas as Revealed by Single Crystal Analysis” *Ilya Bindeman* Department of Geological Sciences University of Oregon Eugene, Oregon, 97403-1272, U.S.A. bindeman@uoregon.edu
9. *Гусева Н.В., Отакулова Ю.А.* Геохимия подземных вод Приташкентского артезианского бассейна (Республика Узбекистан). DOI 10.46566/2225-1545_2021_2_85_489 УДК: 551.49 (575.1)
10. *Расулов А.В. Қаюмов Б.Р.* "Особенности формирования газового состава в подземных водах сейсмогенных зонах Узбекистана" Международной научно-практической конференции «интеграция науки, образования и производства – залог прогресса и процветания», посвященной 5-летию основания Навоийского отделения академии наук республики Узбекистан в Трёх томах. Том I 9-10 июня 2022 года, город навои, республика узбекистан 248-252 бетлар
11. *И. Слесак, Х. Слесак, Й. Крук*, Кислород и перекись водорода в ранней эволюции жизни на Земле: сравнительный анализ биохимических путей in silico. Астробиология 12, 775–784 (2012).
12. «Микросейсмические явления вызывают значительное падение pH в подземных водах» *М. Стиллингс , Р. Дж. Ланн , С. Питарули , З. К. Шиптон , М. Кинали , Р. Лорд , С. Томпсон* Первая публикация: 17 декабря 2020 г. https://doi.org/10.1029/2020GL089885
13. *Дж.Ж. Кендирбаева* Идентификация гидрогеохимических и гидродинамических эффектов с проявлениями сейсмичности на территории Кыргызстана Вестник КРАУНЦ. Физ.-мат. науки. 2020. Т. 33. № 4. С. 209-223. ISSN 2079-6641
14. *Wisnu Arya Gemilang, Gunardi Kusumah, Guntur Adhi Rahmawan* HIDROGEOKIMIA AIRTANAH TIDAK TERTEKAN KAWASAN PESISIR DI PEMUKIMAN NELAYAN KECAMATAN TEUPAH SELATAN, KAB. SIMEULUE, PROVINSI ACEH Ris.Geo.Tam Vol. 28, No.1, Juni 2018 (25-35) DOI: 10.14203/risetgeotam2018.v28.636
15. *Maya Aiko Salsabila Putri, Thomas Triadi Putranto, Narulita Santi Analisis Hidrogeokimia Dan Logam Berat Pada* Air Tanah Menggunakan Metode WQI dan HPI Untuk Keperluan Higiene Sanitasi Kabupaten Belitung Timur Tersedia online di: http://ejournal.undip.ac.id/index.php/teknik TEKNIK, 44 (3), 2023, 211-221
16. *Aldynanda Lesmana, Boy Yoseph CSSSA, T. Yan Waliana Muda Iskandarsyah* KARAKTERISTIK HIDROKIMIA AIR TANAH PADA BAGIAN TIMUR CEKUNGAN AIR TANAH BANDUNG – SOREANG : STUDI KASUS SEBAGIAN KECAMATAN CICALENGKA DAN KECAMATAN CIMANGGUNG, PROVINSI JAWA BARAT Padjadjaran Geoscience Jornal. Vol. 5, No. 6, Desember 2021: 546-561
17. *Wisnu Arya Gemilang, Hendra Bakti Penilaian Hidrokimia* dan Kualitas Air tanah Tidak Tertekan di Kawasan Pesisir Simeulue Timur, Provinsi Aceh Jurnal Lingkungan dan Bencana Geologi, Vol. 10 No. 1, April 2019: 39 – 50

18. *Kepala Bapedalda Propinsi Daerah Istimewa Yogyakarta* PERUBAHAN KUALITAS AIRTANAH DI SEKITAR SUMBER PENCEMAR AKIBAT BENCANA GEMPA BUMI Forum Geografi, Vol. 20, No. 2, Desember 2006: 99 – 119
19. *Malakootian, M., Nouri, J.* Chemical Variations of Ground Water Affected by the Earthquake in bam region Int. J. Environ. Res., 4(3):443-454, Summer 2010
20. *Yeeping Chia, Yuan-Shian Wang, Jessie J. Chiu, Chen-Wuing Liu* Changes of Groundwater Level due to the 1999 Chi-Chi Earthquake in the Choshui River Alluvial Fan in Taiwan Bulletin of the Seismological Society of America, 91, 5, pp. 1062–1068, October 2001
21. *Kei Nakagawa, Zhi-Qiang Yu, Ronny Berndtsson, Takahiro Hosono* Temporal characteristics of groundwater chemistry affected by the 2016 Kumamoto earthquake using self-organizing maps Journal of Hydrology 582 (2020) 124519

К ВОПРОСУ НЕОБХОДИМОСТИ СЕЙСМИЧЕСКОГО МИКРОРАЙОНИРОВАНИЯ В ГОРОДСКИХ ТЕРРИТОРИЯХ (НА ПРИМЕРЕ ГОРОДА ГУЛИСТАН)

Ядигаров Э.М.[1], Хусомиддинов А.С.[1], Исламов Х.А.[1], Мансуров А.Ф.[1]
[1]Институт сейсмологии им. Г.А.Мавлянова АН РУз, Ташкент, Узбекистан
E-mail: ahrorhs1980@gmail.com

Аннотация: *В статье приводится результаты проведенных работ для сейсмического микрорайонировании территории города Карши. Сейсмический интенсивность оценины не только в макросесмических баллах и в пиковых ускорениях грунта. Оценено влияния грунтовых условий на параметры сейсмической интенсивности на основе сейсморазведочных, а также инженерно-геологическими методами с использованием сейсмогрунтовых моделей. Для решения задач СМР города Карши сейсморазведочные работы проводилась в 34 точках по всей территории города. На основе обобщение полеченных инженерно-сейсмологических результатов составлены карты сейсмического микрорайонирования территории города в двух показателях.*

Ключевые слова: *Грунтовые условия, исходная сейсмичность, приращение сейсмичной интенсивности, макросейсмическая шкала, пиковое ускорение.*

1. Введение

Землетрясения принадлежат к величайшим катастрофам, происходящим на земном шаре. Землетрясения как стихийные бедствия представляют собой исключительно сложные, слабоизученные по своим последствиям явления. Главная опасность землетрясении-разрушение зданий и сооружений, влекущее за собой человеческие жертвы. Более 75% территории Узбекистана находятся в сейсмических опасных зонах. Исходя из этого, за последние годы Президентом Республики Узбекистан и Кабинетом Министров нашей Республики разработан комплекс мер, направленных на уменьшение негативных последствий сильных землетрясений и обеспечение сейсмической безопасности населения республики и объектов промышленного и гражданского строительства. Разработка карт сейсмического микрорайонирования (СМР) городов выполняется в рамках Указа Президента Республики Узбекистан от 30 мая 2022 года УП-144 «О мерах по дальнейшему совершенствованию системы обеспечения сейсмической безопасности Республики Узбекистан» и постановления Президента Республики Узбекистан от 16 мая 2023 года ПП-158 «О дополнительных мерах по дальнейшему совершенствованию системы обеспечения сейсмической безопасности населения и территории Республики Узбекистан» (Приложение 1, Пункт 7).

Оценка сейсмической опасности обычно сводиться к вычислению максимально возможных сейсмических воздействий, которые необходимо учитывать при строительстве в сейсмических районах. Сейсмическая опасность отражается на картах сейсмического районирования той или иной территории [1-14]. В нашей стране в зависимости от задач и необходимой детальности картирования сейсмической опасности рассматривается три типа. 1) Общее сейсмическое районирования (ОСР)- для всей территории страны: 2) Детальное сейсмического районирования (ДСР)-для ограниченных площадей и отдельных регионов: 3) Сейсмическое микрорайонирование (СМР)-для городов, населённых пунктов и строительных площадок. В состав сейсмическое микрорайонирование входит комплекс методов позволяющий определить сейсмичность изучаемой площадки с учетом локальных грунтовых

условий по данным инженерно-геологических изысканий. Известно, что балльность района определяемая по картам сейсмического районирования, является величиной, условной для конкретного района, и не решает полностью вопроса о расчётной сейсмической интенсивности, в особенности, когда проектируются и возводятся крупные и ответственные сооружения. Это объясняется осредненностью грунтовых условий и поэтому, в случае необходимости они подлежат уточнению. В настоящее время сейсмическим микрорайонированием пользуются не только для назначения антисейсмических мероприятий при проектировании сооружений, но и при выборе места постройки, для исключения нередко не оправданных экономических расходов.

Сейсмическое микрорайонирование выполняется с целью количественной оценки влияния местных инженерно-геологических условий (состав и свойства грунтов, положение грунтовых вод, особенности рельефа, наличие сейсмоактивных разломов и др.) на сейсмичность с указанием изменения интенсивности в баллах по ГОСТ 34511-2018, а также инженерных параметрах, таких как пиковое ускорения колебания, спектр амплитуд и реакции, длительности колебания. До сегодняшнего дня разработанные нами карты СМР составлялись только в одних параметрах сейсмического измерение, то есть в баллах. В настоящее время карты сейсмического микрорайонирования делается на 2 вида (в макросейсмических баллах и инженерных показателях).

2. Материалы, методы и объект исследования

В настоящее время, с развитием методики СМР предлагается осуществлять на новой научно-методической основе с использованием параметров сейсмических воздействий и грунтовой толщи, непрерывно распределенных в пространстве. Уточнение исходной сейсмичности территорий является неотъемлемой частью работ по сейсмическому микрорайонированию. Оно основано на комплексных сейсмологических, сейсмотектонических и геолого-геофизических исследованиях, направленных на определение интенсивности сейсмических воздействий на территории, для которых осуществляется сейсмическое микрорайонирование. Были построены карты эпицентров инструментально-зарегистрированных землетрясений, её анализ на предмет приуроченности эпицентров к основным тектоническим нарушениям, определяющим сейсмичность на исследуемом объекте. Выделено на основе сейсмотектонических и сейсмологических методов сейсмогенных зон, оказывающих значимый сейсмический эффект на строительную площадку. Расчеты выполнялись, с учетом параметров повторяемости землетрясений (A10, γ) и величины сейсмического потенциала Ммах, периодов повторения сотрясений с заданными значениями пиковых ускорений и выделение на их основе зон не превышения в течение 50-ти лет величин максимальных ускорений с вероятностью P=0.9; P=0.95, P=0.98 и P=0.99.

Для определения категории и состава грунтовых условий проведены полевые инженерно-геологические, геофизические полевые исследования на территории распространения различных литологических типов грунтов. При этом использованы современный цифровой трехкомпонентный сейсмометр CMG-6TD производство Guralp (Великобритание) с частотной характеристикой – равномерная в диапозоне 0,03-50 Гц, сейсморазведочная станция «MAE X610-S» (производство Италия) с применением горизонтальных и вертикальных сейсмоприемников, частотой 4,5 Гц. Обработка и расчеты данных проведены с использованием программных средств: «Reflexw», «Rayfract», «PcLab» (Италия).

Для оценки приращения сейсмической интенсивности площадки использован метод Накамуры [15], более известного, как метод отношений спектров горизонтальной компоненты записи к вертикальной (the Horizontal to Vertical Spectrum Ratio - HVSR) и методы сейсмических жесткостей и инженерно-геологических аналогии.

3. Анализы и результаты

Объект исследования является г. Гулистон. Город Гулистон расположен в центральной части Узбекистана. По своему структурному положению данная территория относится к области перехода от Тянь-Шаньского эпиплатформенного орогена к Туранской платформе. Сейсмичность территории напрямую связана с тектоникой данного региона и проявляется в основном в пределах крупных разломов земной коры, активизированных на современном этапе геологического развития. Области динамического влияния этих разломных зон выделены. [16-17] в сейсмогенерирующие зоны.

Инженерно-геологические данные позволяют классифицировать грунты с точки зрения сейсмического эффекта, проявляемого в рассматриваемом районе. Инженерно-геологическая характеристика пород на основании зданий и сооружений исследуемой территории служат следующие отложения четвертичного периода: Карнабского (QIIkr), Шоркудукского (QIIIsh), Сукайтинского (QIIsk), Амударьинского (QIVad) комплексов, а также современные антропогенные (antQIV). Четвертичные отложения представлены: Карнабский-пролювиальными, Шоркудукский-пролювиальными, Сукайтинский-аллювиальными и аллювиально-пролювиальными, Амударьинский-аллювиальными, антропогенные образования- насыпными грунтами, а также глинистыми осадками ирригационных каналов.

Инженерно-геологических районов в г.Гулистане два. Первый район в геологическом строении принимают участие четвертичные аллювиально-пролювиальные отложения голодностепского комплекса (ap Q3gl). В литологическом отношении на разведанную глубину от 12,0 м до 30,0м участок сложен толщей глинистых грунтов, представленных лёссовидными супесями коричневого цвета, от влажных до водонасыщенных, от мягко пластичной до текучей консистенции. С поверхности земли залегают насыпные грунты мощностью от 0,3 м до 2 м. Насыпные грунты разнородные по составу, плотности сложения и физико-механическим свойствам и в качестве оснований фундаментов не могут быть использованы. В этом районе есть инженерно-геологические подрайоны, под названием I-1. Этот подрайон имеет инженерно-геологические участки, первый участок I-1 - Супеси, в основном, водонасыщенные, текучие, слабые, которые с глубиной замещаются суглинками более плотными, глубина залегания уровня подземных вод на расчетный максимум до 1,0 м. Второй участок II-1 - Супеси пластичные и текучие, слабые, с глубиной замещаются более плотными суглинистыми грунтами, глубина залегания уровня подземных вод на расчетный максимум 1,0-2,0 м, местами до 2,7 м.

Второй район территории кладбищ - исключаются из застройки.

Все существующие методы сейсмического микрорайонирования имеют общую основу: из анализа инженерно-геологических и сейсмологических данных изучаемой площади необходимо выделить так называемый «эталонный грунт». Сейсмическая интенсивность I и III категорий грунтов оценивается увеличением или уменьшением (III категории) относительно ко II категории. Приращение сейсмической интенсивности одного грунта относительно другого с помощью физической характеристики грунта осуществлено С.В. Медведевым.

В инженерно-геологических и гидрогеологических иследованиях в настоящее время получили развитие геофизические изыскания методом многоканального анализа поверхностных волн (MASW). Сейсморазведочные работы проводилась в 34 точках.

По всем точкам были рассчитаны значения V_{s30}. Согласно полученным результатам, скорости V_{s30} для всей площадки лежат в диапазоне 246-330 м/с (рис. 1).

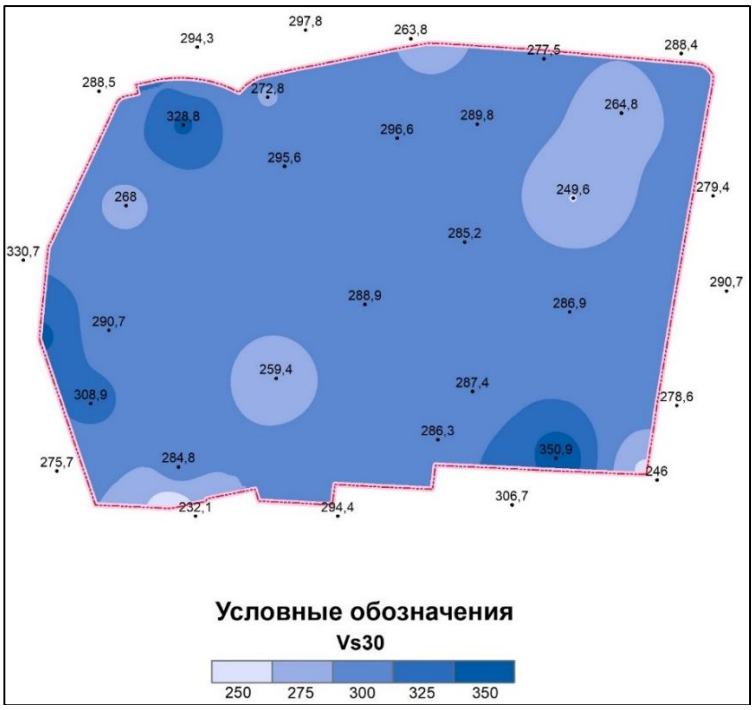

Рисунок 1. - **Карта распределения V_{s30}**

В настоящее время в практике СМР используются скорости поперечных волн, значения которых не зависят от обводненности. По данным о скоростях распространения сейсмических (поперечных волн) волн, полученным сейсморазведочной исследований о плотностях грунтов рассчитаны приращения балльности △I по формуле [18-20]:

$$\Delta I = Klg\frac{V_{эт}\cdot\rho_{эт}}{V_i\cdot\rho_i} \qquad (1)$$

Где *K*- коэффициент пропорциональности. Причем инструкция рекомендует принимать *K* равным 1,67.

При расчетах приращения интенсивности сейсмических воздействий по МСЖ в расчет принималась грунтовая толща мощностью 30 м. Приращения сейсмической интенсивности по МСЖ определялись на основании значений скоростей V_{s30}, полученных результатами сейсморазведки методом MASW с учетом параметров выбранного эталоного грунта (рис.2.).z

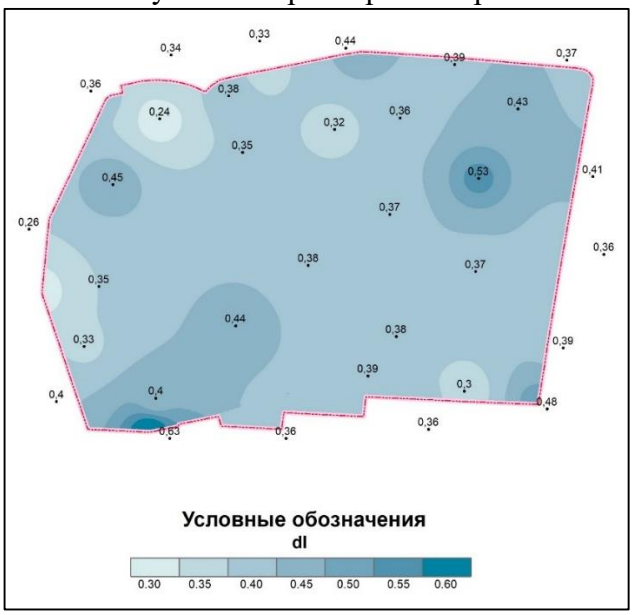

Рисунок 2. - **Карта приращений сейсмической интенсивности по методу сейсмических жесткостей г. Гулистан**

Проведено определение сейсмических жесткостей грунтовых толщ на глубину 30 м, а в некоторых пунктах и более 30 метров, в 34 точках. Обобщенные результаты оценки

показывают изменение приращения сейсмической интенсивности в пределах от +0,24 до +0,48 баллов.

Для расчета воздействий на свободную поверхность необходимо задать исходное колебание, совместимое с целевым спектром реакции на скальное основание. Следующим шагом является построение сейсмогеологических моделей грунтовой толщи площадки.

В таблице 1 приведены значения максимальных ускорений колебаний грунта (PGA, g) для вероятностей P=0.9, P=0.95, P=0.98 и P=0.99 не превышения уровня сейсмических воздействий в течение 50 лет на грунтах I, II и III категории по сейсмическим свойствам.

Таблица 1 - Значения максимальных ускорений колебаний грунта (PGA, g) для различных вероятностей не превышения уровня сейсмических воздействий в течение 50 лет на грунтах I, II и III категории по сейсмическим свойствам. [19,20.]

Таблица 1.

Категория грунта	Значения максимальных ускорений a_{max}, g			
	P=0,9	P=0,95	P=0,98	P=0,99
I категория	0,082	0,111	0,160	0,208
II категория	0,103	0,139	0,200	0,257
III категория	0,130	0,177	0,254	0,327

Обобщенная сейсмогеологическая модель для проведения расчетов на основании инженерно-геологических и сейсморазведочных данных (профили MASW) были построены 100 модели грунтовой толщи. Для учета неопределенностей грунтовых моделей и входных акселерограмм использовался метод Монте-Карло, реализованный в программе Strata. В качестве входных акселерограмм использован набор из 6 штук. Каждая акселерограмма пропускалась через грунтовую толщу. Умножая на количество параметров грунтовой модели, получаем общее число 180 ветвей в расчетах программы Strata. Расчётные методы позволяют определить амплитудно-частотные характеристики слоистой грунтовой толщи и, соответственно, изменённые слоистой средой характеристики колебаний на свободной поверхности площадки или во внутренних точках среды.

Для проведения расчетов по этому методу необходимо определить исходное сейсмическое воздействие, заданное акселерограммой и спектром реакции, и построить сейсмогеологические модели грунтовой толщи. В качестве входных акселерограмм использованы синтезированные акселограммы (рис. 3).

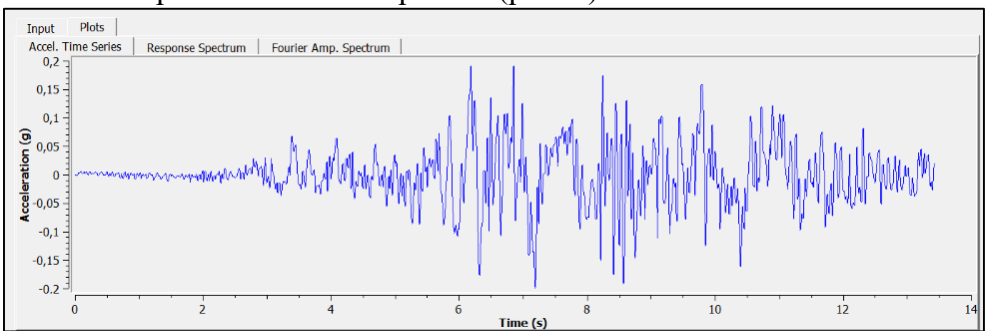

Рисунок 3. - **Синтезированная акселерограмма для территории г. Гулистана**

Акселерограмма были нормализована и приведена к значению ускорения, соответствующего ускорению грунтов первый категории, распространенных на территории города Карши глубинах 100 м, которые представлены плотными конгломератами неогенового возраста. На основании подобного подхода разработаны 100 сейсмогеологических моделей, их расположение в плане приведено на карте точек расположения сейсмогеологических моделей. Здесь необходимо отметить, что при разработке сейсмогеологических моделей использованы результаты сейсморазведки, т.е. изменения V_{s30} в пространстве. Карта сейсмического микрорайонирования была построена на основании медианный, полученных на поверхности Земли по программе Strata (рис.4).

Таким образом, для проектирования высотных зданий динамическими методами разработана карта сейсмического микрорайонирования территории г.Карши по значениям

пикового ускорения (PGA). На исследуемой территории по значениям максимального ускорения колебания грунтовых толщ выделены следующие предельные значения: от 0,18g и до 0,34g. Интенсивность сотрясений на исследуемой площади учетом результатов сейсмического микрорайонирования. Исходные воздействия на площадку на уровне 7,19 баллов.

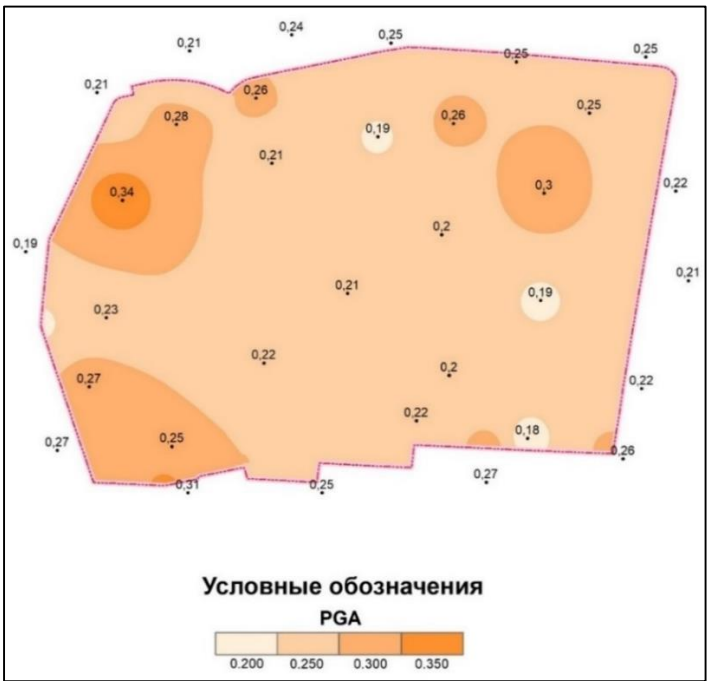

Рисунок 4. - **Карта сейсмического микрорайонирования территории города Карши по значениям пикового ускорения (PGA)**

Рисунок 5. - **Карта сейсмической интенсивности (в макросейсмических баллах)**

В составленной карте сейсмического микрорайонирования территории города Карши в масштабе 1:25 000 выделены только 8-ми балльная зона (рис.5).

4. Заключение

Таким образом, город Карши относится к средней категории по сложности инженерно-геологических условий. В области исследований грунты относятся к третьей категории по сейсмическим свойствам. В рамках сейсмического микрорайонирования территории города Гулистана проведены исследования(сейсморазведка) на 34 геофизических точках. В результате были рассчитаны значения V_{s30} в каждой геофизической точке. На основании полученных результатов были рассчитаны значения приращения сейсмической интенсивности. Значения $\triangle I$ в пределах от + 0,23 до + 0,64. Общая сейсмическая интенсивность составила 8 баллов за счет того, что исходная сейсмичность города Гулистана составила 7,19 балла.

Литература

1. *Алешин А.С.* Континуальная теория сейсмического микрорайонирования. –М.: Научный мир, 2017. 302 с.
2. *Rasulov H.Z., Rasulov R.H., Tashxodjayev A.U., & Babajanov M.B*. (2020). Vibration creep of loess soils. IOP Conference Series: Earth and Environmental Science, 614(1), 012064. https://doi.org/10.1088/1755-1315/614/1/012064.
3. *Artikov T. U., Ibragimov R. S., Ibragimova T. L., Mirzaev M. A., & Artikov, M. T.* (2015). Revealing the seismicity increase in interrelationships in various seismic zones in Uzbekistan as a case study. Geodesy and Geodynamics, 6(5), 351–360. https://doi.org/10.1016/j.geog.2015.03.007
4. *Artikov T. U., Ibragimov R. S., Ibragimova T. L., & Mirzaev M. A.* (2016). Study of modern seismic zoning maps' accuracy (case for Eastern Uzbekistan). Geodesy and Geodynamics, 7(6), 416–424. https://doi.org/10.1016/j.geog.2016.04.015
5. *Artikov T. U., Ibragimov R. S., Ibragimova T. L., & Mirzaev M. A.* (2018). Identification of expected seismic activity areas by forecasting complex seismic-mode parameters in Uzbekistan. Geodesy and Geodynamics, 9(2), 121–130. https://doi.org/10.1016/j.geog.2017.11.005
6. *Artikov T. U., Ibragimov R. S., Ibragimova T. L., Kuchkarov K. I., & Mirzaev M. A.* (2018). Quantitative assessment of seismic hazard for the territory of Uzbekistan according to the estimated maximum ground oscillation rates and their spectral amplitudes. Geodynamics & Tectonophysics, 9(4), 1173–1188. https://doi.org/10.5800/GT-2018-9-4-0389
7. *Artikov T. U., Ibragimov, R. S., Ibragimova T. L., & Mirzaev M. A.* (2020). Complex of general seismic zoning maps OSR-2017 of Uzbekistan. Geodesy and Geodynamics, 11(4), 273–292.
8. *Artikov T. U., Ibragimov R. S., Ibragimova T. L., & Mirzaev M. A.* (2020). Models of the macroseismic field earthquakes and their influence on seismic hazard assessment values for Central Asia. Geodynamics & Tectonophysics, 11(3), 606–623. https://doi.org/10.5800/GT-2020-11-3-0494
9. *Artikov T. U., Ibragimov R. S., Ibragimova T. L., Mirzaev M. A., & Rebetsky Y. L.* (2021). Methods and results of long-term strong earthquakes forecast in the Uzbekistan territory. IOP Conference Series: Earth and Environmental Science, 929(1), 012028. https://doi.org/10.1088/1755-1315/929/1/012028
10. *Atabekov I. U., Artikov T. U., Ibragimov R. S., Ibragimova T. L., & Mirzaev M. A.* (2021). Relationship between Strong Earthquakes and Activation of Deep Faults in Central Asia (Uzbekistan): Numerical Simulation of Stress Field Variations. Geotectonics, 55(3), 377–392. https://doi.org/10.1134/S0016852121030031l2. Золотарев Г.С. Изучение напряженного состояния массивов пород в инженерно-геологических целях Метод. Указания//-Москва: Недра, 1978. - 136 с.
11. *Ibragimova T. L., Ibragimov R. S., Mirzaev M. A., & Rebetsky Yu. L.* (2021). The current stress of earth's crust in the territory of uzbekistan according to focal earthquake mechanisms. Geodynamics & Tectonophysics, 12(3), 435–454. https://doi.org/10.5800/GT-2021-12-3-0532
12. *Ibragimov R. S., Ibragimova T. L., Mirzaev M. A., & Rebetsky Yu. L.* (2023). The probability of a strong (m≥6.0) earthquake in the south Fergana seismic activity zone in the coming years. Geodynamics & Tectonophysics, 14(1). https://doi.org/10.5800/GT-2023-14-1-0688
13. *A.Khusomiddinov, Sh.Yodgorov, F.Sadirov, E.Yadigarov, B.Aktamov, Sh.Avazov*. Estimation of the Seismic Intensity Increments in Tashkent Region. The 1st International Conference on Problems and Perspectives of Modern Science AIP Conf. Proc. 2432, 030034-1–030034-5; https://doi.org/10.1063/5.0089662 Published by AIP Publishing. pp.030034-1-5.
14. *Ismailov V. A., Yodgorov S. I., Khusomiddinov A. S., Yadigarov E. M., Botirovich, A. S., & Aktamov, B. U.* (2023). New classification of soils by seismic properties for the building code in Uzbekistan. Geomechanics and Geoengineering, 1–21. https://doi.org/10.1080/17486025.2023.2296975
15. *C. Zhu, M. Pilz, F. Cotton,* Evaluation of a novel application of earthquake HVSR in site-specific amplification estimation. Soil Dynamics and Earthquake Engineering 139 (2020) https://doi.org/10.1016/j.soildyn.2020.106301
16. *Нурматов У.А., & Юсупджанова У.А.* (2023). Прогноз землетрясений, оценка сейсмической опасности и сейсмического риска в Центральной Азии. XI Казахстанско-Китайский Международный Симпозиум , 209–214.

17. *Нурматов У.А., Садыков Ю.М., & Юсупджанова У.А.* (2023). Геодинамические блоки западного Тянь-Шаня и прилегающих территорий . Материалы Международной Конференции “Актуальные Проблемы Обеспечения Сейсмической Безопасности Населения и Территорий”. - Ташкент, ИС АН РУз, , 218–226.
18. *Алешин А.С.* Континуальная теория сейс мического микрорайонирования. М.: Научный мир, 2017. 300 с
19. *Алешин А.С.* Основные понятия сейсмиче ского микрорайонирования: категория, балл, модель // Сейсмостойкое строительство. Безопасность сооружений. 2013.№5. С.9-13
20. *Алешин А.С.* О грунтовых коэффициентах // Сейсмостойкое строительство. Безопасность сооружений. 2018. №2. С.6-13.

СОДЕРЖАНИЕ

Секция А – Сейсмостойкость зданий и сооружений (теория и эксперимент)

Секция В – Инженерная сейсмология и сейсмический риск